STARBURSTS
AND GALAXY EVOLUTION

XXIInd Rencontres de Moriond : Astrophysics Meeting
Moriond Astrophysics Meeting

Les Arcs, Savoie, France - March 8-15, 1987

STARBURSTS AND GALAXY EVOLUTION

ISBN 2-86332-050-5

EDITIONS FRONTIERES
B. P. 44
91190 GIF SUR YVETTE - France

Printed in Singapore by Kim Hup Lee Printing Co. Pte. Ltd.

STARBURSTS AND GALAXY EVOLUTION

Edited by

TRINH XUAN THUAN
T. MONTMERLE
and
J. TRAN THANH VAN

Editions Frontières

Jacket designed by **Brigitte Tartière**

CONTENTS

FOREWORD

In the last few years has come the realization that a significant fraction of galaxies in the Universe undergo "starbursts". The wealth of ultraviolet, optical, infrared, and radio data obtained by large ground-based telescopes and the IUE and IRAS satellites on our Galaxy and nearby galaxies, has shown that the starbursts are phases when the star formation rate (in a localized region or over the whole galaxy), shows a large increase over the average rate for a period of time short compared to the galaxy's lifetime. The "starburst phenomenon" appears therefore today as a key factor to understand the evolution of galaxies.

Concurrently, there has been increasing observational evidence that starburst activity in galaxies was even more prevalent in the past. Rich concentrated clusters of galaxies at a look-back time of about 4 billion years or greater show an unusual proportion of blue galaxies, which follow-up spectroscopic work reveal to have undergone starbursts. Deep optical and radio surveys probing galaxies in the field at similar look-back times also suggest a large number of starburst galaxies.

Until now, these two lines of investigation, "local" and "cosmological", have been progressing parallel to each other, without much cross-fertilization of ideas. At the same time there have also been important developments in the understanding of the formation and evolution of massive stars in our own Galaxy, as well as of their interactions with the interstellar gas. Since massive stars are one of the main tracers of starbursts, these developments are very relevant to their understanding.

With these thoughts in mind, and with suggestions from R. Joseph, D. Kunth and R. Larson, we designed a workshop program intended to bring together experts on massive stars in the Galaxy, on starbursts in nearby galaxies, and observational cosmologists studying high-redshift star-forming galaxies, in an attempt to present an unifying view of the starburst phenomenon at all redshifts and its implications on galaxy evolution.

The 6-day workshop took place in the lovely setting of Les Arcs, in the French Alps, and was attended by 65 participants from 12 countries. These proceedings contain in camera-ready form all the 57 papers that were presented during the meeting. We have also added a contribution by Jim Condon, who could not attend the meeting but has graciously accepted to write up the talk he would have given. Starbursts are ubiquitous in the Universe. The first four sections are arranged in order of increasing redshift of the starburst environment : from the Galaxy and the Local Group galaxies (section I) to dwarf and HII galaxies (section II) to IRAS and interacting galaxies (section III) to intermediate and high-redshift galaxies and quasars (section IV) . Section V contains theoretical attempts to understand the starburst phenomenon, section VI discusses future instruments, and section VII contains the summary of the conference.

The workshop also included two very interesting joint scientific sessions with the particle physicists attending the concurrent workshop on Electroweak Interactions. The first was on Dark Matter. The second was on the supernova 1987A in the Large Magellanic Cloud. This supernova had the good taste to explode just two weeks before the meeting, making the 22nd Rencontres de Moriond the first international conference to discuss the neutrino, otpical and ultraviolet observations of SN 1987 A. The astronomical aspects were reviewed by J. Lequeux and his contribution is included as an appendix to his paper on the Magellanic Clouds.

The success of this highly productive, yet friendly and relaxed Rencontre de Moriond is largely due to the flawless local organization provided by J. Tran Thanh Van and his team which includes Monique Furgolle, Laurence Massiot, Lucienne Norry and Aida Ramos. Finally, we gratefully acknowledge the financial help provided by the Centre National de la Recherche Scientifique and the Commissariat à l'Energie Atomique.

Trinh X. Thuan　　　　Thierry Montmerle

AVANT-PROPOS

On s'est rendu compte très récemment qu'une proportion importante de galaxies dans l'Univers était le siège de sursauts de formation d'étoiles ('starbursts'). L'abondance des données UV, optiques, IR et radio obtenues au moyen de grands télescopes au sol et dans l'espace (IUE, IRAS), sur notre propre Galaxie et les galaxies proches, a permis d'établir que ces sursauts correspondent à des phases de courte durée où le taux de formation d'étoiles (dans une région localisée ou dans toute la galaxie) est très supérieur au taux moyen. Le phenomène "sursaut de formation d'étoiles" apparaît donc aujourd'hui comme un facteur-clé dans l'évolution des galaxies.

Dans le même temps, l'observation a montré de façon de plus en plus évidente que ces sursauts de formation d'étoiles étaient encore plus importants dans le passé. Des amas de galaxies riches et concentrés, de 4 milliards d'années plus jeunes que la Galaxie, contiennent une proportion étonnament élevée de galaxies bleues. Comme le montre leur spectroscopie, ces galaxies sont en fait passées par une ou plusieurs phases de formation d'étoiles intenses. Des observations profondes en optique et en radio de galaxies de champ, à des époques reculées comparables, montrent également la présence de nombreuses galaxies associées à des sursauts de formation d'étoiles.

Jusqu'à présent, ces deux voies de recherche, "locale" et "cosmologique", ont progressé parallèlement avec relativement peu d'échanges d'idées. Au même moment, sont apparus des développements importants dans notre compréhension de la formation et de l'évolution des étoiles massives dans notre Galaxie, ainsi que de leurs interactions avec le gaz interstellaire. Les étoiles massives étant des indicateurs importants de l'existence de sursauts de formation d'étoiles, ces développements sont en étroite relation avec l'étude de ce phénomène.

A la suite de ces réflexions, et avec le concours de R. Joseph, D. Kunth et R. Larson, nous avons établi le programme d'un colloque qui réunirait des experts de la formation et de l'évolution des étoiles dans la Galaxie et les galaxies proches, ainsi que les observateurs dont les travaux portent sur les galaxies à sursaut de formation d'étoiles très lointaines. Notre but était de présenter une vue unifiée du phénomène "sursaut de formation d'étoiles" dans tous les environnements et jusqu'à une époque lointaine, ainsi que les conséquences de ce phénomène sur l'évolution des galaxies.

Le Colloque a réuni pendant six jours, dans le cadre magnifique des Arcs, 65 participants venant de 12 pays. Le présent volume contient les 57 communications qui y furent présentées. Nous y avons ajouté un article de J. Condon, qui n'a pu assister au colloque mais a très aimablement accepté de rédiger le texte de la communication qu'il aurait souhaité présenter. Les sursauts de formation d'étoiles étant observés partout dans l'Univers, ceci nous a suggéré un plan par ordre de décalage cosmologique croissant : la Galaxie et le Groupe Local (chap. I), les galaxies naines et les galaxies HII (chap. II), les galaxies IRAS et les galaxies en interaction (chap. III), et pour finir, les galaxies de décalage cosmologique intermédiaire puis élevé, ainsi que les quasars (chap. IV). Le chapitre V contient des travaux théoriques récents sur le phénomène "sursaut de formation d'étoiles". Il est suivi d'une présentation des observatoires futurs (chap. VI), et enfin d'un résumé du colloque (chap. VII).

Le colloque a également compris deux sessions conjointes avec des physiciens des particules, qui assistaient en même temps à leur propre colloque sur les Interactions Electrofaibles. La première eut pour objet la "matière noire", la seconde porta sur la supernova 1987A dans le Grand Nuage de Magellan. Cette supernova eut le bon goût d'exploser à peine deux semaines avant le colloque, faisant des XXIIèmes Rencontres de Moriond la première conférence internationale où furent discutées simultanément les observations de neutrinos et les données astronomiques. Un évenement exceptionnel ! Les résultats en optique et UV ont été présentés "à chaud" par J. Lequeux, et la contribution de ce dernier est incluse ici en appendice à son article sur les Nuages de Magellan.

Le succès et l'animation de ces Rencontres de Moriond, leur ambiance amicale et détendue, doivent beaucoup à la perfection de l'organisation sur place, menée par J. Tran Thanh Van et son équipe en particulier Monique Furgolle, Laurence Massiot Lucienne Norry et Aïda Ramos. Enfin, nos remerciements vont au CNRS et au CEA pour leur aide financière.

Trinh X. Thuan Thierry Montmerle

I. STAR FORMATION IN THE GALAXY AND IN LOCAL GROUP GALAXIES

SN 1987 A in the Large Magellanic Cloud

(North is to the top and East to the left - photograph European Southern Observatory)

MASSIVE STAR FORMATION IN THE GALAXY

Peter G. Mezger
Max-Planck-Institut für Radioastronomie,
Auf dem Hügel 69, 5300 Bonn 1, F.R.G.

Summary

I. The galactic disk: We summarize the relevant characteristics of the galactic disk.

II. OB star and total star formation rates and its relation to the mass distribution in the galactic disk: OB star formation rates (SFRs) can be estimated from Lyman continuum (Lyc) photon production rates and warm dust (wd) luminosities, respectively, and total SFRs can be inferred if an Initial Mass Function (IMF) is adopted. We apply this procedure to the galactic disk. Resulting SFRs and lockup rates (i.e. the rate at which interstellar matter (ISM) through star formation is permanently locked up in low mass and dead stars) are compared with predictions made for a closed system ($M_{ISM}+M_{*}$ =const.) and a star formation law of the form $\psi \propto M^{\xi}_{ISM}$. It is found that the present-day SFR, inferred from the observed Lyc photon production rate with a constant IMF, can not be reconciled with the mass distribution of the galactic disk.

III. Bimodal star formation: Bimodal star formation in the galactic disk means that two different mechanisms of star formation are at work: In main spiral arms *induced star formation* is triggered by some global effects and only stars above a critical mass $m_C \sim 3\ m_{\odot}$ are formed. In the interarm region stars in the total mass range $m \gtrsim m_L \sim 0.1 m_{\odot}$ form due to *spontaneous star formation*. In the galactic disk about ~2/3 of all OB stars are formed via induced star formation. The bimodal IMF, together with star formation in a closed system, and spontaneous and induced SFRs being both proportional to the amount of molecular hydrogen, connects the observed present-day OB SFR correctly with the total mass distribution. The total bimodal SFR in the galactic disk is ~ $3 m_{\odot} yr^{-1}$. The average star formation efficiency in molecular clouds is $\varepsilon \sim 10^{-9}\tau_{cl} \sim (1-10)\%$, with estimated lifetimes of molecular clouds ranging from $\tau_{cl} \sim 10^{7}-10^{8}$yr.

I. The galactic disk

Our proto-galaxy was a sphere consisting originally of H and He gas. Formation of the first generation of stars and of a gaseous disk in the plane of rotation of the sphere occurred concurrently. These first generations of stars form today the galactic halo, which contains at least as much mass as the disk. Formation of the disk through accretion of halo gas must have occured over an appreciable fraction of its lifetime, but for the sake of simplicity I adopt in the following an effective lifetime of τ_{disk} ~ 1E10yr. Stars observed in the vicinity of the sun have masses in the range m ~ $(0.1-60)m_{\odot}$, with some stars having masses as high as ~ $100m_{\odot}$. O stars $(19-100m_{\odot})$ and B stars $(3.5-11m_{\odot})$ have MS lifetimes of some 1E6 yr and some 1E7 yr, respectively. In their final evolutionary stages stars return the fraction $r = 1-m_f/m$ of their MS mass m to the interstellar matter (ISM). The average mass of the stellar remnant, m_f, can be that of a white dwarf $(\sim 0.6m_{\odot})$ or of a neutron star $(\sim 1.4m_{\odot})$. It is this circulation of ISM through the interior of massive stars which is responsible for the "chemical evolution" of the Galaxy, i.e. the enrichment of the ISM and younger stars with elements heavier than ^{4}He. Since mainly massive stars with short MS lifetimes contribute to the mass return it is usually considered to occur "instantaneously" at the time when stars are formed. This yields a simple relation between lockup rate dM_*/dt and star formation rate (SFR) $\psi(t)$, in which the time delay between star formation and mass return, in essence the MS lifetime, is neglected

$$dM_*/dt = (1-r)\ \psi(t) \qquad (1)$$

With increasing age of the disk more and more mass is permanently locked up in low-mass and dead stars. Today in our Galaxy and in external spiral galaxies the ISM accounts for not more than a few percent of the total mass. Whenever the gas density exceeds ~ $1E2cm^{-3}$ molecular hydrogen forms on dust grains. Giant molecular clouds with masses as high as $5E6m_{\odot}$ contain most of the molecular hydrogen. They consist of subunits of $\sim(1E4-1E5)m_{\odot}$, which develop dense $(\gtrsim 1E5cm^{-3})$ cloud cores with masses up to some $1E3m_{\odot}$ and which are the locations of massive star formation. Having reached the MS O stars ionize the surrounding gas and form HII regions which emit free-free continuum emission at cm wavelengths. O and B stars heat dust in their surroundings to temperatures of ≳30K. This warm dust (wd) emission attains its maximum at FIR wavelengths ≲ 100μm. The bulk of the interstellar dust is heated by the general interstellar radiation field (ISFR) to temperatures between ~10−25K. Both radio and FIR emission can be observed throughout the Galaxy and therefore are used to trace the distribution of OB stars in the galactic disk.

Table 1: **Characteristics of the Galactic Disk for $R_\odot$ = 8.5kpc**

	Units	$R_{kpc} \leq 0.3$	$1.7 \leq R_{kpc} \leq 8.5$	Disk
Total Mass $M_D(R)$	$m_\odot$	6.5E8	4.4E10	1.2E11
Mass of atomic H	$m_\odot$	-----	0.7E9	1.4E9
Mass of molecular H_2	$m_\odot$	1.1E7	1.5E9	1.8E9
Mass of ISM:X^{-1}[M(H)+M(H_2)]	$m_\odot$	1.5E7	3.1E9	4.3E9
Lyc photon luminosity N_{Lyc}	s^{-1}	1.8E52	1.9E53	2.1E53
Stellar luminosity L	$L_\odot$	7.0E8	3.0E10	3.6E10
Total IR luminosity L_{IR}	$L_\odot$	2.7E8	1.1E10	1.2E10
(wd) Luminosity L_{IR}^{wd}	$L_\odot$	1.7E8	4.1E9	4.7E9
(cd) Luminosity L_{IR}^{cd}	$L_\odot$	5.1E7	4.6E9	5.3E9
Adopted age τ_{Disk}	yr	-----	1E10	-----

In Table 1 are compiled some of the characteristics of the galactic disk. Following the recent IAU recommendations a distance of the sun from the galactic center of $R_\odot$ = 8.5kpc is adopted. We subdivide the disk into nucleus (R≤0.3kpc) and spiral arm region (1.7≤R/kpc≤8.5) where most of the massive star formation occurs. But some molecular clouds together with a modest rate of massive star formation are observed to extend outside the solar circle. The distribution of atomic hydrogen ends at R ~ 16kpc and the distribution of old disk population stars extends even further. We refer the following quantitative discussion on (massive) star formation to the spiral arm region, since only there all relevant parameters are known with sufficient precision.

II. OB star and total star formation rates and its relation to the mass distribution in the galactic disk

1) Star formation rates determined from radio and FIR observations

The creation function

$$C(t,m)dm = \psi(t)\phi(m)dm \tag{2a}$$

yields the number of stars formed per unit time in the mass range m, m+dm. The inital mass function (IMF) is considered to be independent of time and is normalized to unity

$$\int_{m_L}^{m_U} \phi(m)m\, dm = 1 \tag{2b}$$

In the following we use the Miller and Scalo (1978) IMF with $m_L = 0.1 m_\odot$ and $m_u = 60 m_\odot$, but modified for $m \geq 20 m_\odot$ as described below. Integration of the creation function yields the SFR

$$\int_{m_L}^{m_u} C(t,m) m \, dm = \psi(t) \tag{2c}$$

which is, like the lockup rate eq.(1), expressed in $m_\odot yr^{-1}$.

From the free-free flux density the Lyman continuum photon production rate N_{Lyc} can be estimated by applying small corrections for Lyc photons which escape from density-bound HII regions or which are absorbed by dust grains in the ionized gas. This quantity is connected to the present-day SFR by the relation (see Güsten and Mezger, 1983, hereafter referred to as Paper I, and references therein):

$$N_{Lyc}(t_0) = \psi(t_0, m_L) \int_{m_L}^{m_u} \phi(m) dm \int_0^{\tau_{MS}(m)} N_{Lyc}(m,t) dt \tag{3a}$$

with $\tau_{MS}(m)$ the MS lifetime of a star of mass m and $\psi(t_0, m_L)$ the SFR of all stars in the mass range $m_L \leq m \leq m_u$. In the derivation of eq. (3a) it has been assumed that the SFR was constant during the MS lifetime of the stars. Since only stars with $m > 20 m_\odot$ contribute significantly to N_{Lyc} the integral depends on the slope of the IMF for $m \geq 20 m_\odot$. The influence of different slopes in this mass regime and different upper and lower mass limits is discussed in Paper I. A slope of $\gamma = 3.2 - 3.6$ ($\phi(m) \propto m^{-\gamma}$) as originally derived by Miller and Scalo (1978) is probably too steep (Scalo, 1986) and a slope of $\gamma = 2.6$, as suggested by Garmany et al. (1982), appears to be more realistic. We extrapolate the Miller-Scalo IMF for $m \geq 20 m_\odot$ with this slope and refer to it as "modified Miller-Scalo IMF". Evaluation of eq.(3a) with $m_L = 0.1 m_\odot$, $m_u = 60 m_\odot$ yields

$$\psi(t_0) = 2.7 \, (^{+1.3}_{-0}) \, 10^{-53} \, N_{Lyc} \tag{3b}$$

where the upper limit relates to the original Miller-Scalo (1978) IMF, the lower limit relates to the "modified Miller-Scalo IMF" (see Güsten, 1986).

The warm dust luminosity of a molecular cloud is related to its stellar content by

$$L_{IR}^{wd} = \sum_i f_d(m_i) \, L_*(m_i) \tag{4a}$$

with $f_d(m)$ the fraction of the stellar MS lifetime during which a star of mass m is still surrounded by dense ($n_H \sim 1E3 - 1E5 cm^{-3}$) gas and dust. Cox et al. (1986) estimate that B stars contribute most to the (wd) luminosity and that $\langle f_d(m) \rangle \sim 0.15$ when averaged over the stellar mass range $\sim(3-19) m_\odot$. In principle we could proceed as in the case of the free-free emission and express the total OB star luminosity $L_*(m)$ by a relation analoguous to eq.(3a). However, while only stars with masses $m \gtrsim 20 m_\odot$ contribute significantly to the Lyc photon production rate $N_{Lyc}(m,t)$ when integrated over the IMF and the MS lifetime, the corresponding integral with $L_*(m,t)$ substituted for $N_{Lyc}(m,t)$ would monotonously increase with decreasing stellar mass. This would mean that the relation between observed (wd) luminosity L^{wd}_{IR} and SFR $\psi(t_o)$, corresponding to the above eq. (3b), would in essence be determined by the highly uncertain correction factors $f_d(m)$ in eq.(4a) and thus yield accordingly uncertain estimates of SFRs.

However, for normal galaxies with continuously ongoing star formation one can derive an empirical relation between L^{wd}_{IR} and $\psi(t_o)$ using our Galaxy as a calibrator. Multiplication of eq.(3b) with the ratio N_{Lyc}/L^{wd}_{IR} = 4.6E43 Lyc photons $s^{-1}/L_\odot$, taken from Table 1 and valid for the spiral arm region yields

$$\psi(t_o) = 1.3\,(^{+0.6}_{-0})\,10^{-9}\,L^{wd}_{IR} \tag{4b}$$

In star-burst galaxies, where all OB stars are supposedly formed within a relatively short time interval, a larger fraction of massive stars may still be surrounded by dense gas and dust and the factors $f_d(m)$ are therefore probably larger. In this case relation (4b) would overestimate the SFR necessary to produce a given (wd) luminosity.

Figure 1

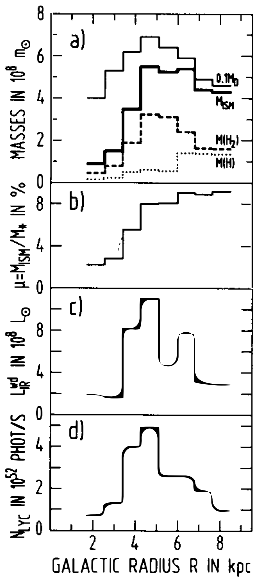

Fig. 1: *The diagrams show as function of the galactic radius R:a) Total mass M_D, mass of interstellar matter M_{ISM} and mass of molecular $M(H_2)$ and atomic $M(H)$ hydrogen. b) The ratio μ = M_{ISM}/M_D. c) The warm dust luminosity L^{wd}_{IR}. d) The Lyc photon production rate N_{LYC}.*

2. Application to the spiral arm region of the galactic disk

Some of the integrated characteristics of the galactic disk from Table 1, such as total mass, mass of the ISM and its constituents, N_{Lyc} and L_{IR}^{Ψ} are given in Fig.1a–d for concentric bins of width $\Delta R = 0.85$kpc surrounding the galactic center. Substitution of N_{Lyc} in eq. (3b) yields the SFR $\psi(t_o)$ shown in Fig.2a. The total "observed" SFR in the spiral arm region obtained with the "modified" Miller–Scalo IMF is

$$\psi(t_o) \sim 5.1 \left({}^{+2.5}_{-0}\right) m_{\odot}yr^{-1} \qquad (5a)$$

As will be discussed in Sect.III this SFR is too high and is ~ $2.6m_{\odot}yr^{-1}$ if bimodal star formation is considered (see eq.11). In the context of the principal topic of this workshop it is of interest to note that about 10% of all massive stars are formed in the central region $R \leq 0.3$kpc.

We compare the above present-day SFR with the average SFR in the spiral arm region

$$\langle\psi(t)\rangle = \frac{1}{(1-r)} \frac{M_D}{\tau_{Disk}} = 7.6m_{\odot}yr^{-1} \qquad (5b)$$

derived for a disk age τ_{disk} = 1E10yr and a return rate of $r = 0.42$ (computed for the Miller–Scalo IMF) and obtain a ratio $\psi(t_o)/\langle\psi\rangle = 1-0.67$ with the above lower and upper limit of $\psi(t_o)$. Both average SFR $\langle\psi\rangle$ and "observed" present-day SFR $\psi(t_o)$ are shown in Fig.2a as function of galactic radius R.

The result $\psi(t_o) \sim \langle\psi\rangle$ does not agree with constraints imposed by the chemical evolution of the Galaxy. On the assumption that most of the enrichment of the ISM with elements heavier than ^{4}He is due to the evolution of massive stars formed in the disk, Maeder (1981) estimates for the solar vicinity a ratio $\psi(t_o)/\langle\psi\rangle = 0.31$. Direct estimates of the SFR of all stars in the solar vicinity (see e.g. von Hoerner, 1968; Miller and Scalo, 1978) yield for the "solar bin" (i.e. in the range of galactic radii $R_{\odot} \pm 0.425$kpc) $\psi_{\odot} \sim 0.14\ m_{\odot}yr^{-1}$, while $\langle\psi\rangle \sim 0.8m_{\odot}yr^{-1}$ computed with eq.(5b) and $\psi(t_o) \sim 0.3m_{\odot}yr^{-1}$ computed with eq.(3b). From this result we conclude that even the "modified" Miller–Scalo IMF still overestimates the total SFR required to produce a given Lyc photon production rate. This conclusion can also be expressed differently, viz. that the Miller–Scalo IMF (and other IMFs as well) overestimate the total mass of a newly formed generation of stars relative to the mass contained in O stars.

3) Comparison with the evolution of a closed system

To allow a simple analytical treatment of the evolution of the galactic disk by successive star formation we assume that all gas had been assembled in the disk when 1E10yr ago the first generation of stars has formed. In a closed system the sum of the total mass of interstellar matter, M_{ISM}, and of matter permanently locked up in low-mass and dead stars, M_*, is constant at any time.

$$M_{ISM} + M_* = M_D \tag{6a}$$

To obtain an analytical expression for the change of the gas content with time it is necessary to adopt a relation between SFR and the amount of ISM available to be transformed into stars, for which we choose the rather general expression

$$\psi \propto M_{ISM}^K \tag{6b}$$

Combination of eqs. (6a and b) yields the well-known solutions for the decrease of the gas content of the disk with time.

$$\frac{M_{ISM}}{M_D} = \mu(t) = \begin{cases} \exp\{-t/\tau\} & k=1 \\ [1+(k-1)t/\tau]^{1/(1-k)} & k\neq1 \end{cases} \tag{6c}$$

τ is the timescale during which more than half of the original gas content of the disk has been permanently locked up in low mass and dead stars. Its meaning as a "star formation efficiency per unit time" becomes more transparent when we express the SFR ψ in terms of μ and τ and thus obtain

$$\psi/M_{ISM} = \tau^{-1}(\mu^{k-1}/(1-r)) \tag{6d}$$

where the expression in brackets is constant for a given exponent k. The left side of eq.(6d) multiplied with a time intervall is then the star formation efficiency.

For a given star formation law (specified by the exponent k in eq. 6b) the ratio $\psi^{pre}/\langle\psi\rangle$ can be expressed as a function of $\mu = M_{ISM}/M_D$, with ψ^{pre} the SFR predicted by the closed system model.

$$\frac{\psi^{pre}(t)}{\langle\psi(t)\rangle} = \begin{cases} \mu\ln\mu^{-1} & k=1 \\ \dfrac{\mu-\mu^k}{k-1} & k\neq1 \end{cases} \tag{6e}$$

Note that for a constant mass return rate r the same relation holds for the lockup rate dM_*/dt.

Substition in eq.(6e) of μ = 0.07 (from Table1) and $\langle\psi\rangle$ = 7.6 $m_\odot yr^{-1}$ (from eq. 5b) predicts the following present-day SFRs for the spiral arm region of the galactic disk:

$$\frac{\psi^{pre}(t_0)}{m_\odot yr^{-1}} = \begin{cases} 7.1 & k=0 \\ 3.0 & k=0.5 \\ 1.3 & k=1 \\ 0.43 & k=2 \end{cases} \tag{6f}$$

Comparison with a present-day "observed" SFR of $\psi\langle t_0\rangle$ = 5.1−7.6$m_\odot yr^{-1}$ favours an exponent k which is close to zero corresponding to a constant SFR. Arguments against such a star formation law have been discussed previously. One might argue in favour of k>0 that the effective disk age could be considerably shorter than 1E10yr due to a gradual build-up of the disk, which would result in a retarded onset of star formation. But even if we introduce an appropriate scaling factor between "predicted" and "observed" SFR (which is equivalent to a decrease of τ_{Disk}), neither the model with k=0 nor that with k=1 (or still higher exponents) can actually reproduce the observed ratio $\psi/\langle\psi\rangle$. This is demonstrated in Fig.2b where the "observed" ratio $\psi(t_0)/\langle\psi\rangle$ (Fig.2a) is compared with the corresponding ratio predicted for closed-system models with k=0 (scaling factor 1) and k=1 (scaling factor 5.1), respectively. Obviously, the simple closed-system model needs some adjustment to obtain agreement between "predicted" and "observed" lockup rates. Bimodal star formation as introduced in Paper I for quite different reasons (viz. to explain galactic abundance gradients), together with a star formation law with k=1, can also solve this problem, as shown in Sect.III.

Figure 2

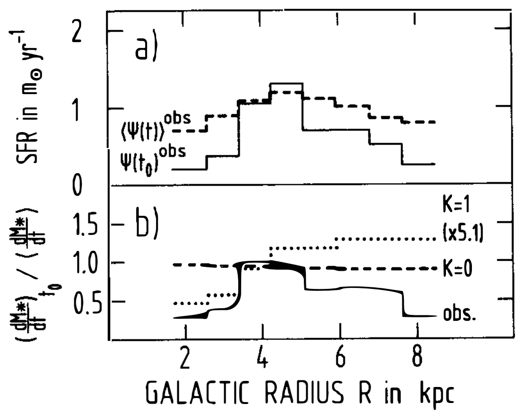

Fig. 2: *The diagrams show as a function of the galactic radius R: a) Average star formation rate (SFR)$\langle\psi(t)\rangle$, computed with eq. (5b), τ_{DISK} = 1E10yr and M_D from diagram 1a; and present-day SFR computed with eq.(3b) for a "modified" Miller-Scalo IMF and N_{Lyc} from diagram 1d. b) Ratio of present-day to average lockup rate, predicted by eq.(6e) for a closed system model for k=0 and 1, respectively, and μ from diagram 1b. The "observed" ratio is obtained from diagram 2a.*

4) "Observed" gas masses and star formation rates in external galaxies

The determination of total masses in our and in external galaxies is based in most cases on the galactic rotation curve. The ISM in galaxies consists of gas and dust, with dust accounting for a few percent of the total mass. The main constituents of the gas are H and ^{4}He, whose relative abundance ratio is primarily determined by big bang nucleosynthesis. Atomic hydrogen is traced by the Hλ21cm line which is nearly always optically thin, allowing straight forward H-mass determinations. Molecular hydrogen on a global scale is traced by rotational transitions of the CO molecule, which in most cases are opaque. Empirical relations are applied to convert observed CO surface brightnesses into column densities of the usually optically thin (but therefore weaker and more difficult to observe) rare isotope molecule ^{13}CO. The extrapolation of this calibration, derived for our galaxy, to external galaxies assumes that their molecular clouds are comparable in size and distribution to clouds in our Galaxy. This assumption is highly uncertain and could therefore introduce large errors in estimates of molecular hydrogen masses.

Dust grains mixed with both atomic and molecular hydrogen absorb stellar light, get warmed up and reemit the absorbed energy as blackbody emission with a quasi Planck spectrum $\nu^m B_\nu(T)$ which peaks at the wavelength $\lambda_{max}/\mu m = 5100/(3/3+m)$. The exponent m is determined by the wavelength dependence of the dust opacity and is m~2 for $\lambda \geq 100\mu m$ and ~1.5 for $100 \leq \lambda/\mu m \leq 40$. Dust heated by the general interstellar radiation field (ISRF) attains values of ~20-25K in the diffuse ISM and ~14K in molecular clouds, corresponding to spectral peaks in the wavelength range λ~100-200μm. Typical observed IR spectra of star forming galaxies, however, are double-peaked (Fig.3) indicating that one deals with two dust components of quite different temperatures. The first peak at submm wavelengths relates to cold dust heated by the general ISRF which is associated with the bulk of the neutral ISM. The second peak at shorter wavelengths arises from warm dust ($T^{wd} \geq 30$K). Model computations (Cox et al., 1986) have shown that only OB stars, which are still surrounded by dense dust shells, contribute significantly to this (wd) emission.

Figure 3

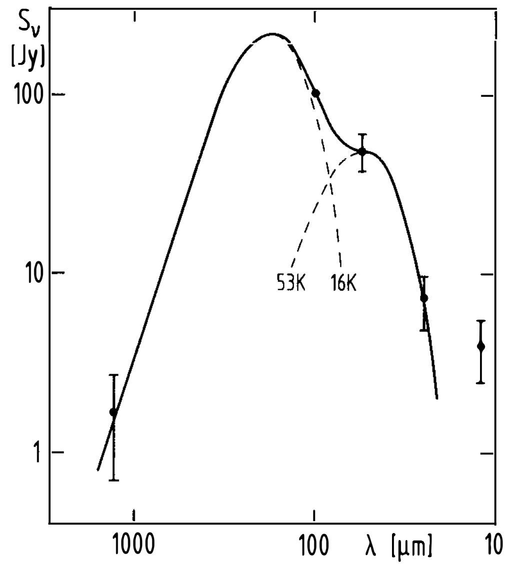

Fig. 3: *Typical observed dust emission spectra of spiral galaxies (Chini et al., 1986), decomposed into contributions from cold and warm dust.*

The possibility of a simple separation of observed IR/submm spectra into contributions from warm and cold dust allows to determine both the total mass of the ISM and the rate of massive star formation of a galaxy in a rather straight forward procedure. L_{IR}^{wd} and hence the massive SFR is in most cases determined with sufficient accuracy by flux densities in the IRAS $\lambda 100\mu m$ and $\lambda 60\mu m$ bands. The submm flux densities at $\lambda \gtrsim 350\mu m$, on the other hand, are usually dominated by cold dust emission. Integrated flux densities of external galaxies at $\lambda 1300\mu m$ can be best obtained with small telescopes. At this wavelength $B_\nu(T^{cd}) \propto T^{cd}$ (i.e. the Raleigh-Jeans approximation can be applied) and the optical depth is always $\tau_{1300} << 1$. With D the distance of the galaxy the mass of both atomic and molecular hydrogen can then be estimated with the relation

$$M_H \propto \frac{D^2 \, S_{1300}}{\sigma^H_{1300} \, T^{cd}} \tag{7}$$

where $\sigma^H_{1300} = \tau_{1300}/[N(H)+N(H_2)]$, the dust absorption cross section per H atom, is known with an estimated uncertainty of about a factor of ~2 (see Mezger et al., 1987).

The Lyc photon production rate N_{Lyc} is the appropriate quantity for quantitative estimates of SFRs. Attempts to separate synchroton and free–free emission in the radiospectrum of external galaxies were, however, with few exceptions not successful, since synchroton emission still dominates at longer mm wavelengths and dust emission starts to dominate at $\lambda \leq 1.3$mm. The warm dust luminosity L^{wd}_{IR}, on the other hand, can be obtained from IRAS observations and can be converted into SFR by means of eq.(4b). One has to be aware of the fact, however, that this is an empirical relation which has been calibrated with N_{Lyc} and L^{wd}_{IR} from our Galaxy. Even more important is to realize that free–free and (wd) emission relate to O and OB stars, respectively, which account for only ~10–30% of the total mass of a newly formed generation of stars. Therefore, the bulk of the mass in "observed" SFRs and lockup rates is inferred via an IMF.

Fig. 4

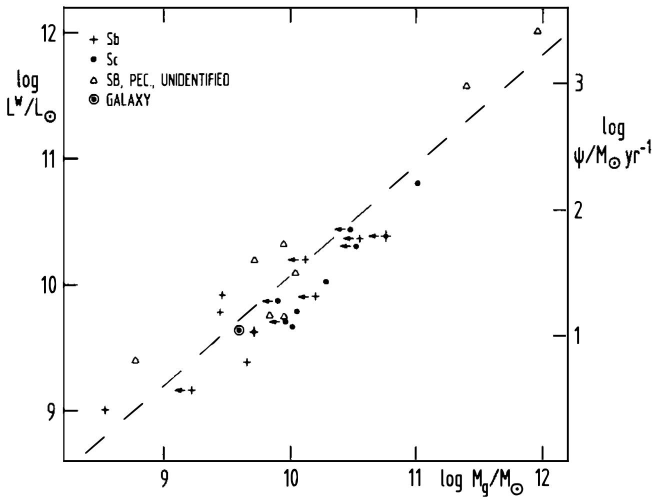

Fig. 4: *The diagram shows for 26 IRAS galaxies warm dust luminosities (left ordinate) vs. total gas content. The SFR (right ordinate) has been computed with eq. (4b), the gas mass with eq. (7) (from Chini et al., 1986).*

Fig. 4 is a diagram from Chini et al. (1986) where L^{wd} vs M_H is plotted for 26 IRAS galaxies. M_H is determined from S_{1300} with eq.(7). We find a linear relationship between L^{wd} and M_H over three decades. Star burst galaxies like M82 and NGC253, on the other hand, combine low gas content with high (wd) luminosity and thus occupy the upper left corner of this diagram. They are not shown in this diagram.

Note, however, that the linear relation between ψ and M_{ISM} for a sample of galaxies is not necessarily equivalent with a linear relationship $\psi \propto$

M_{ISM}, i.e. an exponent k=1 in eq.(6b). If k=0 but the star formation efficiency per unit time τ were constant, all galaxies today would also have the same relative gas content $\mu = (1-t_0/\tau)$.

III. Bimodal star formation

1) The concept of spontaneous and induced star formation

Bimodal star formation means that the births of low and high mass stars involve separate mechanisms. This possibility has first been suggested in two review papers by Herbig (1962) and Mezger and Smith (1977) and was put into a quantitative form by Güsten and Mezger (1983; Paper I) to explain the origin of galactic abundance gradients. Since then bimodal star formation has offered explanations to a number of open questions in galactic evolution (see, e.g. the review by Shuh et al., 1987).

We discriminate between induced star formation (triggered by some external events such as a sudden compression of the ISM by shock fronts, or the formation of GMCs when the gas flows through spiral arms) and spontaneous star formation in quiescent molecular clouds (in our Galaxy e.g.in the interarm region). We assume that in both cases the functional dependence of the IMF on stellar mass is the same, but that the IMF for induced star formation terminates at a critical stellar mass $m_C \sim 3m_\odot$, while the IMF for spontaneous star formation extends to $m_L \sim 0.1m_\odot$. It is shown (Mezger, 1985; hereafter referred to as Paper II) that in the case of induced star formation eqs. (3b) and (4b) are reduced by a factor

$$[1-\Delta(m_C)] = 0.80\ m_C^{-0.4} - 0.23 \tag{8a}$$

valid for $1 \leq m_C/m_\odot \leq 6$. With $m_C = 3m_\odot$ as suggested for induced star formation $[1-\Delta(m_C{=}3m_\odot)] = 0.29$ and

$$\psi^{ind} = [1-\Delta(m_C)]\psi^{spon} = 0.29\ \psi^{spon} \tag{8b}$$

This means that – compared with spontaneous star formation – only ~ 1/3 of the mass of ISM must be converted into stars to sustain a given Lyc photon production rate N_{Lyc} or (wd) luminosity L^{wd}, respectively. A similar reduction is obtained for the fraction of matter of a newly formed generation of stars which gets permanently locked up in low-mass and dead stars. This fraction is (Paper II)

$$(1-r)^{ind} = (0.136 m_C^{-1.4} + 0.008)\ [1-\Delta(m_C)]^{-1} = 0.13 \tag{9a}$$
$$= 0.22\ (1-r)^{spon}$$

with $(1-r)^{spon} = 0.58$. The bimodal lockup rate

$$\left(\frac{dM_*}{}\right)^{ind} = (1-r)^{ind}\ \psi^{ind} = 6.4\ 10^{-2}\ \left(\frac{dM_*}{}\right)^{spon} \tag{9b}$$

amounts to only ~6% of the lockup rate in the case of spontaneous star formation.

2. Bimodal star formation in the galactic disk

Bimodal star formation applied to the galactic disk means that induced star formation occurs in spiral arms and spontaneous star formation occurs in the interarm region (Paper I and references therein). Since observations indicate that massive stars form in dense molecular clouds we make the plausible assumption that the *spontaneous* OB SFR has a power-law dependence on the mass of *molecular hydrogen*, $M(H_2)$, and that the *induced* SFR is proportional to both $M(H_2)$ and the *relative velocity* $R(\Omega_R - \Omega_P)$ with which the ISM flows through the spiral arms. This leads to a formation law of massive stars of the form

$$\psi_{OB}(R) \propto M^k_{H_2}(R)\,[1+\alpha\nu(R)] \qquad (10)$$

with

$$\alpha = \psi^{ind}_{OB}(R_\odot)/\psi^{spon}_{OB}(R_\odot)$$

the ratio of induced to spontaneous star formation at the solar circle, for which observations suggest $\alpha = 1$ (Paper I). $\nu(R) = (\Omega_R - \Omega_P/(\Omega_\odot - \Omega_P)$ is the normalized relative flow speed, for which a numerical expression is given in Paper I. There and in Paper II is also shown that k=1 in eq.(10) yields a good fit between the OB SFR $\psi_{OB}(R) \propto N_{Lyc}$ and $M(H_2)$. The ratio $\alpha=1$ implies that in our Galaxy ~2/3 of all O stars are formed in spiral arms via induced star formation.

Expressions for bimodal IMF, SFR and lockup rate are given in Paper II, eqs. (9a – 12b) together with "observed" SFRs and lockup rates for the case of bimodal star formation. This latter quantity, as taken from column (10), Table 1 of Paper II, but reduced by a factor 2.7/4 = 0.68 to account for the "modified" Miller-Scalo IMF, is shown as solid curve in Fig.5. The bimodal SFR for the spiral arm region of the galactic disk is

$$\psi^{bm}(t_0) \sim 2.6 m_\odot yr^{-1} \qquad (11)$$

and thus is by about a factor of 2 lower than the SFR estimated for a constant IMF which extends from $0.1-60 m_\odot$ (see eq. 5a).

Figure 5

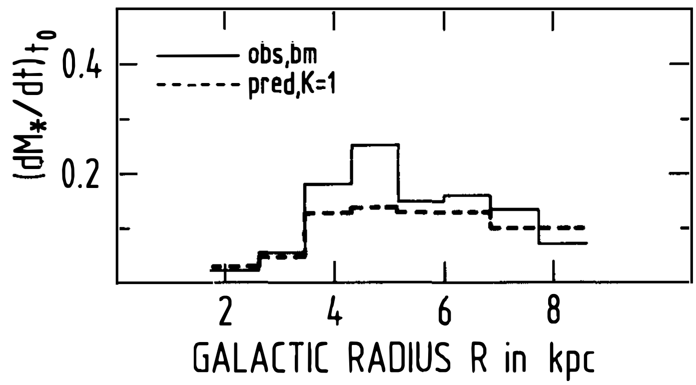

Fig. 5: *Comparison of the lockup rate for bimodal star formation (obs, bm) with that predicted for a closed system with k=1 (see text).*

The dashed curve in Fig.5 is the lockup rate predicted by eq.(6e) for the closed system with k=1 and for values μ as given in the diagram Fig. 1b. The quantitative agreement between the lockup rate predicted by this simple model and the "observed" lockup rate derived for a bimodal IMF appears at first sight amazing. The explanation, however, is given by eq. (9b) which tells us that for $m_c = 3m_\odot$ the lockup rate for induced star formation amounts to only ~6% of the lockup rate for spontaneous star formation. Hence, to a first approximation, it is only spontaneous star formation in the interarm region which contributes to the lockup rate, so that the amplification factor $[1+\alpha\nu(R)]$ in eq.(10) due to induced star formation can be neglected. This means that in the spiral arm region of the galactic disk, where molecular hydrogen is the dominant component of the ISM

$$\left(\frac{dM_*}{dt}\right)^{bm} \sim \left(\frac{dM_*}{dt}\right)^{spon} \propto M(H_2) \sim M_{ISM} \qquad (12)$$

which corresponds to a star formation law (eq.6b) with k=1 and star formation in a closed system model. This fact explains the quantitative agreement between bimodal lockup rate $(dM_*/dt)^{obs,bm}$ and lockup rate predicted by the closed system model with k=1, $(dM_*/dt)^{pred} = (\mu/\ln\mu^{-1})\, M_D(R)/\tau_{Disk}$, shown in Fig.5. In a qualitative way one can state that in the case of spatial bimodal star formation the induced formation of massive stars in spiral arms appears like a (compared to the galactic rotation time) short firework, whose ashes is returned to the ISM within a short time in form of gas enriched with heavy elements. Only a small fraction of the mass of ISM transformed into stars, viz. ~13%, remains permantly locked up in stellar remnants. In the interarm regions, on the other hand, about equal amounts of the mass of ISM transformed into stars are returned "instantaneously" to the interstellar space or permanently locked up in low mass and dead stars. Hence it is spontaneous star formation in the interarm region that accounts for the present-day stellar mass distribution in the galactic disk, while induced star formation in spiral arms is primarily responsible for the chemical evolution of the disk.

The bimodal IMF should have a secondary maximum at $m \sim m_c$ and indications of such a secondary maximum are in fact found in the mass range $m \sim (1-2)m_\odot$ (Scalo, 1986).

3.) Efficiency of star formation

Efficiency of star formation is defined as the fraction of the mass of e.g. a molecular cloud which is transformed into stars. With M_{cl} the total mass of the cloud, $\psi(t)$ its SFR at the time t and τ_{cl} the lifetime of the cloud the star formation efficiency is

$$\varepsilon = M_{cl}^{-1} \int_0^{\tau_{cl}} \psi(t)\, dt \qquad (12a)$$

If the SFR is proportional to the mass of ISM available to be transformed into stars (i.e. if k=1 in eq.(6b)), ε is independent of time (see eq. 6d) and is

$$\varepsilon \sim \psi(t_o)\ \tau_{cl}/M_{cl} \qquad (12b)$$

as long as $\varepsilon \ll 1$. With $X(H)^{-1}\ M(H_2) \sim 2.1E9 m_\odot$ (Table 1 and $X(H) \sim 0.7$) and $\psi(t_o) \sim 2.6\ m_\odot yr^{-1}$ (eq.11) the average star formation efficieny is

$$\varepsilon \sim 10^{-9}\ \tau_{cl} \sim (1-10)\% \qquad (12c)$$

for estimated cloud lifetimes ranging from τ_{cl} ~(1E7-1E8) yr.

4) Relevance for star burst galaxies

During a star burst the SFR $\psi(t_o)$ (at least of massive stars) is considerably higher than the average SFR$\langle\psi\rangle$. A starburst is probably triggered by some large scale effects such as encounters or interactions with other galaxies. In analogy with star formation in spiral arms it appears plausible to assume that most of the starburst would result in induced star formation, with an IMF which terminates at a critical mass m_c. In this case the relation eq.(4b) between ψ and (wd) luminosity becomes

$$\psi^{ind} = 1.3\ 10^{-9}\ L_{IR}^{wd}\ [1-\Delta(m_c)] \qquad (13a)$$

where eq.(8a) yields a numerical expression for $[1-\Delta(m_c)]$. The corresponding lockup rate is given by (eqs. 9a and b). For $m_c = 3m_\odot$ we obtain

$$\psi^{ind} = 3.8\ 10^{-10}\ L_{IR}^{wd} \qquad (13b)$$

and

$$\left[\frac{dM_*}{dt}\right]^{ind} = 3.7\ 10^{-11}\ L_{IR}^{wd} \qquad (13c)$$

The highest IR luminosities observed by IRAS are $L_{IR} \sim 1E12L_\odot$. If they are due to warm dust emission powered by massive stars $m \geq 3m_\odot$ a SFR of $\psi^{ind} \sim 380 m_\odot yr^{-1}$ and a lockup rate of $\sim 37 m_\odot yr^{-1}$ would be enough to sustain this luminosity. This are relatively modest rates compared to the corresponding rates in the case of spontaneous star formation, which are $1300 m_\odot yr^{-1}$ and $754\ m_\odot yr^{-1}$, respectively.

References

Chini, R, Kreysa, E., Krügel, E., Mezger, P.G.: 1986, Astron.Astrophys. 166, L8
Cox, P., Krügel, E., Mezger, P.G.: 1986, Astron.Astrophys. 155, 380
Güsten, R.: 1986, in "Spectral Evolution of Galaxies" C. Chiosi and A. Renzini, eds., p.449
Güsten, R., Mezger, P.G.: 1983, Vistas in Astronomy vol. 26, p.159 (Paper I)
Herbig, G.: 1962, Advanc. Astron. Astrophys. 1, p. 47–103
Maeder, A.: 1981, Astron.Astrophys. 101, 385
Mezger, P.G., Smith, L.F.: 1977, Proc. IAU Symp. No.75 (de Jonge and Maeder, eds.; D.Reidel Publ.Co,) p. 133
Mezger, P.G.: 1985, Proc. IAU Symp. No.116 (de Loore, Willis and Saskarides, eds.; D.Reidel Publ.Co.) p. 479 (Paper II)
Mezger, P.G., Chini, R., Kreysa, E., Wink, J.: Astron.Astrophys. (in press)
Miller, G.E., Scalo, J.M.: 1978, Astrophys.J. Suppl. 41, 513
Scalo, J.M.: 1986, in "Fundamentals of Cosmic Physics" 11, p.1–278
Shu, F.H., Adams, F.C., Lizano, S.: 1987, Ann. Rev. Astron. Astrophys. (in press)
von Hoerner, S.: 1968, in "Interstellar Ionized Hydrogen" (Y. Terzian, ed.), p.101

THE HIERARCHICAL STRUCTURE OF MOLECULAR CLOUDS

Jean-Pierre CHIEZE
Commissariat à l'Energie Atomique
Centre d'Etudes de Bruyères-le-Châtel, Service P.T.N.
B.P.12, F-91680 Bruyères-le-Châtel, France

The mass-radius-velocity dispersion relations observed among the members of cool molecular complexes is interpreted in terms of fragmentation at the gravitational instability threshold in a roughly constant pressure environment. The mass range of the self-similar fragmentation hierarchy is governed by the thermal instability thresholds. Using a realistic equation of state, the gravitational stability of thermally stable clumps is analyzed as a function of both the local gas pressure and extinction of the mean interstellar radiation field.

1. Introduction

The masses of molecular clouds observed in various complexes are tightly correlated with the square of their radii[1),2),3)]. In the range 100 $M_{\odot}$ – 10^7 $M_{\odot}$, the molecular gas is distributed in a self- similar hierarchy of smaller and denser substructures, each one obeying the scaling laws $M \propto R^2$, $\Delta v \propto R^{1/2} \propto M^{1/4}$. But this hierarchy breaks down at the level of several 100 $M_{\odot}$: less massive clouds only exhibit small *dense cores* containing about 10 percent of the total mass[2),4)].

Both thermal and gravitational instability play a major role in the formation of molecular clouds from hot, cooling interstellar gas. The mass of the largest complexes is about the Jeans mass for $T \sim 10^4$ K, while the self-similar hierarchy breaks down at about the critical mass of a medium which has just recovered *thermal* stability. From the analysis of the equation of state of molecular gas[5),6)], it turns out that the threshold of thermal instability is $T_* \sim 90$ K. The limiting mass of thermally stable self-gravitating molecular clouds is $M \approx 100$ $M_{\odot}$.

Thus we are led to distinguish between:

- the formation and the fragmentation of massive structures ($M > 100$ $M_{\odot}$) from hot and thermally unstable gas, and

- the gravitational stability of less massive clouds and dense cores which have recovered thermal stability.

Fig.1 shows, in the mass-radius plane, the location of gravitational and thermal instability thresholds.

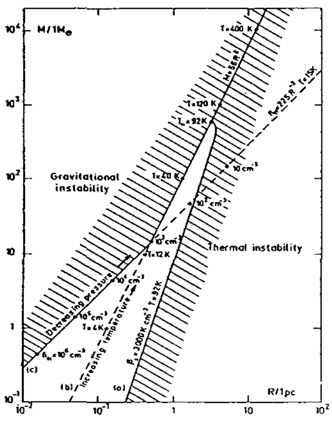

Fig. 1. The approximate stability domain of molecular clumps, limited by gravitational and thermal instability. The region is bounded by self-gravitating structures at the threshold temperature of thermal insta bility (T≈92 K) and, on the left-hand side (straight line of slope 2), by gravitational instability in a $\bar{P}_0 = 3000$ $Kcmm^{-3}$ pervasive medium. Small dense cores are nearly isothermal (T=10-15 K) and experience much larger surface pressure. The relevant gravitational threshold is the straight line of slope 2.

2. Gravitational instability in a hot cooling gas.

We assume that the mean pressure of the interstellar gas is regulated at large scale by some specific mechanisms -such as supernovae explosions[7]. Furthermore, we suppose, as usual, that thermal instability develops at roughly constant pressure $\tilde{P}_0 \equiv P_0/k$, where k is the Boltzman constant. From dimensional considerations, one can conclude that the mass-radius relation of the gravitational critical masses in a constant pressure environment is $M \propto R^2$. Consequently, the internal velocity dispersion scales as $\Delta v \propto L^{1/2} \propto M^{1/4}$. The actual normalizations depends upon the gas equation of state and the ambient pressure P_0.

More precisely, it can be shown[3] that the family of the *critical* self-gravitating poytropic gas spheres is characterized by the scaling:

$$M_* = \left(8\pi \frac{n+1}{n-3}\right)^{1/2} \left(\frac{P_0}{G}\right)^{1/2} R^2 \tag{1}$$

where n is the polytropic index. (Pressure limited polytropic spheres with $0 < n \leq 3$ are unconditionally stable against poytropic perturbations, but are unstable if $-1 < n \leq 0$).

A similar result can be obtained from the traditional Jeans analysis of gravitational stability. One can note in this respect that the definition of the Jeans length supposes a static (infinite) medium. We have shown elsewhere[8] that introducing the infall velocity gradients which develops in a collapsing medium only diminishes the Jeans length by a negligible factor.

Accordingly, Eq.(1) adequately represents the mass-radius relation among the critical self-gravitating condensations in a cooling medium. The internal velocity dispersion in a critical cloud (assumed hereinafter to be isothermal for simplicity) is:

$$\frac{\Delta v}{1\ kms^{-1}} = 0.60 \left(\frac{\tilde{P}_0}{3800\ Kcm^{-3}}\right)^{1/4} \left(\frac{R}{1\ pc}\right)^{1/2} = 0.21 \left(\frac{\tilde{P}_0}{3800\ Kcm^{-3}}\right)^{1/8} \left(\frac{M}{1\ M_\odot}\right)^{1/4} \tag{2}$$

These relations depends rather weakly upon the ambient pressure.

An interesting feature is that the total proton *column density* across it any critical cloud is a constant. Numerically, we have:

$$\frac{\mathcal{N}_H}{1\ cm^{-2}} = 4.\ 10^{20} \left(8\pi \frac{n+1}{n-3}\right)^{1/2} \frac{\mu_H}{1\ amu} \left(\frac{\tilde{P}_0}{3800\ Kcm^{-3}}\right)^{1/2} \tag{3}$$

For an isothermal cloud, adopting[9] $\mathcal{N}_H/A_v = 1.55\ 10^{21} cm^{-2} mag^{-1}$ and $\mu_H = 1.3\ amu$, the extinction at the center of a critical cloud is $Av_c = 1\ mag$.

We suggest that efficient fragmentation should occur in clouds at, or near gravitational instability. Fragmentation may be triggered by the *dynamical* cooling instability which develops in the range $8000\ K \leq T \leq 100\ K$ where thermal balance is not equilibrated[10]. Moreover, the transition from the atomic to the H_2 molecular gas phase which occurs in regions with[11] $Av = 1\ mag$ implies strong UV shielding and thus further destabilization of the thermal balance.

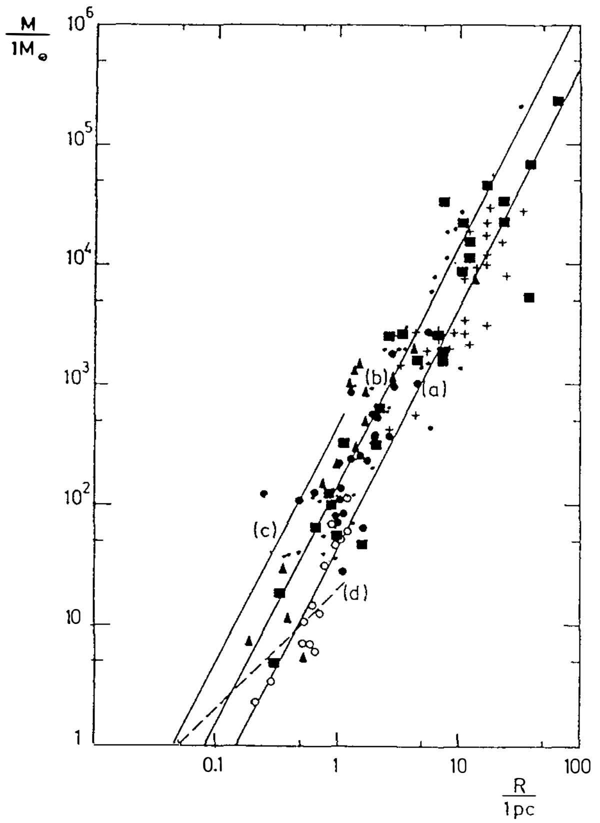

Fig. 2. The mass-radius relation among molecular clouds. a) Equation (1) with $\hat{P}_0 = 3800\ Kcm^{-3}$ and $\beta = 1.$, b) with $\beta = 1.5$.

Further cooling can trigger the formation of a hierarchy of fragments of decreasing masses and increasing densities ($n_H \propto R^{-1}$). If the filling factor of fragments is small, as observed[2),12)], the ambient medium can efficiently pervade the interclump space, so that the hierarchy of the critical masses develops according to Eq.(1) at the typical interstellar medium pressure ($\tilde{P}_0 \sim 3800\ K cm^{-3}$), down to 100 $M_\odot$.

After each fragmentation stage, (i.e. at each level of the hierarchy), violent relaxation of the fragments results in a quasistatic virial equilibrium state with a radius R_{vir} in the range[3)] $R_*/2 \leq R_{vir} \leq 0.86\ R_*$. This process preserves the scaling laws Eqs.(1) and (2), which have then to be renormalized. Adopting a contraction factor $\beta \equiv R_*/R_{vir} = 1.5$, the relaxed configurations obey the relations:

$$\frac{M}{1\ M_\odot} = 140 \left(\frac{R_{vir}}{1\ pc}\right)^2 \tag{4}$$

$$\frac{\Delta v}{1\ kms^{-1}} = 0.20 \left(\frac{M}{1\ M_\odot}\right)^{1/4} = 0.68 \left(\frac{R}{1\ pc}\right)^{1/2} \tag{5}$$

The internal kinetic energy of the parent homogeneous structures has been converted in part into kinetic energy of the macroscopic mass motion of the relaxed fragments.

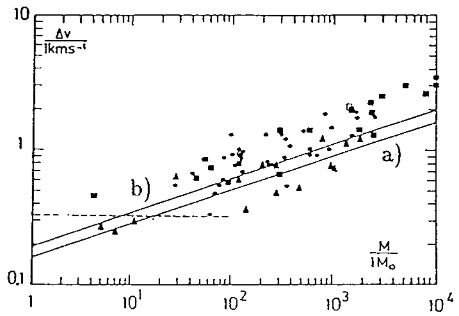

Fig. 3

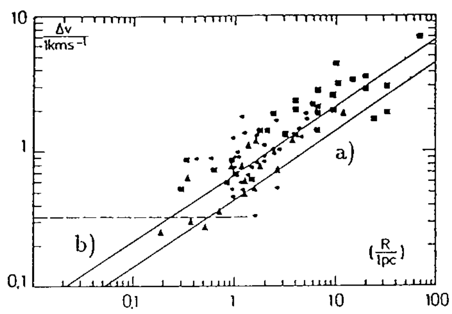

Fig. 4

Fig. 3. The relation between the mass and the internal velocity dispersion for the sample represented on Fig. 1. Same conventions as for Fig. 2.

Fig. 4. The relation between the radius and velocity dispersion for the sample of Fig. 2. Same conventions as in Fig. 2.

3. Gravitational stability of thermally stable gas

We turn now to the study of thermally stable gas, which, *a priori*, is packed into clouds of $\sim$ 100 $M_\odot$. The gravitational stability of molecular clumps depends crucially upon the equation of state. It can be investigated [6] in terms of the local pressure (or the pressure P_s at the surface of a clump) and of the local intensity of the interstellar radiation field (or the extinction Av_s at the surface). These quantities are subject to large variations *inside* a cloud.

As expected, the critical mass decreases as:

- the local pressure P_s increases, and,
- the local extinction Av_s increases.

The critical surface $M_* = M_*(P_s, Av_s)$ is reproduced on fig. 5.

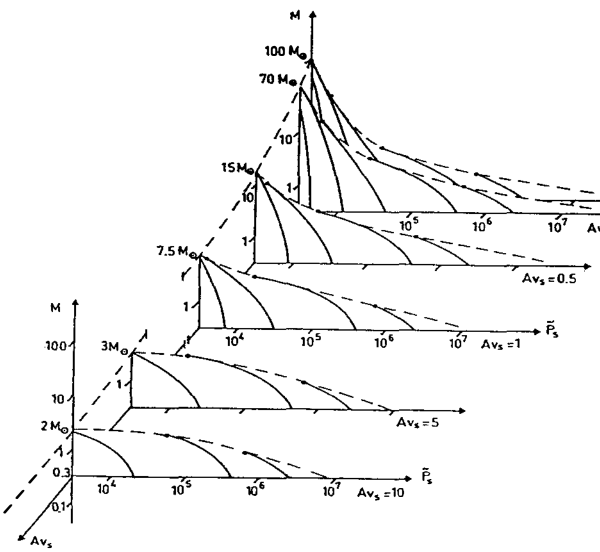

Fig. 5. Thermally stable molecular clumps. The locus of the gravitational limiting masses in the $(M,\ \bar{P}_s,\ Av_s)$ plane is represented by the surface envelope of the dashed lines. Each thick curve represents the mass of stable clumps with a given central density (log n_{Hc}=2.(1.)6. from the left to the right of the figure. Clumps with $n_{Hc} = 10^2 cm^{-3}$ are only reported for $Av_s = 0$ and 0.1 *mag*.)

The maximum mass of a self-gravitating cloud (ignoring turbulence, magnetic fields and embedded young stars) is $M_0 = 100\ M_\odot$. This corresponds to the mass termination of the hierarchy of fragmented clouds. In practice, this is the limiting mass of unshielded molecular clouds, with surface pressure $\tilde{P}_0 = 3000 - 4000\ Kcm^{-3}$.

The mean extinction inside a *molecular complex* is about $Av = 1 - 2\ mag$, (Eq.(3)). Assuming an *intercloud* pressure inside the complex of the same order as above, ,the critical mass drops to $5 - 7\ M_\odot$. In much more shielded regions, $Av \geq 10\ mag$, the critical mass is always less than $2\ M_\odot$, and steeply decreases in regions where the pressure field is in excess of $10^5\ Kcm^{-3}$. Such masses and local conditions are typical of the *low mass molecular cores*[4], found in quasistatic molecular clouds.

4. Conclusion

The self-similar fragmented structure of *cool* molecular clouds, observed in the range $100\ M_\odot \leq M \leq 10^7\ M_\odot$, can be interpreted in terms of fragmentation at the threshold of gravitational instability of thermally instable gas, cooling down at roughly constant pressure.

The completion of the fragmentation mechanism is essentially achieved when the gas recovers thermal stability at $T \sim 90K$. The critical mass is then $M_0 \sim 100\ M_\odot$. Clouds in this mass range are then the basic components of the hierarchy.

Self-shielding among the members of a molecular complex can induce the formation of dense molecular cores ($M \leq 2\ M_\odot$) inside individual clouds.

References

1) R.B. Larson: Monthly Notices Roy. Astron. Soc. **194** (1981) 809
2) E. Falgarone and M. Pérault: in Physical Processes in Interstellar Clouds, (1987) ed. G.Morphill and M.Scholler (Munich)
3) J.P.Chièze: Astron. Astrophys. **171** (1987) 287
4) P.C. Myers: in *Protostars and Planets II* (1985) p.81 ed. D.C. Black and M.S. Matthews, The University Of Arizona Press
5)T. de Jong, A. Dalgarno, W. Boland: Astron. Astrophys. **91** (1980) 68
6) J.P. Chièze and G. Pineau des Forêts: Astron. Astrophys. (1987) in press
7) C.F. Mc Kee and J.P. Ostriker: Astrophys. J. **218** (1977) 148
8) P. Blottiau, S. Bouquet and J.P. Chièze: in preparation
9) R.C. Bohlin, B.D. Savage and J.F. Drake: Astrophys. J. **224** (1978) 132
10) A. Lioure and J.P. Chièze: in preparation
11) S.P. Tarafdar and K.K.S. Swamy: Monthly Notices Roy. Astron. Soc. 200 (1982) 431
12) L. Blitz and A.A. Stark: Atrophys. J. Lett. **300** (1986) L89

A NEW PICTURE OF INTERSTELLAR MEDIUM : CHIMNEY MODEL

Satoru IKEUCHI
Tokyo Astronomical Observatory,
Mitaka, Tokyo 181,
Japan

Many observational facts which indicate a different picture of the interstellar medium from the McKee-Ostriker's three-phase model are accumulated in this decade. Based upon the sequential star formation model in molecular clouds the gigantic superbubbles are formed by sequential supernova explosions. Such superbubbles stand perpendicular to the disk like chimneys and the hot gas can go up to the halo like smoke in chimneys. About one thousand of chimneys smoke in a galaxy along the spiral arms. At the interarm region the classical two-phase model is preferable. Here, several observational evidences for this picture are presented, and some implications to the evolution of galaxies are discussed.

1. Introduction

Almost two decades have passed after Spitzer [1] summarized the fundamental processes in the interstellar medium (ISM). In that book, he presented a picture that the standard HI clouds are confined by pressure of ambient pervasive medium. This picture is formulated and confirmed by Field, Goldsmith and Habing [2] by examining the thermal processes in ISM.

This picture should be modified by the discoveries of hot gas component. One is the discovery of diffuse soft X-ray background due to the thermal emission of hot gas with the temperature $\sim 10^6$ K [3]. Another discovery is the absorption lines in the UV wavelength due to highly ionized ions like OVI [4]. If they are collisionally ionized the gas temperature should be several times 10^5 K, which is a little lower than that of the X-ray emitting gas. Since the column density of OVI ions increases with the distance to the UV source these ions are thought to be interstellar in origin [5].

Since the cooling time of these hot gas components is less than 10^6 years, some continuous bulk heating process is necessiated in order to maintain them. This means that the dynamical and thermal state of ISM is not static but dynamically stirred.

McKee and Ostriker [6] (hereafter referred as MO) presented a revolutionary model of ISM, in which the hot gas component with $T_h \sim 5 \times 10^5$ K and $n_h \sim 3 \times 10^{-3}$ atoms cm^{-3} occupies a large fraction of the volume, and both the cold clouds and the surrounding warm ionized gas are confined by this pervasive hot gas. These three gas components can not be in the static equilibrium locally, but can be in the mass and pressure balance globally. From this view, MO formulated the three-phase model of ISM. Ikeuchi *et al.* [7] tried to calculate the time variation of each component by considering the mutual exchange processes driven by supernova remnants. Their conclusion is that both the two-phase model and three-phase model are right. The structure of ISM is determined by two parameters, the supernova explosion rate, S, and the total gas density, n. As is easily understood, in the low S and/or high n case the two-phase sturcture arises, and in the high S and/or low n case the three-phase structure dominates.

However, in this decade many observational facts have been accumulated, which seem to indicate a different picture of ISM from this MO model. Here, I propose a new picture which is called CHIMNEY MODEL as is seen in the later. Firstly, I summarize several observational evidences for this picture, and then present a rough sketch of it.

2. New Observational Facts

2.1. Evidences for the Chimneys Model

(a) Superbubbles

Cash *et al.*[8] have discovered an extended X-ray (0.1 ~ 0.6 keV) emitting shell with the size ~ 450 pc in the Cygnus region. They called this a superbubble and indicated similar candidates in the Orion-Eridanus region and the Gum nebula. In the former, the X-ray emission is also confirmed and an extended HI and Hα loops with the size ~ 250 pc are reported[9, 10]. From the X-ray spectrum the gas temperature is estimated to be several times 10^6 K at the shells. In addition to this, the probable detection of hard X-ray flux at the Cygnus superbubble is reported by TENMA (Koyama 1986, private communication). Since the iron lines at 6.7 keV is clearly recognized in the spectrum, the presence of hot gas with the temperature ~10^8 K is highly expected. Such a high temperature suggests the energy input within $10^{3\sim4}$ years, which are much shorter than the age of the Cygnus superbubble. The continuous energy supply in the superbubble occurs even now.

(b) Supershells

Heiles[11, 12] have discovered many shells, loops, arcs and filaments by the HI 21 cm lines. He reported about 50 clouds with the size 100 pc to 3 kpc (supershells), and some of them are now expanding and others are stationary. In the filtered pictures for enhancing the small structures, the HI clouds look like worms which crawl out from the disk. These worms and supershells may be originated in multiple supernovae and/or superbubble phenomena. It is confirmed that the geometrical center of a supershell corresponds to the Cygnus OB association, which is the energy source of the Cygnus superbubble. It suggests that the cold HI components are expelled from the disk due to the dynamical processes at OB associations.

(c) GMC/OB Association/HII Region/HI Loop

In three candidates of superbubbles, all set of population I objects, giant molecular cloud, OB association, HII region and HI loop, coexist. Some of them like the Cygnus region and the Orion-Eridanus region associate with supernova remnants, X-ray superbubbles and pulsars. All these facts indicate the sequential star formartion as well as active energy ejection by stellar winds and/or supernovae. Tomisaka *et al.*[13] showed that the superbubbles with the size 300 ~ 1000 pc can be formed if the sequential supernova explosions occur every 10^5 y during the lifetime of a giant molecular cloud, $1 - 2 \times 10^7$ y. Further, if such sequential explosions occur in the plane stratified medium like the Milky Way the superbubble predominantly expands to the halo region like the cylinder perpendicular to the disk as shown by Tomisaka and Ikeuchi [14] (hereafter referred as TI). The HI chimney with the height 1 kpc grows up from the disk and the hot gas goes up through the chimney to the halo.

2.2. Observations of New Hot Gas Component

(a) X-ray Ridge

According to McKee and Ostriker [6] the temperature of hot gas prevailing over the disk is, at most, 10^6 K. Recent observations by EXOSAT [15] and TENMA [16] indicate the presence of hotter gas component than $\sim 10^7$ K, and this X-ray emitting region extends smoothly like a ridge. Such a high temperature gas can not be in a diffuse form because it promptly escapes from the disk. The z-distribution of X-ray flux shows the confinement to the disk like the population I objects. This denotes the X-ray emitting sources to be a number of population I sources. Since the fluctuation of X-ray intensities to different directions is small, the number of sources in a line of sight should be greater than 10 [17]. Koyama, Ikeuchi and Tomisaka [18] examined the possibility that the X-ray ridge is originated in many supernova remnants younger than 10^4 y, and concluded that the supernova explosion rate must be higher than 0.1 SN per year, which seems to be too high. This may suggest that the supernova explosion does not occur randomly but correlatedly like the superbubble model by TI.

(b) Highly Ionized Ions in the Galactic Halo

Analyzing the absorption lines in the halo stars the properties of the galactic gas halo have been studied by using the IUE satellite. Savage and Massa [19] summarized the observational data covering nine years. The clear conclusion is that the detection of CIV, SiIV and NV absorptions due to the diffuse halo gas confirms the presence of the gas with the temperature higher than, at least, several $\times 10^4$ K at the height $z = 2 \sim 3$ kpc. Although the relative importance between the photo-ionization and the collisional ionization is not made clear, both processes seem to work comparably in order to explain the abundances of highly ionized ions [20]. This means that the hot gas supplied from the disk to the halo contributes to the absorption.

(c) Halo Clouds

The halo gas supplied from the disk is cooled within 10^7 y and returns back to the disk as clouds [21), 22)]. Such a fountain model is supported by observations of halo clouds with the positive and negative velocity. van Woerden *et al.* [23)] compared the velocity distributions of halo clouds in the sky with those predicted by Bregman [21)], and confirmed that the velocity pattern agrees with each other. Although it is necessary to reexamine the Yoyo model by Bregman because it seems to be unnatural, the overall behavior of halo clouds can be reproduced by the fountain model.

The above three facts strongly claim that the hot gas formed at the OB associations inevitably escapes from the disk to the halo through chimneys.

2.3. HI Holes in M31

Brinks and Bajaja [24)] have presented an interesting result of their detailed HI survey of M31. They found many HI holes with the size 100 pc to 1 kpc, lining up on the disk plane. If we observe the HI chimneys from outside of our Galaxy, the orifices of chimneys can be seen as HI holes. Of course, the inclination of the disk plane to the line of sight and also the inclination of chimneys to the disk lead to various elliptical figures of HI holes. It will be interesting to compare the distributions of HII regions, continuum radio contours and X-ray sources.

2.4. Big Halos around Distant Galaxies

The absorption line systems in quasars are originated in the intervening materials between quasars and us. Especially, the narrow metallic-line systems are thought to be due to the gas in the halo around distant galaxies. This is confirmed by Bergeron [25)] by discovering the galaxy with the emission lines at the same redshift as the MgII absorption line. In this case, the extension of the halo gas with MgII ions is about 60 kpc because the line of sight to the quasar runs at this distance from the disk. The CIV systems are not directly confirmed as galactic halos like MgII syste, but the two-point correlation of CIV systems shows the similar behavior to galaxies [26)]. Therefore, we may consider the CIV systems to be originated in galaxtic holos. The observed frequency of them indicates the average radius of distant galaxies at $z \sim 2.0$ to be ~ 90 kpc. Then, we may imagine that the galactic halos shrink from the past.

3. Chimney Model of ISM

3.1. Bunched Supernova Explosions

As shown by Tomisaka *et al.*[14] the average time interval of supernova explosions in an OB association is to be

$$\tau_{OB} \sim 2 \times 10^5 \text{ y}. \tag{1}$$

Considering that the lifetime of an OB association is $(2\text{–}4) \times 10^7$ y the expected total number of supernovae is $N_{SN} \sim (1\text{–}2) \times 100$ [27]. If we supose the lifetime of a superbubble is $t_{SB} \sim 10^7$ y the expected number of superbubbles in our galaxy is $N_{SB} \sim N_{OB}/(2\text{–}4) \sim 1000$, where N_{OB} is the total number of OB associations ~ 3000 [28]. As a result the formation rate of superbubbles is estimated as

$$\gamma_{SB} \sim N_{SB}/t_{SB} \sim 10^{-4} \text{ y}^{-1}. \tag{2}$$

The expansion law of a superbubble for $\tau_{OB} \sim 2 \times 10^5$ y is approximated as [13]

$$R_{SB} = 64.3\ n_a^{-0.26}\ t_6^{0.43} \text{ pc}, \tag{3}$$

where n_a and t_6 are the average gas density at the disk and the age of the superbubble in units of 10^6 y. Then, the probability that an arbitrary point in the disk is inside a superbubble with the radius smaller than $R_{SB}(\propto t^{\eta})$ is given by

$$Q = \frac{\gamma_{SB}}{1+2\eta}\left(\frac{R_{SB}}{R_G}\right)^2 t \sim 0.16 \left[\frac{n_a}{1\text{cm}^{-3}}\right]^{-0.52}\left[\frac{t}{10^7\text{y}}\right]^{1.86}\left(\frac{R_G}{10\text{kpc}}\right)^{-2}\left(\frac{\gamma_{SB}}{10^{-4}}\right), \tag{4}$$

where η is 0.43 and R_G is the radius of the disk.

On the other hand, the upward motion of the superbubble is also approximated by equation (1) in the deceleration phase, $t < t_{crit}$, if we replace n_a by the gas density n at the front of the shock wave (TI), i.e.,

$$z_{SB} \sim 64.3\ [\ n(z_{SB})]^{-0.26}\ t_6^{0.43} \text{ pc}. \tag{5}$$

At the critical time, t_{crit}, the upward motion of the shock wave changes to acceleration,

$$(\partial \ln z_{SB}/\partial \ln t) > 1 \text{ at } t > t_{crit}, \tag{6}$$

due to the density stratification. In this acceleration phase, the expansion within disk is limited, and the superbubble predominantly grows up to the halo.

3.2. Chimneys

Within the chimney the hot gas with the density $n_{SB} < 10^{-3}$ cm^{-3} and the temperature $T_{SB} > 3 \times 10^7$ K rises. The total X-ray flux from a superbubble is

$$l_X \sim \pi R_{SB}^2 \cdot z_{SB} \cdot n_{SB}^2 \Lambda(T_{SB})$$

$$\sim 3 \times 10^{34} \left(\frac{n_a}{0.1\mathrm{cm}^{-3}}\right)^{-0.78} \left(\frac{n_{SB}}{10^{-3}\mathrm{cm}^{-3}}\right)^2 \left(\frac{T_{SB}}{3\times10^7\mathrm{K}}\right)^{1/2} \left(\frac{t}{10^7\mathrm{y}}\right)^{1.29} \text{ erg s}^{-1}. \tag{7}$$

The total X-ray flux from $\sim 10^3$ chimneys is $L_X \sim 10^3 l_X \sim 3 \times 10^{37}$ erg s^{-1}, which is a little smaller than the flux of X-ray ridge. Since the space density of chimneys is $N \sim 10^3/\pi(R_G)^2(300\mathrm{pc}) \sim 10^8$ pc^{-3}, this is larger than the lower limit determined from the regularity of X-ray intensity of the ridge [7].

The energy deposited in a chimney is the order of $\sim 3 \times 10^{51}$ erg in the thermal and kinetic energy, respectively (TI). Therefore, the energy supply rate from the disk to halo is

$$\dot{E} \sim E_{th}\, \gamma_{SB} \sim 1\times 10^{40} \left(\frac{E_{th}}{3\times10^{51}\mathrm{erg}}\right) \left(\frac{\gamma_{SB}}{10^{-4}\mathrm{y}^{-1}}\right) \text{ erg s}^{-1}. \tag{8}$$

On the other hand, the gas supply rate to the halo through chimneys is

$$\dot{M} \sim 2(E_{kin}\, \gamma_{SB}) \langle v \rangle^{-2} \sim 0.7 \left(\frac{E_{kin}}{3\times10^{51}\mathrm{erg}}\right) \left(\frac{\gamma_{SB}}{10^{-4}\mathrm{y}^{-1}}\right) \left(\frac{\langle v \rangle}{200\mathrm{km\ s}^{-1}}\right)^{-2} M_\odot \text{ y}^{-1}, \tag{9}$$

where $\langle v \rangle$ is the average rising velocity of hot gas. The scale height of hot gas in the halo is $H_h \sim 3$ kpc, and the dynamical time of the gas to this height is $t_d \sim H_h/\langle v \rangle \sim 1.5 \times 10^7$ y. The average gas density in this region is

$$<n_h> \sim \dot{M}\, t_d/2\pi\, R_G^2\, H_h m_p$$

$$\sim 1.4 \times 10^{-4}\left(\frac{\dot{M}}{0.7\ M_\odot y^{-1}}\right)\left(\frac{t_d}{1.5\times10^7 y}\right)\left(\frac{R_G}{10\mathrm{kpc}}\right)^{-2}\left(\frac{H_h}{3\mathrm{kpc}}\right)^{-1}\ \mathrm{cm}^{-3}. \qquad (10)$$

The cooling time of the halo gas with the temperature $T_h \sim 10^5$ K is

$$t_{cool} \sim 3k\ T_h/<n_h>\ \Lambda(t_h) \sim 2.2 \times 10^7\left(\frac{T_h}{10^5 K}\right)^{1.6}\left(\frac{<n_h>}{1.0\times10^{-4}\mathrm{cm}^{-3}}\right)^{-1}\ \mathrm{y}, \qquad (11)$$

which is comparable to t_d. Therefore, once the gas rises to H_h it returns to the disk after t_d with the negative velocity $\sim$ (1–2) $\times$ 10^2 km s^{-1}. In this way, we can expect the large scale circulation of the gas through the galactic halo. The exact motion of the gas in the halo has not been made clear till now, because the rotation law of the halo is not known.

3.3. Global Picture

The raw woods of chimneys are giant molecular clouds, and they are fired as OB associations. The UV flux and energetic winds ionize the clouds (HII regions), and due to the chain explosions of supernovae a big chimney is formed with the dense cold wall (HI and H_2 gas) and the hot gas. The hot gas goes up to the halo through this chimney, and the average height of hot halo gas is several kiloparsecs. After (2–3) $\times$ 10^7 years, this halo gas cools and returns back to the disk as clouds. Then, the gas circulation time will be (3–5) $\times$ 10^7 years.

The number of chimneys in a galaxy will be $\sim 10^3$, and they stand along the spiral arms because the giant molecular clouds are predominantly accumulated (or formed) at the arm regions. The direction of chimneys depends upon the original height of molecular clouds at the disk, the upper side or the lower side. The chimney walls with the height $\sim$ 1kpc are seen like worms crawling out from the disk [12].

The above picture is described by using the following metaphor. The factories with chimneys are lined up along the arms, and the smoke of hot gas is puffed up from chimneys. In this gas, the metal would be abundant because many supernovae contribute. Such a polluted gas is injected to the halo, and it infalls to the disk like the smoky air with dusts. This global picture resembles to the problem of pollution at the industrial city.

4. Implications

4.1. Gas Circulation

In this picture, the large scale circulation of the gas through the halo occurs with the timescale ~ (3–5) × 10^7 years. This will bring two problems. One is the mixing of heavy elements between the halo and disk, and within the disk itself. Therefore, it makes the gradient of metal abundance small. It should be made clear whether the observed gradient of metal abundances is consistent with this mixing or not. In order to examine this problem, we must follow the motion of rising hot gas and infalling cold clouds exactly.

4.2. Galactic Dynamo

The toroidal magnetic field is wound up by the differential rotation. This field is considered frozen in to the hot gas. Therefore, the wound-up magnetic field is enforced to go up to the halo by superbubbles. The reconnection will occur at the halo, and the cut off field escapes from the galaxy. In this way, the steady magnetic field is maintained. This process is similar to the classical $\alpha\omega$–dynamo, but in the present picture the strengthened part of magnetic field is enforced to lift by the high pressure gas produced by sequential supernova explosions. Therefore, the dynamo action will be very efficient. It is worthwhile to examine this galactic dynamo.

4.3. Propagation of Cosmic Rays

The gas motion between the disk and halo is convective through the chimneys as rising hot gas and infalling cold clouds. The cosmic rays are also associated with these large scale gas motion. The leaky box model is naturally prepared in the present picture. The leaky holes just correspond to the chimneys. The scale length of convective motion would be $H_h \sim 3$ kpc. Till now the propagation of cosmic rays in the medium with such a large scale convective motion has not been studied. It will be interesting to explore the leaky box with chimneys.

I would like to thank G. Field, M. Fujimoto, S. Hayakawa, C. Hayashi, C. Norman, B. Rosner, K. Tomisaka and Y. Uchida for helpful discussion, and H. Suzuki for careful typing of this manuscript.

References

1) Spitzer, L. 1968, *Diffuse Matter in Space* (New York ; Interscence).
2) Field, G.B., Goldsmith, D.W., and Habing, H.J. 1969, *Ap. J. (Letters)*, 155, L49.
3) Tanaka, Y., and Bleeker, J.A.M. 1977, *Space Sci. Rev.*, 20, 815.
4) Jenkins, E.B., and Meloy, D.A. 1974, *Ap. J., (Letters)*, 193, L121.
5) Jenkins, E.B. 1978, *Ap. J.*, 219, 845.
6) McKee, C.F., and Ostriker, J.P. 1977, *Ap. J.*, 218, 148.
7) Ikeuchi, S., Habe, A., and Tanaka, Y.D. 1984, *Month. Notices Roy. Astron. Soc.*, 207, 909.
8) Cash, W. *et al.* 1980, *Ap. J. (Letters)*, 238, L71.
9) Cowie, L.L., Songaila, A., and York. D. 1979, *Ap, J.*, 230, 469.
10) Reynolds, R.J., and Ogden, P.M. 1979, *Ap. J.*, 229, 942.
11) Heiles, C. 1979, *Ap. J.*, 229, 533.
12) Heiles, C. 1984, *Ap. J. Suppl.*, 55, 585.
13) Tomisaka, K., Habe, A., and Ikeuchi, S. 1981, *Ap. Sp. Sci.*, 78, 273.
14) Tomisaka, K., and Ikeuchi, S. 1986, *Publ. Astron. Soc. Japan*, 38, 697.
15) Warwick, R.S. *et al.* 1985, *Nature*, 317, 218.
16) Koyama, K. *et al.* 1986, *Publ. Astron. Soc. Japan*, 38, 121.
17) Koyama, K. 1985, in *X-ray Astronomy* 1984 ed. by M. Oda and R. Giacconi ISAS. p.325.
18) Koyama, K., Ikeuchi, S., and Tomisaka, K. 1986, *Publ. Astron. Soc. Japan*, 38, 503.
19) Savage, B.D., and Massa, D. 1986, *Ap. J.*, 314, 380.
20) Savage, B.D. 1986, *Proceedings of NRAO Conference on Gaseous Go lactic Halos* ed. by J.N. Bregman and F.J. Lockman, p.17.
21) Bregman, J.N. 1980, *Ap. J.*, 236, 577.
22) Habe, A., and Ikeuchi, S. 1980, *Prog. Theor. Phys.*, 64, 1995.
23) van Woerden, H., Schwarz, U.J., and Hulsbosch, A.N.M. 1985, in *IAU Symp. 106 The Milky Way Galaxy*, ed. by H. van Woerden, R. Allen and W.B. Burton, (Reidel. Dordrecht), p.387.
24) Brinks, E., and Bajaja, E. 1986, *Astrop. Astron.*, 169, 14.
25) Bergeron, J. 1986, *Astron. Astrophys.*, 155, L8.
26) Young, P., Sargent, W.L.W., and Boksenberg, A. 1982, *Ap. J. Suppl.*, 48, 455.
27) Bruhweiler, F.C., Gull, T.R., Kafatos, M., and Sofia, S. 1980, *Ap. J.*, 238, L71.
28) Blaauw, A. 1964, *Ann. Rev. Astron. Astrophys.*, 2, 213.

THE ROLE PLAYED BY EVOLVED OB ASSOCIATIONS IN THE GALAXY

Guillermo Tenorio-Tagle

Max-Planck-Institut für Physik und Astrophysik
Institut für Astrophysik
Karl-Schwarzschild-Str. 1
D-8046 Garching b. München

and

C. E. N. Saclay
Service d'Astrophysique
Saclay, France

I. Introduction

The hydrodynamics of remnants caused by the multi-supernova explosions expected from an evolved OB association has become a field of interest in recent years. The motivation has been largely to offer an explanation to the large scale shells and supershells detected in HI in our galaxy (Heiles 1979, 1984). Almost all attempts, have tried exclusively to match the size of the largest structures, disregarding other issues which may be more important. Here I would like to point out several problems regarding the various calculations available in the literature and secondly demonstrate that although supershells cannot be explained by such a mechanism, the multi-supernova explosions from evolved OB associations are still a fundamental event in the realm of interstellar matter.

II. The present "knowledge"

Calculations of supernova remnants in two dimensions have usually been started by placing the presumed energy of the explosion, $E_O \backsim 10^{51}$ ergs, as thermal energy in a small section of the computational grid (Chevalier and Gardner 1974, Bodenheimer et al. 1984). To obtain a reasonable solution, i.e. a remnant that soon joins the Sedov track (with $\backsim$ 1/3 E_O in the form of kinetic energy and $\backsim$ 2/3 E_O remaining as thermal) and that enters the radiative phase at the appropriate time and radius while composing a dense thin shell, one has to care particularly about two things:

I) The numerical resolutions, and

II) about the amount of mass into which the original E_O is deposited. This should be comparable to the amount of mass (Mej) expected to be released during the explosion (say, 5 $M_\odot \leqslant$ Mej $\lesssim$ 10 $M_\odot$).

The latter issue is easy to control, although it is also bound to the numerical resolution and the number of cells into which the initial amount of energy is placed. Test calculations have been made by all authors using this method of simulating the sudden deposition of energy and these have been compared with the well-known analytic or numerical solutions (see Bodenheimer et al. 1984). Here I would like to emphasize however, several aspects which have been overlooked when using the same method to solve other problems. Problems which give their final physical dimension and the finite storage capacity of modern computers, have been calculated with rather poor resolution. A good example is the remnants caused by the large number of supernovae expected in a galactic nucleus or from an evolved OB association. The multi-supernova prolem has been tackled analytically by Bruhweller et al. (1980), Mc Cray and Kafatos (1987) and numerically; in 1D by Tomisaka et al. (1981) and in 2D by Tomisaka and Ikeuchi (1986) and Tenorio-Tagle et al. (1987). The latter presents several calculations with a numerical resolution $\Delta Z = \Delta R = 0.5$ pc of multiple explosions in a constant density medium and in an stratified gas distribution. Calculations with a supernova rate of $2\text{x}10^{-5}$ yr^{-1}, 10^{-5} yr^{-1} and $5\text{x}10^{-6}$ yr^{-1}, which cover the range expected from a "normal" IMF, all led to a similar qualitative result. Namely, to remnants which soon, after a few explosions, become highly irregular as the shell of swept up matter becomes Rayleigh-Taylor (R-T) unstable. The instability occurs once the remnants have grown to a radius $R_{SN} \backsim$ 50 pc, and it is promoted by the sequential deposition of energy (see Tenorio-Tagle et al. 1987). Figure 1 displays the sequence of events that result from one such calculations in a stratified gas distribution. The departures from sphericity of the remnant are first

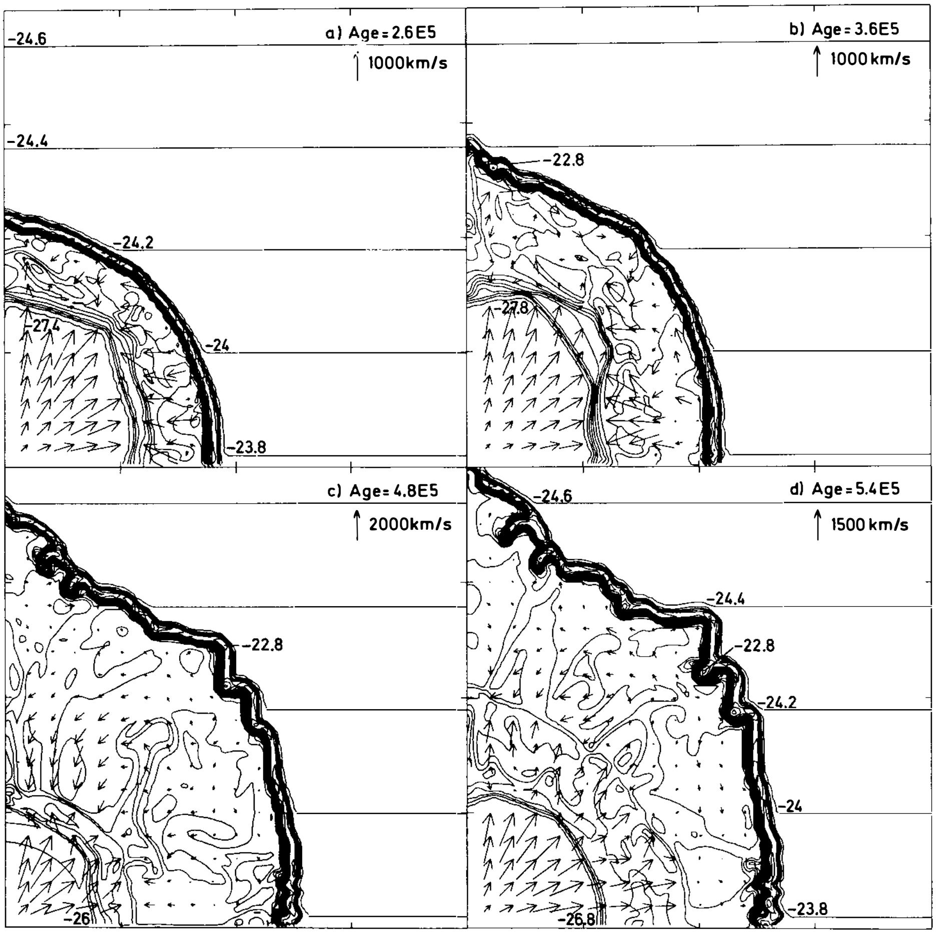

Figure 1:
The evolution of a remnant driven by sequential explosions (rate = $5\times10^{-6}yr^{-1}$) of 10^{51} erg each in a stratified medium (n_0 = 1; H = 150 pc). Evolutionary ages in years are indicated in each frame together with corresponding velocity scales. Constant density lines in the (r,z) plane are plotted on a logarithmic scale, with density contrast $\Delta \log\rho$ = 0.2 between adjacent contours. For some contours the decimal logarithm of the density (in g cm^{-3}) is given. The distance between tick marks on the horizontal and vertical scales corresponds to 25 parsecs.

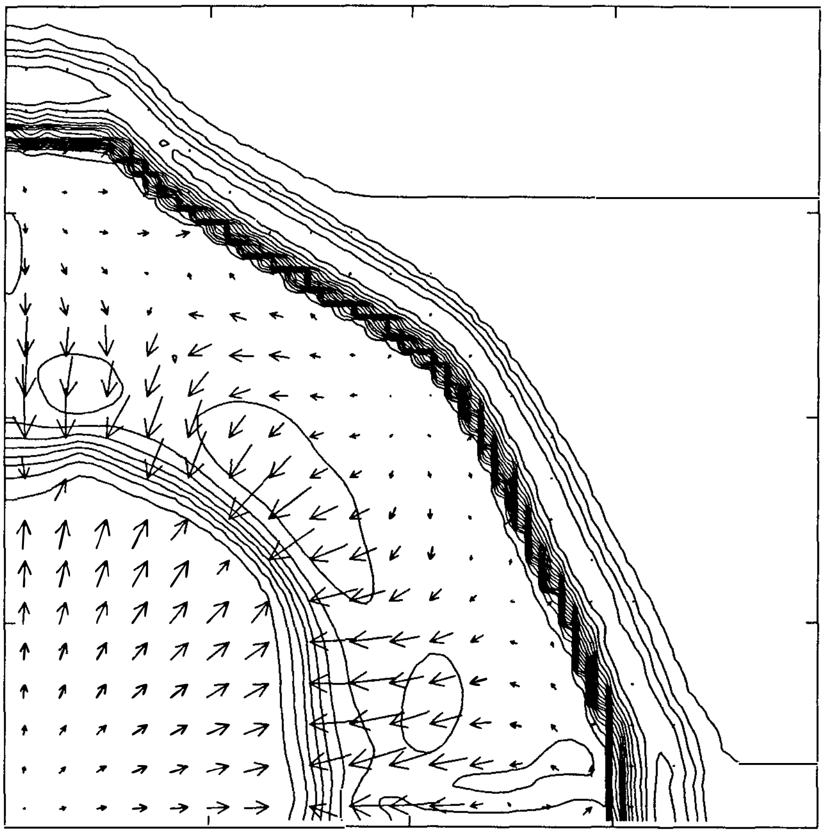

Figure 2:
A low resolution run. Last calculated model for the same conditions as in Figure 1, but for a $\Delta R = \Delta Z = 2$ pc. See Figure 1 for explanation of symbols.

of all caused by the gas distribution which allows the remnant to become elongated in the Z direction. Superimposed on this deformation are also clear signs of the R-T instability which leads to the development of tongues or spikes of dense matter which hang into the remnant interior and lag behind the main shock. Figure 2 on the other hand resulted from an identical calculation, with the same code, but on a grid with lower resolution ($\Delta Z = \Delta R = 2pc$). Evidently, the lack of resolution has inhibited the development of the R-T instability. Note that all performing codes, regardless of resolution, will produce an "answer" to a given initial value problem. However, it should be clear that many of these may have very little to do with reality and particularly the low resolution ones may not be physically sound. Take for example the calculations presented by Tomisaka and Ikeuchi (1986), performed with a numerical grid resolution $\Delta R = \Delta Z = 5$ pc, or 10 pc for the largest grids employed. Clearly the poor resolution has inhibited the R-T instability in all calculations. Instead, their large scale remnants in all cases present very wide shells (width > 100 pc) and consequently throughout their evolution a very poor compression factor (less than a factor of 10, despite radiative cooling) is seen behind the shock. Such odd density distributions make one wonder about the temperature distributions and thus about any detailed comparison that could be made with the observations. Such calculations can only be regarded as a poor, first step towards the true solution of the problem. On the other hand, regarding the issue of supershells in our galaxy (see Heiles 1979, 1984) even such preliminary calculations indicate already the enormous difficulties confronted by the multi-supernova model when invoqued as the mechanism responsible for supershells.

The main issue is the total amount of kinetic energy measured at the final state of evolution, when the remnants have grown to their largest dimension and their expansion velocities have dropped below 8 km s^{-1}; the assumed random speed of motions in the ISM. This amounts to a few times 10^{51} ergs (see Tomisaka and Ikeuchi, 1986, table I) which is too small when compared to the values measured in supershells ($E_K \sim 10^{53-54}$ erg; see Heiles 1979, 1984). This is because of the final size of the largest remnants is at least a factor of two smaller than the dimensions of the largest supershells. This implies that the total amount of swept up matter is almost a factor of 10 of that detected in supershells. The calculations in a low density medium, simulating the conditions at 20 kpc from the galactic center do lead to the largest remnants, but to a smaller amount of mass and velocity compared to supershells. Also these remnants, as noticed by Tomisaka and Ikeuchi, given the increasingly larger speed of the shock in the upward direction promoted by the phenomena of "blow up" which occurs as the shock encounters the lower and lower densities set by the disk stratification, do not lead to an HI shell is the upward direction. Thus, their largest dimension cannot be compared with observed supershells.

The above holds also for the approach of Mc Cray and Kafatos (1987) who solved the multi-supernova problem with an analytical scaled up version of the stellar wind solution. If one drops the assumption of constant density and instead a stratified gas distribution representing our galactic disk is used, then as noticed by Mc Cray and Kafatos (1987), as soon as the radius of the remnant becomes comparable to the density scale height of the disk, the stellar wind approach would break down. This is due to the discharge of the remnant inner pressure into the halo. Under these circumstances the growth of the remnant (in a direction parallel to the galactic plane) would proceed by means of conservation of momentum only.

III. The role played by evolved OB associations

Regardless of the present discrepancy among the solutions found for the multi-supernovae problem, it is clear that large scale remnants will result from such strong depositions of energy into the interstellar medium, and eventually one will be able to track and predict their detailed structure and transendental nature. Presently, however, there is one important feature that all above authors have ignored in their solutions and that is that, if multi-supernova remnants are to evolve for a long time ($4-7\times10^7$ yr, see Bruhweiler et al., table 2) then one has to account also for the fact that interstellar matter is not sitting at rest waiting for the blast wave to overrun it. Rather, at least in our galaxy (and in any other spiral galaxy), it is moving in circular orbits about the galactic center and further it is subjected to a strong differential shear promoted by differential galactic rotation. A first attempt to account for such boundary condition to the multi-supernova problem (Tenorio-Tagle and Palous 1987; paper I) seems to indicate the transendental and true role of evolved OB associations in the galaxy. This is not the build up of supershells or even of large scale remnants but rather the formation of giant molecular clouds ($M > 10^5\ M_\odot$), the future seeds of star formation and thus the link in a well-determined cycle where star formation is a self-regulated event.

Our approach is rather approximate and simple. Facts which can only be justified by the three-dimensional nature of the problem and the various boundary conditions imposed. The calculations are done along the galactic plane only, assuming typical values of density (and disk scale height: H) at 5 kpc, 10 kpc and 20 kpc from the galactic center. Our initial condition assumes that the energies deposited by an OB association (through photo- ionization) has disrupted and evenly spread the cloud where the association formed. Thus at t = 0, which is about 10^7 yr after star formation, the remnant caused by the first supernovae is assumed to have a dimension $R_{SN} \sim H$ and it is at about to discharge its overpressure into the halo. We therefore assumed a cylindrical remnant containing a large amount of energy E_{SN} ($E_{SN} = 10^{53}$ erg $\sim$ 100 supernova explosions each of 10^{51} ergs). 2/3 of this energy is assumed to be in the form of thermal energy inside the cylindrical volume. The remaining 1/3 E_0 is in the form of kinetic energy, stored behind the cylindrical shock, in about 1/2 of the mass originally filling the cylindrical volume V, assumed to have been overrun by the blast wave. The other 1/2 of the mass in the original volume will soon be ejected into the halo from both top and bottom ends of the cylinder. The cylindrical shock moving parallel to the galactic plane has been approximated by a number of plane parallel shocks ($\sim$ 100) running the full thickness of the disk, and having originally an outward velocity u and an overpressure, caused by the initial amount of kinetic and thermal energy in the remnant. The hot gas inside the cylinder is allowed to expand freely (with its own sound speed) into the halo and thus controls the pressure behind the cylindrical shock. The equations of motion of the cylindrical remnant also allowed for the perpendicular and parallel components of the shocked matter velocity which result as the blast wave shears due to the differential galactic rotation imposed in the surrounding gas. For a full description of the method of solution please refer to paper 1.

Figure 3 shows the typical evolution of one of these remnants as a function of time. All evolve into increasingly larger elliptical remnants tilting over 90^o until their minor axis collapses and the remnants are refilled with undisturbed matter. This implies that only very young (age $\lesssim 2 \times 10^7$ yr) multi-supernova remnants would look round, or ring like, in the presence of differential galactic rotation.

Throughout the evolution another important intrinsic deformation takes place behind the shock wave. The overtaken matter slides, by means of differential shear, along the shocked layer towards the tips of the elliptical remnants and accumulates in these locations. We have measured the column density across the remnant shell as a function of time and angle, as it would be seen by an observer sitting at the explosion site (or center of original cylinder). This is

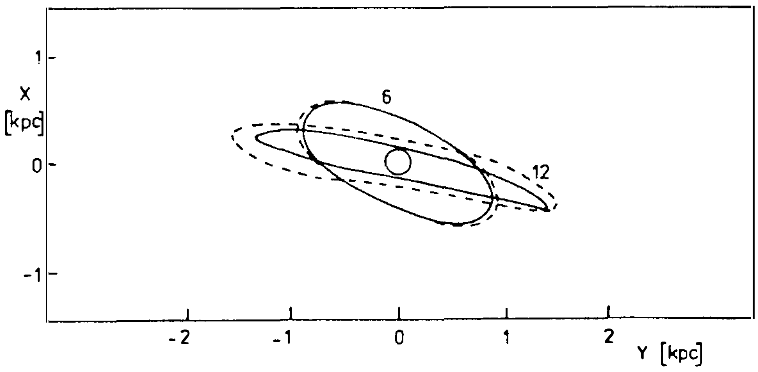

Figure 3:
The time evolution. Face on view of the remnant resultant from the calculations at 10 kpc from the galactic center with (solid lines) and without (dashed lines) self gravity, at the times indicated in units of 10^7 yr. The distance between tick marks equals 1 kpc. Galactic center is downwards and galactic rotation is clockwise.

shown in figure 4 for the calculations at 5, 10 and 20 kpc and are to be compared with the minimum column density derived by Franco and Cox (1987) as required for the formation of molecular clouds. $N_{opacity} = 10^{21}\ Z_{\odot}/Z\ cm^{-2}$. Given the values of Z at 5, 10, and 20 kpc, $N_{opacity} = 2.5\times10^{20}\ cm^{-2}$, $10^{21}\ cm^{-3}$ and $2\times10^{21}\ cm^{-2}$, respectively. All sections of the remnants fulfilling such a criterion would be destabilized to become molecular independently of whether or not self-gravitation sets in. In other words, for molecules to form shielding from the background uv field is the only requirement and this occurs whenever $N > N_{opacity}$.

In the run at 5 kpc the criterion is fulfilled everywhere in the remnant shell irrespectively of direction and long before self-gravity sets in. The remnant still presents two distinct concentrations of matter (at the tips of the remnant) with a

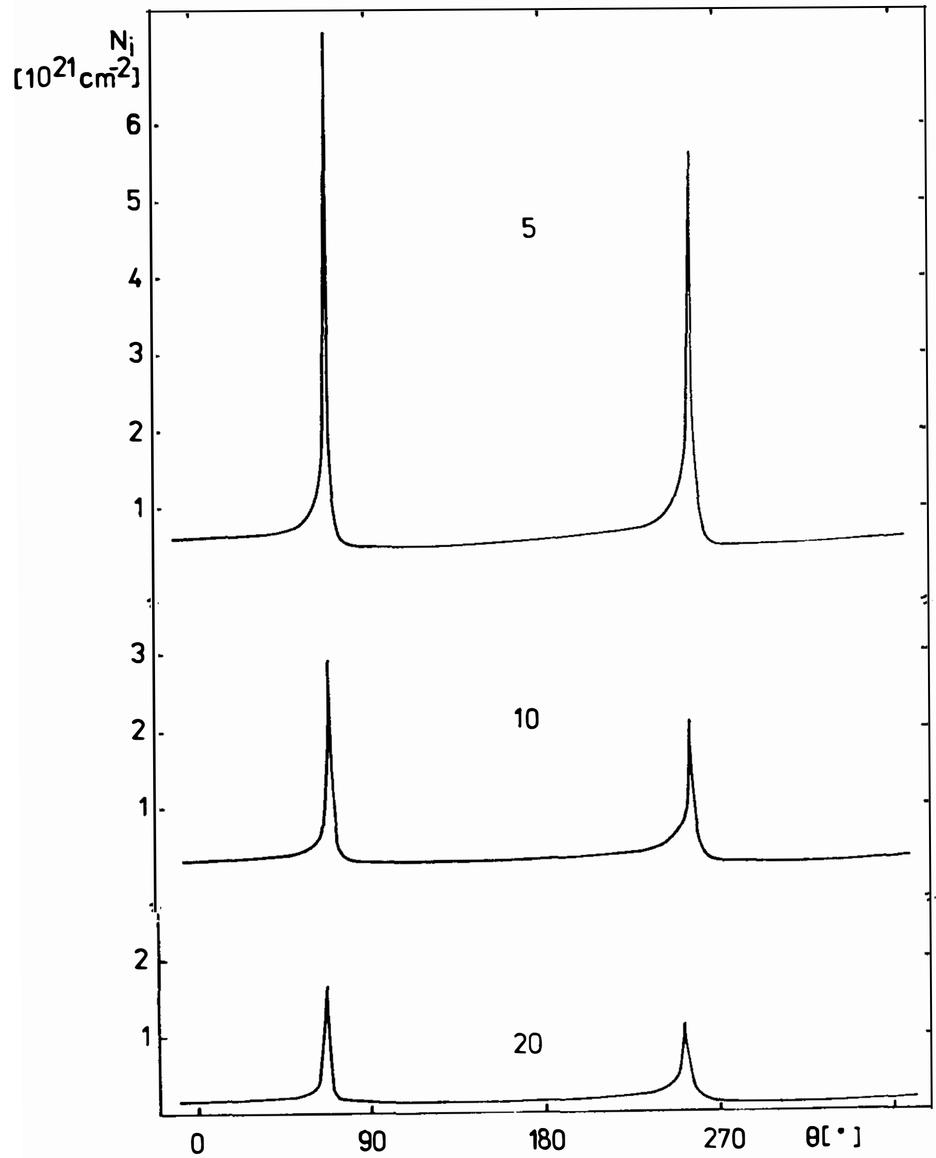

Figure 4:
The run of column density N_i as a function of angle (θ) plotted for the calculations at 5, 10, 20 kpc with selfgravity at $t = t_{final}$, i.e. at 5.5, 10.0 and 18.0 10^7 years. θ runs anticlockwise with direction θ = 0 pointing towards the galactic disk.

larger value of N. In the run at 10 kpc N > $N_{opacity}$ only at the tips of the elliptical remnant and at 20 kpc it would need of self-gravity to take over before the shell column density can exceed the opacity criterion.

In paper I we derived the properties (size, mass, separation) of the resultant giant molecular clouds. These are in good agreement with the observed values. Thus although supernova may have been regarded as a disruptive event, within the present context they end up doing the opposite job. The remnants caused by the supernova power of an evolved OB association, in a differentially rotating disk, lead to the agglomeration of the swept up matter at the tips of the elliptical remnants and with it to the formation of massive molecular clouds. If these clouds are the seeds of a new generation of OB associations, the whole scheme can be regarded as a well-determined sequence of events sustained by a self-regulated process, by star formation.

References

Bodenheimer, P., Yorke, H.W. and Tenorio-Tagle, G. 1984, Astron. Astrophys. 138, 215.

Bruhweiler, F.C., Gull, T.R., Kafatos, M. and Sofia, S. 1980, Astrophys. J. 238, L27.

Chevalier, R.A. and Gardner, J. 1974, Ap. J. 192, 457.

Franco, J. and Cox, D.P., 1986, preprint MPA 258.

Heiles, C. 1979, Ap. J. 224, 533.

Heiles, C. 1984, Ap. J. Suppl. 55, 585.

McCray, R. and Kafatos, M. 1987, Ap. J. (in press).

Tenorio-Tagle, G., Bodenheimer, P. and Rozyczka, M. 1987, Astron. Astrophys. (in press).

Tenorio-Tagle, G. and Palous, J. 1987, Astron. Astrophys. (in press).

Tomisaka, K., Habe, A. and Ikeuchi, S. 1981, Astrophys. Sp. Sci. 78, 273.

Tomisaka, K. and Ikeuchi, S. 1986, Publ. Astr. Soc. Japan 38, 697.

DIFFUSE HIGH-ENERGY RADIATION FROM REGIONS OF MASSIVE STAR FORMATION

Thierry MONTMERLE
Service d'Astrophysique
Centre d'Etudes Nucléaires de Saclay
91191 Gif sur Yvette Cedex, France

ABSTRACT

In the Galaxy, there is evidence that various components of regions of massive star formation (low-mass PMS stars, O and Wolf-Rayet stars, HII regions, molecular clouds) are, together or separately, emitting diffuse high-energy radiation, from sub-keV X-rays to GeV γ-rays. This evidence is briefly reviewed, and the detectability of such radiation from nearby galaxies is examined.

1. INTRODUCTION

In recent years, observational as well as theoretical work has shown that, in the Galaxy, regions of star formation may be associated with high-energy radiation: X-rays, γ-rays, and perhaps even nuclear γ-ray lines. In particular, regions of massive star formation, which are known individually up to very large distances and even in nearby galaxies, may be emitting radiation from various components in the whole ~ 0.1 keV $- \sim 5$ GeV range, i.e., over ~ 7 decades in energy.

The purpose of the present paper is to briefly review what is known in our Galaxy about these links, and examine under what conditions our present knowledge could be extended to nearby galaxies.

Table 1 summarizes the main topics covered in this paper, which will address successively sub-keV X-rays (§ 2), keV and MeV continuum and line emission (§ 3), and $\gtrsim 100$ MeV γ-rays (§ 4). A brief summary and some observational conclusions are presented in § 5.

2. SUB-KEV RADIATION ASSOCIATED WITH MOLECULAR CLOUDS

2.1. Basic observations

Several observations of star-forming regions by the "Einstein" Observatory have shown that pre-main sequence (PMS) stars are strong X-ray emitters. The detections are not limited to the classical T Tauri stars, but include many other stars previously unknown as PMS stars (see reviews by Feigelson 1984, 1987 ; Walter 1987 ; Montmerle 1987a).

The best documented case to date remains the multi-epoch "Einstein" survey (bandwidth ~ 0.1-4 keV) of the ρ Ophiuchi dark cloud region (distance $d \sim 160$ pc) which was not aimed at a particular sample of PMS stars, but at a $\sim 2°\text{x}2°$ area overlapping the cloud using the IPC instrument (Montmerle et al., 1983).

The main results of this study may be summarized as follows:

- among the ~ 50 Rho Oph X-ray ("ROX") sources found, $N_o = 34$ are located in the central $1°\text{x}1°$ overlapping the cloud core;
- variability studies indicate that the X-rays come predominantly, if not only, from solar-type flares, $\sim 10^3$-10^6 times more intense than solar flares;
- the associated bremsstrahlung-emitting hot gas has a typical temperature $kT^* \simeq 0.8$ keV, and the ROX sources have an average luminosity $\langle L^*_x \rangle \simeq 10^{31}$ erg.s^{-1};

TABLE 1 - Links between regions of massive star formation and high-energy radiation in the Galaxy

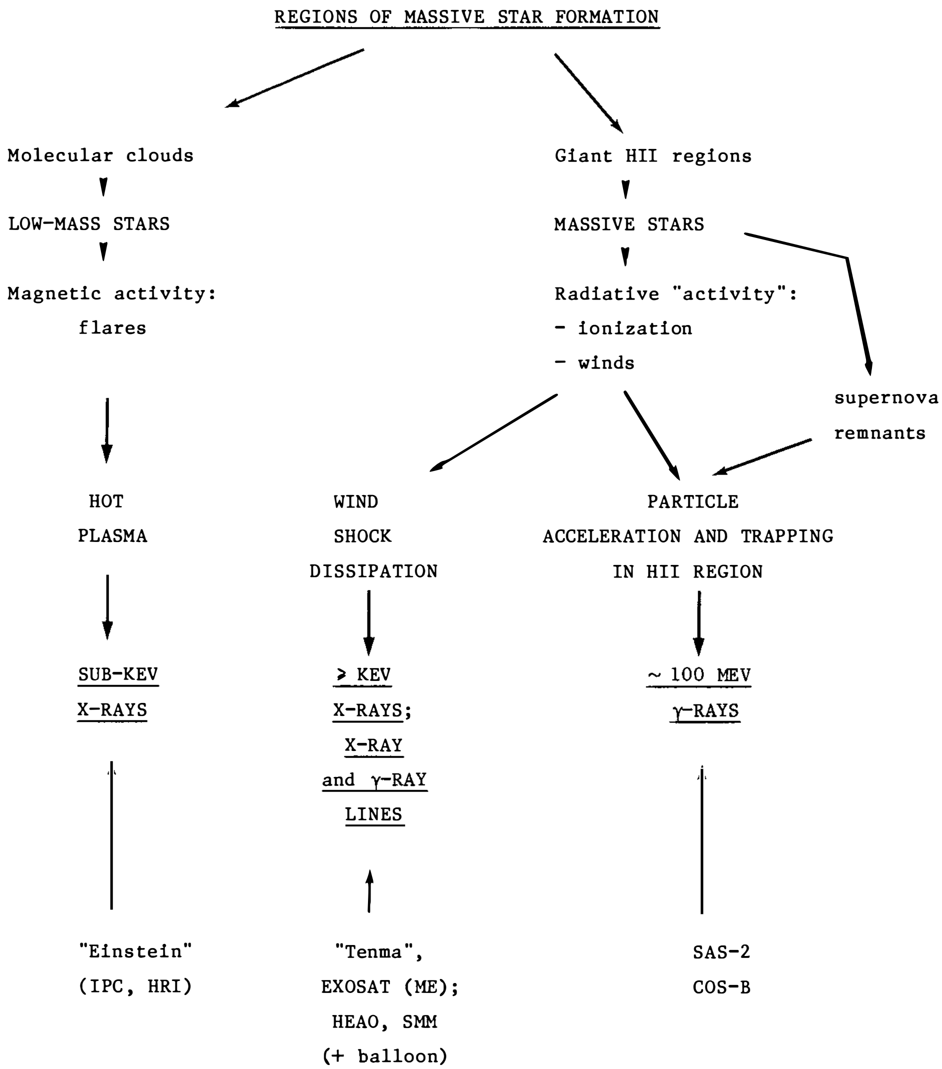

- therefore, the X-ray sources are extincted by interstellar absorption if their $A_V > 3$-5 mag (equivalent hydrogen column density $N_H \gtrsim 10^{21} - 10^{22}\ cm^{-2}$);
- the X-ray emission seems essentially independent of the spectral type, from M to early B;
- the optical counterparts to the X-ray sources, when known, are mostly low-mass PMS stars, many of them proved to be so after X-ray detection (Bouvier, 1987 ; Bouvier and Appenzeller 1987).

For the present paper, the useful conclusions are:

- the large majority of ROX sources are $\lesssim 1\ M_\odot$ PMS stars;
- because of X-ray absorption, ROX sources form a superficial subset of all young stars in the cloud ;
- but they are ~ 3 times more numerous than the classical T Tauri stars already known ; hence, X-rays are a better tracer of low-mass stars than the optical over large areas on the sky.

2.2. ROX-type sources as tracers of low-mass star formation ?

The data on the X-ray emission from PMS stars in nearby ($\lesssim$ 300 pc) molecular clouds are still limited, since the other data concern mainly individual classical T Tauri stars, which we know from the ρ Oph study and a recent study using the "Einstein" archives (Feigelson et al., 1987) are only a minority of the existing visible PMS stars. Nevertheless, altogether the number of known X-ray emitting PMS stars is relatively large (≈ 100).

Hence the following suggestion: if a molecular cloud is far enough, X-rays from neighboring ROX-type sources (which an instrument like the "Einstein" IPC detects with a $\lesssim$ 1' FWHM resolution) will be unresolved, giving rise to an (apparently) diffuse emission. In other words, there should be sub-keV X-ray "glows" around molecular clouds. Such glows could then be used as tracers of low-mass stars in distant clouds, at least in their outer layers (i.e., $A_V \lesssim 3$-5).

In its simplest form, the problem can be formulated as follows. Let $\Phi_{x,o}$ be the total X-ray flux coming from a reference molecular cloud (or from a portion of it), detected over a solid angle $\Omega_{x,o}$, and let Φ_x and Ω_x be the corresponding quantities for another cloud.

Defining a quantity f_x by:

$$f_x = (\Phi_x/\Omega_x)/(\Phi_{x,o}/\Omega_{x,o}) ,$$

f_x is the surface density of ROX-type sources in the outer layers of molecular clouds, normalized to the reference cloud. For this reference, we shall choose the central 1°x1° of ρ Oph:

$\Omega_{x,o}$ = 1 sq. degree, $\Phi_{x,o} = N_o \langle L^*_x \rangle/(4\pi d^2) \simeq 1.2 \times 10^{-10}$ $erg.cm^{-2}s^{-1}$.

For a molecular cloud of extent Ω_g, traced by any means (CO emission, dust etc.), the presence of an X-ray "glow" as defined above implies $\Omega_x \simeq \Omega_g$. In practice, the areas observed today in X-rays are much smaller than Ω_g (several IPC fields, i.e., several sq. degrees at most). To the extent that the PMS star volume density in the outer layers of a molecular cloud is proportional to the density of stars forming in the (invisible) denser regions, f_x becomes a (relative) measure of the efficiency of low-mass star formation in the corresponding molecular cloud.

2.3. Diffuse sub-keV X-ray emission associated with molecular clouds

The hypothesis that sub-keV X-ray glows, related to the gaseous content of molecular clouds, actually exist, is supported by "Einstein" observations of several distant star-forming regions: Orion (~ 0.45 kpc, Ku and Chanan 1979), Carina (~ 2 kpc, Seward and Chlebowski, 1982), and Rosette (~ 1.6 kpc, Leahy 1985).

In the first two nebulae, and in addition to point sources associated with nebular variables and O stars (Orion), or O and Wolf-Rayet stars (Carina), diffuse sub-keV emission is clearly seen. From the published maps and total flux, one finds $f_x \simeq 1$. For the Rosette nebula, the diffuse emission is weak and scattered, and $f_x \leq 0.1$.

On the other hand, the gaseous content along the line-of-sight, for instance traced by CO emission, is not the same for all objects: whereas the X-ray emission surrounds or is close to a local CO maximum, in the cases of ρ Oph, Orion, or Carina, with values of $\int T\,dv$ up to ~ 200 $K.km.s^{-1}$, this quantity is very much smaller for the Rosette nebula ($\int T\,dv \leq 7$ $K.km.s^{-1}$) (see Dame et al., 1987).

Given the widely different content in massive stars of this (admittedly still limited) sample of 4 star-forming regions, running from two early B stars for ρ Oph to 43 O stars (including 6 O3 stars) and 3 Wolf-Rayet stars for the Carina nebula, one can tentatively draw a double conclusion:

(i) sub-keV X-ray glows are closely associated with the molecular gas, and are a good tracer of low-mass star formation, even in distant regions;

(ii) the efficiency of low-mass star formation in a molecular cloud is approximately constant, and independent of its content in massive stars.

Work in progress (Montmerle and Grenier, 1987) is seeking to confirm these conclusions.

Since IR data suggest that star formation still goes on inside clouds at the same time that X-ray emitting PMS stars are present, the implication is that high-mass and low-mass stars appear to form independently of each other, giving some independent support to the "bimodal star formation" concept.

2.4. X-ray glows in other galaxies ?

The preceding conclusion shows the interest of using X-ray observations to determine f_x in other galaxies. Since one needs Ω_g (as well as Φ_x and Ω_x), this will be for some time restricted to nearby objects, for which CO data is available (e.g., Magellanic clouds, M31 etc.)

For an IPC-type detector, again normalizing to the ρ Oph data, glows must generate at least $\Phi_x = \Omega_g\, f_x \times 9.2 \times 10^{-8}$ cts.s^{-1} arc sec^{-2} to be seen. This may be smaller than the instrumental background: for instance, it is a factor 15 too low in the 256" diameter IPC detection cell for the LMC (see Long et al., 1981).

Note that, if $f_x \sim 1$, about 4×10^6 ROX-type sources must be present in a single IPC-type frame pointed at the LMC, resolvable only by a detector with sub-arc sec resolution capability, not achieved by AXAF.

3. DIFFUSE KEV AND MEV RADIATION ASSOCIATED WITH HOT STARS

3.1. Structure of giant hollow HII regions

Giant HII regions are excited by associations of O, B and lower-mass stars. The ionization is usually dominated by a few early O stars, which are also subject to a strong mass loss (typically $\lesssim 10^{-6}$ $M_\odot$ yr^{-1} at v ~ 1500-2500 km.s^{-1}). Owing to the evolution of the most massive O stars, Wolf-Rayet (WR) stars are often also present (see, e.g., Maeder, this volume). If so, they dominate the mass loss, but because their winds are likely powered (up to $\gtrsim$ 3×10^{-5} $M_\odot$ yr^{-1} at 3000 km.s^{-1}) by UV radiation, little is left for them to contribute to the ionization of the surrounding HII region.

The structure of these HII regions is observed to be hollow (internal cavity created by the stellar winds) and thick (outer ionized shell) ; prototypes would be the Rosette nebula, with several O4 stars, and the Carina nebula, with several O3 and WR stars (see also § 2).

The standard "hot interstellar bubble" model describes the interaction between a mass-losing early O star and a dense interstellar gas, but leads to large bubbles of hot X-ray emitting gas surrounded by a thin, compressed HII region (Weaver et al., 1977). Clearly, such a model cannot describe the structure of hollow, thick HII regions.

Dorland et al. (1986) have recently revisited this problem. Two new features were incorporated: effects of stellar evolution (i.e., time-dependent total ionization and mass-loss rates), and complete dissipation of the wind kinetic energy in the shock region (i.e., when the wind becomes subsonic). This last effect turned out to be the most important, with the physical consequence of relaxing the wind pressure on the outer ionized shell and essentially allowing its inner boundary (the observed cavity) to move inwards, very close to the wind shock. By contrast, the standard "hot interstellar bubble" model features an almost adiabatic wind shock ; the only energy loss is the small heating and subsequent evaporation of the HII region by electron conduction at the hot bubble/ionized dense shell interface.

However, as pointed out by Dorland and Montmerle (1987), the linear conduction law, that is, (conductive heat flux) α ∇T, cannot be used as done in the standard model. Indeed, the temperature gradient ∇T between the hot bubble and the ionized shell is too steep, i.e., its scaleheight is smaller than a critical length $\lambda_c \sim 500$ x (hot electron mean free path), as shown by recent work on laser-heated fusion plasmas. Taking into account non-linear effects in the electron conduction, Dorland and Montmerle (1987) have shown that the kinetic energy of the winds of the exciting stars can indeed be radiated over a short distance ($\ll$ thickness of the ionized shell) downstream of the wind shock, in the form of UV and X-rays.

3.2. KeV X-ray emission from HII regions and the "galactic ridge"

It has been known for some time (up to a decade) that several well-known HII regions emit diffuse X-rays of several keV, e.g., Orion (den Boggende 1978), or Carina (Becker et al., 1976). On the other hand, the Dorland-Montmerle model (see also Montmerle 1986) gives the X-ray luminosity L_X and temperature T_X of the thin downstream layer, as a function of the total wind kinetic energy rate L_w and velocity V_w. The model depends on one poorly known conduction-related parameter, not accurately predicted by plasma physics theory, but adjustable to astronomical observations, for instance the observed X-ray luminosity from a reference HII region.

Once this is done, the model predicts $L_x/L_w \sim 1\text{-}2 \times 10^{-4}$ and $T_x \sim 4\text{-}15$ keV, for $V_w \sim 2\text{-}4000$ km.s^{-1}.

These values are consistent with those measured in HII regions like Orion or Carina.

More generally, recent observations by the "Tenma" and EXOSAT satellites (Koyama et al., 1986 ; Warwick et al., 1986) have shown that a large-scale diffuse X-ray emission above several keV is associated with the galactic plane, making up the so-called "galactic ridge". The thermal nature of this emission is attested by the "Tenma" detection of a ubiquitous Fe 6.7 keV line, characteristic of a plasma with $T_x > 2$ keV (and already seen previously in individual regions like Carina, see Becker et al., 1976). The temperatures differ from one line-of-sight to the next. Although it is sometimes difficult to associate the radiation with a specific emitting region, especially inside the solar circle, the facts that the observed temperature range is $\sim$ 2-13 keV, and that excess emission has been noted in the direction of active star-forming regions like Perseus or Cygnus, support the view that the galactic ridge is associated with HII regions excited by mass-losing stars. (For discussions of alternative hypotheses in terms of binary stars, supernova remnants, etc., see discussions in Koyama et al., 1986 and Warwick et al., 1986.)

3.3. Consequences and links with the galactic 1.8 MeV line emission

The total X-ray luminosity of the galactic ridge at several keV, as given by "Tenma" and EXOSAT, is $L_{x,tot} \simeq 1.0 - 1.2 \times 10^{32}$ erg.s^{-1}.

In the framework of the above model, one immediately deduces the total wind kinetic energy rate for the Galaxy (Montmerle, 1986):

$$L_{w,tot} \simeq 6.5 \times 10^{41} \text{ erg.s}^{-1} .$$

Taking the ratio of the number of (wind dominating) WR stars to that of early O stars as $N(WR)/N(O) \simeq 0.2$ (e.g. Maeder, this volume), and average wind energy rates $L_w(WR) \simeq 10^{38}$ erg.s^{-1} and $L_w(O) \simeq 10^{37}$ erg.s^{-1}, one finds the total number of WR stars associated with HII regions which must be present in the Galaxy to account for the galactic ridge in terms of winds from massive stars:

$$N_{WR}(HII) \simeq 4000.$$

This is not an unreasonable number (although on the high end) of WR stars. It is able to account for a sizeable fraction (> 50%) of the observed 1.8 MeV γ-ray line emission from ^{26}Al, if associated with nucleosynthesis in WR stars (see Prantzos and Cassé, 1986).

3.4. Other galaxies: the example of the LMC

This last result can be applied to galaxies: after removal of other sources of keV X-rays like compact objects, supernova remnants etc. (which may not be a trivial task), these X-rays may give directly the total content in massive stars (WR + O) in localized extragalactic HII regions, hence give an independent access to the star-forming efficiency for massive stars.

Is this possible today ? In the LMC, it is known that 81% of all ~ 144 WR stars (Azzopardi and Breysacher, 1985) are in HII regions, hence $N_{WR}(HII) \simeq 120$. Using N(WR)/N(O) = 0.07 (different from our Galaxy because of a different metallicity Z), and $\dot{M} \propto Z^{\frac{1}{2}}$ (see Maeder, this volume), gives $L_{w,tot} \simeq 8.10^{39}$ erg.s^{-1}, hence $L_{x,tot} \simeq 1.6\times10^{36}$ erg.s^{-1}.

This is too low by a factor of ~ 10 to be detected by "Tenma", which has only a wide field-of-view (~ 3.1° FWHM) and no imaging capability. A good target for a future imaging instrument at several keV would be 30 Dor. Only XMM would be suited for that purpose, because of its sensitivity at energies up to ~ 10 keV.

4. DIFFUSE HIGH-ENERGY GAMMA RAYS

4.1. Gamma-ray sources in the Galaxy

A major achievement of the new field of high-energy gamma-rays (~ 50 MeV-5 GeV ; γ-rays, for short) has been the discovery of γ-ray sources by the SAS-2 and COS-B satellites. The main results (see Bignami and Hermsen, 1983 for a review) are as follows:

- ~ 25 sources are known, almost all very close to the galactic plane ;
- the error boxes are typically ~ 1° in radius ;
- the fluxes are in the range ~ 1-10x10^{-6} photons.cm^{-2}.s^{-1}.

They are embedded in an intense ridge of diffuse galactic γ-ray emission. To a first approximation, this ridge can be fully accounted for in terms of interactions between high-energy cosmic rays (essentially protons, electrons, and secondary positrons) of energy density comparable to that in the solar neighborhood, and interstellar matter, as traced by CO and HI surveys (e.g., Bloemen et al., 1986).

Roughly speaking, one can break down the sources in 4 categories (see Montmerle 1985, and references therein, for an update of Montmerle 1979):

- ~ 1/3 are "passive" sources, linked with apparently clumpy molecular clouds, for instance such that their cross-section is in the plane of the sky (e.g., tangent points to galactic spiral arms) ;
- ~ 1/6 are probably or certainly compact, from their observed variability on various timescales (this includes the Crab and Vela pulsars) ;
- ~ 1/6 are yet unidentified ;
- the remaining ~ 1/3 are on the line-of-sight of "active" molecular clouds, i.e., which are the seat of massive star formation and associated energetic objects (WR stars, supernova remnants, etc.).

In these last sources, there is a significant excess (factors ~ 2-5) of γ-rays over what one would expect from the interactions between average-density cosmic rays and the observed matter content.

One model of such a γ-ray source associated with a region of massive star formation features an enhanced cosmic-ray energy density resulting from *in situ* acceleration at the stellar wind shock (or in the stellar winds themselves), or by supernova shock waves, and subsequent trapping of the accelerated particles downstream of the shock, i.e., in the surrounding thick HII region. A trapping mechanism may be resonant Alfvén-wave scattering (Cesarsky and Montmerle, 1983 ; Montmerle 1987b).

In such a "thick cosmic-ray source" (see Lagage and Cesarsky, 1985)—so named because heavy cosmic-ray nuclei cannot leak out of the HII region due to strong nuclear and Coulomb losses - the γ-ray flux at the Sun $\Phi_{\gamma,w}$, resulting from stellar winds, is approximately proportional to the local cosmic-ray flux (itself proportional to the total mass-loss rate) and to the mass of the HII region. Because the acceleration efficiency remains a free parameter, however, one must normalize to a reference object. Once again, the Carina nebula, identified with the γ-ray source 2CG288-00, is a good choice, which allows to compute $\Phi_{\gamma,w}$ in other HII regions, once the exciting stars and gaseous content are known.

4.2. Visibility of LMC HII regions in γ-rays

The Magellanic clouds have not been observed by SAS-2 or COS-B. The 30 Dor region is energized by 25 WR stars, and several hundred O stars, not all known (~ 360 if the average LMC ratio N(WR)/(N(O) is applied). This is about 10 times the stellar content of the Carina nebula, ionizing ~ 10 times as much mass (~ 10^6 $M_\odot$), assuming the same gas densities. The calculated γ-ray flux $\Phi_{\gamma,w}$ for 30 Dor is thus ~ 0.2 x that observed for the Carina nebula. Even taking into account the possible additional contribution of supernova remnants, 30 Dor would probably not have been detected by COS-B. The French-Soviet experiment Gamma-I, due to be launched in late 1988 or early 1989, which has better sensitivity and angular resolution than COS-B, should be able to test this prediction.

5. CONCLUSIONS

The associations between diffuse high-energy radiation and regions of massive star formation in the Galaxy may be summarized as follows:

(i) low-energy (sub-keV) X-ray "glows" directly probe low-mass (PMS) stars, pending confirmation of our finding that their formation efficiency is reasonably constant (f_X ~ 1) ;

(ii) high-energy (several keV) X-rays indirectly probe high-mass stars, through the dissipation of their wind energy in giant HII regions ;

(iii) in the framework of the "thick cosmic-ray source" model, high-energy (~ 100 MeV-5 GeV) γ-rays, associated with in situ cosmic-ray acceleration, probe the interaction of stellar winds (and/or supernova remnants) with the surrounding ionized mass.

In general, these statements cannot yet be tested in nearby galaxies. To test them in the LMC, for instance, requires typically an order-of-magnitude improvement in background rejection, sensitivity, or angular resolution. Hopefully, this goal should be achieved by the planned next generation of high-energy astronomy satellites.

REFERENCES

Azzopardi M., Breysacher J., 1985, Astr. Ap. 149, 213.
Becker R.H., Boldt E.A., Holt S.S., Pravdo S.M., Rothschild R.E., Serlemitsos P.J., Swank J.H., 1976, Ap. J. (Letters) 209, L65.
Bignami G.F., Hermsen W., 1983, Ann. Rev. Astr. Ap. 21, 67.
Bloemen J.B.G.M., Strong A.W., Blitz L., Cohen R.S., Dame T.M., Grabelsky D.A., Hermsen W., Lebrun F., Mayer-Hasselwander H.A., Thaddeus P., 1986, Astr. Ap. 154, 25.
Bouvier J., 1987, in Protostars and Molecular Clouds, eds. T. Montmerle and C. Bertout (Saclay: CEA/Doc), p. 189.
Bouvier J., Appenzeller I., 1987, in preparation.
Cesarsky C.J., Montmerle T., 1983, Sp. Sci. Rev. 36, 173.
Dame T.M., Ungerechts H., Cohen R.S., De Geus E., Grenier I., May J., Murphy D.C., Nyman L.-Å., Thaddeus P., 1987, Ap. J., in press.
Den Boggende A.J.F., Mewe R., Gronenschild E.H.B.M., Heise J., Grindlay J.E., 1978, Astr. Ap. 62, 1.
Dorland H., Montmerle T., 1987, Astr. Ap. 177, 243.
Dorland H., Montmerle T., Doom C., 1986, Astr. Ap. 160, 1.

Feigelson E.D., 1984, in Cool Stars, Stellar Systems, and the Sun, eds. S. Baliunas and L. Hartmann (Berlin: Springer-Verlag) p. 27.
Feigelson E.D., 1987, in Protostars and Molecular Clouds, eds. T. Montmerle and C. Bertout (Saclay: CEA/Doc), p. 123.
Feigelson E.D., Jackson J.M., Mathieu R.D., Myers P.C., Walter F.M., 1987, A.J., in press.
Koyama K., Makishima K., Tanaka Y., Tsunemi H., 1986, Pub. Astr. Soc. Japan 38, 121.
Ku W.H.M., Chanan G.A., 1979, Ap. J. (Letters) 234, L59.
Lagage P.O., Cesarsky C., 1985, Astr. Ap. 147, 127.
Leahy D.A., 1985, M.N.R.A.S. 217, 69.
Long K.S., Helfand D.J., Grabelsky D.A., 1981, Ap. J. 248, 925.
Montmerle T., 1979, Ap. J. 231, 95.
Montmerle T., 1985, 19th Int. Cosmic Ray Conf. (La Jolla), 1, 209.
Montmerle T., 1986, in Advances in Nuclear Astrophysics, eds. E. Vangioni-Flam et al. (Gif-sur-Yvette : Editions Frontières), p. 335.
Montmerle T., 1987a, in Solar and Stellar Physics, eds. E.H. Schröter and M. Schüssler (Berlin: Springer-Verlag), in press.
Montmerle T., 1987b, in Genesis and Propagation of Cosmic Rays, eds. J.P. Wefel and M.M. Shapiro (Dordrecht: Reidel), in press.
Montmerle T., Grenier I., 1987, in preparation.
Montmerle T., Koch-Miramond L., Falgarone E., Grindlay J.E., 1983, Ap. J. 269, 182.
Prantzos N., Cassé M., 1986, Ap. J. 307, 324.
Seward F.D., Chlebowski, T., 1982, Ap. J. 256, 530.
Walter F., 1987, P.A.S.P. 99, 31.
Warwick R.S., Turner M.J.L., Watson M.G., Willingale R., 1985, Nature 317, 218.
Weaver R., McCray R., Castor J., Shapiro P., Moore R., 1977, Ap. J. 218, 377.

MASSIVE STAR FORMATION IN THE MAGELLANIC CLOUDS

James LEQUEUX

Observatoire de Marseille, 13248 Marseille Cedex 04
France

Abstract : The properties of massive star formation in the closest galaxies, the Magellanic Clouds, are reviewed starting from global properties, then going from large scale features (e.g. superassociations) to the exceptional star-forming region 30 Doradus and the smaller clusters. The recent time evolution of massive star formation is discussed shortly.

The Magellanic Clouds are the two closest neighbours of our own Galaxy. They are thus of special interest since the details of the phenomena occurring in these galaxies can be studied almost as easily as in our Galaxy with the bonus that we know that everything in each Cloud is roughly at the same distance, thus avoiding a difficulty that is major in our Galaxy. In particular the massive stars can be studied easily thanks to their high luminosity and the Magellanic Clouds are ideal places to look for massive-star formation. However they do not belong to the same type of galaxy as our own Galaxy, and in particular do not exhibit an obvious spiral pattern. Care should be exercized in generalizing the results obtained on the Magellanic Clouds to other kinds of galaxies: for example, there is no equivalent to 30 Doradus in our Galaxy. On the other hand, the Large Magellanic Cloud (LMC) has about 2 times less heavy elements than our Galaxy and the Small Magellanic Cloud (SMC) almost 10 times less, being one of the lowest-metallicity galaxies known.They offer the possibility of studying the influence of metallicity on star formation, in particular on the initial mass function (IMF), so far as this effect can be separated from others.

In this review I will go from the global scale to smaller scales, first discussing in Part I global parameters related to star formation, then studying large-scale star-formation structures in Part II, and 30 Doradus and smaller active star-forming regions in Part 3. Part 4 reviews briefly our still meager knowledge of the past history of massive star formation in the Clouds.

1. Global properties

I have extensively discussed this point in previous reviews [1], [2] partly based on paper [3]. There has been much debate about the initial mass function in the Clouds, in particular about its upper mass limit. Most of the debate originates in the incompleteness of the catalogues of bright stars and in small-number statistics for the very brightest of them. Moreover, those bright stars often come in small, barely resolved or unresolved groups and this biases the statistics. In fact, there does not appear to exist significant differences between the upper HR diagrams and the upper luminosity functions of the LMC, the SMC and the Solar Neighborhood [3] [4]. Similarly, comparisons of tracers sensitive to different luminosity (or mass) ranges (e.g. the Lyman continuum photons and the far-UV emission) do not suggest important differences. There are however differences in details: the statistics of the evolved stars, in particular of the red supergiants and the Wolf-Rayet stars, are not the same in the three systems for reasons very probably linked to the different metallicities [5] [6]. This should not affect much the gross properties. As far as the evolution of massive stars is the same in the studied systems, the similar luminosity functions and upper HR diagrams suggest similar initial mass functions. However we are still lacking up-to-date stellar evolution models that would allow to check this point, thus a strong statement is not possible.

I now examine the determination of the present day star formation rate (PDSFR) for massive stars in the Magellanic Clouds. Several tracers of massive stars can be used for this purpose [2]: direct star counts, Lyman continuum flux as derived indirectly from the Balmer-line emission of the ionized gas, far-UV emission and far-IR emission. All have drawbacks: the star counts can be very incomplete, we do not really know how much of the Lyman continuum flux of O stars is used to ionize the gas, the far-UV emission is very much affected by far-UV emission; finally there is a sizeable, not well-known contribution from older stars to the heating of the dust thus to the far-IR emission, and also we do not know too well how much of the stellar radiation heats the dust: these points are only beginning to be settled in the solar neighbourhood [7]. Fortunately the three first tracers give consistent results for the Magellanic Clouds when compared to the solar neighbourhood, at least if one uses the star counts of [3] (the counts in [4] are quite incomplete for the Magellanic Clouds, a fact that I did not realize in [2]). Details can be found in [1]. The LMC produces about 1.3 times as many massive stars per unit mass of gas than the solar neighbourhood, and the SMC about 0.3 times only. I personally find misleading to express the PDSFR per unit surface as it is often done, since we do not know well the inclination and the geometry of the Clouds, or the PDSFR per unit mass since the masses of the Clouds are very poorly known, especially for the SMC.

2. Properties of massive-star formation at large scales

It is clear that massive-star formation is neither uniform, nor well correlated with the gas distribution in the Clouds. Massive stars seem to form preferentially in superassociations of kpc size: see e.g. [8]. The sites of star formation move with time over the face of the Clouds: this will be discussed in the last section. However there is also massive star formation in associations and more or less dense clusters (see the next section). Several authors have pointed out massive star formation aligned along "filaments" with lengths up to several kpc in the LMC [9] [10]. These filaments may be connected with the distribution of gas [11] [12] and may also be understood in the framework of the stochastic star formation models [13]. The correlation between massive stars and gas has been discussed by many authors, especially for the LMC: see e.g. [14]. This correlation can be good to fair in some places, but there is anticorrelation in other places, where concentrations of young stars can be entirely devoid of gas. The best example is the Shapley III constellation in the North-East ot the LMC. This is a large concentration of young, massive supergiants with no associated HI and dust (this region appears as a 1°-diameter circular hole on the IRAS 100 μm map). It is surrounded by a ring of HII regions. This description is fully consistent with the model of superbubble formed by the collective effect of several supernova explosions and stellar winds [15]. This is also a case of contagious star formation with a propagation velocity of about 35 km s^{-1} [16]. Another example of a superbubble where the expansion velocity of the ionized and neutral gas is well known is LMC 2, east of 30 Doradus [17].

Recently, accurate radial velocities have been obtained using a correlation spectrometer for most of the red supergiants of both clouds [18] [19]. Preliminary results from this material are the following:

i) the velocity dispersion of stars in superassociations is very small: 5.3 km s^{-1} on the average in 19 areas of the LMC [18], 5.1 km s^{-1} for Shapley III. This is smaller than the velocity dispersions usually quoted for young stars in our Galaxy. However these galactic velocity dispersions have been measured on OB stars for which the accuracy is much poorer and they are probably overestimated in spite of the efforts made for correcting for radial velocity errors. Indeed the velocity dispersion measured on the red supergiants in the Perseus association in the Galaxy is only 4.1 km s^{-1}. These figures are close to the velocity dispersion of giant molecular clouds and smaller than the dispersion for neutral hydrogen, a satisfactory result.

ii) the young-star/gas correlation can be studied better. An interesting case is that of the Shapley II constellation whose stars are pushing the HI with a relative velocity of about 20 km s^{-1}. In the SMC, there is an extended region to the NE where a fraction of the stars are not correlated with the gas.

The outer regions of both clouds are of particular interest. The SMC wing and its extension towards the LMC contains mainly relatively faint blue stars detected either directly on Schmidt plates [20] or through their far-UV emission [12]. The initial mass function in this region appears to be truncated at about 30 $M_\odot$. In the LMC, an extended arc at the extreme south exhibit the same property with a truncation at 25 $M_\odot$ [21]; there are not enough hot stars to ionize the gas. Indeed the high-mass cut-off could be higher if star formation has ceased a few 10^6 years ago, but this is an ad-hoc hypothesis and one may wonder why star formation would have stopped simultaneously over so extended areas.

3. 30 Doradus

30 Doradus is an enormous HII region in the LMC with no equivalent in our Galaxy. However NGC 604 in M33, NGC 2363 in NGC 2366 or the blue compact Galaxy IZw 18 correspond to star formation bursts of similar importance and CM 39 in NGC 4449, the blue compact galaxy IIZw 70 or NGC 5471 and 5461 in M101 are 3 to 20 times stronger: see e.g. [22]. If the IMF is "normal" in 30 Dor, the flux of Lyman continuum photons responsible for the ionization implies the presence of about 300 O stars in the central 2!5 x 2!5 core and of a total of about 700 O stars. The core of 30 Doradus alone contains about 1/8 of all O stars of the LMC. This can be shown in the following ways:

i) The far-UV flux of the core at 1392 A as measured by ANS is 1.48 10^{-11} erg $cm^{-2}s^{-1}A^{-1}$. It is attenuated by dust corresponding to a color excess E(B-V) = 0.38 to 0.46, and the dereddened flux should be in the range 1 - 2.4 10^{-9} erg $cm^{-2}s^{-1}A^{-1}$. This is 1/4 to 1/10 of the total dereddened flux of the LMC at this wavelength [3].

ii) The Lyman continuum flux in the core is 2.5 10^{51} ph s^{-1}. The total flux of the LMC is not known directly but we know that of the SMC [3]; as the LMC contains about 5 times more massive stars than the SMC (see Section 1) its flux of Lyman continuum photons can be estimated as 2 10^{52} ph s^{-1}, 8 times that of the core of 30 Dor.

iii) The core of 30 Dor contains 15 or 16 Wolf-Rayet stars [23], about 1/7 of the total number in the LMC.

30 Dor is the only hypergiant HII region for which we know something directly on the IMF. This IMF turns out to be normal, similar e.g. to that in the field of our Galaxy. There are many very massive stars just because there are a very large number of massive stars! This is discussed in detail in [24] but simple considerations will suffice here. There are about 60 O5 stars or earlier in the core with a mass $M \geqslant 50\ M_\odot$ [25] [26]. If the IMF is $dn(M)/d\log M \propto M^{-1.5}$ up to very high masses this corresponds to a total of 300 O stars (down to 20 $M_\odot$) at least if most of the O stars formed during the burst are still there. That this is the case is shown by the scarcity of evolved stars (there is only one red supergiant in the core). To be fair, one should add to the 50 hottest O stars the 15 or 16 WR which are probably originating from similar high-mass stars, but this would not change much the statistics.

Unfortunately we know very little of the stars with masses somewhat smaller than 20 $M_\odot$, except indirectly through the far-UV flux to which they contribute appreciably. This flux appears to be that of a normal IMF (see earlier) but unfortunately the interstellar extinction is large and the corresponding correction is uncertain. Nothing can be said on still lower-mass stars.

The problem with 30 Dor is thus not in its stellar population which offers nothing exceptional, but in its very existence.

4. Clusters

The Magellanic Clouds are well known for containing compact ("globular") clusters of all ages, including very young ones. They share this property with at least one other galaxy of the Local Group, M33, a system rather similar to the LMC in terms of stellar populations in spite of being a late spiral, and with NGC 55, a galaxy classed as magellanic seen edge-on. Why this is so is not yet understood. Some of these clusters are extremely young, for example NGC 346 which ionizes the HII region N66, the largest in the SMC. The four brightest stars in the core of NGC 346 are O stars and the nearby bright stars Sk 80 (O7 Ia+) and HD 5980 (WN3, eclipsing binary) are probably related [27]. This is a kind of mini-30 Dor. Other clusters in the Magellanic Clouds must contain many O stars. I estimate about 2800 O stars in the LMC and 540 O stars and I guess that a large fraction of those stars (presently under systematic study: see [28]) are in clusters or in very small groups which look like single stars on photographs. R 136 is the most famous example of such a small aggregate now resolved by speckle observations [29] but there are others like R 140 in 30 Dor [23], many binary WR stars that are not necessarily physical binaries, etc. One should be aware of this when studying e.g. the luminosity function since these clusters or aggregates are sources of incompletenesses and biases in the counts. Some small clusters [30] are intermediate between these very compact groups and the normal clusters.

At last point I wish to mention that is relevant to star formation is the age segregation of stars in several clusters in the Magellanic Clouds [31] [32]: the central regions contain younger stars than the periphery, and since the crossing time of the cluster is usually larger than the stellar ages this must reflect conditions at the time of star formation. This is reminiscent of some results in our Galaxy [33].

5. Evolution of star formation in the Magellanic Clouds

As shown a long time ago [34] [35] the UBV colors of a galaxy allow to determined the ratio of the present-day star formation rate (PDSFR) to the integrated star formation rate (SFR) since the birth of the galaxy, provided that the IMF has stayed constant. This property has been extended to any combination of colors by [36] who showed that

$$R = \frac{\text{PDSFR}}{\int_0^{\text{now}} \text{SFR}(t)\,dt} = \begin{array}{ll} 0.10 - 0.14 \ \text{Gyr}^{-1} & \text{for the LMC} \\ 0.045 - 0.11 \ \text{Gyr}^{-1} & \text{for the SMC} \end{array}$$

If the ages of the Magellanic Clouds are 10 - 15 Gyr this is consistent with a uniform past SFR for the LMC and a SFR slightly decreasing with time for the SMC. However this solution is far from unique: any past SFR history giving the same R is consistent with the color observations, and other types of observations are needed. Detailed studies of the field luminosity function and/or (better) of the HR diagram [37] suggest that the bulk of SF in the LMC has started only some 5 Gyr ago, a result which appears to be confirmed by other observations [38] that may however be somewhat controversial: see the discussion after [2]. Also, if the IMF has varied (perhaps because of bimodal SF [39]) this may explain partly the above results. Unfortunately there is no trace of the early massive stars and this hypothesis cannot be checked. A more recent burst of star formation has been advocated by several authors in the LMC e.g. [40], perhaps in relation with an encounter with the SMC that may have occurred 2 10^8 years ago [41], but the evidence appears to me even less convincing. Also, the old (age > 10^9 years) system of globular clusters may have a different kinematics than the younger clusters [42], possibly due to such a gravitational disturbance. However the planetary nebula system, which appears to have a mean age of (2 – 4) 10^9 years, rotates like the young population [43] and the previous result cannot be considered as firmly established.

Another possible approach to the determination of the history of star formation in the Magellanic Clouds is to study the age distribution of star clusters. This has been attempted recently by [44] and [45] for the LMC with roughly consistent results. As in our Galaxy, there are less and less clusters per unit age at old ages. This is clearly the result of cluster disruption, a phenomenon which looks as expected less important in the LMC than in our Galaxy. It is thus impossible to obtain the rate of formation of these clusters as a function of time. What is interesting is that their observed age distribution shows no significant peak within a factor $\sim$ 2 per bin of 0.2 in log (age) [45]. This shows that cluster formation must have been relatively smooth and in particular that no strong burst has occured in the last 10^9 years. Whether this is true for field stars is not clear, and one should not forget that the age scale for clusters is still rather uncertain.

Variations of the star formation in space have been studied by many authors: see discussion and references in [1]. It is clear that the sites of star formation move to large distances in a few 10^7 years, perhaps in agreement with the stochastic star-formation theory [13]. Longer scale variations are also clear at least in the case of the SMC where the carbon stars [46] and the planetary nebulae [47] have a space distribution quite different from the distribution of gas and young stars. This is not unexpected given the disturbed appearance of the SMC.

References

[1] Lequeux, J.: 1984, in Structure and Evolution of the Magellanic Clouds, S. van den Bergh and K.S. de Boer, eds. Reidel, Dordrecht, p. 67.

[2] Lequeux, J.: 1986, in Spectral Evolution of Galaxies, C. Chiosi and A. Renzini, eds. Reidel, Dordrecht, p. 57

[3] Vangioni-Flam, E., Lequeux, J., Maucherat-Joubert, M., Rocca-Volmerange, B.: 1980, Astron. Astrophys. 90, 73

[4] Humphreys, R.M., McElroy, D.B.: 1984, Astrophys. J. 284, 565

[5] Maeder, A., Lequeux, J., Azzopardi, M.: 1980, Astron. Astrophys. 90, L 17

[6] Azzopardi, M., Lequeux, J., Maeder, A.: 1987, Astron. Astrophys. in press

[7] Boulanger, F., Pérault, M.: 1987, Astrophys. J. in press

[8] van den Bergh, S.: 1981, Astron. Astrophys. Suppl. 46, 79

[9] Schmidt-Kaler, Th.: 1977, Astron. Astrophys. 54, 771

[10] Isserstedt, J.: 1984, Astron. Astrophys. 131, 347

[11] Isserstedt, J., Kohl, W.: 1984, Astron. Astrophys. 139, 115

[12] Pierre, M., Viton, M., Sivan, J.P., Courtès, G.: 1986, Astron. Astrophys. 154, 249

[13] Feitzinger, J.V., Glassgold, A.F., Gerola, H., Seiden, P.: 1981, Astron. Astrophys. 98, 371

[14] Martin, N., Prévôt, L., Rebeirot, E., Rousseau, J.: 1976, Astron. Astrophys. 51, 31

[15] Bruhweiler, F.C., Gull, T.R., Kafatos, M., Sofia, S.: 1980, Astrophys. J. Lett. 238, L 27

[16] Dopita, M.A., Mathewson, D.S., Ford, V.L.: 1985, Astrophys. J. 297, 599

[17] Caulet, A., Deharveng, L., Georgelin, Y.M., Georgelin, Y.P.: 1982, Astron. Astrophys. 110, 185

[18] Prévot, L. et al.: 1985, Astron. Astrophys. Suppl. Ser. 62, 23

[19] Maurice, E. et al.: 1987, Astron. Astrophys. Suppl. Ser. 67, 423

[20] Irwin, M.J., Kunkel, W.E., Demers, S.: 1985, Nature 318, 160

[21] Pierre, M.: 1987, Astron. Astrophys. 154, 249

[22] Lequeux, J., Maucherat-Joubert, M., Deharveng, J.M., Kunth, D.: 1981, Astron. Astrophys. 103, 305

[23] Moffat, A.F., Niemela, V.S., Phillips, M.M., Chu, Y-H., Seggewiss, W.: 1987, Astrophys. J. 312, 612

[24] Melnick, J.: 1985, in Star-Forming Dwarf Galaxies and Related Objects, D. Kunth, T.X. Thuan and J. Tran Thanh Van (eds.) Ed. Frontières, Gif sur Yvette, p. 171

[25] Melnick, J.: 1985, Astron. Astrophys. 153, 235

[26] Walborn, N.R.: 1986, in Luminous Stars and Associations in Galaxies, C. de Loore, A. Willis, P. Laskarides (eds.) D. Reidel, Dordrecht, p. 185

[27] Walborn, N.R., Blades, J.C.: 1986, Astrophys. J. Lett. 304, L 17

[28] Conti, P.S., Garmany, C.D., Massey, P.: 1986, Astron. J. 92, 48 and preprint

[29] Weigelt, G., Baier, B.: 1985, Astron. Astrophys. 150, L 18

[30] Lortet, M.C., Testor, G.: 1984, Astron. Astrophys. 139, 330

[31] Meylan, G.: 1982, Astron. Astrophys. 110, 348

[32] Kontizas, E., Kontizas, M., Xiradaki, E., in preparation

[33] Burki, G.: 1980, in Star Clusters, J.E. Hesser (ed.) D. Reidel, Dordrecht, p. 169

[34] Searle, L., Sargent, W.L.W., Bagnuolo, W.G.: 1973, Astrophys. J. 179, 427

[35] Larson, R., Tinsley, B.M.: 1978, Astrophys. J. 219, 46

[36] Rocca-Volmerange, B., Lequeux, J., Maucherat-Joubert, M.: 1981, Astron. Astrophys. 104, 177

[37] Stryker, L.L.: 1984, in Structure and Evolution of the Magellanic Clouds, S. van den Bergh and K.S. de Boer, eds. Reidel, Dordrecht, p. 79

[38] Frogel, J.A., Blanco, V.M.: 1983, Astrophys. J. Lett. 274, L 57

[39] Güsten, R., Mezger, P.G.: 1982, Vistas in Astron. 26, 159

[40] Ardeberg, A.: 1976, Astron. Astrophys. 46, 87

[41] Murai, T., Fujimoto, M.: 1980, Pub. Astron. Soc. Japan 32, 581

[42] Freeman, K.C., Illingworth, G., Oemler, A.: 1983, Astrophys. J. 137, 747

[43] Meatheringham, S.J., Dopita, M.A., Ford, H.C., Webster, B.L.: 1987, preprint

[44] Elson, R.A.W., Fall, S.M.: 1985, Astrophys. J. 299, 211

[45] Chiosi, C., Bertelli, G., Bressan, A.: 1986, Mem. Soc. Astron. Italiana 57, 507

[46] Rebeirot, E., Azzopardi, M., Westerlund, B.: 1987, in preparation

[47] Meyssonnier, N., Azzopardi, M., Lasker, B.: 1987, in preparation

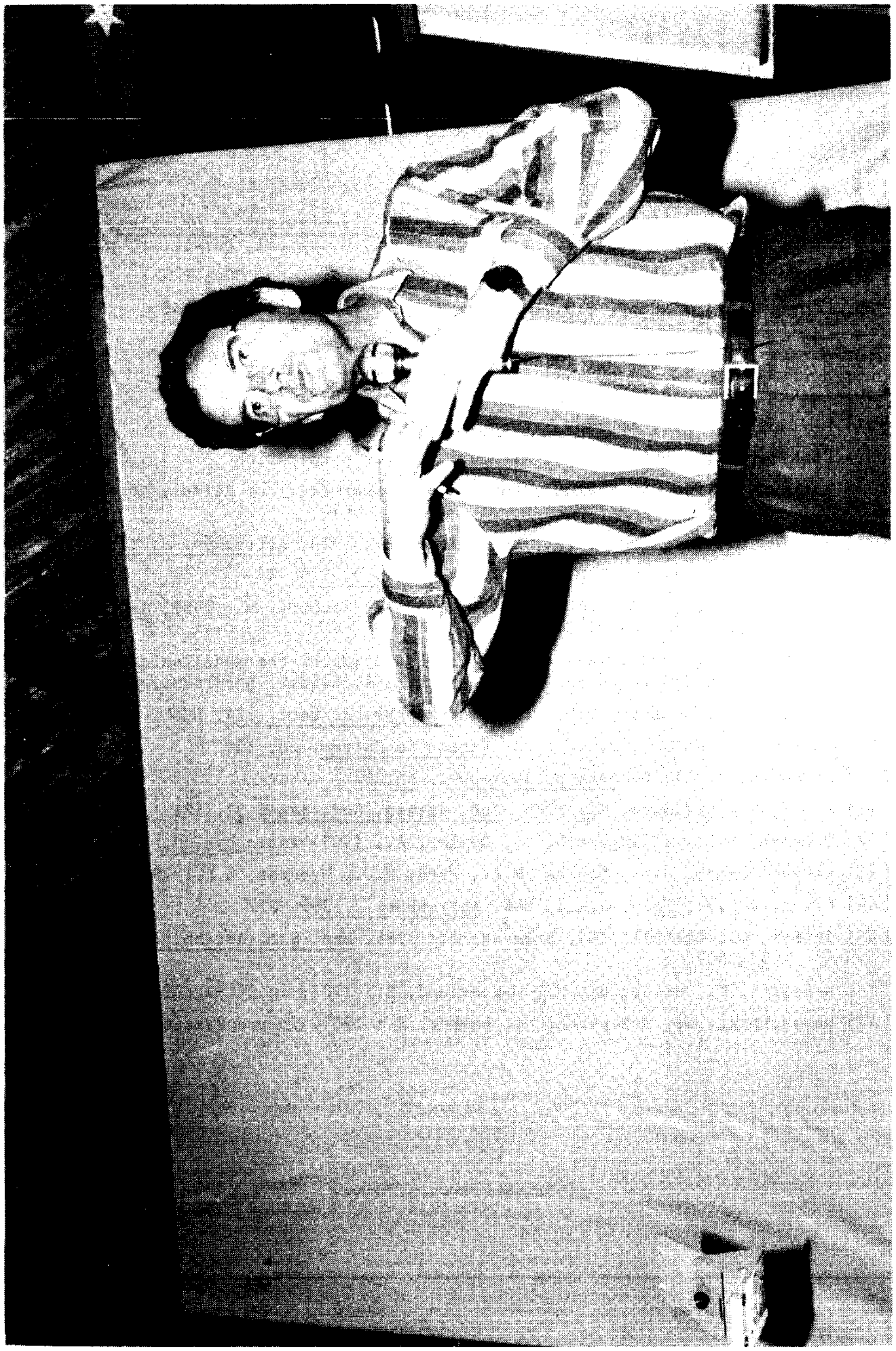

APPENDIX

OBSERVATIONS OF THE SUPERNOVA 1987 A IN THE LARGE MAGELLANIC CLOUD

James LEQUEUX

Observatoire de Marseille
13248 Marseille Cedex 04, France

Observations of the recent supernova 1987 A in the Large Magellanic Cloud up to mid-may 1987 are summarized: light curve and colors, optical, UV and IR spectrum, nature of the progenitor, interstellar lines in the spectrum.
It is shown that this is a somewhat atypical Type II supernova resulting from the explosion of a massive star, but definitive conclusions on the exact nature of its progenitor will have to wait for some time.

1. Introduction

Supernova SN 1987A (the first one discovered in 1987) exploded on February 23 in the Large Magellanic Cloud, one of the satellite galaxies of our own Galaxy, at a distance of 156 000 light-years. This is the first supernova explosion seen with the naked eye since the galactic supernova of 1604 described by Kepler. The brightness of this object and the fact that its distance is rather accurately known (the maximum uncertainty on the distance is of the order of 15%) make its study particularly important. Burst(s) of neutrinos have apparently been observed from this supernova, and this is the birth of neutrino astronomy (although neutrinos are also currently received from the Sun). There is little doubt that the supernova actually exploded in the Large Magellanic Cloud as i) its spectrum shows interstellar absorption lines from gas in our Galaxy and in the Large Magellanic Cloud; ii) the Cloud is sufficiently transparent that if the supernova exploded in a foreground galaxy we would have seen this galaxy on plates taken before the explosion, and iii) the positional coincidence with a star belonging without doubt to the Large Magellanic Cloud in extremely good, as we will see later.

This paper will summarize the observations known to the author by mid-may 1987, 2 1/2 months after the explosion. No attempt is done to provide a bibliography. Much information has been dispatched via the Astronomical Telegrams of the International Astronomical Union. 12 letters to the Editor have been published in Astronomy and Astrophysics vol. 177 (May I, 1987), a few more in Nature but there are also many preprints circulating. Part 2 of the present paper will report on the light curve and evolution in color of the supernova and Part 3 on its spectrum; Part 4 will discuss the problem of the progenitor and Part 5 the interstellar line spectrum. Part 6 will present a discussion about the nature of the object.

2. Light curve and color evolution of SN 1987A

The supernova was discovered on Feb. 24, 1987 independently by I. Shelton in Chile and A. Jones in New Zealand, but actually the first observation was done on 2 short exposures on film by G. Garrad and R. McNaught in Australia on Feb. 23.443 and 23.445 Universal Time. A careful reduction of these films has given a photovisual magnitude $m_{pv} = 6.36 \pm 0.15$. On Feb. 23.62, 4 hours later, the magnitude had increased to 6.11; on Feb. 23.39, 1.3 hour before the first observation, it was fainter than 7 mag. The supernova was not seen on 2 plates taken respectively between Feb. 23.042 and 23.056, and between 23.059 and

23.101. Thus it has exploded between Feb. 23.08 approximately and Feb. 23.443. During this time interval, neutrinos have been reported by the Mont Blanc experiment on Feb. 23.124 and by the Kamiokande and IMB experiments on Feb. 23.316; both may a priori correspond to the explosion, but see later.

The evolution of the luminosity of the supernova has been well followed in the V(visual) band centered on 5500 A by many professional and amator astronomers, resulting in the light curve displayed fig. 1. The best results are accurate to a few hundredths of magnitude. The light has been also followed by the fine-error sensor of the International Ultraviolet Explorer (IUE) satellite, which is more sensitive in the blue (approximately 4500 A). The light curve is slightly different because of the change in color of SN 1987A.

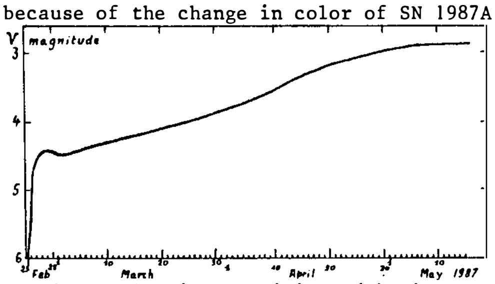

Figure 1: Light curve of SN 1987A in the visible (V) light. This curve has been built on photoelectric measurements and should be accurate to a few hundredth of magnitude.

After a fast rise, the V light curve reached a plateau on Feb. 27-28 at the magnitude V = 4.45 and, after a first broad minimum at V = 4.50 on March 2-3, rised regularly until reaching another plateau at V = 2.90 after May 8. It is likely that this is the maximum light (it was still at the same magnitude on May 15) and that the supernova will decline later. The absolute V magnitude at maximum corrected from interstellar extinction is $M_V = -16.0$, 20.8 mag (2 10^8 times) brighter than the Sun at this wavelength.

The temperature of the emitting layers has also changed during the evolution of the object. The UV emission was very strong at the beginning and was detected down to 1200 angström by the IUE satellite. But emission was already negligible below 1700 A on March 1, 6 days after the explosion. At this date, the energy distribution was not far from that of a 6000 K blackbody, although fainter in the UV, and the effective temperature dropped down to 5200 K on March 11. The total luminosity can be estimated from photometry in a broad range of wavelengths: it increased from 3.2 to 5.5 10^7 solar luminosities between these two dates (1 solar luminosity = 3.8 10^{33} erg s^{-1}); the effective radius (radius of a blackbody with the observed total luminosity and effective temperature) increased from 5600 to 9100 solar radii (1 solar radius = 7 10^{10} cm), due to the expansion of the envelope ejected by the explosion. The further evolution of the energy distribution is more complicated: the UV decrease stopped on March 18 and the object even brightened faster than in the visible after April 26. I have no complete information allowing to calculate recent values for the total radiated energy, but it appears that the maximum in total energy comes later than the maximum in V noted above. Presumably it will reach or pass 10^8 solar luminosities (absolute bolometric magnitude -15.3, emitted energy 4 10^{41} erg s^{-1}).

3. Spectrum of SN 1987 A

The spectrum of SN 1987A, as that of all supernovae, is quite smooth as the lines are very broad. Exceptions are the sharp absorption lines of Na^o, Ca^+ and other elements which are interstellar in origin and will be discussed later. The features in the ultraviolet are time-variable and hard to identify; at some stages the spectrum resembled the UV spectrum of Type-I supernovae (see later for the classification of supernovae). In the visible and the infrared, the spectrum is dominated by the lines of hydrogen (Balmer, Paschen, Brackett and Pfund series), and by a few lines of neutral helium and other elements. These lines have the characteristic so-called P-Cygni profile (from the name of a star where such profiles were discovered): emission near the rest wavelength and blue-shifted absorption. As explained on fig. 2 this profile is characteristic of an expanding envelope with a positive temperature gradient towards the interior.

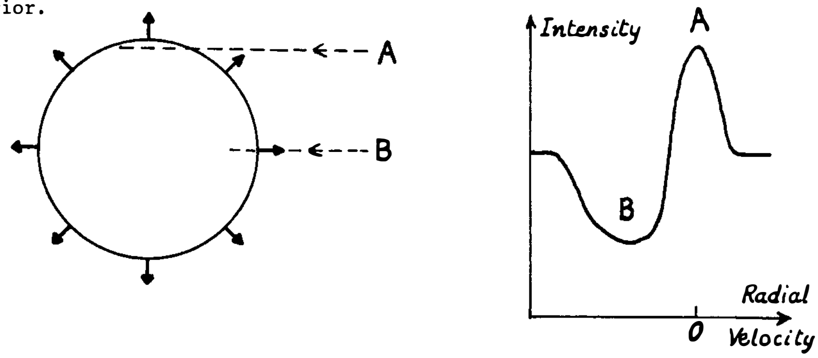

Figure 2: Formation of P-Cygni line profiles in a thick expanding envelope. On the left, a schematic figuration. When looking at the edges (A) one sees material with zero radial velocity which gives an emission line since there is no background emission. The central region (B) gives a blue-shifted line that is seen in absorption over the emission of the hotter background gas of the expanding envelope. The corresponding line profile is indicated on the right. It is seen that the expansion velocity is roughly given by the blue-shift of the absorption dip.

The expansion velocity of the envelope at the depth where the line is formed is roughly given by the blue-shift of the absorption dip (converted into radial velocities). At the beginning, this velocity was as high as 18 000 km s^{-1} for the Hα line, but was smaller for higher lines, 16 000 km s^{-1} for Hβ, 15 500 for Hγ, etc. This only indicates a velocity gradient in the thick expanding material, as we are looking to deeper and deeper levels for higher-energy lines. The dip velocities decreased with time; for example the Hα dip indicated a velocity of 11 000 km s^{-1} on March 10. This is not due to changes in the physical velocities in the atmosphere, but to the fact that we look deeper in the atmosphere while it expands and its optical thickness decreases; in fact, the deceleration is negligible and there might even be an acceleration if energy has been injected after the explosion e.g. through decay of unstable isotopes like ^{56}Ni formed in the explosion.

No X rays or γ rays have been detected, but SN 1987a is a weak radio-source detected first on Feb. 25.4, that reached a maximum 1 or 2 days later then declined. This is not unexpected.

4. The progenitor of SN 1987A

Of course one of the first things done after the discovery of SN 1987a was to look at earlier photographic plates to see what was there before. The surprise was to find a catalogued star named Sk -69°202 right at the position of the supernova (Sk is for the catalogue of Sanduleak, of the Warner and Swasey Observatory). There is only limited material about this star: it is classified as B3I (I for supergiant) and its magnitude and colors are V = 12.24, B - V = 0.04, U - B = -0.65. This is a hot and massive star, with a mass of about 20 solar masses. Is it the progenitor? This is a complicated question that I do not personally consider as completely settled.

Accurate astrometry tells that SN 1987A coincides very well in position with Sk -69°202 within the accuracy of the measurements, a few tenths of an arc second. Figure 3 is a sketch of the immediate surroundings of this star, as revealed by the best previous photographs (see White and Malin, 1987, Nature 327, 36). Star 2 looks similar to the main star (Star 1) but is 2.5 magnitudes fainter. Star 3 is somewhat fainter and redder than star 2. Object 4 is a post-supernova discovery and has not been seen by many authors; it seems to radiate mainly in emission lines and might be a small gaseous nebula.

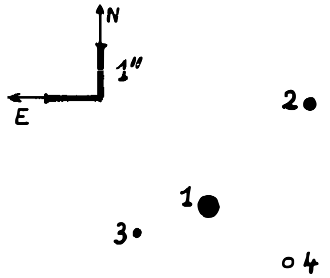

Figure 3: A scheme of the region where SN 1987A exploded. Star 1 is Sk −69°202: the position of the supernova coincides with this star with a high accuracy. This star may itself be double (at least) with 2 components separated by approximately 0."4 NS. Stars 2 and 3 are fainter. Object 4 is apparently visible only in emission lines and is probably not a star, but a small gaseous nebula. The following table recalls the characteristics of the stars.

Star 1:	B3I	V magnitude: 12.24
Star 2:	early B	V magnitude: 15
Star 3:	redder	V magnitude: 16

As said before, the supernova stopped radiating below 1700 A a few days after the explosion. There was something left, low-resolution spectra of which was taken by the IUE satellite: this spectrum shows absorption lines typical of a B3 star, thus it was claimed that Sk −69°202 was still there and is not the progenitor. However a further, more detailed look to what happens in the 5" x 20" entrance aperture of IUE reveals some complication: the source does not appear to be a single star but rather a double object separated by 5" ± 2" in a NW − SE position. This is compatible with those stars being stars 2 and 3 of fig. 3, in which case Sk −69°202 would have disappeared and thus have been the progenitor. Unfortunately the positional accuracy of IUE is not good enough to ascertain the identification directly. If the NW object is an early B star the observed far-UV flux implies that it is fainter than Sk −69°202 by roughly 2 magnitudes in the visible: this is compatible with it being star 2. The other component is twice fainter in the UV and might well be star 3. However −69°202 might be peculiar in the far-UV and be one of the two UV objects.

Another element in the puzzle is the observation from high-quality pre-supernova images that Sk −69°202 might not be a single star itself! The corresponding image is elongated NS, contrary to other images in the field, and suggests that Sk −69°202 is a double star with 2 components separated by roughly 0."4. It may well be that one of these components is the progenitor and that the other is still there: this might explain the faintness of the object seen in the far-UV (if it can be identified with the SE object seen by IUE). If this is true it is very hard to say something about the progenitor as we do not know the individual properties of the two components of Sk −69°202. Thus we cannot yet conclude about the progenitor. There is a good chance that it is a blue massive star, but this might be one of the components of Sk −69°202 (if double) and thus its mass can be somewhat smaller than 20 solar masses and it may not be a normal B3 supergiant. We can however assess that it cannot be a Wolf-Rayet star, i.e. a massive star deprived from its envelope at the end of evolution: these stars have well-recognizeable spectral features that would have been seen in existing objective-prism spectra of the region taken before the explosion.

5. Interstellar lines in the spectrum of SN 1987A

Spectra of SN 1987 show a number of narrow, complex lines formed in the interstellar matter between the object and us: lines from Na^o, Ca^+, K^o in the visible and many elements and ions ranging from Mg^o or C^o to Si^{+++} or C^{+++} in the far-UV; spectra are published in Astronomy and Astrophysics 177, L17 and L37. There are also interstellar diffuse bands. They are similar to what has been observed previously in a number of stars of the Large Magellanic Cloud and have nothing to do with SN 1987A itself, but their observations are of much higher quality as the supernova was so much brighter than the other stars. The lines are produced either in the galactic disk with heliocentric radial velocities 0 to 30 km s^{-1}, or in the Large Magellanic Cloud with velocities 200 to 300 km s^{-1}. Intermediate-velocity components also exist and are generally attributed to gas clouds in the galactic halo.

6. Discussion: the nature of SN 1987A

Supernovae are classified according to their light curves and spectra into two main groups. SNI have well-defined light curves and no hydrogen lines in their spectra; they are supposed to originate in carbon-deflagration of carbon-oxygen white dwarfs, thus in low-mass stars. SNII have a variety of light curves and show hydrogen lines in their spectra. They result from the explosion of massive stars following the collapse of their iron core (for a up-to-date detailed discussion of supernovae in general, see the excellent review by S.E. Woosley in NucleoSynthesis and Chemical Evolution, 16th Advanced Course Saas Fee 1986, sold by Geneva Observatory, CH 1290 Sauverny).

This classification gives an oversimplified view of the reality. Each class is very diverse and encompasses a variety of light curves: actually Zwicky distinguished many more classes. In particular the so-called subtype Ib (sometimes called Type III) corresponds to the explosion of massive stars stripped of their envelopes (e.g. Wolf-Rayet stars). It must be realized that what we see is only the radiation of the external parts of the outer regions of the star ejected by the explosion and that the total amount of visible energy (kinetic and thermal) is only a small fraction of the energy liberated in the supernova phenomenon. For example, the collapse of a massive star produces some 2 10^{53} ergs of gravitational energy which is ultimately converted in neutrinos, and only

10^{51} ergs of kinetic, thermal and radiated energy. No surprise that the light-curve depends much of the properties of the external layers of the star, and of whether it has or not an extended envelope. The larger the envelope, the more energy is converted into radiation and the longer the time scales for light variations. It has become recently possible to predict the evolution of a supernova in some detail: see the cited review by Woosley, and Shaeffer et al. (1987: Astrophysical J. Letters 316, L31).

What can we say on SN 1987A? It shows hydrogen lines in its spectrum and must be Type II or related, in any case a massive object. The fact that its UV spectrum resembled a Type I spectrum at some stages does not seem to be very significant. The neutrino emission also points to a massive object unambiguously, and the Kamiokande - IMB burst has roughly the expected intensity for formation of a neutron star during collapse (Schaeffer et al., 1987, Nature, to be published). It seems even possible to account for observations of two neutrino bursts separated by 4 1/2 hours (the Mont Blanc one and the Kamiokande/IMB one) if the first corresponds to the formation of a neutron star which further collapses as a black hole: this requires an object with a mass $\geq$ 20 solar masses, marginally compatible with the explosion of Sk -69°202 (Hillebrandt et al., 1987 Nature, to be published).

Whatever the details, it is clear that SN 1987A is Type II, and that its progenitor was a massive star of mass $\gtrsim 20\ M_{\odot}$ or somewhat less. The classical progenitor of a Type II supernova is a redsupergiant. This cannot be the case here since this progenitor would have been seen and would moreover have produced a brighter supernova because of more efficient energy conversion in an extended envelope. SN 1987A cannot originate from a totally stripped star like a Wolf-Rayet star although what is observed of its light curve and its relative faintness recall of Type Ib (also called Type III) supernovae which are believed to originate from Wolf-Rayet stars: the lines typical of Wolf-Rayet stars would have been observed. However the progenitor might have been a partially stripped star; the relatively faint magnitude, the plateau a few days after the explosion and the fast initial decrease of photospheric temperature suggest an initial radius $\lesssim 10^{12}$ cm (for comparison, a B3I star has a radius of about $1.8\ 10^{12}$ cm and a Wolf-Rayet star $\gtrsim 1.4\ 10^{11}$ cm): Schaeffer et al., 1987, Nature, to be published. However it is not excluded that the progenitor was a B3I star provided the density structure in the expanding material is given by homologous expansion of the stellar structure (Hillebrandt et al., 1987, Nature, to be published).

Only future observations will tell us more about the progenitor, in particular its degree of stripping. Whatever the result, it is somewhat surprising to find a star with mass $\gtrsim$ 20 solar masses exploding in a stage different from the red supergiant one. Conventional stellar evolution calculations predicts that a star of this mass will become a red supergiant prior to the ignition of core carbon burning which triggers the supernova phenomenon. However if the star is a member of a close binary system it may never reach this stage since its growth towards the red supergiant stage will be limited by capture of the expanding matter by its companion. Recent model calculations of single stars with low heavy-element abundances also find that single stars with masses in the range 15 to 25 solar masses and reduced heavy-element abundances as are stars in the Large Magellanic Cloud can explode as blue supergiants (Hillebrandt et al., 1987, op. cit.).

This conclusion is critically dependent on the treatment of convection in the star.

BURSTS OF STAR FORMATION IN THE MAGELLANIC CLOUDS

M.-C. Lortet, G. Testor
Département d'Astrophysique Extragalactique et de Cosmologie
Observatoire de Paris, Section de Meudon
92195 Meudon Principal Cedex, FRANCE

ABSTRACT

By the comparative study of adjacent stellar associations in the Magellanic Clouds, we were able to follow the spatial and temporal developments of starbursts at the scales of 10 Myr and 500 pc. Most of the known S Dor type stars of the Magellanic Clouds were thus found to have a relatively old environment. We propose to revisit the current ideas on age and evolutionary status of S Dor stars (Hubble-Sandage Variables) and different subtypes of WR stars.

We will summarize here a few results obtained from the study of regions of recent or current star formation, at space and time scales smaller than considered by Lequeux[6]. Few studies up to now have been devoted to the comparison of the physical data pertaining to adjacent star forming regions. Hänel[4] outlined such a study for the complex nebula N 11 in the LMC, from kinematical data ; Dopita[3] discussed the supergiant H II shell Shapley III, where star formation began in the center 15 Myr ago and propagated outward. We studied several cases where star formation propagates more or less linearly[10] as coarsely described by Westerlund[23]. In Sect.1, we recall one of these cases. Consequences on the current ideas about the nature of S Dor type stars are developed in Sect.2 and illustrated by the region Shapley II. The nomenclature used throughout this paper for objects is explained in 7) and 8).

1. TYPICAL CASES OF SEQUENTIAL FORMATION

A clear instance of sequential star formation is provided by the group of stars and nebulae dominated by the nebulae N 83–84, in the Inner Wing of the SMC (see Lortet and Testor[10] and their Fig.2a). Table 1 summarizes a few properties of the different objects, ordered by age. Spatially this sequence extends from SW to NE over a distance of about 500 pc. The analysis of this region of the SMC is made easy and safe because in this direction, this galaxy is made of only one sheet of gas, instead of two or more in the north or in the Bar[12] : thus areas close on the sky are indeed close in space. The oldest objects (cepheids which period is a good age–indicator, red supergiants and the X–ray source SMC X–1) are related to a faint extended filamentary shell DEMS 157 while bright compact H II regions (e.g. N 83A1) host non evolved O stars[19].

On this instance, we see that the contrast in ages of the stellar population is reflected in the properties of the nebulae : faint extended shells/or absence of nebulosity are often associated with evolved stars (as in many instances in the LMC) while compact H II are the place where to look for hotter (unevolved) stars. This remark is important, as it may guide deeper studies of the massive star content of the Magellanic Clouds and of more distant galaxies, where individual stars of moderate luminosity ($M_V \sim -5$) cannot be resolved.

2. THE RANGE IN AGES OF THE S DOR AND WR STARS REVISITED

The WR population is sometimes schematized by statistical properties, for instance that they are relatively young stars (3–6 Myr) with a progenitor of mass larger than 40$\mathcal{M}_\odot$[1),11]. In fact, Schild and Maeder's study for galactic stars[16] and examination of the LMC stellar associations show that some subtypes of WR stars are associated with stars as young as O3–4 stars (in Car OB1) while other ones (for

Table 1 : Sequential star formation in the K1 region in the SMC
(data excerpted from Lortet and Testor, 1987)

Stellar Data		Nebular Data		Age
Star or star cluster	Spectral Type (hottest star)			Myr
Two cepheids P ~ 25d		DEMS 157	faint shell 500pc in diameter centered near SMC X-1	15
SMC X-1	B0 I			
Red supergiants				7–15
NGC 465	O9 I	N 85	very faint	6–7
NGC 460b	[O8–9 V]	N 84B1	[OIII]/Hβ ~ 2	4–5
NGC 456 (part)	[O8–9 V]	N 83C1	[OIII]/Hβ ~ 2	4–5
NGC 456	O6.5–7 V	N 83A1	[OIII]/Hβ ~ 6	2–3
NGC 460a	[O5–7 V]	N 84A1	[OIII]/Hβ ~ 7	2–3

instance early WN) are found in clusters whose hottest stars are of spectral type B1 or even B2. Recently, Schild[15] found the WN9–10 star Brey 18 (= R 84) in the LMC to be 8 or more Myr old. Thus the span in age of WR stars extends up to 8 Myr at least, from the youngest ones (WN 6–7 stars of 30 Dor and Car OB1) to broad lines early WN and WN9–10 stars like Brey 18.

On the other hand, the S Dor type stars, because they are thought to be exceptionally luminous, have been considered so far to be very young, and evolved from massive progenitors who never go through the red supergiant phase[1,11]. However, their high luminosity and mass (and even chaotic light-variability) are now questioned by discoveries such as the binarity of R 81 = Sk −68 63[18], of total present mass about 35 $M_\odot$. Moreover, our studies show that all of them are associated with an older environment than was believed, namely B supergiants, the oldest among WR stars and even, in several cases, red supergiants. This is illustrated in Fig. 1 which shows the distribution of S Dor type stars compared with those of WR stars and red supergiants, for the region of the LMC known as the constellation Shapley II. This is a homogeneous region, poor in gas and dust[6,14], rich in red supergiants of similar spatial velocities[13]. In strong contrast to the star forming region 30 Dor located just to the east[(1)], Shapley II contains few bright nebulae, no WN6–7 stars, and only one WC star located in its youngest part, the nebula N 144. Fig. 1 shows eight S Dor type stars, most of them members of tight clusters.

(1) Notice that SN 1987A is sitting just at the edge of this last one ; the stellar content of the nearby superbubble N 157C has been analysed by Lortet and Testor and its five WR stars are not shown in Fig. 1a.

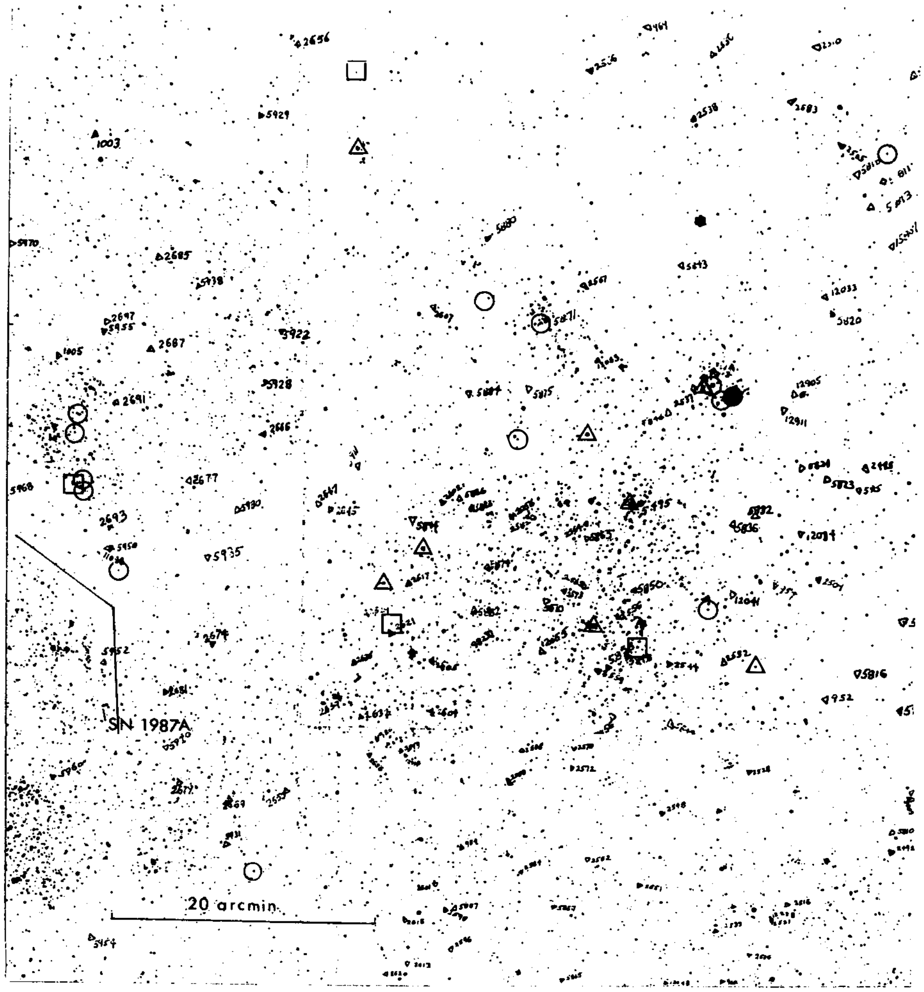

Fig.1 : The "constellation" Shapley II in LMC. The field extends to the NW up to the nebulae N 144 and N 138, to the east up to the stellar associations LH 90, center of the superbubble N 157C, and LH 85+89.

a) Mosaic of Hodge and Wright's B charts. The Wolf–Rayet stars are indicated by circles (early WN), squares (WN8–10), filled circle (WC, one in N 144). The S Dor type stars are indicated by triangles : almost all are members of a cluster (e.g. SL 530 and 552, NGC 1983 and 1994...). The Wolf–Rayet population in N 157C is not indicated (insert). SN 1987A is shown south of N 157C.

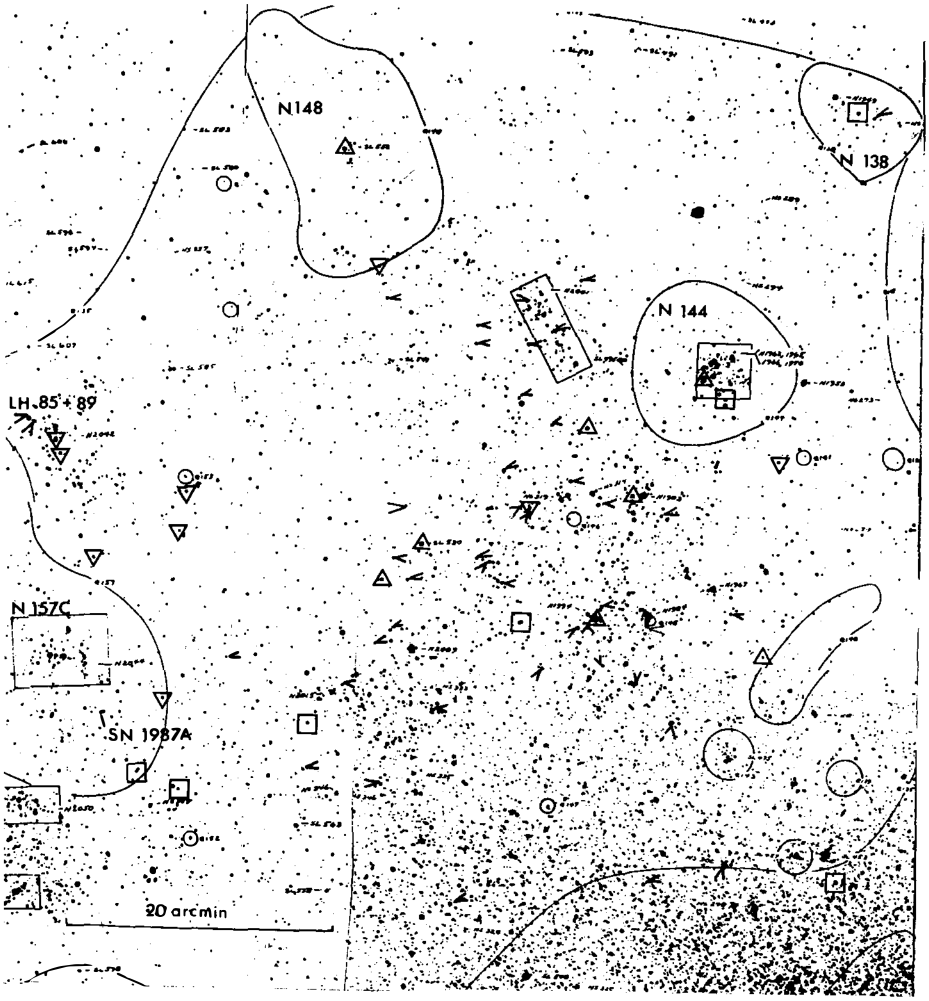

Fig.1b : Mosaic of Hodge and Wright's V charts. S Dor type stars and red supergiants (only those with measured radial velocities). The S Dor type stars are shown as in Fig.1a (upwards triangles). The sign > indicates red supergiants with the range of velocities 267 < V_{hel} < 285 km s^{-1}, typical of Shapley II. More receding velocities are indicated by a triangle downwards, more approaching ones by a square. The curved lines define Henize nebulae. The circles are small nebulae, not stars.

The star Brey 18, quoted in Sect.1, stands as a summary of all the points made above. This star, classified as a S Dor variable of Of-like type[17], has a spectrum OIafpe or WN9–10[22] and a M companion[2], belongs to a stellar association 8 Myr or more old[15], itself surrounded by the filamentary shell DEML 110. Moreover its M companion is dominant in V light, which means that its bolometric luminosity would be surestimated by at least 1.5 – 2 magnitudes if the companion is ignored or were undetected.

3. CONCLUSION

The approach of looking for a sequence of ages in adjacent regions of star formation is promising. The finding of an older environment than believed for S Dor type stars is of utmost importance. The idea that at least a fraction of them is a later evolutionary step following the red supergiant stage cannot be rejected, as other recent data have also questioned their variability, high mass and high luminosity. The question of their multiplicity is a basic one, indeed already raised by Walborn[21] for the candles of the Magellanic Clouds[5] and is now topical for the progenitor of the Supernova in LMC[20].

REFERENCES

1) Chiosi, C., Maeder, A. : 1986, Ann. Rev. Astron. Astrophys. 24, 329.
2) Cowley, A.P., Hutchings, J.B. : 1978, P.A.S.P. 90, 636.
3) Dopita, M.A. : 1986, IAU Symp. 115, 501.
4) Hanel, A. : 1984, IAU Symp. 108, 391.
5) Humphreys, R.M. : 1983, Ap. J. 269, 335.
6) Lequeux, J. : 1987, these Proceedings.
7) Lortet, M.-C. : 1986, Astron. Astrophys. Suppl. 64, 303.
8) Lortet, M.-C., Spite, F. : 1986, Astron. Astrophys. Suppl. 64, 329.
9) Lortet, M.-C., Testor, G. : 1984, Astron. Astrophys. 139, 330.
10) Lortet, M.-C., Testor, G. : 1987, Astron. Astrophys., submitted.
11) Maeder, A., Meynet, G. : 1987, Astron. Astrophys., in press.
12) Mathewson, D.S., Ford, V.L., Dopita, A., Tuohy, I.R., Long, K.S., Helfand, D.J. : 1983, Ap.J. Suppl. 51, 345, Fig. 20.
13) Prévot, L., Andersen, J., Ardeberg, A., Benz, W., Imbert, M., Lindgren, H., Martin, N., Maurice, E., Mayor, M., Nordström, B., Rebeirot, E., Rousseau, J. : 1985, Astron. Astrophys. Suppl. 62, 23.
14) Schwering, P. : 1987, these Proceedings.
15) Schild, H. : 1987, Astron. Astrophys. 173, 405.
16) Schild, H., Maeder, A. : 1984, Astron. Astrophys. 136, 237.
17) Stahl, O., Wolf, B., de Groot, M.J.H., Leitherer, C. : 1985, Astron. Astrophys. Suppl. 61, 237.
18) Stahl, O., Wolf, B., Zickgraf, F.-J. : 1987, ESO Preprint No. 488.
19) Testor, G., Lortet, M.-C. : 1987, Astron. Astrophys. 178, 25.
20) Testor, G., Lortet, M.-C. : 1987, IAU Circ. No. 4352 and in preparation.
21) Walborn, N. : 1977, Ap.J. 215, 53.
22) Walborn, N. : 1982, Ap.J. 256, 452.
23) Westerlund, B. : 1985, in "Birth and Evolution of Massive Stars and Stellar groups, Ed. H. Boland and H. van Woerden, p. 259.

INFRARED PROPERTIES OF THE MAGELLANIC CLOUDS

P.B.W. Schwering
Sterrewacht Leiden, Huygens Laboratorium
Postbus 9513
NL-2300 RA Leiden
The Netherlands

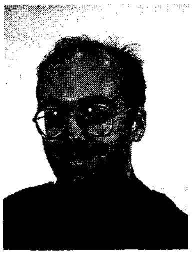

Abstract: Integrated infrared maps of the Magellanic Clouds are shown. The far-infrared spectra of the Magellanic Clouds are very similar and resemble the NGC 4449 spectrum. They show an average dust temperature of 35K. There is less 12 µm 'excess' emission from the Clouds than from M31. The 60 µm luminosity of the LMC equals that of M31. The dust temperature map resembles the infrared map of the Clouds, but there is an anti-correlation between 12/25 µm and 60/100 µm showing that the 12 µm 'excess' is due to the infrared cirrus component. At a resolution of 15' there is a reasonably good correspondence between the dust and HI gas distributions, that breaks down at high intensity levels.

1. Introduction

The Magellanic Clouds are close enough to be used for a detailed comparison with our Milky Way galaxy. On the other hand they are far enough away to obtain integrated properties which can be compared to those of other galaxies. They are dwarf irregular galaxies, having low dust-to-gas ratios, low metal abundances, high atomic gas content and a relatively high present-day star formation rate. The IRAS satellite has obtained various pointed 'Additional Observations' (AOs) on the Clouds in the infrared at 12, 25, 60 and 100 μm (see Israel and Schwering, 1986).

2. Far-infrared images of the Magellanic Clouds

Maps at 12, 25, 60 and 100 μm of the SMC based on IRAS AO data are shown in Schwering and Israel (1987), and of the LMC in Schwering (1987). The infrared data presented in those papers have a resolution of roughly 1' in-scan by 7' cross-scan, in two independent and orthogonal scan-directions. Figure 1 shows the LMC total far-infrared emission (1-500 μm) obtained from extrapolating the 60 and 100 μm emission over the whole infrared range using the 60/100 μm ratio as a line-of-sight dust temperature and assuming a λ^{-1} emissivity law, convolved to 8' resolution. This Figure closely resembles the optical picture of the LMC. The greater Doradus region produces about 50% of the total infrared radiation of the LMC. Other prominent HII-region complexes visible on the map are N11, N44 and N79. The LMC-Bar and Shapley's Constellation III are also clearly visible. The integrated infrared luminosity of the LMC is $L_{IR} = 7 \times 10^8 L_\odot$.

Figure 2 shows the total far-infrared emission map of the SMC obtained in the same manner at the same scale and resolution. The grayscales cut-off at the same intensity value, showing that the SMC is a much weaker (~0.1 x) infrared emitter than the LMC. Note the HII-regions that show up prominently in the infrared: N66, N76 in the NE part of the Bar; N81, N83/84, N88 in the SMC-Wing. The bright emission peak in the SW-Bar is probably a result of a long line-of-sight through the SMC at that position (Mathewson et al., 1986). The SMC is surrounded by low level extended emission. The integrated infrared luminosity of the SMC is $L_{IR} = 7 \times 10^7 L_\odot$.

3. The far-infrared spectrum

The far-infrared spectra of the Clouds are presented in Figure 3. The spectrum of M31 (Walterbos and Schwering, 1986) has been scaled to the distance of the LMC (53 kpc; Humphreys, 1984). In the spectra we note several things. First of all, as already noted, the SMC is a factor of ten weaker than the LMC. The shape of the SMC spectrum is very similar to that of the LMC.

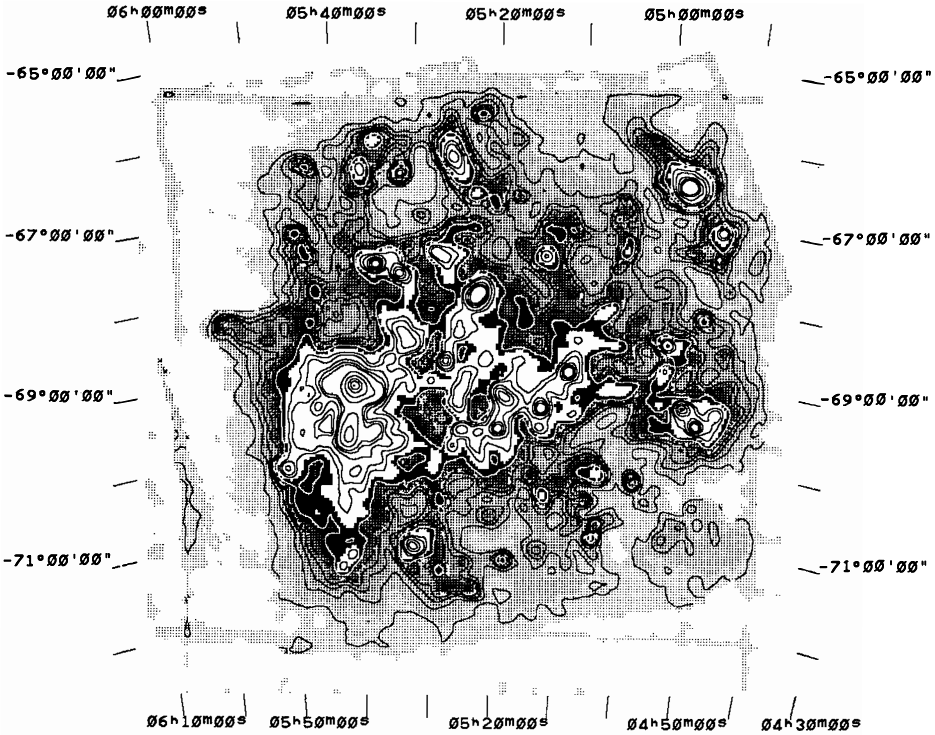

Figure 1: Integrated infrared map of the LMC. Darker grayvalues indicate higher intensity levels but are cut off at the peak.

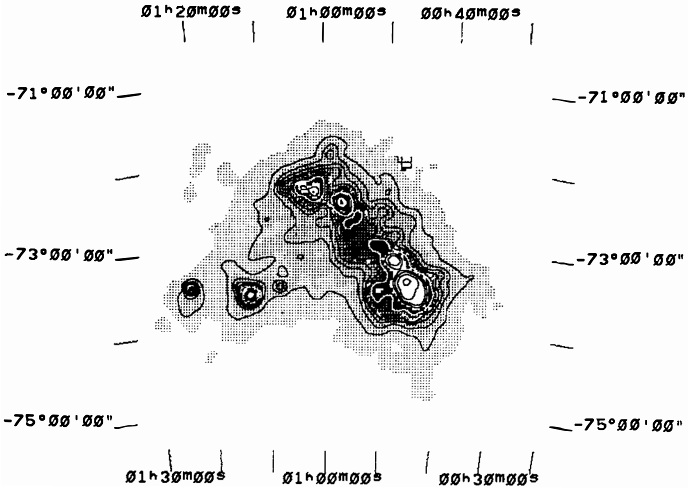

Figure 2: Integrated infrared map of the SMC, at the same scale and resolution as figure 1.

These two spectra are, however, very different from that of M31, but very much like that of the active giant irregular galaxy NGC 4449 (Hunter et al., 1986). Compared to M31 the ratio 60/100 μm is higher (resulting in a 10K higher average dust temperature for the Clouds: T_d~35K), and the 12/25 μm ratio is lower (showing less 12 μm excess). In the Galaxy and in M31 this 12 μm excess is (at least partly) ascribed to small grains (Cox et al., 1986; Walterbos and Schwering, 1986). This would mean that there is a relatively small contribution by such grains in the Magellanic Clouds compared to in the Andromeda galaxy. It is interesting to note that the LMC has the same 60 μm luminosity as the much larger spiral galaxy M31. The value of infrared 'excess' L_{IR}/L_B in the LMC is about three times higher than in the SMC and twelve times higher than in M31 (see Caspers, 1987).

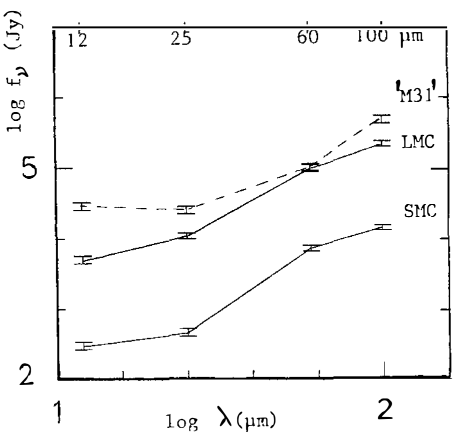

Figure 3. Infrared spectra of the Magellanic Clouds, and M31 scaled to the distance of the LMC.

4. The relation between 12/25 μm and 60/100 μm

Helou (1986) studied the relation between the 12/25 μm and the 60/100 μm ratio of integrated IRAS flux densities of galaxies. The two ratios are in anti-correlation: Galaxies with a high 60/100 μm dust temperature show a low 12/25 μm colour temperature and vice-versa. Anti-correlation in the same way was noted in the ring of M31 by Walterbos and Schwering (1986).

In the Magellanic Clouds the dust temperature is closely related to the infrared emission itself, high dust temperatures coincide with high infrared surface brightness HII-regions (30 Doradus and N11 in the LMC; N66, N76, N81, N83 and N88 in the SMC: T_d=40-50K). The temperature in the bars is enhanced (~35K) compared to the temperature of the diffuse emission (~25K). The 12/25 μm ratio anti-correlates with infrared and dust temperature: High ratios occur in low temperature, low infrared surface brightness regions.

Figure 4 shows the 12/25 μm versus 60/100 μm relation in a colour-colour diagram similar to that of Helou (1986). Here we plotted pixel-value ratios in the infrared maps (with a cut-off at 0.25 MJy/sr). In the SMC there are no low dust temperature areas with strong enough 12 and 25 μm emission resulting in a lack of points in the lower right area of the diagram. The LMC shows the same relation as found by Helou. At the lower right side the LMC-figure contains some horizontal scatter due to the weakness of the 25 μm emission relative to 12 μm at certain positions. The correlation bends down to the Cirrus point (Solar neighbourhood radiation field, marked by X_C).

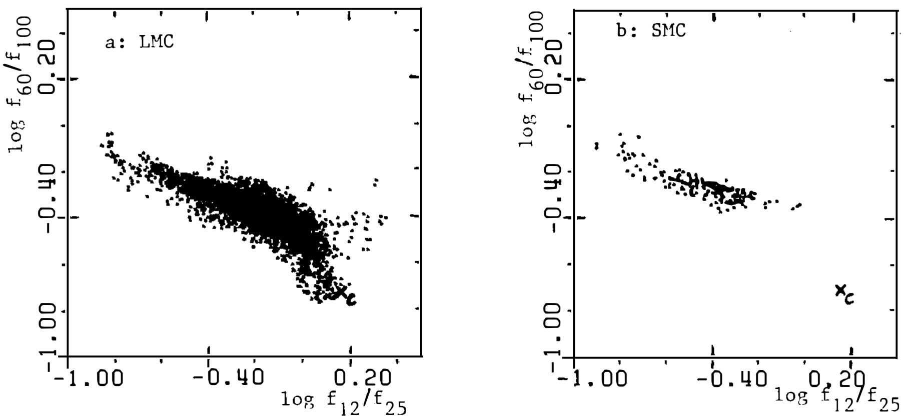

Figure 4: Colour-colour diagram showing the relation between the 12/25 μm and 60/100 μm ratio in the Magellanic Clouds.

5. The relation between dust and neutral hydrogen

From the infrared data and the calculated line-of-sight dust temperatures we have estimated the dust column density. This is an underestimate of the true dust column density because the IRAS satellite is not sensitive to dust colder than about 20K. The maps, with 15' resolution, are shown in Figure 5. The dust column density map is shown as contours, while gray-scales represent integrated HI maps (Rohlfs et al., 1984; McGee and Newton, 1982). In the LMC we see dust concentrations in the 30 Doradus complex. On the whole there exists a reasonable agreement between HI and dust, but there is a 'dust excess' in the HII-regions.

The SMC also shows a good correlation between dust and HI. Dust concentrations occur in the SW Bar (long line-of-sight) and in N83/84, but not in N66. For this HII-region the infrared appears to come from a hot source with a low dust content. The other HII-regions show a mixture of higher dust content and high temperatures.

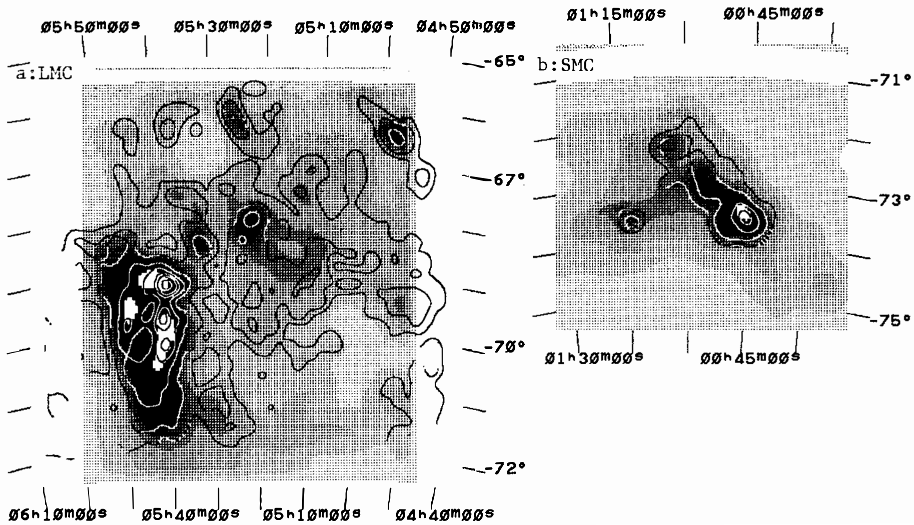

Figure 5: Dust column density contours shown on the integrated HI grayvalues. Higher grayvalues indicate higher column densities. The HI peaks in the 30 Doradus region in the LMC and the SW-Bar in the SMC.

References

Caspers H.C.M.: 1987, these proceedings

Cox P., Krügel E., Mezger P.G.: 1986, Astron. Astrophys. **155**, 380

Helou, G.: 1986, Astrophys J. (Lettres) **311**, L33

Humphreys R.M.: 1984, in 'Structure and Evolution of the Magellanic Clouds', ed. S. van den Bergh, K.S. de Boer, Reidel Dordrecht, 145

Hunter D.A., Gillett F.C., Gallagher III J.S., Rice W.L., Low F.J.: 1986, Astrophys. J. **303**, 171

Israel F.P., Schwering P.B.W.: 1986, in 'Light on Dark Matter', ed. F.P. Israel, Reidel Dordrecht, 383

Mathewson D.S., Ford V.L., Visvanathan N.: 1986, Astrophys. J. **301**, 664

McGee R.X., Newton L.M.: 1982, Proc. Astron. Soc. Australia **4**, 308

Rohlfs K., Kreitchmann J., Siegman B.C., Feitzinger J.V.: 1984, Astron. Astrophys. **137**, 343

Schwering P.B.W., Israel F.P.: 1987, submitted to Astron. Astrophys. Suppl.

Schwering P.B.W.: 1987, in preparation.

Walterbos R.A.M., Schwering P.B.W.: 1986, submitted to Astron. Astrophys.

LUMINOUS STARS IN M31

Peter S. CONTI
Department of Astrophysical, Planetary, and
Atmospheric Sciences, University of Colorado
and
Joint Institute for Laboratory Astrophysics
University of Colorado and National Bureau of Standards
Boulder, Colorado 80309-0440 USA

CCD photometry of several associations in M31 is presented. One may derive the sizes, determine the reddening, identify the youngest stars and discuss the luminosity functions from data such as these. A brief overview of the luminous stellar population in the Magellanic Clouds is also given.

The spiral galaxy M31 represents the closest example of an SB type in which individual stars may be studied. The large angular extent, the unfavorable inclination of the disk to the line of sight, the stellar image crowding, and the variable internal reddening all combine to make stellar studies difficult although not intractable. The recent advent of CCD devices, with their high quantum efficiency and linear detection capability, have now given us the means to investigate the luminous hot star population of this galaxy, and others in the Local Group. For M31 the large size on the plane of the sky restricts present work to only samples of relatively small regions of this galaxy; with larger CCDs now coming into general use, this problem may be somewhat eased. Crowding of stellar images is an important problem for luminous stars as they are mostly found in associations; it is largely solved by using Stetson's crowded-field, point-spread-function fitting program DAOPHOT. It is absolutely critical to be able to resolve close stellar images into their individual components in any population study such as described here.

The work I will depict in this talk is based mostly upon a paper published with my colleagues Phil Massey and Taft Armandroff in which the quantitative data are laid out in more detail (Massey et al 1986 - MAC). I also wish to speak a little near the end of the talk on the current status of studies of the IMF of the massive stars in the Magellanic Clouds and will draw upon the recent work with Phil and with Katy Garmany (Conti et al 1986; Garmany et al 1987). These papers may be consulted for additional information. Here I would like to appraise the essentials of these ongoing population studies of the most massive stars in environments different from the solar vicinity.

We obtained CCD frames, 4 arc minute on a side, of eight regions of M31 containing OB associations (van den Berg 1964). Our choices were selected on the basis of their appearance on the Hodge (1981) atlas as having numerous luminous blue stars present, and the presence of appreciable H-alpha emission as shown by the area survey of Pellet et al (1978). Since we are primarily interested in the O and Wolf-Rayet (W-R) star population, those OB associations with substantial H-alpha are most likely to contain these stars. One of the main objectives was to obtain narrow filter images which isolate the W-R stars (following Armandroff and Massey 1985) and candidates were found in many of the associations in these eight regions.

The main thrust of my talk today will deal with the OB population for which UBV frames of four of these regions were obtained. These were centered on OB associations 8,9, and 10; 48; 78 (NGC206); and 102, respectively. OB8, 9 and 10 are found well inward of the main spiral arms of M31 to the NE of the galactic center; OB48 is somewhat further out in this direction; OB78 is in the opposite

(SW) direction from the center of M31 but well within the main spiral arm structure; finally, OB102 is in the far NE quadrant, well beyond the location of the main stellar population of M31.

The imaging data were obtained at the prime focus of the 4-m telescope at Kitt Peak with an 800×800 Texas Instruments chip. The details of the observational program, and the normal reduction procedure can be found in MAC. For these OB associations we have been able to: (a) ascertain their sizes from their hot luminous star membership; (b) determine the differential reddening among the associations; (c) identify the youngest population, those stars with ages less than 10^7 years of age; (d) consider the luminosity function of these most massive stars. I shall take up each of these findings in turn.

The initial identification of the OB associations and their boundaries was given by van den Berg (1964) using eye estimation of the blue star population outlines on ultraviolet Schmidt plates taken at the Tautenberg Observatory. Many were found to be 300 to 500 pc in size, somewhat larger than those identified in our Galactic system, or in the LMC. Hodge (1986) has recently considered selection effects in determining association sizes. In an interesting experiment, he finds that use of a similar plate scale, color, and limiting absolute magnitude led him to determining essentially identical sizes for sample associations in the LMC and M31. Hodge thus suggested that the apparently larger sizes found by van den Berg in M31 might not be real and he cautioned against selection effects in this regard.

In our work on M31 we are able to isolate the OB population by UBV photometry. When these stars are identified in the associations, their distribution is invariably concentrated towards the centers of the boundaries outlined by van den Berg (1964). We confirm that the associations in this galaxy, as outlined by their OB stars, have sizes similar to those found elsewhere, the largest being typically 100 to 200 pc. Of course, as Hodge (1986) and others have pointed out, there are relatively fewer associations in this SB galaxy, given its total luminosity, compared to SC and Irregular types.

The observed color magnitude diagram for OB 48 is given in Fig. 1. As one can realize by inspection, the number of stars increases with fainter apparent magnitude down to about 21.5, where they diminish; thus we are reasonably complete in counts to about this luminosity limit. An important initial question concerns the number of Galactic stars in this diagram (since we are concerned only with the OB population we cut off the B-V color at +1.0). Foreground galactic stars will hardly contribute to this figure: with a galactic latitude of -21° for M31, the line of sight passes through 1 kpc of our Galactic disc for an assumed disk half-thickness of 350 pc. A galactic main sequence A star would therefore be brighter than V = 10; a G star brighter than 15. The predicted Galactic star counts of Ratnatunga and Bahcall (1985) suggest a foreground contamination of one or two stars per CCD frame. Further down the main sequence the K and M dwarfs would start to appear in somewhat larger numbers but they are not in the abscissa range of our plots and are not important for our discussions.

Although all the stars with photometry in OB48 are plotted in Fig. 1, we found it useful to initially discard those in which the internal statistical uncertainty in either U, B, or V was larger than 0.1 magnitudes. This had the effect of eliminating most of the faintest stars but gave better accuracy in what follows. In Fig. 2 I show the color-color plot for OB48. It is quite obvious that the association is reddened, and the extrinsic uncertainty in the photometry is perhaps 0.2 magnitudes for an individual star given the scatter in the points. At the distance of M31 (Mod = 24.26 according to Welch et al 1986) the faintest main sequence stars correspond to M_V of -3.0, or B0V. Thus we would expect we are detecting main sequence and all luminosity type O stars, B giants, and B and later type supergiants. In Fig. 2 the straight line with the arrow at the end is the reddening line for an O9.5 main sequence star with slope 0.72. The intrinsic colors for main sequence and supergiants (FitzGerald 1970) are indicated.

The stars of Fig. 2 should be dereddened such that the main body of blue stars gives a best fit to the intrinsic colors of the supergiants or to the main sequence O types (near to or above the reddening line). With color-color plots similar to Fig. 2, and trial and error, we thus estimated the mean reddening in each association. Isolating and comparing various regions suggested differential reddening within an association across the CCD frame played no important role in

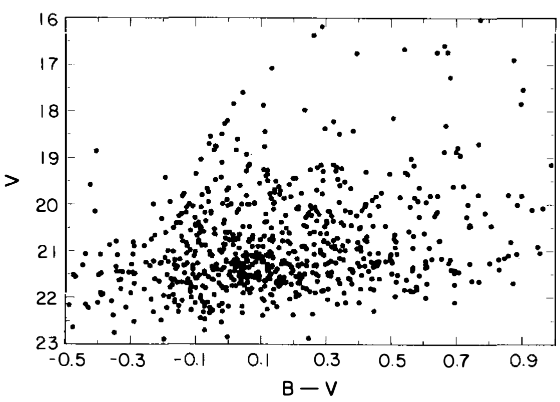

Fig. 1. Color magnitude diagram for all stars with photometry in the field of OB48.

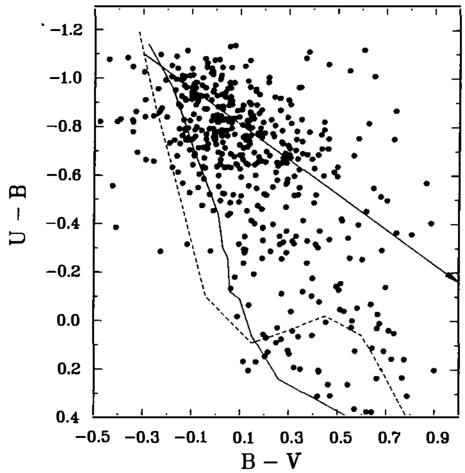

Fig. 2. Two color plot for stars in OB48. The straight line with the arrow at the end is the reddening lines for an O9.5V star. The solid and dashed lines are the intrinsic color for main sequence and supergiant stars, respectively.

the observed photometric scatter. The resultant mean reddening values ranged from E(B-V) = 0.24 for OB48 and OB 8, 9, and 10, to 0.12 for OB78 and 0.08 for OB102. The latter value is similar to the expected foreground reddening from our own galaxy (Humphreys 1979; Burstein and Heiles 1984).

We are now in a position to plot dereddened color-magnitude diagrams for our four CCD fields. We found it useful to use $(U-B)_0$ as the abscissa, rather than the $(B-V)_0$, as this will better isolate the blue star population. In the next few color-magnitude diagrams evolutionary tracks for stellar composition models of 60, 40, 20 and 10 solar masses are also plotted (the former three from Maeder 1987, the latter from Pylyser 1984). The more massive stars include the effects of mass loss, determined empirically. Although overshooting is probably important for stars such as these (e.g. Doom 1982) it is not included in these models. The greatest uncertainty in plotting these tracks is the step in going from the luminosities and effective temperatures of the models to the observed colors and magnitudes, particularly the still uncertain bolometric corrections. The conversion used the calibrations of Flower (1977), Conti (1987), and FitzGerald (1970). The tracks should only be used as a guide to the eye and as a rough indication of the inferred masses and ages of the stars. We included only that portion of the evolutionary track in which the model is carried upwards and to the right towards lower temperatures (primarily the period of core hydrogen burning and the immediately following phases). The post core hydrogen burning stage is critically dependent on the physical basis of the models, but most investigators agree that the most massive stars will turn back to the left hand part of the HRD, while the less massive ones will become red supergiants. These stars, and even lower mass ones, then slowly evolve back and forth across the upper part of the HR diagram, the details of which depend on the input physics to the models and their interpretation which is not completely settled.

Before proceeding to the main results it is important to separate, if possible, the stars of the associations from the background of the M31 galaxy itself. We can only do this in a statistical sense since these stars are all at roughly the same distance. The data for the small associations OB8, 9, and 10 enable us to address the problem since they are contained well inside the CCD frame of that region. Figure 3 shows the de-reddened color-magnitude diagram for the stars <u>outside</u> the boundaries of those associations, whereas Fig. 4 shows the objects <u>inside</u>. Comparing the two figures one can see that the population of blue stars is substantially different; as expected, there are many bright blue stars inside these boundaries yet hardly any outside. This not only nicely confirms the reality of the associations it isolates the background M31 population. We see that this population is composed of stars along the 10 solar mass track; these typically have ages of some tens of millions of years. Inside the association boundaries we see not only this background population but also a

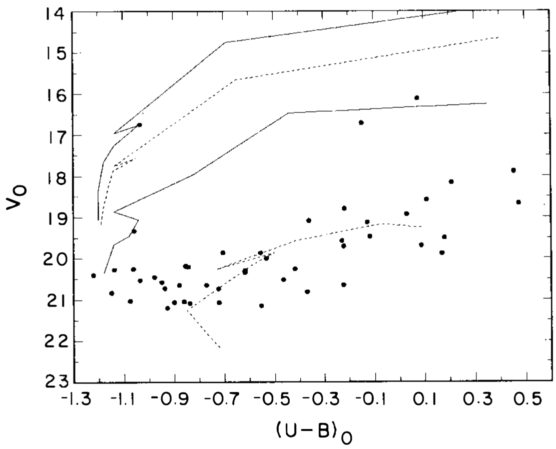

Fig. 3. Dereddened color-magnitude diagram for stars outside the OB8, 9, and 10 association boundaries on the CCD frame. The solid and dashed lines are evolution tracks for stars of 60, 40, 20 and 10 solar masses (see text).

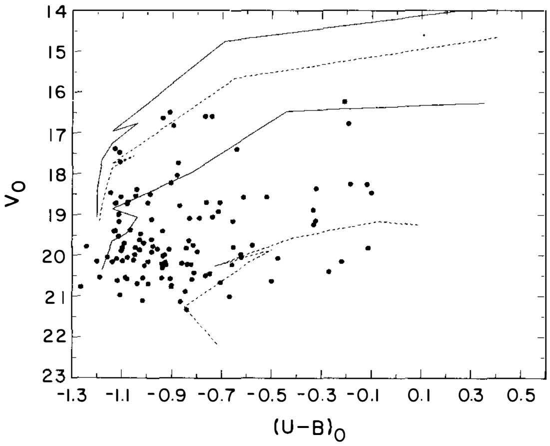

Fig. 4. Dereddened color-magnitude diagram for stars inside the OB8, 9, and 10 association boundaries on the CCD frame. The evolution tracks are as in Fig. 3.

blue "plume" of younger stars with ages typically a few million years (according to the tracks). If our CCD frames went to appreciably fainter luminosity limits, we would detect the even older population of stars in M31 with ages of hundreds of millions to billions of years. With the color and magnitude restrictions of our data, we have been able to isolate only the youngest stars, and our photometry can distinguish among them in a rough fashion.

The boundaries of the other associations as sketched by van den Berg (1964) more or less fill our CCD frames. In hindsight, we could now redraw the boundaries around the bluest and most luminous stars and compare the populations inside and out but that is beyond the scope of my discussion here. In what follows, therefore, all stars on the CCD frames are considered to be members of the associations and all stars with photometry are plotted. The dereddened color-magnitude diagram for OB48 is shown in Fig. 5 and that for OB78 (NGC 206) in Fig. 6. In both associations we see a considerable population of OB stars, particularly those with initial masses greater than 20 solar masses. These are presumably all O stars or B supergiants. We note the substantial numbers of stars at $(U-B)_0$ of order of -1.1 and the difficulty of determining the exact masses from photometry alone (Massey 1985) except in the broadest terms. The higher mass evolution tracks all show a loop near this point which corresponds to the end of core hydrogen burning; appreciable numbers of blue supergiants are found to the right of this theoretical limit. As Maeder (1987) and other have pointed out, this "main sequence widening", analogous to what is seen in Galactic

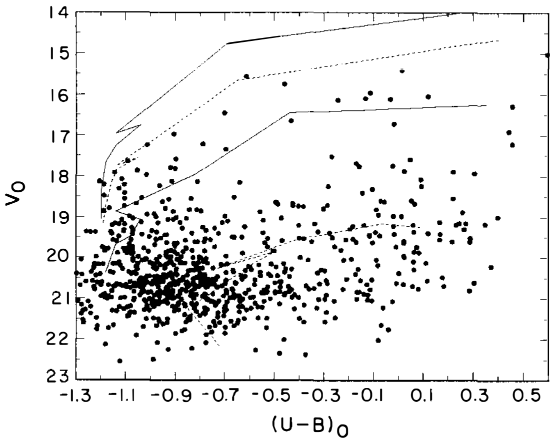

Fig. 5. Dereddened color-magnitude diagram for stars of OB48. The evolution tracks are as in Fig. 3.

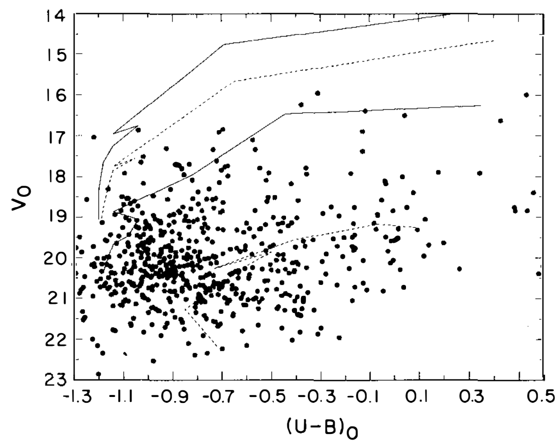

Fig. 6. Dereddened color-magnitude diagram for stars of OB78 (NGC 206). The evolution tracks are as in Fig. 3.

color-magnitude diagrams, is not yet satisfactorily accounted for in the stellar models. Overshooting may play a role in the eventual explanation for this anomaly.

In Fig. 7 I show the color-magnitude relation for the field of OB102. In contrast to the previous three figures, we now find a lack of the most massive, luminous stars. Very few are found with masses inferred to be larger than 20 solar masses. It is clear from this figure that the blue stars are not as

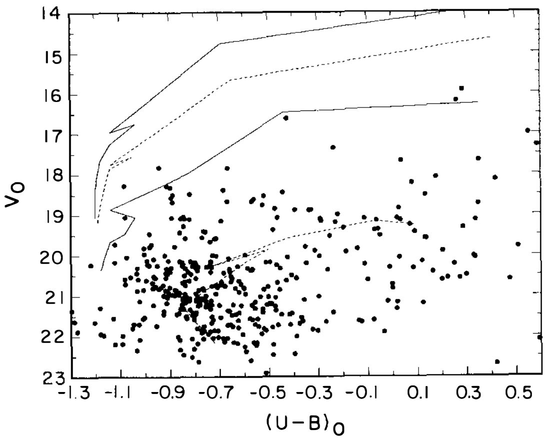

Fig. 7. Dereddened color-magnitude diagram for stars of OB102. The evolution tracks are as in Fig. 3.

luminous as those in the other associations. There are still appreciable numbers of stars between the 10 and 20 solar mass tracks so the straightforward interpretation of these data is that OB102 is older and its more massive stars have already evolved away. It is significant that OB48 and OB78 both contained a half dozen or so W-R candidate stars, whereas OB102 has only two marginal ones. Since W-R stars are the descendants of only the most massive O stars (Conti et al 1983; Humphreys et al 1985) this is what would be expected if OB102 were older than OB48 and OB78. We have thus shown here an ability to segregate the youngest associations of M31 into extreme youth by photometry -- some few million years as represented by OB8, 9, and 10, OB48 and OB78, and one approaching some ten million years, OB102. We could also have predicted this on the basis of the W-R population.

Luminosity functions are often used as a diagnostic for interpreting the properties of a population of stars. These are essentially counts of stars to fainter and fainter apparent magnitude levels. Here we can make use of the derived reddening for each association and use V_0 instead of merely V. Figure 8 gives the results expressed as log N in counts of half-magnitude intervals for our four regions. (Had we ignored the differential reddening effects we would have counted stars in the lightly reddened association OB102 in magnitude intervals which were inconsistent with, say, OB48.) The luminosity functions differ in their ordinate values due to the different numbers of stars in each association. The turnover at V_0 of 21 is due to incompleteness. For a range of 3 magnitudes brighter than this faint limit the functions are parallel. The

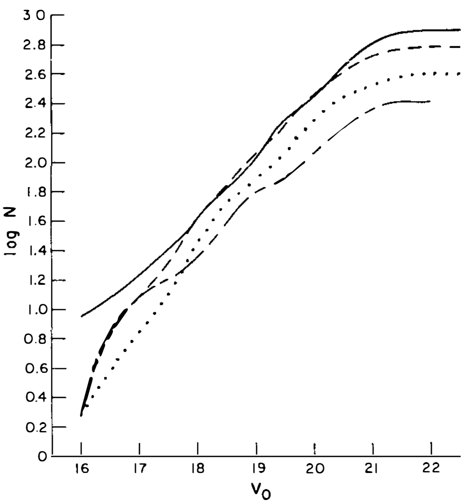

Fig. 8. Luminosity functions (log number brighter than V_0 vs. V_0) for stars in the four fields. Long-short dashed line: OB8, 9, and 10; solid line: OB48; dashed line: OB78; dotted line: OB102.

usual interpretation of such a result is that the IMF are identical within the uncertainties (e.g. Freedman 1985). Is this correct? While it would appear that the parallelism of the luminosity functions between V_0 18 and 21 says something about the massive star content, a look back to Fig. 4-7 will indicate this is not the case. At these V_0 main sequence stars of very different initial masses and ages are being counted together. At V_0 of 18 and fainter the evolved 10 solar mass stars begin to appear as these stars make their traversals back and forth across the upper part of their evolution tracks. It is easy to visualize that these stars, and even lower mass ones, will dominate the statistics of the luminosity function at this and fainter magnitudes. Thus the nearly identical slopes in Fig. 8 say nothing about the massive star population, a point emphasized previously by Massey (1985) and graphically illustrated here. The difference in the luminosity function slopes at brighter magnitudes is probably dominated by the small number statistics and one can infer nothing about the IMF with these data.

The presence of hot, massive stars in M31 is indicated by the numerous HII regions found "strung out like pearls along spiral arms" (Baade 1958). Is strong H-alpha always found with rich collections of O stars? Let us compare the massive star content of OB48 and OB78; I have shown in Figs. 5 and 6 that the luminous stellar populations are similar; we also see parallel populations of W-R stars (MAC). The ages appear to be closely comparable. Yet the H-alpha photographs of these associations (Pellet at al 1978) are distinctly different; little emission is found with OB78, yet considerable H-alpha is connected to OB48. (Unfortunately there are, as yet, no quantitative measures of this emission in M31.) The lack of significant H-alpha led van den Berg (1966) to suggest supernova shells or stellar radiation had cleared the OB78 region of gas; subsequently it was learned that this association sits in a prominent HI hole (Brinks 1981). It seems possible (MAC) that the winds of the numerous hot stars may have created a "superbubble" (following Heiles 1979) in the vicinity of OB78. Why not also in OB48? A potential answer would have to lie in the conditions in the ISM surrounding these two associations since their stellar content seems comparable. If one imagined the medium was less extensive and of lower density surrounding OB78, in contrast to OB48, the observations could be explained. Perhaps the galactic disc is thinner there. In more distant galaxies the star formation rate has been assumed to be proportional to the integrated H-alpha emission. The lack of gas near OB78 indicates a need for caution in deriving massive star statistics from emission measures alone.

What can we learn about star formation in M31 from our data? We have both the W-R statistics (MAC) and the numbers discussed here. Taking into account the inclination of M31 to our line of sight, and the size of our CCD frames, we find the W-R population and the OB stars to be roughly similar to that of the solar neighborhood. There are some regions of M33 where the W-R population is larger than this (Massey 1985) and many where it is similar. On the other hand, we have selected regions of M31 where we expect the number of OB stars to be large. Over most of the face of M31 there are certainly fewer massive stars as the HII regions, and large associations, are mostly concentrated in the annular ring containing OB48 and OB78; overall it would seem that M31 does not have the same fractional population of massive stars as would be inferred if one scaled-up M33. Clearly that is related to the different Hubble types. But there are small regions of M31 where massive star population is as rich as that found near the sun.

Let me turn now to a brief progress report on the stellar population studies in the Magellanic Clouds. This is taken from data presented by Conti et al (1986) and Garmany et al (1987). We intend to eventually complete a census of all the O stars in the SMC and hopefully, also, in the LMC. In the latter galaxy most of the O stars are to be found in the numerous associations (Lucke 1972) for which photometry is still only primitive. CCD frames of many of these associations are now being acquired to enable us to study the luminosity functions and to identify the O star candidates for follow-up spectroscopy. We have new slit spectra of 192 OB stars in the LMC and 120 in the SMC, mostly from stars in the field in which previous photometry was available. Approximately half of each sample were newly identified O stars, the other half being B supergiants. The total numbers of O stars in the SMC will probably turn out to be less than a couple of hundred as we have already found some 50 or so and the number of unstudied associations is small. In the LMC the O star count will probably be over a thousand and we will be have to be content to identify only the more massive ones, which we expect will be found in the numerous associations. Thus the total statistics is uncertain at the present time. However, we have confidence that eventually we will be able to make an accurate count and then we can compare the numbers with other indirect indicators of hot, luminous stars, such as the numbers of W-R stars, the integrated H-alpha emission, or the radio continuum, etc., for calibration purposes.

My numbers given above are only estimates of the massive star population in the Magellanic Clouds but they are based on the actual counts so far. In more distant galaxies the population statistics are indirect; additionally, many methods <u>assume</u> a constant IMF. We hope to eventually address the IMF for the Magellanic Clouds but for now let me just say that I wouldn't be surprised to find it different from the solar vicinity (within 3 kpc). The numbers of HII regions and associations in the LMC seems higher than the similar sized area centered on the sun, whereas that of the SMC seems lower. This is also true for the W-R population, which numbers over 100 for the LMC, 63 or so for the solar vicinity and only 7 or 8 for the SMC. Thus I would expect relatively more massive stars in the LMC and relatively fewer in the SMC, compared to the solar vicinity. If this is related to a slope in the IMF it would be "flatter" in the LMC and "steeper" in the SMC. Possibly upper mass "cutoffs" operate in the lower mass SMC galaxy. For the eventual meaningful comparison, however, one will have to be more careful and to use similar volumes, and masses, and attempt to disentangle the star formation rate from the IMF.

Figure 9 gives the present HR diagram for the LMC (adapted from Conti et al 1986) where all the stars shown have photometry and spectroscopy. The ZAMS track is taken from Pylyser et al (1985) and the upper empirical boundary (the "Humphreys-Davidson limit") has been sketched in. Similarly, Figure 10 gives the HR diagram for the SMC (adapted from Garmany et al 1987) with the Pylyser et al track appropriate to the metal abundance of the SMC. The Humphreys-Davidson limit is sketched also, and it is not the same as that for the LMC, the latter being brighter, although parallel. Recent calculations by Lamers and Fitzpatrick (1987) suggest this limit is related to the "Eddington" limit for radiation pressure, once the correct opacities are included. Their theoretical prediction is qualitatively in agreement with the observed limits shown here although one

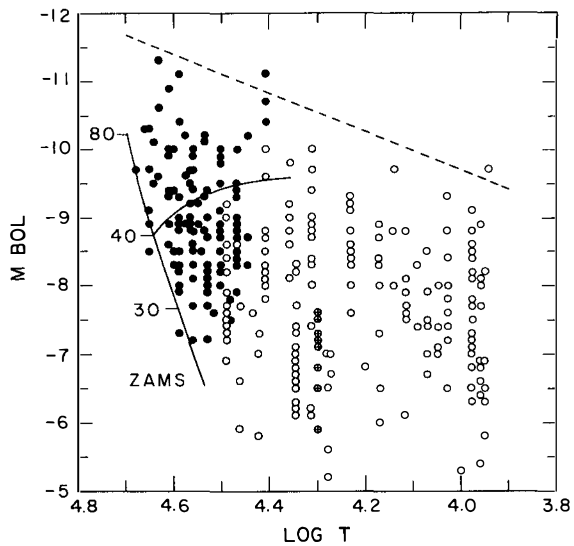

Fig. 9. HR diagram for the LMC for stars with photometry and slit spectral types. The filled symbols are O stars; the open symbols B supergiants; the cross-filled symbols are B emission line objects. The ZAMS and empirical "Humphreys-Davidson limit" are shown (see text).

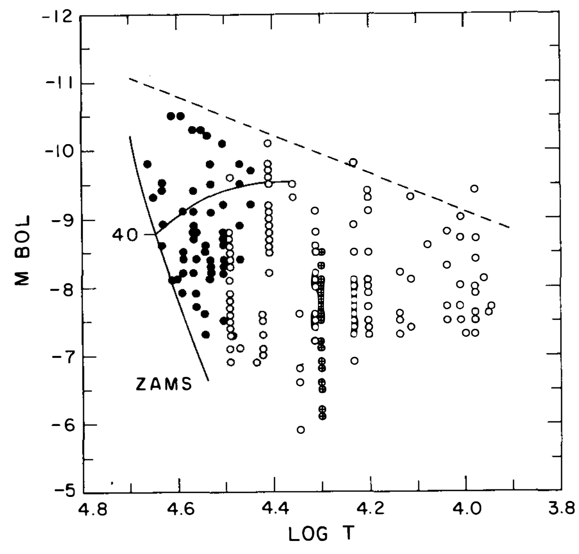

Fig. 10. HR diagram for the SMC for stars with photometry and slit spectral types. The filled symbols are O stars; the open symbols B supergiants; the cross-filled symbols are B emission line objects. The ZAMS and empirical "Humphreys-Davidson limit" are shown (see text).

would then expect that the lower metal abundance in the SMC would result in a brighter limit whereas the opposite effect is seen in our data. Since the census of O stars in incomplete these limits should be considered as preliminary; the SMC might also be constrained by small number statistics although I personally doubt this. I should note that the spectroscopic parallaxes of the O stars in the LMC lead to a distance modulus of 18.3 and that for the SMC one of 19.0; these numbers are used in plotting Figs. 9 and 10.

There are hardly any stars in the SMC with implied masses more than some 80 solar masses according to Fig. 10 (although the stars of NGC 346, the brightest HII region, are not yet plotted having no dependable photometry). Humphreys (1983) has already pointed out the relative lack of massive stars in the SMC based upon a less complete sample than shown here. My suspicion is that when the stellar census is complete, the SMC will be demonstrably deficient in massive stars. Roberta feels this is a statistical cut off due to the low total mass of the galaxy; my personal belief is that it is real and addresses the recent star formation history or the IMF, or both.

What of the massive star population in other stellar systems? Here the data are very preliminary as they are based only on the W-R star population. These are believed to derive from only the most massive stars, some 40 solar masses in the solar vicinity (Conti et al 1983), and tentatively assumed to be similar elsewhere. An important test of this assumption will come from the MC population studies. If we consider only the detected W-R population we have for the Local Group the numbers shown in Table 1 (adapted from Conti 1987 with additions from Moffat and Shara 1987).

Table 1

Wolf-Rayet Statistics in the Local Group

galaxy	actual number	estimated completeness
Solar Vicinity (within 3 kpc)	63	10%
LMC	105	10%
SMC	7 or 8	10%
M33	120	50%
M31	50	factor of a few
NGC 6822	a few	50%
IC1613	a few	50%

Given the respective total masses of these galaxies (our own cannot be accounted for exactly without assumptions concerning the mass distribution) we see that the LMC stands out as having relatively many W-R stars, as does M33 but to a lesser extent. M31 is certainly deficient in W-R stars even with an estimated factor of a few incompleteness, compared to these systems and probably with respect to our own. In the smaller mass systems we are dealing with small number statistics of W-R candidates so any conclusions are preliminary. Armandroff and Massey (1985) have suggested that IC1613, the lowest mass and lowest metal abundance galaxy, does have several W-R candidates. If these are all indeed W-R stars IC1613 would be abnormally rich in these massive star descendants. More data are needed on this issue.

So for now we are left with tantalizing hints (cf. Figs. 9 and 10; Table 1) that the massive star population in the various Local Group galaxies, the only systems for which individual stars can be studied, may differ in ways not strictly proportional to either the total galactic mass or to its overall metal abundance. Whether this is a result of different star formation rates, or various IMFs, is an issue that is not yet settled and will require extensive additional study. For this particular workshop, I know it is an important issue and one for which I would like to leave you with real numbers. My message must instead be to keep an open mind about the ultimate outcome.

I appreciate support for this work from National Science Foundation grant AST 85-20728, and I thank the organizers of this workshop for the opportunity to present some stellar statistics to galactic evolution pundits.

References

Armandroff, T.E., and Massey, P. 1985, Astrophys. J. 291, 685.
Baade W. 1958 in Stellar Populations, edited by D. J. K. O'Connell (North Holland, Amsterdam), p3.
Brinks, E. 1981, Astron. Astrophys. 95, L1.
Burstein, D., and Heiles, C. 1984, Astrophys. J. Suppl. 54, 33.
Conti, P. S. 1987, in O, Of, and Wolf-Rayet Stars, edited by P. S. Conti and A. B. Underhill (NASA special publication, in press).
Conti, P. S., Garmany, C. D., de Loore, C., and Vanbeveren, D. 1983, Astrophys. J. 274, 302.
Conti, P. S., Garmany, C. D., and Massey, P. 1986, Astron. J. 92, 48.
Doom, C. 1982, Astron. Astrophys. 116, 303.
FitzGerald, M. P. 1970, Astron. Astrophys. 4, 234.
Flower, P. J. 1977, Astron. Astrophys. 54, 31.
Freedman, W. L. 1985, Astrophys. J. 299, 74.
Garmany, C. D., Conti, P. S., and Massey, P. 1987 Astron. J. 93, 1070.
Heiles, C. 1979, Astrophys. J. 229, 533.
Hodge, P. W. 1981, Atlas of the Andromeda Galaxy (University of Washington, Seattle).

Hodge, P. W. 1986, in Luminous Stars and Associations in Galaxies, IAU Symposium No. 116, edited by C. W. H. de Loore, A. J. Willis, and P. Laskarides (Reidel, Dordrecht), p.369.
Humphreys, R. M. 1979, Astrophys. J. 234, 854.
Humphreys, R. M. 1983, Astrophys. J. 265, 176.
Humphreys, R. M., Nichols, M. and Massey, P. 1985, Astron. J. 90, 101.
Lamers, H. J. G. L. M., and Fitzpatrick, E. 1988, Astrophys. J. in press.
Lucke, P. B. 1972, Ph.D. thesis, University of Washington.
Maeder, A. 1987, Astron. Astrophys. 173, 247.
Massey, P. 1985, Pub. Astron. Soc. Pac. 97, 5.
Massey, P., Armandroff, T. E. and Conti, P. S. 1986, Astron. J. 92, 1303.
Moffat, A. F. J. and Shara, M. M. 1987, preprint.
Pellet, A., Astier, N., Viale, A., Coutes, G., Maucherat, A., Monnet, G., and Simien, F. 1978, Astron. Astrophys. Suppl. 31, 439.
Pylyser, E. 1984, Licentiaat thesis, University of Brussels.
Pylyser, E., Doom, C., and de Loore, C. 1985, Astron. Astrophys. 148, 379.
Ratnatunga, K. U. and Bahcall, J. N. 1985, Astrophys. J. Suppl. 59, 63.
van den Bergh, S. 1964, Astrophys. J. Suppl. 9, 65.
van den Bergh, S. 1966, Astron. J. 71, 219.
Welch, D. L., McAlary, C. W., McLaren, R. A. and Madore, B. T. 1986, Astrophys. J. 305, 583.

MASSIVE STARS: LIFETIMES AND RELATIVE FREQUENCIES IN NEARBY GALAXIES

André MAEDER
Observatoire de Genève
CH-1290 Sauverny
Switzerland

Some basic properties of massive stars are given, with particular emphasis on the lifetimes obtained in new models with mass loss and moderate overshooting. There are big differences in the relative frequencies of O stars, WR stars, and blue and red supergiants in galaxies. It is shown that this must not necessarily be interpreted as being due to differences in the initial mass function (IMF) or in the star formation rates (SFR) between galaxies. As a matter of fact, the lifetimes in the various post-MS stages seem to be very dependent on the local initial metallicity, probably through the influence of metallicity on the mass loss rates which in turn influence the lifetimes.

1. Introduction

Massive stars, observed either directly or through their effects on gas, are a striking manifestation of starbursts and ongoing star formation. Attention will be focused on new results concerning the lifetimes of massive stars in their various evolutionary stages, in particular in the Wolf-Rayet stage. The lifetimes are an essential property for the determination of the initial mass function (IMF), the star formation rate (SFR) and also for the study of the relative frequencies of blue and red supergiants and WR stars, which show great differences according to galaxies.

2. Recent progress in model construction

The general properties of massive stars were recently thoroughly reviewed [7] and we shall therefore concentrate only on some new results [27] in this field.

A major concern in model building is that of the overshooting distance d_{over}, which is the distance up to which convective mixing really extends above the formal limit given by Schwarzschild's criterion. Overshooting can significantly modify all the model outputs as it is able to increase the amount of nuclear fuel available. The theoretical context for overshooting is still very uncertain. For example, it has been shown [3] that Roxburgh's criterion , extensively used in some recent computations, rests on inconsistent approximations.

To get out of this uncomfortable situation concerning a critical parameter of stellar evolution, an observational approach has been attempted [28]. It is based on the fact that in the HR diagram, the location of the top of the main sequence (MS) is very sensitive to the amount of overshooting. We have collected and analysed data on well-studied clusters, closely analysed for membership, reddening, binarity, rotation and peculiarities. The comparisons between observed sequences and theoretical isochrones in the HR diagram made for 65 clusters and associations of various ages clearly point in favour of moderate overshooting with $d_{over} \simeq 0.25$ to $0.3\ H_p$, where H_p is taken at the edge of the classical core. This result is quite consistent with some other empirical determinations [20, 33], and is also supported by the results on the WR lifetimes (cf. §4).

The mass loss rates $\dot{M}$ are based on recent expressions by de Jager et al. [16], completed by specific rates for LBV and WR stars. Furthermore, up-to-date opacities and nuclear data have been used in the models, which also include the effects of turbulent pressure and acoustic flux in the red supergiant stage.

3. Mass limits and evolutionary connections

The tracks in the HR diagram obtained from these new models [27] are illustrated in Fig. 1.

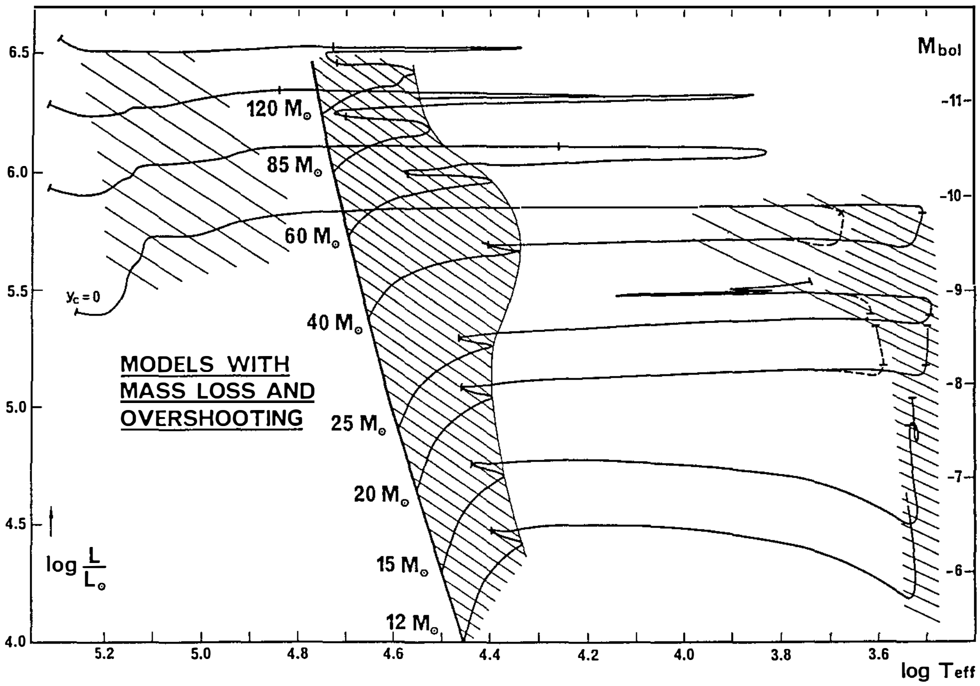

Figure 1. Evolutionary tracks of massive stars with initial composition X = 0.70 and Z = 0.02 evolved with mass loss by stellar winds and overshooting. Hatched areas indicate the main sequence band and the He-burning phase. For red supergiants, the broken lines indicate the tracks computed with $\alpha_p = 1/H_p = 0.3$ while the continuous lines refer to the usual mixing length theory with $\alpha_p = 1/H_p = 1.5$. The first slash along the evolutionary tracks indicates the central exhaustion of H, the second the beginning of the He-burning phase and the last the central exhaustion of He.

On the main sequence (MS) the combination of overshooting and mass loss produces a MS narrowing for the most massive stars (with MS termination in the O-type range, i.e. log $T_{eff} > 4.47$). The reason is that heavy mass loss and overshooting lead the core to be rapidly revealed at the stellar surface: due to the lower H content the opacity is smaller and the star becomes bluer, thus making the MS band narrower. For models with a MS termination in the range of spectral type B0 or later (log $T_{eff} <$ 4.47), the combination of the adopted overshooting and mass loss produces a MS widening, because the relatively large size of the core increases the MS lifetimes as well as the chemical discontinuity in the star models. These models correspond well to the observational requirements [13, 28].

A major result of models with mass loss [e.g. 7] was the existence of three different evolutionary sequences according to the range of initial stellar masses considered. The new models well confirm this view, however the mass limits between the three ranges considered are slightly changed:

for $M \geqq M_1$: O-Of-BSG-LBV-WR-SN

$M_1 > M \geqq M_2$: O-BSG-YSG-RSG-WR-SN (O-BSG-YSG-RSG-BSG-SN for lower $\dot{M}$)

$M_2 > M \geqq M_3$: O-RSG (with or without Cepheid loop)-SN

BSG, YSG and RSG mean blue, yellow and red supergiants respectively. LBV stands for luminous blue variables, WR for Wolf-Rayet stars, SN for supernovae.

The limit M_1 was previously placed near 60 $M_\odot$. Here, M_1 is found to be about 40 $M_\odot$ (maybe up to 50 $M_\odot$), a fact which is in better agreement with the observed upper limit for RSG [12, 14]. M_2 lies between 40 and 30 $M_\odot$; we see that the 25 $M_\odot$ model is very much "hesitating" between a final location in the blue and the red. On the whole, the range of initial masses, where WR stars can be in a post RSG stage, is probably rather narrow, as suggested by Humphreys et al. [15]. M_3, the lower mass limit for O-star formation, is about 15 $M_\odot$.

Let us note that the excursions made by the 60, 85 and 120 $M_\odot$ models to the right of the MS band (region of Hubble-Sandage variables or LBV stars) depend very much on the adopted mass loss rates and on the overshooting. For example, without mass loss, the stars would continuously evolve to the red, never coming back to the blue. On the contrary, models with a very large overshooting [31] never enter the LBV region (say, log $L/L_\odot > 6.0$ and log $T_{eff} < 4.5$). This hints that such models are probably not very appropriate. For average mass loss rates of about 10^{-4} to 10^{-3} $M_\odot$ y^{-1} [19] and the present overshooting, the calculated lifetime in the LBV region is at the most about 10^4 y. Since LBV stars have outbursts with violent mass ejections, an average mass loss rate can hardly be representative of the complexity of LBV stars and the value for the duration of this phase is to be taken with caution.

In these models the formation of WR stars occurs for the models with initial $M \geq 40$ $M_\odot$, in agreement with [15]. However, we notice that in the range of 25 to 40 $M_\odot$ a moderate enhancement of mass loss in previous stages could also marginally lead to the formation of WR stars [32]. The extremely hot location of WR star models in the HR diagram is a consequence of the simple atmospheric treatment used in the models [22]. Substantial developments for matching non-static and non-LTE atmospheric models and internal structure are now in progress. Recently T_{eff} determinations for WR stars have led to a value of about 10^5 K [6, 30].

4. Lifetimes

The lifetimes in the H-, He-, C-burning phases are given in Table 1. The He-phase is defined here from the time of central H-exhaustion to the time of central He-exhaustion. Similarly, the C-phase is considered from central He- to C-exhaustion. The lifetimes in the H-burning phase for stars with initial masses from 15 to 60 $M_\odot$ are given by

$$\log t_H = -.86 \log M/M_\odot + 8.06 \ (\pm .02 \text{ dex})$$

Table 1: Lifetimes in nuclear phases and in the WR stage (in unit of 10^6 y)

Initial mass	H-burning phase	He-burning phase	C-burning phase	WR phase	t_{WR}/t_O	t_{WN}/t_{WC}
120 $M_\odot$	2.9379	.5132	.001051	.508	.17	2.02
85	3.3245	.4998	.001826	.488	.15	1.73
60	3.7108	.6085	.001940	.542	.17	1.34
40	4.7912	.6395	.004884	.492	.12	1.22
25	7.0887	1.1718	.007164	—	—	—
20	8.8064	1.2574	.009136	—	—	—
15	12.1052	1.6329	.017900	—	—	—

where t_H is given in years. As is well known, both mass loss and overshooting increase the MS lifetimes [7].

From the models and up-to-date temperature calibrations [17], we may assign an upper limit to the ages of stars of a given spectral type:

Table 2: Spectral types vs age calibration for O-stars

Sp O4	age	$\leq 1.4 \cdot 10^6$ y
O5		1.6
O5.5		2.0
O6		2.4
O6.5		2.7
O7		3.0
O8		4.0
O9		5.0
B0	age	$\leq 7.0 \cdot 10^6$ y

The ratios t_{He}/t_H of the lifetimes in the He- and H-burning phases lie here in the range of 14 to 18%. In the literature, the ratios obtained by various authors range from about 8 to 19% [7].

Let us examine the effects of overshooting on the t_{He}/t_H ratios. Lifetimes generally depend on the ratio of the available fuel reservoir q_{cc} M to the luminosity L (q_{cc} is the mass fraction of the convective core). Overshooting increases both quantities. Thus, the lifetime in a given nuclear phase may be increased or decreased by overshooting depending on the relative change of both terms in the ratio q_{cc} M/L. In the H-burning phase, the net effect is an increase of the lifetime t_H. However, for the He-burning phase the lifetime t_{He} is decreased by overshooting [4, 20]: the main reason is that models with overshooting evolve at a higher luminosity. On the whole, overshooting through its effects on t_{He} (decrease) and t_H (increase) reduces the t_{He}/t_H ratio. Thus, we may understand why the present t_{He}/t_H ratios are slightly smaller than in the corresponding models without overshooting [24]. This is also partly the reason why models [31] with (too) large overshooting find t_{He}/t_H equal to about 8% which is about half of the ratio found in the present models, which are in better agreement with observations (cf. §5).

The C-burning phase only lasts a few thousand years and typically represents $3 \cdot 10^{-4}$ to $1.5 \cdot 10^{-3}$ of the MS phase. Thus stars in this stage, with copious neutrino flux, should be quite rare: in fact, at the most one could exist among the 160 known galactic WR stars.

WR lifetimes, WN and WC subtypes

Various analyses of the evolutionary status of WR stars [e.g. 7] have led to the identification of WR stars with bare cores, exhibiting CNO processed elements (WN stars) and products of partial He-burning (WC stars). For practical reasons, we have to adopt a single definition of what we consider to be a bare core even if in fact the appearance of the WR phenomenon may be more complex. Owing to the fact the H/He ratios in number up to two (X_s = 0.33) are observed in WN stars [9], we consider that a star enters the WR stage when X_s < .3 and log T_{eff} > 4.5 on the final bluewards track. The condition on log T_{eff} and the final track should allow to avoid considering stars in the LBV region as WR stars. This restriction is, however, not critical since the LBV stage is short; the effect of different definitions on the lifetime of a WR star will be discussed below.

The WR lifetimes t_{WR} are given in Table 1. The values of t_{WR} are typically about $5 \cdot 10^5$y [e.g. 25, 31]. We consider that once a star has entered the WR stage, it stays there up to the final supernova explosion. Table 1 also shows that the differences (t_{He}-t_{WR}) increase with decreasing masses; this is to be explained by the fact that for lower initial masses, a larger fraction of the He-lifetimes t_{He} is spent in the yellow or red stages.

Changes of the limiting value of X_s for defining the entry in the WR stage generally do not modify t_{WR} very much. As an example, for the 60 $M_\odot$ the limits X_s=0.40 and 0.20 give respectively WR lifetimes of 0.604 and 0.537 instead of 0.542 for the adopted limit X_s=0.30.

Physically, t_{WR} depends on mass loss and overshooting in several ways. 1) Both effects make the star enter the WR phase at an earlier time and thus increase t_{WR} for a given model. 2) Severe mass loss in the WR stage also increases t_{WR} by reducing the total mass and thus the central temperature as well as nuclear rates. 3) High mass loss and overshooting in the previous stages reduce the lower mass limit leading to the formation of WR stars, which contributes to an increase of the expected number of WR stars.

The values of the ratio t_{WR}/t_O of the lifetimes in the WR and O stages range from 12% to 17% (cf. Table 1). The main trend is a decrease with decreasing stellar masses. However, the ratio t_{WR}/t_O for the 60 $M_\odot$ model is slightly higher. This is due to the fact that the overshooting sufficiently widens the MS band for this model so that only part of the MS lifetime is spent as an O-star, which contributes to an increase of the t_{WR}/t_O ratio. The remaining fraction of the MS band is spent in this case in the range of types B0-B2. The present values of t_{WR}/t_O are higher than those generally found, which are about 0.06-0.10 [7]. The present values are quite close to the observed ones (cf. Table 3, and ref. 8).

The ratios t_{WN}/t_{WC} of the duration of the WN and WC stages can also be estimated (cf. Table 2). The transition between both stages is clearly defined, while the beginning of the WN stage is subject to the same remarks as above. For the 40 and 60 $M_\odot$ models, i.e. in the range where most WR stars are likely to originate [15], the ratios t_{WN}/t_{WC} amount to 1.22 and 1.34. The ratio t_{WN}/t_{WC} is very sensitive to mass loss and overshooting. High $\dot{M}_{WR}$ and large overshooting reduce the WN phase and cause a more rapid entrance into the WC stage; thus both effects favour small t_{WN}/t_{WC}. The comparison with models by Prantzos et al. [31] is enlightening. These authors have used nearly the same $\dot{M}_{WR}$ as we did, but they request very large convective cores. For models of initial mass 50 and 60 $M_\odot$ they obtain $t_{WN}/t_{WC} = 0.34$ and 0.21. This clearly illustrates the sensitivity of t_{WN}/t_{WC} to overshooting.

The observed number ratio WN/WC of WN and WC stars in the solar neighbourhood is about 1.2 (cf. Table 3). This is in remarkable agreement with our results, which for the adopted $\dot{M}_{WR}$ well supports our choice of the overshooting parameter $d_{over}/H_p = 0.25$, as found from the HR diagrams of young associations.

5. Massive stars in galaxies and metallicity

The large differences in the relative frequencies of O-stars, blue and red supergiants and WR stars in galaxies have been discussed by several authors [e.g. 21]. Table 3, based on [2, 29], shows some interesting number ratios. The recent observations by Azzopardi et al. [2] have greatly clarified the situation. Table 3 shows impressively large changes in some number ratios according to the galaxies considered.

A critical point frequently disputed in the literature [5, 11] is whether the observed differences originate from differences in the IMF or from chemical effects [2, 26]. Table 3 convincingly supports the view that the large changes in the number ratios are somehow correlated with the initial Z content. A second argument is that a ratio like N_{WR}/N_{OBA}

Table 3: Number ratio of massive stars in galaxies

	Z	$\frac{N_{WR}}{N_{OBA}}$	$\frac{N_{WC}}{N_{WN}}$	$\frac{N_M}{N_{WR}}$
GALAXY 7.5-11 kpc	.029	.24	1.1	.2
9 -11 kpc	.020	.17	0.8	.4
M33	.02	.10	$\lesssim$ 1	-
GALAXY 11-12.5 kpc	.013	.07	0.7	3.5
LMC	.006	.07	0.22	9
NGC 6822	.005	.08 :	≤0.17	-
SMC	.002	.03	0.14	24
IC 1613	.002	.03	-	-

expresses the number ratio of a given kind of star with respect to its progenitors and such a ratio is essentially independent of the IMF. Similarly for the N_{WC}/N_{WN} ratios, stars of both subtypes originate from a very similar (although not necessarily totally identical) range of initial masses. These arguments support the view that the large changes exhibited by Table 3 originate from intrinsic stellar properties, most likely related to the initial metallicity at their place of birth [2, 26].

Let us now turn towards the possible theoretical interpretation. Direct structural effects due to metallicity are probably of limited importance in massive stars, since the main opacity source is electron scattering. However, the models show that the fractions of the He-lifetime spent in the various sub-stages (blue, red supergiant, WN, WC) critically depend on the mass loss rates (cf. Table 4, based on ref. 21).

The question now is whether metallicity influences the mass loss rates. This question was answered negatively [10], however the relevant observations may not have been sufficiently accurate in view of the size of the effects. Theoretically, an almost linear relation $\dot{M}$ vs Z was predicted [1], while more recent models [18] suggest a dependence of approximately $\dot{M}$ vs $Z^{1/2}$. Any such direct connection, whether linear or not, allows to account qualitatively why the regions of high Z have a higher relative frequency of WR stars, and a higher WC/WN ratio. The construction of detailed models necessary for providing quantitative lifetime ratios for massive stars at different metallicity is now in progress.

Table 4: Effects of mass loss on blue and red supergiants and WR lifetimes

★ $t_{He} \simeq t_{BSG} + t_{RSG} + t_{WR}$, sharing varies with $\dot{M}$

★ *BLUE SUPERGIANTS (BSG):*

no $\dot{M}$: $t_{He} \simeq t_{BSG}$

with $\dot{M}$: $\left\{\begin{array}{l}\text{He - phase moves to red}\\ \text{Blue loops reduced}\end{array}\right\}$ $t_{BSG} \downarrow$

★ *RED SUPERGIANTS (RSG):*

$$\left.\begin{array}{ll}\text{moderate } \dot{M} \Rightarrow & \dfrac{t_{RSG}}{t_{OBA}} \uparrow \\ \text{(for low } \dot{M} \text{ : lack of RSG)} & \\ \text{high } \dot{M} \Rightarrow & \dfrac{t_{RSG}}{t_{OBA}} \downarrow \end{array}\right\} \quad \dot{M} \uparrow \Rightarrow \quad \frac{t_{RSG}}{t_{OBA}} \nearrow\searrow$$

★ *WOLF-RAYET STARS (WR):*

$$\left.\begin{array}{l}\dot{M} \text{ incrases } t_{WR} / t_{OBA} \\ \quad \text{lowers threshold mass for} \\ \quad \text{forming WR stars (most} \\ \quad \text{from } M_{initial} \geq 40\ M_{\odot}\text{)}\end{array}\right\} \quad \dot{M} \uparrow \Rightarrow \quad \frac{N_{WR}}{N_{OBA}} \uparrow\uparrow$$

As a general conclusion, we emphasise that the very large differences in the populations of massive stars (blue, red supergiants, WR stars) in galaxies must be interpreted with great care and cannot be attributed directly as being due to changes in the IMF or SFR.

REFERENCES

1. Abbott, D.C. 1982, Astrophys. J. 259, 282
2. Azzopardi, M., Lequeux, J., Maeder, A. 1987, Astron. Astrophys. in press
3. Baker, N.H., Kuhfuss, R. 1986, preprint Max-Planck-Institut für Phys. und Astrophys., no 256
4. Bertelli, G., Bressan, A., Chiosi, C., Angerer, K. 1986, Astron. Astrophys. Suppl. Ser. 66, 191

5. Bertelli, P., Chiosi, C. 1981, in The Most Massive Stars, ESO Workshop, Ed. S. D'Odorico, D. Baade, K. Kjär, p. 211
6. Cherepashchuk, A.M., Eaton, J.A., Khaliollin, K.F. 1984, Astrophys. J. 281, 774
7. Chiosi, C., Maeder, A. 1986, Ann. Rev. Astron. Astrophys. 24, 329
8. Conti, P.S., Garmany, C.D., de Loore, C., Vanbeveren, D. 1983, Astrophys. J. 274, 302
9. Conti, P.S., Leep, E.M., Perry, D.N. 1983, Astrophys. J. 268, 228
10. Garmany, C.D., Conti, P.S. 1984, Astrophys. J. 284, 705
11. Garmany, C.D., Conti, P.S., Chiosi, C. 1982, Astrophys. J. 263, 777
12. Humphreys, R.M. 1983, Astrophys. J. 269, 335
13. Humphreys, R. 1984, in Observational tests of the stellar evolution theory, IAU Symp. No. 105, Ed. A. Maeder and A. Renzini, Reidel Publ., p. 279
14. Humphreys, R., Davidson, M.K. 1979, Astrophys. J. 232, 409
15. Humphreys, R.M., Nichols, M., Massey, P. 1985, Astron. J. 90, 101
16. de Jager, C., Nieuwenhuijzen, H., van der Hucht, K.A. 1986, in Luminous stars and associations in galaxies, IAU Symp. 116, Ed. C.W.H. de Loore, A.J. Willis, P. Laskarides, p. 109
17. Kudritzki, R.P., Hummer, D.G. 1986, in Luminous stars and associations in galaxies, IAU Symp. 116, Ed. C.W.H. de Loore, A.J. Willis, P. Laskarides, p. 3
18. Kudritzki, R.P., Pauldrach, A., Puls, J. 1987, Astron. Astrophys. 173, 293
19. Lamers, H.J.G.L.M. 1986, in Luminous stars and associations in galaxies, IAU Symp. 116, Ed. C.W.H. de Loore, A.J. Willis, P. Laskarides, p. 157
20. Langer, N., El Eid, M.F. 1986, Astron. Astrophys. 167, 265
21. Lequeux, J. 1985, in Birth and infancy of stars, Les Houches XLI, Ed. R. Lucas, A. Omont, R. Stora, North Holland Publ., p. 6
22. de Loore, C., Hellings, P., Lamers, H. 1982, in Wolf-Rayet stars: observations, physics and evolution, IAU Symp. 89, Eds. C. de Loore and A.J. Willis, Reidel Publ., p. 53
23. Maeder, A. 1981, Astron. Astrophys. 102, 401
24. Maeder, A. 1987, Astron. Astrophys. 173, 247
25. Maeder, A., Lequeux, J. 1982, Astron. Astrophys. 114, 409
26. Maeder, A., Lequeux, J., Azzopardi, M. 1980, Astron. Astrophys. 90, L17
27. Maeder, A., Meynet G. 1987, Astron. Astrophys. in press

28. Mermilliod, J.C., Maeder, A. 1986, Astron. Astrophys. 158, 45
29. Meylan, G., Maeder, A. 1983, Astron. Astrophys. 124, 84
30. Pauldrach, A., Puls, J., Hummer, D.G., Kudritzki, R.P. 1985, Astron. Astron. Astrophys. 148, L1
31. Prantzos, N., Doom, C., Arnould, M., de Loore, C. 1986, Astrophys. J. 304, 695
32. Schild, H., Maeder, A. 1984, Astron. Astrophys. 136, 237
33. Stothers, R.B., Chin, C.W. 1985, Astrophys. J. 292, 222

INFLUENCE OF METALLICITY ON THE POPULATION OF WR STARS

P. ARNAULT, D. KUNTH
Institut d'Astrophysique, 98bis, bd Arago, 75014 Paris, France

H. SCHILD
Royal Greenwhich Observatory, Herstmonceux Castle,
Hailsham, East Sussex BN27 1RP, England

Abstract.

We present synthetic populations of massive stars for the solar neighbourhood, the LMC and the SMC and compare the results with the observed stellar populations. We particularly concentrate on calculated and observed numbers of Wolf-Rayet stars in different chemical environments. We conclude that present WR scenarios and models of stellar evolution can reproduce these numbers reasonably well. The agreement is obtained if binaries are excluded.

1. INTRODUCTION

Star formation processes at large scales are best studied in Irregular and blue compact dwarf galaxies (BCDGs). Observationnally these objects offer the opportunity to study both the present-day star formation rate and the upper IMF (initial mass function) over scales of about 1 kiloparsec and under a wide range of metallicity conditions. We thus decided to develop a model that could reproduce the observational signatures of the ongoing star formation in late type and compact galaxies. In particular we require our model to match the ultraviolet stellar absorption lines that are observed in IUE spectra as well as the Wolf-Rayet optical bands detected in the optical around 4686 Å.

The framework of such a study is to construct an evolutionary model that assumes the IMF and a star formation scenario. The evolution of all the stars is calculated using theoretical stellar evolutionary tracks. The composite spectrum of the stellar population can then be computed as a function of time with the aid of a stellar spectra library. With such a tool we can study, as a backup, quantities such as the Lyman continuum photon production, the metallicity enrichment, the supernovae rate, the effective temperature of the ionizing cluster since a snapshot gives the exact distribution of stars according to types as a function of time.

Here we only aim to discuss the stellar evolutionary prescriptions of our model. One way to test our understanding of massive star evolution is to compare the model predictions with available observed massive star counts catalogues. Not only can we test the validity of the stellar evolutionary tracks but also the treatment of mass-loss, overshooting and their dependence on the metallicity. Once these tests are successfully conducted will we apply our models to distant galaxies such as the Irregulars and BCDGs.

2. STAR COUNTS

Counts of stars with masses larger than 15 $M_\odot$ are available for the Magellanic Clouds and the solar neighborhood within 3 kpc around the Sun. The most serious problem attached to these counts is that of completeness in particular for the Magellanic Clouds. For this reason we only considered stars with initial masses greater than 30 $M_\odot$ for the neighborhood zone (hereafter $\odot$) from Humphreys and Mc Elroy (1984). Counts for the Magellanic Clouds were derived from Lequeux (this conference) and obtained using the number of stars per kpc^2 in the solar neighborhood multiplied by the ratio of the integrated 1690 Å intrinsic luminosities $L_{1690}(\mathrm{LMC})/L_{1690}$ (1 kpc^2, $\odot$), Vangioni-Flam *et al.*, 1980). These star numbers are larger by a factor of about 10 with respect to those of Humphreys and Mc Elroy (1984). The numbers of WR stars n(WR) in the ⊙, the LMC and the SMC are taken from Hidayat *et al.* (1982), Breysacher (1981) and Azzopardi and Breysacher (1979) respectively. Table 1 lists all the adopted values. For the 3 regions the R ratios between n(WR) and the number of stars n(O) with masses $M > 30\ M_\odot$ will be compared with our model predictions. They are directly related to the upper mass limit of the IMF and the present-day star formation rate. They are also expected to depend on the metallicity through mass-loss and overshooting.

Table 1 : Star counts in the solar neighborhood and in the magellanic clouds.

		⊙	L M C	S M C
N (star > 30 $M_\odot$)		383	1800	340
N (WN)	single	13	59	2
	double	7	22	5
N (WC)	single	21	8	0
	double	9	10	1
References		1) 3)	2) 4)	2) 5)

References : 1) Humphreys and Mc Elroy; 2) Vangioni-flam et al.; 3) Hidayat et al.; 4) Breysacher; 5) Azzopardi and Breysacher.

3. THE MODEL

a) The stellar evolutionary tracks

The stellar evolutionary tracks are taken from Maeder for the ⊙ (1986, 1987). A grid of evolutionary tracks for a metallicity $Z = 1/10\ Z_\odot$ was kindly provided to us by Maeder to reproduce the star counts of the SMC. The WR scenario stems from Maeder's models where, at solar metallicity, stars more massive than $60\ M_\odot$ follow Conti's scenario whereas if $25\ M_\odot < M < 60\ M_\odot$ the stars leave the main sequence and reach the WR phase after they became RSG (Maeder 1981, 1986).

For SMC metallicities only stars with $M > 60\ M_\odot$ reach the WR stage. Note that at this point we have no scenario leading to WR in binary systems. The influence of metallicity in mass loss has been parametrized as

$$\dot{M} = (\dot{M})_{\odot} Z^{-0.5}$$

where $(\dot{M})_{\odot}$ is the mass loss in solar unit (Maeder, case B).

WR subtypes have been assigned following Maeder (1983) prescriptions on surface abundances.

b) The star–formation scenarios

We first checked that the influence of variations in the slope x and the upper mass M_{up} of the IMF was unimportant in relation to the quantities investigated here. We thus adopted x=2, M_{up}=120 $M_{\odot}$ and a lower limit cut–off of 15 $M_{\odot}$ to describe the IMF as a simple power–law function. The star formation rate has been described using two extreme scenarios :

— an "instant" burst (IB) where stars formed during the first 0.5×10^6 years and evolve along the HR diagram.

— a "continuous burst" (CB) where stars are formed at a constant rate. Computations are performed until the stellar population of massive stars reaches a steady phase. This occurs after about 7×10^6 years.

The results of the models are shown in Fig. 1 and 2 for stellar evolution at $\odot$ metallicity, including mass loss and overshooting effects. Figure 1 displays the R ratio of the number of WR stars with respect to that of stars more massive than 30 $M_{\odot}$ as a function of time for the IB scenario. After 3×10^6 years the first WR stars appear (WNL subtypes) and their number reaches a maximum at 5×10^6 years after the onset of the burst. At about 7×10^6 years no WR stars remain. During a short transition period of about 1 Myr the ratio raises to 0.5. At variance with this result the CB scenario shown in Fig. 2 indicates a constant R ratio of only 0.1 after a timescale of about 7×10^6 years. This R value is significantly smaller than that of the IB model. When SMC evolutionary tracks are used, only WN–types are produced and the R ratio decreases by a factor of about 20 with respect to solar metallicity models. As we emphasized before, the influence of the IMF slope is negligible to the R ratio. The same applies to the influence of M_{up} when varying within a reasonable range. We note however that for higher M_{up} the WR stars occur as early as 2×10^6 years after the onset of the burst.

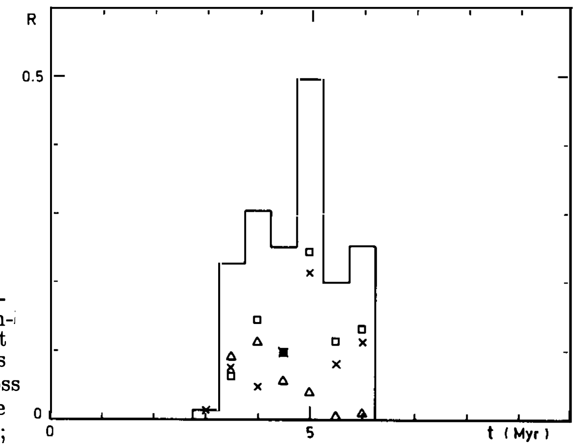

Fig.1:
Time evolution of the R ratio of WR over massive stars numbers for the instantaneous burst model. The evolutionary tracks include overshooting and mass loss effects at solar metallicity. The symbols used are : X ≡ WNL ; Δ ≡ WNE ; □ ≡ WC.

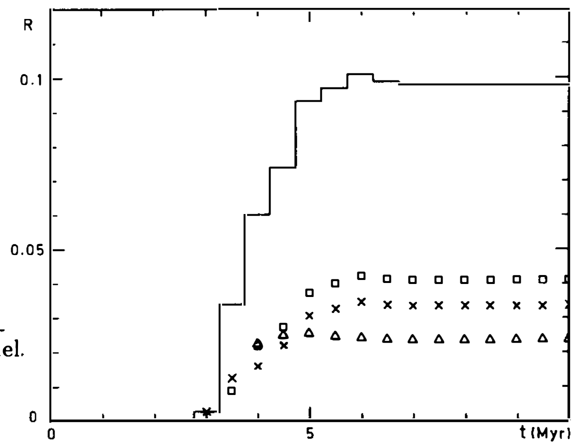

Fig.2 :
Time evolution of the R ratio of WR over massive stars numbers for the continuous burst model. The evolutionary tracks include overshooting and mass loss effects at solar metallicity. The symbols used are : X ≡ WNL ; Δ ≡ WNE ; □ ≡ WC.

4. COMPARISONS WITH OBSERVATIONS

In order to compare with star counts over large regions we have first considered the predictions of the CB models. This is partly because the occurrence of WR stars in the IB models seem implausibly too short therefore the agreement with observed values could be fortuitous. In Table 2 we give the available data for the ⊙, the LMC and SMC.

We have distinguished the single WR from the binaries WR since our models have no inference onto the binary formation. Note that for the SMC, Massey (1985) argues that only 2 out of the 8 known WR seem to be single. In the ⊙ and the LMC the ratio single/binary is estimated to be of the order of 0.5. With this word of caution regarding binarity we find that the CB models reproduce fairly well the observations for the 3 regions. This agreement is only obtained if binaries are excluded. It is conceivable that binary scenarios are increasingly important in very low metallicity environments and actually dominate the formation of WR stars.

Table 2 : Observed and theoretical ratios between WR and massive stars in the solar neighborood and in the magellanic clouds.

	⊙	L M C	S M C
Metallicity Z :	0.02	0.01	0.002
$R = N(WR)/N(star>30M_\odot)$:			
CB model	0.107	{0.057} {0.041}	0.0045
Observations	0.13 (0.02)	0.055 (0.004)	0.024 (0.005)
Without binary WR	0.09 (0.02)	0.037 (0.003)	0.0059 (0.002)

Note : { } These values of R are obtained from an interpolation between the calculated values for the ⊙ and the SMC. The upper value corresponds to a linear interpolation. The lower value corresponds to power-law approximation $R \propto Z^{1.37}$

( ) Values in parentheses are estimated statistical 1 σ errors on the star counts.

On the other hand, the IB models seem to be more adapted to star formation over small scales. Indeed because of the grainy nature of star formation processes, objects such as giant HII regions typified by 30 Dor or NGC 604 are not experiencing star formation events over periods longer than few 10^6 years (see Lequeux *et al.*, 1981). In other words an HII region is a local burst of star formation "in essence". Using Moffat *et al.* (1987) WR counts in 30 Dor and Lequeux's estimate of the number of O stars within the same region (this conference) we find that the R ratio is roughly 4 to 8 times greater than in the rest of the LMC. This leads to an age of 5×10^6 years according to the IB model. In this context the short-lived massive stars such as the WR can be used as age indicator of a small star forming region.

REFERENCES

- Azzopardi, M., Breysacher, J., 1979, Astron. Astrophys. 75, 120
- Breysacher J., 1981, Astron. Astrophys. Suppl. 43, 203
- Hidayat B., Supelli, K., Van der Hucht, K.A., 1982, IAU Symposium 99, 27
- Humphreys, R.M., McElroy, D.B., 1984, Ap. J. 284, 565
- Lequeux, J., Maucherat–Joubert, M., Deharveng, J.M., Kunth, D., 1981, Astron. Astrophys. 103, 305
- Maeder, A., 1986, Preprint
- Maeder, A., Meynet, G., 1987, Preprint
- Maeder, A., 1981, Astron. Astrophys. 102, 401
- Maeder, A., 1983, Astron. Astrophys. 120, 113
- Massey P., 1985, P.A.S.P. 97, 5
- Moffat, A.F.J., Niemela, V.S., Phillips, M.M., Chu, Y., Seggewiss W., 1987, Ap.J. 312, 612
- Vangioni–Flam, E., Lequeux, J., Maucherat–Joubert, M., Rocca–Volmerange, B., 1980, Astron. Astrophys. 90, 73

II. STAR FORMATION IN DWARF AND HII GALAXIES

STARBURSTS IN BLUE COMPACT DWARF GALAXIES

Trinh X. Thuan
Astronomy Department, University of Virginia

Abstract

We summarize all the arguments for a bursting mode of star formation in blue compact dwarf galaxies (BCD). We show in particular how spectral synthesis of far-ultraviolet spectra of BCDs constitutes a powerful way for studying the star formation history in these galaxies. BCD luminosity functions show jumps and discontinuities. These jumps act like fossil records of the star-forming bursts, helping us to count and date the bursts.

1. Introduction

Ever since their discovery by Sargent and Searle[1], blue compact dwarf (BCD) galaxies ($M_B \gtrsim - 18$) have been known to make massive stars in bursts: during a time short compared to the lifetime of the galaxy, the star formation rate (SFR) in some localized region or over the whole galaxy exceeds by several orders of magnitudes the SFR averaged over the lifetime of the BCD. Star formation in BCDs cannot be continuous but must proceed by bursts because of several observational contraints:

1) the amount of neutral gas available to feed the star formation process is $\sim 10^8\ M_\odot$[2]. Conversion rates of gas into stars in these galaxies are between 0.1 and 1 $M_\odot\ yr^{-1}$[3,4], so that the rate of star formation in the current burst cannot be maintained for more than $10^8 - 10^9$ years before the gas is depleted.

2) BCDs are all metal-deficient as compared to the solar neighborhood. They have metallicity ranging from $\sim 1/3$ to $\sim 1/30$ of the solar metallicity, with the abundance distribution peaking at $\sim 1/10$ of the solar value and dropping off sharply for metallicities less than $\sim Z_\odot/10$[5]. Assuming no removal of the metals from the regions where they are produced, star formation at the rate presently observed in BCDs would produce too much metals after $\sim 10^8$ years. In the case of the BCD IZw 18 = MKN 116 which is the most metal deficient BCD known ($Z \sim Z_\odot/30$), the amount of metals produced in the present burst of star formation already exceeds the amount observed after $\sim 4 \times 10^6$ years. Of course, the metallicity constraint on the age of bursts in BCDs is not as stringent if processes such as galactic winds can remove metals from these galaxies[6].

3) Optical-infrared colors of BCDs put strong constraints on the burst ages. Near-infrared colors are direct probes of the underlying older stellar population known to exist in BCDs[7,8,9,10], while optical colors are sensitive to the young stellar population responsible for the ionization of the gas. Infrared magnitudes, when combined with optical magnitudes, give infor-

mation on the relative importance of the young and old stellar populations, and hence on the past and present history of star formation in BCDs. Figure 1, taken from Thuan[8)], shows the location of different types of dwarf galaxies in the (U-B, V-K) plane.

To interpret the optical-infrared colors, the models of Struck-Marcell and Tinsley[11)] are used. These models describe the color evolution in time of a star formation burst of duration 2×10^7 yr, with a solar neighborhood initial mass function and superposed on an old galaxy with colors similar to that of E and SO galaxies (U-B = 0.56, V - K = 3.22). Each point in the (U-B, V-K) plane is characterized by two parameters: the first is the strength b of the burst, defined as the ratio of the mass of stars made during the burst to the

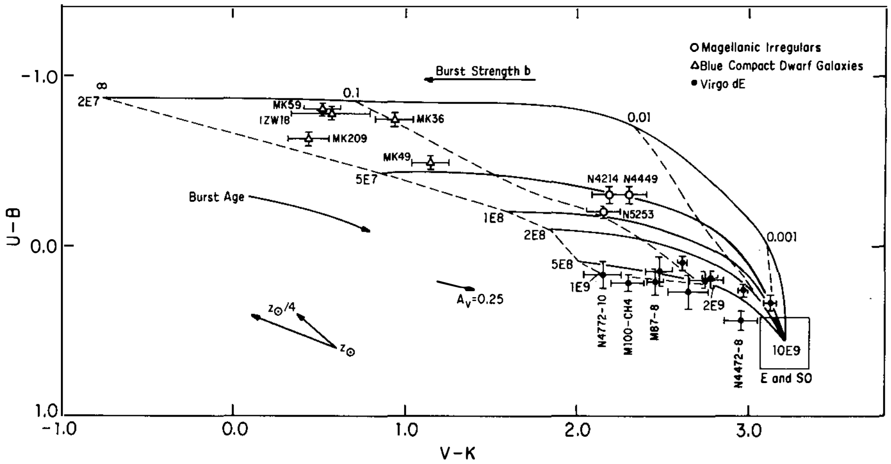

Figure 1. The infrared-optical (U-B, V-K) color-color diagram for dwarf galaxies [8)]. Burst models from Struck-Marcell and Tinsley[11)] have been drawn. The star formation bursts have a duration of 2×10^7 yr, are described by a solar neighborhood IMF, and occur in an old galaxy with U-B = 0.56 and V-K = 3.22. Each dashed line is the evolutionary track of a burst of strength b passing through the ages indicated on each solid line. Arrows indicate the effect of interstellar reddening and two estimates of the effect of reducing the metallicity by a factor of 4.

mass in the old galaxy, and the second is the time elapsed since the beginning of the burst, or its age. We should note that Struck-Marcell and Tinsley's models do not include the light contribution from red supergiants and therefore overestimate the real burst strengths. The numbers derived for b should thus be considered as upper limits. The burst ages should be accurate.

It is clear from Figure 1 that, of all dwarf galaxies, BCDs have the smallest burst ages τ (all less than $\sim 5 \times 10^7$ yr) and the largest burst strengths b (more than one tenth of the mass of the galaxy participates in the burst). Then come, in order of increasing burst ages and decreasing burst strengths, the dwarf magellanic irregulars ($10^7 \lesssim \tau \lesssim 10^8$ yr, $0.01 \lesssim b \lesssim 0.1$) and the Virgo dwarf elliptical galaxies ($10^9 \lesssim \tau \lesssim 8 \times 10^9$ yr, $b \gtrsim 0.1$). Thus optical-infrared colors of BCDs imply that bursts of star formation in these galaxies do not last much longer than $\sim 5 \times 10^7$ yr.

4) Finally, the young stellar populations as probed by ultraviolet spectra of BCDs can provide strong constraints on the star formation history in these galaxies[12]. Spectral synthesis of IUE BCD spectra also strongly supports the idea that star formation in BCDs occurs in bursts, as shown in detail in the next section.

2. Starbursts in BCDs: Constraints from far-UV spectra

A detailed review of the properties of far-ultraviolet spectra of BCDs, has been given by Thuan[12]. Two complementary approaches have been adopted to extract information from these spectra. The first approach, called 'evolutionary synthesis', consists of using the best available stellar evolutionary tracks and stellar atmospheres to calculate the time evolution of a composite spectral energy distribution (SED). The resulting SED depends on a small number of parameters which characterize a particular evolutionary scenario (for example continuous star formation or bursts) such as the slope of the initial mass function (IMF) and the e-folding time for star formation. The evolutionary models[13] which best fit the BCD data are those in which massive star formation occurs in bursts lasting between 1 and 5 x 10^6 years and with an IMF slope similar to that found in the solar neighborhood ($x \sim 1.5$ to 2 where x is defined by $dN/dM \propto M^{-(x+1)}$). There is no attempt in this approach to adjust the population parameters to obtain optimal fits to the SED.

The second approach, called 'optimizing synthesis', consists of deriving the stellar populations which best fit a SED, using linear or quadratic programming techniques which, in contrast to the evolutionary synthesis approach, permit to explicitly evaluate the goodness of fit and the uncertainties in the derived parameters. I report here some recent results obtained, in collaboration with M. N. Fanelli and R. W. O'Connell, by applying the optimizing synthesis method to the far ultraviolet spectra of a few BCDs, in particular, that of IZw36 = MK 209 [4] ($M_B = -14.0$) and of Haro 2 [2] ($M_B = -18.1$). Details on how to set up a far ultraviolet stellar library and on how to apply the linear programming techniques have been described elsewhere [12,14].

The results are shown graphically in Figure 2, in the upper panels for MK209 and in the lower panels for Haro 2. The horizontal axes show the 8 main-sequence groups in which the library stellar spectra have been binned. These groups were chosen by minimzing the cosmic dispersion of the stellar spectra within a group while maximizing the difference with neighboring groups without leaving gaps along the main sequence, and are intended to represent specific locations in the color-magnitude diagram[14]. Although giant and supergiant groups were also included in the stellar library, the synthesis program did not pick them out in the specific cases of MK209 and Haro 2. The horizontal axes also give the mean absolute visual magnitude corresponding to each main-sequence group. The vertical axes give the numbers of stars within the 10" x 20" IUE aperture in each group as derived from the spectral synthesis of the far-UV spectra, divided by the range in absolute visual magnitude ΔM_V of each stellar group. In other words, the vertical axes give the stellar luminosity function in each BCD.

The open circles correspond to the best unconstrained model obtained by

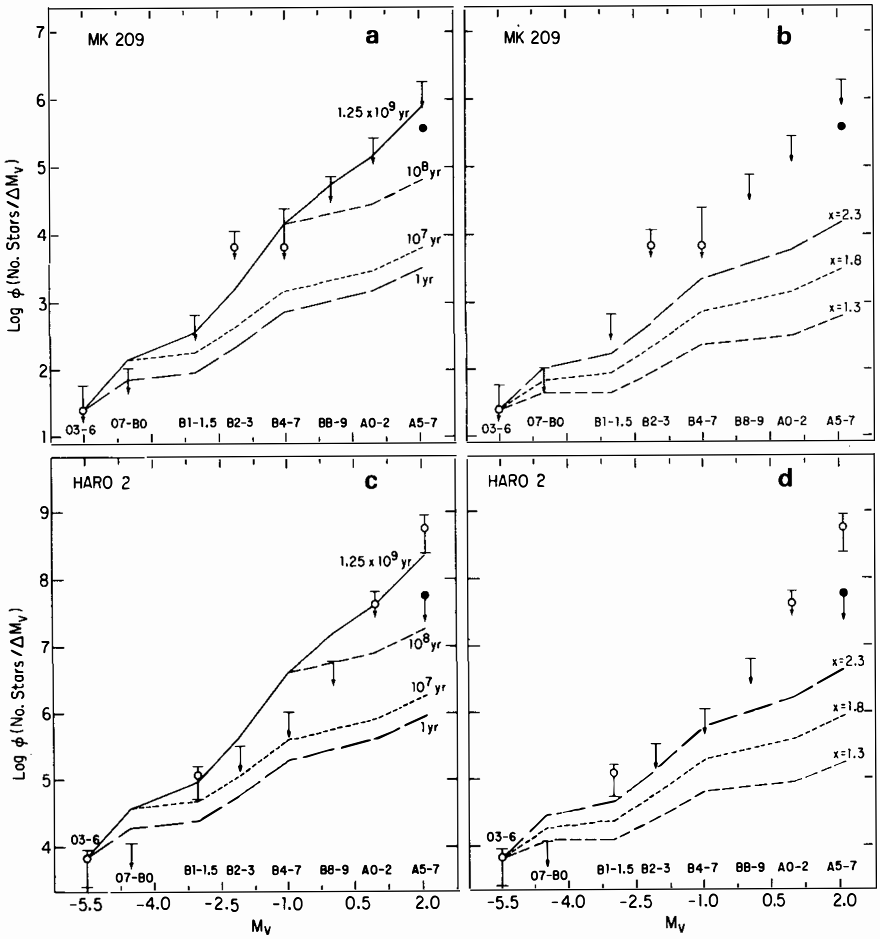

Figure 2. The luminosity functions (open circles) derived from spectral synthesis of the far-UV spectra of the BCDs MK209 (Figures 2a and 2b) and Haro 2 (Figures 2c and 2d). The filled circles represent the number of A5-7V stars when optical color constraints are added. The error bars correspond to 3σ limits (see text). Two sets of star formation models normalized to the O3-6V group have been superposed on the data points: a) a set of continuous star formation models with durations 1 yr, 10^7 yr, 10^8 yr and 1.25 x 10^9 yr and an IMF with x = 1.8 (Figures 2a and 2c) and 2) a set of infinitely short burst models with IMF slopes characterized by x = 1.3, 1.8 and 2.3 (Figures 2b and 2d).

varying the amount of intrinsic extinction E(B-V) until the best fit to the observed spectrum is obtained. This is done by minimizing the quantity $\varepsilon = 100 \sum r_i$ where r_i is the absolute fractional flux residual between the model and the observed galaxy spectrum at the i^{th} wavelength. The best fits are obtained for E(B-V) = 0 for MK209 and E(B-V) = 0.15 for Haro 2. These extinctions are much lower than the values of 0.24 (MK209) and 0.33 (Haro 2) derived from the Balmer decrement method and corrected for extinction from the Galaxy. The ultraviolet light, in contrast to the optical light, comes from regions nearly devoid of extinction.

The most important results of the synthesis work can be clearly seen in Figure 2: the best fit models give invariably a stellar luminosity function which is discontinuous. In the case of MK209, the synthesis program picks out the O3-O6V group, rejects the next two groups (O7-B0V and B1-1.5V), picks out the B2-3V and B4-7V groups, but rejects the B8-9V, A0-2V and A5-7V groups. For Haro 2, only the O3-O6V, B1-1.5V, A0-2V and A5-7V groups are selected. The remaining groups are rejected. The reality of these breaks is demonstrated by forcing the program to produce smooth luminosity functions. The resulting fits are always much worse.

In order to compare the synthesis results with simple star formation models, it is useful to provide error bars to the open circles in Figure 2. 'Maximum allowable' or 'minimum allowable' amounts of a given population component can be determined by forcing the best model to include or exclude successively larger light contributions from it until ε is increased or decreased by a factor of 3. In the linear programming fitting procedure, this is equivalent to a 3σ upper or lower limit in the conventional least-squares technique[15]. For some open circles, especially in the case of MK209, a lower limit cannot be obtained because the corresponding stellar group can be removed completely without exceeding the 3ε limit. This situation occurs more often for MK209 than for Haro 2, because the best fit model for MK209 has an ε twice as large as that for Haro 2 (ε = 7.2 compares to 3.5). This larger value of ε is due to the difference in metallicity between the stars in the library ($Z \sim Z_\odot$) and MK209 ($Z \sim Z_\odot/10$). The fit is better for Haro 2 because it has a metallicity nearer to solar ($Z \sim Z_\odot/3$). The data point in the last bin, the number of A5-7V stars, is very uncertain because of the very small light contribution of this stellar group to the BCD far-ultraviolet spectra. We have used the BCD optical colors[2] to reduce the uncertainty in the A5-7V stellar group. The data points resulting from this added constraint are plotted as filled circles in Figure 2.

To interpret the synthesis results, we consider two limiting types of models for star formation[4]. The first type of model examines the case of continuous star formation (CSF) where stars are formed continuously with a constant star formation rate during a time τ. Models with 4 different τ varying from 1 yr to 1.25×10^9 yr have been computed. All CSF models have an IMF slope with $x = 1.8$. This is the slope of the solar neighborhood mass function in the stellar mass range of interest[16] ($2 \lesssim M/M_\odot \lesssim 100$). The second type of model examines the case of an infinitely short burst (ISB). IMF slopes with x varying from 1.3 to 2.3 have been considered in ISB models. All models have been normalized to the data point corresponding to the O3-6V stellar group.

We first compare the synthesis results with the CSF models. The most stringent constraint on these models comes from the absence of the O7-BOV group in both BCDs. This absence excludes all CSF models in the case of Haro 2 (Figure 2c). CSF models with $\tau \lesssim 10^7$ yr can accomodate the upper limit for the O7-BOV group and also all the remaining groups in the case of MK209 (Figure 2a). We next discuss the ISB models. Again, all the ISB models can account for the MK209 data points when the error bars are taken into account (Figure 2b), although the IMF cannot have a slope much steeper than $x = 2.3$. In the case of Haro 2, ISB models with $x > 1.3$ fail to account for the absence of the O7-BOV group. The ISB model with $x = 1.3$ can barely accomodate the upper limit for the O7-BOV group, but fails to predict enough stars in the B1-1.5V group (Figure 2d).

In summary, neither CSF nor ISB models can account for the discontinuities in the stellar luminosity function of Haro 2. To account for these jumps, several independent bursts of star formation must be postulated. The O3-6V stars would be formed in the present burst. The B1-1.5V stars would come from a burst which happened ∿ 15 million years ago while the A0-2V stars would have their origin in a burst occuring ∿ 5×10^8 years ago. In this scenario, the jumps in the luminosity function are like fossil records of all the previous bursts in the past history of the BCD.

The story for MK209 is not as clear-cut because of the lack of lower limits to the data points. Nevertheless, its stellar luminosity function can be explained by a single burst (the present one) with an age $\tau \lesssim 10^7$ years and with an IMF whose x ∿ 1.8. The preceding burst age is consistent with the one derived using optical-infrared colors[7)] (Figure 1). The amount of metals produced during that time scale is also in good agreement with that observed[4)]. If we accept the interpretation that the present burst is the first one in the lifetime of MK209, then the presence of an underlying older stellar population which is much more spatially extended than the star-forming region would imply a bimodal mode of star formation in the BCD, where massive and low mass star formation are decoupled[10)].

We conclude that spectral synthesis of ultraviolet spectra offers a very powerful way for studying the star formation history in BCDs. Not only can we count the number of bursts in each BCD but we can also date them by the location of the jumps in the luminosity function.

Acknowledgements

I am grateful to R. W. O'Connell and M. N. Fanelli for allowing me to present our joint work. This work has been supported in part by NASA grant NAG 5-257 and by Air Force Office for Scientific Research grant AFOSR 85-0125.

References

1) Sargent, W. L. W. and Searle, L. 1970, Ap. J. (Letters), 162, L155.

2) Thuan, T. X. and Martin, G. E. 1981, Ap. J., 247, 823.

3) O'Connell, R. W., Thuan, T. X. and Goldstein, S. J. 1978, Ap. J. (Letters), 226, L11.

4) Viallefond, F. and Thuan, T. X. 1983, Ap. J., 269, 444.

5) Kunth, D. and Sargent, W. L. W. 1986, Ap. J., 300, 496.

6) Vader, J. P. 1987, Ap. J., 317, 128.

7) Thuan, T. X. 1983, Ap.J., 268, 667.

8) Thuan, T. X. 1985, Ap. J., 299, 881.

9) Loose, H. H. and Thuan, T. X. 1986, in Star-Forming Dwarf Galaxies and Related Objects, eds. D. Kunth, T. X. Thuan and T. T. Van (Editions Frontieres), p. 73.

10) Thuan, T. X. 1987, in Nearly Normal Galaxies, ed. S. Faber (Springer Verlag), in press.

11) Struck-Marcell, C. and Tinsley, B. M. 1978, Ap. J., 221, 562.

12) Thuan, T. X. 1986, in Star-Forming Dwarf Galaxies and Related Objects, eds. D. Kunth, T. X. Thuan and T. T. Van (Editions Frontieres), p. 105.

13) Lequeux, J., Maucherat-Joubert, M. Deharveng, J. M. and Kunth, D. 1981, Astr. Ap., 103, 305.

14) Fanelli, M. N., O'Connell, R. W. and Thuan, T. X. 1987, Ap. J., in press.

15) O'Connell, R. W. 1980, Ap. J., 236, 430.

16) Miller, G. E. and Scalo, J. M., Ap. J. Suppl., 41, 513.

NEW HIGH-RESOLUTION HI OBSERVATIONS OF I Zw 18 AND I Zw 36

F. Viallefond[1,2], J. Lequeux[3], G. Comte[3]

[1] Observatoire de Meudon, DEMIRM, F-92195 Meudon Principal Cedex, France

[2] Visiting Astronomer, Very Large Array, National Radio Astronomy Observatory Socorro, New Mexico, NM 87801, U.S.A.

[3] Observatoire de Marseille, 2 place Le Verrier, F-13248 Marseille Cedex 04, France

ABSTRACT

The blue compact galaxies I Zw 18 and I Zw 36 have been observed in 21 cm line with the configurations B and C of the Very Large Array* synthesis telescope, achieving resolutions of 5" x 5" x 12 km s^{-1}. The new maps reveal extremely dense HI clumps located on the edge of the locus of the stellar formation bursts. The mass derived from the ordered part of the velocity field is of the order of 13 times the total HI mass in I Zw 18.

*The Very Large Array is one of the facilities of the National Radio Astronomy Observatory, operated by Associated Universities, Inc., under contract with the National Science Foundation.

Introduction

The blue compact galaxies (BCG's) I Zw 18 and I Zw 36 are by now considered as prime examples among the large class of star-forming dwarf objects. Let us simply recall that one of the chief interests in studying BCG's is the search for genuine "primeval" or "young" galaxies, that is, objects being forming their very first generation of stars from the primeval purely gaseous protogalactic clumps.

I Zw 18, whose interstellar metallic abundance is only 1/40 of the solar one, exhibits the case for the most metal-poor active star-forming galaxy known to date, and yet its abundance is still too large for its gas not having been contaminated by some enrichment from stellar nucleosynthesis products[1,2,3]. Obviously, the study of the dynamical state of the gas in some extreme cases of BCG's could shed some light on the processes of formation and early evolution of galaxies; the important gaseous content of BCG's[4,5,6] favors 21 cm line observations.

Following previous 21 cm line supersynthesis at Westerbork with about 35 arc seconds resolution[7,8], we have undertaken a new program with the Very Large Array, devoted to higher spatial and spectral resolution observations of I Zw 18 and I Zw 36; we report here some preliminary results.

The observations were conducted in 1986 with the B and C configurations of the antenna array, yielding respective FWHM beams of 5".2 x 5".2 and 12" x 12" at 21 cm. The velocity resolution was fixed at 12 km s^{-1}. Data cubes produced by both configurations were merged to produce final maps with enhanced signal-to-noise ratio.

I Zw 18

The Westerbork observations[7] delineated an extended, elongated HI cloud of 2 x 1 arc minutes at the detection threshold of 95 K.km s^{-1} (1.7 10^{20} at.cm^{-2}), some structure was evident throughout this cloud; a provisional interpretation was given, based on the convolution of the beam with six clumps, two of which being extended. The main HI core was found only approximately centered on the brightest optical patch.

The new VLA map is displayed in Fig. 1, with a final resolution of 8 x 8 arc seconds, and a detection threshold of 100 K.km s^{-1} (1.8 10^{20} at cm^{-2}). A lot of substructure is present within a principal, elongated cloud of 60"x30", surrounded by several small clumps whose individual extents are about one beam area, one of them being larger, as an appendage at the SW end of the main cloud.

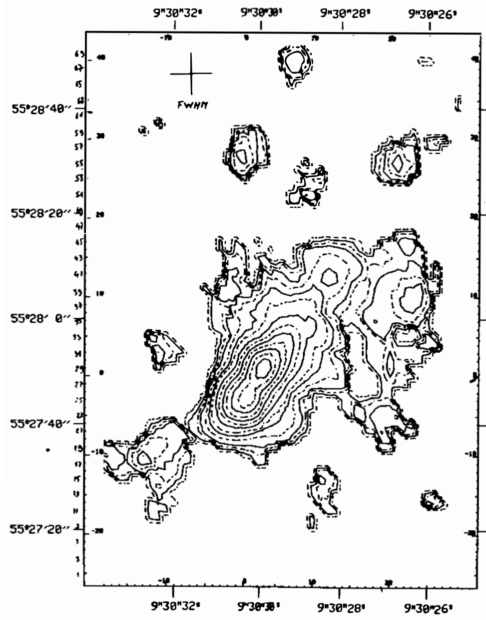

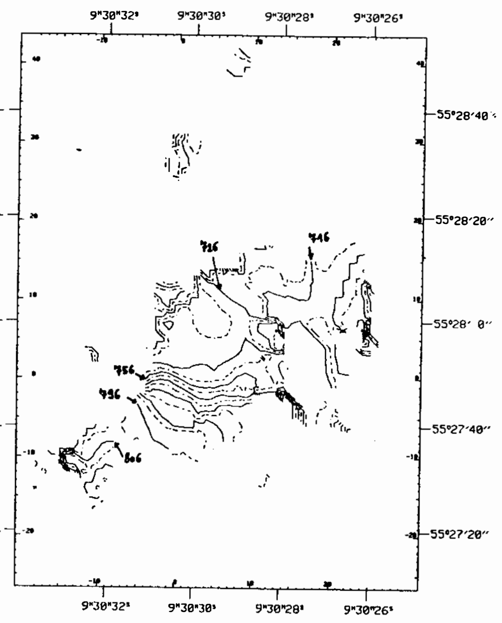

Fig. 1

Fig. 2

I Zw 18: total HI (left) and velocity field (right)

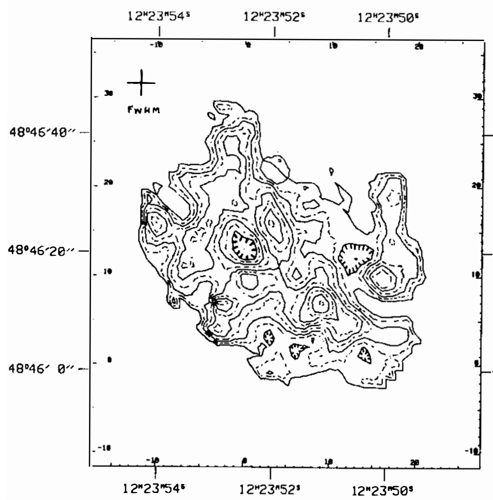

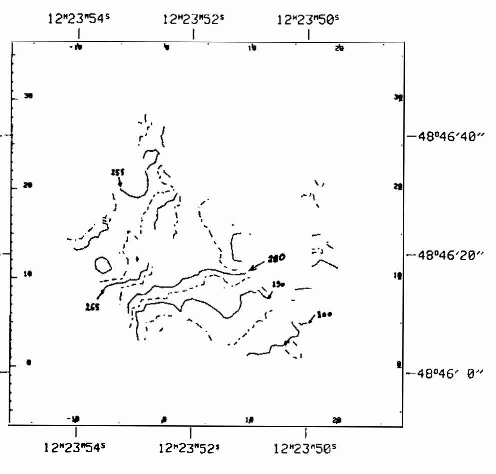

Fig. 3

Fig. 4

I Zw 36: total HI (left) and velocity field (right)

The main cloud encompasses all the detected optical structure of the galaxy; at the detection threshold, its outer limit coincides roughly, in its southern half, with an outermost isophote on a very deep CCD blue frame taken in 1982 with the Canada France Hawaï 3.6 m telescope (courtesy L. Vigroux), whose limiting surface brightness is about 27.5 B mag arc sec^{-2}. The HI is more extended than the optical image on the west. The peak HI density is clearly displaced from the peak optical brightness; the secondary faint optical patch at the NW also coincides with a depression in HI surface density. (Positional accuracy of the optical features with respect to the radio map was insured by astrometric measurements of a dozen stars in the field, enabling a precision of about 0.3 arc sec r.m.s.)

The peak value of the HI column density, in the core of the main HI cloud, is extraordinarily high: more than 3800 K.km s^{-1} on Fig. 1, but on the original 5".5 x 5".5 B configuration full resolution map it reaches 5500 K.km s^{-1} (about 10^{22} at. cm^{-2}), is still unresolved, and it is likely that the line is saturated, in which case these figures are only lower limits to the column density. This unresolved clump, whose diameter at 10 Mpc is smaller than 270 pc (B configuration projected FWHM beam), contains more than 4.4 10^6 $M_\odot$ of HI gas with a mean volumic density larger than 18 cm^{-3}.

The velocity field across I Zw 18 is displayed in Fig. 2; an overall fairly regular radial velocity gradient is seen over the main HI cloud; assuming that this gradient is due to rotation we derive a Keplerian spherical mass of 8.9 10^8 $M_\odot$ within a radius of 31" (1.55 kpc), about 13 times the total HI mass of 6.7 10^7 $M_\odot$ [7]. However, a position-velocity cut along what could be called the optical major axis (best major axis of the principal optical feature in P.A. 328°) shows blobs of gas departing conspicuously from the main ridge associated with the regular velocity gradient, suggesting lots of turbulent and/or infall motions.

I Zw 36

The Westerbork observations[8] showed a large HI cloud 3' x 2' in extent, about 4 times larger as the optical image seen on the Palomar Observatory Sky Survey, with evidence for several subcomponents, and a rather chaotic velocity field. A companion cloudlet with no optical counterpart was detected at 2' NE. The detection threshold was 40 K.km s^{-1} (7.5 10^{19} at. cm^{-2}).

The VLA map, pictured in Fig. 3, has 5".2 x 5".2 resolution and a detection threshold of 300 K.km s^{-1} (5.5 10^{20} at. cm^{-2}): any low-brightness extended emission seen on the Westerbork map is thus likely to be lost on this map.

The overall HI distribution is approximately elliptical in shape, with a series of high-density clumps and a deep hole, marginally resolved, in the northeast half. The centroid of the optical emission coincides with a minimum in the HI distribution; the maximum HI density peaks at 3100 K.km s^{-1} (5.7 10^{21} at. cm^{-2}) in a marginally resolved clump containing about 1.3 10^6 $M_\odot$ of HI gas with a mean density of 28 cm^{-3}.

The velocity field in the central part is once more fairly regular (with some evidence for non-rotating motions on a major axis position-velocity cut) and yields a Keplerian spherical mass of 7.7 10^7 $M_\odot$ at 4.6 Mpc over a 18" radius (or .8 kpc), to be compared to a total HI mass for the central cloud only of $\sim$ 2.2 10^7 $M_\odot$ [8].

As a comparison with I Zw 18 and I Zw 36, we recall that the major extragalactic HI complexes known to date have much lower mean densities:[9] NGC 604 contains 1.6 10^6 $M_\odot$ in an 300 pc diameter cloud with $\langle n_H \rangle \simeq 7$ cm^{-3}, cloud L16 in NGC 4449 contains 3.7 10^6 $M_\odot$ in an 410 pc diameter cloud with $\langle n_H \rangle \simeq 8$ cm^{-3} and NGC 5471 in M101 has 8.6 10^7 $M_\odot$ in an 1640 pc diameter cloud with $\langle n_H \rangle \simeq 1.2$ cm^{-3} only.

Acknowledgements

We are deeply indebted to many people at the VLA site for obtaining and calibrating a considerable part of the data in absentee observing mode.

References

1) Searle, L., Sargent, W.L.W. 1972, Astrophys. J. 173, 25
2) Davidson, K., Kinman, T.D. 1985, Astrophys. J. Suppl. Ser. 58, 321
3) Kunth, D., Sargent, W.L.W. 1986, Astrophys. J. 300, 496
4) Gordon, D., Gottesman, S.T. 1981, Astron. J. 86, 161
5) Thuan, T.X., Martin, G.E. 1981, Astrophys. J. 247, 823
6) Kinman, T.D., Davidson, K. 1981, Astrophys. J. 243, 127
7) Lequeux, J., Viallefond, F. 1980, Astron. Astrophys. 91, 269
8) Viallefond, F., Thuan, T.X. 1983, Astrophys. J. 269, 444
9) Viallefond, F., Goss, W.M., Allen, R.J. 1982, Astron. Astrophys. 115, 373

SOME IDEAS FOR THE CHEMICAL EVOLUTION OF IZw18

Irini Pantelaki and Donald D. Clayton
Department of Space Physics and Astronomy
Rice University, Houston, Texas 77251

Abstract. We present calculations of a simple scenario for dwarf irregular galaxies like IZw18 that can explain the apparent paradox of having very low concentrations of CNO in HII regions of a current starburst and yet have nearly solar ratios for C/O and N/O. We calculate concentrations in a hot ambient medium containing primordial clouds, whose collisions initiate new starbursts, and then argue that about 1% of today's clouds have been admixed from that hot medium.

1. Introduction

Observation of ultraviolet emission lines of [NII] and [CIII] from the dwarf irregular galaxy IZw18 by Dufour [1] has motivated the study of chemical evolution to be reported here. Despite the extremely low concentration X_0 of oxygen in the HII regions, the abundance ratios N/O and C/O are even greater than in other moderately metal-poor dwarf galaxies (e.g. LMC and SMC). This observation alone rules out the possibility that the present starburst in IZw18 is its first one, just as it also rules out the suggestion by Kunth and Sargent [2] that the HII regions observed are contaminated by supernova ejecta from its present starburst. A galaxy characterized by almost solar ratios C:N:O at concentrations some forty times smaller than solar poses a severe and interesting problem in the chemical evolution of galaxies. We propose here an interesting historical scenario that may find application to the problems of dwarf irregular galaxies in general and of IZw18 in particular. Our approach will be to consider a two-phase interstellar medium, HI clouds surrounded by a matrix of hot unseen gas, and to specify assumptions that allow us to calculate the chemical compositions of both. Our postulated hot medium continuously loses mass by way of a coronal wind, whereas the otherwise primordial HI clouds are only slowly enriched in CNO by admixing from the surrounding hot matrix.

Consider the following configuration today for a dwarf irregular galaxy. Past bursts of star formation have left a mass $M \gtrsim 10^8\ M_\odot$ of mostly low-mass stars in some irregular elliptical bulge. This gravitating system supports about $M_g \sim 10^5\ M_\odot$ of hot ($T \sim 10^6$ K) gas throughout a volume somewhat larger than that of the stars. This hot medium is however continuously flowing away in a coronal type wind and is also continuously being replaced by mass loss from the stars formed in prior starbursts. The hot medium is kept hot even between starbursts by mechanical heating from Type I supernovae and by the kinetic energy imported to the mass lost from intermediate mass stars by the random ($v \approx 100$ km/sec) velocities of the old stars. These power inputs are found to be adequate to continuously remove the mass of hot medium, leaving only the $\sim 10^5\ M_\odot$ of hot gas that is in hydrostatic equilibrium in the gravitational potential of the stars. Also contained within the system is $\geq 10^7\ M_\odot$ of HI clouds, envisioned as some modest number of discrete units orbiting the center of mass of the stars. These HI clouds are considered by us to be remnants of compressed gas that remained unchanged by the initial starburst, which turned around the inflow and set the mass of a dwarf elliptical system [3]. Subsequent smaller starbursts are imagined to occur as a result of collisions of these clouds, which are, for the moment, considered to retain their initial primordial composition. This construction is consistent with star formation at late times in essentially primordial matter, as observed in IZw18.

The interpretation of the very low but nonzero CNO abundances observed in today's starburst is then interpreted by us as follows. The hot ambient medium contains large and usually variable concentrations X_O and X_C, which we calculate below. This ambient gas is mixed very slowly into the clouds, so that today about 1% of the cloud mass was gathered from the hot medium by mixing, resulting in cloud concentrations similar to those observed in IZw18.

2. Calculation for the proposed scenario

To be specific we assume that the dwarf galaxy has experienced six separate starbursts, spaced 10^9 yr apart, and thus having an age today of 5×10^9 yr. The first and largest starburst was associated with galaxy formation and limited the total mass by stopping and reversing infall [3]. The five subsequent smaller starbursts are in our calculations taken to be equal to the burst of star formation today, $2 \times 10^5\ M_\odot$. This mass for today's starburst results from taking a normal initial mass function and by creating enough O stars to provide the Lyman continuum. We took the initial starburst to be $7 \times 10^8\ M_\odot$.

Two other arbitrary characteristics were added to each starburst. Because it did not seem physically plausible to form each star at the same moment, we spread each starburst out uniformly over 10^7 yr. This seems a reasonable dynamic timescale for colliding clouds. We also must specify the mass of primordial cloud gas that was dispersed into the hot medium by the star formation process. We took $10^9\ M_\odot$ of hot gas created by the initial $7 \times 10^8\ M_\odot$ starburst, whereas the smaller subsequent bursts added $10^6\ M_\odot$ to the mass of the hot medium at that time. This dispersed cloud mass is removed from the galaxy by the supernova power, but, because its mass exceeds the $10^5\ M_\odot$ maintainable in hydrostatic equilibrium, it acts as a buffer to first absorb the early nucleosynthesis products of each starburst.

For this exploratory study we did not treat realistic hydrodynamics for a configuration that is, in real cases, poorly defined. We took a much simpler approach in order to facilitate rapid results. We assumed that the mechanical power P(t) in stellar ejecta is converted, after correction for radiative losses L(t), to wind power, so that we write

$$P(t) - L(t) = \frac{GM}{R} W(t) \qquad (1)$$

where W(t) is the mass loss rate from the galaxy of mass M and radius R. We take the wind W(t) to respond instantaneously to the power P(t), even though in realistic cases the supernova shocks first create bubbles of overpressure that only later drive winds. Another approximation made for simplicity is that the hot medium is well mixed at all times, so that the rate of loss of oxygen mass, for example, can be set equal to $X_0W(t)$. In truth, of course, a SNII creates an O-rich pocket that requires time for distribution throughout the volume. But the multiple occurrence of SNII, overlapping in the hot medium, vitiates this problem. We take the volume to be a sphere of radius R = 650 kpc. A simple calculation shows that in the large initial burst, supernovae collide before they cool, so that we take $P - L = 10^{51}$ ergs per supernova in Eq. (1). In the smaller later bursts we also ignored radiative cooling on the rather uncertain grounds that they expand into an already hot medium in their burst out of the HII complex.

It is easy to see that the SN power in a 2×10^5 $M_\odot$ starburst is adequate to remove the 10^6 $M_\odot$ of gas cloud dispersed by it into the hot medium, because that starburst produces 950 Type II supernovae having a total mechanical input of $\sim 10^{54}$ ergs, which, for a dwarf of this size is adequate to remove 10^7 $M_\odot$ of medium. As a result, the wind following each starburst drives the medium mass down to the 10^5 $M_\odot$ remaining hydrostatically. Between the starbursts the intermediate mass stars are shedding a lot of mass into the medium, but the mechanical power associated with it and with a steady rate of Type I SN is found to be adequate to continuously drive the medium away. The chemical effects will be great, however, because between bursts the O-rich supernova ejecta is replaced by C-rich and N-rich ejecta from the intermediate-mass stars, producing a concentration history that is novel in studies of chemical evolution.

During the bursts we calculate a mass for the hot medium, taking it to satisfy

$$dM_g/dt = E(t) - W(t) \tag{2}$$

where E(t) is the ejection rate from stars, and where the boundary condition on M_g for each burst is determined by the mass of cloud that was dispersed into it by the starburst. The well-mixed metallicity Z of the hot medium derives from

$$\frac{d}{dt}(ZM_g) = E_z(t) - Z(t)\,W(t) \tag{3}$$

where $E_Z(t)$ is the ejection rate of element Z. With the aid of Eq. (2) this equation is transformed to $M_g\ dZ/dt = E_z(t)-Z(t)E(t)$, which is the equation that we integrate. The Type II SN are derived from 10-100 $M_\odot$ progenitors whose deaths are not mass ordered because of the spread of 10^7 yr in the starburst. The oxygen yield and supernova power are therefore distributed over a 3×10^7 yr period beginning with the explosion of a massive star formed near t = 0 in the burst and ending with explosion of a 10 $M_\odot$ star that was born at t = 10^7 end of the burst.

It is an important ingredient of our calculation that carbon is produced in both SNII and in intermediate-mass stars. We take the yields to be such that when averaged over the entire mass spectrum, as in a normal continuously evolving galaxy, half of the carbon originates in SNII and half of it in the intermediate-mass stars. We calculate explicitly the time dependence of carbon production because the deaths of those stars are mass ordered. This carbon ejection has the effect of maintaining the concentration of carbon in the hot medium, even as it replaces the gas ejected earlier in each starburst from the SNII.

Figure 1 illustrates the magnitude and time dependence of both oxygen and carbon concentrations in the hot medium. The behavior of X_O is remarkable. Its rapid rise is normally expected as Type II supernovae begin; but the peak value, $X_O = 0.3$, is exceedingly large for such short times, and the subsequent precipitous fall is, as far as we know, unprecedented. How are these surprises to be interpreted? The key is the large wind driven by the SNII. It causes the hot-ISM mass to decline rapidly. The mass fraction X_O reaches a very large value very quickly precisely because it measures the concentration in the medium still remaining. The huge SN yield in the face of falling M_g results in the quick rise. This changing identity of the mass under discussion is also responsible for the equally sudden decline in X_O. The intermediate stars eject large amounts of mass after termination of the SNII, and that ejecta is oxygen free. The wind keeps carrying the medium away and diluting the rapidly declining amount of oxygen remaining with this oxygen free ejecta. The mechanical power can support a wind capable of holding M_g at 10^5 $M_\odot$ despite the $\sim 10^8$ $M_\odot$ of intermediate-mass-star ejecta placed into it during the first 10^9 yr after the termination of SNII from the initial starburst.

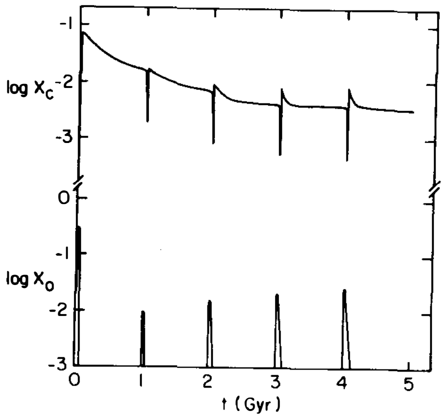

Figure 1. Concentrations of O and C in the hot medium as a function of time.

The situation for carbon is somewhat different. The value of X_C increases suddenly during the SNII bursts, but the intermediate-mass-star winds that drive down both oxygen and SNII carbon contain new carbon themselves. Therefore X_C does not fall to a low value between bursts. The sudden dip in X_C at the beginning of each burst, very narrow in time in Fig. 1, appears because we flooded the ISM at that moment with the mass of primordial cloud that is liberated to the hot medium in each starburst.

3. Discussion

Suppose that the primordial clouds move through the hot medium. Some of the hot medium will slowly mix through them by turbulence within the clouds. If we envision that admixing occurs at a constant rate over 5×10^9 yr, the resulting abundance in the clouds would be proportional to a time average of the abundance in Fig. 1, which yields a carbon abundance five times that of oxygen. According to Dufour's results for IZw18 the oxygen abundance is actually larger than the carbon abundance by a factor of 3. Although it is, therefore, very easy to explain within this scenario the surprisingly large abundance of C with respect to O, constant mixing yields an excessive C/O ratio. But a constant mixing rate may not be appropriate. During the bursts of star formation mixing may be enhanced owing to the enhanced turbulence in the hot medium. Oxygen-rich supernova shells may even cool and partially condense on the surfaces of the primordial clouds, giving C/O the observed value. The condensation of the SNII ejecta on the clouds may also have been enhanced by their position relative to these primordial clouds. It is reasonable to assume that the SNII products get ejected close to the HI clouds which presumably remain concentrated in the central region of the galaxy where the cloud collisions and starbursts occur, whereas the intermediate mass stars release carbon and nitrogen after their migration away.

A non-zero initial oxygen concentration may also produce more realistic C:N:O ratios. This may happen if we imagine pristine matter falling between outflowing channels of material from the initial burst of star formation. Turbulence between infalling and outflowing channels may change the composition of the former, which therefore reaches the galaxy with nonzero oxygen concentration and subsequently participates in the condensation of the clouds where the smaller bursts later occur. Much of todays C and N may then have been admixed as we described.

This research was supported by the Robert A. Welch Foundation

4. References

[1] R. J. Dufour, Publ. Astron. Soc. Pac., 98, 1025 (1986).
[2] D. Kunth and W. L. W. Sargent, Astrophys. J., 300, 496 (1986).
[3] R. B. Larson, Mon. Not. Roy. Astron. Soc., 169, 229 (1974).

Hα FABRY-PEROT INTERFEROMETRIC OBSERVATIONS OF BLUE COMPACT DWARF GALAXIES

Trinh X. Thuan
Astronomy Department, University of Virginia

T.B. Williams
Physics Department, Rutgers University

and

E. Malumuth
Space Telescope Science Institute

Hα Fabry-Pérot interferometric observations of the two blue compact dwarf galaxies (BCDs) 7 Zw 403 and 1 Zw 49 are presented. The velocity field of 7 Zw 403 shows no clear large-scale organized motion but the velocity field is not completely chaotic either. The gas associated with the 8 HII regions in 7 Zw 403 has neither the highest nor lowest velocities. The BCD 1 Zw 49 is dominated by a single HII region which is ~ 50 times brighter than any other feature in the galaxy. There is a chain of fainter HII regions extending across the galaxy. The velocity field is well ordered along the HII region chain, but it is very complex around the dominant HII region, suggesting Hα loops and filaments around the latter. Both BCDs show velocity gradients of ~ 25 km s^{-1} on scales of ~ 10 pc in 7 Zw 403 and of ~ 50 pc in 1 Zw 49. These velocity discontinuities compress the gas and are probably responsible for the star formation.

I. Introduction

It is now generally agreed that blue compact dwarf galaxies (BCDs) manufacture massive stars in intense bursts of star formation[1]. BCDs are ideal laboratories for studying close at hand the starburst phenomenon, because their masses are too small ($\lesssim 10^9\ M_\odot$) to sustain density waves and hence the study of starbursts in BCDs is not complicated by density-wave triggered star formation, as is the case in the Milky Way. Moreover, the high gaseous content[2] and low metallicity[1] of BCDs suggest that they are relatively young systems. This expectation is born out by detailed studies of their stellar populations (Loose and Thuan[3] found that the oldest stars in the BCD Haro 2 are only $\sim 4 \times 10^9$ yr old) and of their neutral gas spatial distribution which shows a clumpy, unrelaxed structure[4,5,6]. Thus BCDs may be prototypes of young galaxies and studying star formation processes in BCDs may help us to understand galaxy formation.

The triggering mechanisms of starbursts in BCDs are still completely unknown. It is clear that an understanding of such mechanisms can only be acquired through an understanding of the kinematics and dynamics of the atomic and molecular gaseous component in these galaxies. The neutral atomic hydrogen component can be studied with radio interferometers such as the Westerbork and the Very Large Array telescopes. These HI interferometric studies[4,5,6] have already given very interesting general results. The HI gas shows an irregular structure with very high density clumps and holes in the HI distribution. The gas density in these clumps can reach ~ 30 H atoms cm^{-3}, as compared to the range of 1-8 H atoms cm^{-3} found in HI complexes in nearby galaxies[5]. Although the main HI complex to which the starburst region is associated generally possesses a regular velocity gradient consistent with rotation, expansion or contraction motions, the velocity field of the outlying gas is not inconsistent with the notion that neutral hydrogen is infalling into the galaxy, creating a large-scale disturbance to its interstellar medium[4]. Larson[7] has argued that indeed both a high gas surface density and a large-scale disturbance to the interstellar medium of the BCD are necessary to trigger a burst of star formation. The high gas density shortens the star formation time scale and increases the efficiency for star formation. The large-scale disturbance feeds rapidly the gas into the starburst region.

The study of the ionized gas component in BCDs is a necessary complement to that of the neutral gas component. The ionized gas probes directly the kinematics of the starburst region and detailed comparison of the kinematics of the neutral and ionized gas can pinpoint the possible influence of stellar winds, supernovae and ionization on star formation. We discuss here the preliminary results of a program to obtain Hα Fabry-Pérot interferometric maps of blue compact dwarf galaxies. BCDs are particularly appropriate objects to study with a Fabry-Pérot interferometer because of their very strong and narrow Balmer emission lines and because their star-forming regions occupy nearly the entire galaxy or a large fraction of it.

II. Fabry-Pérot maps of blue compact dwarf galaxies

The objects were chosen from the list of Thuan and Martin[2] which gives the HI width for each BCD, an information which is useful for deciding the velocity range and resolution for our interferometric observations. Other criteria of selection included large angular size, strong Balmer line emission and interesting optical structure. We report here on the observations of 2 BCDs:

7 Zw 403 (V_H = - 92 km s^{-1}, M_B = - 13.5, d_{25} = 1'.7, Δv_{50} (HI) = 43 km s^{-1}) and 1 Zw 49 = MK59 = U8098 = Arp 266 = N4861 + I3961 (V_H = 905 km s^{-1}, M_B = - 17.3, d_{25} = 4'.1, Δv_{50} (HI) = 92 km s^{-1}). In the morphological classification scheme of Loose and Thuan[8], 7 Zw 403 belongs to the most common type of BCD, the iE type, with several centers of star formation and irregular (i) isophotes in the central region but with elliptical (E) outer isophotes. 1 Zw 49 belongs to the class of "cometary" galaxies, with a large dominant HII region in the "head", and a chain of smaller HII regions in the "tail".

The observations were carried out on the Mayall 4m telescope of the Kitt Peak National Observatory on the nights of April 26-30, 1986. The instrument used was the Rutgers Imaging Fabry-Pérot Spectrometer with a Texas Instruments 800x800 CCD detector, kindly loaned to us by Dr. J. Gunn. Briefly, the spectrometer accepts a 25 mm diameter field of view (~ 2.5' on the 4m), collimates the light, passes it through an order-selecting interference filter and a Fabry-Pérot etalon, and re-images onto the detector. The etalon used for these observations had a FWHM resolution of 0.82 Å at Hα and a free spectral range of 25 Å. The CCD detector operated with approximately 50% quantum efficiency at Hα, and with 12 electrons effective readout noise (including the photon noise of the approximately 100 electrons pre-flash employed). The image scale was 0.33" per pixel.

Both galaxies were observed in the Hα emission line and both had 11 exposures of 900s each. The exposures were spaced by 0.5 Å and went from 6558.2 Å to 6564.0 Å for 7 Zw 403 and from 6580.4 Å to 6586.9 Å for 1 Zw 49 to cover the emission line and nearby continuum. The images were corrected with flat-field and bias frames, and were spatially shifted so that all frames were aligned.

A line profile was extracted at each pixel in the image and the line was fit with a Gaussian of four parameters: line intensity, continuum intensity, velocity, and line width. Velocities accuracies, estimated both by the internal error parameters of the Gaussian fit and by the agreement of nearby, independent pixels, are better than 5 km s^{-1}, over most of the map.

Maps of the Hα line intensity and velocity are presented for the two galaxies. Figures 1 and 2 show the results for 7 Zw 403. The maps cover a region about 45" in size. This galaxy is dominated by 8 bright HII regions, immersed in fainter diffuse Hα emission. The peak of the brightest HII region is about 800 photons $pixel^{-1}$, while the diffuse emission is typically 50 photons $pixel^{-1}$ (Figure 1). The HII region diameters range from ~ 37 pc to ~ 92 pc, adopting for 7 Zw 403 the distance of the M81 group of 3.2 Mpc[9]. The spatially more extended underlying older stellar population clearly visible in a deep B CCD picture[8] is absent in the Hα picture.

The velocity map (Figure 2) is encoded with black at ~ -70 km s^{-1} and white at ~ -110 km s^{-1}. The Hα lines are generally unresolved ($\Delta v \lesssim 36.5$ km s^{-1}). It is clear from figure 2 that there is no simple over-all organization to the velocity field in 7 Zw 403. Along the major axis of the galaxy, black and white zones alternate with each other and there is no clear systematic variation of the ionized gas velocity from one end of the galaxy to the other. There is no overall rotation and turbulent random motions must be important. But although there is no clear large-scale organized motions, the velocity field is not clearly chaotic on smaller scales either. The Hα velocities show evident coherence in directions perpendicular to the major axis as can be seen by the bands of the same shading running across the galaxy. These bands

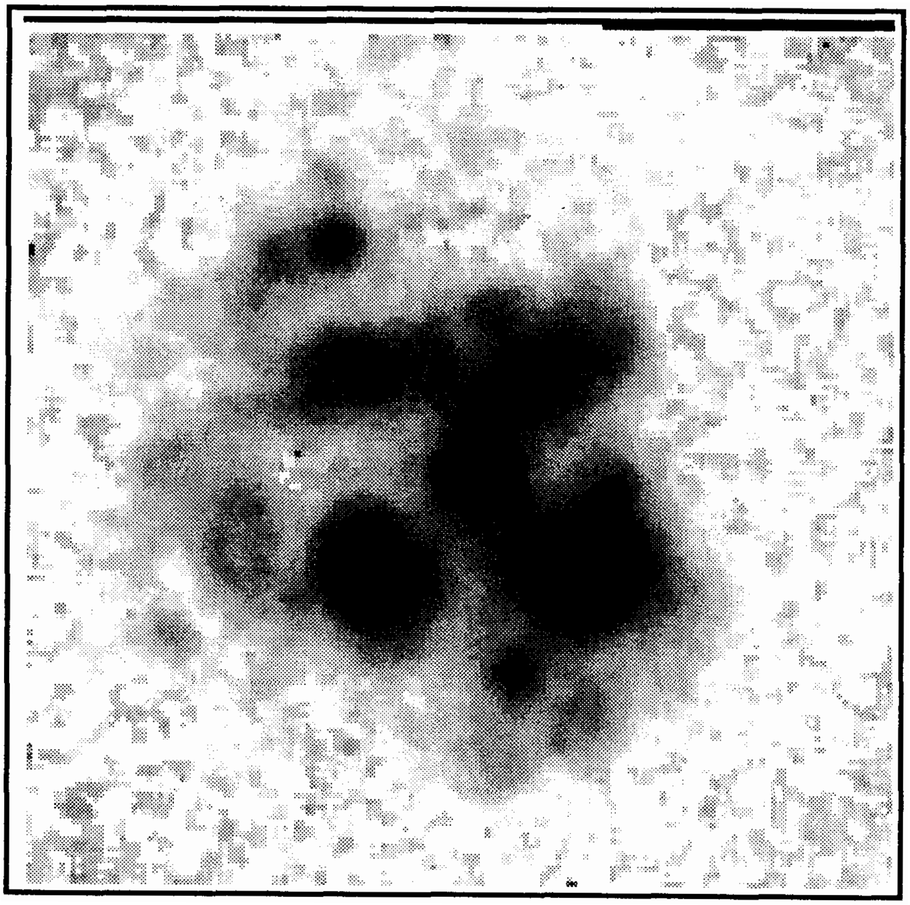

Figure 1 - Hα intensity map of 7 Zw 403. North is at bottom and East to the right. The map is 45"x45" in size. The galaxy is dominated by 8 bright HII regions, immersed in fainter diffuse Hα emission. The peak of the brightest HII region is about 800 photons pixel^{-1}, while the diffuse emission is typically 50 photons pixel^{-1}.

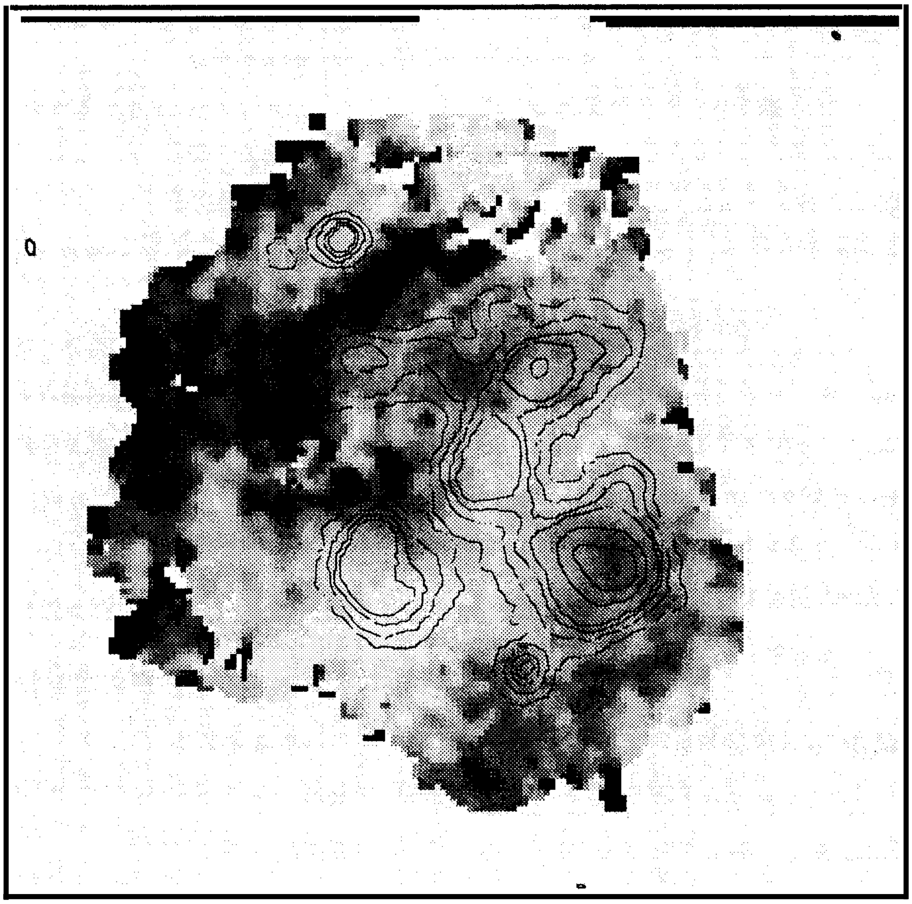

Figure 2 - Hα velocity map of 7 Zw 403 with the same orientation and scale as in figure 1. The velocity map is encoded with black at a heliocentric velocity of -70 km s^{-1} and with white at -110 km s^{-1}. There is no simple over-all organization to the velocity field. The Hα intensity contours are overlaid.

have sizes of ~ 70 x 320 pc. On yet smaller scales (10 to 20 pc), there are locations in the BCD where there are velocity gradients larger than 30 km s^{-1}. The corresponding dynamical time scale is only $\lesssim 10^6$ years, as compared to a burst age between ~ 2 x 10^7 and ~ 5 x 10^7 yr[1)]. A complex velocity field in such a predominantly gaseous system cannot be maintained much longer than several dynamical time scales. Thus the ionized gas in 7 Zw 403 cannot be in an equilibrium state and must have been stirred up by the ongoing starburst.

Figure 2 also shows the contours of the 8 HII regions superposed on the velocity map. An intriguing fact is apparent: the gas associated with the HII regions, sites of the youngest stellar populations in the BCD tends to have intermediate velocities, while both the highest and lowest velocity areas occur in the diffuse gas between the HII regions.

Figure 3 shows the Hα intensity map of 1 Zw 49. The longer dimension of the galaxy in Hα is ~ 65". There is a dominant HII regions whose diameter is ~ 185 pc, adopting a redshift distance of 7.2 Mpc (H_o = 75 km s^{-1} Mpc^{-1}) and which is ~ 50 times brighter than any other feature in the galaxy. This HII region is surrounded by complicated loops and filaments of Hα, suggestive of past supernova events. This impression is reinforced by the presence of large holes in the Hα distribution, with diameters varying from ~ 50 pc to ~ 280 pc, also suggestive of explosive events. A chain of 14 fainter and smaller HII regions with diameters between ~ 60 and 100 pc extends across the body of the galaxy. The HII region chain strongly suggests some type of self-propagating star formation which was stopped at the edge of the galaxy. The largest HII region in the Large Magellanic Cloud, 30 Doradus, may be very similar to the dominant HII region in 1 Zw 49, if the LMC was seen more

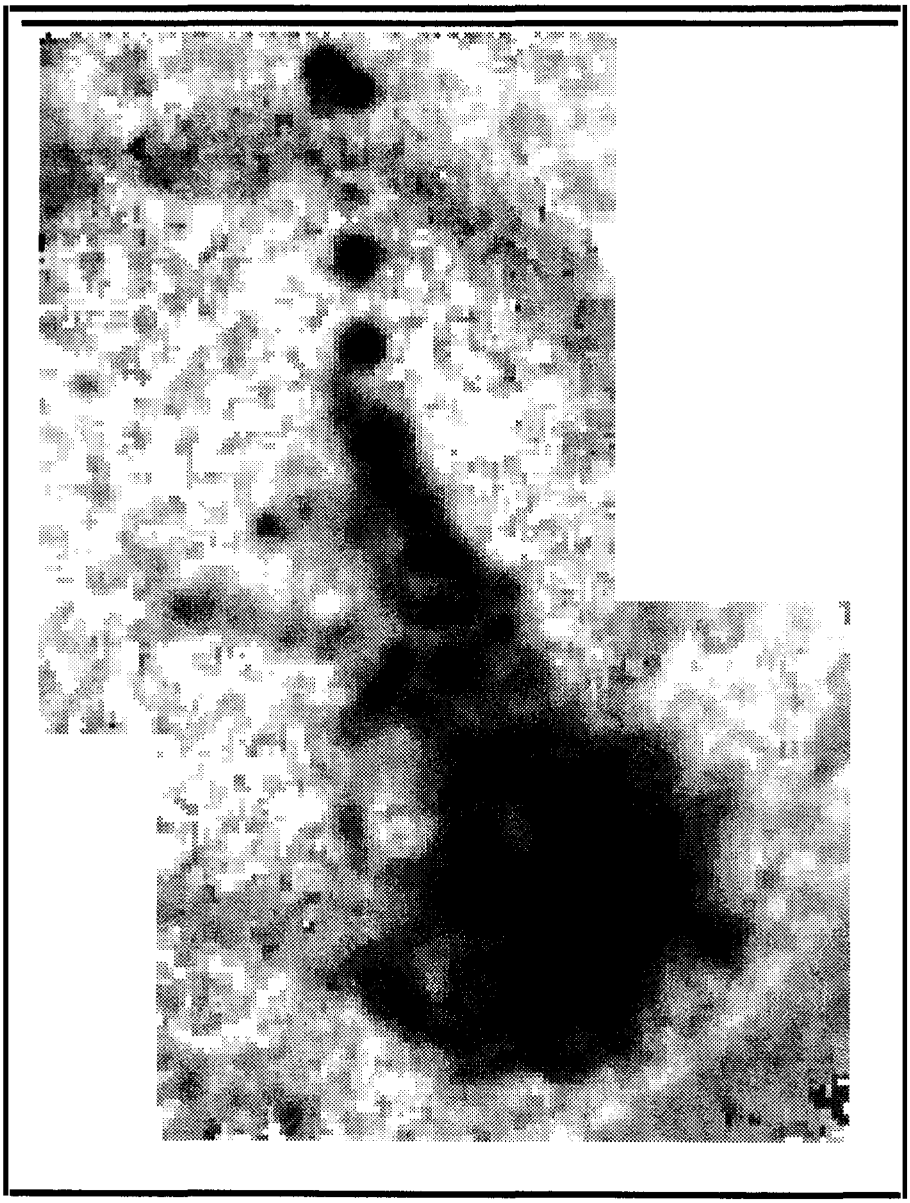

Figure 3 - Hα intensity map of 1 Zw 49. North is at the top and East to the left. The longer dimension of the object is ~ 65" in size. There is a dominant HII region followed by a chain of smaller HII regions immersed in diffuse emission. Hα loops and filaments can also be seen.

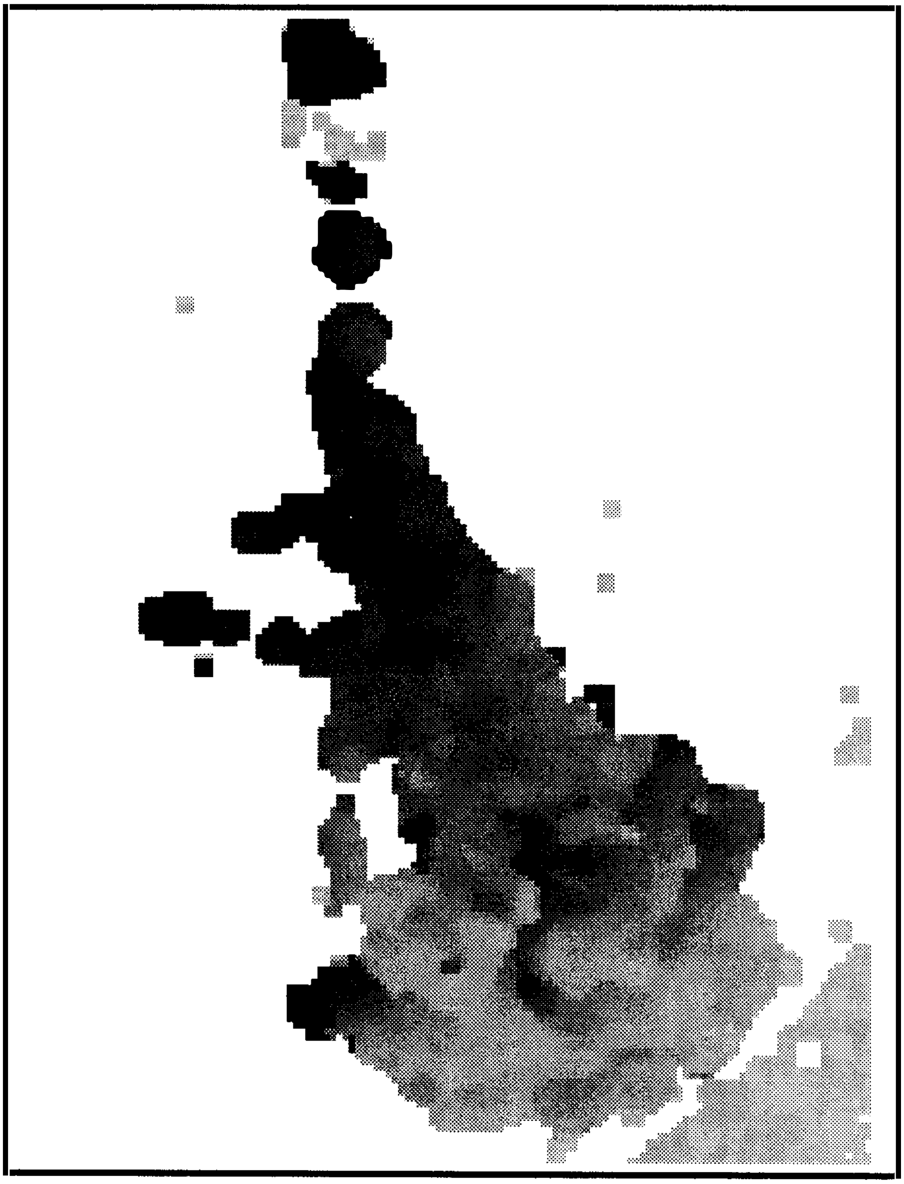

Figure 4 - Hα velocity map of I Zw 49 with the same orientation and scale as in figure 3. The velocity field is well-ordered along the HII region chain ranging from a heliocentric velocity of 848 km s^{-1} at the dominant HII region to 913 km s^{-1} at the other end. The velocity field around the dominant HII region shows a very complex structure, probably caused by the presence of Hα filaments lying either in front or behind the rest of the emitting gas.

edge-on. All HII regions, including the dominant one, are embedded in much fainter diffuse Hα emission. As in the case of 7 Zw 403, the much more extended older stellar populations clearly visible in a deep B CCD frame[8)] and whose diameter is ~ 4ʹ.1 is not seen in the Hα picture.

Figure 4 shows the Hα velocity field of 1 Zw 49. Contrary to the case of 7 Zw 403, the change of shading is more gradual and systematic along the major axis of the galaxy, reflecting a well-ordered velocity field along the chain of HII regions, ranging from a heliocentric velocity of 848 km s^{-1} at the very bright HII region to 913 km s^{-1} at the farthest end. This velocity field can be understood as the rotation of a disk galaxy viewed edge-on, with the bright end approaching and the faint end receding.

On this overall regularity in the velocity field on large scales, are superposed disordered motions on smaller scales. The velocity field around the dominant HII region is very complex. Detailed examination of the line profiles in this region suggests that they are double-peaked, which indicates that the filaments are distinct kinematic entities, probably lying either in front of or behind the rest of the emitting gas. We have not yet fitted two-component gaussians to the line profiles in this part of the galaxy, and thus the velocities displayed in figure 4 are averages over the double-valued velocity field in this region, doubtless giving rise to much of the complicated appearance of the velocity map here. As in 7 Zw 403, there are sharp velocity gradients ($\Delta v \sim$ 25 km s^{-1}) on scales of ~ 50 pc in some locations, again suggesting that the gas is not in equilibrium there. These sharp velocity gradients on small scales appear to be a general feature of star-forming dwarf galaxies. They are also seen in the blue irregular galaxies NGC 4214 and NGC 4449[10)]. These complex velocity fields are probably responsible for the star formation itself. The velocity jumps compress the gas, causing it to collapse and form stars.

Clearly, the Fabry-Pérot interferometric Hα intensity and velocity maps are rich in information and can teach us a great deal about star formation in blue compact dwarf galaxies. Their high spatial (~ 1".5 or 23 pc in 7 Zw 403 and 52 pc in 1 Zw 49) and velocity (~ 2.5 km s^{-1}) resolutions allow to probe smaller scales than is possible with the HI interferometric maps (the VLA beam with the B configuration is ~ 5" x 5", with a velocity resolution of 12 km s^{-1}) and to study the effects of the young stellar populations on the gas: dynamics of HII regions, effects of supernovae causing filamentary structure and holes, etc... These maps will also permit to ask such questions as: can the cloud motions be sustained by supernovae explosions or are additional sources of momentum needed such as infall of the outlying gas seen in HI maps[4,5] or merger with another galaxy[10]?

Acknowledgements

TXT has been partially supported by NASA grant NAG 5-257 and by Air Force Office for Scientific Research grant AFOSR 85-0125.

References

1) Thuan, T.X., 1987, this volume.

2) Thuan, T.X. and Martin, G.E., 1981, Ap. J., 247, 823.

3) Loose, H. and Thuan, T.X., 1986, Ap. J., 309, 59.

4) Viallefond, F. and Thuan, T.X. 1983, Ap. J., 269, 444.

5) Viallefond, F., Lequeux, J. and Comte, G., 1987, this volume.

6) Brinks, E. and Klein, U. 1986, in Star-Forming Dwarf Galaxies and Related Objects, eds. D. Kunth, T.X. Thuan and T.T. Van (Editions Frontières), p. 281.

7) Larson, R.B., 1987, this volume.

8) Loose, H. and Thuan, T.X. 1986, in Star-Forming Dwarf Galaxies and Related Objects, eds. D. Kunth, T.X. Thuan and T.T. Van (Editions Frontières), p. 73.

9) Sandage, A. and Tammann, G.A. 1976, Ap. J., 210, 7.

10) Hartmann, L.W., Geller, M.J. and Huchra, J.P. 1986, A.J., 92, 1278.

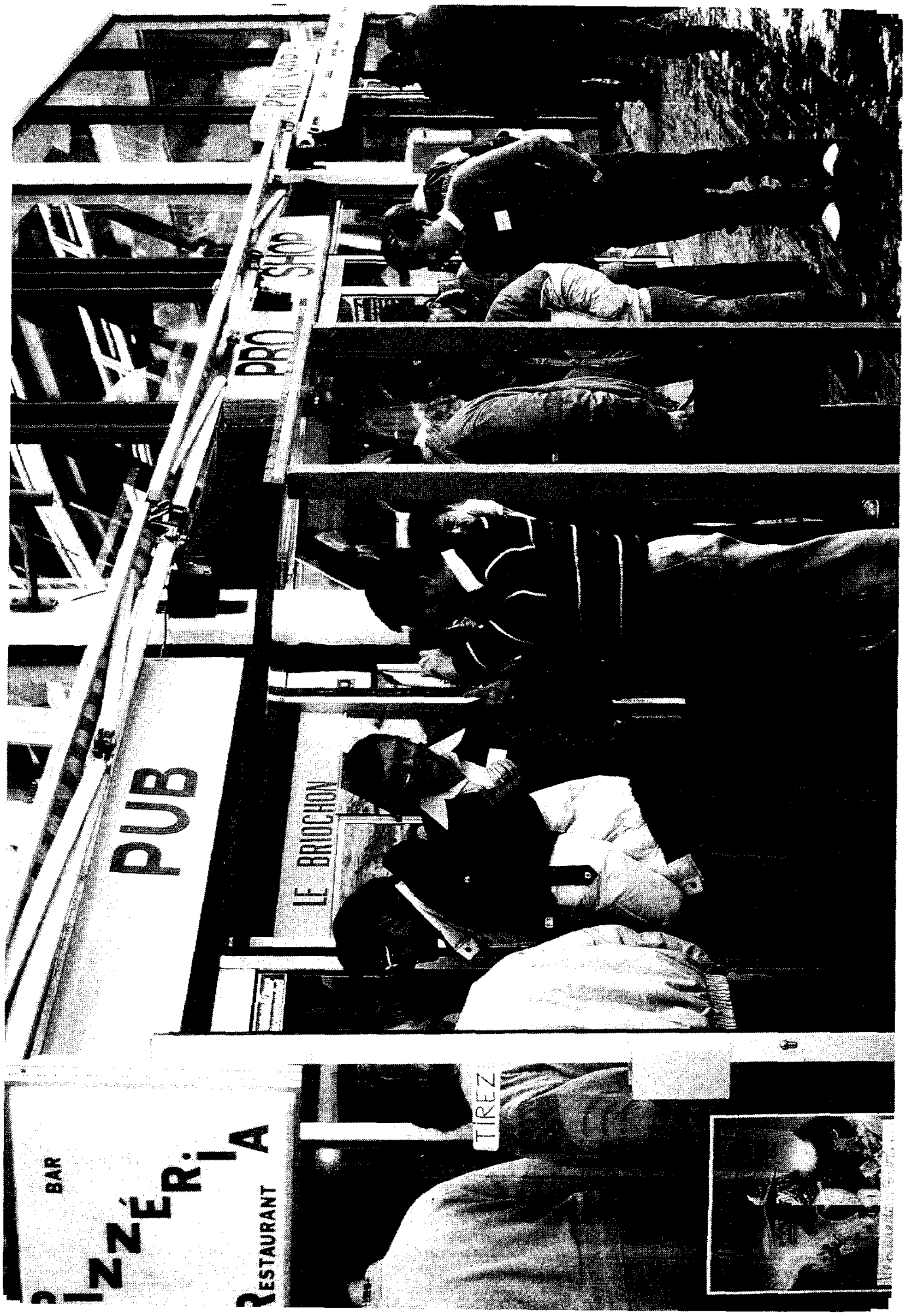
PUB
PRO SHOP
LE BRIOCHON
TIREZ
BAR

HENIZE 2-10: A STARBURST DWARF GALAXY

Hans Zinnecker
Royal Observatory, Edinburgh, Scotland
present address: Max-Planck-Institut für extraterr. Physik, 8046 Garching, FRG

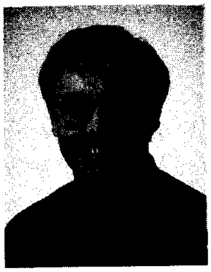

New observational results on He 2-10 are described, including 2 μm spectroscopy, 10 μm mapping, and CCD imaging (in B, Hα, SII, OIII). Strong Bγ emission a 2.17 μm, CO–absorption at 2.3 μm, and the Q–branch of molecular hydrogen at 2.41 μm have been detected. The centre of the galaxy is clearly resolved in Hα into a stellar–like core of size 1.8"x2.5" (50 pc x 75 pc at the adopted distance of 6 Mpc). This is consistent with the 10 μm map which shows a central point source unresolved at the 4" resolution level. IRAS data indicate that about half of the total luminosity is in the 12–100 μm range and that the mass of hot dust is $\approx 10^5$ $M_\odot$ [T(dust) $\approx$ 50 K]. The nucleus seems to dominate the emission. The ionizing radiation is equivalent to $\sim$ 2500 06V star. The NIR continuum comes from starlight (red supergiants). H_2 emission could be due to shock excitation caused by supernova remnants. The starburst models of Telesco [20]are used to deduce that the burst must have occurred $\sim 1 \cdot 10^7$ yr ago. The observed WR features in the integrated spectrum suggest a similar age of the young population, while the nonthermal radio flux could come from a few "radio–supernovae". The burst may have been triggered by the collision of two dwarf galaxies.

Introduction

He 2-10 (or PK 248+8-1 or ESO 495-G21) is a peculiar blue compact emission line galaxy [1] originally mistaken as a planetary nebula [2,3]. The galaxy is interesting because is is a dwarf galaxy undergoing a star burst. It is bright enough to observe, and the literature on it is growing [4, 5, 6, 7]. I will summarize below (Section I) what is known about this object before I am going to describe new observational data (Section II). The previous and the new data together can be used to give a preliminary analysis of the starburst but I cannot include this analysis here for lack of space, except for the result which is stated in the abstract.

I. Previous Data

1. Optical image and colours

Allen, Wright, and Goss (1976) [1] published a prime-focus AAT plate of He 2-10 taken in the blue on which the galaxy looks double. This is suggestive of a merger of two dwarf galaxies. The galaxy measures 20" x 30" on the sky corresponding to $\approx$ 1.0 kpc x 1.5 kpc in linear size if the distance is of order 10 Mpc ([1,7]). The colours are rather blue (B-V $\sim$ 0.5 and U-B $\sim$ - 0.3) in a large aperture getting bluer towards the very centre (B-V $\sim$ 0.4 and U-B $\sim$ - 0.6) [7].

2. Distance, absolute magnitude, and surface brightness

The distance is not well known, anything in the 5-15 Mpc is possible, the recent low values [7] more likely than the original high values [1]. In this paper a distance of 6 Mpc will henceforth be adopted [7]. The recent optical data [7] give V $\approx$ 12.2 in a 43" diaphragm yielding M_v = - 16.7 at the adopted distance ($M_{v,o} = -$ 17.3). Thus L_v is estimated to be $\sim 7 \cdot 10^8 L_\odot$, the distance-independent visual surface brightness is of the order of $10^9 L_\odot/kpc^2$. The data also indicate [7] that the visual surface brightness in the central part (4" or 120 pc in diameter) is still an order of magnitude higher ($10^{10} L_\odot/kpc^2$). These values are very high by any standard and are indicative of starburst activity [8] or nuclear activity [9].

3. Optical spectrum

He 2-10 was the first galaxy in which Wolf-Rayet features such as broad bands of NIII, NIV and HeII were discovered [1] in the integrated spectrum (confirmed by [4,5]). These are indicative of a large population of WN stars. From the strengths of the features several hundred to several thousand WN stars are needed to produce the observed bands [1, 4, 7] depending on the distance. Since the progenitors of WR-stars are young massive O stars, the large number of WR-stars points to a burst of (massive) star formation a few million years ago (ie corresponding to the age of WR-stars). Another characteristics of the optical spectra is appearance of the higher Balmer lines in absorption indicating a large population of B and A stars [1]. The emission line spectrum is of moderate excitation. The equivalent width of Hβ emission is 33 Å [1,7], thus there must be a strong blue continuum possibly due to many blue supergiants.

4. Internal extinction and metal abundance

Total extinction has been estimated [7] to be $A_v \approx 0.85$ mag from the Balmer decrement after correcting for the underlying stellar absorption lines (the uncorrected Hα : Hβ ratio is 6.2). Menzel Case B was assumed. Foreground extinction in the direction of He 2-10 is estimated to be $A_v \sim 0.6$ mag, therefore the internal extinction in the visual is around 0.25 mag.

The oxygen abundance is 0.5 $\pm$ 0.3 times solar and the nitrogen abundance is 1.0 $\pm$ 0.3 solar [7]. Thus the heavy element abundance seems somewhat below solar but not by as much as was originally thought [1].

5. Non–thermal radio emission

He 2-10 is one of the two dwarf galaxies which exhibits non-thermal radio emission (spectral index = – 0.6 $\pm$ 0.15). The second dwarf galaxy of this kind is II Zw40 with which He 2-10 shares many other similarities (cf. [10] for II Zw40). The non–thermal flux (55 mJy at 5 GHz) could either be due to supernova remnants associated with a starburst or a nuclear engine (mini–AGN). The former hypothesis is favoured, not least because the observed WR-features prove the presence of massive stars. An intriguing alternative way to explain the nonthermal radio flux is a population of a few "radio supernovae" [11] (like SN 1979c) which would require a current supernova rate in He 2-10 of about 3-5 per decade, a high but not an impossible frequency.

6. Neutral hydrogen and total mass

He 2-10 is fairly rich in neutral hydrogen [1]. The 21 cm flux is about 0.1 Jy which implies a total HI mass $\approx 1.5 \cdot 10^8 M_\odot$ (i.e. $M_{HI}/L_v \sim 0.2$). The FWHM of the 21 cm line is 160 km/s which leads to an estimate of the total gravitating mass $M_{tot} \approx 4 \cdot 10^9 M_\odot$ (R/2.5 kpc) inside a radius R. The radius r of the HI emission is not known, and a VLA HI map would be very useful. Assuming r = 5 kpc the average HI surface density would amount to $\sim 20 M_\odot/pc^2$ or $\sim 3 \cdot 10^{21} Hatoms/cm^2$. This is quite high, and would imply a gas-to-dust ratio much in excess of the Galactic value (by on order of magnitude) to match the low internal extinction.

II. New Data

1. The infrared spectral energy distribution

The spectral energy distribution of He 2-10 in the near- and far infrared is shown in Fig. 1 kindly provided by Pat Roche. It is seen that the bulk of the integrated infrared luminosity comes from the far-infrared implying that substantial amounts of dust are present to intercept and reradiate the UV-light from massive young stars. The IRAS fluxes in the 12, 25, 60, and 100 μ bands are 1.1, 6.5, 24, and 27 Jy, respectively, while the NIR measurements at UKIRT (20" beam) yielded K = 9.60, J-H = 0.68, H-K = 0.35.

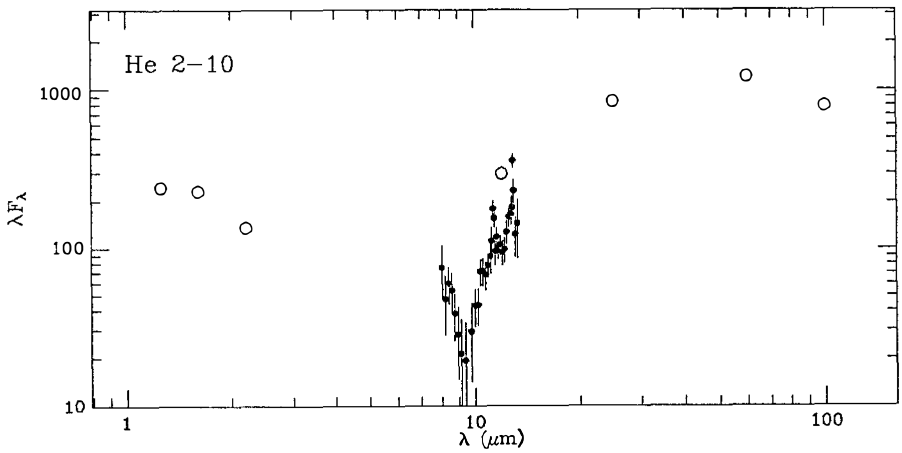

Fig. 1: Infrared energy distribution of He 2-10 (from P. Roche)

The H-K colour is much redder than is typically observed for galaxies dominated by old stellar populations (for those, H-K =0.20) indicating either a significant population of intermediate age carbon stars (from a previous starburst) or, more likely, an enhanced population of young cool M supergiants associated with the present starburst (the latter interpretation is further strengthened by the strong CO-index at 2.3 μm[12]; see below). The ratio between the luminosity in the K-band and the integrated luminosity in the 4 IRAS bands is 0.05 (where $L_{IRAS} = 2 \cdot 10^9 L_\odot$ and $L_K = 10^8 L_\odot$ for the adopted distance of d = 6 Mpc). L_{IRAS}/L_B = 2 implying that there is an important fraction of radiation that is not intercepted by dust perhaps related to a reduced dust-to-gas ratio. (This could be an important hint regarding the search for starburst proto-galaxies.) The temperature of the dust grains is $\approx$ 50 K estimated from the ratio of the 60 to 100 μm flux. This is rather hot compared with most other galaxies of a representative subsample of Shapley-Ames galaxies observed by IRAS (cf. Fig. 2 in [13]). This could be due to a population of small grains, for which the observed 3.28 μm feature also provides some evidence. On the other hand, the grains in He 2-10 might be hotter than usual because of the unusually high radiation field in the central starburst region. A dust mass of $\sim 10^5 M_\odot$ is calculated from the far-infrared luminosity and the dust temperature following Gondalekhar et al. [14]. It is possible that there is a lot more dust at low temperatures which would only show up at submm wavelengths.

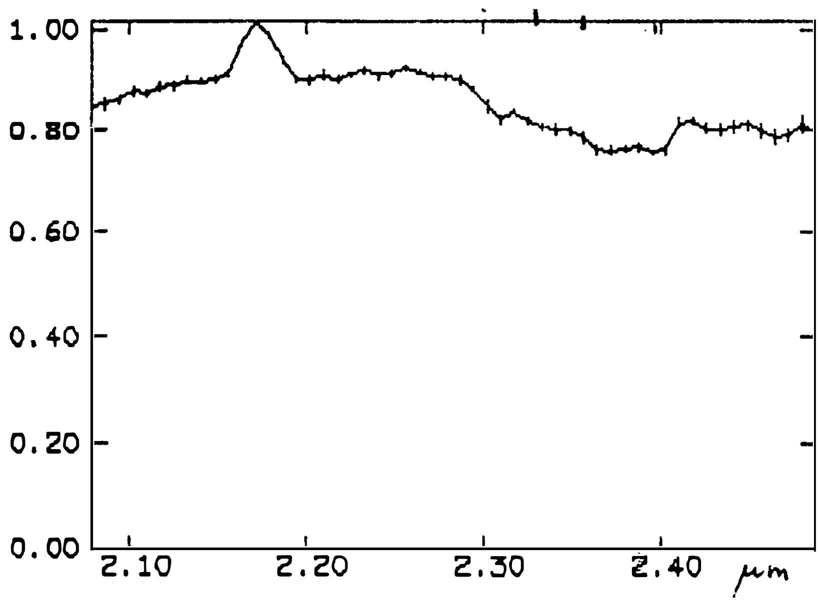

Fig. 2: 2 μm spectrum of He 2-10 obtained at UKIRT

2. 2 μm–spectroscopy

An infrared spectrum between 2.05-2.45 μm for He 2-10 was obtained at UKIRT in November 1986 and improved in February 1987 (using a 20 arcsec diameter beam and a circular variable filter with a resolution of about 100). The spectrum is shown in Fig 2. It is seen that there is strong Brackett gamma emission at 2.17 μm strong CO absorption in the 2.3 μm region, and significant emission at 2.41 μm; the latter feature is identified as the v = 1-0 Q-branch of molecular hydrogen, and we therefore claim we have detected shocked molecular hydrogen in this dwarf galaxy, although the v=1-0 S(1) line at 2.12 μm is not present in the spectrum. There are reasons why this line might escape detection, both instrumental and physical reasons, e.g., the low spectral resolution and/or the differential extinction as well as the lesser intrinsic strength (factor 3 or so) of the S(1) line compared with the Q- branch.

The presence of CO absorption proves that the 2 μm continuum is starlight. The depth of the CO-absorption (ie the CO-index) is indicative of cool, low-gravity stellar atmospheres, that is red giants or red supergiants . Here an interesting question arises: since the depth of the CO absorption not only depends on the luminosity class of the evolved stars (it is larger for supergiants than for giants) it is possible to explain a given CO-index by either lower metallicity supergiants or higher metallicity giants. Although the metallicity has been estimated to be around half-solar from the optical spectrum, that spectrum reflects the post-starburst chemical composition of the HII regions. The pre-starburst composition could, however, have been somewhat more metal-poor when the progenitor stars of the giants or supergiants were born (factor 2 or so). This consideration tends to favour the supergiants as the source for the near-infrared light.

Finally, let us discuss the Bγ which must rank among the strongest detections in any galaxy (S/N = 50). The large ratio F(Bγ)/F(H2 S(1)) $\geq$ 10 that comes from the nil detection of the H_2 S(1) line at 2.12 μm is surprisingly different from cases of massive starburst galaxies like Arp 220 or NGC 6240 in which Bγ is comparable in strength to the H_2 S(1) line or much smaller [15, 16, 17]. The flux in the Bγ line is $\sim 1 \cdot 10^{-20} W cm^{-2}$ which corresponds to the production of about $5 \cdot 10^{50} B\gamma$ photons per second which in turn corresponds to a Lyc production rate of $4.2 \cdot 10^{52}$ photons/sec (assuming $N_{Lyc} = 84\ N_{B\gamma}$ [18]predicted by recombination theory). This is equivalent to the output of about 2500 O6V stars. The ratio of the observed Bγ flux to the Hα flux is 1:6 which implies a total extinction of $A_v \approx 0.8$ mag (assuming Case B recombination) in good agreement with the total extinction value derived from the Balmer decrement Since the galactic foreground extinction is estimated to be $A_V \approx 0.6$ mag in the direction of He 2-10 [7], the internal extinction is estimated to be $A_V \approx 0.2$ mag. Since most of the ionizing flux originates in the 2-3 arcsec nucleus of the galaxy (see II.3), the different sizes of the diaphragms used for the Hα and the Bγ measurements (4 arcsec versus 20 arcsec) should not affect the physical ratio of the Hα/Bγ in the central region.

3. CCD imaging

CCD images in Hα, OIII, SII, and the broad-band B filters of He 2-10 have been obtained at the ESO 2.2 m telescope in February 1987. The images have been taken by R. Mundt. Previously, only direct photographic plates in Hα, OIII and the broad-band filters B and R had been taken [4]. The new data resolve the Hα bright stellar-like core of the galaxy; the FWHM of the core is 1.8" x 2.5", that is 50pc x 75pc. The asymmetry results from a weak second component 2-3 arcsec to the west of the main component, a feature that has not been

4. 10μm mapping

In March 1987, He 2-10 was mapped at 10μm at the IRTF using Telesco's 5x4 element bolometer. The observations were made by Dr. Telesco. The galaxy does not appear to be resolved at the angular resolution of the instrument (4 arcsec). Thus the peak flux density (measuring 0.30 $\pm$ 0.02 Jy) should be that of the point source which is, however, about a factor of 3 below the IRAS value in the 12 μm band (1.1 Jy). The colour correction for the difference in the wavelengths between the bolometer (10.8μm) and IRAS (12μm) is probably 20-30 % (i.e. the colour corrected bolometer flux is $\approx$ 0.4 Jy); it is unlikely that observational or calibrational uncertainties account for the difference of the bolometer flux and the IRAS flux. Possibly there is low-level, diffuse emission which fell below the bolometer noise level. The fact that the 10μm nucleus is not resolved is consistent with the fact that the nucleus is just resolved in Hα due to the smaller pixel size in the optical CCD. It may be worth mentioning that He 2-10 exhibits an unidentified 11.25 μm feature [19], a feature not observed in IIZw40, thus an interesting difference between two otherwise similar objects.

Acknowledgments

I wish to thank R.D. Cannon (for supporting the origins of the present investigation), T.G. Hawarden (for obtaining an improved 2 μm spectrum during UKIRT Service Observing Time), R. Mundt (for taking the CCD data at ESO at my request), P. Roche (for providing Fig. 1), C.M. Telesco (for obtaining the 10 μm map at the IRTF), and M. Rosa for critically reading the manuscript. Finally, I would like to congratulate the organizers of the XXIIth Rencontre de Moriond for a most enjoyable and profitable conference.

References

[1] Allen D.A, Wright, A.E., and Goss, W.M. 1976. MNRAS 177, 91
[2] Henize, K.G., 1967. Astrophys. J. Suppl. 14, 125 and 154
[3] Cohen, M. and Barlow, M.J., 1974. Astrophys. J. 193, 401
[4] Hutsemekers, D. and Surdej, J., 1984. Astron. Astrophys. 133, 209
[5] D'Odorico, S., Rosa, M., and Wampler, E.J., 1983. Astron. Astrophys. Suppl. Ser. 53, 97
[6] Moorwood, A.F.M., 1986. Astron. Astrophys. 166, 4
[7] Johansson, L., 1987. Astron. Astrophys. 182, 179
[8] Zinnecker, H.,1985. 1st IRAS conference, ed. Israel, p. 271
[9] Wynn-Williams, C.G., 1987. IAU-Symp. No. 115, p. 587
[10] Wynn-Williams, G. and Becklin, E.E., 1986. Astrophys. J. 308, 620
[11] Weiler, K.W., Sramek, R.A., Panagia, N., van der Hulst, J.M., Salvati, M., 1986. Astrophys. J. 301, 790
[12] Baldwin, J.R., Frogel, T.A, and Persson, S.E., 1973. Astrophys. J. 184, 427
[13] de Jong, T. et al., 1984. Astrophys. J. 278, L67
[14] Gondalekhar, P.M., Morgan, D.H., Dopita, M., and Ellis, R.S., 1986. MNRAS 219, 505
[15] Joseph, R.D., and Wright, G.S., and Wade, R., 1984. Nature 311, 132
[16] Rieke, G.H., et al., 1985. Astrophys. J. 290, 116
[17] DePoy, D.L., Becklin, E.E., and Wynn-Williams, C.G., 1986. Astrophys. J. 307, 116
[18] Beck, S.C., Beckwith, S., and Gatley, I., 1984. Astrophys. J. 279, 563
[19] Phillips, M.M. , Aitken, D. K., and Roche, P.F., 1984. MNRAS 207, 25
[20] Telesco, C.M., 1985. Proc. RAL-Workshop "Extragalactic Infrared Astronomy", p. 87

INFRARED PROPERTIES OF NEARBY DWARF IRREGULAR GALAXIES

Henk CASPERS
Sterrewacht Leiden Observatory
Postbus 9513
NL-2300 RA LEIDEN
The Netherlands

Abstract: Far-infrared IRAS detections for a number of nearby dwarf irregular galaxies extend the hitherto known L_{IR}/L_B properties for galaxies to very low values and show a large spread in dust temperatures and L_{IR}/L_B values.

1. Introduction

The IRAS mission resulted in a large database of broadband emission at 12, 25, 60 and 100 μm (IRAS, 1984). In galaxies without active nucleus the far-infrared emission is mainly caused by thermal re-emission by dust grains of UV and optical radiation absorbed from the interstellar radiation field. This emission can be modelled by essentially two thermal components. A hot component due to direct heating of dust by nearby stars and a colder cirrus component due to dust heated by the diffuse interstellar radiation field. Although much of the latter emission may be radiated at wavelenghths larger than 100 μm and both components tend to overlap at 60 μm, the S_{100}/S_{60} flux density ratio is a useful indicator for the relative importance of star formation activity and dust content in these galaxies.

2. Observations

From the Leiden IRAS (CRDD) database 60 and 100 μm flux-densities were extracted off a large number of nearby dwarf galaxies of Hubble type Sd to Im. Most of these are systems with very low far-infrared luminosities. This survey yielded a number of 23 (out of 80) detections of galaxies with L_{IR} between 10^6 and 10^8 $L_\odot$.

3. The Infrared Properties

In Figure 1 the luminosity ratio L_{IR}/L_B is plotted for these galaxies versus the flux ratio S_{100}/S_{60} as described by De Jong et al. (1984). Here L_{IR} represents the interpolated luminosity at 80 μm. For comparison a sample of blue compact galaxies as described by Kunth and Sèvre (1985) and a number of nearby galaxies of various morphological types are also plotted (data for M31 from Walterbos and Schwering, 1986; for LMC and SMC from Schwering, 1987). The solid line corresponds to the correlation found by De Jong et al. (1984) in a sample of RC2 spiral galaxies.

As can be seen, the dwarf irregular galaxies populate a large part of the diagram and do not correlate with the spiral galaxy sample. They are less luminous in the infrared and tend to have higher colour temperatures at 100 to 60 μm.

The interpretation of this diagram is hazardous as it depends on a combination of warm and cold dust as well as extinction effects, but one may speculate on the general characteristics. The explanation of the location of the blue compact sample with respect to the spiral galaxies seems straightforward: this sample very likely represents dwarf galaxies which are

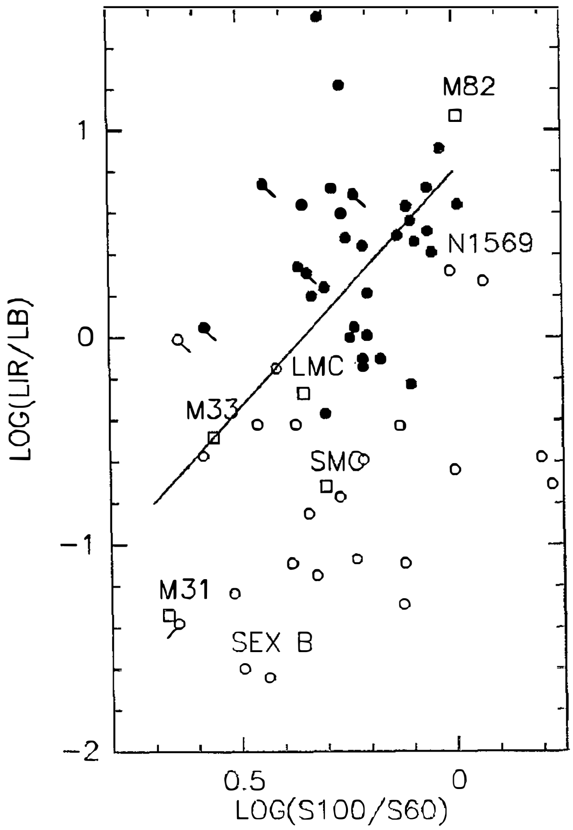

Figure 1: Plot of infrared to blue luminosity ratio versus 100 μm to 60 μm flux density ratio for the sample of nearby dwarf irregular galaxies (see text, open circles), a sample of blue compact galaxies (Kunth and Sèvre, 1985, dots) and a number of nearby galaxies of various morphological types (squares). The line represents the correlation shown by a sample of spiral galaxies (De Jong et al. 1984). Stripes indicate upper limits.

in a stage of enhanced star formation and therefore have a higher dust temperature caused by the more intense interstellar radiation field. In this way one may expect to find the more active galaxies in the diagram at higher L_{IR}/L_B and lower S_{100}/S_{60} values, shifted along the spiral galaxy correlation line.

Another factor is the total gas-to-dust ratio in the galaxy. Removal of dust, thereby causing a decrease in the absorption optical depth of the galaxy may result in a shift in the diagram perpendicular to the correlation line. Removal of dust causes fewer photons to be absorbed. Individual grains are less in number but on average hotter as they are heated more effectively by a stronger interstellar radiation field.

Especially for dwarf irregulars, one expects this mechanism to be related to the metallicity of the system as this influences the stellar mass-loss rate, and therefore with the star formation history. This hypothesis finds some support in the labelled dwarf irregulars in the plot. For example NGC 1569 shows the characteristics of a recent star formation burst (Gallagher and Hunter 1984, Israel and De Bruyn 1987) and a metallicity between that of the LMC and SMC. The metallicity of the Sextans B system is considerably lower than the other three (Vigroux, Stasińska and Comte 1987)

4. Conclusion

In their far-infrared properties, nearby dwarf irregular galaxies are distinct from spiral galaxies in the diagram. Generally the far-infrared emission at 60 and 100 μm implies higher dust temperatures and lower luminousity. This is probably related to the low gas-to-dust ratio, and generally low metallicities in these systems.

References

De Jong, T, Clegg, P.E., Soifer, B.T., Rowan-Robinson, M., Habing, H.J., Houck, J.R., Aumann, H.H., Raimond, E.: 1984, Astrophys. J. **278**, L67

Israel, F.P., De Bruyn, A.G.: 1987, submitted to Nature

IRAS: 1984, Explanatory Supplement, ed. Beichman, C.A., Neugebauer,G.,Habing, H.J., Clegg, P.E. and Chester T.J.

Kunth, D., Sèvre, F.: 1985, in 'Star forming Dwarf Galaxies and related objects', ed. D. Kunth, T.X. Thuan, J. Tran Thanh Van, Editions Frontières, Paris 1985

Schwering, P.B.W.: 1987, these proceedings

Vigroux, L.,Stasińska, G., Comte, G.: 1987, Astron. and Astrophys. **172**, 15

Walterbos, R.A.M., Schwering, P.B.W.: 1986, submitted to Astron. and Astrophys.

The Young face of the BCG ESO 400-G43*

Nils Bergvall
Uppsala Astronomiska Observatorium
Sweden
Steven Jörsäter
Stockholms Observatorium
Sweden
Kjell Olofsson
Uppsala Astronomiska Observatorium
Sweden

We briefly discuss the results of a multifrequency study of the blue compact galaxy ESO 400-G43. This galaxy, one of the most luminous BCG:s known, is embedded in a massive HI cloud and shows clear signs of a global burst of star formation. There are substantial evidence that this is the first grand star formation epoch in the history of this galaxy.

*Based on observations made at the European Southern Observatory, La Silla, Chile and on IUE observations collected at the Villafranca ESA Satellite Tracking Station, Madrid, Spain

1. Introduction

Blue compact galaxies (BCG:s) frequently show conspicuous bright knots revealing ongoing active star formation. At lower light levels, however, a majority of the BCG:s show a smooth extended structure[1,2]. A few of the known BCG:s display an irregular morphology in the near IR combined with a very short scale length of the optical luminosity profile. Such cases are of particular interest since these galaxies might be experiencing their first major star forming event, thus lacking an underlying old stellar disk.

Here we briefly report on results from a study of one such galaxy, ESO 400-G43, based on observations obtained at ESO (visual, near IR), the Very Large Array (VLA) of the NRAO* and with the IUE satellite[3], and from a study of spectral evolutionary synthesis[4]. It is one of the most luminous BCG:s known (M_V = −20.4) and it has low metal abundances (~1/8 $Z_\odot$), typical of this class of objects[5]. The galaxy was detected by IRAS at 60 μm and 100 μm. The fact that $S_{60} > S_{100}$ indicates that it contains dust of unusually high temperature, even for BCG:s[6]. We assume that hot stars are responsible for the heating of the dust. This is reasonable since $F_{FIR} \sim F_B$; thus is the energy in the stellar flux sufficient. Fig. 1. shows a CCD Gunn I image of the galaxy.

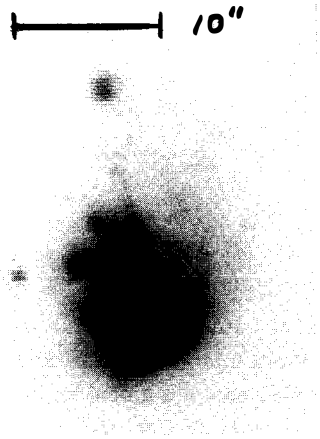

Fig. 1. A CCD image of ESO 400–G43 obtained through a Gunn I filter (~8000 Å) with the MPI 2.2 m telescope at ESO, La Silla, Chile. For an H_0 of 75 kms^{-1}Mpc^{-1} 1" corresponds to 380 pc.

*The National Radio Astronomy Obervatory is operated by Associated Universities Inc., under contract with the National Science Foundation

2. The Stellar Population

Slit spectra obtained at ESO reveal gaseous emission across the whole main body of the galaxy. The excitation reaches a maximum in the hot spot north of the main body. Stars with masses up to 100 $M_{\odot}$ are required in order to explain the observed line intensities in this area. A slightly lower level of excitation is found close to the luminosity maximum. We have also obtained a spectrum of ESO 400-G43 with the IUE satellite using the SWP camera. This spectrum, shown in Fig. 2 is rich in absorption features characteristic of young massive stars.

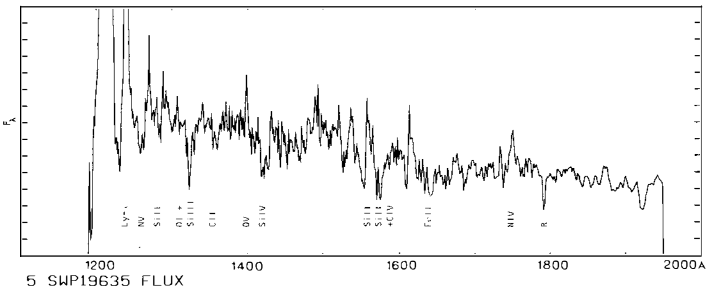

Fig. 2. A low resolution IUE spectrum of ESO 400-G43

The observed UBVRIJHK fluxes, [OIII]/Hβ-ratio and the Hβ equivalent width in emission, $W(H_{\beta})$, were compared to predictions from an evolutionary model of a metal poor star forming region. All observations were corrected for extinction based on an averaged Hα/Hβ ratio in a long slit spectrum across the galaxy (after compensating for underlying absorption lines). The corrected continuum distribution in the optical/near-IR region is displayed in Fig. 3. This figure also shows a model continuum of a young stellar population with an age of 20 Myrs and a constant star formation rate (SFR). We used a Salpeter IMF[7] and a mass range of 0.1 - 50 $M_{\odot}$, constraining the model so that the predicted W(Hβ) and [OIII]/Hβ ratio agree with the observations. From the evolutionary model we calculate the total mass in young stars and ionized gas (obtained from the total Hβ flux) to be 1.2 10^{9} $M_{\odot}$ and $M/L_B = 0.1$. A critical parameter in models of this type is the adopted lifetime of red supergiants. In this case the lifetime was estimated from statistics made on bright stars in the SMC[8]. Models of this kind clearly depend on several parameters whose values are rather uncertain. Here we merely intend to illustrate that it is *possible,* adopting commonly accepted values of the parameters of the mass function, to explain the observed properties of the stellar component without invoking old stars.

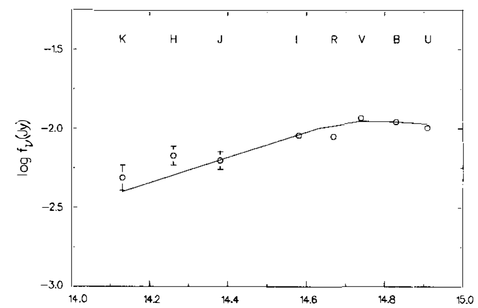

Fig. 3. Johnson UBVJHK and Cousins IR broadband photometry of ESO 400-G43. The aperture diameter was 30". The solid line shows the predicted continuum distribution for a burst of an age of 20 Myrs, a Salpeter IMF and an upper mass limit of 50 $M_\odot$. A constant SFR was assumed.

A conclusive test of the presence of an old stellar population may be obtained from spectroscopic observations in the near IR. The spectral energy distribution was calculated using evolutionary tracks and synthetic spectra of metal poor stars[4]. Continuous gaseous emission from H^+ was included. The model spectrum is shown in Fig. 4. A calculated spectrum for an old burst is also shown. We see that red supergiants dominate the spectrum of the young burst. If young stars dominate the mass features like the CO bands should be well above typical detection limits, e.g. a 4σ detection in a 2 hour observation using the ESO 3.6 m telescope and IR spectrograph (IRSPEC). Such observations are evidently of crucial importance.

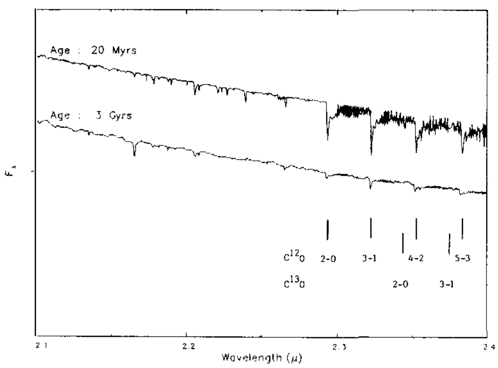

Fig. 4. A plot of the predicted profiles at 20 Myrs and 3 Gyrs (normalized on the former) using the model described in the text. The CO bands are identified.

3. Radio continuum and 21 cm line

In 1985 observations of ESO 400-G43 were carried out in the 6 and 21 cm continuum and in the 21 cm line of HI with the VLA in the B+C hybrid configuration[3]. The spectral index between the continuum bands was found to be -0.4. After subtraction of the thermal contribution derived from the model we obtain a spectral index of -0.7, a typical value for SNR.

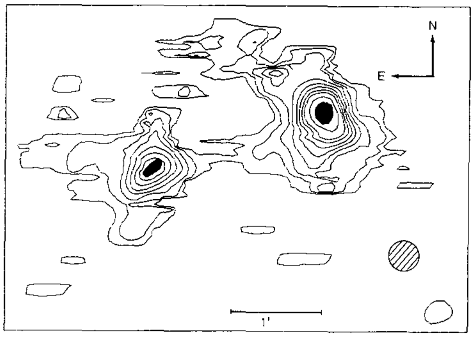

Fig. 5. The integrated HI distribution of ESO 400-G43 and its companion obtained with the VLA. The synthesized beam size (20"x 20") is indicated in the figure as well as the optical extent.

The integrated HI map is shown in Fig. 5. ESO 400-G43 is evidently a member of a double system where both galaxies are surrounded by extensive HI halos. We derive a total HI mass of the system of 1.1 10^{10} $M_{\odot}$, of which the principal component constitutes 50 %. Optical spectra of the companion show striking similarities to those of ESO 400-G43. The velocity difference between the two components is negligible.

The HI distribution of ESO 400-G43 has a fairly regular morphology. The cloud is showing rotation and the rotation curve is plotted in Fig. 6. We assume an inclination of 50° and a p.a. of the major axis of 200°. The mass derived for the optical disk is less than 2 10^9 $M_{\odot}$.

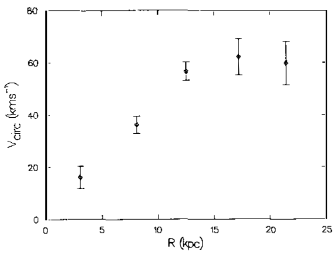

Fig. 6. The rotation curve of ESO 400-G43 as deduced from HI observation. Note that the beam smearing effects is substantial in the inner parts.

4. Conclusions

The spectroscopic and photometric data as well as the dynamical arguments presented above are consistent with a young stellar population dominating the mass in the optical region of ESO 400-G43. The relative fraction of HI gas mass is extremely large. When considering the present rate of gas consumption in the galaxy one finds that the ongoing starburst cannot be very old. The low metal abundance leads to the same conclusion. To summarize, we consider ESO 400-G43 to be a prime candidate of a galaxy presently experiencing its first major burst of star formation.

References

1) Loose, H.H., Thuan, T.X.: 1986 in *Star forming dwarf galaxies*, **73**, ed. Kunth, D., Thuan, T.X. and Tran Thanh Van, J., Instititut d'Astrophysique, Paris
2) Kunth, D., Martin, J.M., Maurogordato, S., Vigroux, L. : *ibid.*, **89**
3) Bergvall, N, Jörsäter, S. : 1987 To be submitted to *Nature*
4) Olofsson, K.: 1987, in preparation
5) Kunth, D.:1986 in *Star forming dwarf galaxies*, **183**, ed. Kunth, D., Thuan, T.X. and Tran Thanh Van, J., Instititut d'Astrophysique, Paris
6) Kunth, D., Sevre, F.: *ibid.*, **331**
7) Salpeter, E.E.: 1955, *Ap. J.***121**, 161
8) Humphreys, R.M., McElroy, D.B.: 1984, *Ap.J.* **284**, 565

SPECTROPHOTOMETRY OF A BCG. IZW 207

J. Masegosa and M. Moles
Instituto de Astrofísica de Andalucía
SPAIN

ABSTRACT

We present spectroscopic observations of the Blue Compact Galaxy IZW 207. When comparing with HII galaxies and High Luminosity ones it appears more similar to HLG in chemical abundances and infrared properties suggesting different histories of star formation in both.

I. INTRODUCTION.

Since the pioneering work of Zwicky[16] important effort has been devoted to discover galaxies of as low metallicity as IZW 18 (1/50 Z⊙) (Kunth and Sargent[10], Kinman and Davidson[9], Lequeux et al.[11]) but not sucess has been obtained till now. In the spectroscopic catalogue of HII galaxies (Terlevich et al.[15]) which includes about 500 Blue Compact Galaxies we could extend the known low metallicity BCG up to 1/30 Z⊙ but we did not find any galaxy with lower metallicity.

The aim of the present investigation was to get the spectroscopic properties of IZW 207, in particular to obtain the metallicity in different regions of the galaxy. IZW 207 was discovered by Zwicky[16] and Sargent[14] classified it as a galaxy with sharp emission lines. Moles et al.[12] have found that the broad band colours of IZw 207, as compared with other spectroscopically similar BCG, are unusual in the sense that it is significantly bluer in B−V and U−B and redder in V−R and V−I. They suggested that the red colours could be produced by the presence of a great proportion of supergiants. However, as its extreme blue colours are similar to the ones found for IZW 18 (Huchra[7]), we suspected to be another candidate of low metallicity, but after the spectroscopic observations were made it came out not to be the case. Thus the blue colours could only reflect the presence of a very young burst.

II. OBSERVATIONS AND DATA REDUCTION

We got long slit spectra of IZw 207 with the Isaac Newton 2.5 m telescope at the Observatorio del Roque de los Muchachos, La Palma (Spain). The 235 mm focal length camera was used with the IPCS as detector. The setup of the instrument resulted in a spatial resolution better than 2 arcseconds and a spectral resolution of 1 Å/channel.

Data reduction was carried out in the standard way using the SPICA package at the VAX 11/750 of the IAA. Three standard stars from the list by Oke (1974) were observed to get flux calibrated results. Internal consistency between the calibration curves from each star indicates that the fluxes are in error by less than 15% . The line intensities were measured with ALICE, an interactive program kindly supplied to us by Jorge Melnick. Assuming that the main source of error is the positioning of the continuum they amount to 5 and 30 % depending on the intensity of the line.

III. RESULTS

The spatial distribution of the Hβ flux along the slit for the three spectra we got is shown in figure 1, with the different regions marked on it. The distributions of [OIII] and Hα are similar to that of Hβ and are not presented here.

The spectra, shown in figure 2, are typical for HII regions ionized by hot stars. These figures illustrate well the differences between the different regions. Particularly noticeable are the strong absorptions in the Balmer lines present in regions C and E of the knot 2 indicating that it could be in a more evolved state that knot 1.

The redshift of IZw 207 is found to be 0.0187, in agreement with the value given by Sargent[14] . We checked for velocity differences between both regions in the galaxy using cross correlations techniques with negative result. The upper limit to any redshift difference is 30 km/s.

To correct for extinction we have estimated the reddening from the Balmer decrement and the Withford law has been assumed. The reddening can only be estimated in knot 1 where the Balmer lines do not present absorption components. Considering case B recombination for Te=10000°K and $n_e = 100cm^{-3}$, a consistent solution has been found for c_β= 0.36 for the three regions in knot 1. For the second knot we have assumed the same reddening. For region C this seems to be a reasonable guess since the (uncorrected) [OII]/[OIII] ratio is similar to that found in knot 1. For region E however that ratio is 30% lower in C and assuming the same reddening would result in a higher excitation for this region, what does not look very realistic in view of its spectrum. The reddening we found is almost completely internal in origin since the external extinction only amounts to E(B−V) = 0.04.

The electronic density was estimated from both the [OII]$\lambda\lambda$3726,3729 and [SII]$\lambda\lambda$6717,6731 doublets for the regions with good S/N ratio. To deblend the [OII] lines we used an iterative deconvolution program assuming that both lines are gaussians with a FWHM equal to that of the [OIII]λ5007. It is to note that when both doublets are available for the density determination the values from the [OII] lines are always smaller than those from the [SII] lines. These differences have also been noticed by Deharveng et al.[2] and Danks and Manfroid[1] for some HII regions.

No direct electronic temperature determination can be made except for region A where an upper limit could be set to [OIII]λ4363. The temperature we found from the [OIII]$\lambda\lambda$4959,5007/[OIII]λ4363 ratio is Te=10000°K. For the other regions, B and D, coming from the same knot in the galaxy, the temperature was set equal to that value. An indirect estimation was obtained from the Pagel calibration (Edmunds and Pagel[1]). Both results are in good agreement and are presented in table 2. For the knot two only the indirect method can be used for region C and E. In those regions the strong absorption in Hβ, particularly noticeable in C, give an overestimation of the [OII] + [OIII]/Hβ ratio and consequently an overestimation of the temperatures.

The ionic chemical abundances were derived assuming the same temperature for low and high ionization species and the total abundances for heavy elements were obtained following Peimbert and Costero[13] and are given in table 1.

For the Helium abundance we have used HeI 5876 since HeI 4471 is not detected. We estimate that assuming the HeI 5876/HeI 4471 recombination value, HeI 4471 should have an equivalent width well below 1 Å. We have corrected the HeI 5876 line for collisional effects after Ferland[5] . Finally to compute the Helium total abundance we have used the ionization correction factor given in Kunth and Sargent[10]. The final value for the helium abundance is given in table 1.

IV. DISCUSSION

The first point to note is that the excitation does not seem to change in a given knot. Due to the fact that the reddenning in knot 2 cannot be estimated it is possible that a difference in excitation between both knots is present, in particular regarding region E, as we note before. We consider that could be due rather to a difference in extinction than in the excitation. In any case, the differences, if any, cannot be very important.

Considering only the knot 1, regions A and D present the same physical conditions and metallicities but region B shows some important differences. We have pointed out that the same temperature can be assumed for the three regions but the density in B is a factor of three greater than in the other. It also presents an overabundance in Nitrogen and Neon by factors of 1.5 and 2 respectively. This result is difficult to interpret because if Ne and O are supposed to be produced by the same stars the oxygen abundance should show the same differences and that is not the case. Moreover the similarity in excitation and in the equivalent width of Hβ between the three sections seems to indicate that the stellar content of the three regions is similar. This situation is at variance with the results by Diaz et al.[3] for NGC 604 where they find no differences in heavy element abundances between different parts of the nebula. Marked spatial differences are however found by them in excitation, which they discuss to be the result of evolutionary effects.

These possible anomalies could be an artifact produced by a bad choice of the temperature since we have no a direct estimation of it. We have considered the resulting temperature in region B from the calibration of Pagel but that does not change very much the situation since it is not far from the previously adopted value.

In fact to avoid an overabundance in Ne we should rise the temperature but in that case the overabundance of N would become larger. It is then clear that some kind of anomaly is present in IZw 207.

The results can be compared with those for other Blue Compact Galaxies (French[6], Kinman and Davidson[9], Kunth and Sargent[10] and Terlevich et al.[15]). Among them the class of High Luminosity Galaxies (HLG) defined by French are particularly interesting in that context. With respect to excitation and anomalies in the Ne and N abundances IZw 207 is similar to the HLG with the same oxygen abundance, in particular to Mkn 168 for which the overabundances of Ne and N are less marked.

The plot Ne/O versus N/O for HII galaxies, HII regions and High Luminosity Galaxies is presented in figure 3. The HLG stand out from the others no matter their metallicity is. In figure 4 the distribution of Ne/N values for the same galaxies is also shown. As we can see all types of galaxies displays the same range of Ne/N values and on that basis they are no differences between all of them. Thus overabundances of N and Ne go together and can be very important for not very metal rich galaxies.

The star forming activity of IZW 207 can be compared with that of other star forming galaxies on the basis of their respective Hα and IRAS fluxes. In table 2 the relevant parameters for that galaxy, Blue Irregulars from the sample by Hunter and Gallagher[8] and the HLG from the list of French are given. Unfortunately no IRAS data are available for Mkn 168 since it is confused with that of UGC 06441. The other three HLG have larger IRAS fluxes than IZw 207 but this galaxy has on its side a larger IRAS flux than the low luminosity Blue Compact Galaxies and Irregulars.

The high formation rate for IZw 207 becomes moderate if we normalize to the blue luminosity. Thus the relative importance of the present burst of star formation in IZw 207 is smaller than in other HLG or even smaller than in HII galaxies, taken IIZw 40 as a good representative. This is illustrated in figure 5. It can be inferred that the star formation in IZw 207 was very important from the last $10^8 - 10^9$ yr till now. This high rate could not be sustained from its very beginning and in that sense IZw 207 can be considered a "lazy Galaxy" but not as much as IIZw 40 for example. In that case the very red V$-$R and V$-$I colors found for IZw 207 are the result of an important contribution from giant stars from the previous bursts with some contribution from supergiants.

A point to note is that IIZw 40, a low metallicity HII galaxy has the highest normalized rate of star formation whereas it is not clear if it is forming stars with a higher efficiency or it is producing more bright stars than the HLG the situation is compatible with the IMF becoming flatter for metallic poor galaxies as suggested by J. Melnick (this meeting).

Also interesting are the differences between the normalized star formation rates for HLG. As their metallicities are similar, differences in their respective IMF cannot reasonably be invoked. We are then lead to admit very different efficiencies in the gas to stars conversion process. They are all three in interaction and this seems to be a candidate to explain those differences.

The L_{IR} to L_{α} ratios for HLG are always greater than for other objects in the table. As a consequence the star formation rates derived respectively from the IRAS flux and from the Hα flux are very different for HLG whereas they are much more similar for the other galaxies. Then whereas in IIZw 40 what is observed in the optical and the IR ranges is essentially the same process, in HLG including IZw 207 only a small fraction of the star formation process can be observed at optical wavelengths. This result could means that for IZW 207 and HLG the dust is also heated by reradiation from hot stars embebed in molecular clouds which do not contribute to the Hα luminosity, in agreement with the inferences previously quoted from the L_{IR} to L_B data. Further work on HLG is needed to look for differences in the star formation process comparing with HII galaxies, which in this context appear to be "lazy" galaxies with not much star formation in the past.

ACKNOWLEDGEMENTS

We thank the support staff at the INT telescope. The Isaac Newton telescope is operated on the island of La Palma by the Royal Greenwich Observatory at the spanish Observatorio del Roque de los Muchachos of the Instituto de Astrofisica de Canarias. We also thank A. del Olmo and J. Perea for their help during the preparation of this manuscript.

REFERENCES

1) Danks, A.C. and Manfroid, J. 1976, Astron. Astrophys. 48,63

2) Deharveng, L., Israel, F.P., Mauchrat, M. 1976, Astron. Astrophys. 48,213

3) Diaz, A.I., Terlevich, E., Pagel, B.E.J., Vilchez, J.M. Edmunds, M. 1987, Mon. Not. Roy. Astron. Soc. 226,19

4) Edmunds, M. and Pagel,B.E.J. 1984, Mon. Not. Roy. Astron. Soc. 211, 507

5) Ferland, G.J. 1986, preprint

6) French, H.B., 1980 Astrophys. J. 240, 41

7) Huchra J.P., 1977, Astrophys. J. Supp. Ser. 35, 171

8) Hunter, D.A., Gillett, F.C., Gallagher, J.S., Rice, W.L. and Low, F.J. 1986, Astrophys. J. 303, 171

9) Kinmam, T.D. and Davidson, K. 1981, Astrophys. J. 243, 127

10) Kunth, D. and Sargent, W.L.W. 1983, Astrophys. J. 273, 81

11) Lequeux, J., Peimbert, M., Rayo, J.F., Serrano, A. and Torres-Peimbert, S. 1979, Astron. Astrophys. 80, 155

12) Moles, M., Garcia-Pelayo, J.M., del Rio, G. and Lahulla, F. 1987, Astron. Astrophys. (in press)

13) Peimbert, M. and Costero, R. 1969, Bol. Obs. Ton. y Tacu. 5, 3

14) Sargent, W.L.W. 1970, Astrophys. J. 160, 405

15) Terlevich, R., Masegosa, J., Melnick, J. and Moles, M. 1987 "Spectroscopic Catalogue of HII Galaxies". In preparation.

16) Zwicky, F. 1964, Astrophys. J. 273, 81

Table 1

Parameters/Region	A	B	C	D	E
LOG (3727/5007)	0.04	0.05	-0.01	-0.01	-0.18
LOG (5007/Hβ)	0.048	0.042	0.72	0.47	0.66
LOG (6584/Hα	-1.17	-0.98	-0.29	—	—
LOG (F Hβ)	-14.66	-14.91	-16.07	-14.54	-14.95
EW(Hβ)	30.	26.	2.	34.	19.
[OII]+[OIII]/Hβ	0.87	0.80	1.10	0.84	0.98
N ([SII])	100	300	—	—	—
N ([OII])	100	100	—	170	100
T	9600	8800	—	9100	11400
12+LOG(O/H)$_{Pagel}$	8.38	8.44	—	8.38	8.20
12+LOG(O/H)	8.35	8.28	—	8.37	8.41
12+LOG(O^+/H^+)	8.09	8.03	—	8.03	8.04
12+LOG(O^{++}/H^+)	7.99	7.93	—	8.11	8.17
12+LOG(N^+/H^+)	6.50	6.69	—	—	—
12+LOG(N/H)	6.75	6.94	—	—	—
LOG (N/O)	-1.60	-1.34	—	—	—
12+LOG(Ne^{++}/H^+)	7.13	7.48	—	7.26	—
12+LOG(Ne/H)	7.48	7.83	—	7.53	—
LOG(Ne/O)	-0.87	-0.45	—	-0.84	—
He	0.081	0.084	—	—	—
Y	0.273	0.280	—	—	—

Table 2

GALAXY	LOG(S_{100}/S_{60})	LOG L_{IR}	LOG(L_{IR}/L_B)	LOG(L_{IR}/L_α)	SFR_{IR}	SFR_α
DDO 47	0.70	40.19	-0.52	2.64	0.002	0.0002
DDO 50	0.15	41.20	-0.38	1.67	0.020	0.02
N 4449	0.30	42.87	0.38	1.90	0.990	0.65
N 1569	0.00	42.69	0.46	1.50	0.650	1.10
IIZW 40	-0.10	42.73	1.23	1.32	0.720	1.80
N 3690	0.02	45.30	1.16	3.87	267.0	1.90
N 7714	-0.006	44.21	0.47	3.07	22.0	1.00
IZW 207	0.26	43.69	0.23	2.98	6.56	0.36

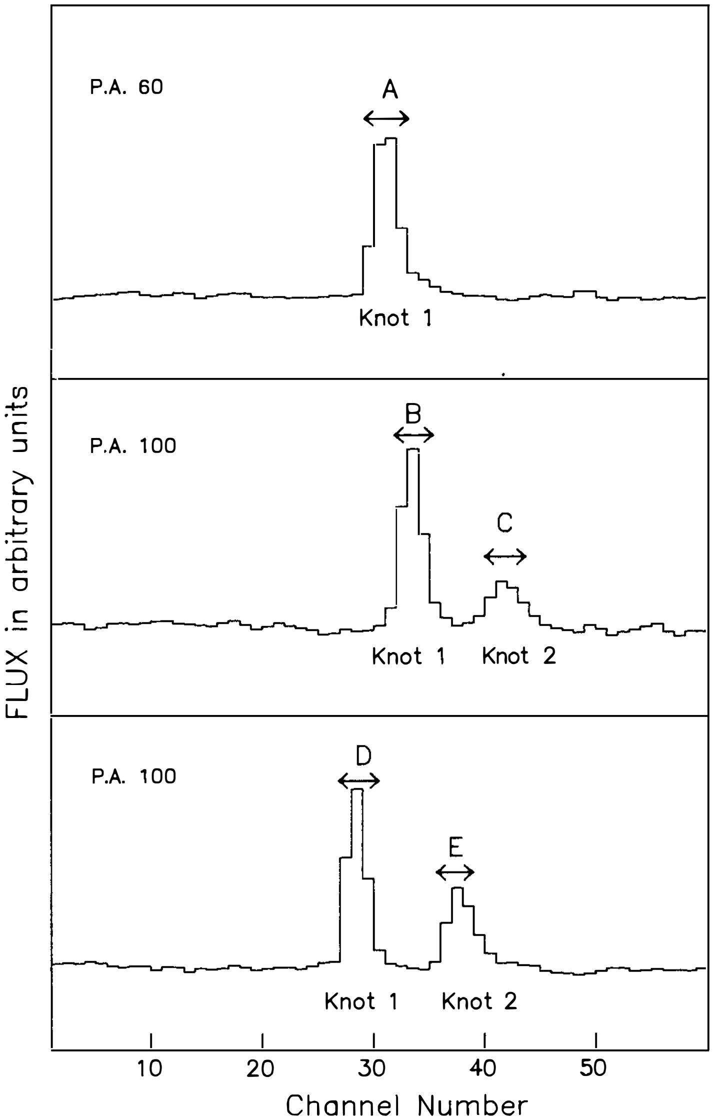

Figure 1.- The Hβ flux distribution along the slit for the three position angles. The different regions analyzed are indicated.

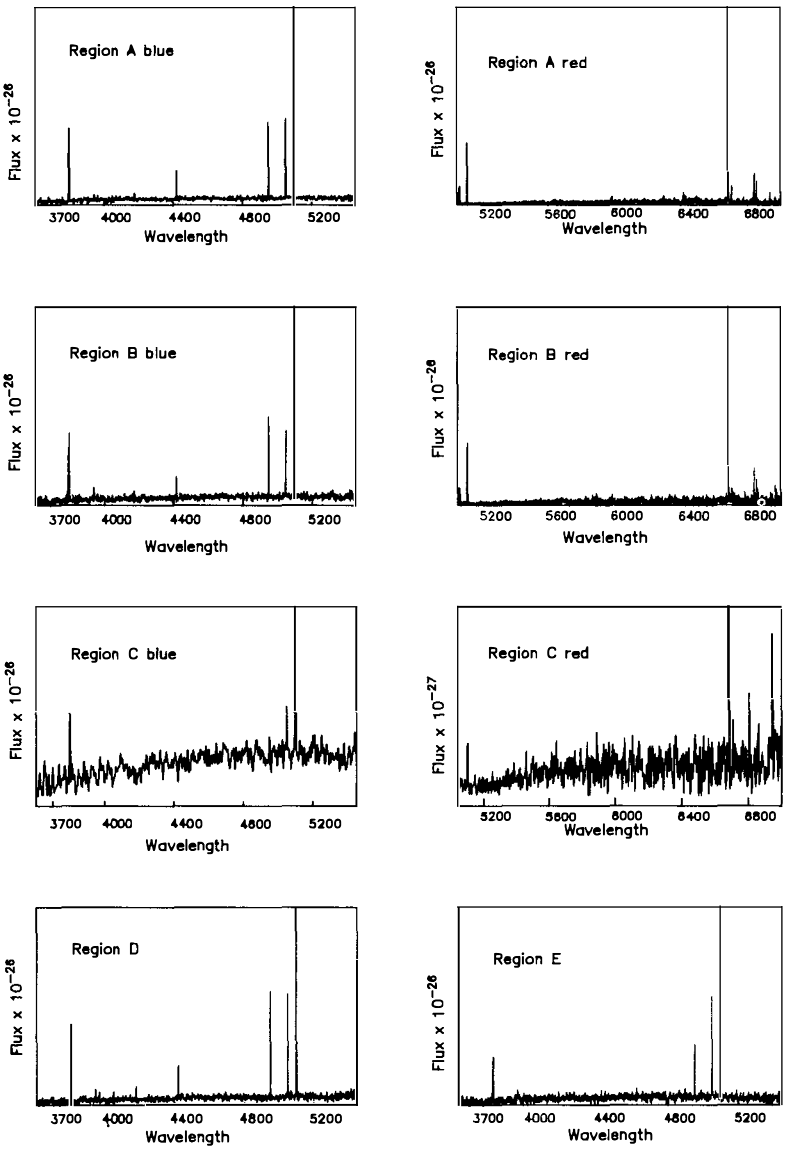

Figure 2.- The blue and red spectra for regions A to E. The flux units are ergs s^{-1} cm^{-2} Hz^{-1}.

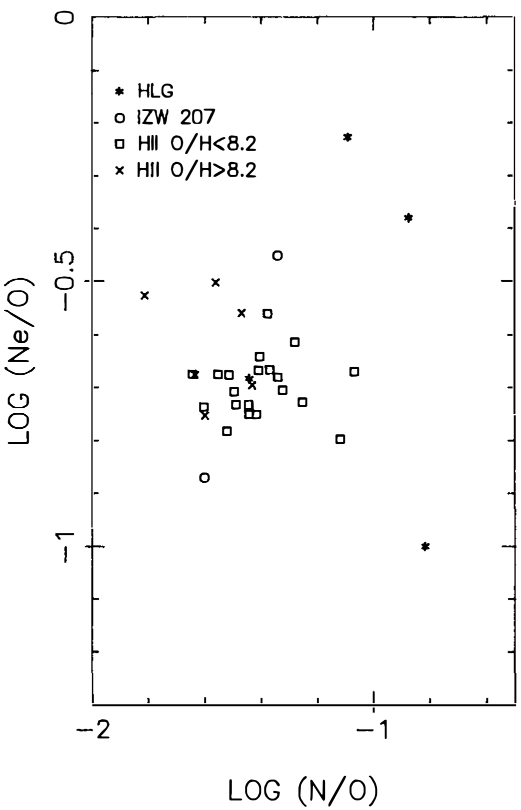

Figure 3.- Neon to Oxigen versus Nitrogen to Oxigen ratios for High Luminosity Galaxies, HII galaxies and IZw 207.

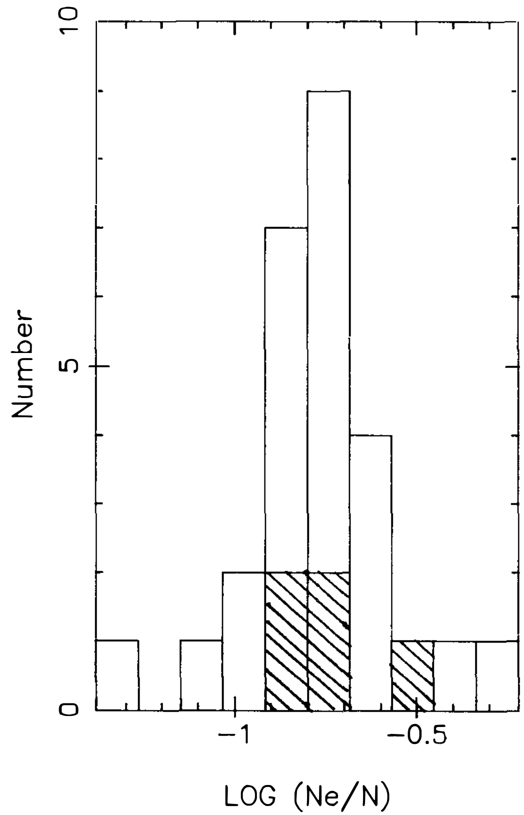

Figure 4.- Neon to Nitrogen ratio distribution for HII galaxies and High Luminosity ones (hatched histogram).

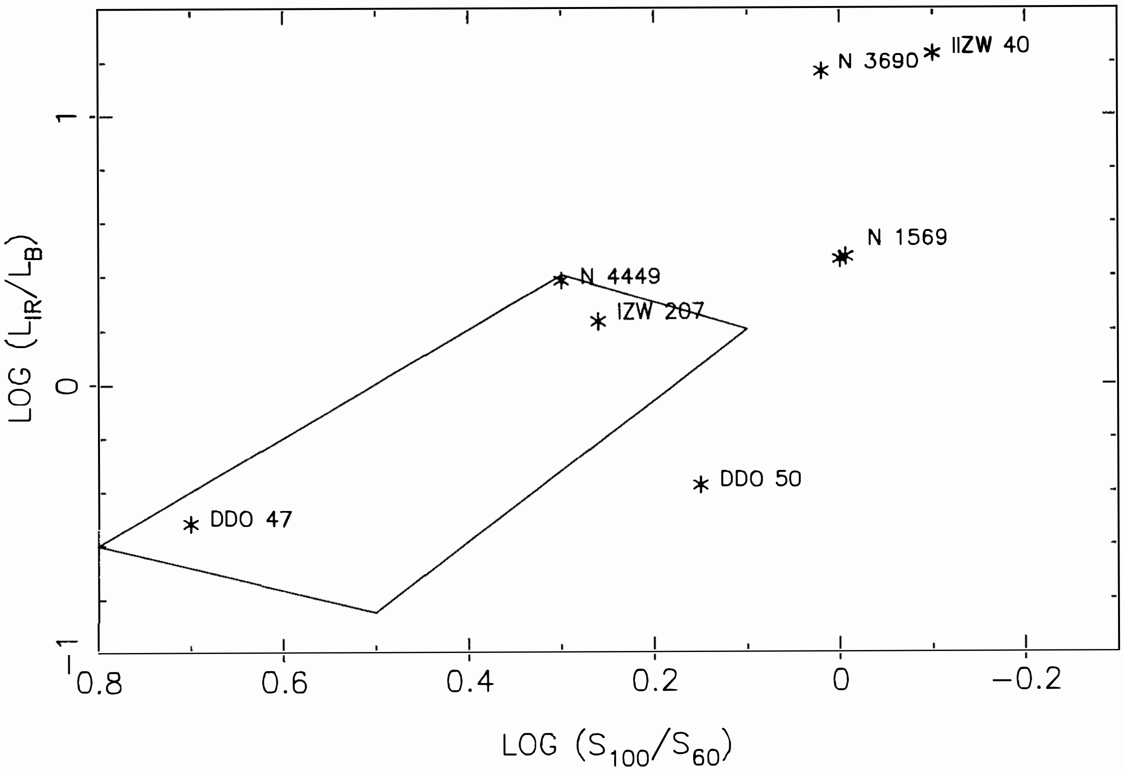

Figure 5.- Infrared to blue luminosity ratios versus far infared flux density ratios. It is also shown the locus for the Shapley Ames galaxies.

MM-OBSERVATIONS OF MARKARIAN GALAXIES

R. Chini
Max-Planck-Institut für Radioastronomie,
Auf dem Hügel 69, 5300 Bonn 1, F.R.G.

Abstract
We present high sensitivity continuum measurements at 1300μm of 14 Markarian galaxies. The spectral index between 100 and 1300μm clearly indicates that the emission must be thermal radiation from dust. We find a relation $L \propto M_g^{0.72}$ between M_g and the total luminosity L of the galaxies. At the low luminosity end classical star burst galaxies like M82 or NGC253 also follow this relation. This implies that the basic parameter for the strength of the activity is the gas mass.

Recently, a very similar dependence $L \propto M_g^{0.9}$ was found to hold for nonactive galaxies and visually obscured HII regions, but with L/M_g a factor of 20 lower. We conclude that a galaxy can be in either one of two modes: active or inactive. In both modes the luminosity is roughly proportional to the gas mass and therefore originates from star formation.

1. Introduction

The first Byrakan Spectral Sky Survey is a catalog of 1500 active galaxies which exhibit a strong UV continuum and an emission line spectrum. About 10% of the objects are Seyferts and a large fraction are so-called star burst and HII region galaxies. Extensive references to the Markarian objects are compiled by Mazzarella and Balzano (1986) and we use the information given in their tables thoughout this paper.

Our sample consists of 14 galaxies with strong FIR emission and turnover wavelength around 100μm. We investigate their spectral appearance at 1300μm. The only selection criterion for our sample was a flux density at 100μm greater than 10Jy. The sample contains two Seyfert 1, two Seyfert 2, eight star burst or HII region galaxies. Two remaining objects have not been classified, but they probably also belong to one of these classes. The observations were carried out at the 30m MRT on Pico Veleta, Spain, using the bolometer system developed at the MPIfR (Kreysa 1985). The HPBW of the Gaussian shaped beam was 11".

(1) Mrk number	(2) α(1950)	(3) δ(1950)	(4) $S_{1.3mm}$ (mJy)	(5) spectral index	(6) color temp.	(7) D (Mpc)	(8) $\log(M_g/M_\odot)$	(9) $\log(L/L_\odot)$	(10) activity class
158	105601.6	614746	6.1±2.8	2.95	33.1	27.6	8.21	10.46	SB
171	112542.8	585023	23.6 2.7	3.29	46.1	41.6	8.99	11.77	HII
188	114453.9	561457	<7	>2.87	>31.3	32.0	<8.43	10.52	
201	121139.9	544820	<9	>3.09	>37.5	33.6	<8.49	10.98	SB
231	125405.0	570837	42.7 4.6	2.61	26.1	164.0	10.73	12.52	Sy1
273	134251.2	560820	<18	>2.76	>28.9	149.0	<10.21	12.14	Sy2
603	030625.6	-30843	26.6 2.4	2.48	24.3	36.0	9.24	11.06	SB
617	043135.5	-84042	10.9 3.2	3.11	37.9	62.8	9.11	11.66	SB
620	064537.5	605413	12.3 2.6	2.61	26.2	26.0	8.58	10.70	Sy2
769	122253.9	164449	8.6 2.7	2.82	30.1	22.8	8.24	10.41	SB
1034	022024.0	315814	18.1 9.0	2.83	25.4	134.0	10.19	12.20	Sy1
1093	050519.5	-80459	7.0 2.2	2.91	32.1	60.0	8.96	11.35	SB
1194	050906.6	50826	28.5 4.7	2.34	22.6	63.2	9.80	11.34	SB
1466	120537.4	30922	6.0 1.8	2.92	32.2	17.6	7.83	10.65	

Table 1: *The spectral index (5) and the color temperature (6) refer to the wavelength interval from 100 to 1300μm and are explained in section 2. In column (10) "SB" stands for star burst galaxy and "HII" for HII region galaxy. Upper limits in column (4) are 3σ values.*

2. Results

Our 1300μm fluxes (see Table 1) together with the IRAS points allow us to determine the spectral index between 100 and 1300μm; α is defined by $S_\nu \propto \nu^\alpha$. The mean α of our sample (Table 1) is 2.83 ± 0.26, so most likely the radiation is due to thermal emission from dust. The temperature T_d (Table 1) has been derived as a color temperature asuming the dust emissivity to vary like $\nu^2 B\nu(T_d)$. For the distance determination we used a Hubble constant of 75km s^{-1} Mpc^{-1}. The total luminosity L was obtained by integrating the fluxes as available in the literature. Generally, most energy is emitted in the IRAS bands. We convert the flux at 1300μm into a gas mass as described in

Chini et al. (1987, paper I) and find that the luminosity L increases with the gas mass M_g; a least-square fit yields (Fig.1)

$$\log (L/L_\odot) = (0.72 \pm 0.11) \log(M_g/M_\odot) + (4.70 \pm 0.98). \quad (1)$$

Our Markarian galaxies are all unresolved by IRAS and listed in the IPC so that their sizes are smaller than 30" at 12μm and smaller than 120" at 100μm. Their mean optical diameter on the Palomar plates, as given in the original tables by Markarian and coworkers, is only 26"± 14". We may therefore expect that the region which emits the bulk luminosity is contained in our 11" beam at 1300μm. In other words, we assume that all flux densities refer to an 11" area and the juxtaposition of L vs. M_g is thus meaningful.

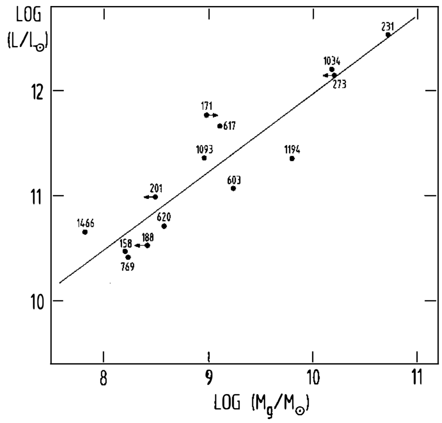

Fig.1: *Luminosity L vs. gas mass M_g for our sample of Mrk galaxies. L was obtained by integrating the flux densities as available in the literature. M_g was derived from the 1300μm point as described in Chini et al. (1987). Arrows pointing to the left are on those galaxies with only upper flux limits at 1300μm. The solid line is a least-square fit given by Eq.(1).*

3. Discussion

Before we proceed with the interpretation of Eq.(1) it is useful to recall that a relation $L \propto M_g^{0.9}$ has recently been established for optically invisible HII regions (paper I) and bright IRAS galaxies, mostly late type spirals (Chini et al. 1986, paper II). It is valid over eight orders of magnitude and it was obtained in the same manner as here by comparing the 1300μm flux with the integrated spectrum. There are two straight-forward conclusions from this remarkable dependence. First, the luminosity is always due to the formation of massive stars and, second, there is a fair proportionality between star formation rate and gas mass, no matter whether one is dealing with a humble HII region or a giant galaxy.

The present Eq.(1) has a similar slope as the above mentioned relation of paper I and II, but it yields some twenty times larger luminosities. This leads to a new definition of activity: Active galaxies have a high ratio L/M_g of order 100 (in solar units) in contrast to the nonactive with L/M_g around 5. In this definition it is not the absolute luminosity that counts, but the luminosity per available gas mass. So we argue, for example, that Arp 220, which is the most luminous member of the sample of paper II, is not a star burst galaxy, but derives its enormous luminosity from the prodigious amount of internal gas. On the other hand, the two classical star burst galaxies M82 and NGC253, for which 1mm fluxes have been obtained by Elias et al. (1978), follow Eq.(1) for active galaxies (see Fig.2).

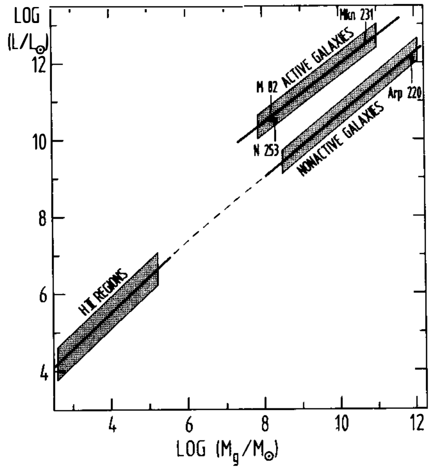

Fig.2: *Here the relation between luminosity and gas mass is shown for our Mrk sample as well as for inactive galaxies and optically obscured HII regions (papers I and II). HII regions and inactive galaxies lie on the same line, i.e. they have the same luminosity or star formation rate per unit of gas mass. In active galaxies the star formation rate is some twenty times higher.*

Fig. 1 shows L vs. M_g and the best fit line for the Markarian objects. Fig.2 displays in addition the optically obscured HII regions of paper I and the nonactive galaxies of paper II. A few prominent sources are indicated. The extragalactic sample is limited, but unbiased, as our only selection criterion is strong apparent 100μm luminosity. Fig.2 therefore suggests that galaxies exist in two modes: active and inactive. In either mode the luminosity is roughly proportional to the gas mass. We naturally conclude that the origin for the luminosity is star formation. The idea that star formation is at the root of infrared galaxies was first proposed by Harwit and Pacini (1975).

In active galaxies the star formation efficiency is extremely high, probably for two reasons: an increased efficiency for converting interstellar matter into stars and a bias of the initial mass function (IMF) towards higher masses. Both effects are needed to explain the brightness of the nuclei in NGC7714 (Weedman et al., 1981) and in NGC253 and M82 (Rieke et al., 1980; Kronberg et al., 1985).

To maintain a luminosity of $10^{10}L_\odot$ from steady state star formation, a few solar masses of gas have to be transformed annually into stars for a typical Miller-Scalo IMF. The activity stage is therefore time-limited because all the available interstellar matter will be used up in less than 10^8yr (see Eq.(1)). So an active galaxy eventually resettles into the nonactive mode and, conversely, an inactive galaxy is occasionally pushed into activity.
The important question is: what triggers the activity? The fashionable answer

says: merging of galaxies. Indeed, almost half of the present Mrk objects have "some sort" of companion according to the list of Mazzarella and Balzano (1986). While the idea of dynamical interaction to explain star bursts is very suggestive, no details have been worked out so far. In the classical process by Toomre and Toomre (1972), which is always cited in this context, the tidal forces during the collision lead to an inflow of mass into the nuclear (a few kpc) region thus providing the fuel for the star burst. No further analysis of how this fuel is transformed into stars is available. Contrary to this, we argue on the basis of Fig.2 that it cannot only be fuel which is needed for activity because for a given gas mass we find both active and inactive galaxies. The effects of merging that are conducive to star formation can lie only in the stirring up of the interstellar medium.

Merging cannot be the sole cause for activity and its importance may sometimes be overestimated. A number of cautioning remarks in this direction have been made by Mazzarella and Balzano (1986). It must be realized that a considerable fraction of active galaxies are singles. Eight objects in our sample do not show signs of close pair interaction. In those isolated systems star bursts have to occur through some intrinsic mechanism. Two scenarios with periodic star formation have been worked out quantitatively.

First, Loose et al. (1982) propose a dynamical scheme for a galactic nucleus (~1 kpc diameter), where the gas swings in the gravitational field of the central stars like a piston. The inward motion is caused by gravitational attraction and proceeds through the dissipation of turbulent cloud motion (and the transportation of angular momentum through viscosity). It is stopped when the gas density is high enough for rapid star formation to occur. The outward motion of the gas is driven by the subsequent supernova explosions. The period of the burst is determined by the rate at which gas is replenished by mass loss from (old) population II stars (or by the inflow rate of gas from the disk) and by the life-time of the progenitor stars of supernovae. A typical period is 10^8yr, of which the activity stage comprises some 25% of the time. The transition phase, where a galaxy would be observed between the two lines of Fig.2, is less than 10%. This would explain why we do not observe objects there. In the models the activity stage is terminated by the dispersive effects of the supernovae and not by an exhaustion of gas mass. This may explain why we do not detect objects above the upper line of Fig.2. The observed increase in luminosity from inactivity to activity by a factor of 20 is also qualitatively correctly reproduced in the Loose et al. scenario.

Second, Ikeuchi et al. (1987) investigate a simple balance equation for the destruction and creation processes of giant molecular clouds. These giant molecular clouds are assumed to be the site of star formation and the analysis leads to periodic solutions in their surface density and thus also to a periodicity of star formation itself. Whether such a process would work in the nuclear regions of galaxies needs, however, further investigation.

4. Conclusions

We have detected 1300μm continuum radiation at the 10mJy level from Markarian galaxies. From the relation between gas mass M_g and luminosity L found in this and in two preceding papers (I and II) we draw the following conclusions:

The star formation rate per unit gas mass is the same in individual HII regions as well as in nonactive (spiral) galaxies, irrespective of the luminosity. Markarian galaxies, which comprise a variety of activity types including Seyferts, are also powered by star formation, but with a very enhanced efficiency. Nonthermal point sources in such galaxies can therefore only be a byproduct, but not the cause of the activity. In the (L, M_g)-plane the distinction between active and inactive galaxies is very clear. The large fraction of isolated active systems suggests that merging of galaxies cannot be the only reason for activity. Alternative scenarios are discussed. In those cases where merging is responsible, the activity is not generated by the increase in gas mass, but by some other mechanism.

References

Chini, R., Kreysa, E., Krügel, E., Mezger, P.: 1986, A&A **166**, L10 (paper II)
Chini, R., Krügel, E., Wargau, W.: 1987, A&A in press (paper I)
Elias et al.: 1978, ApJ. **220**, 25
Harwit, M., Pacini, F.: 1975, ApJ. **200**, L127
Ikeuchi, S.: 1987, IAU Symp. **115**, 691
Kreysa, E.: 1985, URSI Proc. "Int. Symp. on mm and submm wave radio astronomy"(Granada 11.-14.9.84), p.153
Kronberg, P.; Biermann, P., Schwab, F.,: 1985, ApJ. **291**, 693
Loose, H., Krügel, E., Tutukov, A.: 1982, ApJ. **105**, 342
Mazzarella, J., Balzano, V.: 1986, ApJ. Suppl. **62**, 751
Rieke, G., Lebofsky, M., Thompson, R., Low, F., Tokunaga, A.: ApJ. **238**, 24
Toomre, A., Toomre, J.: 1972, ApJ. **178**, 623
Weedman, D., Feldman, F., Balzano, V., Ramsey, L., Sramek, R., Wu, C.: 1981, ApJ. **248**, 195

UV, OPTICAL AND INFRARED PROPERTIES OF STAR FORMING GALAXIES

John P. Huchra
Harvard-Smithsonian Center for Astrophysics
Cambridge, MA
U.S.A.

The UVOIR properties of galaxies with extreme star formation rates are examined. These objects seem to fall into three distinct classes which can be called (1) extragalactic HII regions, (2) clumpy irregulars, and (3) starburst galaxies. Extragalactic HII regions are dominated by recently formed stars and may be considered "young" galaxies if the definition of young is having the majority of total integrated star formation occuring in the last billion years. Clumpy irregulars are bursts of star formation superposed on an old population and are probably good examples of stochastic star formation. It is possible that star formation in these galaxies is triggered by the infall of gas clouds or dwarf companions. Starburst galaxies are much more luminous, dustier and more metal rich than the other classes. These objects show evidence for shock induced star formation where shocks may be caused by interaction with massive companions or are the result of an extremely strong density wave.

1. Introduction

The zoo of star forming galaxies (SFG's) contains many creatures. In fact almost every type of galaxies is forming stars, some albeit slowly. For the purposes of this talk however, I will restrict the use of that definition to those galaxies that are currently involved in "significant" episodes of star formation. One finds that there are basically three classes of object which meet that slightly loose definition. These are the Clumpy Irregulars (named by Heidmann and Casini), the Extragalactic HII Regions (named by Sargent and Searle 1970), and the so called Starburst Nuclei or Starburst Galaxies (named by Weedman). All of these objects are basically undergoing a current burst of star formation that dominates their observed properties.

As in any review, I think it is important to describe what we are trying to learn about the subject. The problems in question are (1) the *age* or timescale of the star formation episode - are there young galaxies? how often do such epidemics of star formation occur? (2) the *Initial Mass Function* (IMF), especially as a function of environment, eg. metallicity, parent galaxy luminosity, galaxy interaction rate, etc., (3) the *Star Formation Rate* (SFR) that describes the history of the galaxy, (4) the *Metallicity* and its role indetermining the SFR and IMF, and (5) the role of *dust*. In particular, all of this information is required to understand the MECHANISMS responsible for star formation in galaxies, including our own galaxy.

Also of interest to me is the connection between nearby star forming galaxies and cosmology. Studies of bursts of star formation in local systems give cosmologists important clues about galaxy evolution and the expected appearance of objects at high redshift and of primeval galaxies. By definition, this is important for understanding deep galaxy counts.

Since an excellent recent general review of star formation in dwarf galaxies and related objects already exists (Kunth, Thuan and Tran Than Van 1986), I will not try to duplicate that work but instead concentrate on several different insights and observations that I think are important in understanding extreme episodes of star formation in galaxies.

2. The Program at CfA

Inorder to try to answer some of the above mentioned questions, I have been involved for over a decade in programs to study galaxies undergoing intense bursts of star formation. This work has been in collaboration with L. Hartmann and M. Geller (at CfA), M. Aaronson (at the University of Arizona), J. Gallagher and D. Hunter (now at Lowell Observatory), and P. O'Brien and R. Wilson (of University College London). The basic data consist of UV-IR energy distributions (SED's) and spectroscopy for objects from each class obtained with IUE, the MMT, at Kitt Peak and from the literature. Some examples of galaxies in each class are:

Eg HII: Mk 36, I Zw 18 = Mk 116, Mk 59, II Zw 70

Clumpy Irr: NGC 4214, NGC 4670, NGC 5253

Starburst: NGC3310, NGC 7714

In addition to our own observations, the IUE archives contain a wealth of data obtained for similar purposes by Thuan, Oke, Peimbert and others. An excellent compilation can be found in Rosa et al. (1984). The primary use of these SED's is for comparison to evolutionary models which will be described in more detail below. Some representative spectra of galaxies from the three above-mentioned classes are shown in Figures 1 and 2. We have made special effort to observe several higher redshift starburst galaxies to measure Ly α emission for comparison with primeval galaxy models.

In addition to SED's, we are also obtaining detailed internal kinematics for

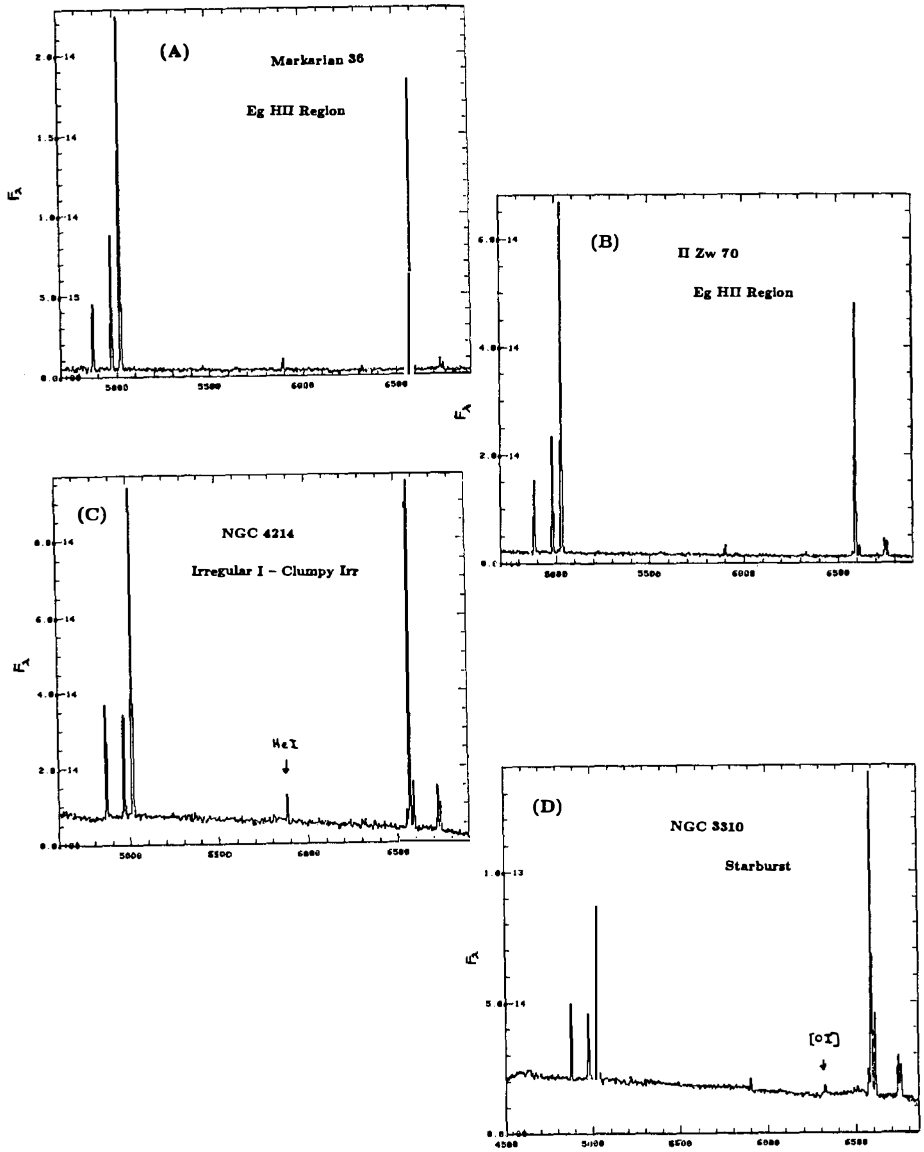

Figure 1. Optical spectra of star forming galaxies of different types. (A) and (B) Markarian 36 and II ZW 70, both extragalactic HII regions with spectra dominated by [OIII] and Balmer emission lines and with very weak [NII] and [SII] lines. (C) the clumpy irregular NGC 4214, and (D) the starburst galaxy NGC 3310. Note the presence of a relatively strong [OI] $\lambda 6300$ line in NGC 3310. Note also the stronger continua in both (C) and (D) compared to (A) and (B).

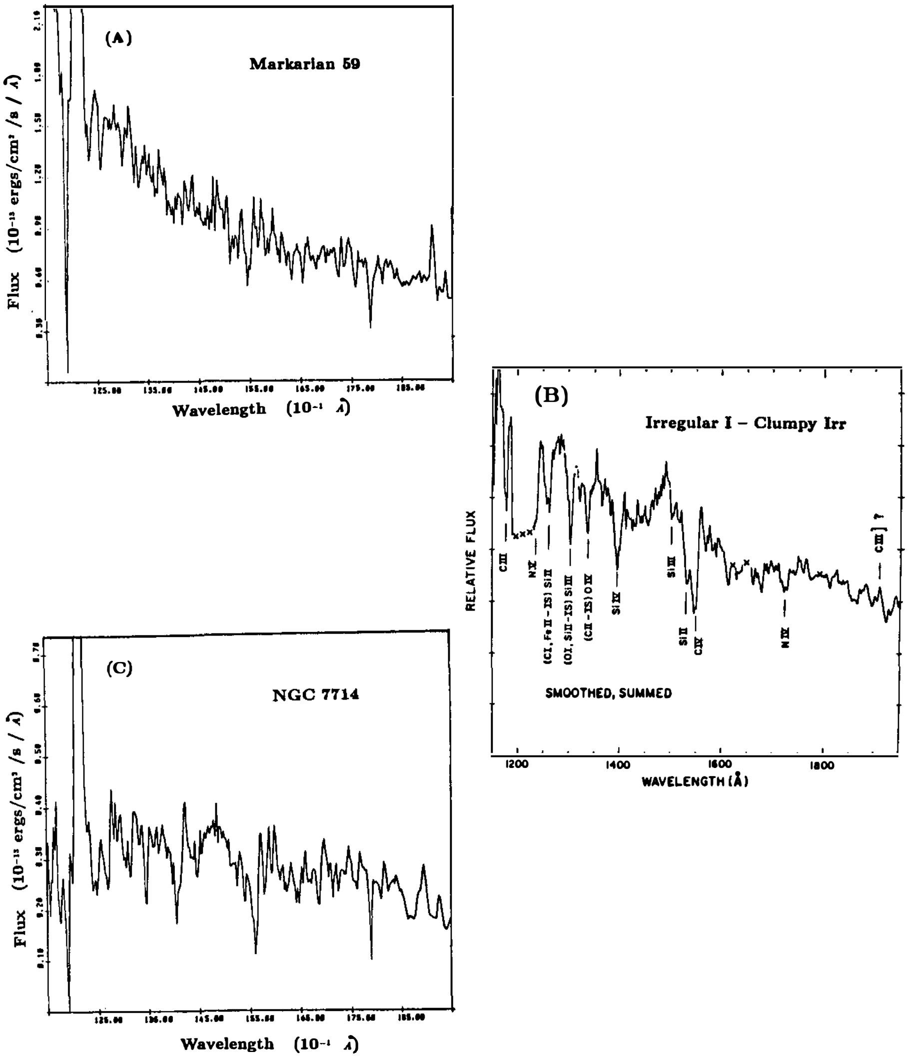

Figure 2. UV spectra (obtained with IUE) of star forming galaxies. (A) Markarian 59 from J. B. Oke is an example of an Eg HII galaxy. (B) is the composite spectrum of NGC 4214 and NGC 4670 from Huchra et al. (1983), clumpy irregular galaxies. Note the P Cygni profiles in the CIV and SiIV lines. (C) NGC 7714 from C. Wu, the archtypical starburst galaxy. It also shows the normal UV absorption lines seen in O and B stars, but the spectral shape is much flatter than those in (A) and (B).

several of the nearest and thus most spatially resolved objects using echelle spectrographs at Mt. Hopkins. Other kinematical and morpohological studies of SFG's have recently been started (eg. Thuan in this conference and Loose and Thuan 1986), and these will be important in sorting out the various dynamical mechanisms that can be responsible for star formation.

3. The Classes of Star Forming Galaxies

The in troduction of a taxonomy for objects is only of use if it enlightens one about differences in physical processes between objects. The first steps in understanding such processes, however, is often just recognizing that differences may exist. In this section I would like to outline the major differences I see between the three general classes of star forming galaxies mentioned above. Later, we will discuss possible differences in evolutionary states and the physical mechanisms of star formation in these classes.

The optical colors of galaxies of the three classes are similar. The Clumpy Irregular (CI) and Starburst (SB) galaxies are onlyslightly redder than the Extragalactic HII regions (Eg HII); all three classes are significantly bluer than more normal spiral and irregular galaxies (Huchra 1977a). The differences between the classes become much more obvious in the infrared and ultraviolet. The Eg HII are much, much bluer in V-K and have ultraviolet continua that are still rising strongly below Ly α. The SB galaxies have spectra that are nearly flat in the UV. Both the CI and SB galaxies have strong stellar absorption lines in the ultraviolet; the C IV and Si IV lines are in P Cygni. The Eg HII have no *strong* lines in the ultraviolet — neither absorption nor emission.

The optical spectra of Eg HII are completely dominated by emission from hot gas; they have only a weak continuum and extremely weak metal absorption lines.

The optical spectra of CI and SB galaxies are cooler, more metal rich, and more dominated by the underlying stellar continua. In addition, 'nonthermal,' or shock excited lines like those of [OI] are usually strong in SB galaxies.

The far infrared properties of SFG's can be studied using data from the IRAS survey. Starburst galaxies, in fact, account for a large fraction of extragalactic IRAS sources. If the 60-100μ color is simply interpreted as a dust temperature, the CI's are only slightly warmer than ordinary late type spiral galaxies, but still fairly cold, $F_{60} < F_{100}$. The starburst galaxies, on the other hand, are warmer with $F_{60} \sim F_{100}$. Few of the catalogued Eg HII galaxies have other than upper limits in the IRAS point source catalog, which could be due either to their generally low apparent luminosities or, more probably, to their low metallicity which implies a lower dust to gas ratio. In the SB galaxies, it is interesting to note that F_{60}/F_{100} increases with infrared luminosity, L_{60}, while F_{12}/F_{60} decreases with L_{60}.

Morpologically, the Eg HII galaxies are usually very compact objects, sometimes multiple. They are usually of very low luminosity although examples have been found that are as luminous as the Milky way. CI galaxies are Magellanic irregulars that are undergoing excessive star formation. In general, star formation activity is proceeding vigorously over the whole of the galaxy, unlike, for example, the LMC where most of the very recent star formation is centered only on 30 Doradus. The CI's are generally more luminous than the Eg HII, but are rarely more luminous than the Milky Way. SB galaxies tend to be distorted spirals, and are often interacting. In most of the cases I have examined, vigorous star formation is not confined to the nuclear regions, but proceeds over most of the disk. For example, their U-B color does not decrease significantly with radius (Huchra 1977a). SB's are generally luminous objects.

Statistically, in a B magnitude limited sample (eg. the CfA Redshift Survey galaxies selected from the Zwicky catalog), Eg HII galaxies constitute less than 1% of the sample, CI's are a few % of the sample and SB's are approximately 10% of the sample (Burg 1987). SFG's are not as rare as originally thought although the extreme examples (Eg HII's) are.

4. Evolutionary Models

The integrated spectral energy distributions of the three classes of galaxies can be compared with simple evolutionary models to try to determine ages, star formation rates and possibly IMF's. The simplest such models just integrate over the contributions of stars at different points in their lifetimes (Huchra 1977b, Tinsley 1968, Struck-Marcell and Tinsley 1978). The galaxy flux at time t in the ith band, $F_G(i,t)$, is given by

$$F_G(i,t) = \Sigma_j \Sigma_k [\Psi(k,j) \int F_k(i,t')\, dt'] \quad (1)$$

where $F_k(i,t')$ is the flux of star of type k in bandpass i at age t', and $\Psi(k,j)$ is the birthrate function for stars of type k in jth timestep.

The contribution from gaseous emission can be computed assuming Stromgren sphere ionization (i.e. assuming the HII regions are ionization bounded). The continuum emission is given by

$$F_\lambda = N_e N_+ \gamma_\lambda(T_e) V \; ergs\; s^{-1}\; \AA^{-1} \quad (2)$$

where V is the volume ionized and γ is the continuous emission coefficient. The Balmer line emission is calculated following Zanstra (1931) where $N(H_0)$

$$F_{H_\beta} = 4.1x10^{-12}\; ergs\; s^{-1}\; N(H_0) \frac{\alpha^{eff}_{H_\beta}(T_e)}{\alpha_E(T_e)} \quad (3)$$

is the number of ionizing UV photons and the α's are the H_β and total recombination coefficients. An ionization bounded Stromgren Sphere implies

$$\alpha_E(T_e) N_e N_+ \approx N(H_o) \quad (4)$$

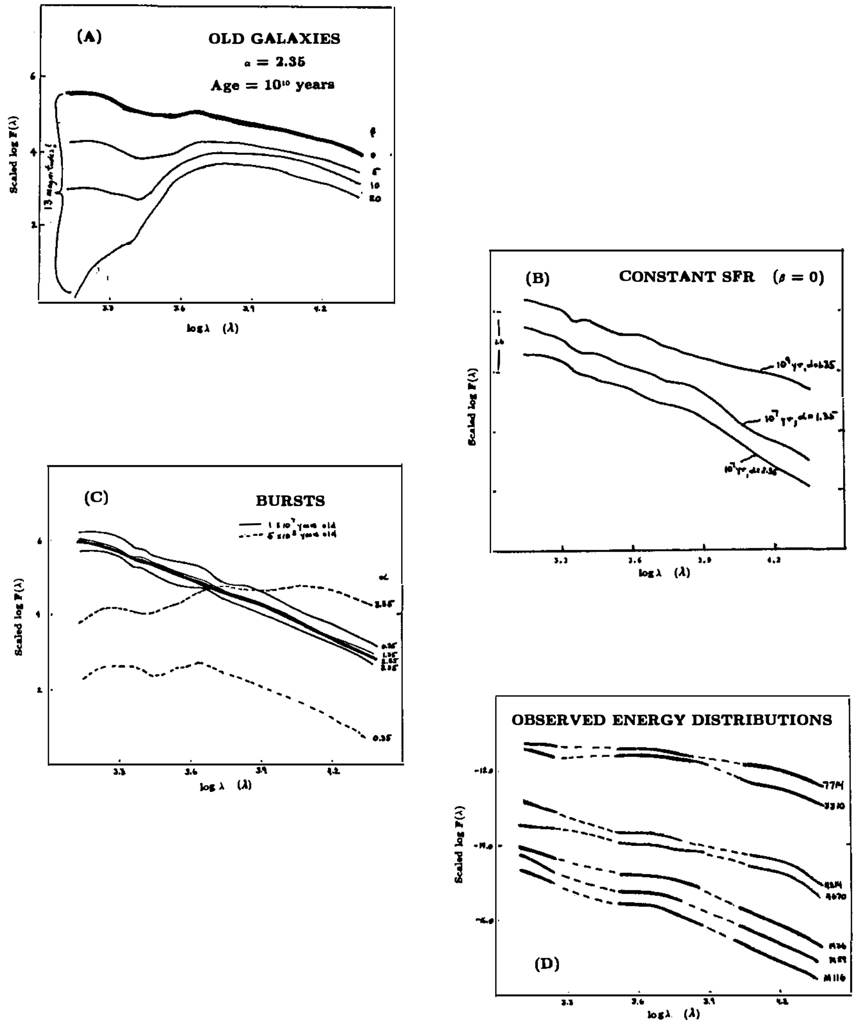

Figure 3. Spectral energy distributions computed for a variety of population models of galaxies (A) old galaxies, (B) galaxies with constant SFR's, and (C) bursts of star formation. (D) shows the observed SED's of representative galaxies for each of the classes Eg HII(Mk36, Mk59, Mk116), CI (N4214 and N4670), and SB (N7714 and N3310). Note the steepness of the SED's for the EG HII galaxies.

$$\rightarrow \; F_\lambda \; = \; N(H_o)\frac{\gamma_\lambda(T_e)}{\alpha_E(T_e)} \qquad (5)$$

With these assumptions, the total emission from gas is **only** a function of the number of ionizing photons $F(N(H_o))$; it does *not* depend very strongly on the gas temperature T_e.

For evolved (old) galaxies, the birthrate function is usually parameterized as

$$\Psi(m,t) \; = \; m^{-\alpha} \, e^{-\beta t/t_0} \qquad (6)$$

where the IMF is assumed to be a powerlaw. For example, in the Solar neighborhood, $\alpha \sim 2.35$, the Salpeter slope. The star formation rate is assumed to be exponential in time; if $\beta = 0$, the SFR is constant, if β is large, most of the star formation takes place while the galaxy is very young.

Figure 3 presents the energy distributions calculated for 3 different types of models as well as examples of the observed overall spectral energy distributions for objects in the three classes of SFG's. These energy distributions cover the range 1200 Åto 2.2 μ. The models shown are for old galaxies with different exponentially decreasing SFR's and the same IMF; galaxies with constant star formation rates but different ages and different IMF's; and pure bursts of star formation (burst duration = 25 million years) with different IMF's seen after 10 million and 50 million years. Note that these models differ significantly from the models of Struck-Marcell and Tinsley (1978) in that they include both the effects of gaseous emission and the very important contribution from red supergiants. Our yougest and bluest burst models never reach U-B = 0.0, whereas the bluest SMT models have U-B = -0.5.

Some interesting and important features of these models are that (1) the bursts become red very fast after they turn off, (2) the IMF has little or no effect on the SED of a burst although objects with steep (low mass star enriched) IMFs will redden faster after the burst turns off, and (3) the SED of a galaxy with a constant

SFR will redden slowly with time.

Observers often use color-color plots to detect and quantify subtle differences in SED's. One such plot useful for distinguishing the properties of the differenct classes of SFG's is the infrared-optical V-K versus the ultraviolet-optical U_1-V plot. U_1 is the magnitude at 1400 Å. Figure 4 shows this diagram for a variety of models as well as selected objects from the three classes. There is a clear separation of the Eg HII galaxies from the other two classes; the CI's are less well separated from the SB's, but are noticeibly bluer in U_1-V than the SB's. The properties of this diagram will be discussed further below.

Another very important diagnostic for star formation in galaxies is their emission line properties. I introduced the notion of using the equivalent width of Hβ to try to measure the slope of the IMF (Huchra 1977b). Kennicutt (1983) has shown that the total Hα flux of a galaxy is a good measure of its integrated star formation and has used this to derive SFR's for a large number of spiral galaxies. More recently, Campbell, Terlevich and Melnick (1986, preprint 1987, and Melnick in this volume) have used gas temperatures and equivalent widths to show that the IMF in SFG's is a function of metallicity, with low metallicity galaxies forming stars with flatter or high mass star enriched IMF's.

5. Results from Energy Distributions and Spectra

Eg HII galaxies are dominated by low metallicity O Stars. From the extensive work of the Piemberts, Pagel, Kunth and others (eg. Kunth 1985) we know that [Fe/H] ≤ 0.1 in these objects. Mk 36, for example, contains 300 O stars and perhaps 1 M supergiant or 100 K-M giants (Huchra et al. 1982). These objects are almost pure bursts of star formation and could even be called *young* galaxies. Most of the star formation that has **ever** taken place in the galaxy has happened recently. If we adopt a quantitative definition of "young" as having more than 50% of their

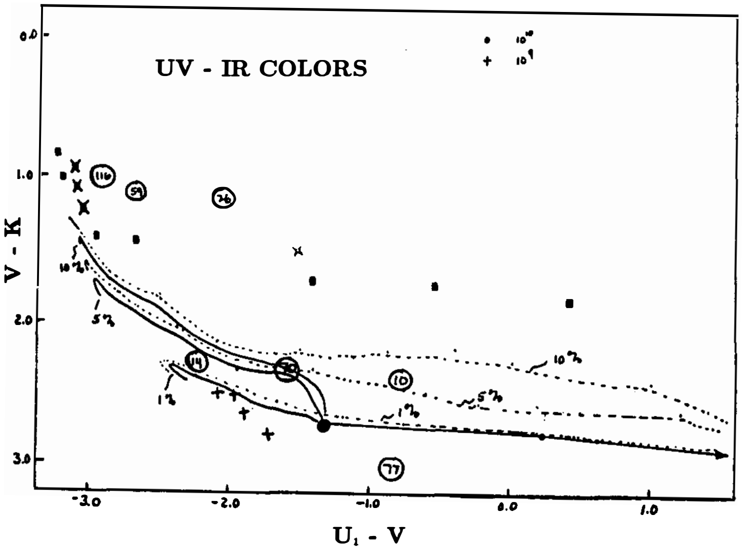

Figure 4. The V-K versus U_1-V color-color diagram for several models plus the actual observed colors for the galaxies in figure 3 (d). The galaxies are shown as large circles with their identification enclosed (14 = NGC 4214; 10 = NGC 3310; 77 = NGC 7714; 70 = NGC 4670 and the others are Markarian numbers). The crossed boxes are pure burst models; the straight solid line near the bottom represents the locus of old galaxies with slightly declining SFR's; the solid circle is a galaxy with a constant SFR; the dotted lines and solid curving lines are loci of models with bursts of star formation superposed on old populations. The percentages refer to the fraction of mass involved in recent star formation.

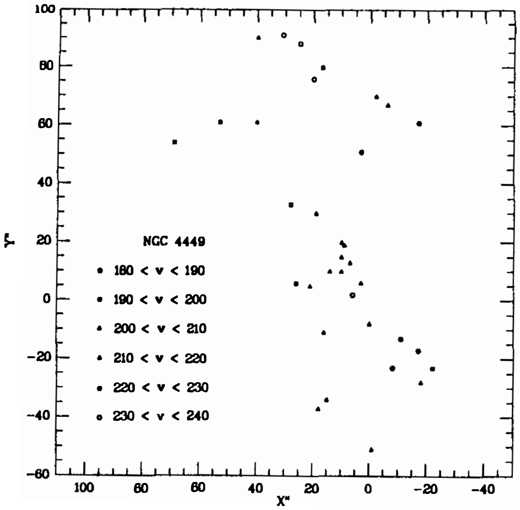

Figure 5. The observed velocity field map for NGC 4449 from observations at the Whipple Observatory 1.5-m.

integrated star formation in the last 10^9 years, these galaxies are it. The average age of the dominant population is $\sim\ 5x10^7$ years (and depends slightly on the IMF). The only alternative to the "young" galaxy hypothesis is that population II stars (low metallicity) never evolve into red supergiants or giants.

In the color-color plot of figure 4, these galaxies lie near the tip of the pure burst branch in V-K but are slightly redder than predicted in U_1-V. This could easily be due to a very small amount of reddening, A_V's of 0.1 to 0.2, since $E_{(U_1-V)} \sim 5\ A_V$. This is consistent with their low metallicity and with other measures of internal extinction.

The CI's are also dominated by O stars, but are more metal rich. 50% of their UV continua is from O stars of mean spectral type O6 or O7. The observed P Cygni profiles are indicative of normal population I stars with mass loss. Morphologically, these galaxies are dominated by giant HII regions. In NGC 4670 there are the equivalent of 2000 O5 stars, in NGC 4214 ther are $\sim$ 500 O5 stars, and the observed radio emission is free-free (Huchra et al. 1983). These galaxies are best described by a burst of star formation superposed on a 'well developed' old population. A few % of the galaxy's mass is involved in the current episode of star formation.

The SB's are much like the CI's in stellar content. They are slightly more metal rich and dustier (larger IRAS fluxes and a position further to the red in U_1-V). They are more luminous. Radio emission is partly Synchrotron, probably from supernova remnants. A major difference w.r.t the other two classes of galaxy is the strong [OI] lines which are usually indicative of significant amounts of shocked gas. Morphologically many of these galaxies are interacting with relatively massive neighbors, although a small fraction are apparently isolated.

6. The Internal Kinematics of Irregulars

An important diagnostic of possible causes of the enhanced SFR in galaxies is their kinematics. We have been obtaining high precision (1 km s^{-1}) echelle velocities for HII Regions in NGC4214, NGC4449 (Hartmann, Huchra and Geller 1986) and several other galaxies. Similar work has been described at this conference by Thuan and collaborators using a scanning Fabry-Perot. Figure 5 is the velocity map for NGC 4449.

In the galaxies we have studied, which are primarily clumpy irregulars, we find that chaotic motions dominate on small scales. The velocity dispersion (Chaotic) is of the same magnitude or larger than any systematic motions (eg. Rotation) seen. $\sigma_{gal} \sim 20\ to\ 30\ kms^{-1}$. In addition, the line widths of individual HII regions in the clumpy irregulars are $\sim 20\ kms^{-1}$. The masses of NGC 4214 and NGC 4449 in HI are both $\sim 10^9$ $M_\odot$. The momentum input from the stellar population (winds from O and B stars plus supernovae) is $\sim 5 \times 10^{46}$ g cm s^{-1}, which is only enough to move 10^7 $M_\odot$ at 20 km s^{-1}. The mass in the central regions of the galaxies is $> 10^8$ $M_\odot$. Clearly additional momentum input is needed. Both NGC 4214 and NGC 4449 have dwarf, gas rich companions. We have suggested that the intense star formation seen now in such galaxies is the result of recent mergers or collisions with gas clouds or gas-rich dwarf galaxies (Hartmann, Huchra and Geller 1986).

7. Summary

I have made the case that SFG's fall into three distinct classes: (1) extragalactic HII regions, (2) clumpy irregulars, and (3) starburst galaxies. Extragalactic HII regions are dominated by recently formed stars. If the definition of a "young" galaxy is one where the majority ($>$ 50%) of its total integrated star formation has occured in the last billion years, Eg HII galaxies are probably "young" galaxies. Clumpy irregular galaxies are bursts of star formation superposed on an old population. The star formation pattern in these galaxies is chaotic and they may be examples of stochastic star formation. The few detailed kinematical studies that have been done suggest that star formation in these galaxies is triggered by the infall of gas clouds or dwarf companions. Starburst galaxies are much more luminous, dustier and appear to be more metal rich than the other classes. These objects show evidence for shock induced star formation. Since many of these galaxies are interacting with massive (as opposed to dwarf) companions, the shocks are almost certainly caused by dynamical interaction and/or gas transfer from the companion. In those SB galaxies that do not show evidence for interaction, I think the enhanced star formation may be the result of an extremely strong density wave.

This work has been supported by NASA grant NAG-5-87.

References

Burg, R. 1987, *Ph. D. Thesis*, Massachusetts Institute of Technology.

Campbell, A., Terlevich, R. and Melnick, J. 1986, *M. N. R. A. S.* **223**, 811.

Kunth, D., Thuan, T. X. T. and Tran Than Van, J. eds. 1986, *Star Forming Dwarf Galaxies and Related Objects*, (France: Editions Frontieres).

Hartmann, L., Huchra, J., and Geller, M. 1986, *A. J.* **92**, 1278.

Huchra, J. 1977a, *Ap. J. Suppl.* **35**, 171.

Huchra, J. 1977b, *Ap. J.* **217**, 928.

Huchra, J., Geller, M., Hunter, D. and Gallagher, J. 1982, in *Advances in Ultraviolet Astronomy: Four Years of IUE Research*, ed. Y. Kondo, (NASA).

Huchra, J., Geller, M., Gallagher, J., Hunter, D., Hartmann, L., Fabbiano, G. and Aaronson, M. 1983, *Ap. J.* **274**,

Kennicutt, R. C. 1983, *Ap. J.* **272**, 54.

Kunth, D. 1986, in *Star Forming Dwarf Galaxies*, (Editions Frontieres), p 183.

Loose, H. and Thuan, T. X. 1986, in *Star Forming Dwarf Galaxies*, (Editions Frontieres), p 73.

Rosa, M., Joubert, M. and Benvenuti, P. 1984, *Astron. and Ap. Suppl.* **57**, 361.

Sargent, W. L. W. and Searle, L. 1970, *Ap. J. Lett.* **162**, L155.

Struck-Marcell, C. and Tinsley, B. 1978, *Ap. J.* **221**, 562.

Tinsley, B. 1968, *Ap. J.* **151**, 547.
Zanstra, H. 1931, *Pub. Dom. Ap. Obs.* **4**, 234.

HII GALAXIES

Jorge Melnick
European Southern Observatory
D-8046 Garching bei München, F.R.G.

HII galaxies are the simplest systems where the starburst phenomenon can be studied at galactic scales. Some relevant properties of HII galaxies are reviewed and new results on the morphology and environments of these objects are presented. About 50% of the HII galaxies studied are starlike and isolated. They are promising candidates for being young galaxies.

1. INTRODUCTION

HII galaxies are a class of blue compact galaxies (BCG's) characterized by having giant HII region-like spectra. This class was first identified by Sargent and Searle[1] who called them Isolated Extragalactic HII Regions. Since, however, not all HII galaxies are isolated, we prefer to call them HII galaxies.

In this contribution I would like to review some of the generic properties of HII galaxies. In particular, I will present some statistical results from our "Spectrophotometric Catalogue of HII Galaxies" (henceforth the SCHG)[2], I will briefly review the results on the IMF of HII galaxies and discuss recent results on the kinematics of HII galaxies and their application as distance indicators. To conclude I will present new results on the morphology of HII galaxies based on recent CCD imagery.

Most of the work I will describe has been done in collaboration with Roberto Terlevich and Mariano Moles. Bernard Pagel (this volume) has described the results of using the HII galaxies of the SCHG to determine the primordial abundance of helium.

2. STATISTICAL PROPERTIES OF HII GALAXIES

The SCHG contains close to 1000 spectra of somewhat more than 400 HII galaxies selected from objective prism surveys, mostly in the southern hemisphere. Most of the spectra in the SCHG are low resolution either IDS or RETICON observations aimed at determining fluxes and redshifts as well as a spectral classification. About one hundred objects were selected for higher resolution studies with the purpose of determining abundances and gas kinematics (from line profile analysis). I will discuss these results in the following two sections.

The only result from the low resolution data I would like to present here is the absolute magnitude distribution. This is shown in Figure 1. The absolute blue magnitudes were computed as[3],

$$M_B = -2.5 \log \frac{L(H\beta)}{W(H\beta)} + 79.4$$

where $L(H\beta)$ is the integrated $H\beta$ luminosity, corrected for reddening and $W(H\beta)$ the equivalent width of the line. The large luminosities of HII galaxies reflect their large star formation rates. Using the equations of Terlevich and Melnick[3], one estimates that after the massive stars disappear, HII galaxies will be on average 4 magnitudes fainter than the present values and thus the "evolved" values for the absolute magnitudes will range from M_B = -19 to -9 which is the range of values commonly assigned to dwarf galaxies[4].

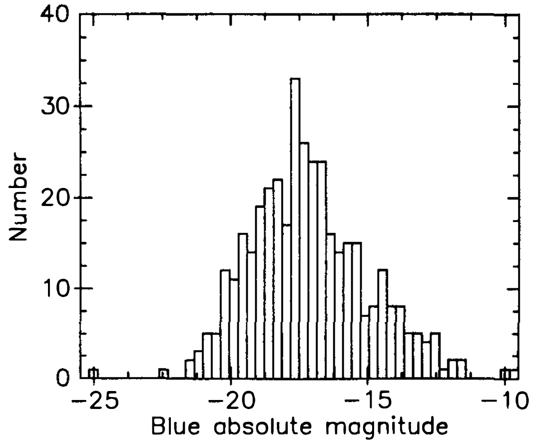

Fig. 1. Distribution of absolute blue magnitudes for more than 400 HII galaxies in the SCHG.

Figure 2 shows a series of representative spectra of HII galaxies compared to the spectrum of the prototypical giant HII regions 30 Doradus. The similarities are evident. Figures 1 and 2 illustrate the observational basis of the classification of HII galaxies as giant HII region-like dwarf galaxies.

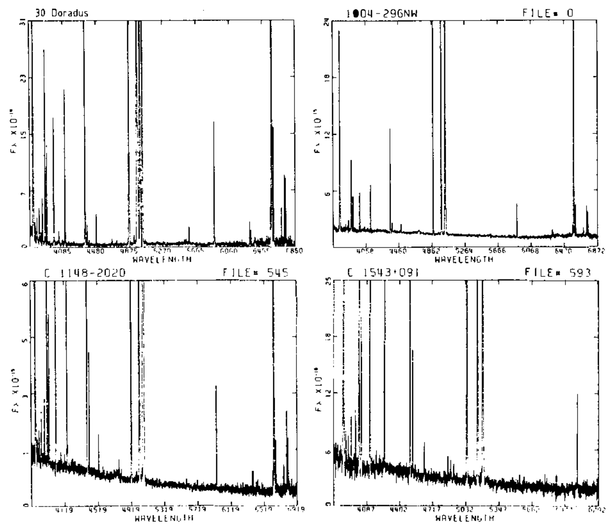

Fig. 2. Spectra of three representative HII galaxies and of the prototype giant HII region 30 Doradus.

3. THE IMF OF HII GALAXIES

Richness and stochastic effects[5,6] preclude most efforts to determine stellar initial mass functions (IMF) from the luminosity function of isolated parts of galaxies and lead to questioning the meaning of a galaxy-wide IMF[7]. The only places where the stellar IMF can be directly observed are very young, massive, star clusters where stochastic effects are minimal and where the full mass range may be realized. In the Galaxy, the IMF of the largest open clusters has been studied by Taff[8] and Burki[9], and I[10] have studied the luminosity function of the 30 Doradus cluster in the LMC. The general conclusion of these studies is that the IMF of these systems differs significantly from the Salpeter function.

Terlevich and I have argued in several different papers[3,5,11,12] that the slope of the IMF in giant HII regions and HII galaxies must decrease as the metallicity of these systems goes down. I would like to review here very briefly the evidence for this conclusion. More detailed discussions of these issues can be found in the above references and in the papers by Melnick et al.[13] and Campbell et al.[14].

3.1. Dynamical results

The integrated Hβ luminosities of HII galaxies correlate with the velocity dispersion of the nebular gas, σ, as[14],

$$L(H\beta) \propto \sigma^{4.5\pm0.5}$$

The same correlation is valid for giant HII regions and in fact this is one of the defining properties of giant HII regions[13]. These correlations are illustrated in figure 3. In fact L(Hβ) depends not only on σ but also on the oxygen abundance of the nebular gas (O/H). A multi-parameter analysis shows that the (L(Hβ),σ,O/H) relation has the functional form[14],

$$L(H\beta) \propto \frac{\sigma^5}{(O/H)} \tag{1}$$

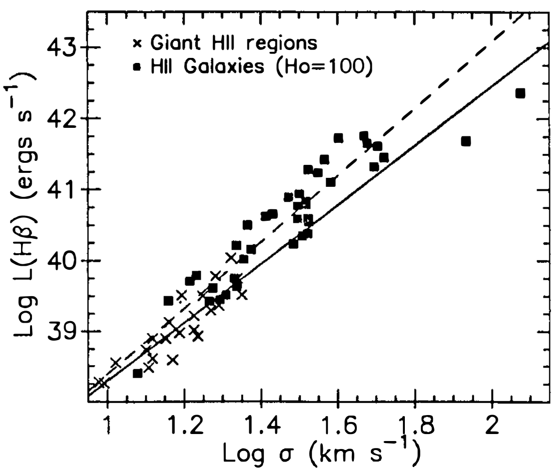

Fig. 3. Correlation between integrated Hβ luminosity and velocity dispersion for giant HII regions and HII galaxies. A Hubble constant of H_o = 100 km s^{-1} Mpc^{-1} has been used to compute the luminosities of HII galaxies.

Giant HII regions exhibit the same correlation except that there $L(H\beta) \propto R_c\sigma^2/(O/H)$ [13]. Both results are equivalent since (for giant HII regions) the core radii, R_c, scale as σ^3. Thus, if we assume that giant HII regions and HII galaxies (that is the HII region component) are gravitationally bound and that $R_c\sigma^2$ measures their total masses, eq. 1 implies that the ratio between the stellar mass and the ionizing luminosity of starburst clusters increases approximately linearly with oxygen abundance. We have computed population synthesis models to investigate the origin of this correlation[15], and concluded that it can only be explained if the IMF gets steeper with increasing metallicity[11]. Of course, this conclusion is valid only if the gas motions are due to gravity. The case for nebular turbulence driven by stellar winds has not yet been convincingly made but remains an intriguing possibility that must be investigated further[13].

3.2. Spectrophotometric evidence

There are about 70 HII galaxies in the SCHG for which we have oxygen abundances based on a direct measurement of the strength of the [OIII]λ4363 line. From these data we arrive at results which cannot (at least easily) be explained by models with constant IMF. Figure 4 presents a plot of the electronic temperature of the ionized gas, T_e, as a function of oxygen abundance. The

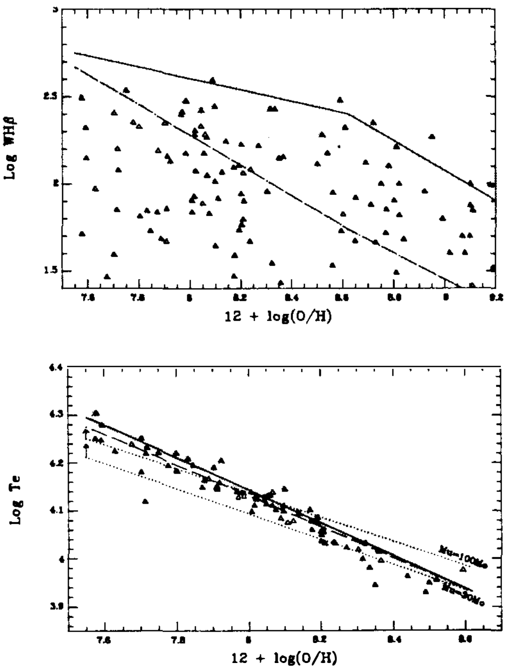

Fig. 4. (upper) Relation between electronic temperature and oxygen abundance for HII galaxies (adapted from Terlevich[5]). (lower) Distribution of Hβ equivalent widths as a function of abundance for HII galaxies. The shaded area represents the locus of zero-age clusters.

dotted lines represent the predictions of models with a fixed IMF for 2 different values of the upper mass limit (M_U = 30 $M_\odot$ and M_U = 100 $M_\odot$) and the dashed line represents a model with variable M_U between 30 and 150 $M_\odot$. The solid line shows the fit of a variable slope using the relation between IMF slope and metallicity derived by Terlevich and Melnick[11)] from the mass to light ratios. Both the variable M_U and the variable slope models are seen to fit the data reasonably well. The lower panel in figure 4 shows a plot of the equivalent width of the Hβ line, W(Hβ), plotted against abundance. Since W(Hβ) depends on the age and on the luminosity of the underlying stellar component one does not expect a correlation between W(Hβ) and abundance but a broad distribution with an upper envelope corresponding to zero-age clusters with no underlying galaxy[5)]. Variable M_U models for ZAMS stars (dashed line) are a poor representation of the data while the variable slope model (solid line) fits remarkably well the zero age envelope. Therefore in order to simultaneously fit both the (T_e,O/H) and the (W(Hβ),O/H) diagrams either both the upper and the lower cutoffs of the IMF must change with metallicity or the slope must change with abundance. If the lower cutoff M_L is varying, in order to explain the large values of W(Hβ) observed for the most metal poor HII galaxies M_L must be close to 10 $M_\odot$ [11)]. If globular clusters are the descendants of starburst clusters, as seems to be suggested by the continuity in the properties of LMC clusters of ages ranging from less than 10^7 yrs to a Hubble time[6)], a strong metallicity dependence of M_L can be ruled out.

4. HII GALAXIES AS DISTANCE INDICATORS

The rms dispersion of the L(Hβ),σ,(O/H) relation is 0.55 magnitudes, comparable to the scatter of the best available distance indicators. Thus the

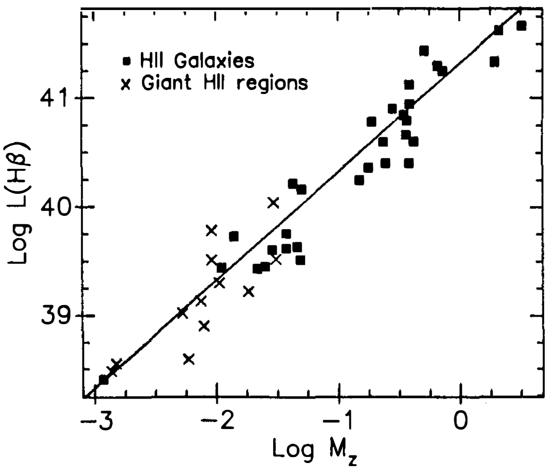

Fig. 5. Relation between Hβ luminosity and the distance indicator parameter and $M_z = \sigma^5/(O/H)$. H_0 = 100 km s^{-1} Mpc^{-1} was used to compute HII galaxy luminosities.

parameter $M_z = \sigma^5/(O/H)$ can be used to predict the luminosities of HII galaxies and thus to estimate their distances. Figure 5 shows a logarithmic plot of L(Hβ) versus M_z for the same HII galaxies as shown in figure 4. Also shown in this figure are 14 giant HII regions with accurate metallicities and distances known from Cepheid variables which we used as zero point calibrators. Notice that the shift of HII galaxies relative to giant HII regions which was apparent in the (L(Hβ),σ) plot (figure 3) has disappeared. This is because the HII galaxies in our sample are on average a factor of 1.6 times oxygen poorer than the calibrating HII regions. From these data we obtain a "raw" value of H_0 = 110 km s^{-1} Mpc^{-1} which, after correction for Malmquist bias and for the motion of the sun relative to the Cosmic Microwave Background, yields a final value of H_0 = 89±10 km s^{-1} Mpc^{-1}, compatible with some previous determinations[16,17] and incompatible with others, notably with that of Sandage and Tammann[18]. A complete discussion of these results will be presented elsewhere[14].

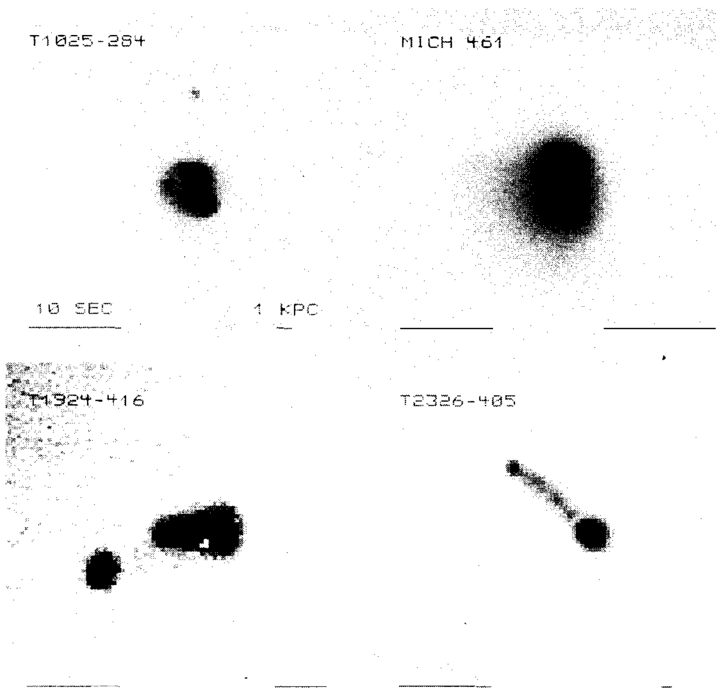

Fig. 6. CCD images of four HII galaxies of multiple morphology. North is at the top, west is to the left. The linear and the angular scales of each picture are also shown.

5. THE MORPHOLOGY OF HII GALAXIES

Using the Danish 1.5m telescope at La Silla we have recently obtained CCD pictures of 30 HII galaxies with the purpose of measuring diameters and studying their morphology and environments. On the basis of these data HII galaxies can be divided into three broad morphological types:

a) Multiple systems: These galaxies are dominated by more than one giant HII region. The small radial velocity differences between the components indicates that they are not parts of interacting systems. Four examples of this class are shown in figure 6.

b) Interacting systems: Here the HII galaxy is part of an interacting system characterized by tidal tails and/or distortion. Examples of this class are shown in figure 7.

c) Isolated objects: The HII galaxies in this class are isolated and in most cases stellar or semi-stellar. Typical examples are shown in figure 8.

A fourth class of objects which lies at the boundary of what we would call HII galaxies are amorphous galaxies with one or several giant HII regions in

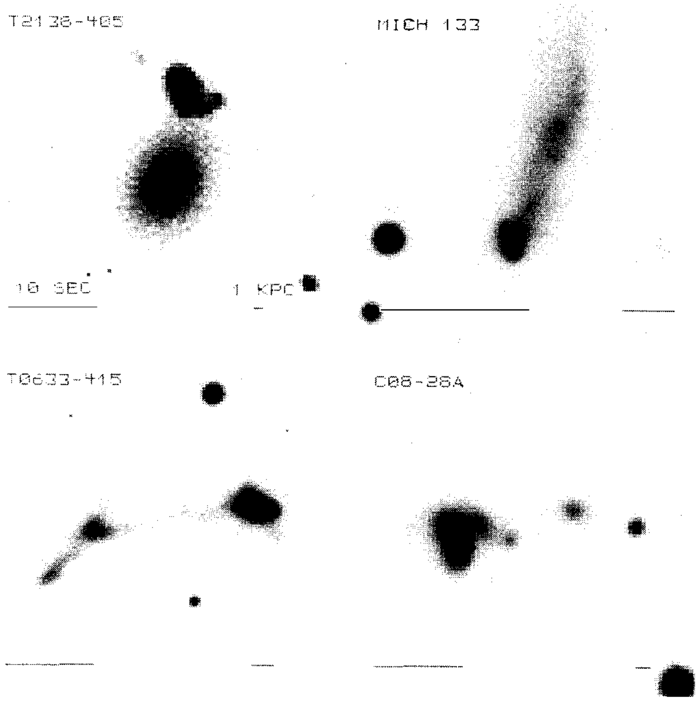

Fig. 7. CCD images of HII galaxies in interacting systems.

their central parts. Three examples of this class are shown in Figure 9. The starburst component of NGC 1705 has no emission lines but is a massive, young (~ 10^7 yrs) starburst cluster[19]. The spectrum of this cluster, shown in figure 9, illustrates the evolutionary connection between giant HII regions, starbursts. and young globular clusters in irregular galaxies.

In total, 20% of the objects surveyed appear to be parts of interacting systems, 30% have double or multiple HII region components and 50% are isolated with stellar or semi-stellar morphology. These results show that galaxy collisions and mergers are an important but by no means unique mechanism to induce starburst activity. In fact, the isolated semi-stellar objects which comprise half of our sample are probably the best candidates for being young galaxies.

CONCLUSION

The study of HII galaxies opens a number of urgent questions about violent star formation (starbursts). Particularly intriguing are the suggestion that the

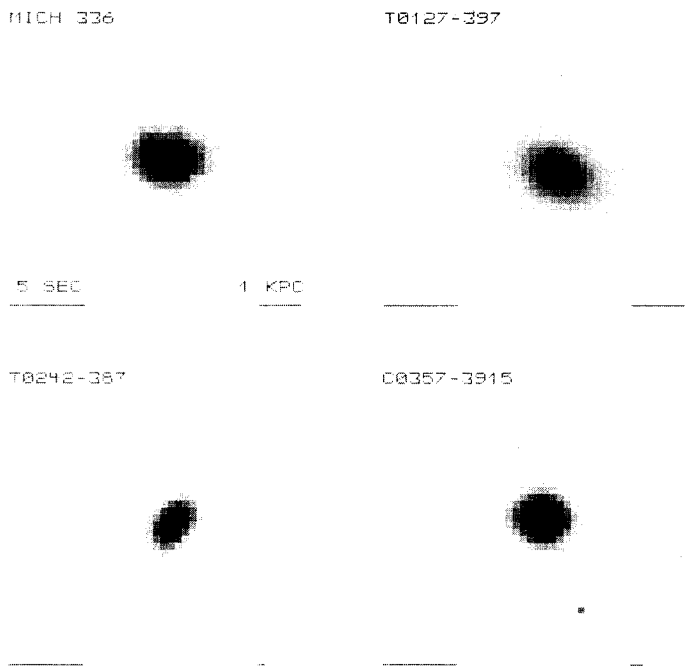

Fig. 8. CCD images of typical isolated HII galaxies.

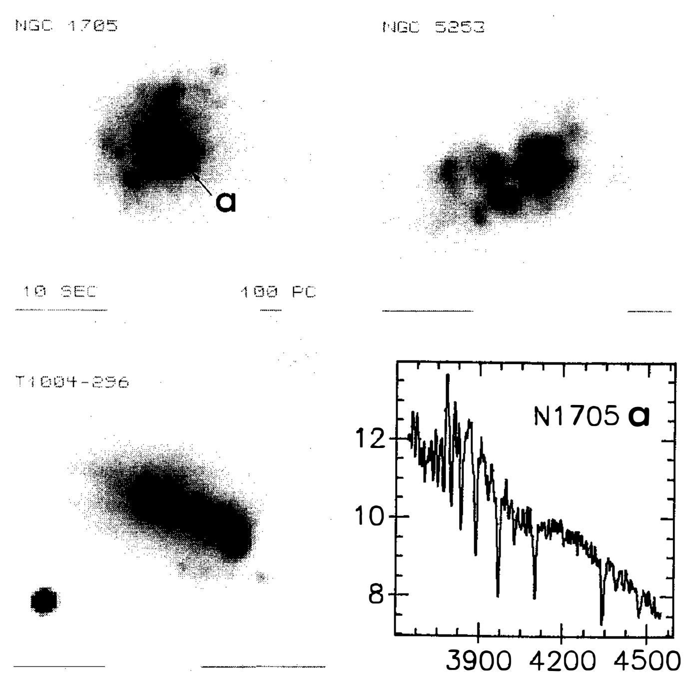

Fig. 9. Amorphous galaxies with HII region spectral characteristics. The starburst component of NGC 1705 is a massive young cluster, the spectrum of which is shown in the figure.

IMF of starbursts depends on chemical composition and the fact that a large fraction of HII galaxies are isolated and stellar and therefore may be young galaxies. High resolution 21 cm maps are badly needed to investigate the role of collisions between intergalactic neutral hydrogen clouds in the formation of these objects.

The galaxies with multiple morphology are also very interesting; in general the different components have different ages (as evidenced by their excitations and Hβ equivalent widths) and in many cases there are age gradients across the galaxies. This strongly suggests that violent star formation self-propagates in gas-rich dwarf galaxies.

I conclude with the usual plea for more observations; detailed 21 cm maps of HII galaxies are absolutely essential to progress further in our understanding of how HII galaxies, the simplest galaxies, are formed.

REFERENCES

1. Sargent, W.L.W., and Searle, L., 1970, Astrophys. J. (Letters), **162**, L155.
2. Terlevich, R., Melnick, J., Masegosa, J., and Moles, M., 1987, "Spectrophotometric Catalogue of HII galaxies", in preparation (SCHG).
3. Terlevich, R., and Melnick, J., 1981, MNRAS, **195**, 839.
4. Sandage, A., 1985, in "Star Forming Dwarf Galaxies and related objects", eds. Kunth, Thuan and Tran Thanh Van, Paris, Frontières, p. 31.
5. Terlevich, R., 1985, in "Star Forming Dwarf Galaxies ...", p. 395.
6. Chiosi, C., 1985, in "Star Forming Dwarf Galaxies ...", p. 449.
7. Melnick, J., 1987, preprint.
8. Taff, L.G., 1974, Astron. J., **79**, 128.
9. Burki, G., 1980, in "Star Clusters", IAU Symp. 85, ed. J. Hesser, p. 123.
10. Melnick, J., 1985, in "Star Forming Dwarf Galaxies ...", p. 171.
11. Terlevich, R., and Melnick, J., 1983, ESO preprint **264**.
12. Melnick, J., and Terlevich, R., 1986, Observatory, **106**, 69.
13. Melnick, J., Moles, M., and Terlevich, R., 1987, ESO preprint **444**, MNRAS, in press.
14. Campbell, A.R., Terlevich, R., and Melnick, J., 1986, MNRAS, **223**, 811.
15. Melnick, J., Terlevich, R., and Eggleton, P.P., 1985, MNRAS, **216**, 255.
16. Aaronson et al., 1986, Astrophys. J., **302**, 536.
17. de Vaucouleurs, G., and Peters, W.L., 1986, Astrophys. J. **297**, 27.
18. Tammann, G.A., 1987, ESO Preprint 489 and references therein.
19. Melnick, J., Moles, M., and Terlevich, R., 1985, Astr. Astrophys. **149**, L26.

STARBURSTS AND THE CHEMICAL EVOLUTION OF HII GALAXIES: AGES OF BURSTS VS LOCAL ENVIRONMENTAL POLLUTION

B E J Pagel
Royal Greenwich Observatory, Herstmonceux Castle,
Hailsham, East Sussex BN27 1RP

Summary

Results previously published for oxygen, nitrogen and helium abundances in HII galaxies are revised to allow for collisional contributions to the helium lines and a few further objects added. The relationships found are similar in general to those found previously, though with fewer objects departing from the dY/dZ relation derived by Peimbert and his colleagues, and are confirmed by a principal component analysis which shows that O/H accounts for about half of the variation in helium, but N/H for essentially all of it.

These effects are consistent with an additional component of helium and secondary nitrogen, superposed on primary nitrogen, with the additional component either coming from low-mass stars made in very old bursts or resulting from local pollution of the observed HII regions by winds from massive stars within them. Evidence from different regions of POX 4 and NGC 5253 gives some slight support to the latter hypothesis.

1. Introduction

Chemical evolution of gas-rich dwarf galaxies may in some ways be especially simple in the light of correlations of abundance with gas fraction and mass [1-4] but in other ways complicated by the discrete nature of starbursts[5-7]. In most cases, furthermore, information on their abundances comes from HII regions which may be locally polluted by newly synthesised elements in winds[8] or supernova ejecta[9]. Such pollution by winds has been observed in WN ring nebulae[10][11] and in a small outlying region of 30 Doradus[12]. In this paper I discuss peculiarities resulting from starbursts in HII regions and HII galaxies with well known helium, as well as nitrogen and oxygen, abundances[8][13-21].

2. The data

In previous work[8] [19], new data for HII galaxies by Terlevich and Melnick[22] [23] were used to study the primordial helium abundance Y_p and the relationship between Y, O and N. While confirming the existence of a dY/dZ slope against oxygen abundance O/H, as maintained by Peimbert *et al.*, we found this to be greater for HII galaxies than for HII regions in nearby irregulars, but that both kinds of objects fitted a single relation between Y and N/H. We suggested local pollution of HII regions in HII galaxies by winds from massive stars. Since then we have added further objects and made an agonising reappraisal of the helium abundances to allow for a collisional contribution following Ferland[24]. This is usually less than 5 per cent, and the results are described in detail elsewhere[21]. Fig 1 shows the new (He, O/H) and (He, N/H) relationships, which are qualitatively similar to those derived before[8], but the outstanding high-weight objects in the upper panel are few in number (to wit: 1214-277, NGC 5253A and marginally II Zw 40) and they need not be distant HII galaxies; nor is there any correlation with the visibility of WR features.

3. Statistical analysis

Roberto Terlevich has carried out ML and PC analyses for the data in Fig 1 using the program TABU written by J. Melnick. Linear maximum likelihood solutions (with 1σ errors) are (excluding NGC 604)

$$Y = .2297 + 135\,(O/H),\ \text{rms}\ .0092 \qquad (1)$$
$$\quad \pm\ 54 \quad \pm\ 45$$
$$= .2320 + 2730\,(N/H),\ \text{rms}\ .0083 \qquad (2)$$
$$\quad \pm\ 40 \quad \pm\ 820$$

confirming our previous findings[8] that the HII galaxy sample gives a larger value of dY/dZ than the value of about 3.2 found for nearby irregulars compared with one another[1] or with Galactic HII regions[25] and that helium is better correlated with N/H than with O/H. Without the three high-weight objects lying above the line in the upper panel of Fig 1 we would have dY/dZ ≃ 4 in accord with Peimbert[25], but differing from Vigroux et al. [26] who used very poor data.

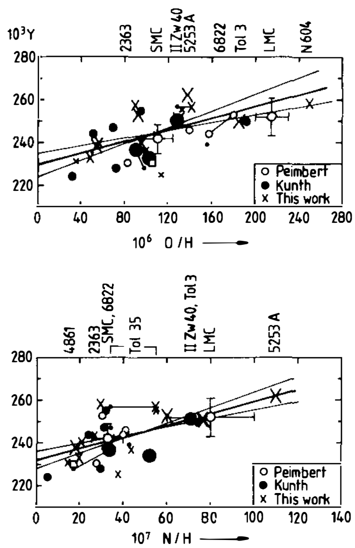

Fig. 1. Helium mass fraction Y plotted against O/H and N/H. Lines are maximum-likelihood regressions with ± 1σ error limits. Sizes of symbols are inversely related to the errors.

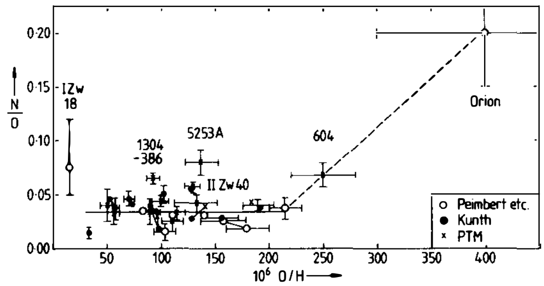

Fig. 2. N/O plotted against O/H for the objects in Fig. 1, with a few others (I Zw 18[30], NGC 604[20] and Orion[31]) added for purposes of illustration.

4. Discussion

Theoretically[27], C and N production peak for stars around 2.5 $M_\odot$, lifetime ~ 500 Myr, and He near 5 $M_\odot$, lifetime ~ 100 Myr, both long compared to HII region, but shortish on galactic, time-scales. However, some of all three elements comes from massive stars, in winds or supernova ejecta. Matteucci and Tosi[6] explain lack of correlation between N/O and O/H in irregular galaxies on the basis of primary N from stars below 5 $M_\odot$ combined with a bursting mode of star formation which gives enough time since the last burst to enable this nitrogen to swamp secondary N from high-mass stars. However, the nitrogen in subdwarfs seems also to demand primary production in massive stars at some stage[7]. This still leaves open the origin of the scatter in N/O (Fig 2), which could quite readily be associated with age differences[28] among the bursts but for the close association that we now find with helium which is produced in the normal way in about 1/5 of the time scale for nitrogen.

How much of the scatter in N/O is real? Fig 2 shows that in most cases the data are consistent with a constant value 0.034. Tol 65[29] and NGC 4861[13] are over 2σ below, which might be due to recent starbursts, but their errors may be underestimated. This leaves our three objects with abnormally high helium for their oxygen as the only ones standing out significantly with a corresponding excess of nitrogen. In principle this could be due to pollution by stellar winds[8] or just possibly the starbursts in these galaxies could be so exceptionally old that there has been time for stars with little over $1M_\odot$ (like the red giants in globular clusters[32]) to have contributed extra N and He. In both cases the additional nitrogen is secondary, but the consequences in the two cases are not identical. Only in the case of winds from WN stars we have the straightforward situation that all the original hydrogen has been changed into helium and all the CNO into nitrogen[27]. If such material is mixed with ambient interstellar gas with original mass fractions X of hydrogen and Z_{CO} of C + O, then the changes satisfy the simple relationships

$$\Delta Y/\Delta X_N = X/Z_{CO} \tag{3}$$

and

$$\Delta Y/\Delta(N/H) = 14X(X-\Delta Y)/Z_{CNO} \tag{4}$$

Table 1 shows that equation (4) fits our best data and the WR ring nebulae fairly well, consistent with the idea of local pollution[8] [19].

Table 1

He and nitrogen enrichment in WR nebulae and an HII galaxy

	Orion[11]	RCW58[11]	RCW104[11]	MR26[11]	NGC5253 A[21]
$10^4 \frac{O}{H}$	3.5	3.5	3.3	3.3	1.4
$10^5 \frac{N}{H}$	2.5	26	17	5.6	1.1
$10^5 \Delta(\frac{N}{H})$	.0	23.5	14.5	3.1	0.64
Y	.29	.54	.45	.36	.262 ± .007
ΔY	.00	.25	.16	.07	.017
Z_{CNO}	0.006	0.006	0.006	0.006	0.002:
$\Delta Y/\Delta(N/H)$ observed		1100	1100	2250:	2700
$\Delta Y/\Delta(N/H)$ from eq(4)		735	880	1030	3600:

The alternative (youth vs age of the underlying population) is more difficult to test, except in cases where one can compare abundances in different parts of one galaxy: age implies uniform abundances while pollution implies excess He and N in the affected HII region. The data in Table 2 are far from conclusive, but they give a little support to pollution and suggest the need for further careful long-slit observations.

Table 2

Evidence for nitrogen and helium gradients

	10^6(O/H)	10^7(N/H)	ΔY
POX 4 (nucleus)	90 ± 5[29] 96 ± 8[21]	35 ± 3[29] 34 ± 3[21]	.00 [21]
POX 4 (NW)	98 ± 12[29]	17 ± 4[29]	-.01:[21]
NGC 5253A	137 ± 15[21] 160 [33]	110 ± 15[21] 100: [33]	.02 [21]
NGC 5253B	200 ± 60[22]	62 ± 15[22]	?

I thank Roberto Terlevich and Jorge Melnick for supplying observational data and for carrying out the statistical analysis.

References

1) Lequeux, J., Peimbert, M., Rayo, J. F., Serrano, A., and Torres-Peimbert, S. 1979, Astr. Astrophys., **80**, 155
2) Kinman, T. D., and Davidson, K. 1981, Astrophys. J., **243**, 127
3) Pagel, B. E. J. 1986a, in Cosmogonical Processes, W. D. Arnett, C. J. Hansen, J. W. Truran and S. Tsuruta (eds), Utrecht: VNU Science Press, p. 66
4) Pagel, B. E. J. 1986b, in Highlights of Astronomy, J. P. Swings (ed), Reidel, p. 551
5) Matteucci, F., and Chiosi, C. 1983, Astr. Astrophys., **123**, 121
6) Matteucci, F., and Tosi, M. 1985, Mon.Not.R.astr.Soc., **217**, 391
7) Matteucci, F. 1986, Pub. Astr. Soc. Pacific, **98**, 973
8) Pagel, B. E. J., Terlevich, R. J., and Melnick, J. 1986, Pub. Astr. Soc. Pacific, **98**, 1005
9) Kunth, D., and Sargent, W. L. W. 1985, Astrophys. J., **300**, 496
10) Kwitter, K. 1984, Astrophys. J., **287**, 840
11) Rosa, M. 1986, in IAU Symposium no. 122, Heidelberg, in press
12) Rosa, M., and Mathis, J. S. 1987, Preprint
13) Dinerstein, H., and Shields, G. 1986, Astrophys. J., **311**, 45
14) Peimbert, M., and Torres-Peimbert, S. 1974, Astrophys. J., **193**, 327
15) Peimbert, M., and Torres-Peimbert, S. 1976, Astrophys. J., **203**, 581
16) Peimbert, M., Torres-Peimbert, S., and Peña, M. 1986, Astr. Astrophys., **158**, 266
17) Dufour, R.J., Shields, G., and Talbot, R. 1981, Astrophys. J. **252**, 461
18) Dufour, R. J., 1983, in IAU Symposium no. 108: Structure and Evolution of the Magellanic Clouds K. S. de Boer (ed), Reidel, p. 351
19) Pagel, B. E. J., 1987a, in Advances in Nuclear Astrophysics, E. Vangioni-Flam and J. T. T. Van (eds), Paris: Ed. Frontieres
20) Diaz, A. I., Terlevich, E., Pagel, B. E. J., Vilchez, J. M., and Edmunds, M. G., 1987, Mon. Not. R. astr. Soc., **226**, 19
21) Pagel, B. E J. 1987b, in First ESO-CERN School on Astro-Particle Physics, Erice, A. de Rujula, D. Nanopoulous and P. A. Shaver (eds) Singapore: World Scientific Publishing Co., in press
22) Campbell, A., Terlevich, R.J., and Melnick, J. 1986, Mon. Not. R. astr. Soc., **223**, 811
23) Terlevich, R. J., Melnick, J., Masegosa, J., and Moles, M. 1987, in preparation
24) Ferland, G. J., 1986, Astrophys, J., **310**, L67
25) Peimbert, M. 1985, in Star Forming Dwarf Galaxies, D. Kunth, T. X. Thuan and J. T. T. Van (eds), Paris: Ed. Frontieres, p. 403
26) Vigroux, L., Stasinska, G., and Comte, G. 1987, Astr. Astrophys., **172**, 15
27) Maeder, A. 1984, in Stellar Nucleosynthesis, C. Chiosi and A Renzini (eds), Reidel, p. 115
28) Edmunds, M. G., and Pagel, B. E. J., 1978, Mon. Not. R. Astr. Soc., **185**, 77P
29) Kunth, D., and Sargent, W. L. W. 1983, Astrophys. J., **273**, 81
30) Dufour, R.J. 1986, Pub. Astr. Soc. Pacific, **98**, 1025
31) Simpson, J.P., Rubin, R. H., Erickson, E. F., and Hass, M.R. 1986, Astrophys. J., **311**, 895
32) Kraft, R. P. 1985, in Production and Distribution of the CNO Elements, I. J. Danziger, F. Matteucci and K. Kjär (eds), ESO, Garching, p. 21
33) Webster, B. L.,and Smith, M. G. 1983, Mon. Not. R. astr. Soc., **204**, 743

III. STAR FORMATION IN IRAS AND INTERACTING GALAXIES

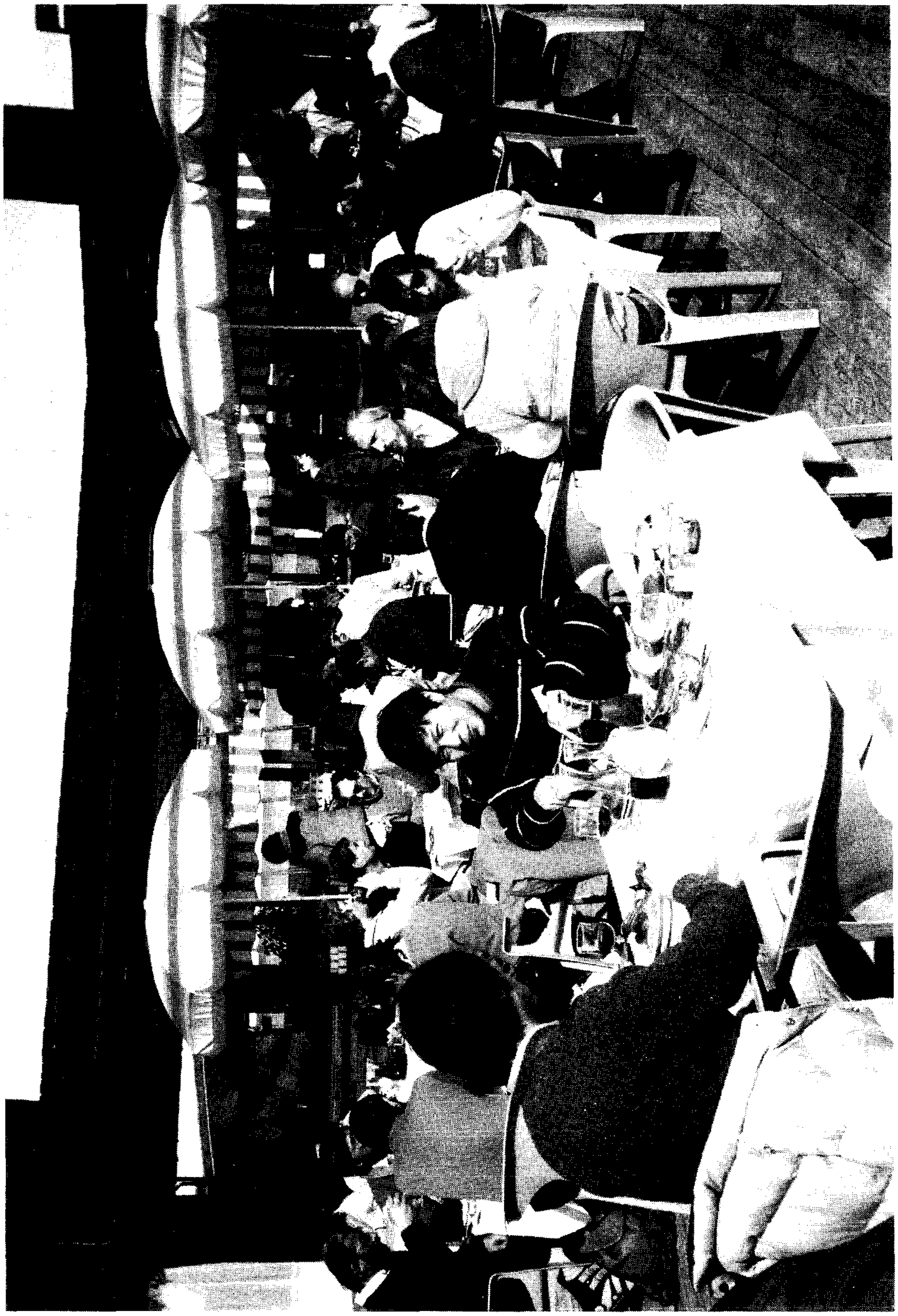

INFRARED PROPERTIES OF IRAS GALAXIES

M. Rowan-Robinson

Theoretical Astronomy Unit,
Queen Mary College,
Mile End Road, London, E1 4NS

ABSTRACT. The infrared emission from IRAS galaxies is modelled in terms of 3 components: a normal disc component, due to interstellar 'cirrus'; a starburst component, modelled as hot stars in an optically thick dust cloud; and a Seyfert component, modelled as a power-law continuum immersed in an $n(r) \propto r^{-1}$ dust cloud associated with the narrow-line region of the Seyfert nucleus. The correlations between the luminosities in the different components, the blue luminosity and the X-ray luminosity of the galaxies are consistent with the model. Spectra from 0.1 to 1000 μm are predicted and compared with available observations. The models are compared with those of other workers.

1. INTRODUCTION

The main properties we have to explain are:
(i) the great range of far infrared luminosities in IRAS galaxies, from $4 \times 10^7 - 4 \times 10^{12}$ $L_\odot$ at 60 μ (Fig 1).
(ii) the great range of ratio of far infrared to optical luminosity, in IRAS galaxies, from 0.05 to several hundred (Soifer et al 1984, Rowan-Robinson et al 1986),
(iii) the correlation of L_{FIR}/L_{opt} with S(100μ)/S(60μ) (de Jong et al 1984, Rowan-Robinson et al 1986),
(iv) the distribution of IRAS galaxies in the IRAS colour-colour diagrams,
(v) the fact that many Seyferts show a peak at 25 μ (Miley et al 1984, de Grijp et at 1985).

Far infrared (10-100 μ) radiation can be expected from a normal spiral galaxy due to a variety of mechanisms. Dust in interstellar neutral hydrogen clouds, illuminated by the general interstellar radiation field, radiates prominently at 100 μ and in our Galaxy has been called the infrared 'cirrus' (Low et al 1984). The cirrus is also seen at 60 μ and more recently has been found to be radiating surprisingly stongly at 25 and 12 μ (Gautier and Beichman 1985, Boulanger et al 1985). To radiate significantly at 12 μ, interstellar grains must include a grain population much hotter than the thermal equilibrium temperature and it has been postulated that this

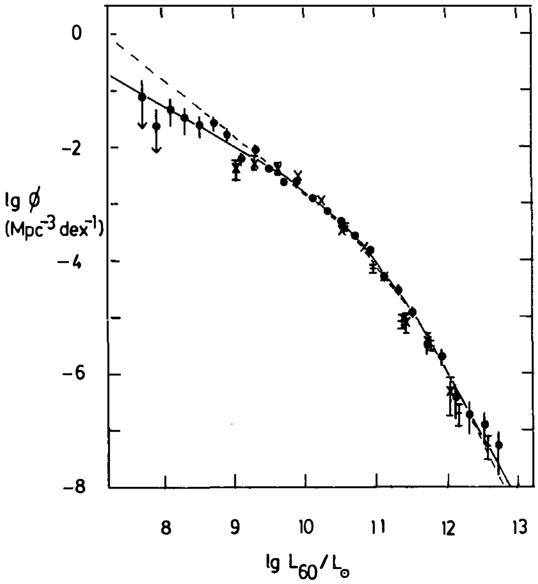

<u>Fig 1</u> 60 μm luminosity function for IRAS galaxies: filled circles (Lawrence et al 1986), crosses (Soifer et al 1986), x's (Rieke and Lebofsky 1986, assuming their $L_{IR} = 2.7\ L_{60}$), calculated for $\Omega = 1$, $H_0 = 50$. The solid curve is the two power-law fit of Lawrence et al.

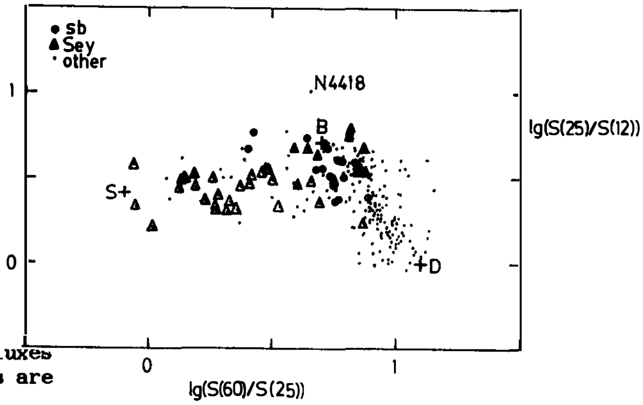

(a) lg{S(25)/S(12)} v.lg{S(60)/S(25)},

<u>Fig 2</u> IRAS colour-colour diagrams for unresolved IRAS galaxies with high-quality fluxes in all 4 bands. Circled dots are star-burst (or HII) galaxies, triangles are Seyferts, dots are neither of these or unclassified to date. The crosses labelled D, B, S, are the adopted colours of the 'disc', 'starburst' and 'Seyfert' components used to synthesize the observed far infrared spectra.

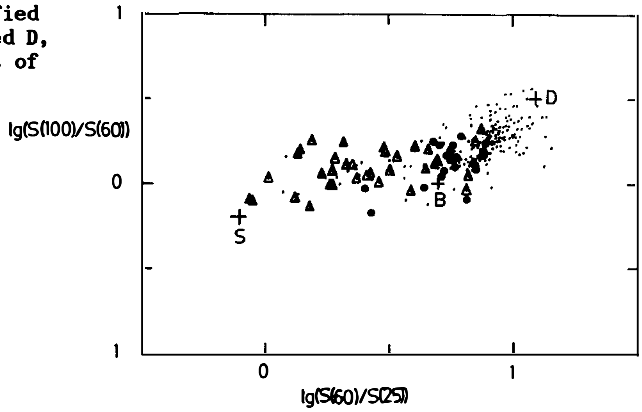

(b) lg{S(100)/S(60)} v.lg{S(60)/S(25)}.

population consists of very small grains (radius 0.001-0.003 μ, ~ 50 atoms) or, alternatively, or large molecules (Sellgren 1984, Leger and Puget 1984). Dust in the surface layers of molecular clouds will also be heated by the interstellar radiation field and in addition may be heated by young OB associations recently formed from the cloud complex. However uv photons will not be able to penetrate further than $A_V \sim 1$ into the clouds, so the bulk of the dust within molecular clouds should be at a temperature significantly lower than that in the HI clouds. Dust in the vicinity of protostars and newly formed stars embedded in molecular clouds will also radiate strongly in the far infrared. Crawford and Rowan-Robinson (1986) have shown that compact, high surface-brightness IRAS sources in the Galactic plane, many of which are associated with compact HII regions, can be modelled as hot stars embedded in a high optical depth dust cloud.

Finally high optical-depth circumstellar dust shells around late type stars, OH-IR sources and young planetary nebulae, form a related population of far infrared emitters which dominate the 12 and 25 μ emission from the bulge of our Galaxy (Habing et al 1985, Rowan-Robinson and Chester 1986) and could make a significant contribution to the 10-25 μ emission from the discs of some quiescent spirals like M31.

Turning to active galaxies, some categories like 'starburst' galaxies (Balzano 1983) may differ from normal spirals in the far infrared only in the relative proportions of the different ingredients discussed above. On the other hand galaxies with a quasar-like nucleus, eg Seyfert 1 galaxies, might be expected to produce additional far infrared radiation. Both quasars and Seyferts are known to have power-law spectra in the wavelength range 1-10 μ, with spectral index α ($S(\nu) \propto \nu^{-\alpha}$) in the range 0.5 -2 (Neugebauer et al 1979, Ward et al 1986). At visible and ultraviolet wavelengths quasars also have roughly power-law continua with a mean spectral index around 0.5 (Richstone and Schmidt 1980, Cheney and Rowan-Robinson 1981). Where such a nuclear source is located in a galaxy containing dust, for example a spiral galaxy, some of this visible and ultraviolet light will be absorbed by dust and reemitted in the far infrared.

2. DECOMPOSITION OF INFRARED SPECTRA INTO COMPONENTS

2.1 The Sample Studied

Rowan-Robinson and Crawford (1986, 1987 a,b) have selected from the IRAS Point Source Catalog all those sources which have high-quality fluxes in all 4 IRAS bands (12, 25, 60, 100 μ), which are not flagged as associated with months-confirmed small extended sources (SES) in any band, and which are associated with catalogued galaxies. Associations were only accepted if they were within 2′ of the IRAS position. Where accurate optical positions are available for the galaxy the positional agreement with the IRAS source is generally better than 10″ for this sample. After deletion of 2 sources whose far infrared spectra were clearly those of stars (and for which there were also stellar associations), of the source 15463-2845 which is flagged as confused and of the planetary nebula NGC 6543, which picked up a spurious association with a nearby galaxy, the sample consisted of 227 galaxies.

The SES-flag condition was necessary both to eliminate contamination by cirrus emission and to ensure that the fluxes measured by IRAS represent the total flux from the galaxy. Where the emission from a galaxy is extended with respect to the IRAS beam the fluxes reported in the Point Source Catalog may be seriously underestimated and corresponding IRAS colours will be distorted.

175 have measured velocities. For the 52 which do not, we clearly have no information on their activity type either (see below). 24 are elliptical or lenticular, 129 are spiral or irregular, 74 are of unknown Hubble type, 18 are starburst or HII galaxies, 15 are Seyfert 1, 23 are Seyfert 2. Arp, Vorontsov-Velyaminov and Zwicky compact galaxies appear to be represented on a basis proportional to their frequency in the general galaxy population.

2.2 IRAS Colour-Colour Diagrams

Figures 2 a,b show the 12-25-60 and 25-60-100 μ colour-colour diagrams for the sample, with different symbols for starburst (+HII), Seyfert and other galaxies. Some striking features of this distribution are immediately apparent. (a) The starburst galaxies occupy well-defined areas of the 2 diagrams and in fact have colours very similar to those of compact HII regions in our Galaxy (Crawford and Rowan-Robinson 1986); (b) the bulk of the 'normal' galaxies (non-Seyfert, non-starburst) lie in a band stretching from the zone occupied by the starburst galaxies towards warmer S(25)/S(12) colours in Fig 2a and towards cooler S(100)/S(60) colours in Fig 2b; (c) the Seyferts spread out from this band towards lower values of S(60)/S(25), indicating the presence of a component peaking at 25 μ. Such a component was first noticed by Miley et al (1984) in 3C390.3. Low values of S(60)/S(25) have been successfully used as a criterion for selecting Seyfert galaxies by de Grijp et al (1985).

2.3 A 3-Component Model for Far Infrared Spectra of Galaxies

As a first step towards understanding the range of galaxy far infrared spectra implied by Fig 2, we postulate that these spectra can be considered as a mixture of 3 components: (1) a normal 'disc' component, (2) a 'starburst' component, (3) a 'Seyfert' component. The colours adopted for these 3 components are indicated in Fig 2 by the letters D, B and S, and Fig 3 shows the corresponding spectra of the 3 components normalised to 12 μ, after colour-correction for the effect of the IRAS pass-bands. We now discuss models for each of these 3 components.

In Fig 4a the spectrum of the 'disc' component is compared with the spectrum of an isolated piece of cirrus in our Galaxy, a small cloud of interstellar neutral gas and dust with $A_V \sim 0.15$ presumably illuminated by the interstellar radiation field (Boulanger et al 1985). The agreement is remarkably good, showing that it is plausible to

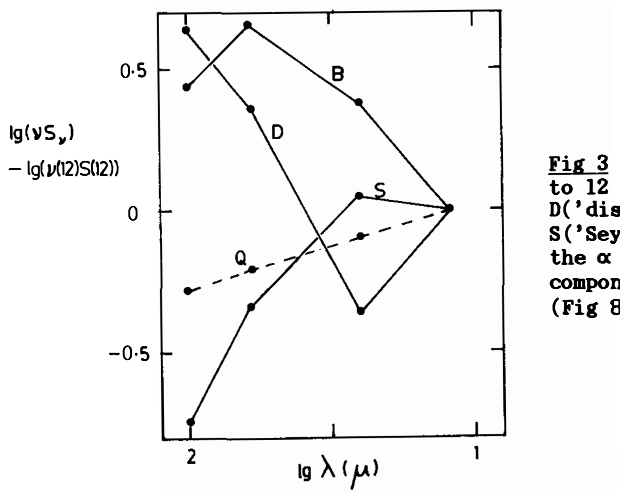

Fig 3 12-100 μ spectra, normalized to 12 μ, of adopted model components: D('disc'), B('starburst') and S('Seyfert'). The broken curve Q is the α = 0.7 power-law ('quasar') component considered for 3C273 (Fig 8c).

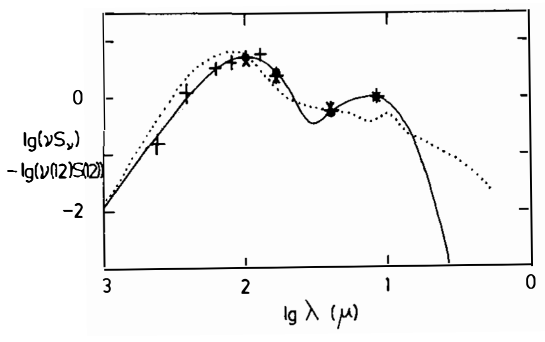

Fig 4 Model fits to the spectra of the adopted components (filled cirlces). (a) 'disc' component. The x's denote the spectrum of an isolated cirrus cloud in our Galaxy studied by Boulanger et al (1985). The crosses are the composite spectrum of our Galaxy compiled by Cox & Mezger (1987). The dotted curve is the interstellar grain model of Draine and Anderson (1985). The solid curve is an empirical fit of the form $S_\nu = \alpha\nu B_\nu(30K) + \beta\nu B_\nu(210K)$.

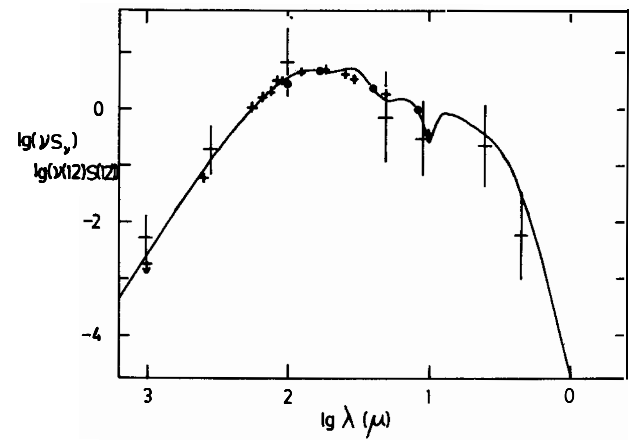

(b) 'starburst' component. The small crosses are the data of Telesco et al (1984) for th 3-kpc ring in NGC 1058, which they attribute to a starburst. The large crosses are the average spectrum for regions of massive star formation in our Galaxy derived by Rowan-Robinson (1979). The solid curve is a simple model for a star-forming region of the type discussed by Crawford and Rowan-Robinson (1986), a uniform spherically symmetric dust cloud illuminated by a hot star (T_s=400000K), with optical depth τ_{uv} = 100, ratio of inner to outer cloud radius r_1/r_2 = 0.0015.

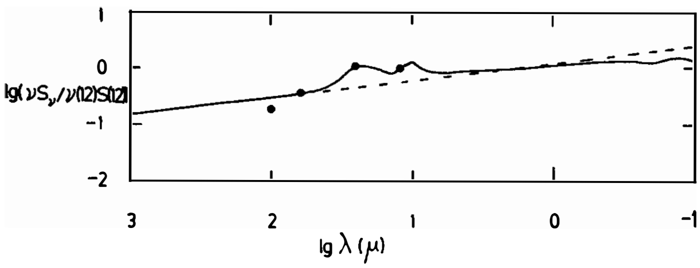

(c) 'Seyfert' component. The solid curve is a model consisting of an α = 0.7 power-law continuum source (indicated by the broken line) embedded in a spherically symmetric dust cloud with density distribution $n(r) \propto r^{-1}$, $r_1 < r < r_2$, optical depth τ_{uv} = 1 (A_V=0.23), temperature of the hottest grains T_1 = 1000K, and r_1/r_2 = 0.0055.

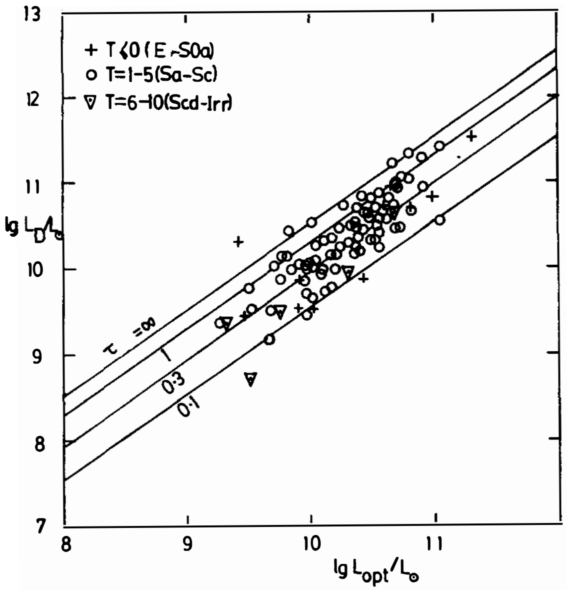

Fig 5 The correlation of the luminosity in the 'disc' component, L_D, in solar units, versus the blue luminosity of the galaxy. H_0 = 50 km s^{-1} Mpc^{-1}, and Ω_0 = 1, throughout this paper. Different symbols are used for different ranges of galaxy types, based on the parameter T of de Vaucouleurs et al (1976): + E-S0a, ʘ Sa-Sc, ∇ Sd-Irr.

The solid lines give values of the characteristic optical depth τ derived from eqn (8).

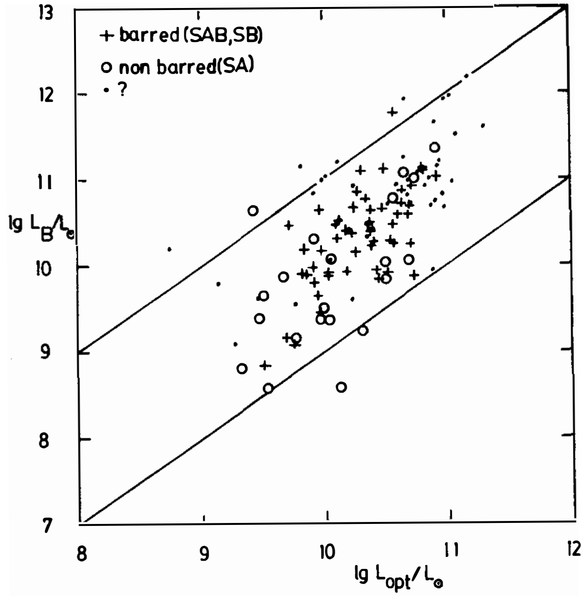

Fig 6 The correlation of the luminosity in the 'starburst' component, L_B, in solar units, versus the blue luminosity of the galaxy. The symbols denote: + barred galaxies (SB or SAB), ʘ un-barred galaxies (SA), · bar-type unknown or not relevant. Seyferts have been excluded from this figure.

regard the 'disc' component as radiation from interstellar dust in the galaxy illuminated by the general galaxy starlight. Rowan-Robinson and Chester (1986) have estimated that emission from the bulge component identified by Habing et al (1985) would not make a significant contribution to the integrated flux from most galaxies at 12–100 μ. We have also shown an empirical fit to the 'disc' component spectrum of the form $\alpha\nu B_\nu$ (30K) + $\beta\nu B_\nu$ (210K). The cool component gives a good representation of the 30–100μm emission from larger (0.01–0.1 μm) grains modelled by Rowan-Robinson (1986), but the hot component will give only a very approximate representation of the emission from very small grains or large molecules.

Fig 4b shows the spectrum of the 'starburst' component compared with the spectrum of the 3 kpc disc observed in NGC1068 by Telesco et al (1984), with the average spectrum of star-forming clouds in our Galaxy calculated by Rowan-Robinson (1979) and with a simple model for a cloud containing a newly-formed massive star (stellar temperature T_s = 40000K, grain condensation temperature T_1 = 1000 K, uniform density, ratio of inner radius of dust cloud, r_1, to outer radius, r_2, r_1/r_2 = 0.0015, composite interstellar grain properties adopted by Rowan-Robinson (1982), ultraviolet optical depth, τ_{uv} = 100). The latter model is one from a sequence used by Crawford and Rowan-Robinson (1986) for high surface brightness sources in the Galactic plane associated with star-forming regions and compact HII regions.

The agreement of the 'starburst' component spectrum with the model, with the average spectrum for star-forming clouds in our Galaxy, and with the 3 kpc disc in NGC1068 which Telesco et al (1984) argue to be a burst of star formation, is excellent.

Fig 4c compares the spectrum of the 'Seyfert' component with a simple model consisting of a central source with a power-law continuum extending from λ = 0.1 μ to 1 mm embedded in a dust cloud with density distribution $n(r) \propto r^{-1}$, T_1 = 1000 k, r_1/r_2 = 0.0055, τ_{uv} = 1 (A_V = 0.23). The agreement is satisfactory. The spectral index α = 0.7 was selected because quasars detected by IRAS appear to have 12 – 100μ spectral indices centred on this value (Neugebauer, Soifer and Rowan-Robinson 1986). Models with α = 0.5, 0.9 also give a reasonable fit. The dust is presumably located in the narrow-line region of the quasar-like object (see section 7). We were not able to obtain a satisfactory fit with $n(r) \propto r^{-2}$ or $n(r)$ = constant.

We conclude that there is a reasonable observational and theoretical basis for the separation into the 3 components of Fig 3 and that this separation may give valuable insight into the nature and energetics of infrared-emitting galaxies.

2.4 Deconvolution into Components

Let $\Delta\nu_i$, i = 1–4, be the effective bandwidths for the IRAS 12, 25, 60 and 100 μ bands (i.e. 13.48, 5.16, 2.58 and 1.00 x 10^{12} Hz respectively, IRAS Explanatory Supplement 1984) and suppose S_i are the fluxes in Jy in each band for a particular galaxy.

Let $$S_{tot} = \sum_{i=1}^{4} S_i \ \Delta\nu_i \qquad (1)$$

and $$y_i = S_i / S_{tot} \ , \ i = 1\text{–}4. \qquad (2)$$

For the 'disc' component (j = 1), 'starburst' component (j = 2) and 'Seyfert' component (j = 3), let the flux in band i be $T_{j,i}$ (Jy) and let

$$T_{j,tot} = \sum_{i=1}^{4} T_{j,i} \ \Delta\nu_i \qquad (3)$$

$$t_{j,i} = T_{j,i} / T_{j,tot}. \qquad (4)$$

We then look for the least-squares solution of the over-determined set of equations

$$y_i = \sum_{j=1}^{3} \alpha_j \ t_{j,i} \ , \ i = 1\text{–}4, \qquad (5)$$

to determine the relative proportions, α_j, j = 1-3, of the spectrum attributable to component j. If any of the α_j are found to be negative, the most negative is set to zero and the equations re-solved with one fewer variable. If one of the α_j is still negative, the remaining one is set to be 1.

Table 1 summarizes the number of each mixture combination for each galaxy type. All Seyferts but one have a 'starburst' component and all but 3 have a 'Seyfert' component. The 3 exceptions are all Type 2 Seyferts.

2.5 Correlations Between Luminosities in Components

To calculate the far infrared luminosities in each component we need to apply a correction for the incomplete wavelength coverage of the IRAS bands. Lonsdale et al (1985) have shown that the quantity $1.26(S_3 \ \Delta\nu_3 + S_4 \ \Delta\nu_4)$ is an excellent approximation to the 42.5-122.5 μ integrated spectrum of sources with blackbody or powerlaw spectra. The great range of spectral behaviours over the wider range 10-100 μ make it impossible to achieve as good a result over this whole wavelength range. However the quantity

$$1.26 \ S_{tot} = 1.26 \sum_{i=i}^{4} S_i \Delta\nu_i \qquad (6)$$

is a good approximation to the integrated spectrum from 10-120 μ of the 'Seyfert' component model adopted here and is within 15% for the 'starburst' model, so we adopt this as a measure of the 10-120 μ far infrared flux from galaxies.

We have then calculated luminosities in each component, using

$$L_j = 1.26\ \alpha_j\ S_{tot}\ .4\ \pi d^2 \qquad (7)$$

where d is the luminosity distance calculated in an $\Omega = 1$ universe for H = 50. We have also calculated optical luminosities based on $\nu\ S_\nu$ in the B-band applying the de Vaucouleurs et al (1976) internal extinction correction. Corrections for interstellar extinction have been derived from the maps of Burstein and Heiles (1978), assuming $A_B = 4\ E(B-V)$. Optical luminosities have not been quoted for galaxies with $/b/ < 10^o$ unless direct estimates of interstellar extinction are available.

Fig 5 shows the correlation of L_D, the luminosity in the 'disc' component, with L_{opt}, the B-band optical luminosity, for non-Seyfert galaxies with $L_B/L_{opt} < 4$, with different galaxy types indicated by different symbols. If the 'disc' component is interpreted as emission from interstellar dust as a result of absorption of starlight, then the ratio of these two luminosities can be interpreted in terms of a characteristic optical depth in dust

$$L_D/L_{opt,tot} \simeq (1 - e^{-\tau}) \quad , \qquad (8)$$

where $L_{opt,tot} = \int_{opt-u\nu} L_\nu d_\nu = 3.3\ L_{opt}$ by integration over the interstellar radiation field model of Mathis et al (1983). Lines of constant τ as given by (8) are indicated in Fig 5. As might be expected, early-type galaxies (E and L) have lower values of L_D/L_{opt}, consistent with a low dust content. Any contribution from dust near newly-formed stars or from circumstellar dust shells would also be lower for early-type galaxies. The values of τ are consistent with internal extinction formula of de Vaucouleurs et al (1986). We see that there is no evidence for exceptionally high internal extinction in these galaxies. For galaxies with $L_B/L_{opt} > 4$, one third of the galaxies have values of $L_D/L_{opt} > 3.3$, inconsistent with eqn. (8) for any τ. Either part of the illumination of the cool 'disc' component is provided by the starburst (but without enhancing L_{opt}) or the internal extinction is considerably higher than that given by the de Vaucouleurs et al formula (cf Moorwood et. al. 1986, de Jong and Brink 1987).

Fig 6 shows the correlation of L_B, the luminosity in the 'starburst' component with L_{opt}. Here there is a great deal of scatter, consistent with the idea of a transient, high luminosity event. There is clear evidence that barred spiral galaxies have significantly more luminous starburst components than non-barred spirals and this is the explanation of the correlation of far infrared colour with the presence of a bar, found by Hawarden et al (1985).

A broad correlation is found between L_S, the luminosity in the 'Seyfert' component, and L_B suggesting that there may be a common cause (for example, the sudden feeding of a galactic nucleus with gas) for the starburst and power-law continuum source. Fig 7, L_S versus L_X, the X-ray luminosity, shows a good correlation, consistent with the idea that the 'Seyfert' component is dust illuminated by the central quasar-like source. Seyferts appear to have rather low values of L_D/L_{OPT}, even when they are spirals.

Of the 14 galaxies in our sample which have $L_{IR} > 3.10^{11}L_0$ the far infrared spectra of 11 are dominated by starburst components (including the galaxy NGC6240 studied by Joseph et al 1984, Becklin et al 1985). The exceptions are the quasar 3C273, the Seyfert 1 galaxy I Zw 1, and the Seyfert 2 galaxy Mk 463.

2.6 Model Fits to Infrared Spectrum of Selected Galaxies

For several galaxies in our sample the spectra are known at wavelengths outside the 12-100 μ range studied by IRAS, in some cases covering the range from ultraviolet wavelength to 1 mm. These spectra provide a strong test of our models. The main conclusion of this comparison is that while our models give an excellent fit to the infrared spectra of more than 60% of the galaxies with good spectral data, the remainder require modification to give a good fit in the range 1-10 μ. These cases are almost all Seyfert galaxies and the modification required is that the optical depth across the dust cloud in the narrow-line region should be $\gg 1$.

There are 2 other galaxies which require an additional ingredient to bring their predicted spectra into line with observations. Arp 220 (not actually in our sample) and NGC 4418 both have anomalously high {S(25)/S(12)} ratios, most easily understood as due to heavy extinction by interstellar dust in the parent galaxy.

We now discuss these 3 classes of galaxy in turn:

2.6.1. Galaxies for which the models of section 4 are a good fit. Fig 8a,b shows the visible to far infrared spectra of several galaxies for which the basic model of section 4 gives a good fit. These include the galaxy NGC 6240, for which we attribute most of the far infrared emission to a starburst component (α_2 = 0.95). The contribution of starlight can be seen at wavelengths shorter than 3 μ (except for NGC 7469, for which it has been subtracted). Fig 8c shows the data for 3C273 compared with our 3-component model and for a model with an additional pure power-law component. Although the latter improves the fit to the IRAS data, the fit to the overall spectrum is not improved. Although we can not resolve the issue of whether dust is present in the emission line region of 3C273, the IRAS data do point to the existence of a starburst in this galaxy.

2.6.2. Galaxies for which a higher optical depth Seyfert component is required. The best observed galaxy in this category is NGC 1068. Fig 8d shows the spectrum of the core ($\lessdot$100 pc) of this galaxy compared with our standard 'Seyfert' component and with a high optical depth model (β=1, T_1=500K, τ_{uv}=75, r_1/r_2=0.00215). The latter model, which involves a dust mass of $3x10^5$ $M_\odot$ distributed between 4 and 180 pc from the central power-law source, is a much better fit to

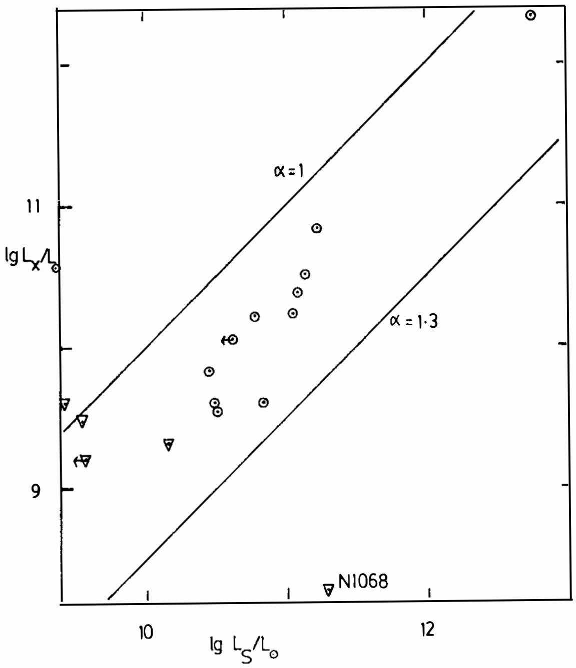

Fig 7 The correlation of the 2-10 keV ('hard') X-ray luminosity, in solar units, with the luminosity in the 'Seyfert' component. Seyferts of type 1 and 2 are denoted by circles and triangles, respectively. The straight lines are labelled with the infrared to X-ray spectral index.

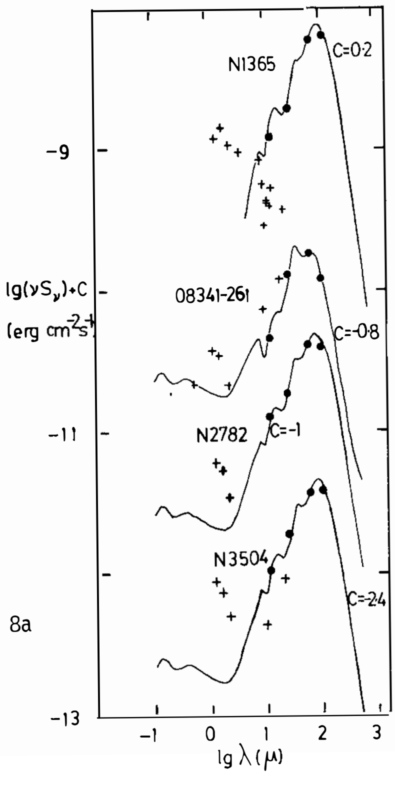

Fig 8a

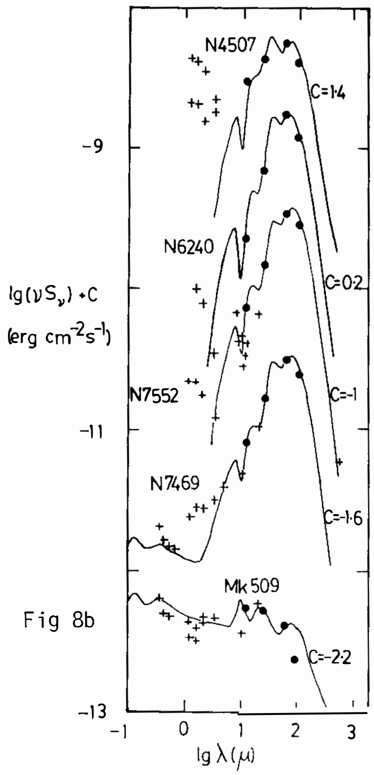

Fig 8b

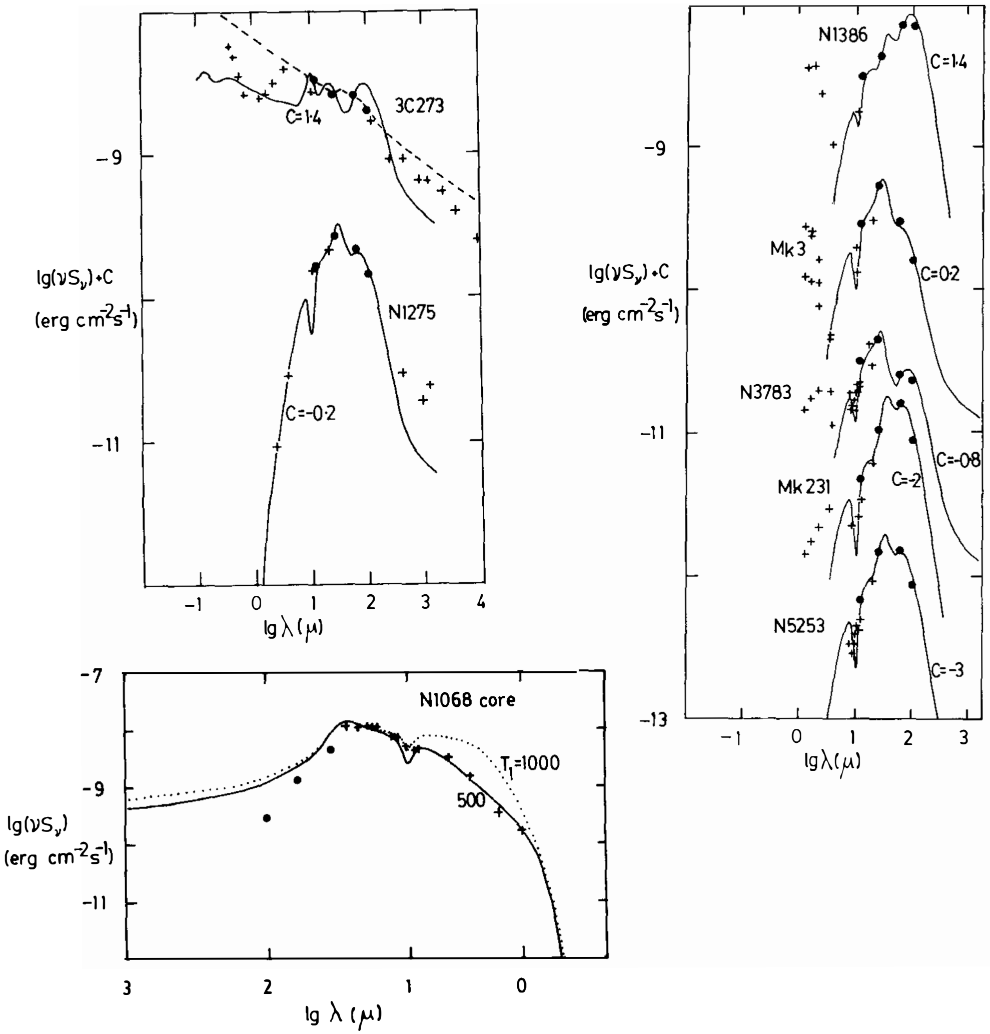

__Fig 8__ Ultraviolet to millimetre wavelength spectra predicted by the models of the present paper, compared with observations, for selected galaxies. The filled circles are the colour-corrected IRAS data, to which the models were fitted.

(a) NGC 1365, 08341-261, NGC 2782, NGC 3504.

(b) NGC 4507, 6240, 7552, 7469 and Mk 509.

(c) Contemporaneous observations of 3C273 (solid curve: 3-component model, broken curve: 'starburst' plus α = 0.7 power-law model) and NGC 1275 (τ_{uv}=75, T_1=500K model, see Fig 9d), the latter with the contribution of starlight subtracted.

(d) The core of NGC 1068 (data from Telesco et al 1984) compared with τ_{uv}=75 Seyfert model, with T_1 = 1000K (dotted curve) and 500K (solid curve).

(e) Galaxies for which the τ_{uv} = 75, T_1 = 500K model of Fig 9d gives a better fit to the overall spectrum than our standard model: NGC 1386, Mk 3, NGC 3783, M, 231, NGC.

the observations.

On rerunning our deconvolution programme with this higher optical depth Seyferts model, there are several other galaxies for which this gives a much better fit to the overall spectra: NGC 1275, 1386, 3783, 5253 and 6764 and Mrk 3 and 231, illustrated in Fig 8c and e.

These high optical depths can not, however, apply to the line-of-sight to the central source, since uv excesses are seen in several cases. The dust must be clumped into clouds which do not cover the central compact source.

2.6.3. Arp 220. Fig 9 shows two possible models for the unusual galaxy Arp 220. This galaxy does not actually qualify for the sample studied in the present paper, since the 12 μ flux is not of sufficient quality, but the interest generated by it (Soifer et al 1984) warrants trying to understand its far infrared spectrum within the framework of the present paper.

The IRAS colours of this galaxy are unique (for example, $\mathrm{Log}\{S(25)/S(12)\}=1.25$) and it cannot be understood as a mixture of the 3 components used in section 4. It can however be modelled either as a starburst behind very strong (A_V = 78 mag.) interstellar extinction (arising perhaps because the galaxy is seen virtually edge-on) or as a quasar embedded in a high optical depth (τ_{uv} = 186, A_V = 40) dust cloud. The predicted outer angular radii of the dust clouds are $1\overset{''}{.}7$ for the starburst model with extinction and $0\overset{''}{.}37$ for the embedded quasar model, and since the 20 μ emission tends to come from the inner edge of the dust cloud these are both consistent with the $<$ 1" size at 20 μ reported by Becklin et al 1986.

2.6.4. NGC 4418. This galaxy has an unusually high S(25)/S(12) ratio and a very deep 10 μ absorption feature (Roche et al 1986), both of which suggest exceptionally high extinction. It is located at l=290, b=61, where the interstellar extinction is low. Our model for this (Fig 8f) consists of a pure starburst model with an additional A_V=37 magnitudes of extinction, most of this presumably due to internal extinction in NGC 4418, which would again have to be almost edge-on.

2.7 Discussion

The model fits to the far infrared spectra of the assumed components, illustrated in Figure 3 can be used to estimate the dimensions and masses of the dust clouds responsible for the infrared emission. For the 'starburst' and 'Seyfert' component models, which involve a specific optical depth in dust, the angular and linear radius of the dust cloud can be derived from the integrated flux, S_{tot} (eqn (1)) and the luminosity L_j (eqn (7)) respectively.

For the 'starburst' model we find, for a spherically symmetric cloud illuminated by a central cluster of stars,

$$\lg \theta_2('') = -7.83 + 0.5 \lg (1.26\, \alpha_2\, S_{tot})$$

and (9)

$$\lg r_2(\mathrm{cm}) = 14.59 + 0.5 \lg (L_B/L_\odot)$$

The inner edge of the dust cloud is defined by

$$r_1/r_2 = 0.0015.$$

The corresponding dust mass is

$$\lg(M_d/M_\odot) = -6.32 + \lg(L_B/L_\odot). \qquad (10)$$

For the galaxies in the present sample, r_2 lies in the range 3 pc to 250 pc, so the starburst activity is confined to a small region of the galaxy, presumably in most cases the nucleus. However our assumption of spherical symmetry clearly underestimates the extent if the stars are distributed through the cloud or if the starburst is actually located in a ring. For example for the NGC 1068 'starburst' component we find $\theta_2 = 3''$ and $r_2 = 30$ pc, considerably smaller than the observed 3 kpc diameter ring. The very high light-to-mass ratios implied by eqn (10) means that the starburst involves only high-mass stars and that the efficiency of star-formation must be very high.

For the 'Seyfert' model we find

$$\lg \theta_2('') = -7.32 + 0.5 \lg (1.26\, \alpha_3\, S_{tot})$$

and (11)

$$\lg r_2(\mathrm{cm}) = 15.11 + 0.5 \lg(L_S/L_\odot)$$

with a corresponding dust mass

$$\lg (M_D/M_\odot) = -7.81 + \lg(L_S/L_\odot). \qquad (12)$$

The inner edge of the dust cloud is defined by

$$r_1/r_2 = 0.0055.$$

For the galaxies in the present sample r_2 lies in the range 30 pc to 400 pc, consistent with the dust being located in the narrow line region of the Seyfert nucleus. The gas in Seyfert narrow-line regions is known to be highly clumpy, with a very low filling factor and, as we saw in section 2.6.2, the same must be true for the dust.

For the 'disc' model we assumed $\tau_\nu \propto \nu$, but the model does not involve any specific value of τ_{uv} so we can only calculate $\tau_{100}{}^{1/2}\, \theta_2$, where $\tau_\nu = \tau_{100}(100\mu\mathrm{m}/\lambda)$ is the optical depth in 30K grains. We find

$$\lg \{\tau_{100}{}^{1/2}\, r_2(\mathrm{cm})\} = 16.02 + 0.5 \lg(L_D/L_\odot)$$

or (13)

$$\lg\{\tau_{100}^{1/2}\,\theta_2('')\} = -6.90 + 0.5\,\lg\,\{1.26\,\alpha_1\,S_{tot}\}.$$

The optical depth at 12 μ in 210 K grains, τ_{12}, is related to that in 30 K grains by $\tau_{12} = 0.98 \times 10^{-4}\,\tau_{100}$. For a source to be a point source at 60 and 100 μ, the full width to half-power cannot be greater than 1'. Galaxies with $\alpha_D > 0.5$ yield $\tau_{100}^{1/2}\,\theta_2('')$ in the range 0.''6 to 1.''2 and this implies $\tau_{100} > 0.0004$. Using the interstellar grain model of Rowan-Robinson (1986), we can translate this lower limit on τ_{100} to one on A_V and find $A_V > 0.8$. This is broadly consistent with the optical depth estimates derived from Fig 5. As many of the galaxies in the present sample have Holmberg diameters considerably greater than 1', we must presume that the bulk of the far infrared emission comes from the inner part of the galaxy. This is still consistent with being reemission of starlight obscured by interstellar dust, since the halfpower width of the optical light is much smaller than the Holmberg diameter.

3. OTHER STUDIES

(i) de Jong and Brink (1987)
de Jong and Brink decompose the far infrared energy distribution into two $Q_\nu B_\nu(T)$ components with $Q_\nu \propto \nu$ and the dust temperatures T = 15, 60 K.

The warm component is heated by recently formed stars (T_s=30000 K) inside molecular clouds. 50% of the luminosity of these stars is assumed to be absorbed inside the clouds and 50% is assumed to escape and contribute to the cool component.

The cool component is heated partly by older disk stars (T_s=7000 K) in the general interstellar medium and partly by light from recently formed stars which escapes from the molecular clouds where the stars have formed.

They solve for A_B^o, the face-on extinction, L_1, the luminosity of the disk stars, and L_2, the luminosity of recently born stars, such that the IRAS 60 and 100 μ fluxes and the observed blue magnitude are reproduced. The calculation takes account of the inclination of the galaxy and the λ^{-1} dependence of extinction (so there are different optical depths for 30000 and 7000 K radiation). The analysis has been applied to two samples: a representative sample of 120 galaxies from the Revised Shapley Ames Catalog, and a subset of 20 minisurvey galaxies studied in detail by Moorwood et al (1986).

de Jong and Brink conclude that:
(i) A large fraction of the disk infrared luminosity is emitted at wavelengths >100 μm.

(ii) For the RSA galaxies the values of A_B^o and their dependence on galaxy type agree well (within a factor of two) with those derived from optical data by Sandage and Tammann (1981) and by de Vaucouleurs et al (1976).

(iii) The minisurvey galaxies show enhanced star formation (higher values of L_2/L_1), higher values of A_B^o (50% of the sample have $A_B^o>1$, compared with 9% for the RSA sample), and a tendency to be more highly inclined (40% of the sample have a/b > 2.5 compared with 15% for the RSA sample). The minisurvey sample can be subdivided into 40% which are highly inclined normal galaxies and 60% which have ~3 times larger star formation rates. Galaxies in the latter group are about twice as dusty as normal galaxies.
(iv) The model gives a natural explanation of the distribution of galaxies in the L_{IR}/L_{BT} versus S(100)/S(60) diagram.

(ii) Helou (1987)
The sample studied by Helou consists of all galaxies in 'Catalogued Galaxies and Quasars Observed in the IRAS Survey' (Lonsdale et al 1985) having high quality fluxes in all four IRAS bands and not flagged as extended. Most galaxies with S(60)/S(25) < 5.5 are Seyferts (de Grijp et al 1985) and are not considered further by Helou. In a plot of S(60)/S(100) versus S(12)/S(25), 'normal' galaxies (those with S(60)/S(25) > 5.5) spread out along a band such that the warmer they are in S(12)/S(25), the cooler they are in S(60)/S(100).

The band corresponds to progressively greater star formation activity as it proceeds from the lower right hand corner to the upper left hand corner of the diagram. Galactic cirrus (Low et al 1984, Gautier 1986, Leene 1986) is found at the lower end of the band, together with very quiescent spirals such as M31 and M81. In contrast the upper end of the band is occupied by starburst galaxies like NGC 6240 (Wright, Joseph & Meikle 1984) and blue compact galaxies or 'extragalactic HII regions' such as Mrk 158, and compact Zwicky galaxies (Kunth and Sevre 1986, Wynn-Williams and Becklin 1986). This interpretation is supported by a model in which a realistic mixture of grains including polycylic aromatic hydrocarbons (PAH) is subjected to increasingly intense radiation fields (Desert 1986).

Two other samples of IRAS galaxies confirm the reality of the band in the colour-colour diagram: a sample of Virgo cluster spirals complete to B = 12.8 (Helou 1986b), and a sample of near-by galaxies, roughly complete to an apparent diameter of 10' (Rice et al 1986). However the restriction to unresolved galaxies in the Helou and Rowan-Robinson and Crawford studies does lead to underpopulation of the low surface brightness, cooler (in S(60)/S(100)) end of the band.

Helou argues that the spread across the band implies that a simple mixing of two fixed components, C ('cirrus') and A (active component related to HII regions) is inadequate. He argues that two physical parameters are required to characterize the distribution: the intensity in its active regions, A, and the ratio A/C, where C is the (fixed) cirrus component. As the ambient radiation field goes from solar neighbourhood intensity to several hundred times this value, A traces out the upper envelope to the observed band so the model is capable of explaining all galaxy colours.

The C component is due in large part to older disk stars and cannot be identified with recent star formation. The close relation between non-thermal radio and far infrared emission becomes even more intriguing, as it seems to apply independent of IRAS colour (Helou, Soifer and Rowan-Robinson 1985).

5. DISCUSSION

The 3 models reviewed here for the observed normal galaxy - starburst sequence are strikingly different in their predictions of the optical properties of IRAS galaxies. In the Rowan-Robinson and Crawford model, the starburst component is immersed in over 50 magnitudes of visual extinction, so there would be virtually no additional radiation observed in the visible. de Jong and Brink allow 50% of the radiation from the starburst to escape, so that IRAS galaxies with strong starbursts should differ in colour and intensity profile from normal galaxies. Helou's calculation (curve D in Fig 9b) is essentially an optically thin one, so would imply drastic changes to the visible appearance of a strong IRAS starburst galaxy. However Helou (1986a) argues that the dust optical depth must in fact increase for strong starburst galaxies because of the high value of L_{IR}/L_{opt}. Further study is needed to establish whether the presence of a strong, warm component at 60 and 100 μ is accompanied by changes in the visible appearance of the galaxy. My impression of the work published to date is that there is in general no drastic change. A preliminary look at the distribution of L_D/L_{opt} versus L_B/L_{opt} in the model of Rowan-Robinson and Crawford shows no evidence of the strong correlation that would be expected in the de Jong and Brink model.

The question raised by de Jong and Brink as to whether galaxies with high values of infrared-to-optical luminosity ratio also have abnormally high internal extinction deserves further study, as also does the question of whether edge-on-galaxies are over-represented (de Jong and Brink) or under-represented (Burstein 1986) in the IRAS survey. My own recommendation is that these studies should not be carried out on the minisurvey sample, much of which lies near the Ophiucus and Taurus molecular clouds, where the magnitude of interstellar extinction in our own Galaxy cannot be reliably estimated. Finally it is clear that the current star formation rate in a galaxy can not be calculated simply by multiplying the far infrared luminosity by an appropriate constant.

Finally it is clear that the current star formation rate in a galaxy can not be calculated simple by multiplying the far infrared luminosity by an appropriate consant.

REFERENCES

Balzano V.A., 1983, Astrophys.J. 268, 602

Becklin E.E., De Poy D.L. and Wynn-Williams C.G., 1985, Proceedings of the Infrared Detector Workshop, Laramie, Wyoming

Boulanger F. Baud B. and van Albada G.D., 1985, Astron.Astrophys 144, L9

Burstein D., 1986, preprint
Burstein D. and Heiles C., 1978, Astrophys.J. 225, 40
Cheney J. and Rowan-Robinson M., 1981, Mon.Not.R.astr.Soc. 195, 831
Crawford J. and Rowan-Robinson M., 1986, Mon.Not.R.astr.Soc., in press
Cox P. and Mezger P., 1987, Star formation in Galaxies, ed C.J. Lonsdale (NASA Printing Office) p.23.
Desert F.X., 1986, in 'Light on Dark Matter', First IRAS Symposium, ed. F. Israel (Reidel) p. 213
Draine B.T. and Anderson N., 1985, Astrophys.J. 292, 494
Gautier T.N. III, 1986, in 'Light on Dark Matter', First IRAS Symposium, Noordwijk, ed. F. Israel (Reidel), p. 49
Gautier T.N. and Beichman C.A., 1985, BAAS 16, 968
de Grijp M.H.K., Miley G.K., Lub J. and de Jong T., 1985, Nature 314, 240
Habing H.J., Olnon F.M., Chester T., Gillett F., Rowan-Robinson M. and Neugebauer G., 1985, Astron.Astrophys. 152, L1
Hawarden T., 1985, in 'Light on Dark Matter' ed. F.P. Israel (Reidel)
Helou G., 1986a, Astrophys.J. (in press)
Helou G., 1986b, in 'Star Forming Dwarf Galaxies and Related Objects', ed. Kunth D., Thuan T.X., and Tram Thank Van, J. (Gif-sur-Yvette; Editions Frontiers)
Helou G., Soifer B.T., and Rowan-Robinson M., 1985, Astrophys.J. 298, L7
IRAS Explanatory Supplement, 1984, C.A.Beichman G.Neugebauer, H.J.Habing, P.E.Clegg and T.J.Chester (eds), JPLD-1855
de Jong, T., et al, 1984, Astrophys.J., 278, L67
Joseph R.D., Wright G.S. and Wade R., 1984, Nature 311, 132
Lawrence A., Walker D., Rowan-Robinson M., Leech K.J., and Penston M.V., 1986, Mon.Not.R.astr.Soc. 219, 687
Leene A., 1986, Astron.Astrophys. 154, 295
Leger A. and Puget J.L., 1984, Astron.Astrophys. 137, L5
Lonsdale C.J., Helou G., Good J.C., and Rice W., 'Catalogued Galaxies and Quasars Observed in the IRAS Survey', 1985, Preprint -1932, Jet Propulsion Laboratory
Low F.J. et al, 1984, Astrophys.J. 278, L19
Miley G.K., Neugebauer G., Clegg P.E., Harris S., Rowan-Robinson M., Soifer B.T. and Young E., 1984, Astrophys.J. 278, L79
Moorwood A.F.M., Veron-Cetty M.-P. and Glass I.S., 1986, preprint
Neugebauer G., Becklin E.E., Oke J.B. and Searle L., 1976, Astrophys.J., 205, 29
Neugebauer G., Soifer B.T. and Rowan-Robinson M., 1986, in 'Structure and Evolution of Active Galaxy Nuclei', ed. G. Giuricin et al (Reidel). p.11
Neugebauer G., Oke J.B., Becklin E.E. and Matthews K., 1979, Astrophys.J. 230, 79
Rice W.L., et al 1986, preprint
Rieke G.H., and Lebofsky M.J., 1986, Astrophys.J. 304, 326
Richstone D.O. and Schmidt M., 1980, Astrophys.J. 235, 361
Roche P.F., Aitken D.K., Smith C.H., and James S.D., 1986, preprint
Rowan-Robinson M., 1979, Astrophys.J. 234, 111
Rowan-Robinson M., 1982, Mon.Not.R.astr.Soc. 201, 289
Rowan-Robinson M., 1986, Mon.Not.R.astr.Soc. 219, 737
Rowan-Robinson M., Helou G. and Walker D., 1986, Mon.Not.R.astr.Soc. (in press)

Rowan-Robinson M. and Chester T., 1986, Astrophys.J. in press
Sandage A. and Tammann G.A., 1981, 'Revised Shapley Ames Catalog of Bright Galaxies' (Carnegie Inst. Washington)
Sellgren K., 1984, Astrophys.J. 277, 623
Soifer B.T. et al, 1984, Astrophys.J. 283, L1
Soifer B.T. et al, 1986, Astrophys.J. 303, L41
Soifer B.T. et al, 1985, Astrophys.J. 278, L71
Telesco C.M., Becklin E.E., Wynn-Williams G.G., 1984, Astrophys.J. 282, 427
de Vaucouleurs G., de Vaucouleurs A. and Corwin H.Jr, 1976, '2nd Reference Catalogue of Bright Galaxies' (Univ. of Texas, Austin)
Ward M., Elvis M., Fabbiano G., Carleton N., Willner S.P., Lawrence A., 1986, preprint
Wright G.S., Joseph R.D., and Meikle W.P.S., 1984, Nature 309, 430
Wynn-Williams C.G., and Becklin E.E., 1986, Astrophys.J. (in press)

Table 1: numbers of galaxies with different combinations of 'disc' (D), 'starburst' (B) and 'Seyfert' (S) components

type	number	
D	5	(NGC 2076, 4750, 5078, 5530; 23260-4136)
B	6	(NGC 1614, 4418; UGC 8335; 10039-3338, 20551-4250, 23128-5919)
S	1	(IC 4329A)
DB	138	
DBS	55	
DS	7	(NGC 4047, 5656, 7624, 7817; 01091-3820, 02069+2339, 20243-0226)
BS	15	(NGC 1275, 1377, 4253, 5253, 6552; UGC 3426, 4203, 8058, 8850 9412; 003449-334, 08171-2501, 08341-2614, 13197-1627, 20481-5715)

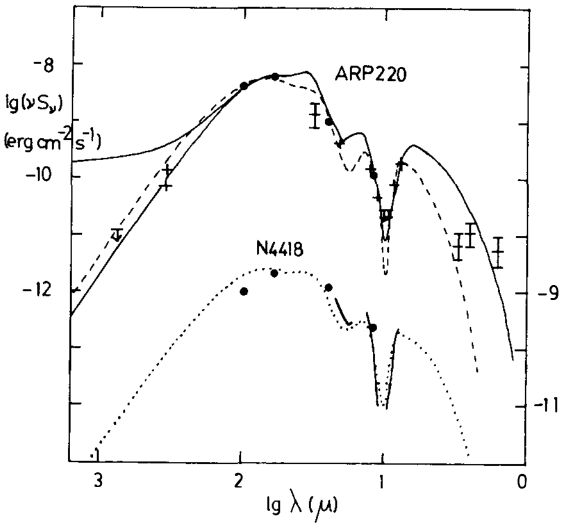

Fig 9 Models for Arp 220 (broken curve: 'starburst' model with 'an additional A_V = 78 mag. of extinction by interstellar dust. Solid curve: power-law (α=0.7) continuum source embedded in uniform spherically symmetric dust cloud with τ_{uv} = 186 (A_V=40). The upper and lower solid curves at larger wavelengths correspond to whether the power-law source continues beyond 100 μ or not.) and NGC 4418 (dotted curve: 'starburst' model with an additional A_V = 39 mag. of extinction by interstellar dust).

STARBURSTS AND IRAS GALAXIES

Patrick BELFORT
Institut d'Astrophysique de CNRS
98 bis, bd Arago F-75014 Paris
France

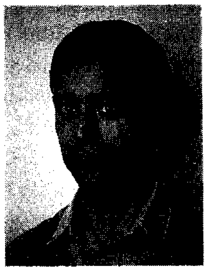

Abstract : Several observational hints suggest that most of the IRAS galaxies are undergoing bursts of star formation. A simple photometric model of starburst galaxy was developed in order to check whether starburst events are really able to account for the far-infrared and optical properties of all the IRAS galaxies with HII region-like spectra. FIR activities up to a few hundred are actually easily reached with rather small bursts in red host-galaxies, and L_{IR}/L_B, EW(Hα) and (U$-$B) versus (B$-$V) diagrams can be used to estimate burst strength and extinction. But more observations are required to conclude about the most extreme cases. Four typical infrared-selected IRAS galaxies are presented and their burst strength and extinction estimated.

1. Introduction

The existence of galaxies exhibiting infrared-to-blue luminosity ratio (L_{IR}/L_B) up to 100 or even more, while "normal" galaxies show ratios of the order of unity, has been one of the most striking IRAS discoveries. Regarding their spectral energy distribution (from near-infrared to radio wavelengths), UV, optical and infrared spectra, near-infrared colors and the tight correlation found between far-infrared emission and nonthermal radio emission, most of these galaxies have been proposed to be starburst galaxies [1].

So, it was interesting to check whether a simple photometric model of starburst galaxy is really able to account for the far-infrared (FIR) and optical properties of all the IRAS galaxies with HII region-like spectra, or whether an other mechanism is responsible for generating at least a part of the FIR emission in some cases.

Such a model was developed at the Institut d'Astrophysique de Paris, in collaboration with R. Mochkovitch [2]. The FIR luminosity is computed as the starlight absorbed by dust throughout the galaxy from 912 to 9000 Å and the energy of Lyman continuum and Lyman alpha photons absorbed by dust within HII regions. The amount of dust is described by the extinction $E_1(B-V)$ for stars less massive than 20 $M_\odot$ and $E_2(B-V)$ for stars more massive. This selective extinction is required to account for the Hα equivalent width in normal galaxies. The fraction of Lyman continuum photons directly absorbed by dust in HII regions is described by the factor $(1-f)$. Typically, in normal galaxies $E_1(B-V)=0.05$ and $E_2(B-V)=0.40$, $(1-f)=0.3$.

Several FIR and optical quantities are computed : L_{IR}/L_B ratio (sometimes referred as FIR activity), reddened UBV colors and Hα equivalent width, infrared excess, etc ...

2. Normal galaxies

Before discussing the starburst and IRAS galaxies, the model has been applied to a sample of 44 normal galaxies. Figure 1 shows their distribution in the diagram L_{IR}/L_B versus $(B-V)$. The FIR luminosities are deduced from the IRAS Point Source Catalog [3] and Small Scale Structure Catalog [4] fluxes, according to the relation given by Boulanger et al. [5], and the blue luminosities and $(B-V)$ colors are from the RC2 [6]. The two theoretical lines correspond to the model predictions with the IMF proposed by Kennicutt [7] and two choices for the extinction : an extinction which is rather large for normal galaxies and a small one.

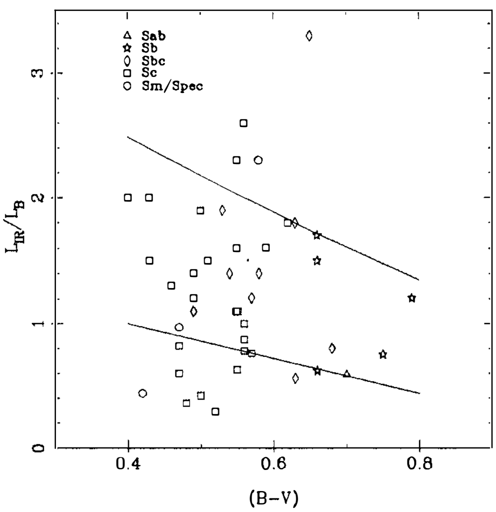

Figure 1 : L_{IR}/L_B versus $(B-V)$ diagram for normal galaxies.
upper line : $E_1(B-V)=0.10$ and $E_2(B-V)=0.80$.
lower line : $E_1(B-V)=0.025$ and $E_2(B-V)=0.20$.

The agreement between the predictions and the observed FIR activities is quite good since most of the galaxies lie within the area delimited by the curves. The galaxies above and below can be easily accounted for by slightly larger or smaller extinctions, except for NGC 4666 and NGC 6574, which FIR activities ($\sim$ 4.7 and 3.3, respectively) likely require a slightly enhanced star formation.

3. Starburst galaxies

In the starburst model, burst have been assumed in progress for $2\,10^7$ years. The strength b is the ratio of the mass of stars formed in the burst to the mass of stars ever formed in the underlying galaxy, as proposed by Larson and Tinsley [8]. The extinction $E_b(B-V)$ is the same for all the stars in the burst and the burst IMF is that of the host-galaxy.

The Figure 2 shows the FIR activity of starburst galaxies as a function of b and $E_b(B-V)$. Heavy lines correspond to burst strengths of 0.005, 0.01 and 0.05 with a 3-magnitude extinction. The blue luminosities and (B$-$V) colors are then those of the underlying galaxies, while the FIR emission is dominated by the burst. On the contrary, when $E_b(B-V)$ decreases, the contribution of the burst to the optical range becomes important. The (B$-$V) color becomes bluer and the FIR activity lowers (thin lines).

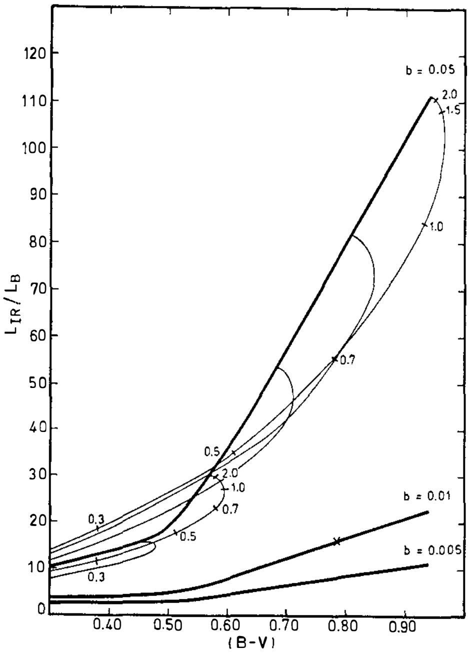

Figure 2 : L_{IR}/L_B versus (B$-$V) diagram for starburst galaxies.
heavy lines : b=0.005, 0.01, 0.05 and $E_b(B-V)$=3.
thin lines : b=0.05 and $E_b(B-V)$ decreasing from 3 to 0.3 magnitude.

At a given burst strength, the FIR activity is naturally larger for red host-galaxies but even weak bursts in blue host-galaxies produce L_{IR}/L_B ratios greater than 3. Furthermore, FIR activities up to 100 are easily reached with very reddened bursts of a few percent in red host-galaxies, and even larger values will be reached if the underlying galaxy is also very dusty [9].

Such a diagram can be used to estimate the strength of a possible burst in IRAS galaxies with known (B$-$V) colors, but it is also possible to estimate the burst extinction if an other color is available. Figure 3, for instance, shows the effects of different bursts on the Hα equivalent width as a function of the extinction. Heavy lines correspond to "normal" sequences, thin lines show the effect of decreasing extinction and dashed lines are sequences of identical extinction.

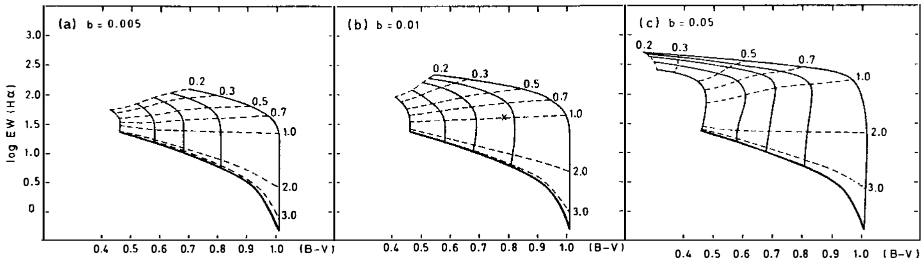

Figure 3 : log EW(Hα) versus (B−V) for starburst galaxies : (a) b=0.005, (b) b=0.01, (c) b=0.05

As an example, if the cross on Figure 3b corresponds to a galaxy with a FIR activity suggesting a burst strength of ~1% (Fig.2), the extinction E_b(B−V) can be estimated about 1 magnitude. Of course, UBV color diagrams may be used in the same way, and burst strength and extinction have been estimated for a sample of 51 starburst, interacting and blue compact galaxies by Belfort, Mochkovitch and Dennefeld [2, 10].

4. IRAS galaxies

In order to study the IRAS galaxies as a class, about 30 infrared-selected IRAS galaxies have been observed through BVI and Hα filters by M. Dennefeld (IAP) and P. Bouchet (ESO) with the CCD camera of the ESO 2.2-meter telescop. Four of them, typical of the complete sample, are shown in Figure 4.

On the first image (a), the IRAS galaxy lies between the ticks, while an other large spiral with the same velocity is visible on the right. IRAS 09111−1007 presents the largest FIR activity of the sample galaxies ($L_{IR}/L_B \sim 210$), suggesting a rather large, strongly reddened burst. IRAS 09234−1146 (b) corresponds to a pair of highly interacting galaxies, but with a small FIR activity of only ~2, suggesting that interactions do not systematically imply bursts of star formation. IRAS 12422−2009 (c) does not show any companion or interaction. However, its Hα equivalent width indicates a small burst with a rather small extinction, which explains its moderate FIR activity (~3). And the last image (d) shows a nearly edge-on IRAS galaxy (IRAS 12481−2005, between the ticks) with at least one faint companion and a large spiral in the foreground. Its FIR activity is about 47, which corresponds to a burst of a few percent.

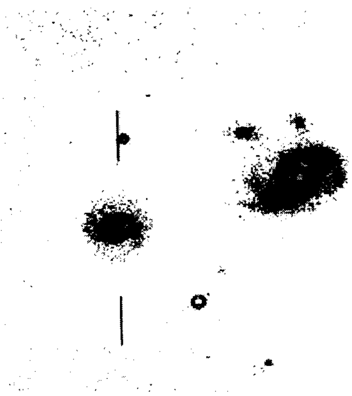

(a) IRAS 09111−1007

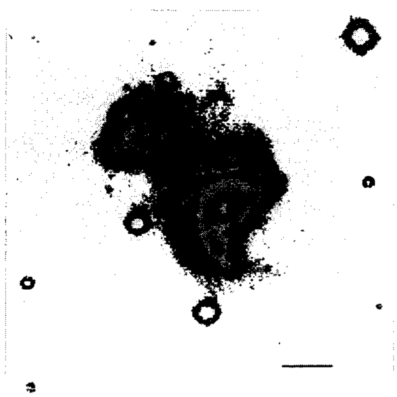

(b) IRAS 09234−1146

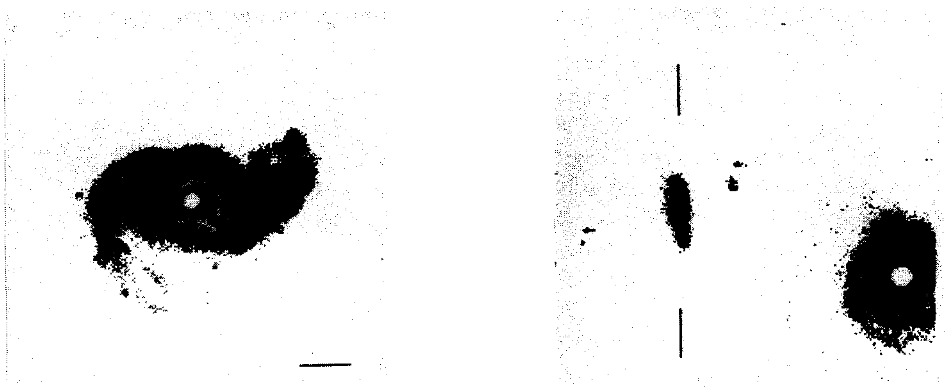

(c) IRAS 12422-2009 (d) IRAS 12481-2005

Figure 4 : B-images of four typical IRAS galaxies with HII region-like spectra. North is at top and east is on the right. The length of the ticks represents 10". (observations made by M. Dennefeld and P. Bouchet at ESO)

The FIR and optical properties of these four IRAS galaxies are summarized in the following table, together with the corresponding estimates of their burst strength and extinction.

IRAS	L_{IR}/L_B	(B−V)	EW(Hα)	b	E_b(B−V)
09111−1007	210	1.07	33 Å	∼ 0.05	∼ 1.5
09234−1146	1.9	0.40	25 Å	0	—
12422−2009	3.4	0.76	23 Å	< 0.003	∼ 0.5–1
12481−2005	47	0.93	56 Å	∼ 0.02	∼ 1

5. Conclusion

A simple photometric model of starburst galaxy is actually able to account for the far-infrared and optical properties of IRAS galaxies with L_{IR}/L_B ratios up to a few hundred. It is difficult to conclude about the most extreme IRAS galaxies [11, 12] because their (B−V) colors are unknown, but starbursts forming only massive stars and occuring in very dusty host-galaxies could produce such FIR activities [2, 9].

References

[1] Soifer, B.T., Houck, J.R., Neugebauer, G. : 1987, IPAC preprint n° 0024
[2] Belfort, P., Mochkovitch, R., Dennefeld, M. : 1987, Astron. Astrophys. **176**, 1
[3] IRAS Point Source Catalog : 1985, Washington D.C.: US Government Printing Office
[4] IRAS Small Scale Structure Catalog : 1986, Washington D.C.: US Government Printing Office
[5] Boulanger, F., Baud, B., van Albada, G.D. : 1985, Astron. Astrophys. Letters **144**, L9
[6] de Vaucouleurs, G., de Vaucouleurs, A., Corwin, N.C. : 1976, Second Reference Catalog of Bright Galaxies, Austin, University of Texas Press
[7] Kennicutt, R.C. : 1983, Astrophys. J. **272**, 54
[8] Larson, R.B., Tinsley, B.M. : 1978, Astrophys. J. **219**, 46
[9] Belfort, P. : 1987, thesis (in preparation)
[10] Belfort, P., Mochkovitch, R., Dennefeld, M. : 1987, "Star Formation in Galaxies", Washington D.C.: US Government Printing Office (in press)
[11] Aaronson, M., Olszewski, E.W. : 1984, Nature **309**, 414
[12] Houck, J.R., Schneider, D.P., Danielson, G.E., Beichman, C.A., Lonsdale, C.J., Neugebauer, G., Soifer, B.T. : 1985, Astrophys. J. Letters **290**, L5

OPTICAL OBSERVATIONS OF IRAS-SELECTED GALAXIES

Ulrich KLAAS
Max-Planck-Institut für Astronomie
Heidelberg
West Germany

ABSTRACT

Some examples of an optical study of faint IRAS-selected galaxies are presented. Deep, direct CCD images have been obtained for 100 fields. In many cases one or several galaxies with extremely peculiar structure are found at the IRAS positions. Long-slit CCD spectra show emission lines typical for HII and starburst galaxies. Obvious interactions are very common among these objects. Redshifts between 0.01 and 0.24 have been measured in 40 fields. Broad band CCD B and R photometry results in absolute B magnitude M_B of quite normal galaxies between -19 mag and -21 mag. All objects are very powerful in the far infrared, luminosities between 40 µm and 120 µm ranging from 10^{10} up to $1.5 \cdot 10^{12}$ $L_\odot$. Thus the ratio L_{FIR}/L_B extends from 1 to extreme values of about 100. Very red regions in the B-R colour maps are supposed to indicate the sites of the far infrared radiation sources.

1. Introduction

The IRAS all-sky survey has revealed a class of extragalactic objects which are bright in the infrared - mainly at 60 and 100 µm - but optically faint, e.g. the minisurvey galaxy sample described by Soifer[1]. We have started to search for similar, previously unidentified objects in other selected sky regions and to study their physical properties in detail. In order to obtain a large sample and simultaneously detect faint structures in the galaxies, the recently installed 3.5 m telescope of the Max-Planck-Institut für Astronomie on Calar Alto, Spain was used for all observations.

2. Selection of sources

The search for infrared-bright galaxies in the IRAS Point Source Catalog[2] was restricted to two areas: a ten degree-wide strip around the northern pole (RA: 0 h - 24 h, DEC: $+80^{\circ}$ - $+90^{\circ}$); and a field south of the galactic plane within the boundaries RA: 0 h - 2 h 30 m and DEC: $+30^{\circ}$ - $+40^{\circ}$. All objects in these fields have $|b| > 20^{\circ}$ and could be easily observed from Calar Alto during the available telescope time. A second motive for choosing these regions was that the source identifications were possible in two areas not covered by other large survey programs[3,4].

The IRAS point sources had to fulfill the following selection criteria: no positional match with other catalogues; and high flux quality in the 60 and/or 100 µm band. If the 25 µm flux had a high quality level, the 60 µm flux had to be larger by a factor of at least two. This demand for an increasing flux towards longer infrared wavelengths and the high galactic latitude of the sources gives a high probability to discriminate galaxies from stars and other galactic objects[1]. If only the 100 µm flux was of good quality, the sum of the two cirrus flags CIRR1 + CIRR2 had to be less than or equal to 10 (see IRAS explanatory supplement[5] for a detailed description). A total number of 320 IRAS galaxy candidates was selected. We tried to identify all sources on the Palomar Sky Survey Prints by plotting overlays with source positions and error boxes, but about 20% could not be definitely identified on POSS, mainly those which were only detected at 100 µm. It is probable that a large part of these unidentified 100 µm sources are infrared cirrus, because the selection criteria were not very severe.

3. Direct imaging

Deep, direct imaging was performed using the prime focus CCD camera

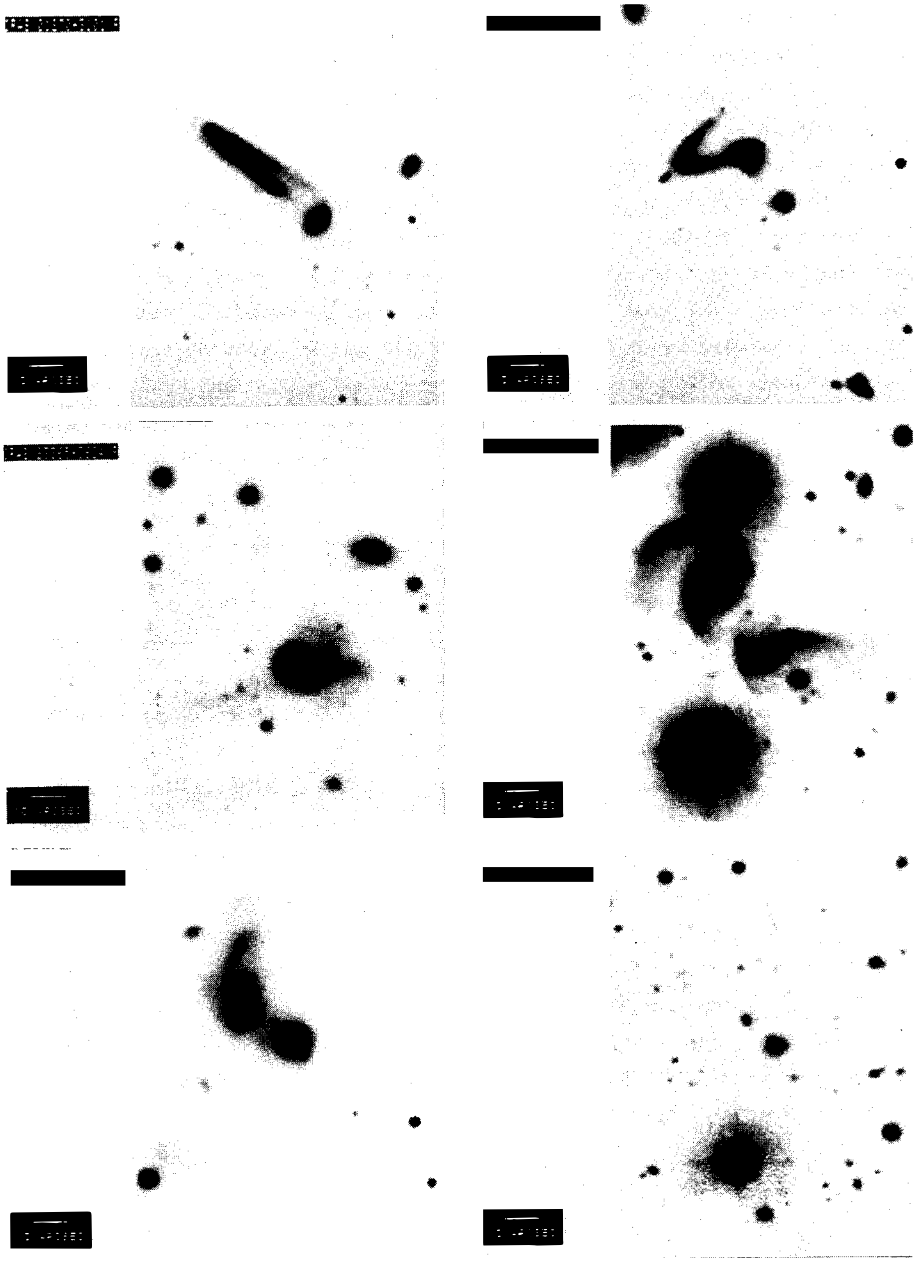

Fig. 1: Morphology of IRAS galaxies. Peculiar fine structures are still found for the most distant galaxy in this sample, which is IRAS 04203+8120 (bottom right) at a redshift of z = 0.24. For each image the orientation on sky is north to the left and east to the bottom. The grey scale display is logarithmic.

equipped with an RCA chip. Typical exposure times were between 1500 and 2000 sec. The objective of the imaging was

1. to find peculiar fine structures in the morphology of the candidate galaxies, and
2. to search for possible galaxy candidates in those fields where either only objects at the plate limit or no objects were found on POSS.

Thus far, 77 fields have been observed in broad band B and R filters (25 additionally in an I filter) and 23 only in the R filter. The results obtained from this sample are that galaxy candidates can be found for all IRAS sources with high flux quality at 60 μm or 60 and 100 μm. In about 50 fields one or several objects with peculiar morphology - tidal tails and arms, faint light bridges, double nuclei, bright knots outside the center or disturbances in the isophotal structure stretching out from the core - are observed (Fig. 1).

4. Spectroscopy

Long-slit, low resolution (10 - 15 Å) spectroscopy was performed in the wavelength range 4700 - 7300 (8200) Å with the Boller and Chivens spectrograph attached to the Cassegrain focus of the 3.5 m telescope. A 1024 x 656 pixel RCA-CCD detector was used. The expectation was to find emission line objects within the IRAS position uncertainty ellipse

1. to confirm the galaxy candidate as well as associated or interacting companions,
2. to determine the excitation mechanisms and classify the galaxy among the different types of active galaxies,
3. to derive distances, sizes and absolute luminosities, and
4. to get the spatial dependence of emission lines and line ratios.

74 spectra have been taken in 50 fields together with corresponding flux standards. In nearly all observed fields galaxies with strong emission lines are detected (Fig. 2). The high percentage of interacting galaxies in this sample found by direct imaging is confirmed. The spectra are typical of HII-region and starburst galaxies. The redshifts of the objects range between 0.01 and 0.24, yielding far infrared luminosities mainly in the range 10^{10} to 10^{11} $L_{\odot}$. However, there are a few objects of the Arp 220 class which reach IR luminosities of more than 10^{12} $L_{\odot}$. Some objects show several discrete emission regions which coincide with the nucleus and the bright optical knots found in the direct images (Fig. 2). Line intensities of these objects often differ in the individual emission regions.

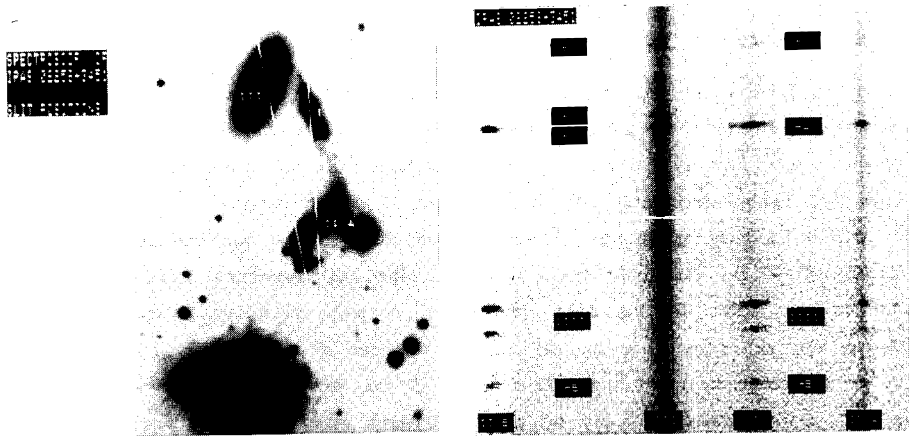

Fig. 2: Spectroscopy of IRAS 02258+3451. The direct image shows a group of three galaxies, two having a very disturbed appearence. Two spectra of this object have been obtained, the slit orientations are drawn in the image and the object positions are marked. From both spectra, the wavelength regions around H_α and the [OIII]/H_β line complex respectively are displayed. All three galaxies show strong emission lines, having the same redshift.

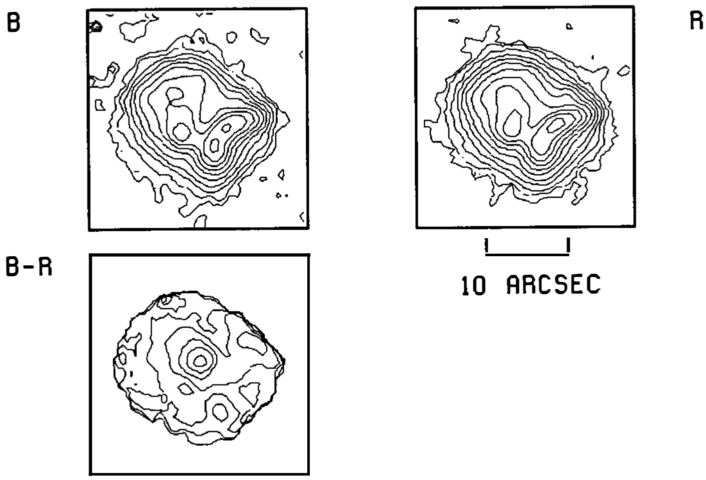

Fig. 3: Photometry of IRAS 14168+8256. The two upper images show the red (right) and blue (left) surface brightness. Isophotal contours between 20.5 and 27 mag/arcsec^2 are displayed. For this object a L_{FIR}/L_B ratio of 8 has been deduced. There are two prominent regions in this butterfly-shaped object, where strong line emission is observed, too. Colours between -0.1 and 1.3 mag are displayed in the B-R colour map. The reddest region (B-R = 1.4 mag) is situated in the gap between the two optically brightest regions. This may indicate the location of a dust layer, which is the source of the far infrared radiation.

5. Photometry

In addition to the exposures of the object fields, CCD standard star fields published by Christian et al.[6] were observed, several per night, at different air masses to enable the determination of surface brightness and integrated brightness and the construction of colour maps.

The half hour exposured direct images allow us to outline the galaxies to a limit of 27 - 27.5 mag arcsec^{-2}. The optical absolute brightness of the objects turn out to be like those of normal galaxies, with M_B between -19 mag and -21 mag. However, all these sources show a large infrared excess, with the ratio L_{FIR}/L_B extending from 1 to extreme values of about 100. The B-R colour maps of many of these objects show striking structures, e.g. relatively red central regions, reddened bars, significantly redder as well as bluer regions which may have a rather complex form (Fig. 3), whereas other galaxies have a quite diffuse appearence with B-R colours larger than 2 or 3 magnitudes. We assume, that these colour maps give us some hints where dusty regions as well as star forming sites are located.

I thank Drs. H. Elsässer and F.V. Hessmann for a critical reading of the manuscript.

References

1) Soifer, B.T., Rowan-Robinson, M., Houck, J.R., de Jong, T., Neugebauer, G., Aumann, H.H., Beichman, C.A., Boggess, N., Clegg, P.E., Emerson, J.P., Gillett, F.C., Habing, H.J., Hauser, M.G., Low, F.J., Miley, G., and Young, E., 1984, Astrophys. J. Lett. 278, L71
2) IRAS Point Source Catalog, 1985, Joint IRAS Science Working Group
3) Wolstencroft, R.D., Savage, A., Clowes, R.G., Mac Gillivray, H.T., Legett, S.K., and Kalafi, M., 1986, Monthly Notices Royal Astron. Soc. 223, 279
4) Lawrence, A., Walker, D., Rowan-Robinson, M., Leech, K.J., and Penston, M.V., 1986, Monthly Notices Royal Astron. Soc. 219, 687
5) IRAS Catalogs and Atlases, Explanatory Supplement 1985, edited by Beichman, C.A., Neugebauer, G., Habing, H.J., Clegg, P.E., and Chester, T.J., Washington, D.C.: U.S. Government Printing Office
6) Christian C.A., Adams, M., Barnes, J.V., Butcher, H., Hayes, D.S., Mould, J.R., and Siegel, M., 1985, Publ. Astron. Soc. Pac. 97, 363

RADIO AND OPTICAL STUDIES OF HIGH LUMINOSITY IRAS GALAXIES

R.D. Wolstencroft*, S.W. Unger+, A. Pedlar+, J.N. Heasley†, Q.A. Parker*, J.W. Menzies×, A. Savage*, H.T. MacGillivray*, S.K. Leggett* and R.G. Clowes*

* Royal Observatory, Edinburgh, Scotland
\+ Royal Greenwich Observatory, Herstmonceux Castle, East Sussex, England
\+ Nuffield Radio Astronomy Laboratories, Jodrell Bank, England
† Institute for Astronomy, University of Hawaii, USA
× South African Astronomical Observatory, Capetown, South Africa

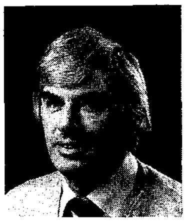

Follow-up observations of a complete sample of 154 IRAS galaxies, optically identified down to B=21, indicate that between 3 and 9% of the sample are ultraluminous ($L_{IR} > 10^{12}\ L_{\odot}$) depending on the choice of H_o (75 to 50 km s^{-1} Mpc^{-1}). VLA observations at 20 cm of the complete sample indicate that 85% are detected above 1mJy and for the most part the radio emission is centrally concentrated. The tight linear relation between radio and infrared luminosities is valid at the highest luminosities. Of the 11 most luminous objects one is a quasar : it fits the radio infrared relation very well which suggests that the infrared and radio emission has the same origin as in the other IRAS galaxies, ie. it probably originates primarily in regions of star formation in the host galaxy. The other 10 very luminous galaxies are either close but resolved mergers or double galaxies, presumably interacting. Radio observations of the 10 original empty field sources in our sample with no optical counterpart ($B \leqslant 21$) allow us to conclude that 4 of these are fainter galaxies just outside the IRAS error ellipse with high values of L_{IR}/L_B. One other object, with a radio source at the edge of the error ellipse but no optical counterpart brighter than B = 23, may prove to be a highly luminous galaxy with $L_{IR}/L_B \gtrsim 1250$.

1. Introduction

We are carrying out a comprehensive program of optical identification of all sources in the IRAS Point Source Catalogue in the South Galactic polar cap at $|b| \gtrsim 60^\circ$. Optical identifications down to a limiting magnitude of B = 21 yield a candidate within the IRAS error ellipse for 97.5% of *all* catalogued sources : we refer to the remaining 2.5% of sources as empty field objects. Wolstencroft et al. [1] have described the identification methods used and the results obtained in a study of a small area (304 deg^2) (the small SGP sample) which is part of the survey field covering a total area of about 2600 deg^2 (the large SGP sample). The objects identified in the three main classes are :

Sample	Area (deg^2)	All	Number of objects Stars	Galaxies	Empty Fields
Small SGP	304	312	148	154	10
Large SGP	2600	2800	1480	1255	65

The figures for the large SGP sample are still preliminary but are unlikely to change by more than 1%.

We have been carrying out follow-up studies of galaxies and empty field sources in the small SGP sample with the principal aims of (a) determining an infrared luminosity function for a complete sample of IRAS galaxies, (b) understanding the source of the very high luminosities of some of these galaxies and (c) seeking to obtain identifications of the empty field objects. The following data are being gathered : spectra, typically at 5 Å resolution, to give redshifts and emission line strengths; broad band CCD images of the highest luminosity galaxies; and 20 cm radio continuum maps.

2. The Highest Luminosity Galaxies in the Small SGP Sample

Redshifts have so far been obtained for about 130 (85%) of the galaxies: the median and maximum values are z = 0.03 and 0.33 respectively. These redshifts have been used to calculate distances, using $H_o = 75$ km s^{-1} Mpc^{-1} and $q_o = 0$, and far infrared luminosities, L_{IR}. The histogram of $L_{IR}/L_\odot$ peaks between 10^{10} and 10^{11}. If we define ultra-luminous IRAS galaxies to be those with $L_{IR} > 10^{12}$ $L_\odot$ ($H_o = 75$) then from a sample that is 85% complete there are 4 such galaxies (3.1%) out of 130: for reference it is worth noting that Arp 220 is not ultraluminous on this definition since on our scale its luminosity is 8.00×10^{11} $L_\odot$. In their IRAS bright galaxy sample Sanders et al. [2] found 3.1% were ultraluminous, identical to our figure. Note that because Sanders et al. define L_{IR} in the range 8 to 1000μm whereas we define it between 43 and 123 μm (eg they find $L_{IR} = 1.55 \times 10^{12}$ $L_\odot$ for Arp 220), the fraction of ultraluminous galaxies in the two samples are not exactly comparable. This fraction depends sensitively on the assumed value of H_o : if $H_o = 50$ is adopted, the fraction of ultraluminous galaxies in our sample becomes 11 or 8.5% of the sample. In our large (small) SGP sample there are 1255 (154) galaxies, and we therefore expect to find 39 (107) galaxies with $L_{IR} > 10^{12}\ L_\odot$ for $H_o = 75$ (50) in the large sample. For the remainder of this paper L_{IR} is calculated using $H_o = 75$.

A provisional infrared luminosity function, $\Phi\ (L_{IR})$, based on the 85% complete sample has been determined. We find a change of slope of the luminosity function at $L_{IR} \simeq 10^{10}\ L_\odot$ with $\Phi(L_{IR}) \propto L^{-2.4}$ at $L_{IR} > 3 \times 10^{10}\ L_\odot$ and a shallower slope at $L_{IR} < 10^{10}\ L_\odot$: because there are relatively few galaxies with $L_{IR} < 3 \times 10^9\ L_\odot$ the exact value of this shallower slope is uncertain. This result is consistent with the luminosity function derived by Lawrence et al. [3] for a sample in the north galactic polar cap.

During July and October 1986 we mapped all 154 galaxies and 10 empty fields at 20 cm with the B/C array of the VLA. 131 (85%) of the galaxies were detected above 1mJy of which 120 were classified as compact and 11 as extended based on a visual inspection of the maps. 38 of the optically smaller galaxies (diameter $\lesssim$ 20 arc sec) were mapped at higher resolution with the A/B array (~ 4 arc sec FWHM beam) and 78% of these show the same flux in the two arrays. These results imply that the radio flux from most IRAS galaxies is centrally concentrated and that the great majority of IRAS galaxies are 20 cm radio sources at flux levels above 1mJy. Radio luminosities, L_{RAD}, derived for those galaxies with redshifts, range between 5×10^{20} and 2×10^{24} w Hz^{-1} and correlate extremely well with L_{IR}. The correlation is consistent with the relation $L_{RAD} \propto L_{IR}$ holding over a very wide range of luminosities with no signs of saturation at the highest values of L_{RAD} : the dispersion is very narrow with 50% of the sample having a value of log (L_{IR}/L_{RAD}) within 0.15 of the mean value. A full description and interpretation of these radio results will be presented elsewhere (Unger et al., 1987).

The four ultraluminous galaxies in our sample are :

IRAS Name	$L_{IR}/L_\odot$	z	L_{IR}/L_B	F_{60}/F_{100}	B
23515-2917	$>1.18\times10^{12}$	0.334	>42	>0.47	19.3
00275-2859	1.45×10^{12}	0.279	23	0.85	18.3
00406-3127	1.07×10^{12}	0.246	119	0.72	20.0
00441-2221	1.83×10^{12}	0.314	11	0.41	17.3

Three of these four objects are double and one, IRAS 00275-2859, is single. This latter object is atypical of the sample and is in fact a quasar : we discuss it later. If we consider a larger sample, namely the 10 most luminous galaxies (excluding the quasar) ($L_{IR} > 4.4\times10^{11}\ L_\odot$), we find that all 10 are double galaxies. Based on optical morphology alone 5 of these doubles are well separated galaxies (50 to 135 kpc), with the optically brighter galaxy identified as the IRAS source, and 4 are close interactions or resolved mergers with clear evidence of tidal disruption ; one galaxy is a radio double but optically single with a separation of 103 kpc. 2 of the 10 are both radio and optical doubles and 7 are optical doubles only. The projected separations of some of these 10 double galaxies are surprisingly large, ranging from 6 to 135 kpc with a median value of 53 kpc. If a recent interaction is the source of the high luminosity of these galaxies then, assuming a relative velocity of 150 km s^{-1}, the earliest time of closest approach for a pair with the median separation would have been $3.5 x 10^8$ yrs ago. This is consistent with estimates [5,6,7] of T_{max}, the time between closest approach and maximum infrared luminosity, of a few x 10^8 years. However in the case of interactions producing ultraluminous galaxies we expect that the onset of starbursts in individual molecular clouds would need to occur in a narrow time 'pulse' which could bias T_{max} to smaller values. For the 3 double galaxies with *projected* separations between 90 and 135 kpc it becomes more difficult to argue that the corresponding smallest values of T_{max}($5.9 x 10^8$ and $8.9 x 10^8$ yr) are consistent with a previous close encounter. The extreme case of IRAS 23515−2917 almost certainly requires a different explanation. The optically brightest of the two galaxies, A, which is identified with the IRAS source, is a radio source (5.1 mJy) ; the optically fainter companion, B, which is 20 arc sec (135 kpc) SSE of A, is also a radio source (2.2mJy) and has a close, still fainter companion, C, 5 arc sec due N. One possible explanation is that galaxy A is currently undergoing a merger or close encounter which at a scale of 6.7 kpc per arc sec cannot be resolved in the CCD image, and that any past interaction that may have occurred between A and the galaxy pair B and C is not influencing the present emission for A. Such an explanation in terms of unresolved mergers might also explain the two other pairs with separations greater than 90 kpc. A variation on the above explanation might be to suppose that the current merger or close interaction is more effective because the tidal disruption produced by the earlier encounter (with the now distant companion) was still very evident when the second event began, ie the target was 'primed'.

IRAS 00275−2859 has a spectrum totally different from that of all other objects in our sample. Our spectrum between 4750 and 6250Å shows that the Hβ emission line is very broad (3500 km s^{-1} FWHM), with an absorption trough 180 Å wide on its blue side reminiscent of broad line absorption quasars (see eg [8]). Other emission lines seen are [OII] 3727Å and [Ne III] 3869Å. This source was discovered independently by Vader and Simon [9] to be a quasar, who noted the presence of strong Fe II lines in its spectrum. Our measurement of the 20 cm radio flux of 3.6mJy places the quasar firmly on the narrow radio−infrared luminosity relation found for our sample. This suggests that the radio and infrared emission originate in regions of star formation in the host galaxy.

3. Empty Field Sources

Radio sources are very valuable guides in the identification of empty field IRAS sources, i.e. sources with no optical counterpart (B<21) within the 95% confidence IRAS error ellipse. This is because (a) 85% of IRAS galaxies are radio sources above lmJy, (b) the chance of finding an unrelated radio source with F(1.4 GHz) > 1mJy within the IRAS error ellipse is low, and (c) the ratio of infrared to radio luminosity lies in the narrow range established for the identified IRAS galaxies. Thus empty field sources due either to cirrus or faint cool stars are not expected to be radio sources. The identification of galaxies just outside the error ellipse of an empty field which coincide in position with a radio source can be confirmed : note that our optical and radio positions differ on average by about 2 arc sec in both right ascension and declination. We expect to find about 5% of our identifications just outside the 95% confidence error ellipse.

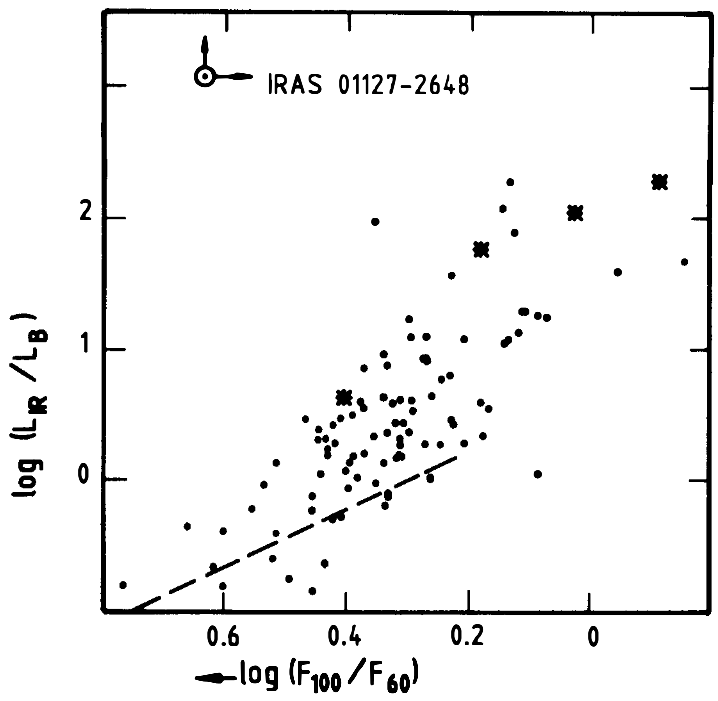

Figure 1

Relation between L_{IR}/L_B and the 100 to 60μm flux density ratio for those galaxies with good or moderate quality fluxes at both 60 and 100μm (taken from [1]). The asterisks show the 4 empty field objects identified with galaxies just outside the error ellipse. The dashed line is the relation for an optically selected sample of Sbc galaxies [10].

We obtained the following results for the 10 original empty field sources : 4 are galaxies just outside the error ellipse ; 1 is a merger of 2 nearby infrared sources resulting in a spurious IRAS position ; 1 is a peculiar M star ; 3 are cirrus sources ; and 1 is an object with a radio source at the edge of the error ellipse and no optical counterpart brighter than B = 23. This latter object, IRAS 01127−2648, is the most interesting of the empty field sources : the radio source which may be its radio counterpart lies 46±3 arc sec from the IRAS position on the major axis of the error ellipse. The infrared to radio ratio based on the 60μm flux density (the 100μm flux density is an upper limit) is consistent with the correlation found for IRAS galaxies. The relation between L_{IR}/L_B and the ratio of 60 to 100μm flux density provides a further test of the credentials of an IRAS galaxy. This is shown for our sample in fig 1 : the 4 empty field objects identified with galaxies just outside the error ellipse (shown as asterisks) fit the relation well, but in the case of IRAS 01127−2648 the 100μm upper limit and lower limit on B (and hence L_{IR}/L_B) complicate the interpretation. If the radio source is truly the radio counterpart of IRAS 01127−2648 then the most conservative assumption would be that it is an ultraluminous galaxy with B ≈ 23, $L_{IR}/L_B \approx 1250$ and, $F_{60}/F_{100} \simeq 1.6$. Deep CCD imaging to identify the radio counterpart, plus spectroscopy and coaddition of the IRAS data will be carried out to settle this question.

References

[1] Wolstencroft, R.D. Savage, A., Clowes, R.G., MacGillivray, H.T., Leggett, S.K., and Kalafi, M. 1986. Mon. Not. Roy. Astro. Soc. 223, 279.

[2] Sanders, D.B., Soifer, B.T., Elias, J.H., Madore, B.F., Matthews, K., Neugebauer, G., and Scoville, N.Z. 1987. Astrophys. J. (in press).

[3] Lawrence, A., Walker, D., Rowan-Robinson, M., Leech, K.J., and Penston, M.V. 1986. Mon. Not. Roy. Astr. Soc. 219, 687.

[4] Unger, S., Wolstencroft. R.D., Savage, A., Pedlar, A., Parker, Q.A. MacGillivray, H.T., Leggett, S.K., and Clowes, R.G. 1987. In preparation.

[5] Byrd, G.G., Valtonen, M.J., Sundelius, B., and Valtaoja, L. 1986. Astron. Astrophys. 166, 75.

[6] Byrd, G.G., Sundelius, B., and Valtonen, M. 1987. Astron. Astrophys. 171, 16.

[7] Noguchi, M., and Ishibashi, S. 1986. Mon. Not. Roy. Astr. Soc. 219, 305.

[8] Hazard, C., Morton, D.C., Terlevich, R., and McMahon, R. 1984. Astrophys. J. 282, 33.

[9] Vader, P., and Simon, M. 1987. Nature 327, 304.

[10] Davies, R.D., Wolstencroft, R.D., Pedlar, A., Hummel, E., and Van der Hulst, J.M. 1987. In preparation.

OH MEGAMASERS IN IRAS GALAXIES

Jean-Michel MARTIN
OBSERVATOIRE DE PARIS-MEUDON
Département de Radioastronomie
92190-MEUDON
FRANCE

Huge extragalactic hydroxyl masers have recently been discovered with the Arecibo, Nançay, Jodrell Bank and Parkes radio telescopes. These objects seem to belong to a very peculiar class and are called megamasers, regarding their high 1667 Mhz OH line luminosity witch can be greater than one thousand solar luminosities, in contrast to the masers appearing in molecular clouds and in circumstellar shells which are detectable only at distances less than a few kpc and are thus several order of magnitude less powerful. Most of these galaxies were first detected by the IRAS satellite and are characterized by a strong far infra red luminosity. They would be undergoing strong bursts of star formation, giving rise to a number of short-lived massive stars which are responsible of a strong UV radiation field and radio continuum emission, through supernovae formation, the UV radiation field heating the dust particles witch radiate in the far IR, at 60 and 100 μm. An OH and HI survey is carried out with the Nançay radio telescope and additional high resolution data (VLA and MERLIN) have been obtained. These observations will provide essential data for a better understanding of these objects.

INTRODUCTION

The first extragalactic OH absorption has been discovered by Weliachew in NGC253 (1971). Narrow emission features have been detected later in the same galaxy (Whiteoak and Gardner, 1976) and in M82 (Rieu et al. 1976).

More recently, galaxies showing nuclear continuum emission were searched for OH absorption (Rickard et al. 1982, Baan et al. 1985, Kazès and Dickey, 1985). The OH 1667 MHz line optical depth has been found increasing with the inclination of the galaxy upon the plane of the sky as expected for absorption lines originating in a molecular disk (Baan et al. 1985). In the course of these surveys, a huge OH emission has been discovered in Arp220 (=IC4553) at Arecibo and in Mrk231 and NGC3690 at Green Bank (Baan, 1985, Baan,Wood and Haschick, 1982). These galaxies were detected by the IRAS satellite as strong far infra-red (FIR) emitters, and thus have large FIR/B luminosity ratios with total FIR luminosities reaching 10^{12} L_0. They obviously belong to a new class of masers, and are called "megamasers". It is therefore of great interest to detect other such powerful galaxies and also less luminous OH maser sources, in order to make a statistical study and to compare with other galaxies which have the same FIR and optical properties but have not been detected in the OH lines.

A survey of selected luminous IRAS galaxies, catalogued and uncatalogued, is being conducted with the Nançay radiotelescope, in connection with optical spectroscopy and photometry (ESO and OHP). 5 megamasers have been found in both catalogued and uncatalogued sources: Mrk273, IRAS1720-0014, Zw1510+0724, Arp148 and IIZw96 (Bottinelli et al. 1985a,b,1986). Additional data have been obtained on IRAS1720-0014 with the VLA array and MERLIN interferometer.

THE MAIN PROPERTIES

The OH emission lines are different from what is observed in our Galaxy:

The galactic source W3(OH) is stronger in the 1665 MHz and is highly polarized, its luminosity is of about 5×10^{-6} L_0. On the other hand, megamasers have stronger 1667 MHz line with a 1667/1665 ratio between 3 and 5, except for IRAS1017+0828 and IIIZw35 (Mirabel and Sanders, 1987) and no polarization has been found in IRAS 1720-0014, within a confidence level of 15% (fig. 1,3). These lines are strong, with isotropic luminosities ranging from a few solar luminosities to 1200 L_0 in IRAS 1720-0014, compared with M82 which luminosity is only 0.1 L_0. Moreover, these lines are always broader than 100 km/s, with in some cases, two or more emission and/or absorption components, and also high velocity features were detected in Mrk231 and in Mrk273 (L. Staveley-Smith et al. 1987).

T' ɜ HI content has been measured in most of the megamaser galaxies. Wide HI osorption has been detected in Arp220 , Mrk231 , NGC3690 , Mrk273 (bottinelli et al. 1985a) and IRAS 1720-0014 (600km/s, fig.2, Bottinelli et al. 1985b). This suggest the existence of unusual HI clouds infalling, or being ejected along the line of sight, in addition to rotation velocities. In the other sources, either narrower emission or absorption profiles have been measured.

The brightest megamasers are also very luminous in the FIR, the FIR luminosity ranges from 1.2 to 11×10^{11} L_0 but there is another property which must be pointed out: the megamasers' FIR colors are different from other IRAS galaxies, as is has been shown by S.W. Unger et al. (1986). We found a similar criterion for selecting the candidates for our survey. The 12/25 μm flux ratio is greater for megamasers than for other spiral galaxies (>2) and the 60/100 μm flux ratio equals about 1. Arp220 has a bigger 12/25 μm ratio which is greater than 16.

Most of the megamasers are distant (≈100Mpc) and their apparent size is small. However, the optical images display galaxies with various morphologies: half of them are clearly interacting objects, like NGC3690, Mrk231 and mergers like Arp220 and Arp148 which is a ring galaxy. Mrk273 has a long tail with no visible cause as it is mentionned in the Vorontsov-Velyaminov catalogue (1977) but it might be the result of the merging of two galaxies.

The optical spectra of the megamasers are similar to other IRAS galaxies, revealing low-ionization emission lines (Dennefeld et al. 1985) and also a large reddening derived from the Balmer decrement: in Zw1510+0724's spectrum the Hß line is not detected.

All these observational properties fit well the simple model which has been presented by Baan (1985). In this scenario, a starburst galaxy is needed. The UV radiation field heats the neighbouring dust which radiates again in the FIR. The OH molecular clouds are then inverted by the FIR radiation field, according to Baan (1985) and Norris et al. (1986). This point is under investigation. The OH molecules amplify the radio continuum emission from the supernovae remnants. In fig. 4, the OH and FIR luminosities are well corelated.

HIGH RESOLUTION OBSERVATIONS

We observed IRAS1720-0014 in march, 1986 with the VLA radio telescope (A-array). The beam's size was one arcsecond. After data reduction has been done on the site, we found that the source is not resolved in continuum and in the line channels at a wavelenth of 18 cm (fig.5). This result is strengthening the interpretation that the continuum radio emission from central parts of the galaxy is amplified by the neighbouring OH molecular gas. We made also a continuum map of the same galaxy with the MERLIN radiotelescope in december, 1986: The nucleus is unresolved at an angular resolution of 0.25 arc second (fig. 6). We need higher angular resolution to understand the structure of the masing regions, first to find their physical properties, to explain the dynamics of the molecular clouds around the nucleus and the masing amplification process.

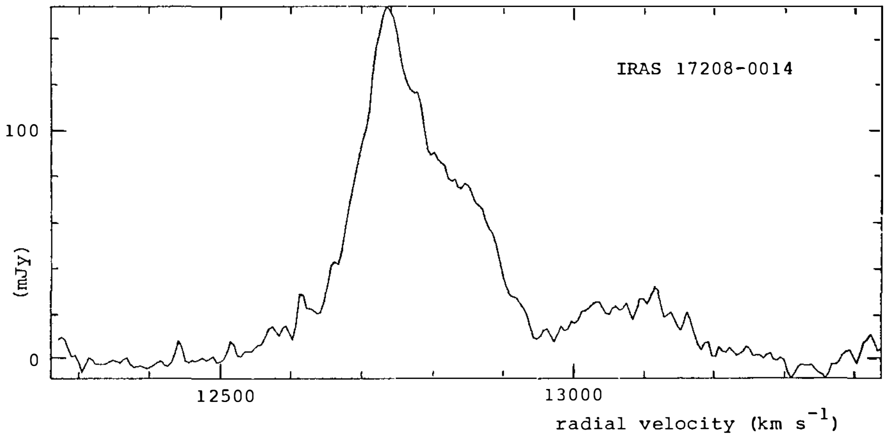

Fig. 1:average (linear H and V polarizations) OH spectrum of IRAS 1720-0014 with a resolution of 4.5 km/s. Radial velocities are given in terms of heliocentric optical redshift. The central feature corresponds to the 1667 MHz transition, the redshifted secondary feature corresponds to the 1665 MHz transition.

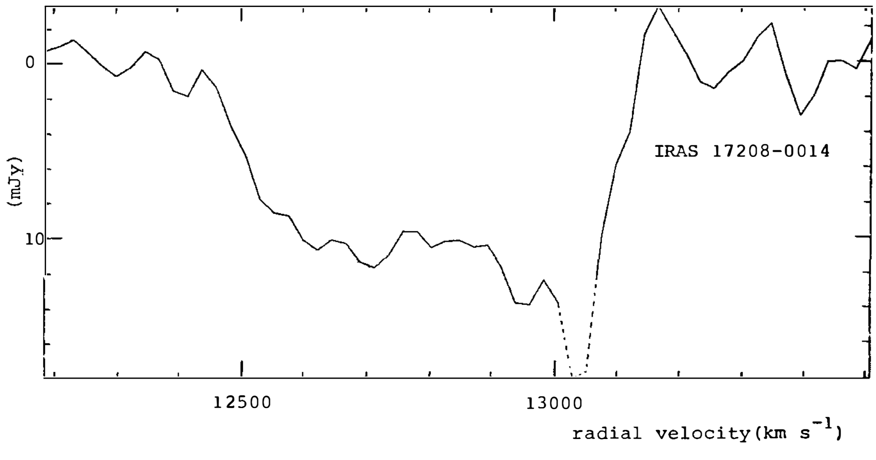

Fig. 2:HI profile of IRAS 1720-0014 with a velocity resolution of 21 km/s. The dashed part corresponds to an external interference spike.

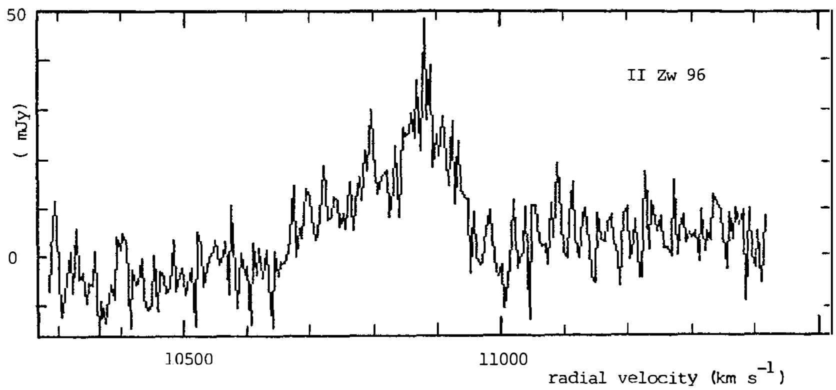

Fig. 3: OH spectrum of IIZw96 centered for the rest frequency of the 1667 MHz transition with a velocity resolution of 4.5 km/s. Radial velocities are given in terms of the heliocentric optical redshift. No instrumental baseline was removed. The 1665 MHz transition is not detected.

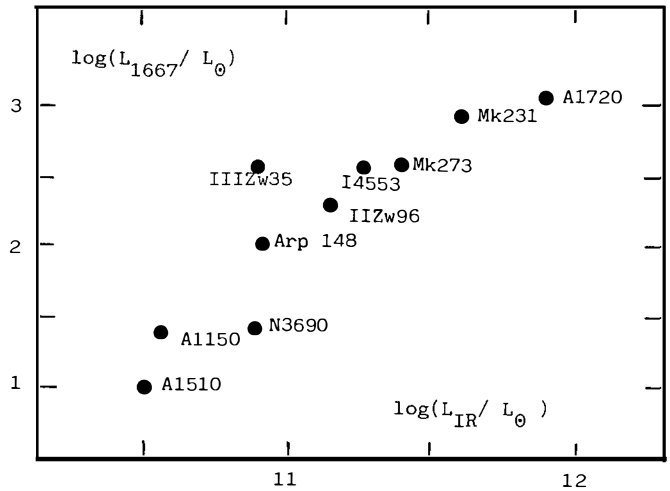

Fig. 4: Isotropic luminosity at 1667 MHz vs. far infrared luminosity determined from IRAS data for megamaser galaxies.

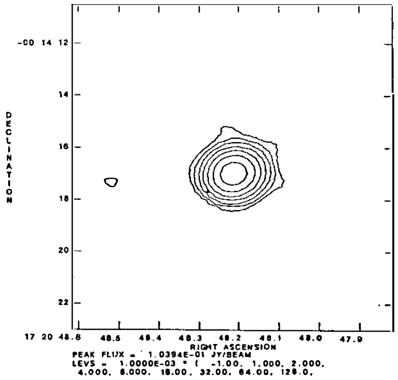

Fig. 5: VLA-A array 18 cm OH lines + continuum map of IRAS 1720-0014. The beam size is 1". The source is clearly unresolved. The r.m.s. noise is of 0.3 mJy/ beam.

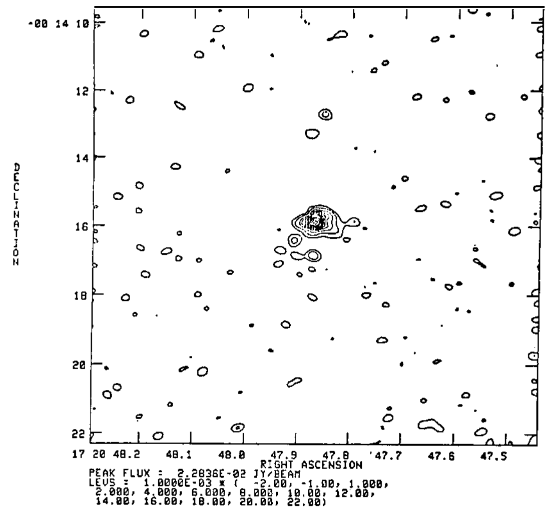

Fig. 6: MERLIN phase referenced continuum map of IRAS 1720-0014. The beam size is 0.25". The r.m.s. noise is of 0.4 mJy/beam. Only the central feature is real. This observation has been made in collaboration with S.W. Unger, J.M. Chapman, R.J. Cohen, and L. Staveley-Smith.

REFERENCES

Baan,W.A., Wood,P.A., Haschick,A.D., 1982 Astrophys. J. 260,L29

Baan,W.A., 1985 Nature, 315,26

Baan, W.A., Haschick, A.D., Schmeltz J.T., 1985, Astrophys. J. 298,L51

Bottinelli,L., Fraix-Burnet,D., Gouguenheim,L., Kazès,I., Le Squeren,A.M., Patey,I.,Rickard,L.J.,Turner,B.E.,1985a Astron.astrophys.151,L7

Bottinelli,L., Gouguenheim,L., Le Squeren,A.M., Dennefeld,M., Paturel,G., 1985b IAU Circ. 4106

Bottinelli,L., Gouguenheim,L., Le Squeren,A.M., Martin J.M., Dennefeld,M., Paturel,G.,1986, IAU Circ. 4231

Dennefeld et al., 1986, in "Star forming Dwarf Galaxies and related objects", ed. by D. Kunth, IAP Atrophysics meeting, p 351

Kazès,I., Mirabel, I.F., Sanders D.B.,1987 IAU Circ. 4362

Kazès,I., Dickey, J.M., 1985,Astron.astrophys.152,L9

Mirabel I.F., Sanders, D.B.,1987, Astrophys. J. *(in press)*

Norris,R.P., Whiteoak J.B., Gardner F.F., Allen D.A., Roche P.F., 1986, Mon. Not. R. astr. soc. 221,51p

Rickard, L.J., Bania, T.M., Turner, B.E., 1982, Astrophys. J., 252, 147

Rieu, N.Q., Mebold, U., Winnberg, Guibert, J.,Booth, R.,1976, Astron.astrophys.52,467

Staveley-Smith,L., Cohen, R.J., Chapman J.M. , Pointon, L.,Unger S.W.1987, Mon. Not. R. astr. soc., *(in press)*

Unger,S.W., Chapman, J.M., Cohen, R.J., 1986,Mon. Not. R. astr. soc. 220, 1p

Vorontov-Velyaminov, B.A., 1977, Astron.astrophys. Suppl. Ser. 28,1

Weliachew L., 1971, Astrophys. J., 167, L47

Whiteoak J.B., Gardner F.F., 1976,Mon. Not. R. astr. soc. 176, 25p

THE GAS CONTENT IN STARBURST GALAXIES

I.F. Mirabel
Instituto de Astronomía y Física del Espacio, Argentina
and University of Puerto Rico

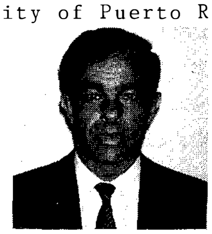

and

D.B. Sanders
Palomar Observatory, California Institute of Technology

The results from two large and homogeneous surveys, one in HI, the other in CO, are used for a statistical review of the gaseous properties of bright infrared galaxies. A constant ratio between the thermal far-infrared radiation and non-thermal radio emission is a universal property of star formation in spiral galaxies. The current rate of star formation in starburst galaxies is found to be 3-20 times larger than in the Milky Way. Galaxies with the higher far-infrared luminosities and warmer dust, have the larger mass fractions of molecular to atomic interstellar gas, and in some instances, striking deficiencies of neutral hydrogen are found. A statistical blueshift of the optical systemic velocities relative to the radio systemic velocities, may be due to an outward motion of the optical line-emitting gas. From the high rates of star formation, and from the short times required for the depletion of the interstellar gas, we conclude that the most luminous infrared galaxies represent a brief but important phase in the evolution of some galaxies, when two galaxies merge changing substantially their overall properies.

1. Introduction.

Among the extragalactic sources detected by the Infrared Astronomical Satellite (IRAS), the most luminous far-infrared galaxies are very interesting objects, since they host several unusual phenomena. Their study is important because they are the best sample to explore the link between starburst objects on one hand, and quasars and active galaxies on the other hand. There are indications that Superluminous Far-infrared galaxies represent a brief but important phase in the evolution of some galaxies, when a galaxy mass of interstellar matter is rapidly converted into stars. The morphology and kinematics of the gas in these galaxies suggest that they are the results of galaxy-galaxy interactions. The most energetic objects, like Mrk 231, IRAS 1211+03, or Arp 220, appear to be advanced mergers.

In this note, after a summary of the correlations found by Sanders and Mirabel [1] between the far-infrared, the total radio continuum, and the CO fluxes, we describe the main results from a neutral hydrogen survey of bright IRAS galaxies, recently finished at the Arecibo Observatory. 96 sources from the Bright Galaxy Sample [2] with far-infrared luminosities in the range of $2 \times 10^{10} - 2 \times 10^{12}$ solar luminosities, observable from Arecibo were surveyed in the 21 cm line of atomic hydrogen. The results from this survey are combined with the results from the CO surveys by Sanders and collaborators [1,3,4], to determine statistical properties of the IRAS bright galaxy sample, such as the mass of atomic hydrogen, the kinematics of the gas, and the molecular to atomic gas content. One of the advantages of this comparative study between the content of molecular gas and the content of atomic gas is that we use only data from two large and homogeneous surveys.

2. Radio continuum and far-infrared fluxes.

The far-infrared flux from spiral galaxies is a good indicator of star formation, since it comes from dust heated by stellar radiation. If the nonthermal radio emission is an indication of the number of supernovae, a correlation between the far-infrared flux and radio emission should be expected. Figure 1 from Sanders and Mirabel [1] shows that the radio flux

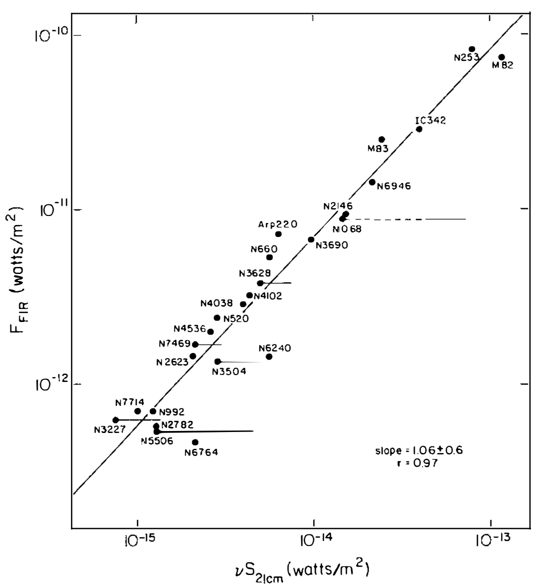

Figure 1. Total far-infrared flux determined from IRAS data vs. the total radio continuum flux at 1.4 GHz for bright radio spirals. Compact radio components less than 100 pc in size were substracted (horizontal lines) from the total flux in several galaxies.

at 21 cm and the thermal FIR flux coming from the discs of spiral galaxies are strongly correlated. This implies that bright radio spirals are among the strongest far-infrared extragalactic sources, further strengthening the argument that bright radio spirals are powered by energetic starbursts.

A similar correlation was found by Helou et al. [5] for a larger sample of spiral galaxies. Figure 1 shows that the ratio between the radio and FIR fluxes is similar for high luminosity galaxies like Arp 220, and lower luminosity galaxies like M 83. In figure 1, the poinlike (d smaller than 100 pc), and jetlike radio sources, usually associated with active nuclei, were substracted from the total radio flux. The nearly constant ratio between far-infrared and radio emission in the discs of spiral galaxies seems to be a universal property of massive star formation in extragalactic systems. The fraction of massive stars seems to be independent from the global star formation rate.

3. The molecular gas.

CO observations of bright radio and far-infrared galaxies [1] have shown that this type of galaxies have masses of molecular hydrogen in the range of 3×10^8 to 4×10^{10} solar masses. The galaxies with the broadest CO emission lines are strongly interacting contact pairs. Furthermore, the galaxies with the higher far-infrared IRAS fluxes at 60 and 100 μm have the higher CO intrinsic luminosities.

In figure 2 is made a comparison of the far-infrared luminosity with the CO luminosity for the sample of galaxies initially studied by Sanders and Mirabel [1]. The far-infrared and CO luminosities in bright IRAS galaxies appear to be similar to the values found for the classic starburst galaxies M 82 and NGC 253. The ratio $L_{FIR}/M(H_2)$ provides a measure of the current rate of star formation and it is found to be 3-20 times larger in these galaxies than for the ensemble of molecular clouds in the Milky Way. This larger $L_{FIR}/M(H_2)$ ratio implies that the total star formation in starburst galaxies is determined by; (i) the total amount of molecular gas, and (ii) an enhanced efficiency of star formation when compared with the Milky Way and other spiral galaxies. Similar conclusions have been reached more recently by Young et al. [6].

High resolution observations of the CO in Arp 220 [7], and NGC 3690 [8] show that more than 40 % of the molecular gas is concentrated in regions smaller than 2 kpc in diameter, with densities 10-100 times greater than in the inner 1 kpc of the Milky Way. The abnormally large concentrations of molecular gas in the cores of superluminous far-infrared galaxies is likely to be the result of galaxy-galaxy interactions between spiral galaxies. The current star formation rates from the $L_{FIR}/M(H_2)$ ratios imply that the molecular gas will be depleted in less than 10^8 yrs. This time is of the same order as the dynamical time required to concentrate most of the interstellar gas in the merger nucleus of two colliding spiral galaxies.

4. The atomic gas

One of the most striking results from the 21 cm line survey of bright infrared galaxies is the frequent presence of velocity broad absorption. The absorption signals arise in the HI located in front of the bright radio

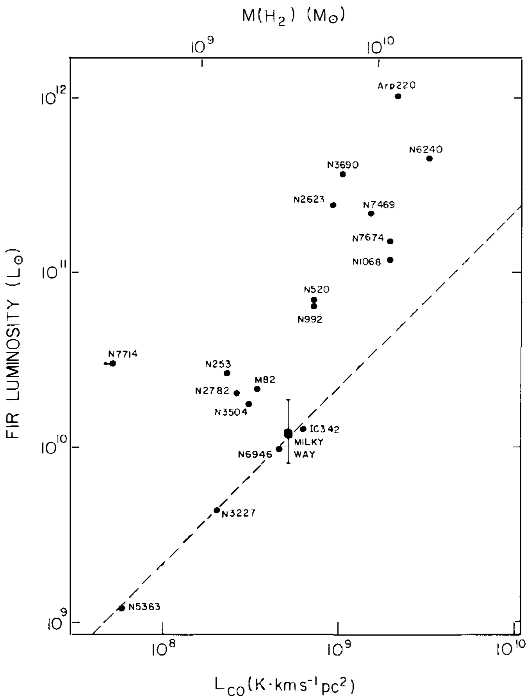

Figure 2. The total far-infrared luminosity determined from IRAS data vs. CO luminosity and the total mass of H_2 in molecular clouds. The vertical bar for the Milky Way represents the range of total FIR luminosity, and the dashed line represents the locus of points with $L_{FIR}/M(H_2)$ equal to that found for the Galaxy.

cores. In the Arecibo survey, we have detected 15 galaxies with HI absorption, up to redshifts of 22,000 km/s.

The absorption may be as broad as 900 km/s. The galaxies IRAS 1211+03, IRAS 1056+24 and Arp 220 show absorption features with fluxes greater than 3 rms extending over velocity ranges of 700 to 900 km/s. This result is indicative of high turbulent, non-circular motions along the line of sight to the nuclear radio source. The high turbulent motions of the interstellar gas detected in HI are consistent with the optical morphology of these galaxies as strong interacting systems and advanced mergers.

To estimate the column density and mass of the absorbing HI, a nuclear radiocontinuum source of 2 kpc in diameter can be assumed. This assumption is justified by VLA continuum maps made by Condon [9] of several of the brightest galaxies of our sample. Furthermore, VLA-A observations of the HI in Arp 220 [10], show that the HI in this galaxy has an extension of 1.5

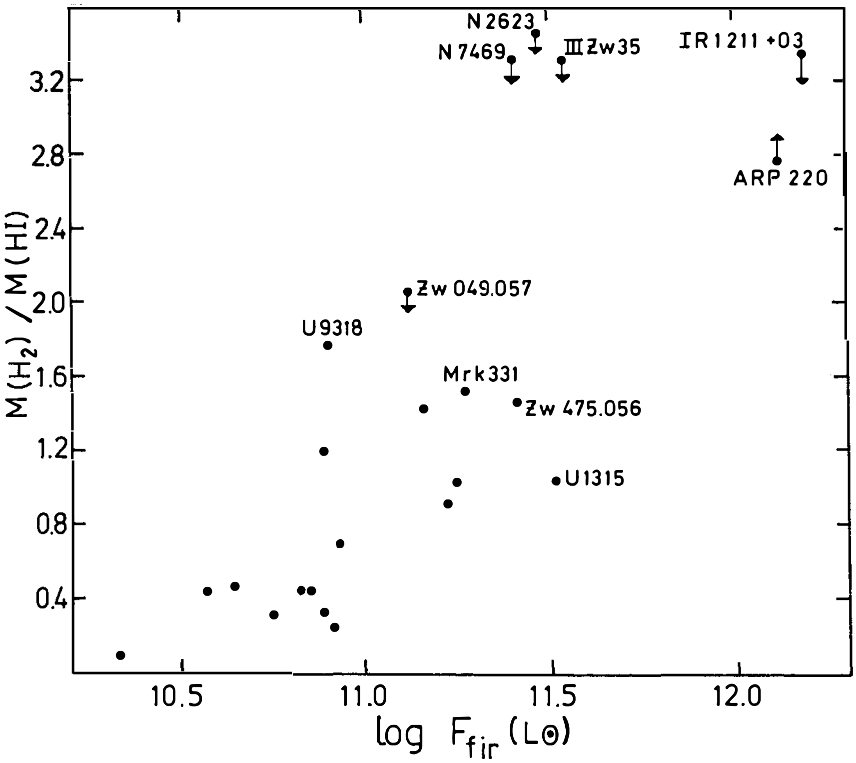

Figure 3. Total molecular to atomic mass ratios vs. far-infrared luminosities for the sources unresolved by the telescope beams. For galaxies with strong HI absorption, only limits of the $M(H_2)/M(HI)$ ratios are given.

kpc. Assuming that the absorbing HI covers uniformly the nuclear radio-sources, column densities of atomic neutral hydrogen in the range of 10^{19}–10^{20} T_s atoms/cm^2 are found. These column densities are more typical of the column densities found along the discs of spiral galaxies, rather than of the column densities in neutral hydrogen high velocity clouds, which are about two orders of magnitude lower than those values. The masses of the absorbing HI in the galaxies of our sample are smaller than 3 x 10^8 solar masses, if T_s= 100 K.

The HI masses and far-infrared luminosities seem to be only loosely correlated. For a given far-infrared luminosity we find galaxies with HI masses that differ by as much as a factor of 50. This large scatter implies that star formation depends more from the total amount of molecular gas, as shown in figure 2, than from the total amount of atomic gas.

Among the galaxies surveyed in HI at Arecibo, there are 23 galaxies with well determined total CO luminosities by Sanders and collaborators [1,3,4]. These 23 galaxies are at redshifts greater than 4,000 km/s, and are unresolved by the 21 cm Arecibo telescope beam, as well as by the 2.6 mm beam of the 12-m telescope at Kitt Peak. For this sample of galaxies we find tight correlations that are important for our understanding of starburst galaxies.

In figure 3, the molecular to atomic gas content versus the far-infrared luminosities are plotted. For five galaxies with HI absorption, only the upper limits of the molecular to atomic gas ratios can be given, since the absorption signals against the nuclear continuum flux may neutralize the detection of hydrogen emission. The lower limits of HI mass were calculated multipling a flux equal to 3 times the rms by a velocity width of 300 km/s. The cancellation of emission signals by the absorption would result in an underestimation of the total mass of HI, and therefore, in an overestimation of the molecular to atomic gas ratio. Because of beam dilution effects, the HI observations of bright radio spirals at high redshifts are more sensitive to the absorbing HI, which contributes, at most, 3×10^8 solar masses to the total mass of atomic hydrogen.

Despite of the previous considerations, there are indications that the relative deficiency of HI in the most luminous far-infrared galaxies is real. Hydrogen emission was searched in Arp 220 by Mirabel at Arecibo, and by Baan et al. [10] using the VLA-C configuration. A limiting mass of 4.6×10^9 $M_\odot$ was found. There is a striking absence of HI emission in Arp 220 as compared with the estimated amount of molecular gas. A lower limit for the HI to H_2 mass ratio can also be found from models of the H_2CO maser detected in Arp 220 by Baan et al. [11]. Similarly, for the galaxy IRAS 1017+08 we find an upper limit for the mass of atomic hydrogen of 3.2×10^9 $M_\odot$. Although these are not stringent upper limits for the HI masses, they put these galaxies on the lower edge of the observed HI distribution in irregulars and early spirals.

We find that the star formation rate per unit of interstellar mass and the molecular to atomic mass ratios are correlated. A high fraction of gas in molecular form must be a condition for a high rate of star formation. Figure 4 shows that the molecular to atomic gas ratio is proportional to

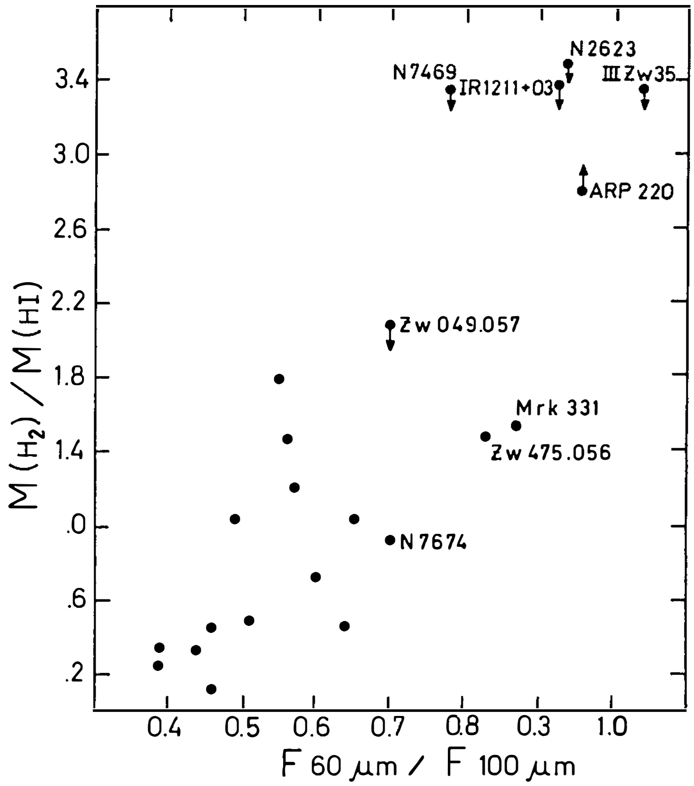

Figure 4. Total molecular to atomic gas ratios vs. the IRAS 60 to 100 microns flux ratio. The molecular to atomic mass ratio is correlated with the dust temperature.

the far-infrared color, namely, to the temperature of the dust. A higher fraction of molecular gas must be a condition for the production of the stellar photons that heat the dust.

5. Discussion.

A striking finding from the neutral hydrogen profiles is a clear preponderance for the HI absorption to be redshifted relative to the optical systemic velocity of the brighter far-infrared galaxies. In figure 5a a histogram of the $V_{HI\ ABS} - V_{OPT}$ difference is shown. This difference is positive for 14 galaxies, and it is negative only for one galaxy. For the 15 galaxies with HI absorption, a mean difference of 106 km/s is found. The HI velocities were calculated following the optical definition. They are the unweighted mean radial velocities of the absorption signals greater than 3 times the rms. The optical redshifts are from Palomar, [12] and [13].

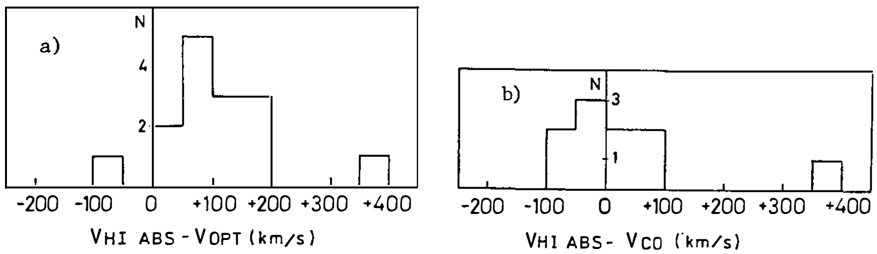

Figure 5. a) Histogram of the difference between the redshifts of the HI absorption and optical lines in bright far-infrared galaxies. b) Histogram of the difference between the HI absorption redshifts and the CO emission redshifts.

From the analysis of the data we conclude that the trend for the HI absorption velocity to be greater than the optical is not a consequence of systematic errors in the HI velocities. There are two possibilities which we now discuss in turn. (i) The HI velocity does not represent the systemic velocity of the galaxies, and this trend is due to the infall of HI towards the nuclear radio source. This possibility is unlikely. A comparison of the HI redshifts with the CO systemic velocities show no significant trend. Figure 4b shows a histogram of the radial velocity difference between the HI absorption and the CO emission for 10 galaxies. Since no significant trend is found when comparing the HI and CO redshifts, we conclude that the velocities of the HI absorption represent more accurately than the optical, the systemic velocity of the galaxies.

(ii) We tentativelly favor a real difference between HI and optical redshifts, due to gas moving radially, probably outward, in the central regions of these galaxies. If the outwardly moving line-emitting gas is mixed with dust, the attenuation of optical emission from the far side leads to an optical redshift below systemic. Mirabel and Wilson [14] have claimed that this effect takes place in Seyfert galaxies. More recently, Hutchings et al. [15] have found a similar trend in quasars. The interpretation of the statistical blueshift of the optical radial velocities in terms of outflowing gas is consistent with the discovery of superwinds in Starburst galaxies by Heckman et al.[16] and McCarthy et al. [17]. The wind's ram pressure may drive slow shocks into high density clouds, producing optical line emission.

It is tempting to speculate that the relative deficiency of neutral atomic hydrogen in the most luminous far-infrared galaxies could be due to ionization, and/or the removal of HI by supernovae induced winds coming from the nuclear regions. However, a substantial contribution to the relative deficiency of HI could also be a consequence of an enhanced efficiency in the formation of molecular gas in nuclear regions having abnormally large concentrations of gas and dust.

The extraordinary star formation rates in super starburst galaxies must cause the depletion of the interstellar gas in the environs of the nuclear regions in less than 10^8 years, leaving the system void of interstellar gas. In this context, we find attractive the idea that bright infrared galaxies may be the predecessors of some kind of early type galaxies.

Acknowledgements: I.F.M. is a member of CONICET, Argentina. This work was supported by NSF Epscor program at UPR. D.B.S. is supported in part through the IRAS extended mission program.

6. References.

1. Sanders, D.B. and Mirabel, I.F. 1985, Ap.J., 298, L31.
2. Soifer, T.B., Sanders, D.B., Madore, B.F., Neugebauer, G., Danielson, G. E., Elias, J.H., Persson, C.J., Rice, W.L., 1987, Ap.J. in press.
3. Sanders, D.B., Scoville, N.Z., Young, J.S., Soifer, B.T., Schloerb, F.P Rice, W.L., Danielson, G.E. 1986, Ap.J. 305, L45.
4. Sanders, D.B., Scoville, N.Z., and Soifer, B.T. 1987, Ap.J. in press.
5. Helou, G., Soifer, B.T., and Rowan-Robinson,M. 1985, Ap.J. 298, L7.
6. Young, J.S., Kenney, J.D., Tacconi, L., Claussen, M.J., Huang, Y.-L., Tacconi-Garman, L., Xie, S., Schloerb, F.P. 1986, Ap.J. 311, L17.
7. Scoville, N.Z., Sanders, D.B., Sargent, A.I., Soifer, B.T., Scott, S.L. Lo, K.Y. 1986, Ap.J. 311, L47.
8. Sargent, A.I., Sanders, D.B., Scoville, N.Z., Soifer, B.T., 1987, Ap.J. 312, L35.
9. Condon, J.J. 1980, Ap.J. 242, 894.
10. Baan, W.A., van Gorkom, J.H., Schmelz, J.T., Mirabel, I.F., 1987, Ap.J. 313, 102.
11. Baan, W.A., Güsten, R., Haschick, A.D. 1986, Ap.J. 305, 830.
12. Huchra, J. 1986, Center for Astrophysics redshift survey, preprint.
13. Palumbo, G.G.C., Tanzella-Nitti,G., Vettolani,G. 1984, A catalogue of radial velocities of galaxies.
14. Mirabel, I.F., and Wilson, A.S. 1984, Ap.J. 277, 92.
15. Hutchings, J.B., Gower, A.C., Price, R. 1987, A.J. 93, 6.
16. Heckman, T.M., Armus, L., Miley, G.K. 1987, A.J.,93, 276.
17. McCarthy, P.J., Heckman, T., van Breugel, W. 1987, A.J., 93, 264.

STARBURSTS IN INTERACTING GALAXIES

R D JOSEPH
Astrophysics Group
Blackett Laboratory
Imperial College of Science & Technology
London SW7, England

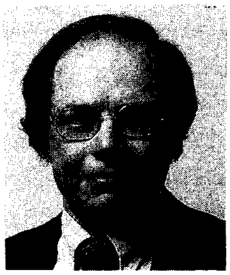

JHKL and 10 μm photometric studies of interacting galaxies show that interactions between galaxies produce mass-to-light ratios smaller than can be understood in terms of a normal popoulation of evolved stars. We will then investigate whether starbursts or 'monsters' are likely to be the energy source powering the IR activity in these galaxies. Using available IR, optical, radio, and ultraviolet observations we show that, in general, starbursts appear to be ubiquitous in interacting galaxies. Finally, we investigate the larger implications of interaction-induced starbursts. Such starbursts are likely to have played a major role in the spectral, chemical, and morphological evolution of many galaxies. They are also likely to figure prominently in the physics of other types of activity in galactic nuclei, although the way in which they do remains unclear.

1. Introduction

One of the most fundamental and most neglected questions elicited by the discovery of 'activity' in the central regions of galaxies is, what triggers this activity in its manifold variety of forms? One of the most obvious possibilities is that interactions between galaxies could provide such a trigger, and several of us have been exploring this idea from various points of view over the past few years. The tidal perturbations resulting from an interaction should disturb the quiescent equilibrium conditions in a disc galaxy and might be expected to promote cloud-cloud collisions, leading to shocks, gas compression, and an enhanced star formation rate. Dissipative processes could result in material falling toward the bottom of the gravitational potential of the galaxy, and if there is a compact object present in the galactic nucleus, accretion of this material onto the object could fuel Seyfert-type activity. Thus interactions might be expected to be associated with either 'starbursts' or 'monsters'[1]. In either case, it should be evident that interacting galaxies are a seminal class of galaxies to study to investigate the origin of activity in galaxies.

2. Infrared activity in interacting galaxies

Before embarking on a search for activity in interacting galaxies, it may be prudent to pause and consider just what we are looking for. I shall take as a working definition of activity in galaxies that used by Balick & Heckman[2]: 'qualitatively unusual, quantitatively energetic, compared to the evolution of normal stars.' One useful indicator of such activity is the mass-to-light ratio, M/L. For a thermonuclear energy source,

$$M/L = M/(0.007\varepsilon Mc^2/\tau), \qquad (1)$$

where ε is the fraction of the mass undergoing hydrogen burning and the lifetime is τ. For $\varepsilon = 10\%$ and $\tau = 10^{10}$ yr, $M/L = 1\ M_\odot/L_\odot$. Thus, we have activity in the central regions of a galaxy if $M/L < 1$. If the luminosity is dominated by the IR emission, we have IR activity if $M/L_{IR} < 1$. In As examples the 'starburst' galaxies M82 and N253 have M/L_{IR} ratios of 0.04 and 0.001 respectively, whereas a 'normal' galaxy like M31 has a ratio of 48.

The principal observational approach to measuring L_{IR} has been to do photometry at 10 μm. However, to obtain good sensitivity at 10 μm is difficult, and to do it for a large sample of galaxies requires more telescope time than is easily obtainable. We therefore, undertook JHKL photometry (1.2, 1.6, 2.2, & 3.8 μm), and we used a K-L colour excess over normal galaxy colours as an indication of the rising IR spectrum which characterises large IR luminosity and, perhaps, small M/L_{IR}. We observed the central 8 arcsec of a sample of 22 pairs of interacting galaxies from the Arp [3] Atlas with representation of several morphological types. Two conclusions emerged from this study[4].

i) There is a K-L excess over normal galaxy colours (i.e. K-L > 0.5) for one member of an interacting pair for ~ 85% of the sample.

ii) In no case does more than one member of a pair exhibit a K-L excess.

Thus, if a K-L excess is a good indicator of a large IR luminosity and a small M/L_{IR}, it appears that interactions are extremely efficient in triggering IR nuclear activity in galaxies.

We have followed up this study with 10 μm photometry of galaxies in the JHKL sample. This data, in addition to other 10 μm data in the literature[5),6)] provides a sample of ~ 40 interacting and merging galaxies for which 10 μm luminosities in 5-8 arcsec apertures is available[7]. With this data we can investigate more quantitatively the evidence for IR activity in the central regions of interacting galaxies.

2.1 Continuum energy distribution

The continuum spectra of a few of these galaxies are displayed in Fig. 1, along with that for N253. It may be seen that they all have the quasi-thermal spectra typical of galactic HII regions: a steep rise, but slower than a Planck function, indicating thermal emission from dust at a range of temperatures. By comparison, the mid-IR spectra of quasars and Seyfert 1 galaxies are generally much flatter[8].

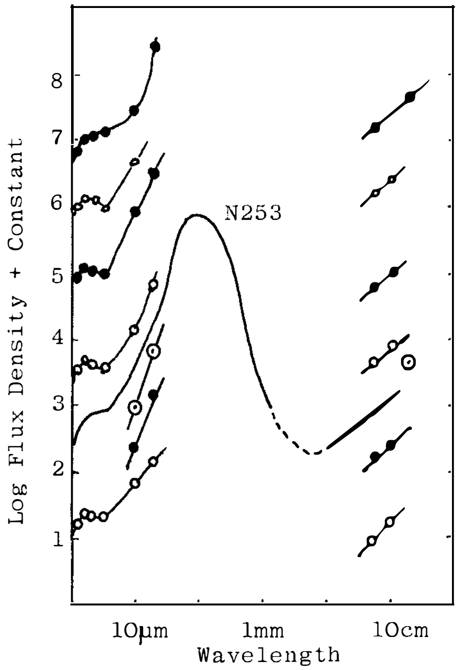

Fig. 1. Continuum energy distributions for several interacting galaxies.

2.2 IR luminosities

The IR luminosities of these interacting galaxies are large. In Table 1 the 10 µm luminosities of interacting and merging galaxies are compared with other classes of galaxies--Seyferts, classic starbursts, and bright spirals. It is evident that the interacting galaxies are at least an order of magnitude more luminous than the bright spirals, and substantially more luminous than the classic starbursts. Mergers are more luminous than non-merging interacting galaxies by nearly another order of magnitude, and are essentially as luminous as the Seyferts at 10 µm.

Table 1. Luminosities at 10 μm for various classes of galaxies.

Class of galaxy	N	Range ($L_\odot$)	Mean ($L_\odot$)
Interacting	24	$4x10^7$-$7x10^9$	$2.5x10^9$
Merging	9	$4x10^9$-$5x10^{10}$	$2x10^{10}$
Seyferts	50	$4x10^8$-10^{11}	$4x10^{10}$
Starbursts: M82		10^9	
NGC253		$6x10^8$	
NGC2903		$1x10^8$	
Bright spirals	17	10^5-$7x10^8$	$2x10^8$

2.3 Mass-to-IR luminosity ratios

There are rotation curves available for nine of the galaxies in the sample, and it is possible to place upper limits on the masses of two more. In Table 2 the M/L_{IR} ratios are listed for these eleven galaxies. Note that these ratios are for the mass and total IR luminosity within the same aperture, usually either 5 or 8 arcsec. All the M/L_{IR} ratios are subsantially < 1. Clearly, then, on the criterion stated at the outset, there is IR activity in every galaxy in this sample for which we can estimate a mass.

Our conclusions from this data are:

i) There is IR activity, indicated by a $M/L_{IR} << 1$, in the central few arcsec of every interacting galaxy for which the appropriate data is available.

ii) The emission mechanism appears to be thermal emission from 'warm' dust, like that in galactic HII regions.

Table 2. Mass-to-IR luminosities for interacting galaxies.

Galaxy NGC	Arp	M/L (solar units)
520	157	<0.01*
1614	186	0.003
2798	283	<0.4*
2992	245	0.001
3227	94	0.02
3256		0.01
3396	270	0.002
3395	270	0.007
4088	18	0.02
4194	160	0.03
5194		0.3
6240		<0.08*
7714	284	0.01

3. The energy source

There have been two proposals for the energy source which powers this IR activity in the central regions of interacting galaxies: a rapid burst of star formation ('starbursts'), or accretion onto a compact object ('monsters'). Undoubtedly both processes are often present, but whether one or the other dominates is an outstanding controversy which rages as intensely for interacting galaxies as it does for spiral galaxies generally. In the following I will summarise the variety of observational approaches which have been undertaken to distinguish between these two energy sources.

3.1 The spatial extent of the mid-IR emission

Imagine a dust grain at a distance R from a luminosity source. The dust grain which reach an equilibrium temperature T at which its thermal emission equals the rate of absorption of energy from the luminosity source:

$$\langle Q\rangle_{UV}\pi a^2 L_S/4\pi R^2 = \sigma T^4 \langle Q\rangle_{IR} 4\pi a^2. \quad (2)$$

For typical grain parameters this gives

$$R \approx 50 T^{-5/2} L_S^{1/2}(L_\odot) \text{ pc}. \quad (3)$$

If there is a single central source of luminosity ~ 10^{10} $L_\odot$, i.e. a monster, it can heat dust grains to T ~ 300 K, i.e. hot enough to that they radiate at 10 μm, only out to a distance of ~ 3 pc. Thus, if there is measurable spatial extent at 10 or 20 μm, it cannot be due to heating by a single, central source i.e. a monster, and must be due instead to distributed sources of luminosity, i.e. a starburst.

We have been pursuing an observing programme along these lines, and the result is shown in Fig. 2 for the interacting galaxy N2798. It exhibits spatial extent at 10 μm (similarly at 20 μm, compared to an unresolved star, at a 5 σ significance. If we include data in the literature[7)], four interacting galaxies, N2798, N3227, N3690, and N5194, and five merging galaxies, N6240, N1614, N3256, N3310, and IC883, have measured spatial extent at 10 μm. Thus 25% of the sample is resolved at 10 μm. This suggests rather strongly that the 10 μm emission in these galaxies is powered by a single quasar-like nucleus, while starbursts rather naturally produce such spatial extent.

3.2 Optical spectra

Another approach to determining the underlying energy source is to use diagnostic diagrams for various optical line intensity ratios, such as those developed by Baldwin, Phillips & Terlevich[9)], and others. There are the required optical spectra in the literature for ~ 31 of the interacting galaxies in the sample, and we have plotted [OIII]/Hβ vs. [NII]/Hα line intensity ratios for these in Fig. 3. The areas outlined in the diagram are those which Baldwin et al. identified as regions of excitation characteristic of HII regions, Liners, and Seyferts. For 21 of the interacting galaxies, the excitation is characteristic of HII regions, 4 are like Liners, and 6 are like Seyferts. Thus the excitation spectrum is characteristic of HII regions

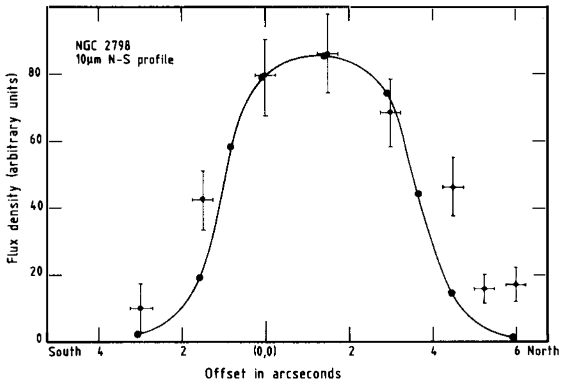

Fig. 2. The spatial extent of N2798 at 10 μm compared to that of an unresolved star. The telescope was moved in 0.75 arcsec steps alternately north and south while chopping east-west for both the star and the galaxy.

in two-thirds of the cases, and thus strongly indicative of an associated starburst. In Section 4.4 I shall consider the possibility that 'Warmers', extreme Wolf-Rayet stars whose existence is inferred by Terlevich & Melnick[10)], account for some of the associations found between interactions and Seyfert-type activity. If there were such a stellar evolutionary phase, it would be natural to find some excitation characteristic of a harder spectrum present as the consequence of a starburst, and therefore it would not be unlikely that the 10 non-HII galaxies have also experienced a starburst which has now evolved to the 'Warmer' phase a la Terlevich & Melnick.

3.3 Radio data

The characteristics of the radio emission from these galaxies provide another approach to distinguishing starbursts from monsters as the underlying energy sources in interacting galaxies. The hallmarks of radio emission from Seyfert-like nuclei are flat spectra and small, usually unresolved sizes. By contrast, steep spectra and extended nuclear radio emission would be expected for the supernovae and supernova remnants associated with a starburst.

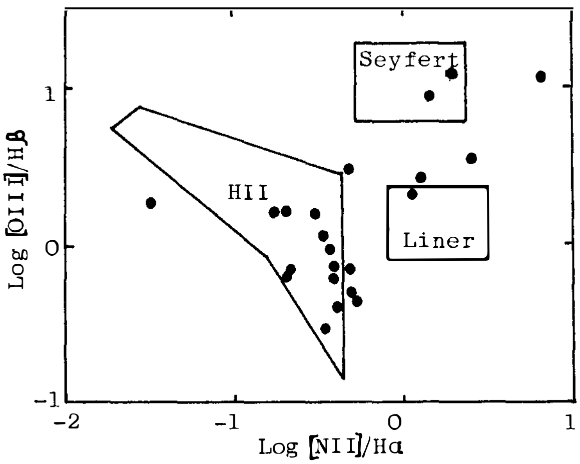

Fig. 3. Optical line ratios for interacting galaxies.

Radio data is available for three-fourths of the sample of interacting galaxies[7]. Virtually all of these have a steep spectra index, ~ -0.7. For ~ 80% of the sample the nuclear radio source is resolved, and the sizes are of the order of several arcsec. These radio features are not characteristic of monsters, but qualitatively consistent with the supernova activity subsequent to a starburst.

3.4 Ultraviolet spectral features

The presence of strong UV emission lines due to CIV, HeII, and CIII is one of the hallmarks of Seyfert-type activity in galaxies. By contrast, one might expect starbursts to show absorption features due to CIV and SiIV, since these features are characteristic of giants and supergiants. In fact, SiIV absorption is luminosity dependent--strongest in supergiants and about zero in dwarfs [11]. We have devoted an entire observing shift on IUE to the most nearby example of an ultraluminous merging galaxy, N3256[12]. The low resolution spectrum shows that the most prominent UV features are those due to SiIV and CIV, and there are no emission features typical of Seyfert-type activity. This is strong supporting evidence, from a rather different observational perspective, that there is strong starburst activity in this copybook example of a merging galaxy.

In summary, we have adduced observational evidence with the broad perspective provided by insights from variety of UV, optical, IR, and radio measurements. All of these observational approaches point toward the ubiquitous presence of starbursts in these luminous IR galaxies. These data do not exclude the concurrent presence of a monster in some or all of these galaxies. However, it is difficult to avoid the conclusion that, in the large majority of cases, starbursts are the dominant energy sources driving the large IR luminosities we have shown to be a common feature of these galaxies. Apparently, interactions produce starbursts.

4. Wider issues and implications

4.1 How prominent are interacting galaxies among luminous IR galaxies?

There has been anecdotal evidence presented in recent years suggesting that interacting galaxies are unusually luminous in the IR[5,6,13]. In particular, Joseph & Wright[14] argued that mergers of disc galaxies produce ultraluminous IR galaxies. Supporting evidence for these ideas is continuing to accumulate. Allen et al.[15], in their studies of optically faint IRAS sources, find many to be strongly disturbed or interacting galaxies. Soifer et al.[16] have identified a sample of the 15 most luminous IRAS galaxies, and their CCD images indicate that most, if not all, are strongly interacting.

There is an apparent 'age effect' in the sample of mergers studied by Joseph & Wright[14] which is related to this question. They classified their sample of mergers into 'young', 'middle-aged', and 'old' on morphological criteria. They found the 'middle-aged' group to have an average IR luminosity ~ 10^{12} $L_\odot$, whereas the other two categories were about 5 times less luminous. they suggested that some of the spread in IR luminosities may be due to this 'age effect', and that luminosities ~ 10^{12} $L_\odot$ may be more typical of the peak starburst activity in mergers of large, gas-rich galaxies.

4.2 Formation of ellipticals from mergers of disc galaxies

Lynden-Bell[17] and Toomre[18], among others, have pointed out that the violent stellar dynamical relaxation which results from a merger will produce a light distribution very much like an elliptical galaxy. If this scheme is correct, one must find a way for the merged remnant to rid itself of the interstellar gas it inherits. If mergers produce starbursts of the very large spatial extent described above, then galactic winds driven by the associated supernovae should sweep the remnant free of gas and dust over a similar spatial extent. Graham et al.[19] show that a starburst with $M/L_{IR} < 1$ (for a typical supernova pregenitor of $\sim 10\ M_{\odot}$) to be energetically adequate, and that such a process may be underway in N3256.

4.3 Spectral evolution of galaxies

On the most simple assumptions, the frequency of interactions between galaxies will be proportional to the galaxies' peculiar velocities divided by the interaction mean free path. This frequency will scale with redshift, z, roughly as $(1+z)^4$. Thus, if we see about 5% of galaxies interacting now, most galaxies will have experienced one interaction at $z \sim 1$. While this is probably too naive an analysis, it indicates that we might expect to see the effects of interaction-induced starbursts in the spectral and chemical evolution of most galaxies.

4.4 Relation to other forms of activity in galaxies

It is becoming increasingly more evident that galaxy interactions are associated with other classes of galactic nuclear activity. Seyfert galaxies frequently exhibit tidal distortions and have companions[2,20] Lilly & Longair[21] describe evidence of the effects of starbursts at high redshifts based on the optical-IR colours they find for 3CR radio galaxies. Smith et al.[22] find that in their deep CCD images of low redshift quasars, about half are hosted by morphologically peculiar galaxies. And recently Heckman et al.[23] have shown that powerful radio galaxies are associated with morphologically disturbed galaxies.

One possible link between interaction-induced starbursts and some of these other forms of activity is provided by the proposed existence of 'Warmers' by Terlevich & Melnick[10] (and cf. Terlevich elsewhere in this volume). These authors argue that such stars can account for most of the high excitation spectral features which characterise Seyfert galaxies and quasars. Since interaction-induced starbursts are apparently efficient in producing high mass stars, one can see that interactions might play a major role in producing these high excitation, high luminosity galactic nuclei.

Another suggestion which has been current is that the interactions provide fresh fuel for accretion onto a compact object lurking in the centre of a galaxy (e.g. Heckman et al.[23]). However, if interaction- induced starbursts do have the large spatial extent which seems to be typical, strong galactic winds driven by the ensuing supernovae should very quickly sweep a large central region free of gas, thereby depriving the monster of any more food.

Although it is clear that there is an association between interactions and non-thermal nuclear activity in galaxies, the physical and causal connections are not at all clear. However, it is likely that the powerful starbursts triggered by interactions are an important clue.

References

1) Gunn, J. E., 1979. Active Galactic Nuclei, p. 213, eds. Hazard, C. & Mitton, S., Cambridge University Press, Cambridge, UK.

2) Balick, B. & Heckman, T. M., 1982. Ann. Rev. Astr. Astrophys., **20**, 431.

3) Arp, H. C., 1966. Atlas of Peculiar Galaxies, California Institute of Technology, Pasadena.

4) Joseph, R. D., Meikle, W. P. S., Robertson, N. A. & Wright, G. S., 1984. Mon. Not. R. astr. Soc., **209**, 111. (Paper I)

5) Lonsdale, C. J., Persson, S. E. & Matthews, K., 1984. Astrophys. J., **287**, 95.

6) Cutri, R. M. & McAlary, C. W., 1985. Astrophys. J., **296**, 90.

7) Wright, G. S., Joseph, R. D., Robertson, N. A., James, P. A. & Meikle, W. P. S., 1987. Submitted to Mon. Not. R. astr. Soc.

8) Lawrence, A., Ward, M., Elvis, M., Fabbiano, G., Willner, S. P.,

Carleton, N. P. & Longmore, A., 1985. Astrophys. J., **291**, 117.

9) Baldwin, J. A., Phillips, M. & Terlevich, R., 1981. Pub. Astron. Soc. Pacific, **93**, 5.

10) Terlevich, R. & Melnick, J., 1985. Mon. Not. R. astr. Soc., **213**, 841.

11) Walborn, N. R. & Panek, R. J., 1984. Astrophys. J. (Letters), **280**, L27.

12) Joseph, R. D., Wright, G. S. & Prestwich, A. H., 1986. New Insights in Astrophysics, ESA SP-263, p. 597.

13) Joseph, R. D., 1986. Light on Dark Matter, p. 447., ed. Israel, F. P., Reidel, Dordrecht, Holland.

14) Joseph, R. D. & Wright, G. S., 1985. Mon. Not. R. astr. Soc., **214**, 87. (Paper II)

15) Allen, D. A., Roche, P. F. & Norris, R. P., 1985. Mon. Not. R. astr. Soc., **213**, 67P.

16) Soifer, B. T., Sanders, D. B., Neugebauer, G., Danielson, G. E., Lonsdale, C. J., Madore, B. F. & Persson, S. E., 1986. Astrophys. J. (Letters), **303**, L41.

17) Lynden-Bell, D., 1967. Mon. Not. R. astr. Soc., **136**, 101.

18) Toomre, A., 1977. Evolution of Galaxies and Stellar Populations, eds Tinsley, B. M. & Larson, R. B., p.401, Yale University Observatory.

19) Graham, J. R., Wright, G. S., Meikle, W. P. S., Joseph, R. D. & Bode, M. F., 1984. Nature, **310**, 213.

20) Keel, W. C., Kennicutt, R. C., Hummel, E. & van de Hulst, J. M., 1985. Astr. J., **90**, 708.

21) Lilly, S. J. & Longair, M. S., 1984. Mon. Not. R. astr. Soc., **211**, 833.

22) Smith, E. P., Heckman, T. M., Bothun, G. D., Romanishin, W. & Balick, B., 1986. Astrophys. J., **306**, 64.

23) Heckman, T., Smith, E. P., Baum, S. A., van Breugel, W. J. M., Miley, G. K., Illingworth, G. D., Bothun, G. D. & Balick, B., 1986. Astrophys. J., **311**, 526.

STAR FORMATION IN INTERACTING GALAXIES

William C. Keel
Sterrewacht Leiden
Postbus 9513
2300 RA Leiden, The Netherlands

Optical spectra, Hα images and photometry, and IRAS data have been used to compare star-forming properties of otherwise similar interacting and non-interacting spiral galaxies. Star formation on all linear scales is enhanced during interactions, particularly in very close encounters. Comparison of continuum colors and Hα equivalent widths with simple models indicates that either the bursts of star formation induced by close interactions are very brief (less than 10^7 years) or that they are enriched in the most massive stars. These processes are minor effects on the evolution of a typical galaxy now; whether they were ever dominant depends on yet-unknown dynamical properties of binary galaxies.

1. Introduction

Several lines of evidence have been used to support links between galaxy interactions and strong bursts of star formation. The optical colors [1], radio luminosities [2] and infrared properties [3] of known interacting systems, as well as the occurrence of obviously interacting galaxies in radio [4] and infrared-selected [5] samples, all indicate that at least some interacting galaxies have much higher star-formation rates than their more isolated cousins. It is thus important both to know the range of phenomena which can be induced by interactions, and to have a quantitative statistical picture of the results of these processes. Individual systems may be altered greatly, but are these processes important in the evolution of a "typical" galaxy? This report summarizes several studies dealing with these questions, primarily undertaken in collaboration with R.C. Kennicutt, Jr., J.M. van der Hulst, and E. Hummel. I deal in turn with star-forming properties of galactic nuclei, disks, individual H II regions, and effects on galactic evolution.

2. Nuclear H II regions and starbursts

We have already published results of optical spectrophotometry of the nuclei of 160 interacting spirals, in comparison with noninteracting ones [6]. We examined three samples of galaxies: one selected for probability of a companion's being physically associated, without consideration of morphology; one drawn from the Arp atlas, consisting of strongly disturbed systems; and a group of more isolated spirals in a magnitude-limited sample. We may thus probe several interaction regimes, and do so in a differential way. The most relevant results here are:

Star formation rates determined from Hα are systematically higher in nuclei of interacting spirals than noninteracting ones. The degree of enhancement has a large range, with the greatest excess (factors > 10, starbursts) found preferentially in "contact" pairs having projected separations less than the combined de Vaucouleurs radii.

The emission spectra of these nuclear star-forming regions indicate either excess massive stars (relative to a Salpeter IMF) or considerably lower abundances in the gas than normally seen in such nuclei.

There is a mild dependence of normalized star-formation rate (from the Hα equivalent width) on projected pair separation, after taking selection effects into account [7].

Enhanced nuclear star formation is present for galaxies separated by as much as 50 kpc; a fairly weak tidal disturbance can have noticeable consequences. The preference of strong bursts for very close pairs sets an immediate limit of order $5x10^7$ years on the duration of optically prominent bursts, in accord with model fits for the surrounding disks (below).

Note that only a fraction ~25% of closely interacting systems show very strong nuclear (or disk) star formation. While such systems are strongly represented in flux-limited samples selected in the UV, IR, emission-line or radio surveys, it should be remembered that most interactions, as seen at a given moment, do not have strong effects on star formation.

3. Disk star formation: enhancements and extensive bursts

We have estimated disk star-formation rates for most of the galaxies in the nuclear samples via Hα images and large-aperture photometry; crude comparison was possible with IRAS measures, mostly for pairs taken together. Full details are given elsewhere [8]. Our primary conclusions are:

As with nuclei, a small subset of disks show strong responses; most are only slightly enhanced above normal for their morphological type.

In strong interactions, both members of a pair show similar disk responses, independent of orientation or morphology; in such pairs, the dynamics of the interaction itself has overridden each disk's initial conditions. This is a version of the Holmberg effect [9] first seen in broad-band colors.

Disk and nuclear enhancements of star formation occur together only in the most strongly enhanced systems. Strong disturbances produce simultaneous responses in all parts of a galaxy.

The inner disks (within 3 kpc) seem to respond to interactions more readily than the outer parts, perhaps due to timescale differences; this is seen also in the work of Bushouse [10]. This effect may blend with that seen for nuclei [6]; the distinction may reflect convention rather than physically distinct nuclei and inner disks.

The UBV colors and Hα equivalent widths may be fit by models of old populations with superimposed bursts. The results indicate either burst durations less than 10^7 years, or an excess of very massive stars. The bursts may have long tails up to 10^8 years, but if the IMF is normal, the peak duration must be small.

Using the IRAS fluxes (particularly 25-60 microns) as rough indicators of star-formation rate broadly confirms the Hα results; details cannot be tested independently because too few pairs can be separated in the IRAS data, even after extensive reprocessing.

4. H II regions in interacting galaxies

Our Hα images allow quantitative measure of the spatial and luminosity distributions of the H II regions in nearby systems, as long as differential extinction across a galaxy is not strong. Such data can, in principle, be used to address both the preferred sites of induced star formation (locations of shock fronts [11], effect of the direction of tidal disturbances [12, 13]) and any preferred scale for such star formation. The derived Hα luminosity functions must be interpreted with care; resolution differences can dominate physical changes.

From preliminary analysis, it appears that most interacting galaxies share the power-law form for the H II region luminosity function seen in such normal spirals as NGC 628 [14]. A few (NGC 275, 5474, 7714) show different slopes or "bumps". These features suggest differences in scale, but whether this pertains to individual H II regions or their clumping cannot be determined with available resolution. Work on further objects is in progress.

The spatial distribution of H II regions likewise shows a variety of forms. Many objects, again, show nothing remarkable. Some (NGC 4038/9, NGC 3690) show active star formation along the expected contact surface between two disks. In some cases, strong arcs are seen, as predicted by the cloud-collision models of Noguchi and Ishibashi [11]. There is no strong, general preference of H II regions for the side of a galaxy towards or opposite a companion (when the space orientation can be reconstructed); summing the final results for all such systems should allow weak trends of this kind, or time-lag effects, to be uncovered.

5. Interactions and galaxy evolution

From these data, we may address the question of whether interaction-induced star formation is important in the evolution of a typical galaxy (which issue is distinct from dynamical effects and merging). For spirals comprising an approximately volume-limited sample, interactions account for 6±3% of current OB stars, with errors mostly from such factors as Hubble type and luminosity dependences. A substantial fraction of spirals have probably undergone significant bursts of induced star formation at some time, but this is not an crucially important process at its current rate.

Interactions were almost certainly common in the early history of galaxies, and one might consider whether their effects were ever likely to be dominant. An important uncertainty is in what kinds of systems mostly produce interactions. Encounters of completely unrelated galaxies are not important, as there are too few, with velocities too high for maximum tidal influence. Initially bound systems or subsystems are more likely prospects, but the crucial issue - how strongly bound - is nearly immune to observational testing. Tightly bound pairs will have a different interaction history than marginally bound ones, which may only now be approaching one another for the first time. Given the current uncertainties, induced star formation might have been dominant, or trivial, compared to internally regulated star formation early in galactic history. Further approaches, both observational and theoretical, to this problem are urgently needed.

Individual systems, however, can clearly have their star-forming histories strongly affected by interactions. Not only can mergers induce such strong bursts as to clear the remnant of gas [15], but some exceptionally long-lived episodes may be triggered by companions. A case in point is II Zw 23. This luminous blue compact shows an early-type stellar population and gaseous filaments that are apparently infalling [16]. The integrated properties indicate that star formation at the present rate has been going on for several 10^8 years; this will exhaust the available H I in a comparable time if it continues, analogous to some phases of galaxy formation. A candidate companion is present, whose disturbance might have precipitated instabilities in the H I envelope leading to the observed star-forming episode. Events in numerous merging systems may proceed in a similar, but more rapid, fashion.

6. Summary

Galaxy interactions, as seen in spirals, may have important temporary effects on both nuclear and disk star formation (induced starburst). A small fraction have very strong bursts, which are well seen in several kinds of surveys, but they are not representative of the average situation. Uncertainties in the dynamics of binary galaxies limit extrapolation of local results to early galactic evolution.

1. Larson, R.B., and Tinsley, B.M. 1978, Astrophys. J. 219, 46.
2. Stocke, J.T. 1978, Astron. J. 83, 348.
3. Joseph, R.D., Meikle, W.P.S., Robertson, N.A., and Wright, G.S. 1984, Mon. Not. R. Astron. Soc. 209, 111.
4. Condon, J.J., Condon, M.A., Gisler, G., and Puschell, J.J. 1982, Astrophys. J., 252, 102.
5. Lonsdale, C.J., Persson, S.E., and Matthews, K. 1984, Astrophys. J. 287, 95.
6. Keel, W.C., Kennicutt, R.C., Jr., van der Hulst, J.M., and Hummel, E. 1985, Astron. J. 90, 708.

7. Sharp, N.A., and Keel, W.C. 1987, Astron. J. (submitted).

8. Kennicutt, R.C., Jr., Keel, W.C., van der Hulst, J.M., Hummel, E., and Roettiger, K. 1987, Astron. J. 93, 1011.

9. Holmberg, E. 1958, Medd. Lunds Astron. Obs. ser 2, 136.

10. Bushouse, H.A. 1986, Ph.D. diss., Univ. of Illinois.

11. Noguchi, M., and Ishibashi, S. 1986, Mon. Not. R. Astron. Soc. 219, 305.

12. Arp, H.C. 1973, Astrophys. J. 183, 411.

13. Hodge, P.W. 1975, Astrophys. J. 202, 619.

14. Kennicutt, R.C., Jr., and Hodge, P.W. 1980, Ap. J. 241, 573.

15. Graham, J.R., Wright, G.S., Meikle, W.P.S., Joseph, R.D., and Bode, M.F. 1984, Nature 310, 213.

16. Keel, W.C. 1987, in preparation.

DYNAMICAL TRIGGER OF STAR FORMATION IN SPIRAL GALAXIES

Françoise COMBES
Observatoire de Meudon, France
and Ecole Normale Supérieure, Paris

It is now well-known that interactions between galaxies or the presence of a bar in the center of a spiral can induce two-arms density waves in a galactic disk. The consequent increase in interstellar cloud collisions, the formation of giant molecular clouds giving birth to stars, and the formation of rings by angular momentum transfer, could explain the starbursts phenomena in spiral galaxies.

Starbursts appear to be related to dynamical phenomena, like bar waves in galaxies or tidal interactions and mergers. This concerns mainly spiral galaxies, which I only consider here. The case of blue compact dwarfs might be different, since, because of their small masses, these systems could be dominated by stochastic star formation (one giant HII region). What are the mechanisms that link dynamics and star formation?

Evidences for dynamical trigger

1. Interacting galaxies

In 1978, Larson & Tinsley compared the color diagrams of a sample of interacting galaxies with a control sample, and concluded that tides were triggering bursts of star formation in interacting galaxies. From H_{alpha} emission, Bushouse (1986) reaches the same conclusions. The tidal interaction seems to favor also nuclear activity (Keel et al 1985). The IRAS survey has now added overwhelming evidence for enhanced star formation in interacting galaxies (de Jong et al 1984, Soifer et al 1984). According to Sanders et al (1986), most galaxies with far infrared luminosities larger than 10^{11} L☉ are interacting galaxies or mergers.

Young et al (1986) have studied in the CO line a sample of 26 galaxies: 13 isolated and 13 interacting. They notice first that their molecular content is similar, according to their similar ratio of blue luminosity to total molecular mass (L_B / MH_2). This point is interesting since we can distinguish two steps in the star formation triggering: first the gas density (either atomic or molecular) could be enhanced, and second the star formation efficiency for a given gaseous mass could also be enhanced. From the sample here, there seems to be no evidence that the global molecular content of interacting galaxies is different from that of the isolated galaxies. The dynamical action is concentrated mainly on the star formation efficiency: The dust temperature obtained from the ratio 60μ/100μ emissions is multiplied by a factor 2 in interacting galaxies; the star formation efficiency (SFE) as qualitatively measured by the ratio L_{IR}/ MH_2 is about 7 times higher in interacting galaxies (this is coherent with the larger dust temperature).

Joseph & Wright (1985) claim that mergers are a class of ultraluminous infrared galaxies (at 10μ); their luminosity (4 10^9 L☉– 5 10^{10} L☉) reaches the level of Seyfert's, much brighter than ordinary starburst galaxies (5 10^8–10^9 L☉), while bright spirals range between 10^5 -7 10^8 L☉ in luminosity.

To determine which triggering mechanism is at play, it is necessary to know precisely **where** in the galaxy is going on the starburst: this requires that we know the SFE (L_{IR} / MH_2) with high spatial resolution. This becomes now available with near-infrared observations, and mm CO observations with large single dishes or interferometers.

o Arp 299

From interferometric CO observations of these merging galaxies, Sargent et al (1987) found two compact molecular regions, each 1.4 10^9 M⊙ of H_2. One is coïncident with the nucleus of IC694, but the other one is a region of a spiral feature, possibly formed by the tide. The first region has L_{IR} / MH_2 of 280, it has a flat radio spectrum, that requires a nonthermal source. In the spiral arm region the SFE ratio is 40, typical of a starburst region (for the Milky Way, the mean SFE is ~3).

o Ring galaxies

These galaxies contain only a nucleus and a ring feature, the archetype is the Cartwheel; they are likely to have suffered head-on collisions (cf Theys & Spiegel 1976; Lynds & Toomre 1976). The ring is a density wave, born in the collision, where star formation occurs: Appleton & Struck-Marcell (1987) have studied the ratio between far-infrared and blue luminosities in a sample of ring galaxies; they found that rings are starburst regions, with color temperatures of the dust higher than normal. The location of these starburst is non ambiguous; in some ring galaxies, even the nucleus has been separated from the rest of the disk.

o NGC3628

In this edge-on galaxy, part of the Leo Triplet, Boissé et al (1987) found a discrepancy between the IRAS position and the CO maximum, also coïncident with the continuum position. It is likely that star formation has been enhanced outside the central region by the tides (inducing gas infall and shocks).

2. Barred galaxies

In the IRAS survey (de Jong et al 1984, Soifer et al 1984) barred galaxies are also strong far-infrared emitters. According to Hawarden et al (1986), barred galaxies have twice as much infrared luminosities than non-barred galaxies; they are also easily distinguished in infrared color-color diagrams. Barred galaxies often possess resonant inner rings, that are regions of starbursts (hot spots in H_{alpha}).

According to recent high resolution CO observations of the nucleus of some bright spirals, the molecular gas reveals as a very good tracer of bar waves and nuclear rings: examples are NGC253, M82 (Lo et al 1987), NGC6946 (Ball et al 1985, Weliachew et al 1987), NGC1068 (Myers & Scoville 1987), NGC1097 (Gérin et al 1987). Interesting enough, in most of these examples, the bar is present together with a companion.

How do these mechanisms work?

A central bar and a passing-by companion, both have similar actions in the disk of the perturbed spiral galaxy: bisymmetrical forces (in cos(2 θ), θ being the azimuth in the disk). These forces generate a two-arms density wave in the disk (see e.g. Toomre 1977).

Once the density-wave developped, the accumulation in density in the arms, and the crowding of orbits, creating systematic encounter velocities between gas clouds, favorise cloud collisions. Collisions between molecular clouds are highly inelastic, and coalescence forms giant molecular clouds (GMC), where young star associations are produced.

Noguchi & Ishibashi (1986) have simulated such a scenario, with a passing-by companion perturbing a disk of colliding test-particles. Assuming the star formation rate proportional to the collision rate, they found in their best model that star formation is increased by a factor of about 8 with respect to normal, 3 10^8 years after perigalactic passage. They also found that, after several galactic rotations, particles loose their angular momentum and settle down into a ring.

The occurence of a bar is much more frequent: 2/3 of the spiral galaxies are classified as barred, and oval components are very frequently observed even in non-barred systems (Zaritsky & Lo, 1986). The oval potential generates a spiral structure in the gaseous component. With a collisional model involving a mass-spectrum of molecular clouds, we have shown (Combes & Gérin 1985) that GMC were formed preferentially in the bar-induced spiral arms, implying an enhancement of star formation there.

The torque exerted by the bar on the spiral arms transfers angular momentum: outside corotation, particles flow towards the outer Lindblad resonance (OLR), and inside corotation, they flow towards the inner resonance (ILR) if present. The gas settles into rings, where it is no longer subject to torques (Schwarz 1984). In our molecular clouds simulations, we found the formation of inner rings very efficient, occuring within a few rotations with a strong bar; the position of the ring could be very close to the nucleus, according to the angular velocity of the bar (cf Fig. 1.). Simulations carried on with a passing-by companion, with the spiral disk as an orbit plane, give similar results (cf Fig. 2).

A passing-by companion reinforces the bar action, provided that the collision is not head-on. We have run N-body simulations (Gérin, Combes, Athanassoula 1987) to test the gravitational influence of a companion on a barred galaxy. Provided that the perigalactic passage of the companion is not too close, that the stars contributing to the bar are not ejected by the tides, the tidal action always reinforces the bar (cf Fig. 3). When the bar is not yet settled (models where the apparition of the bar is postponed by the presence of a massive hot bulge), the companion passage destabilises the disk with respect to bar formation (Fig. 4.).

These cumulated actions could be at play in many starburst galaxies (NGC1068, NGC1097...), and must be invoked to explain the sudden increase in activity of the bar; indeed, the starburst phenomenon is necessarily short-lived, and a stationnary bar could not be the origin.

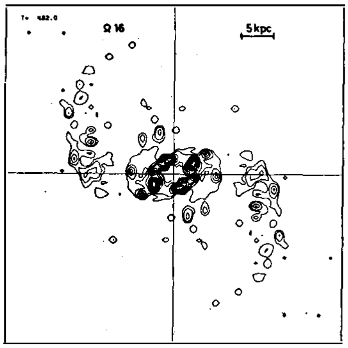

Figure 1: Formation of a nuclear ring in a barred galaxy. Contours of the amount of energy dissipated in cloud collisions are represented here for an angular velocity of the bar of 16 Km/s/kpc.

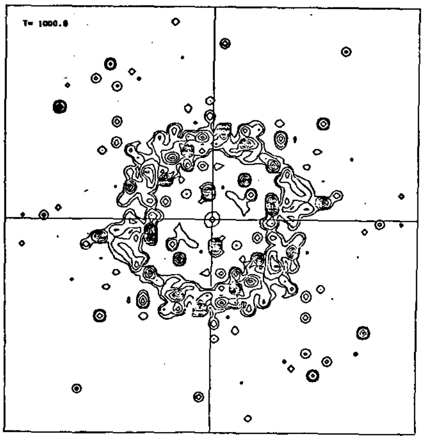

Figure 2: Same representation for an axisymmetric model for the galactic disk, perturbed by a companion.

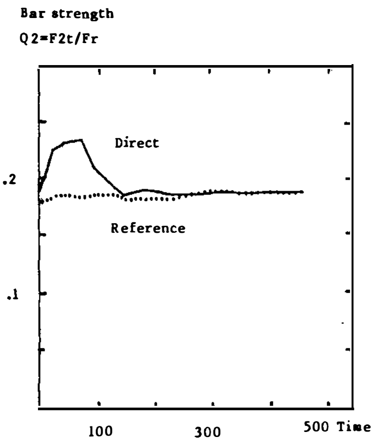

Figure 3: N-body simulations of a disk of stars having already formed a bar by previous evolution; comparison of the bar strength in function of time for two cases: — with a perturbing companion; - - - reference run of the isolated disk.

Q_2 is the strength of the bar measured by the maximum ratio of the tangential force (provided by the 2nd harmonic) to the total radial force.

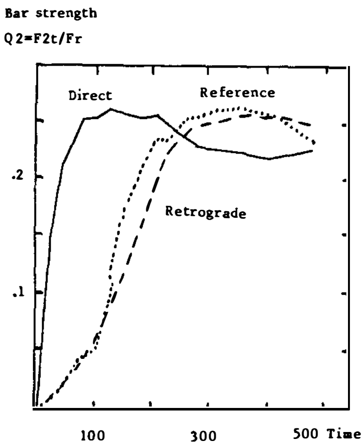

Figure 4: Similar diagrams for a disk of stars perturbed by a passing-by companion, before the formation of the bar (cf Gérin et al 1987).

References

Appleton P.N., Struck-Marcell C., (1987) Ap.J. 312, 566
Ball R., Sargent A.L, Scoville N.Z., Lo K.Y., Scott S.L., (1985) Ap.J. 298, L21
Boissé P., Casoli F., Combes F., (1987) A&A 173, 229
Bushouse H.A. (1986) PhD Thesis, University of Illinois, Urbana
Combes F., Gérin M., (1985) A&A 150, 327
Gérin M., Combes F., Athanassoula E. (1987) A&A in prep
Gérin M., Nakai N., Combes F., (1987) A&A in prep
Hawarden T.G., Mountain C.M., Leggett S.K., Puxley P.J. (1986) M.N.R.A.S. 221, 41P
de Jong T., Clegg P.E., Soifer B.T., Rowan-Robinson M., Habing H.J., Houck J.R., Aumann H.H., Raimond E., (1984) Ap.J. 278, L67
Joseph R.D., Wright G.S. (1985) M.N.R.A.S.214, 87
Keel W.C., Kennicutt R.C., Hummel E., van der Hulst J.M. (1985) A.J. 90, 708
Larson R.B., Tinsley B.M., (1978) Ap.J. 219, 46
Lo K.Y., Cheung K.W., Masson C.R., Phillips T.G., Scott S.L., Woody D.P. (1987) Ap.J. 312, 574
Lynds B., Toomre A. (1976) Ap.J. 209, 382
Myers S.T., Scoville N.Z. (1987) Ap.J. 312, L39
Noguchi M., Ishibashi S., (1986) M.N.R.A.S. 219, 305
Sanders D. B., Scoville N.Z., Young J.S., Soifer B.T., Schloerb F.P., Rice W.L., Danielson G.E. (1986) Ap.J. 305, L45
Sargent A.L, Sanders D.B., Scoville N.Z., Soifer B.T. (1987) Ap.J. 312, L35
Schwarz M.P. (1984) M.N.R.A.S. 209, 93
Soifer B.T. et al (1984) Ap.J. 278, L71
Theys J.C., Spiegel E.A. (1976) Ap.J. 212, 616
Toomre A. (1977) A.R.A.A. 15, 437
Weliachew L., Casoli F., Combes F., (1987) A&A sub
Young J.S., Kenney J.D., Tacconi L., Claussen M.J., Huang Y.L., Tacconi-Garman L., Xie S., Schloerb F.P., (1986) Ap.J. 311, L17
Zaritsky D., Lo K.Y. (1986) Ap.J. 303, 66

COMPOSITE DISK/HALO MODELS OF SPIRAL GALAXIES

E. Athanassoula and A. Bosma
Observatoire de Marseille
2 Place Le Verrier
13248 Marseille Cedex 04, France

We briefly discuss mass models of spiral galaxies involving decomposition into disk and halo components using rotation curves and radial luminosity profiles. Suitable models are obtained by assuming constant mass-to-light ratio in the disk (and bulge, if present), and constraining the value of this ratio by spiral structure theory.

1. Introduction.

Several dynamical quantities are required for the study of the chemical evolution of spiral galaxies, e.g. the mass surface density in the disk as function of radius, the mass-to-light ratio as function of radius, and the relative distribution of disk and halo material. The observable quantities from which these can be obtained are the light distribution in the galaxy and the velocity field. Several modeling procedures have been used so far, such as

a) assuming all the mass is in the disk, e.g. the Monnet-Simien models [13], used by McCall is his compilation [12] ; or the Nordsieck [14] models. The Monnet-Simien models attempt to fit a rotation curve with an $r^{1/4}$-bulge and an exponential disk, each with constant mass-to-light ratio, and thus fail in the outer parts of a galaxy, where the rotation curve stays flat. The Nordsieck models imply a strong increase of the mass-to-light ratio in the outer parts (e.g. [4]). Neither is very satisfactory to use.

b) assuming 'nothing', i.e. use only considerations about the global form of the rotation curves [5]. This does not help us for detailed analysis of individual galaxies.

c) using some scheme to decompose a galaxy in a disk and a halo component. We will review here briefly the procedures used sofar, and focus on a particularly promising scheme, which we intend to use in the future to examine questions like e.g. the ratio of gas to total mass in a disk as function of radius, and its relation with the observed oxygen abundance gradients.

2. Disk/halo decompositions

The general outline of the modeling procedure is given as a block diagram in figure 1. The basic assumption is always that the mass-to-light ratio of the disk is constant with radius. This seems justified by the fact that there are no appreciable color gradients (e.g. [19, 7, 10]). An independent, but still constant, mass-to-light ratio is considered for the bulge, whenever this component exists. Following a method pioneered by Kalnajs [9], the rotation curve for the disk (and for the bulge, if necessary) can be calculated from the observed radial luminosity profile, using the mass-to-light ratio(s) as free parameter(s). If there is a difference with the observed rotation curve,

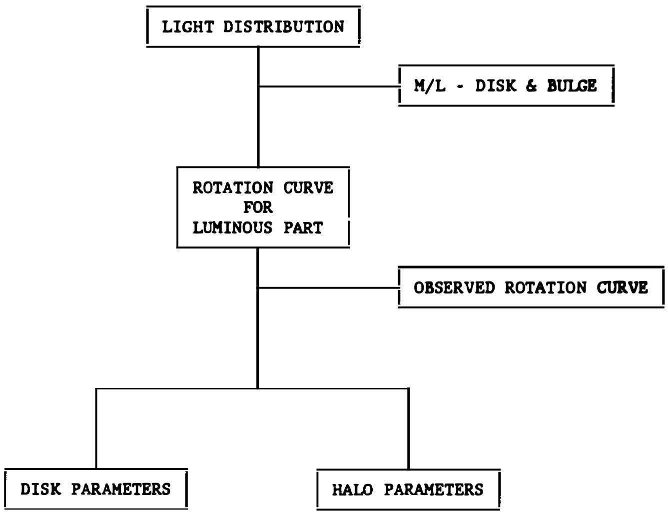

Figure 1. Schematics of the modeling prodecure.

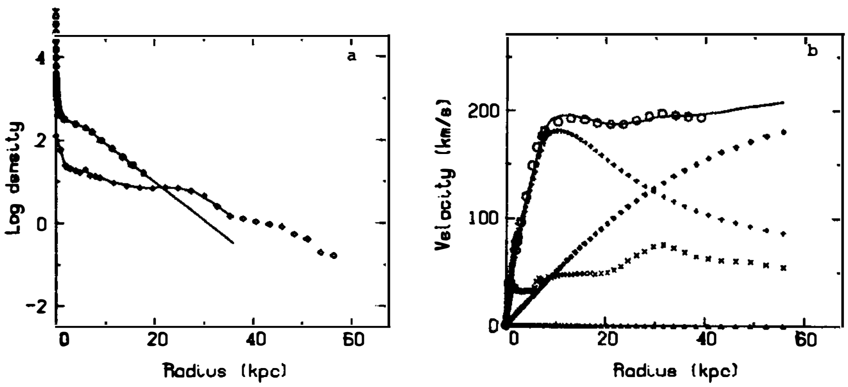

Figure 2. Mass model for IC 342 a) Radial luminosity profile (from Ables 1971) and gas profile (from Newton 1980; Young and Scoville 1982) b) Composite mass model.

as is always the case in the outer parts of the galaxies provided the velocity data extend sufficiently far out, the difference is attributed to a halo component. The rotation curve for the halo can, once determined, be parametrized. For this a particular shape, e.g. spherical, and sometimes a particular mass distribution, e.g. isothermal, must be assumed. However, since these assumptions influence only the halo parameters and not those of the visible material, we will not discuss them here any further. In many cases [6, 2] the gas has been included as a separate component. An example of such a model is given in figure 2.

To escape an infinity of models with different mass-to-light ratios choices have to be made to fix this parameter. Several ways have been proposed :

a) 'best fit' models [10,11], where a least squares fitting to a predetermined halo function is obtained. This has the disadvantage of prejudicing our knowledge about halos, without justification.

b) 'maximum disk models'. Two such classes can be distinguished.

b1) The 'truely maximum disk', considered e.g. in [9] and [10], where the mass-to-light ratio is taken as high as possible without overshooting the central parts of the observed rotation curve. In such cases a halo, if present, has a hollow core.

b2) The 'maximum disk without a hollow core', for which the mass-to-light ratio has been somewhat lowered so as to allow a more reasonable halo profile ([17] and [1]).

c) Constraints on the mass-to-light ratio of reasonably symmetric two armed spiral galaxies can be set from the theory of swing amplification [16] (cf. [1]). This shows that a massive halo, unless it is cold and responding, inhibits spiral structure and that the halo mass necessary for this is a function of the number of arms in the galaxy. Thus a disk-halo decomposition such that most of the mass is in the halo is incompatible with the existence of spiral structure. If one considers consecutively larger and larger disk mass-to-light ratios one will reach a threshold; values below this excluding two armed spirals and values above it allowing it. This we will call "no m=2" solution. If we continue raising the disk M/L we will reach a second threshold, between M/L values excluding or allowing m=1 spirals or asymetries. In a number of cases the "maximum disk without a hollow core" solution has been reached before the m=1 instabilities become allowed and in most cases the two solutions are very close [1]. We will, for the purposes of this talk, not distinguish between them. One can thus define an allowed region bracketed by two extrema: on the lower side the 'maximum disk with no m=2' and on the upper side the 'maximum disk with no m=1' [1]. We have submitted the 'maximum disk with no m=1' to a number of tests to check whether it is a reasonable solution. We find that

- It gives good fits to the observed velocities
- It allows the observed spiral structure, both in number of arms and in radial extent
- It gives reasonable gas fractions
- It gives reasonable mass-to-light ratios, agreeing both with the stellar populations models and with values obtained from different dynamical constraint (i.e. the vertical equilibrium of galactic disks, [18]).

These arguments and the corresponding analysis can be found in [1] for the sample analyzed in that paper.

For one galaxy of that sample, NGC 488, measurements of the velocity dispersion are available [8], while an extended HI rotation curve has been recently obtained [3]. It is thus possible to build a mass model and calculate its axisymetric stability parameter Q [15]. A preliminary analysis shows that the Q values obtained from the 'no m=1' model are reasonable.

Although the above tests cannot constitute absolute proof they certainly provide strong indication that the 'maximum disk with no m=1' is a good model and can be used for further studies, in particular those of dynamical or chemical evolution and population models. We are much less favourable to the model corresponding to the lower limit, 'maximum disk with no m=2', since this is faring less well for a couple of the above issues. Finally we cannot, at this stage, assess any intermediate model.

References :

1. Athanassoula, E., Bosma, A., Papaioannou, S. : 1987, Astr. Ap. 179, 23
2. Athanassoula, E., Bosma, A. : 1987, I.A.U. Symp. 130 (in press)
3. Bosma, A., Athanassoula, E. : (in prep.)
4. Bosma, A., Van der Kruit, P.C. : 1979, Astr. Ap. 79, 281
5. Burstein, D., Rubin, V.C. : 1985, Ap. J. 297, 423
6. Carignan, C., Freeman, K.C. : 1985, Ap. J. 294, 494
7. Elmegreen, D.M., Elmegreen, B.G. : 1984, Ap. J. Suppl. 54, 127
8. Illingworth, G., Kormendy, J. : (priv. comm)
9. Kalnajs, A.J. : 1983, in "Internal Kinematics and Dynamics of Galaxies",

11. Kent, S.M. : 1987, A. J. 93, 816

12. McCall, M.L. : 1982, "The Chemistry of Galaxies", University of Texas publications in Astronomy No. 20

13. Monnet, G., Simien, F. : 1977, Astr. Ap. 56, 173

14. Nordsieck, K.H. : 1973, Ap. J. 184, 719

15. Toomre, A. : 1964, Ap. J. 139, 1217

16. Toomre, A. : 1981, in "The Structure and Evolution of Normal Galaxies", eds. S.M. Fall and D. Lynden-Bell, Cambridge Univ. Press, p. 111

17. Van Albada, T.S., Bahcall, J.N., Begeman, K., Sancisi, R. : 1985, Ap. J. 295, 305

18. Van der Kruit, P.C., Freeman, K.C. : 1986, Ap. J. 303, 556

19. Wevers, B.M.H.R. : 1984, PhD Thesis, University of Groningen

COLLISIONS BETWEEN GALAXIES: GRAVITATION AT PLAY

Françoise COMBES
Observatoire de Meudon, France
and Ecole Normale Supérieure, Paris

Galaxies are not isolated systems of stars and gas, "independent universes" as believed by astronomers about ten years ago, but galaxies are formed and evolve by interaction with their environment, mainly with their nearest neighbors. Gravitational interactions produce enormous **tides** in the disk of spiral galaxies, generate spiral arms and trigger bursts of star formation. Around elliptical galaxies, the collision with a small companion produces a series of waves, or **shells**. A galaxy interaction leads, in most cases, to the coalescence of the two colliders: second generation galaxies are therefore still forming now by galaxy mergers, essentially elliptical galaxies, but also compact dwarfs. Collisions between galaxies could also trigger activity in nuclei for radiogalaxies and quasars...

Galaxies are formed in groups and clusters, and this increases considerably the frequency of interactions: an evaluation of this frequency based on the mean galaxy density, as if their repartition was homogeneous in the Universe, underestimates totally the phenomenon. In average, it can be extrapolated from observations that a massive galaxy has swallowed several small companions in a Hubble time. Gravitational interactions considerably perturb the disk of spiral galaxies, and are often the cause of their peculiar spiral morphology (cf the case of Messier 51, fig.1.). These interactions brake the galaxies on their relative orbit, and the companions merge to form a new system, possibly an elliptical galaxy: we are still witnessing such merging events today. Their study is fundamental to our knowledge of galaxy formation.

The physical nature of galaxy interactions

It is only very recently that the nature of galaxy interactions has been elucidated; in the 1940's, the swedish astronomer Erik Holmberg had yet already established the basis of the right interpretation, but his pioneer work had little impact. He predicted the giant tides generated by the interaction, the consequent merging of the galaxies: he even carried out analogic simulations of the phenomenon! With the help of light bulbs, which intensity decreases as the square of the distance, and therefore can simulate the gravitational forces, he computed the behaviour of an ensemble of interacting stars : he solved the N-body problem. Two systems of 74 bulbs mobile on a table simulated two interacting galaxies.

During the following 30 years, the theory only stepped backwards: astronomers were convinced that the long and very thin filaments observed around interacting galaxies (cf fig. 2) could not come from tides, but they believed in a hydromagnetic origin, since thin filaments were reminiscent of matter collimation by the force tubes of the magnetic field. The more familiar tides in the solar system, and in particular the earth tides, could not indeed lead to imagine such filamentary perturbations: tides on earth act only on solid or liquid materials with strong cohesion, while galaxies are a very loose ensemble of stars and gas, without any cohesion except by self-gravitation. After the 1964 discovery of quasars, these extremely energetic phenomena in galactic nuclei, it was even thought that the centers of galaxies were the seat of giant explosions, which could be at the origin of the filaments.

The famous article by the Toomre brothers in 1972 brought to an end all these hypothesis. Alar Toomre was at this time searching for a mechanism to generate spiral structure in galaxies; he had just demonstrated that density waves were transient, and could not maintain themselves since galaxy formation. Gravitational galaxy interactions could be such a mechanism. The numerical simulations that he

Figure 1: The galaxy Messier 51, from the constellation Canes Venatici. The companion NGC5195 at the top left would be the cause of the M51 spiral structure. Composite photograph, enhancing the weak luminosity levels, by Burkhead (1978).

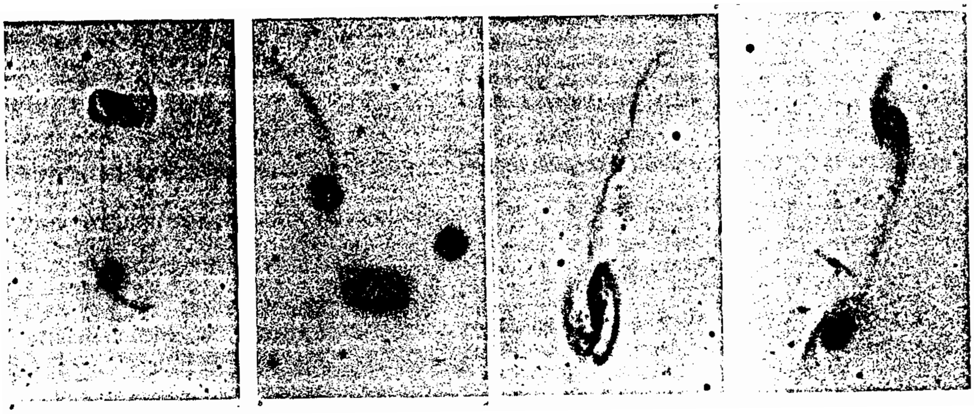

Figure 2: The tidal interaction between galaxies forms very thin filaments joining the parent galaxies. These filaments were believed to be matter collimated by the magnetic field lines. (from Arp Atlas, 1961)

undertook then with his brother established the efficiency of the mechanism, but also the gravitational nature of all galaxy interactions: gravity alone was able to produce long and thin filaments in intergalactic space.

A very simple numerical model

The simulations of the Toomre brothers could have been achieved long ago, they were technically feasible, requiring very little computing power: they are based on the restricted 3-body problem. All stars of the target galaxy and of the companion are represented by test-particles, of negligible mass. They are subject to the mean gravitational field of the two galaxies, whose relative orbits are computed in the frame of the 2-body problem. It is justified to neglect the self-gravitation of particles, since the tidal perturbations affect mainly the external parts of galaxies, less gravitationally bound.

Tidal forces have a bipolar symmetry in the perturbed galactic disk: they represent the differences over the whole disk of attraction forces from the companion; an attraction excess on one side, and a corresponding lack in the other side, disrupt the disk. This bipolarity, which explains the existence of two earth tides in 24H, is at the origin of the two-arms spiral structure of most spiral galaxies. A typical exemple is the galaxy Messier 51, of the constellation Canes Venatici: Fig. 3 shows how the companion NGC5195 has generated one of the greatest spiral structure in the sky.

When the two interacting galaxies have equal mass, the two internal spiral features form a bridge, which will soon be accreted by one of the galaxies; the two external spiral arms are spread out in two antennae, which will subsist during one or two billion years, genuine remnants of the past interaction. Two famous exemples are presented in Fig. 4 -5: The Antennae (NGC 4038-9) and The Mice (NGC 4676 A-B). these two systems are close to merging, final step of the interaction. The simulations show that stars in the antennae reach the escape velocity: they will disperse in intergalactic space in a near future. But at the tip of one of The Antennae, dense gaseous complexes have formed, as revealed by interferometric radio-observations of atomic hydrogen (fig 4b). These complexes have also large quantities of ionised gas, suggesting an enhanced star formation; it is likely that this activity has been triggered by the encounter of the antennae with the intergalactic medium. Once separated from the parent galaxies, the dense complexes will form dwarf compact galaxies, of second generation.

Galaxies warped like pancakes

Our own galaxy, The Milky Way, is itself in interaction with the Magellanic

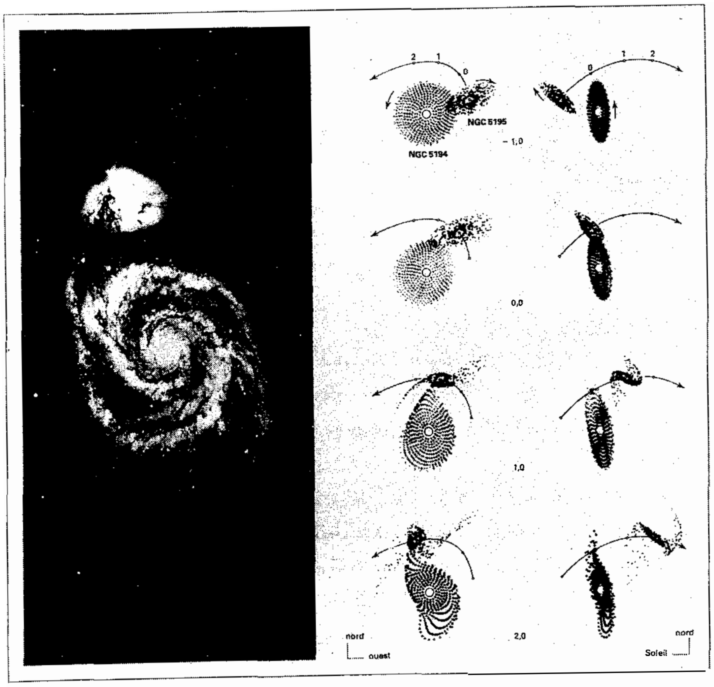

Figure 3: Numerical simulation of the tidal interaction between Messier 51 and its companion by the Toomre brothers (1972). The initial state consists in two homogeneous disks. The two spiral arms generated in each galaxy are due to the bipolar geometry ($\cos 2\theta$) of tidal forces.

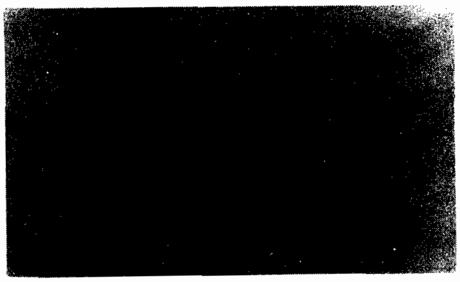

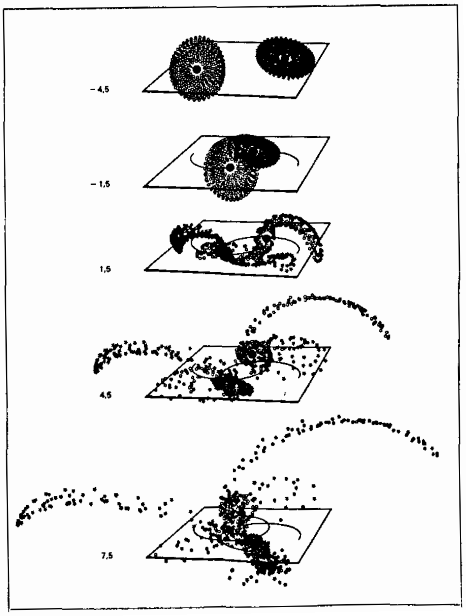

Figure 4: The interactive system NGC4038-4039 called The Antennae a) Comparison of photograph and numerical simulations

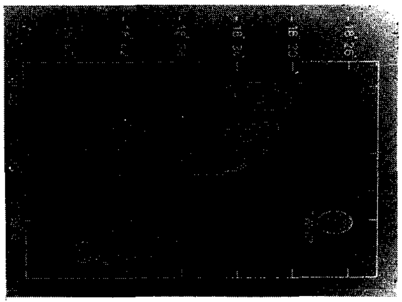

Figure 4: b) isophotes of atomic hydrogen emission observed by interferometry at 21cm wavelength (from van der Hulst 1978).

Clouds. A gaseous loop links like a bridge these two irregular galaxies to the Milky Way, and is called the "Magellanic Stream", observed in atomic hydrogen at 21cm wavelength. Numerical simulations, intricated by the presence of three galaxies, can still account for the observations (Fig. 6).

Another manifestation of this interaction is the deformation of the plane of the Milky Way like a pancake: from a galactocentric distance corresponding to the Sun, the disk plane is warped upwards, and downwards in the diametrically symmetric regions. This warp is observed in most spiral galaxies, and is of course more easily defined in edge-on galaxies (cf Fig. 7); in galaxies of different inclinations, it is the perturbed dynamics that reveals the phenomenon. The deformation is not static, the warping is in fact an oscillation of the plane around the equilibrium position, which is the plane defined in the central regions. The restoring force is the gravitational attraction from the unperturbed disk of stars. The phenomenon has been a problem for a long time, because the rate of differential oscillation of the disk is very fast: the vertical oscillation period of matter depends upon the galactic center, and after a few mean periods, the stars no longer oscillate in phase, and the disk would look like a corrugated plane, which is not observed even for "isolated" galaxies without near neighbors (for which the interaction is not recent). What is the mechanism that could extend the oscillation period, until it becomes of the same order as a Hubble time (ten billion years) ? One solution is to add some unseen mass as a halo around spiral galaxies: this dark matter is already suspected by the flat rotation curves of atomic hydrogen far from the galactic centers. But these rotation curves do not yield any clue on the 3 dimensional distribution of the dark matter, which could also be confined in the disk. To solve the problem of persistence of warps, the dark matter must be distributed spherically: the more flattened the mass distribution, the stronger the restoring force, and the shorter the oscillation period (in the extreme case, in a spherically symmetric potential, there is no longer any oscillation).

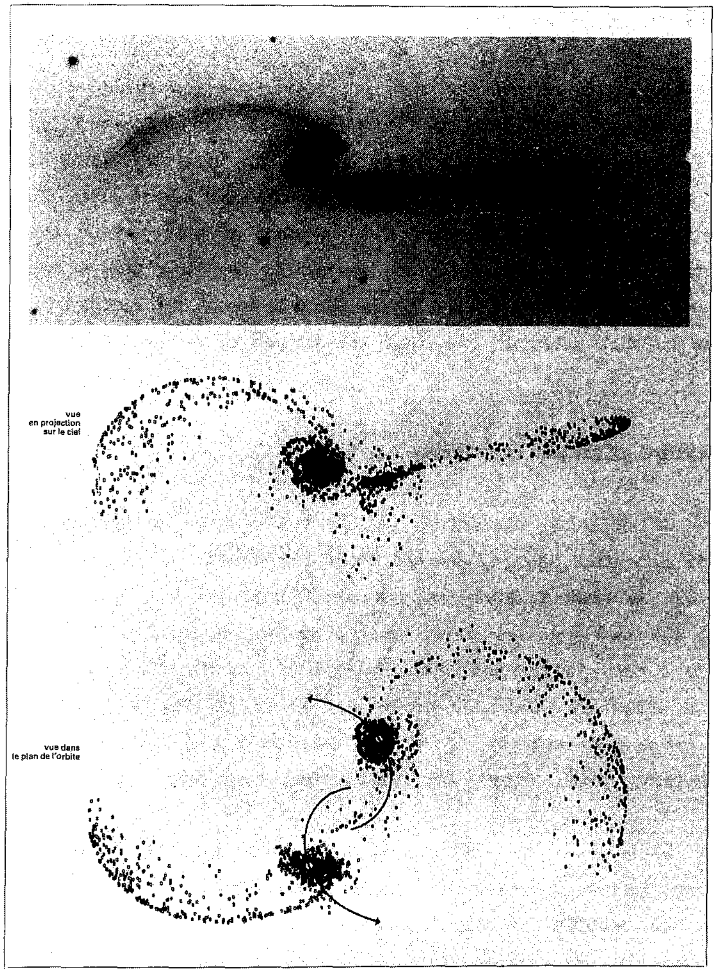

Figure 5: The galaxies NGC4676A and B are well known as the Mice. They are two galaxies of comparable mass, similar to the Antennae. These systems could give birth to dwarf compact galaxies, after dispersion of the tails in intergalactic space.

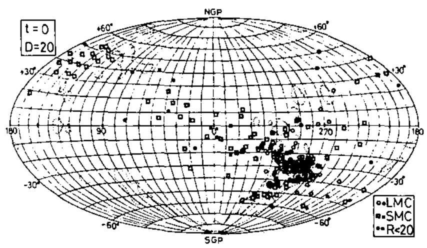

Figure 6: Our own galaxy, The Milky Way, is in gravitational interaction with the two Magellanic Clouds (LMC and SMC). One evidence is the "Magellanic Stream", a loop of atomic gas observed around the Milky Way plane, and numerically simulated here (Fujimoto & Sofue 1977). Another manifestation of the tidal interaction is the warping of the plane of The Milky Way, from a galactocentric distance corresponding to the Sun.

A nucleus remover for galaxies

When the impact parameter of the collision is varied, the generated spiral arms are more or less wound, and they close on themselves in a ring for a head-on collision, as shown in Fig. 8. Though a much rarer event, the ring formation is however observed in a certain number of galaxies, such as the Cartwheel (Fig. 9). Most often, the companion at the origin of such a morphology is observed on the minor axis, confirming the almost head-on collision; sometimes the ring galaxy has completely lost its nucleus, which might be found further out towards the companion. When the two companions are disk galaxies, two rings are formed by reciprocity (cf II Hz 4, Fig. 10).

A theory of formation of elliptical galaxies

What is the fate of violently interacting galaxies? The large perturbations involved require a lot of potential energy, pumped from the kinetic energy of the relative orbit. Each galaxy is braked down by dynamical friction, and spirals in towards the barycentre. The two galaxies merge, and a violent relaxation of stars begins: the final system is a mass distribution which looks like a truncated isothermal system, very similar to an elliptical galaxy. In the object NGC7252 (Fig. 11), where the two long tails attest of a past interaction, the two galactic nuclei are merged in one radial mass distribution, which obeys the well-known luminosity profile of ellipticals.

If it looks very likely that the merging of two spiral galaxies forms an elliptical galaxy, could tidal interaction be at the origin of all ellipticals? This would be one solution to the old problem of ellipticals formation. In the conventional interpretation where all galaxies are formed at about the same time, just after the Big-Bang, the existence of two types of galaxies, spheroids and disks, is explained by a two-speeds star formation: stars in elliptical galaxies are formed very efficiently out of the protogalactic cloud, before much dissipation of the gas component. Stars in spiral galaxies, on the contrary, are formed more slowly from gaseous clouds, which had time to condense and flatten, forming a disk by rotation. In the merging theory, all galaxies would form as spirals first, which is attractive.

It is possible to estimate the number of merging galaxies since the Big-Bang. Based on the observed number of today merging systems with long tails (cf NGC7252), and on the known duration of this merging period of 1-2 billion years, one can extrapolate to 10-20 % the fraction of merged galaxies since the beginning of the Universe. This percentage corresponds to the observed fraction of elliptical galaxies in the sky! Yet this theory of formation of ellipticals has faced a large number of objections: the very large abundance of globular clusters in ellipticals could not be

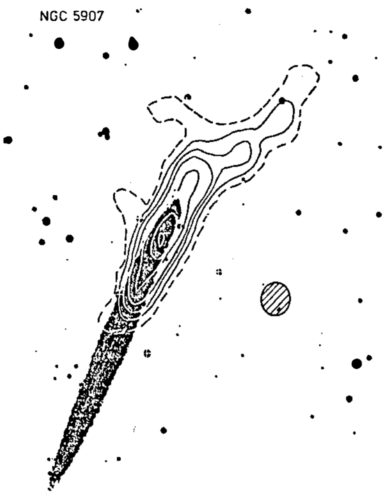

Figure 7: On this edge-on spiral galaxy NGC5907, the warping of the plane is clearly visible, from the atomic hydrogen isophotes (21cm) (from Sancisi 1976).

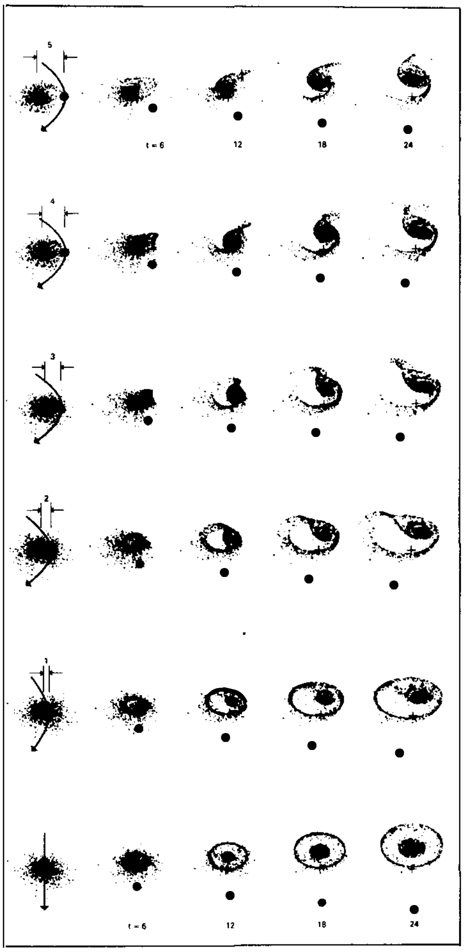

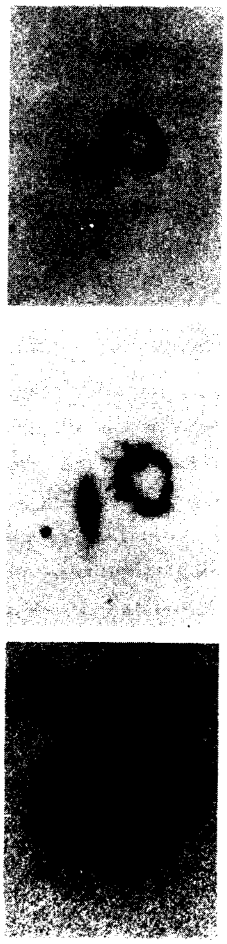

Figure 8: When the impact parameter of the collision is progressively reduced, the generated spiral arms are transformed in a ring head-on collision), (from Toomre 1977); the unit of time is here 100 million years. The photographs at right display a few exemples of ring galaxies observed in the sky.

explained by the merging of two spirals, where globular clusters are much less numerous; the merging of two diffuse star-systems could not lead to the formation of a very concentrated elliptical galaxy; dwarf elliptical could not be formed by the same mechanism.

Recent observations and theoretical work now bring new arguments in the debate, and in particular the phenomenon of shells around ellipticals.

Galaxies surrounded by shells

Already in 1961 H. Arp had observed very thin structures like rings around some elliptical galaxies, but it is mainly the two australian astronomers Malin and Carter in 1983 which revealed the phenomenon, in observing 137 shell galaxies (cf Fig. 12). With the help of filtering techniques (unsharp masking, namely) more and more elliptical galaxies (from 20 to 40% according to some authors) are observed with these thin star structures like arcs, interlocked up to ten galactic radii, reaching a number as high as 25 around the same galaxy. The observation of shells by Schweizer (1983) around merging systems, where the tidal interaction is evident (cf NGC7252, Fig. 13), suggests that the collision between two galaxies could be at the origin of shells formation.

The numerical simulations by Quinn (1984) of the accretion of a small companion by a massive elliptical confirm this hypothesis: the companion has a nearly radial orbit (almost head-on collision) towards the central elliptical galaxy; it is dispersed by tidal forces, and its stars then independently oscillate in the gravitational potential well of the massive galaxy. When the stars reach their apocenter (maximal elongation of their pendular motion), their velocity is zero, there is an accumulation point: this is a shell. If there exists shells at various distances from the center, this is provided by the spread in energy of the companion stars, and their consequent spread in apocenters. The distribution of shells is discrete, since the stars have different oscillation periods, they do not oscillate in phase, and they do not reach their apocenters (shells) at the same time (cf. Fig 14).

The results of simulations agree perfectly with observations, the model explains for instance the interleaving of shells in those shell systems which are aligned with the major axis of the elliptical galaxy. This allows the determination of important physical quantities of elliptical galaxies: in particular the 3 dimensional shape and the mass repartition in the shell galaxies. Fig. 14 displays the results of two simulations of shell formation with two different shapes for the massive elliptical: oblate and prolate spheroids: in the prolate case, shells are aligned with the apparent major axis of the central galaxy, and interleaved in radius; in the oblate case, shells are spread in all azimuths around a galaxy observed round in projection (face-on). Shells can therefore help to deduce the real geometry of the underlying elliptical.

Figure 9: The archetype of ring galaxies: The Cartwheel. This structure is due to a companion present today near the ring axis, at the top right.

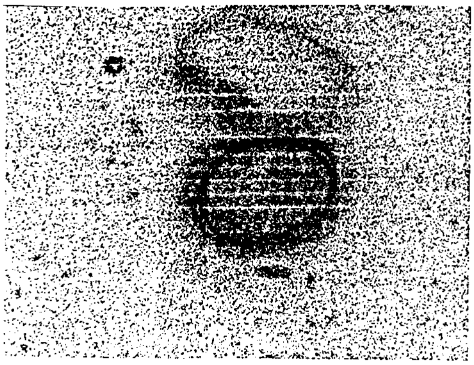

Figure 10: In a head-on collision, when the two protagonists are disk galaxies, a ring is formed symmetrically in the two systems: II Hz 4 is an exemple of a double ring (cf Lynds & Toomre 1976).

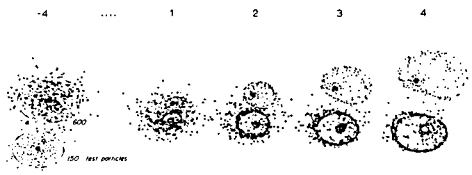

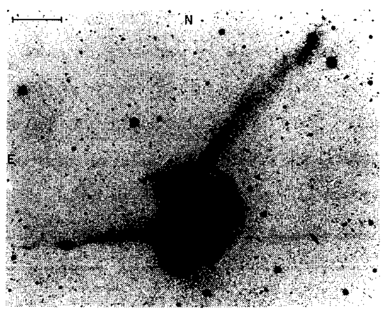

Figure 11: The archetype of merging galaxies NGC7252; the two long tails coming out of this unusual object, a mixing of galactic nuclei, attest of the tidal interaction at the origin of the merger (cf Schweizer 1982).

Indeed it is well-known since 1978 that elliptical galaxies are not rotating systems: their apparent flattening cannot be attributed to rotation as for spirals, but probably to an anisotropic velocity dispersion. Their 3 dimensional shape could then be oblate (pancake), or prolate (cigar) or even triaxial.

Besides, in the same manner as iron filings are used to trace the magnetic field lines, shells could be used to test the gravitational potential around elliptical galaxies; namely they can be used to test the radial repartition of mass and determine the presence of any hypothetical unseen matter, therefore to play the role of the atomic gas in spiral galaxies. For the few shell galaxies for which we possess enough information, there does not seem necessary to add any dark matter to account for the radial distribution of the shells. This result has to be confirmed with a larger number of shell galaxies.

Statistics on the observed shell geometries together with the efficiency of shell formation obtained in the simulations, allow to deduce several conclusions: there would exist in the Universe twice as much oblate than prolate elliptical galaxies; and when taken into account the high fraction of shell galaxies in the sky and the low efficiency of shell formation, one can estimate at 4 or 5 the mean number of swallowed companions by each massive elliptical galaxy. The accretion phenomenon is thus very common.

When the capture of small companions is taken into account, the formation of elliptical galaxies by merging is not yet finished! Several recent arguments have given a boost to the old debate around the merger theory of formation of ellipticals: the merging of two gaseous systems, in contrast to star systems, by dissipation would allow the formation of concentrated distributions; also the far-infrared observations carried on by the satellite IRAS in 1984 have revealed that the brightest objects in the sky at these wavelengths were the mergers and interacting galaxies. The far-infrared flux is directly related to the rate of star formation, since it is emitted by the dust heated by very young stars, still embedded in their interstellar clouds where they were born. Huge bursts of star formation are therefore occuring in merging galaxies. This active star formation could easily explain the large abundance of globular clusters in the final elliptical, and also the depletion of gas, swept away by the galactic wind generated by supernovae and gas ionisation.

There remains this convincing argument of Alar Toomre in 1977: if merging of galaxies are not the origin of ellipticals, where are gone the remnants of mergers, whose archetype is NGC7252? These mysterious objects would represent, as we have already estimated, at least 10% of galaxies in the Universe!

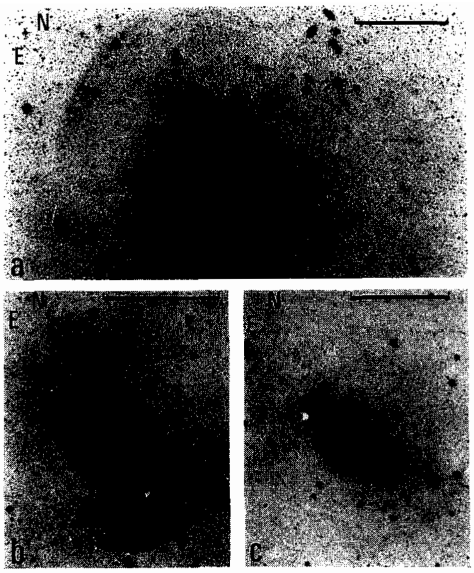

Figure 12: Three photographs at different exposure times, and different scales, of the elliptical galaxy NGC3923: 25 shells are observed around this galaxy, aligned with the major axis, and interleaved in radius. Shells are very sharp structures, very weak in luminosity, consisting only of stars (from Malin & Carter 1983).

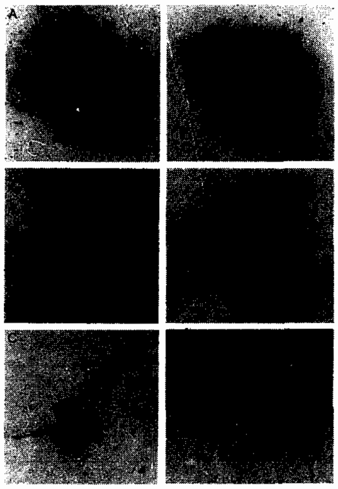

Figure 13: Three merging systems A) Fornax A, B) Centaurus A, C) NGC7252, observed directly in the left column, and after unsharp masking in the right column. This filtering of low spatial frequencies enhances the shell contrast. Shells are present in the three systems, which suggests a link between tidal interaction and the shell phenomenon, from Schweizer (1983).

References

Burkhead M.S. (1978) Ap.J. Supp. 38, 147

Dupraz C., Combes F., (1986) A.& A. 166, 53

Fujimoto M., Sofue Y., (1977) A.& A. 61, 199

Lynds B., Toomre A., (1976) Ap.J. 209, 382

Malin D.F., Carter D., (1983) Ap.J. 274, 534

Quinn P.J. (1984) Ap.J. 279, 596

Sancisi R., (1976) A.& A. 53, 159

Schweizer F. (1982) Ap.J. 252, 455

Schweizer F., (1983) I.A.U. 100, 319

Toomre A. (1977) Yale Conference

Toomre A., Toomre J. (1972) Ap.J. 178, 623

van der Hulst (1979) A.& A. 71, 131

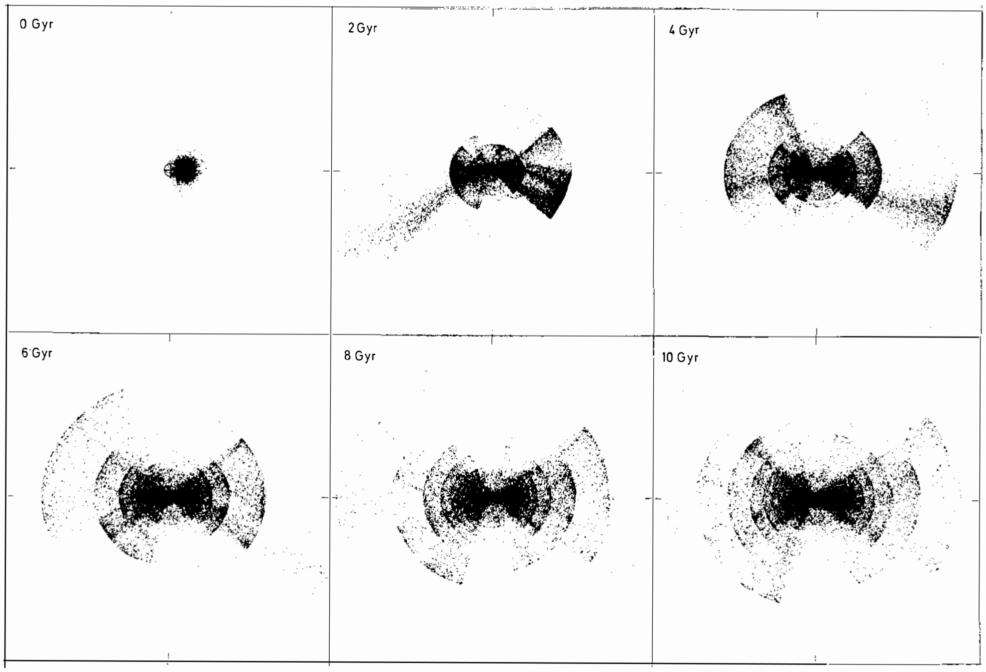

Figure 14: Numerical simulations of the accretion of a small companion by an elliptical galaxy, from Dupraz & Combes (1984): a) the massive elliptical is prolate (cigar-shape), shells are aligned along the major axis; b) the oblate case (pancake), where shells are randomly spread around the galaxy.

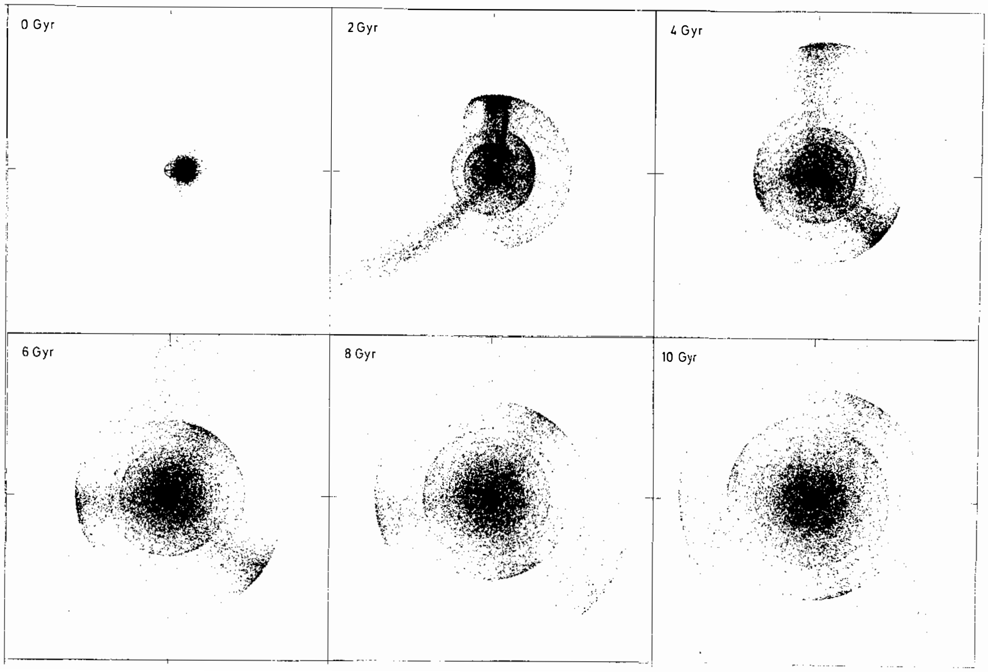

IV. STAR FORMATION AT INTERMEDIATE AND HIGH REDSHIFT

AN OBJECTIVE PRISM Hα SURVEY OF NEARBY CLUSTERS: MASSIVE STAR FORMATION IN CLUSTER SPIRALS

C. Moss*
Institute of Astronomy
Cambridge, U.K.

An objective prism survey has been made of galaxies in the clusters Abell 347 and Abell 1367 to detect global combined Hα + [NII] emission as an indicator for the current rate of massive star formation. Strong emission correlates with a disturbed morphology for the galaxy, and there is an indication that in tidally disturbed galaxies the emission is more concentrated towards the galaxy centre than for non-disturbed galaxies. One explanation of the results is that massive star formation is triggered by gravitational interactions between spiral galaxies falling onto the cluster.

* Visiting Astronomer, Kitt Peak National Observatory, operated by the Association for Research in Astronomy, Inc., under contract with the National Science Foundation. Observations were made with the Burrell Schmidt of the Warner and Swasey Observatory, Case Western Reserve University.

1. Introduction

The global Hα emission of a galaxy is recognised as a useful indicator of the current star formation rate for massive stars [1,2]. Using the Burrell Schmidt telescope on Kitt Peak equipped with a ten degree objective prism, a survey has been made of galaxies in the clusters Abell 347 and Abell 1367 for galaxies with strong global combined Hα + [NII] emission (λλ 6563, 6584 Å) in order to investigate the effect of environment on massive star formation in cluster spirals [3]. The survey was made over an area of approximately 5 degrees in diameter centred on each cluster using an RG 630 (or alternatively an RG 645) filter and hypersensitised IIIaF emulsion. A typical exposure time was 2 hours, and two plates of excellent quality were obtained for each cluster. For the statistical analysis which follows, those galaxies which were detected in emission on both plates of a cluster plate pair will be used.

Approximately 20% of CGCG galaxies were detected in emission, and approximately 33% of the detected galaxies are fainter than the limit of this catalogue. There are 72 CGCG galaxies in the surveyed area of Abell 347, and 117 such galaxies in the surveyed area of Abell 1367. Morphological types have been independently determined for these galaxies by Whittle from high quality Palomar Schmidt plates (Abell 1367) or PSS glass copies (Abell 347) [4]. These CGCG galaxies will comprise the sample to be used for the statistical analysis which follows, with the omission of 6 galaxies whose spectra overlapped stellar spectra, and 4 galaxies which are double with both components fainter than m_p = 15.7.

The objective prism spectra of the detected emission-line galaxies were digitised using the PDS microdensitometer of Kitt Peak Observatory, and Hα equivalent widths and fluxes were measured. For a sample of galaxies in Abell 1367 Hα equivalent widths and fluxes have also been obtained by Kennicutt, Bothun and Schrommer [5] from wide aperture photometry and these are in good agreement with the values obtained from the objective prism spectra [3]. The detection limits in equivalent width and flux for the present survey are $W_\lambda > 20$ Å and log f > -13.0 respectively, where f is the Hα flux in erg cm^{-2} sec^{-1}.

2. Properties of the emission-line galaxies

No E or E-SO galaxies are detected in emission, and the fraction of galaxies of type SO and later detected in emission increases towards later types as expected. This is shown in Table 1. In the Table, N_T denotes the total number of galaxies of a given type and f denotes the fraction of these galaxies detected in emission.

Galaxies have been designated as tidally disturbed or interacting by Whittle [4]. As is seen from the second section of Table 1, there is a strong correlation between strong Hα emission and tidal disturbance of a galaxy.

TABLE 1

RELATION OF Hα EMISSION TO GALAXY MORPHOLOGY

		Type class				
		2	3	4	5	6-8
All galaxies	N_T	54	25	28	26	23
	f	4%	12%	32%	46%	43%
Tidally-disturbed galaxies	N_T	4	6	6	8	9
	f	25%	50%	50%	50%	78%
Other	N_T	50	19	22	18	14
	f	2%	0%	27%	44%	21%

NOTE TO THE TABLE. Type classes are: 1 - E, E-SO; 2 - SO; 3 - SO-a; 4 - Sa, Sab; 5 - Sb, S...; 6 - Sbc, Sc; 7 - Sc-Im, Im; 8 - pec., unclassified.

Finally, there is some suggestion that the emission or star forming regions are more centrally concentrated in the tidally disturbed galaxies. This is shown in Table 2. The sample of emission-line galaxies has been divided into tidally disturbed and non-disturbed galaxies, and according to the visual appearance of the emission in the objective prism spectrum. As is seen, the tidally disturbed galaxies tend to have more compact emission. This effect is significant at the 2% level.

TABLE 2

GALAXY MORPHOLOGY AND SPECTRAL APPEARANCE OF EMISSION-LINE GALAXIES

Spectrum	Tidally-disturbed galaxies	Other galaxies
V. diffuse, diffuse	4	12
'Normal', compact, v. compact	14	6

3. Comparison of cluster and field emission-line galaxies

Kennicutt and Kent have measured global Hα equivalent widths and fluxes for a large sample of field spirals [6]. Assuming the detection limits for the present survey given above, the percentage of cluster galaxies detected in emission may be compared with the percentage expected if the cluster spirals were similar to field spirals. This comparison is shown in Figure 1. This Figure is a histogram showing the percentage of cluster galaxies of various types detected in emission (hatched area), in comparison with the fraction of field spirals of the same type expected to be detected in emission at the distance of the two clusters (open area). As is seen, early type spirals (types S0-a to Sb) in the clusters are significantly more likely to be detected in emission than field spirals of the same types. Some uncertainty in this result arises from the difficulty of accurately establishing galaxy types from Palomar Schmidt plates. Further, some galaxy types are more uncertain because the galaxies are tidally disturbed. However it seems unlikely that these effects can explain the higher fraction of early-type cluster galaxies detected in emission than expected. This result is in agreement with the detection of an enhancement of star formation in cluster spirals, which was found from radio data for Abell 1367 and the Coma cluster by Gavazzi and Jaffe [7].

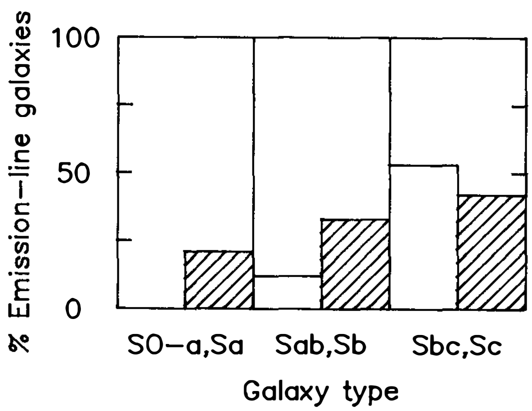

FIGURE 1.

A comparison of the observed fraction of cluster spirals of different types detected in emission (hatched area) with the fraction of field spirals at the distance of the clusters which are expected to be detected (open area).

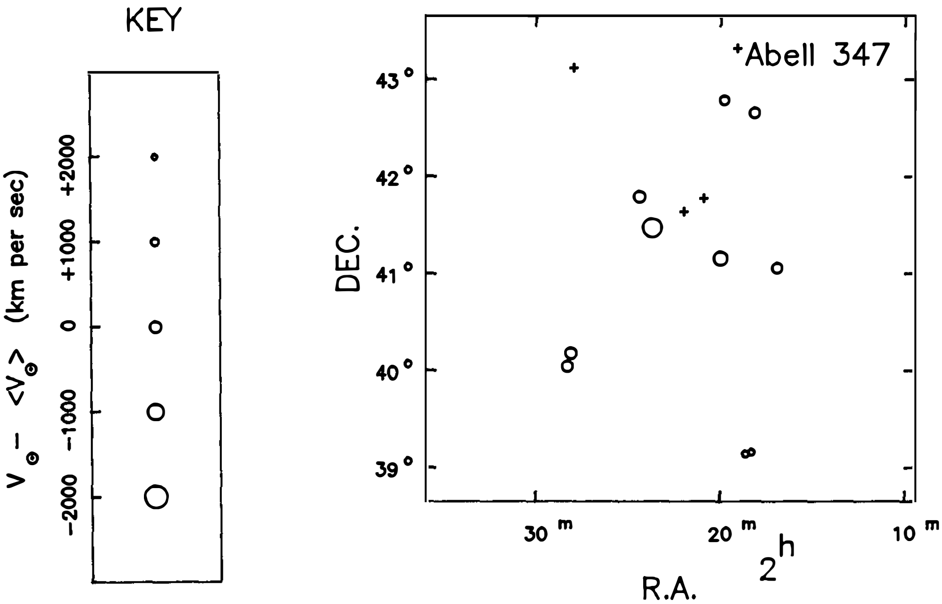

FIGURE 2

The distribution of disturbed and interacting galaxies and galaxies noted as peculiar in Abell 347. Velocities of galaxies with respect to the cluster mean are represented by the size of the circle denoting each galaxy as shown in the Key. Galaxies with no measured velocity are represented by crosses.

FIGURE 3 (opposite)

Distribution of disturbed, and interacting galaxies, and galaxies noted as peculiar in Abell 1367. The symbols are the same as in Figure 2.

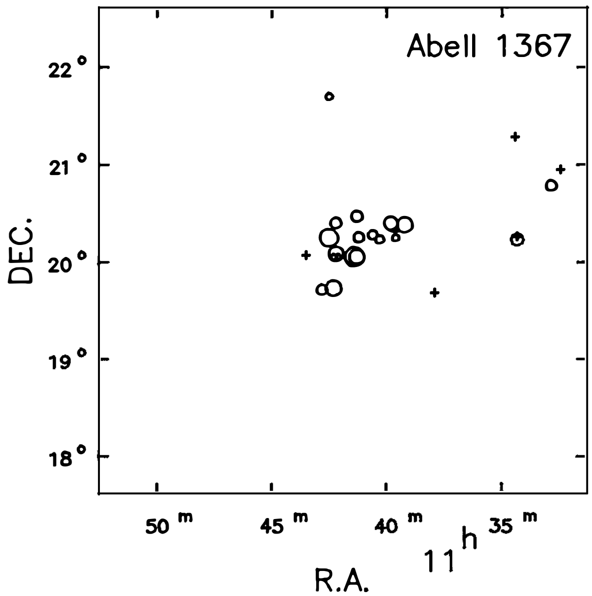

4. Triggering of star formation in cluster spirals by tidal interaction

Previous surveys have accumulated considerable evidence for enhanced star formation in interacting galaxies [e.g. 8,9,10,11]. The observed strong correlation between detection of strong Hα emission and tidal disturbance for the present sample of cluster galaxies might seem to indicate that the enhanced star formation observed in cluster spirals is also due to galaxy-galaxy interactions. However the velocity dispersion of emission-line galaxies in each of the two clusters is approximately 1000 km sec^{-1}, which is too large for tidal interaction to be significant if the spirals are distributed randomly in position and velocity in the clusters. In Figures 2 and 3 the distributions are shown of disturbed and interacting galaxies and galaxies noted as peculiar in Abell 347 and Abell 1367 respectively. Velocities of the galaxies with respect to the cluster mean have been represented by the size of the circle denoting each galaxy, as shown by the Key in Figure 2. Galaxies with no measured velocity are represented by crosses. It is readily apparent that the galaxies shown in each of the Figures may easily be grouped in pairs or small groups with low velocity dispersion, although the velocity dispersion of the whole sample for each cluster is high. This suggests that tidal interaction is responsible for triggering star formation in a significant fraction of the emission-line galaxies detected in the clusters. Finally it may be noted that such interaction is precisely what would be expected to occur in a shell of galaxies falling onto the cluster, and thus the observed enhanced star formation in cluster spirals may be evidence of continuing galaxy accretion by the clusters.

References

[1] Kennicutt, R.C. 1983. Astrophys. J., **272**, 54.
[2] Gallagher, J.S., Hunter, D.A. & Tutukov, A.V. 1984. Astrophys. J., **284**, 544.
[3] Moss, C., Irwin, M. & Whittle, M. 1987. In preparation.
[4] Moss, C. & Whittle, M. 1987. In preparation.
[5] Kennicutt, R.C., Bothun, G.D. & Schommer, R.A. 1984. Astr. J., **89**, 1279.
[6] Kennicutt, R.C. & Kent, S.M. 1983. Astr. J., **88**, 1094.
[7] Gavazzi, G. & Jaffe, W. 1985. Astrophys. J. Lett., **294**, L89.
[8] Larson, R.B. & Tinsley, B.M. 1978. Astrophys. J., **219**, 46.
[9] Wasilewski, A.J. 1983. Astrophys. J., **272**, 68.
[10] Lonsdale, C.J., Persson, S.E. & Matthews, K. 1984. Astrophys. J., **287**, 95.
[11] Kennicutt, R.C. & Roettiger, K.A. 1986. Preprint.

SPECTROSCOPY OF GALAXIES IN A370 : A STUDY OF THE CLUSTER CONTENT

Geneviève SOUCAIL
Observatoire de Toulouse
14, avenue E. Belin
31400 TOULOUSE
France

After a brief review of the observations of distant clusters of galaxies ($z > 0.2$) and the evolutionary effects already detected, I will present the data obtained by the Toulouse Observatory team on the cluster Abell 370 ($z = 0.37$), both with photometry and spectroscopy. A first analysis leads to the conclusion that the cluster content is different than the one expected for a rich cluster and that 50 % of spiral-like galaxies are identified.
An interpretation in terms of burst of star formation is proposed for the blue galaxy excess detected in A370.

1. Introduction: Observations of distant clusters of galaxies

Since the beginning of the eighties, the observation of distant clusters of galaxies has become possible with the development of new instruments such as CCD detectors or more sensitive photographic plates, used on large telescopes. Numerous observational data on clusters are now available, mainly photometric ones.

The first large statistics was obtained by Butcher et al.[1,2] on more than 15 clusters with z varying from 0.1 to 0.5. The sample of clusters with photometric data was then increased mainly by Couch, Ellis, Newell ...[3,4,5,6], Le fèvre [7], up to more than 30 distant clusters presently investigated in deep photometry.

For all observers, the main goal was a search for evolutionary effects in clusters of galaxies younger than the well-known nearby ones: Coma, Virgo ... The first result stressed by Butcher and Oemler in 1978 was the evidence of an increasing fraction of "blue objects" with the redshift, known as the Butcher-Oemler effect (see § 2.b). In the beginning, it was controversed because it could be suspected to result from a contamination of field galaxies (foreground galaxies are generally bluer than most of the galaxies belonging to the cluster) [8,9], but now the B.O. effect is well confirmed and detected for most distant clusters, even if it is not well understood [10].

The nature of the "blue objects" in clusters began to be studied spectroscopically a few years ago, as multi-object spectroscopic systems were developed for several large telescopes. The first confirmation of the B.O. effect was obtained by Dressler and Gunn, on the clusters 3C 295 [11] and Cl 0024+1654 [12], when they determined the membership of nearly half the blue objects.

Presently, about 10 distant clusters have been investigated spectroscopically, with redshifts from 0.2 to 0.54: 3C 295, Cl0024+1654, Cl 0016+16 [13], Cl 1447+2619 [14], AC 103 [15], A223, A963 and A2111 [16]. The main interest is to identify the nature of the "blue objects" of the clusters. This population differs from cluster to cluster, but it can be separated in two classes: active galaxies (Seyfert 1 or 2), and galaxies with strong star formation (burst or post-starburst) [16].

A few years ago, the Toulouse Observatory has developed an on-line multispectroscopic system called PUMA for the 3.6m C.F.H.Telescope and for E.S.O. [17]. It is well suited to the study of distant clusters of galaxies as it is possible to obtain simultaneously more than 20 spectra of objects in the same field. This is the reason why we began this study, and mainly the observation of the cluster Abell 370 (z=0.374) .

2. Spectroscopy of galaxies in the A 370 cluster

a. The data

They have been collected during 3 observing runs at C.F.H.T. (3.5 nights in September of 1985 and 3 nights in November of 1986) and at E.S.O. on the spectrograph EFOSC mounted on the 3.6m telescope (2.5 nights in November of 1986). The use of a focal reducer allows one to obtain direct imagery of the field. After the data reduction, about 330 objects have been measured in photometry with B,V and R filters, in a field of 5'x7'. The completeness limit is roughly R=21 and the brightest cluster member has R≈17.4 .

With the multispectroscopic system PUMA, it has then been possible to do spectroscopy of 88 objects in the same field (with a dispersion of 10 Å/pixel) [18], and the radial velocities have been measured for 47 galaxies belonging to the cluster.

We should point out that this amount of data is one of the largest collected on a distant cluster of galaxies. It allows a precise study of its content and its evolution, and the main results have presented elsewhere [19]. Note that a catalogue is in preparation and will be soon published.

b. Description of the cluster

A 370 is the Abell cluster with the largest measured redshift (z=0.374). It is a bright, compact and very rich cluster, which can be characterised by the parameter $N_{0.5}$ [20]. The value $N_{0.5}=31$ can be compared with the one measured for the Coma cluster ($N_{0.5}=28$). Another similarity between these two clusters is the presence of two dominant giant galaxies in the center, the presence of two substructures or clumps, even if the ones in A370 are not significantly correlated with redshifts. The X-ray luminosity of the cluster has been detected and it corresponds to $L_x = 1.45\ 10^{45}$ erg/s in the 0.7-6keV band, in the cluster frame.

With the redshifts of 47 member galaxies, we have been able to derive a velocity dispersion inside the cluster: $\sigma \approx 1350$ km/s with an accuracy better than 200 km/s. This value is typical for rich nearby clusters.

All these characteristics stress the fact that A370 is a cluster similar to the Coma cluster, a sort of "sosie", but observed 5 Gyrs before. Moreover it seems to be quite evolved dynamically [19], with evidences of luminosity segregation.

But the main difference appears in the color content of the cluster: Butcher and Oemler have shown that A370 is a rather blue cluster [10], contrary to the rich nearby ones. Quantitatively, they define the blue galaxy fraction as the fraction of galaxies in a sample corrected statistically from the field contamination, with the criteria:

- absolute V-manitude $M_V \leqslant -20.00$
- color index $(B-V)_{rest-frame} \leqslant (B-V)_{Elliptical} - 0.2$
- distance to the center $d \leqslant R_{30}$
  (where R_{30} is the radius containing 30% of the objects of the cluster)

With this definition f_B is a distance-independant coefficient, allowing a statistic work on a sample of clusters of different redshifts and their comparison. In the case of A370, $f_B \approx 21\%$.

Finally, it should be noted that A370 presents a strange ring-like structure in its center, for which the photometry has been obtained [21], showing a giant luminous structure , very blue and thin (see § 3.d).

c. Morphological content

With the spectra of more than 50 galaxies belonging to the cluster, we have tried to determine the spectral content of each object. To do so, we have compared the spectral energy distribution of the galaxies (measured with a dispersion of about 10 Å/pixel, from 4500Å to 7500Å) with different synthesized spectra obtained with the evolutionary model of Guiderdoni and Rocca-Volmerange [21]. The spectral identification of each galaxy led us to classify them in three groups: elliptical and lenticular galaxies (E/S0), red spirals (SA and SB), and blue spirals (SC, SD and Irregular).

The main result derived from this work is the observation that 50 % of the galaxies in the cluster are spiral-like, in a radius of 0.7 Mpc and a R-magnitude range 17-19.5 , compared to only 3 % in the Coma cluster for a similar sample. This striking result must be interpreted in terms of an evolutionary effect, as A370 is roughly 5 Gyrs younger than nearby clusters.

3. Analysis of the content of the cluster

a. The spirals in A370

First, it is important to note that these galaxies are "normal spirals" and that no galaxy with AGN has been found in this cluster, contrary to some others distant clusters such as 3C 295 [11].

As for their position in the field, they appear less concentrated in the center than the elliptical ones, an effect confirmed by the color segregation shown in the photometric data. This is the first confirmation of a morphological segregation (assuming that the spectral type corresponds to the morphological type) in such a distant cluster, and it reveals different dynamical states for the two populations.

Furthermore, there are still about 30 % of spirals in a radius of 350 kpc around the center. If it is a projection effect, this means that the morphological segregation is even stronger and that the spirals are falling on the cluster, and if not , we have to explain their survival in the dense environment of the cluster center.

b. Evolution of the galaxies

As A370 presents so many similarities with Coma, it is rather natural to imagine than it is evolving towards a Coma-like cluster, and that the main differences between the two clusters must be smoothed in 5 Gyrs. We thus have to determine the mechanism of "disappearance" of the spiral galaxies and their probable evolution towards lenticular galaxies (or even elliptical ones).

First, tidal stripping can be invoked as such a phenomenon, mainly in the dense core of the cluster. But the most efficient encounters require low relative velocities, which is rather incompatible with the high velocity dispersion (σ=1350 km/s). On the contrary, the sweeping mechanism is more and more efficient when the galaxies have high velocities through the cluster. Moreover, A370 has a strong X-ray luminosity, and consequently a dense Intra-Cluster Medium. So, this mechanism is probably occuring in the center of the cluster, leading to a morphological segregation, interpreted here as an evolutionary effect (and not an "ab initio" effect).

c. The B.O. effect

In our spectroscopic sample, we have identified 8 "blue objects" (using the B.O. definition). As only 4 of them belong to the cluster, we can say that in our sample, slightly smaller than the B.O.'s one, we have measured a blue galaxy fraction $f_B \approx 13\%$. But what are these galaxies ?

First of all, none of them is a Seyfert galaxy nor an AGN. On the contrary, they present strong Balmer absorption lines, have been identified as late-type spirals (Sc or Irregular Magellanic), and some of them present the [OII] 3727Å emission line. All these parameters are indicators of a strong star formation, having occurred recently, or still occurring. They suggest that a burst of star formation could accompany the gas removal process in galaxies when they travel for the first time accross the Intra-Cluster Medium.

d. The "arc" in A370

Finally, we would like to present briefly the recent results obtained on the giant luminous "arc" lying in the center of the cluster [21]. The size of this structure is roughly 150 kpc long and less than 10 kpc large (assuming H_0= 50 km/s/Mpc). The multi-color photometry has shown that it is bluer than any other galaxy in the cluster. Furthermore, we have obtained a spectrum of the East-end of the arc (with a rather poor S/N ratio), and identified it with the spectrum of a galaxy at z=0.59.

So our best interpretation of the nature of the arc is the gravitational lensing of a galaxy at z=0.59, by the cluster core of A370. Using a multi-point-mass model, it is possible to reproduce very satisfactorily the structure of the arc, taking into account the mass of the cluster core ($\sim 2.10^{14}$ M_0) and the masses of the secondary deflectors lying along the arc. Moreover, as we should observe two symmetric arcs in this configuration, we can explain easily the fading of the Northern one (which should lie near the Northern Giant galaxy) as an effect of this galaxy, if its mass is above 3.10^{12} M_0. The details of this model, and a discussion of the other interpretations of the nature of the arc have been presebnted in a paper submitted recently [23]. We are expecting new spectroscopic data this summer, in order to confirm or infirm the gravitational lensing hypothesis.

Conclusion

With the data presented here on A370, we would like to try to discuss the different time-scales for the evolution of clusters of galaxies:

- First, the dynamical evolution seems to have been rapid after the formation of the cluster, as several cases of segregation are detected in clusters 5 Gyrs younger than the nearby ones.
- But the evolution of the morphological content is more surprising, as we have detected a large proportion of spiral-like galaxies in A370. Moreover, the confirmation of the Butcher-Oemler effect can be discussed in terms of evolution, too, even if the mechanisms occuring in the clusters are not well understood.

References

[1] - Butcher, H., and Oemler, A., Jr. 1978, Astrophys. J., **219**, 18
[2] - Butcher, H., Oemler, A., Jr., and Wells, D.C. 1983, Astrophys. J., Suppl., **52**, 183
[3] - Couch, W.J., Ellis, R.S., Godwin, J., and Carter, D. 1983, Mon. Not. R. Astr. Soc., **205**, 1287
[4] - Couch, W.J., and Newell, E.B. 1984, Astrophys. J. Suppl., **56**, 143
[5] - Couch, W.J., Shanks, T., and Pence, W.D. 1985, Mon. Not. R. Astr. Soc., **213**, 215
[6] - Ellis, R.S., Couch, W.J., Mac Laren, I., and Koo, D.C. 1984, Mon. Not. R. Astr. Soc., **217**, 239
[7] - Le fèvre, O. 1986, Ph.D Thesis, Université de Toulouse
[8] - Mathieu, R.D., and Spinrad, H. 1981, Astrophys. J., **251**, 485
[9] - Dressler, A., and Gunn, J.E. 1982, Astrophys. J., **263**, 533
[10] - Butcher, H., and Oemler, A., Jr. 1984b, Astrophys. J., **285**, 426
[11] - Dressler, A., and Gunn, J.E. 1983, Astrophys. J., **270**, 3
[12] - Dressler, A., Gunn, J.E., and Schneider, D.P. 1985, Astrophys. J., **294**, 70
[13] - Dressler, A. 1985, Spectral Evolution of Galaxies. Proceedings of the fourth workshop of the advanced school of astronomy, March 1985. Reidel Publishing Company.
[14] - Butcher, H., and Oemler, A., Jr. 1984a, Nature, **310**, 31
[15] - Sharples, R.M., Ellis, R.S., Couch, W.J., and Gray, P.M. 1985, Mon. Not. R. Astr. Soc., **212**, 687
[16] - Lavery, R.J., and Henry, J.P. 1986, Astrophys. J., **304**, L5
[17] - Fort, B., Mellier, Y., Picat, J.P., Rio, Y., and Lelièvre, G. 1986, Proc. S.P.I.E., "Instrumentation in Astronomy VI", Vol **627**, March 1986

[18] - Soucail G., Mellier, Y., Fort, B., Picat, J.P., and Cailloux, M. 1987a, Astron. Astrophys., in press
[19] - Mellier, Y., Soucail, G., Fort, B., and Mathez, G. 1987, submitted
[20] - Bahcall, N.A. 1981, Astrophys. J., 247, 787
[21] - Soucail G., Fort, B., Mellier, Y., and Picat, J.P. 1987b, Astron. Astrophys., 172, L14
[22] - Guiderdoni, B., and Rocca-Volmerange B. 1987, Astron. Astrophys., in press
[23] - Soucail, G., Mellier, Y., Fort, B., Hammer, F., and Mathez, G. 1987c, submitted

STAR FORMATION IN COOLING FLOWS

A.C. Fabian

Institute of Astronomy

Cambridge

United Kingdom

A cooling flow can deposit large quantities of gas around the central galaxy in a cluster. These are then the largest nearby regions of star formation if the gas forms into stars. The process also operates in most elliptical galaxies at a much reduced rate. Optical magnitudes and spectra of central cluster galaxies show that only a small fraction of the gas is converted into 'normal' stars. Most of it presumably forms low-mass stars. The evidence for star formation from cooling flows, both near and distant, is discussed.

Introduction

The hot gas in the cores of many clusters of galaxies, and in elliptical galaxies, is cooling by emission of X-rays. A cooling flow is established as the density of the gas is forced to rise by the weight of the overlying atmosphere (see Fabian, Nulsen & Canizares 1984; Sarazin 1986) . The rate at which cooled gas is deposited, and presumably forms stars, is substantial, ranging from $1\,\mathrm{M}_\odot\,\mathrm{yr}^{-1}$ for isolated ellipticals up to $500 - 1000\,\mathrm{M}_\odot\,\mathrm{yr}^{-1}$ for some rich clusters. These last figures suggest that cooling flows are the largest regions of star formation at the current epoch.

The mass accumulated over a Hubble time,

$$\dot{M}t = 2 \times 10^{12} \left(\frac{\dot{M}}{100\,\mathrm{M}_\odot\,\mathrm{yr}^{-1}}\right) \left(\frac{H_o}{50\,\mathrm{km\,s}^{-1}\ \mathrm{Mpc}^{-1}}\right)^{-1} \mathrm{M}_\odot.$$

The limits on neutral hydrogen and molecular gas in cluster cores (Jaffe 1987) are much less than this ($\leq 10^9 - 10^8\,\mathrm{M}_\odot$) so that the gas must cool into some form of condensed matter such as stars. The magnitudes and colours of the central galaxies in cooling flows directly rule out any 'standard' initial-mass-function for most of these stars and low-mass stars are generally assumed to be formed. There is at present no direct evidence for a large population of such stars in cooling flow galaxies. Nevertheless, there is some evidence for high total masses and high mass-to-light ratios, so the galaxies do possess dark matter. The X-ray data indicate that cooled matter is deposited in a manner consistent with the distribution of the dark matter and so it is possible that the dark matter consists of low-mass stars formed in the cooling flow.

There is some optical evidence for gas and star formation in cooling flow galaxies. This is the main subject of this review (see also O'Connell 1987). Less than ten per cent, and typically less than one per cent, of the mass deposited is currently detectable in this way. Indeed, the mass-to-light ratio of the deposited matter is similar to that inferred by other means for the central galaxies. Whereas the interpretation of star formation in late-type galaxies proceeds mainly from the light emitted and the associated mass is inferred indirectly, the situation for cooling flows is mostly reversed. There we 'see' the mass going into stars (or at least cooling below X-ray emitting temperatures) and we are left to infer, or puzzle over, where the light is.

2. Mass Deposition in Cooling Flows

The observational evidence for cooling flows is primarily derived from the X-ray waveband. Images from the Einstein Observatory show that highly-peaked X-ray surface brightness profiles are common in 50 per cent of rich clusters (Jones & Forman 1984; Arnaud 1985; Stewart *et al.* 1984b) and are sometimes found in poor clusters (Canizares *et al.* 1983). Such profiles are deprojected and the count emissivities converted to gas density and temperature (see Fabian *et al.* 1981). They indicate high central gas densities and strong cooling. Where X-ray spectra are available of the cores of cooling clusters then low temperature components are found. The emission lines from gas around 10^7 K are particularly important (Cowie 1981). Solid State Spectrometer data (Mushotzky *et al.* 1981) and recent NRL Spartan results (Ulmer *et al.* 1987) on the Perseus cluster show clear evidence for cooling gas in the cluster core. The emission measures of cool gas deduced from the spectra agree well with those estimated from the images.

The rate at which matter is deposited as cooled gas, $\dot{M}$, is essentially deduced from the total luminosity, L, emitted within the region where the cooling time of the gas is less than some age ($\sim H_o$).

$$L \approx \frac{5kT}{2\mu m}\dot{M}.$$

T is the temperature from which the gas has cooled (typically that at the edge of the cooling region) and the factor of 5/2 includes the PdV work done on the cooling gas (*i.e.* it is the enthalpy). The above expression is only approximate as gravitational work is done on the gas if it flows inward through the cluster core and into the central galaxy.

We actually measure the surface brightness profile and thus $L(r)$ so $\dot{M}(r)$ can be determined. This mass deposition rate within radius r always increases with r. Typically $\dot{M}(r) \propto r$. The gas must be inhomogeneous in order that some gas can cool rapidly at large radii whilst other gas cools slowly there and flows into the centre. We have pursued several schemes for taking this into account, from 2 phases at each radius (Fabian *et al.* 1985) to a full multiphase analysis where the number of separate phases equals the number of radial bins into which the X-ray counts are divided (Thomas *et al.* 1987). Nulsen (1986) has developed the theory for an inhomogeneous gas with a continuous density variation. This density variation at the outer radius, together with the gravitational potential, determine how gas is deposited at smaller radii. Our results show that a relatively small spread in density (factor$\sim$ 2) is sufficient. A major problem at the moment is understanding the shape and origin of this distribution. As the intracluster gas is enriched by heavy elements some of it must have been processed through stars and it may not be surprising that it is inhomogeneous. In a typical cluster cooling flow we find mass deposited at a rate of $\sim 1\,M_\odot\,yr^{-1}\,kpc^{-1}$ out to 200 – 300 kpc where the flow time is about a Hubble time. If the spread in density persists throughout a cluster, then small amounts of matter may be cooling at very large radii ($\geq$ 500 kpc).

The whole of this Section so far assumes that the gas is cooling and that the only heat source is gravitational work. Alternative heat sources are cosmic rays (Tucker & Rosner 1982), perhaps associated with a central radio source, galaxy motions (Miller 1986) and supernovae (Silk *et al.* 1986).

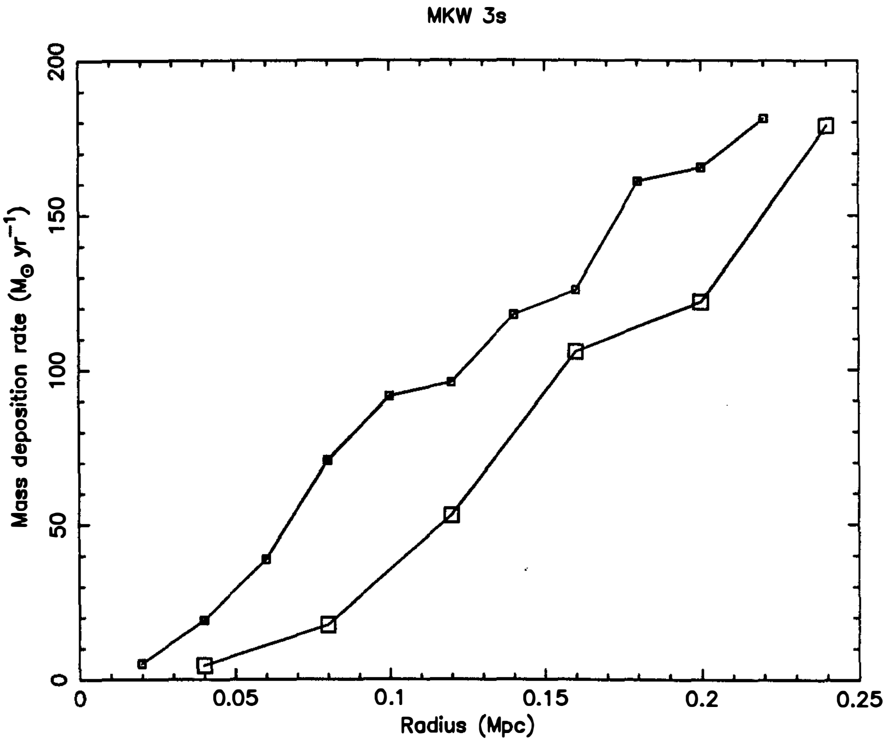

Figure 1. Profiles of mass deposition rate (*i.e.* mass cooling rate within that radius) inferred from the *Einstein Observatory* images of the poor cluster MKW3s (Thomas *et al.* 1987). The upper curve is from HRI data, the lower from IPC data which is of poorer angular resolution.

None of these addresses the problems of stability of the gas (Stewart *et al.* 1984a) or of why cooling flows occur in such a wide variety of conditions. Moreover, the total energy required over a Hubble time is 10^{62} ergs in a typical cluster flow, which corresponds to $\sim$ 100 times the (minimum) energy in the Cygnus A radio source.

The large temperature gradients set up by cooling do suggest conduction as a major heat flow. Bertschinger & Meiksin (1986), in particular, have shown that reasonable agreement with the imaging data can be obtained if (reduced) Spitzer conduction is occurring. The mass flow rate is reduced by about a factor 5 from that estimated without conduction. They do not, however, account for the low temperature spectral components that are observed or explain why X-ray peaked clusters should be common. It is shown in Stewart *et al.*(1984a) that conduction is generally either dominant in which case the gas is almost isothermal, or irrelevant. Only if the gas density is within a range of a factor of 2 of some critical value can both cooling and conduction operate. The data show clear evidence for cooling. A weak tangled magnetic field can easily reduce thermal conductivity by large factors. Such fields are surely expected in enriched intracluster gas.

I shall continue to assume that the mass deposition rates deduced without heat sources other than gravity are correct.

3. Star Formation

It is generally assumed that matter deposited in cooling flows forms into low-mass stars. The colours and magnitudes of the central elliptical galaxies are inconsistent with large rates of 'normal' star formation (Cowie & Binney 1977; Fabian, Nulsen & Canizares 1982; Sarazin & O'Connell 1983; Romanishin 1986; O'Connell 1987). By 'normal' star formation, we mean with an initial-mass-function (IMF) similar to that inferred for the Solar Neighbourhood (see *e.g.* Miller & Scalo 1979). The immediate question then is why there should be a different IMF. Some differences between cooling flows and the conditions in spiral galaxies are a) the pressure is between 10 and 1000 times higher; b) dust is unlikely to be present in the gas which cools from X-ray emitting temperatures, and c) the size of most cooled clumps may be much smalller than the Giant Molecular Clouds associated with the formation of massive stars in our Galaxy. Without a good theory of star formation we cannot be at all specific, but all of the above effects will tend to reduce the stellar mass. The average mass of the low-mass stars must be less than about $0.2\,M_\odot$ from the observed dwarf-to-giant ratio (see Arnaud & Gilmore 1985). This raises the question of whether we are chauvinists with regard to star formation and only recognise that which obviously occurs in our own Galaxy.

There is some evidence for massive stars, in particular A stars. These are seen or inferred in those cooling flows which have extensive optical emission line filaments. Perhaps only there do large clumps of cooled gas occur. A stars have been observed in NGC 1275 for some time (Rubin *et al.* 1977; Wirth *et al.* 1983) and up to 2 per cent of $\dot{M}$ may pass into massive stars (Fabian, Arnaud & Nulsen 1984; Gear *et al.* 1985). Clear evidence for a few per cent of massive star formation is found in A1795 (O'Connell 1987); NGC 6166 (Bertola *et al.* 1986) and M87 (Gunn, Stryker & Tinsley 1981). Further evidence for a small population of massive (A stars) stars in cooling flow galaxies is obtained from observations of the 4000Å spectral break (Johnstone, Fabian & Nulsen 1987). This break is weakened by hotter stars and is found to correlate with $\dot{M}$. It measures mainly the influence of main-sequence stars of a few solar masses. Ultraviolet observations are required to infer the presence of OB stars.

Johnstone, Fabian & Nulsen (1987) suggested that some OB stars are present and that they provide the ionizing radiation required to explain the high brightness of the emission line filaments.

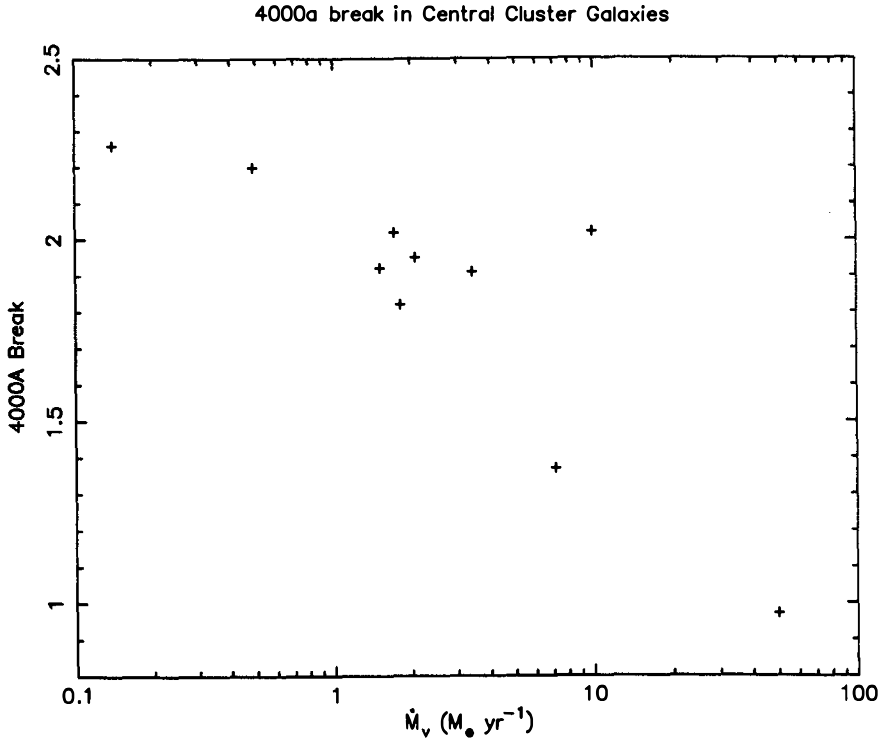

Figure 2. The 4000Å break plotted against $\dot{M}_v$, the X-ray inferred mass-deposition rate in the spectrograph slit, from Johnstone, Fabian & Nulsen (1987). Galaxies with large mass-deposition rates have less break which indicates more massive stars. The galaxy with $\sim 10\,\mathrm{M_\odot\,yr^{-1}}$ and a break of ~ 2 is in A2029 which also shows no optical line emission.

Straightforward recombination or (single) shocks predict a luminosity in the Hβ line,

$$L(\mathrm{H}\beta) \leq 10^{39} \left(\frac{\dot{M}}{100\,\mathrm{M_\odot\,yr^{-1}}} \right) \mathrm{erg\,s^{-1}},$$

which is generally unobservable. Measured values of $L(\mathrm{H}\beta)$ are typically 10 to 10^3 times larger. Whilst an IMF extending up to $60\,\mathrm{M_\odot}$ stars can explain $L(H\beta)$ in much the same way that it is explained in late-type galaxies (Kennicutt 1983), it cannot explain some of the other emission lines, in particular [OI]λ6300. This point .was made by Robinson *et al.* (1987), who show that an ionizing spectrum characterized by a 150,000 K blackbody gives a better fit to the line ratios. They suggest that the hot blackbody spectrum is radiated by the galaxy nucleus. It does have the advantage of being (mostly) unseen as the blackbody peaks in the extreme ultraviolet.

We (Johnstone & Fabian, in preparation) have done further work on the ionizing radiation from

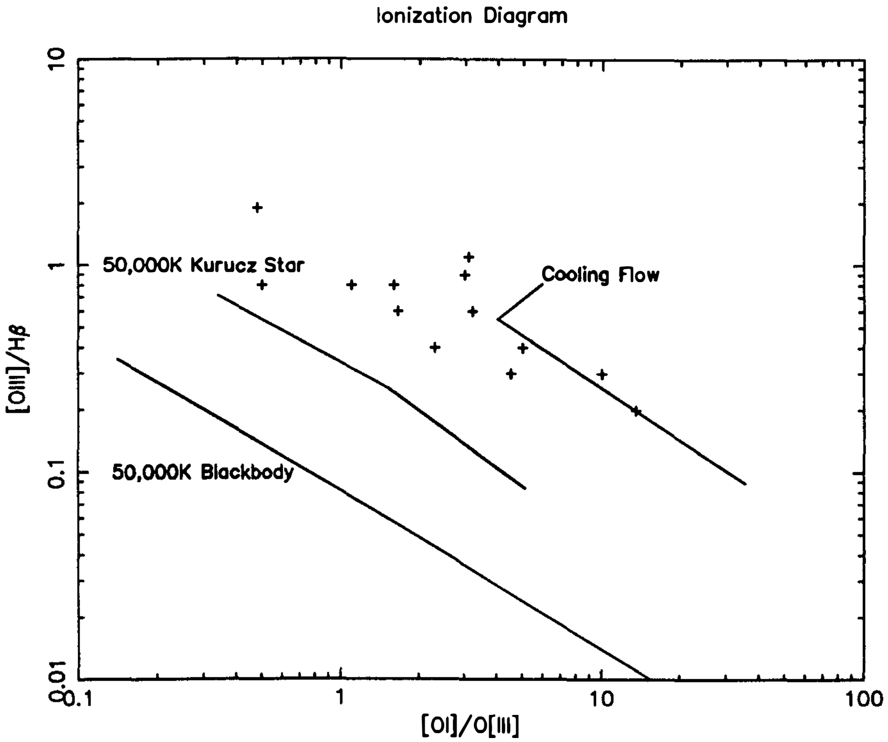

Figure 3. Oxygen line ratios expected from various ionizing sources. The choice of emission lines follows that of Robinson *et al.* (1987). The points represent observed line ratios from cooling flows.

the gas cooling immediately around large blobs. This is enhanced and gives acceptable line ratios (see Fig.3). We therefore suspect that *in situ* ionization occurs from the cooling gas and that radiation from the nucleus is not always necessary.

The overall conclusion of this work is that up to a few per cent of the mass deposition rate passes into stars more massive than $0.2\,M_\odot$. Only in PKS 0745-191 do we find any substantial rate of normal star formation at $\sim$ 10 per cent around $30 - 100\,M_\odot\,yr^{-1}$. This fraction passing into massive stars appears to be associated with optical filaments and large blobs. It is possible that isochoric cooling in these blobs allows lower pressures to transiently occur and so raise the Jeans mass. More plausible perhaps is the notion that massive stars form in massive clouds and low mass stars form in low mass clouds (Larson 1982). This is somewhat akin to the bimodal star formation discussed elsewhere in these Proceedings. It is interesting that

$$\frac{\dot{M}(\text{`normal' IMF})}{\dot{M}(\text{low} - \text{mass IMF})} \approx \frac{M(\text{visible})}{M(\text{dark})}$$

in the central galaxies. The reason for this ratio (say, large clouds to small clouds) is not understood at all at present.

There is some other evidence for star formation in cooling flows. The galaxy NGC 4406 (M86) appears to be plunging through the Virgo cluster at $\sim 1500 - 2000\,\mathrm{km\,s^{-1}}$. Its hot interstellar medium is being pushed out by the ram pressure of the Virgo intracluster gas and appears as a 'plume' of emission Forman *et al.* (1979). Nulsen & Carter (1987) find an optical asymmetry of M86 which matches this plume and they suggest that it is due to star formation in the cooling gas in the plume. The mean mass of stars created there must be 1 $M_{\odot}$. Perhaps turbulence in the gas, which is experiencing a large stress, causes small gas blobs to coalesce so that larger blobs are created. Disturbances within the cooling gas in more isolated ellipticals may have a similar effect and produce observable stars. If the disturbance propagates from the centre of the galaxy then it can create shells such as those found by Malin & Carter (1980). Providing that the disturbance triggers observable star formation on less than a galactic free-fall time, then phase-wrapping (Quinn 1984) gives the shells (Loewenstein, Fabian & Nulsen 1987). The rate of star formation is typically one hundred times greater in the centre of a cluster cooling flow, so the supershells recently discovered by Soucail *et al.* (1987) and Petrosian & Lynds (1986) could also have a similar origin.

4. Distant Cooling Flows

Galaxies consisted orginally of large clouds of gas. If a large fraction of that gas was ever virialized before cooling then the conditions must have been very similar to those in nearby cooling flows. The dense core of such a cloud need not have been virialized and may well have rapidly collapsed into massive stars which exploded and enriched the whole cloud with gas. The dark haloes around many galaxies, which represents most of their mass, is then formed by cooling flows. This implies that flows of hundreds to tens of thousands of solar masses per year must have once been common. Unfortunately, most of the energy release is in the unobservable ultraviolet.

What we can search for is indirect evidence of large cooling flows in the past. One possible class of candidates are the 3CR galaxies observed out to a redshift, z, of ~ 1.8 (McCarthy *et al.* 1987) and perhaps even PKS1614+051 at z ~ 3.2 (Djorgovski *et al.* 1985). Spinrad & Djorgovski (1984a, b), McCarthy *et al.* (1987), Heckman *et al.* (1987) and Stockton & MacKenty (1987) have all found extensive optical line filaments around radio galaxies and quasars. Principally, they interpret the

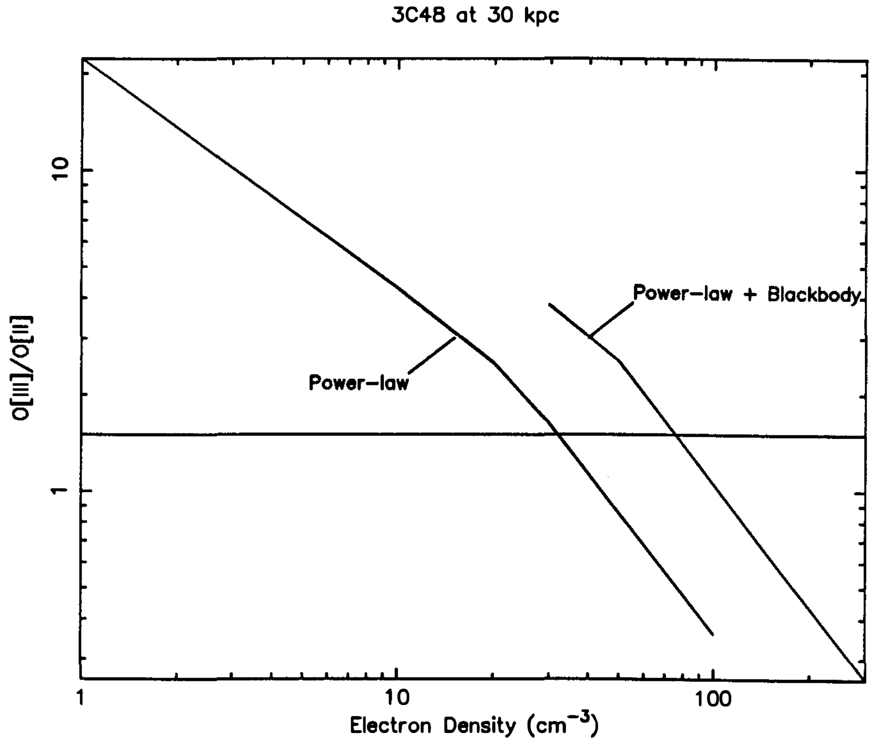

Figure 4. Dependence of the ratio of oxygen lines on gas density in the ionizing radiation expected at 30kpc from 3C48 (see Fabian *et al.* 1987 for details).

emission as due to mergers. In many respects, however, the emission regions show strong resemblances to the filaments around NGC 1275 in the Perseus cluster. This is particularly true of 3C275.1 (Hintzen & Romanishin 1986). Perhaps the best support for a cooling flow interpretation, apart from extended X-ray emission, would be evidence of a high gas pressure ($nT \geq 10^5$ cm^{-3} K; Fabian *et al.* 1986).

We (Fabian *et al.* 1987) have obtained indirect evidence for a high surrounding pressure in the case of the z = 0.37 quasar, 3C48. The ionization state of the emission line filaments, which extend to 35 kpc radius, is relatively low in the sense that the ratio [0III]λ5007: [0II] λ3727 is$\sim$ 1.5. We assume that in this case the quasar nucleus provides the ionizing radiation since its luminosity L_Q is $10^{46}\,\mathrm{erg\,s^{-1}}$ and its ultraviolet and X-ray spectrum (Wilkes & Elvis 1987) is similar to that of 3C273. The ionization state of the gas depends on L_Q/nR^2, so knowing L_Q and the radius of the gas from the nucleus, R, we can determine the gas density, n, through a photoionization balance computation. We used Ferland's code for this and deduce that $n \sim 30\,\mathrm{cm}^{-3}$. The conditions and

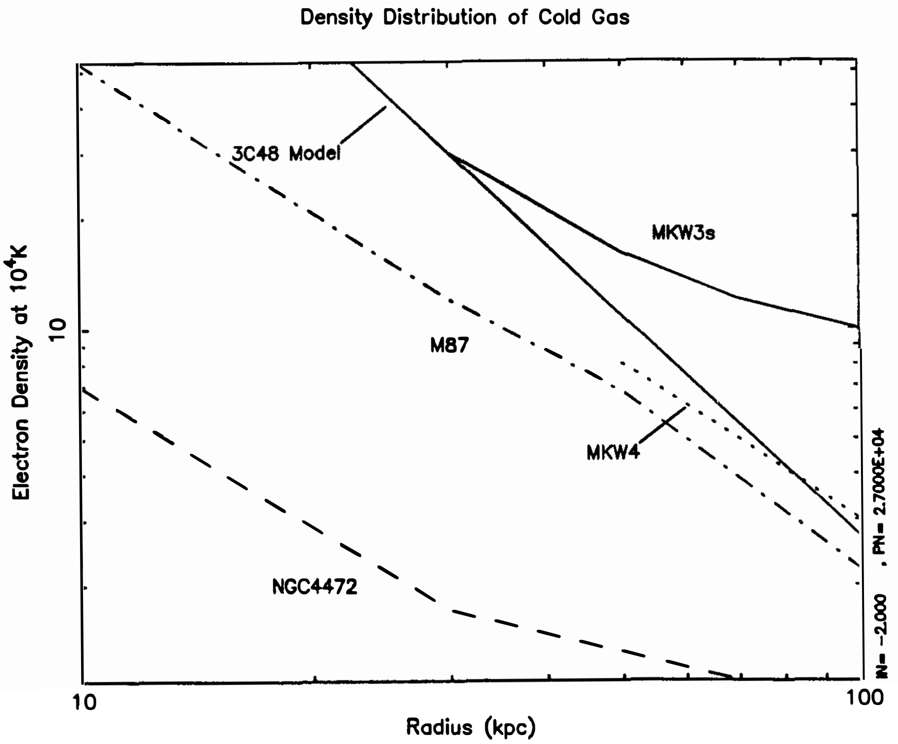

Figure 5. Density of gas at 10^4K in pressure equilibrium with the surrounding hot gas observed with X-rays for MKW3s ($100\,M_\odot\,yr^{-1}$), MKW4 ($30\,M_\odot\,yr^{-1}$), M87 ($10\,M_\odot\,yr^{-1}$) and NGC4472 ($1\,M_\odot\,yr^{-1}$). The density inferred for the optically detected gas around 3C48 is indicated by the power-law of slope -2.

pressure ($T \sim 10^4$K for the optical gas) are then very similar to those in the poor cluster cooling flow in MKW 3s ($\dot{M} \sim 100\,M_\odot\,yr^{-1}$; Canizares *et al.* 1983).

The total mass of cooled gas detected in our slit is $\sim 3 \times 10^8\,M_\odot$ and it must lie in blobs or sheets thinner than 10 pc in order to be ionized sufficiently. If these blobs are due to a collision or merger, as commonly supposed, then the gas would be unconfined and dissipate on $\sim 10^6$ yr. As the emission extends by more than 50 kpc and a merger is unlikely to take place at velocities greater than $100\,km\,s^{-1}$, it seems that the emission must last for at least 5×10^8 yr. Otherwise just a small patch of emission would light up at any given time. Consequently, the merger hypothesis requires ≥ 500 times more gas, (which must also be exceptionally dense), so that $\geq 10^{11}\,M_\odot$ of gas is needed in all. There is probably much more gas outside our slit. This seems to us to be an unacceptably large mass of gas for any known type of galaxy, and casts strong doubt on the merger hypothesis. Whether we can be equally specific about other quasars remains to be seen and depends on detailed spectroscopy being available.

A rate of $100\,M_\odot\,yr^{-1}$ around a relatively nearby quasar does not explain all quasar 'fuzz'. It can help to explain some of the blue colours and star formation. Boroson & Oke (1984) have found clear spectral evidence for A stars around 3C48. To go further we need to spatially resolve the emission from more distant objects. An alternative approach is to rely on absorption lines. If large cooling flows are common then they may cover a significant fraction of the sky and the cooled gas may give narrow absorption lines in background QSOs (Crawford *et al.* 1987). Such lines are, of course, observed (Weymann, Carswell & Smith 1981) and otherwise remain a puzzle. Multiple lines are easily explained as due to filaments suspended in the hot gas.

An even more tantalizing possibility is that of Lyα clouds observed by their absorption of the light from background QSOs. These clouds are normally considered to be low-pressure fluffy things with sizes of ~ 10 kpc. Barcons & Fabian (1987) have shown that they can alternatively be thin sheets with a major axis of only a few parsec. This allows them to be at high pressure and explains the observed column density distribution (Carswell *et al.* 1986). These thin clouds could be the blobs that form the low-mass stars in distant cooling flows. Non-spherical blobs are extremely likely to collapse into sheets, as in supernova remnants (Schwarz *et al.* 1972) and the number of such clouds expected at around 10^4 K in a large cooling flow allow for a reasonable covering fraction. There is a major problem in this hypothesis, however, in that the clouds must present a much smaller covering fraction as the cooling slows below 10^4 K. It is possible that the sheets continue to collapse transversely and are rolled up into spheres so that their surface area is much reduced. This is, of course, necessary if they are to eventually condense into stars. More work is needed.

5. Conclusions

a) Cooling flows are common and represent large regions of star formation, especially of low-mass stars.

b) (Some) dark matter is baryonic and is forming into low-mass objects now.

c) Star formation is multimodal and depends upon environment. The formation of massive stars may be peculiar to spiral arms and irregular galaxies.

d) Cooling flows provide nearby examples of dissipational galaxy formation.

e) We badly need more X-ray data!

Acknowledgements Peter Thomas, Roderick Johnstone and Carolin Crawford are thanked for much help and discussions.

References

Arnaud, K.A., 1985. *PhD thesis*, University of Cambridge.
Arnaud, K.A. & Gilmore, G., 1986. *Mon. Not. R. astr. Soc.*,**220**, 759.
Barcons, X. & Fabian, A.C., 1987. *Mon. Not. R. astr. Soc.*,**224**, 675.
Bertola, F., Gregg, M.D., Gunn, J.E. & Oemler, A., 1987. *Astrophys. J.*, **303**, 624.
Bertschinger, E. & Meiksin, A., 1986. *Astrophys.J*, **306**, L1.
Boroson, T.A. & Oke, 1984. *Astrophys. J.*, **281**, 535.
Canizares, C.R., Stewart, G.C. & Fabian A.C., 1983. *Astrophys. J.* , **272**, 449.
Carswell, R.F., Webb, J.K., Baldwin, J.A. & Atwood, B., 1987. *Astrophys. J.*, in press.
Cowie, L.L., 1981. in *X-ray Astronomy with the Einstein Satellite*, ed. R.Giacconi, 227, (Reidel).
Cowie, L.L. & Binney, J., 1977. *Astrophys. J.*, **215**, 723.
Crawford, C.S., Crehan, D.A., Fabian, A.C. & Johnstone, R.M., 1987. *Mon. Not. R. astr. Soc.*, **224**, 1007.
Djorgovski, S., Spinrad, H., McCarthy. P. & Strauss, M.A., 1985. *Astrophys. J.*, **299**, L1.
Fabian, A.C., Hu, E.M., Cowie, L.L & Grindlay, J.,1981. *Astrophys. J.*, **248**, 47.
Fabian, A.C., Nulsen, P.E.J. & Canizares, C.R., 1982. *Mon. Not. R. astr. Soc.*, **201**, 933.
Fabian, A.C., Nulsen, P.E.J. & Canizares, C.R., 1984. *Nature*, **311**, 733.
Fabian, A.C., Nulsen, P.E.J. & Arnaud, K.A., 1984. *Mon. Not. R. astr. Soc.*, **208**, 179.
Fabian, A.C. *et al.*, 1985. *Mon. Not. R. astr. Soc.*, **216**, 923.
Fabian, A.C., Arnaud, K.A., Nulsen, P.E.J. & Mushotzky, R.F., 1986. *Astrophys. J.*, **305**, 9.
Fabian, A.C., Crawford, C.S., Johnstone, R.M. & Thomas, P.A., 1987. *Mon. Not. R. astr. Soc.* in press.
Forman, W., Schwarz, J., Jones, C., Liller, W. & Fabian, A.C., 1979. *Astrophys. J.*, **234**, L27.
Gear, W.K., Gee., G., Robson, E.I. & Nott, I.G., 1985. *Mon. Not. R. astr. Soc.*, **217**, 281.
Heckman, T. *et al.*, 1986. *Astrophys. J.*,**311**, 526.
Hintzen, P. & Romanishin, W., 1986. *Astrophys. J.*,**311**, L11.
Jones, C. & Forman, W., 1984. *Astrophys. J.*, **276**, 38.
Jaffe, W., 1987. *Astr. Astrophys.*, ,.
Johnstone, R.M., Fabian, A.C. & Nulsen, A.C., 1987. *Mon. Not. R. astr. Soc.*, **224**, 75.
Kennicutt, R.C., 1983. *Astrophys. J.*, **272**, 54.
Larson, R.B., 1982. *Mon. Not. R. astr. Soc.*, **200**, 159.
Loewenstein, M., Fabian, A.C. & Nulsen, P.E.J., 1987. Preprint.
Malin, D. & Carter, D., 1980. *Nature*, **280**, 643.
McCarthy, P. *et al.*, 1987. Preprint.
Miller, L., 1986. *Mon. Not. R. astr. Soc.*, **220**, 713.
Miller, G.E. & Scalo, J.M., 1979. *Astrophys. J.Supp*, **41**, 513.
Mushotzky, R.F., Holt, S.S, Smith, B.W., Boldt, E.A. & Serlemitsos, P.J., 1981. *Astrophys. J.*, **244**, L47.
Nulsen, P.E.J., 1986. *Mon. Not. R. astr. Soc.*, **221**, 377.
Nulsen, P.E.J. & Carter, D., 1987. *Mon. Not. R. astr. Soc.*, **225**, 939.
O'Connell, R.W., 1987. in *Proc. I.A.U. Symp. No. 126*, in press.
Petrosian, V & Lynds, R., 1986. *B.A.A.S.*,**18**, 1014.
Quinn, P., 1984. *Astrophys. J.*, **279**, 596.
Robinson, A., Binette, L., Fosbury, R.A.E. & Tadhunter, C., 1987. *Mon. Not. R. astr. Soc.* in press.
Romanishin, W., 1985. *Astrophys. J.*, **289**, 570.
Rubin, V.C., Ford, W.K., Peterson, C.J. & Oort, J.H., 1977. *Astrophys. J.*, **211**, 693.
Sarazin, C.L., 1986. *Rev. Mod. Phys.*, **58**, 1.
Sarazin, C.L. & O'Connell, R.W., 1983. *Astrophys. J.*, **258**, 552.
Schwarz, J., McCray, R. & Stein, R.F., 1972. *Astrophys. J.*, **175**, 673.
Silk, J., Djorgovski, G., Wyse, R.F.G. & Bruzual, G.A., 1986. *Astrophys. J.*, **307**, 415.
Soucail, G., Fort, B., Mellier, Y. & Picat, J.P.,1987. *Astr. Astrophys.*, **172**, 44.
Spinrad, H. & Djorgovski, G., 1984a. *Astrophys. J.*, **280**, L9.
Spinrad, H. & Djorgovski, G., 1984b. *Astrophys. J.*, **285**, L49.
Stewart, G.C., Canizares, C.R., Fabian, A.C. & Nulsen, P.E.J., 1984a. *Astrophys. J.*, **278**, 536.
Stewart, G.C., Fabian, A.C., Jones, C. & Fabian, A.C., 1984b. *Astrophys. J.*, **285**, 1.
Stockton, A. & MacKenty, J.W., 1987. *Astrophys. J.*, **316**, 584.
Thomas, P.A., Fabian, A.C. & Nulsen, P.E.J., 1987. *Mon. Not. R. astr. Soc.* in press.
Tucker, W.H. & Rosner, R., 1982. *Astrophys. J.*, **267**, 547.
Ulmer, M. *et al.*, 1987. Preprint.
Weymann, R.J., Carswell, R.F. & Smith, M.G., 1981. *Ann. Rev. Astr. Astrophys.*,**19**, 41.
Wirth A., Kenyon, S.J. & Hunter, D.A., 1983. *Astrophys. J.*, **269**, 102.

STAR FORMATION IN ELLIPTICAL GALAXIES AT HIGH REDSHIFT

Robert W. O'CONNELL
Astronomy Department
University of Virginia
Charlottesville, VA 22903 USA

ABSTRACT

The evidence that star formation continued in some elliptical galaxies until recent epochs, $\sim$ 5-8 Gyr ago or z $\sim$ 0.5-1.5, is reviewed with emphasis on observations of nearby systems and the intepretation of high redshift colors. Starbursts may have been a factor in the evolution of all types of galaxies in the relatively recent past.

I. Introduction

Elliptical galaxies, unlike most of the systems discussed at this conference, typically exhibit little outward evidence of star formation. In fact, the conventional view is that they have been quiescent for most of a Hubble time, having completed formation in a rapid collapse and spectacular starburst at high redshifts, $z > 5$. If this is true, we will be deprived of a detailed observational understanding of this event for many years to come because the technical difficulty in studying objects at such high redshifts is formidable.

Fortunately, there is now strong evidence that this conventional view is incorrect, in the sense that star formation in some ellipticals continued until recent epochs, $z < 1.5$. Therefore, the prospects for direct observation of important (if not initial) evolutionary processes in ellipticals at $z \sim 0.5$-1.5 are good. The evidence is based on observations of both local and high redshift systems, and I will review that here with emphasis on the former. In their talks, Djorgovski and Soucail will describe high redshift observations in more detail, including the detection of objects at $z \lesssim 3$ which bear a remarkable resemblance to proto-galaxies.

II. The Conventional View: Ancient Elliptical Galaxies

The conventional interpretation is that all significant star formation was completed in E galaxies not long after the globular cluster formation epoch, 14-16 Gyr ago. This interpretation rests mainly on the following four areas of evidence:

a) Pop II in M32 and the bulge of M31. The resolution of Pop II giants in these nearby galaxies was the final stimulus for the concept of stellar populations formulated by Baade [1]. This was such a powerful, unifying interpretation [2] that its apparent implication--namely that E galaxies and spiral bulges were old, metal deficient, Pop II systems--held sway long past the point when it became clear that this could not be the whole story.

b) The homogeneity of E/SO colors and spectra. The colors and spectra of E/SO's are remarkably uniform, and their cool, red character suggests that these are old systems with a small dispersion of star formation histories formed by a common mechanism [3,4].

c) Continuity of globular clusters and E/SO galaxies. There is an impressive continuity between globulars and E/SO galaxies in some photometric and spectroscopic properties [e.g., 5,6], which suggests that these are all systems of similar age but different chemical content, with the galaxies being more metal rich. I think this is the strongest evidence in support of the conventional interpretation.

d) Synthesis models of E galaxies. Evolutionary synthesis models produced by a number of different investigators agree that the broad-band colors of E/SO's are consistent with ages of 10-15 Gyr if the metal abundance is solar or below ($Z \leq Z_{\odot}$) [7].

III. Difficulties with the Conventional View: Late Evolution of E Galaxies

Until the last few years, the foregoing evidence had not been subjected to critical examination, and perhaps there was no reason to do so. Newer work, however, casts significant doubt on all four pillars of the conventional view. Let me cover this in the same order:

a) Pop II in E galaxies. While there are certainly metal poor Pop II giants in E galaxies and spiral bulges, they represent only a minority component, a bright "frosting" on the color-magnitude diagrams (CMD's). It has been clear since the work of Morgan and Mayall [8] and Baum [9] that the dominant population is metal rich, with $Z \gtrsim Z_{\odot}$. Recent CMD studies of the Galactic bulge [10] and M32 [11] show that the giant branch extends to very cool, metal rich objects (M7 III equivalent in the case of M32).

b) Homogeneity. The implications of color homogeneity must be considered quantitatively. As discussed below in Sec. V, the colors of older galaxies evolve slowly. For example, the FWHM of the U-R histogram for E/SO galaxies in the sample of Sandage and Visvanthan [4], which is fully corrected for metal abundance effects, is only 0.3 mag, but this corresponds to a factor of 2 in age for systems with a given chemical composition.

c) Continuity. Newer studies of both broad band colors and individual spectral features show important differences between globular clusters and galaxies (reviewed in [12,13]). These represent unambiguous and model-independent evidence that globulars and E galaxies do not form a physical continuum and hence do not necessarily have similar ages.

d) Synthesis models. The solar-abundance synthesis models for E/SO's cited above are inappropriate because their nuclei have high metallicities ($Z \gtrsim 2\text{-}3\ Z_\odot$)and shallow line strength gradients indicate possibly supersolar abundance for their integrated light as well [14,15]. For a given set of photometric properties, the inferred age of a population decreases as Z increases [16]. When proper account of this effect is taken, one finds that both evolutionary studies and detailed optimizing spectral synthesis studies yield ages for the last epoch of star formation in E galaxies in the range 5-8 Gyr. No evidence is found for a large 15 Gyr-old component. This work has been reviewed recently in some detail [13,16,17,18], and I do not wish to dwell on it here. I will take the opportunity, however, to respond in Sec. IV to some recent criticisms of these techniques.

Collectively, items (a)-(c) remove the basis for supposing that E galaxies are physically similar to globular clusters--i.e. ancient systems with a small age dispersion. The models cited in (d) indicate that star formation in at least some E/SO's (those near enough to obtain high precision spectrophotometry, typically with $V \lesssim 3000$ km sec^{-1}) continued until recent epochs. For technical reasons explained in [16], it is difficult to determine the earlier history of star formation in E's or to strongly constrain the age of the first generation of stars, which could well be 15 Gyr.

One cannot ignore in this context the wealth of information on stellar populations and dynamics in the disk and bulge of our own Galaxy. The classical interpretation of this data is that the Galaxy formed in a rapid collapse 15 Gyr ago [2,10].

Nonetheless, I think one ought to be careful in extrapolating these results to E's. The history of star formation in the Galactic disk is obviously not similar to that in E's, and the CMD results for the Galactic bulge are controversial [e.g. 38] and demand careful separation of abundance effects (including blanketing) from age effects. Spiral bulges may in any case not closely resemble E's [20].

Furthermore, dynamical revisionists are hard at work rewriting the history of both the Galactic disk [21] and bulge [22] and in particular suggesting that some of the metal poor components, which in the classical scenario form during the initial collapse, were actually accreted from outside after the Galactic disk was in place. Finally, new results on the age of the disk as determined from white dwarf luminosities yield low values $\lesssim$ 10 Gyr, comparable to those cited above [23].

I conclude that the conventional view of E galaxy histories is not supported by the evidence for local E's and that their star formation was not completed during the globular cluster formation epoch. The best evidence is that this continued until as recently as 5-8 Gyr ago.

IV. Concerns About Synthesis Modeling

This conclusion is controversial and, while it is only one of several lines of evidence, the validity of the synthesis modeling described in (d) above has occasionally been questioned, most recently by Renzini [19]. One issue he discussed was the effect of metallicity mixtures on synthesis models, but these, though surely present, appear not to influence the age-dating strongly [16,18]. I think it is worthwhile responding here to several of the other concerns Renzini raised.

Renzini's most serious criticism was that the age of a stellar population cannot be reliably determined from the color of its main sequence turnoff, and, since this is the basis of synthesis age-dating techniques, these are suspect. He claimed that estimating the age of the globular 47 Tuc by this method leads to an unacceptably young value and that a similar problem affects the E galaxy ages quoted above. This argument, if generalized, would render a very large body of integrated light work on galaxies questionable, and much is clearly at stake here.

Renzini's argument overlooks the problem of differential blanketing in converting the observed color of 47 Tuc's turnoff to an effective temperature. He used a $Z = Z_\odot$ color/T_e conversion, whereas for 47 Tuc, $Z = 0.20\ Z_\odot$. After making appropriate blanketing corrections, which, of course, decrease the inferred T_e at turnoff, one finds an age for 47 Tuc comparable to those of other globulars, 14-16 Gyr. The turnoff color-dating method thus appears to be reliable.

Renzini's other major criticsm involved the theoretical isochrones used to calibrate ages derived by the synthesis method. It is well known that the Yale isochrones, widely used in synthesis work, require temperature corrections because they assumed too small a convective mixing length. Renzini argued, correctly, that the simple adjustments made to the Yale isochrones by most authors were inadequate and that a self-consistent treatment of convection in cool stars could significantly affect the dating calibration. Calibrations with an improved treatment of convection by VandenBerg [24] and VandenBerg and Laskarides [25] are shown in Figure 1, and, indeed, the slope of the newer calibration is significantly different than the corrected Yale calibration. Fortuitously, however, the VandenBerg calibration yields the *same turnoff ages* as the older calibration for the (B-V turnoff color, Z) values appropriate for well-studied E galaxies, (0.50, $Z_\odot$) for M32 and (0.65, 2-3 $Z_\odot$) for gE's. Thus, this isochrone recalibration does not alter the conclusion reached by the synthesis studies for the star formation history of E galaxies.

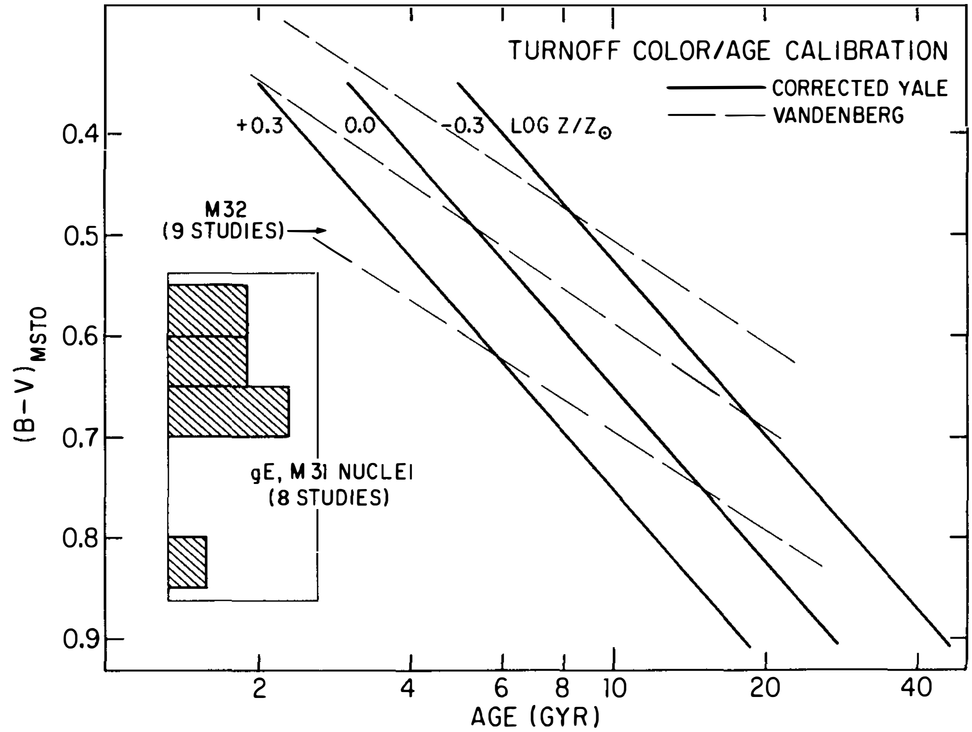

Figure 1: Calibration of the main sequence turnoff color-metallicity-age relation based on the corrected Yale isochrones and on newer calculations by VandenBerg. The slope of the two calibrations is significantly different, presumably because of different treatments of convection and the temperature-color conversion. At the left are turnoff colors derived from a number of synthesis studies for M32 and gE galaxies [see 16]. For the particular mean turnoff colors and metallicities of these objects, the VandenBerg calibration yields the same age dating as the corrected Yale calibration. The log $Z/Z_{\odot}$ = + 0.3 VandenBerg calibration plotted does not include correction for the (unidentified) effect which produces a mismatch with observed cluster main sequences and with the sun [24]. This might shift the line another 0.05 mag redward in B-V, yielding yet younger gE turnoffs.

I am sure this controversy will continue. At present, however, I see no promising way to reconcile the data on local ellipticals with star formation completion ages of order 15 Gyr.

V. Interpretation of Colors of High Redshift Systems

What do direct observations of systems in earlier phases of evolution say about this problem? One fundamental difficulty is that we have very little morphological information on distant galaxies, and the type of objects being observed (E, SO, spiral, or other) is largely conjectural. Even worse, mergers and other interactions can change the morphology of galaxies, so that the ancestor of a local E may not resemble it at all.

It is now well established that the color distribution of bright galaxies changes unexpectedly quickly with redshift (the "Butcher-Oemler" effect), so that by $z \sim 0.3-0.5$, unusually blue objects appear in clusters and the field (see the review by Oemler [26]). These changes are inconsistent with the "standard" evolutionary model for galaxies, which assumes that all galaxies evolve in isolation, are 15 Gyr old, and experience an exponentially declining star formation rate with a range of e-folding times. Evolutionary mechanisms rather different from those which dominate now must be prevalent at even these modest lookback times.

An important feature of the available observations of high redshift systems is the existence of a "red envelope" in the color-redshift diagrams [e.g. 28]. This presumably consists of systems which have been quiescent for a sufficiently long period. It is usually identified with elliptical galaxies and is taken to imply that most E's completed star formation at an early epoch.

What I think may not be widely appreciated is how short this "sufficiently long period" can be. The photometric evolution of quiescent systems to the vicinity of the red envelope is very rapid, taking place in only 1-2 Gyr. Very little color evolution occurs later. The effect is present, for example, in the evolutionary models of Bruzual [29] and Wyse [30], who find that the colors of gE galaxies for $z \lesssim 0.5$ are fitted equally well by ages of 8 Gyr or of 15 Gyr, with even younger ages favored if gE's have supersolar mean metal abundances.

To be somewhat more quantitative, the precision with which photometric measures have been made on high redshift galaxies is only about 0.2 mag (2σ). Various photometric indices of galaxy age evolve so slowly for $t > 1$ Gyr that this observational uncertainty translates into significant age uncertainty. The following table is based on single generation population models by several authors [28,31,33], and the age error factors are obtained by converting the 0.2 mag observational error into an age ratio.

Quantity (Restframe)	$\partial Q/\partial \log t$	Age Error Factor
U-R	0.95	1.6
4000 A Break (mag)	0.37	3.5
B-V	0.33	4.0
V-K	0.47	2.7

It is clear from these error factors that existing observations of systems near the "red envelope" permit a wide range of star formation histories.

This point is also illustrated in Figure 2, where I plot the U-V evolution of bursts of star formation. The plot is in the form often used to display observational results (color vs. z) but is given for the color in the restframe to avoid the complications arising from K corrections. Two burst times are shown, $z = 1.5$ and $z = 0.75$ (corresponding to lookbacks of 7.8 and 5.6 Gyr in the adopted cosmology). The most notable aspect of the plot is the very rapid color decay of the burst with redshift. The burst has a full width at "half color peak" of only about 0.05 in z. Even when 30% of the mass of the galaxy is involved in the $z = 0.75$ burst, the color is within 0.2 mag of a quiescent object by $z = 0.3$. It should be noted that restframe U-V is somewhat more sensitive to the effects of the burst than the laboratory frame B-V and V-R colors which are usually displayed in this kind of plot.

Thus, the existence of a well defined "red envelope" does not preclude major star forming activity in E galaxies as recently as $z \sim 0.5$-1.5, and the

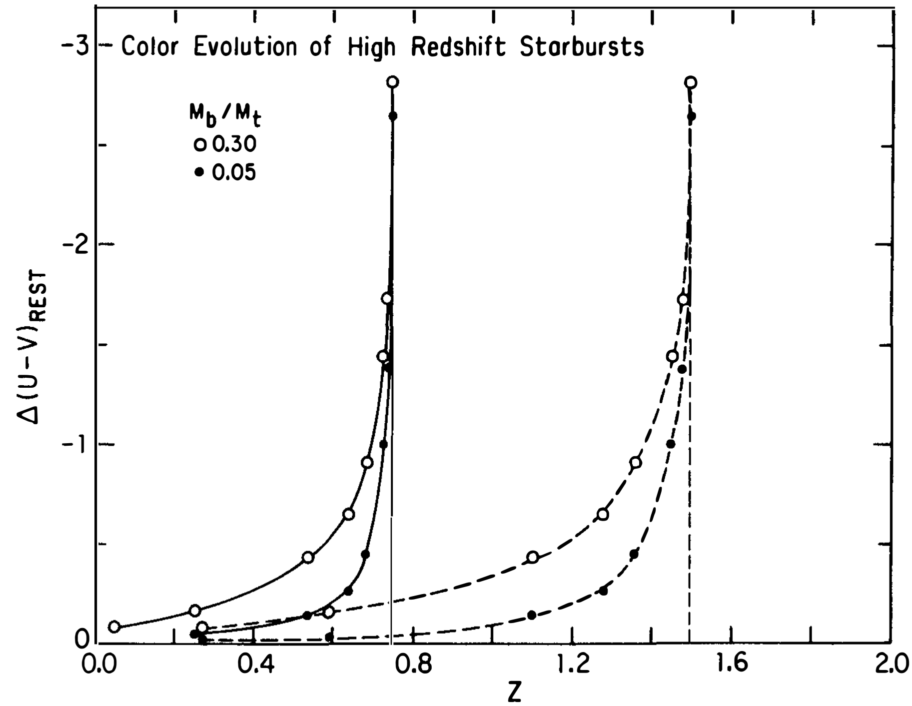

Figure 2: Redshift evolution of the broad band U-V color in the restframe for starbursts occurring in old gE galaxies. Starburst colors are taken from Larson and Tinsley [31]; the burst is assumed to last for 0.01 Gyr. Two burst times, z = 0.75 and z = 1.50, and two burst strengths, 5% and 30% of the galaxy (visible) mass, are shown. The color of the undisturbed gE was taken to be (U-V) = 1.66. H_o = 75 km s^{-1} Mpc^{-1} and q_o = 0 were adopted. Note the extremely rapid decay of the color of the galaxy. Effects of emission lines are not included. These would probably not have strong effects on the restframe U-V evolution but could significantly affect the color excursions exhibited by bursts in the laboratory frame, depending on the redshift involved and filters used.

local evidence appears to require this. Some of the anomalously blue high redshift objects are certainly E's [27,32,36]. It is not impossible that most E's experienced significant late epoch star formation.

A number of workers have pointed out that significant color excursions can be produced by a burst of star formation involving only a small fraction of a galaxy's mass (e.g. 26,27). A glance at the U-V evolution in Figure 2 of a burst involving only 5% of the mass confirms that remark. However, the lifetime of a large color excursion is also very short, so that if a large fraction of a sample of high redshift galaxies exhibit color anomalies, this implies a significant net star formation rate. A statistical analysis of the color distribution in the context of burst models would be worthwhile.

Overall, I think the evidence discussed here supports the view that environmental interactions (infall, tidal encounters, mergers, gas flows, etc.) importantly shape the evolution of galaxies at moderate lookbacks and that E galaxies are not immune to these processes. Ellipticals which happen to complete star formation ealry will occupy the red envelope at high redshifts, but others may experience a prolonged series of star forming episodes which might continue to $z \lesssim 0.5$. Some of these events might well qualify as the kind of "starbursts" discussed in the context of other types of galaxies at this conference. Rapid photometric evolution following the last episode will leave the E's with the cool, reddish colors familiar in nearby systems. It is worth pointing out that recent theoretical studies of galaxy formation are consistent with this evidence for late evolution of ellipticals [37].

VI. Conclusion

On the basis of detailed studies of local systems and the color distribution of high redshift galaxies, it appears that some E galaxies continued forming stars until relatively recent epochs, 5-10 Gyr ago. The prospects for direct observation of basic evolutionary processes in elliptical systems at low redshifts, $z \lesssim 1.5$, where considerable observational firepower may be brought to bear, are therefore quite good. The kind of starbursts we observe only under unusual circumstances at the current epoch may have been common in all types of galaxies in the relatively recent past.

REFERENCES

1. Baade, W. 1944, Ap. J. 100, 137.
2. Sandage, A. 1986, Ann. Rev. Astr. Ap., 24, 421.
3. Lasker, B. M. 1970, A J., 75, 21.
4. Sandage, A. and Visvanathan, N. 1978, Ap. J., 225, 742.
5. McClure, R. D. and van den Bergh, S. 1978, A. J., 73, 313.
6. Faber, S. M. 1973, Ap. J., 179, 731.
7. Tinsley, B. M. 1980, Fund. Cosmic Phys., 5, 287.
8. Morgan, W. W., and Mayall, N. U. 1957, P.A.S.P., 69, 291.
9. Baum, W. A. 1959, P.A.S.P., 71, 106.
10. Whitford, A. E. 1985, P.A.S.P., 97, 205.
11. Seitzer, P. O., and O'Connell, R. W. 1987, in preparation.
12. Burstein, D., Faber, S. M., Gaskell, C. M., and Krumm, N. 1984, Ap. J., 287, 586.
13. O'Connell, R. W. 1986, in [35], p. 321.
14. Faber, S. M. 1977, in Evolution of Galaxies and Stellar Populations, eds. B. M. Tinsley and R. B. Larson (New Haven: Yale University Observatory), p. 157.
15. Baum, W. A., Thomsen, B., and Morgan, B. L. 1986, Ap. J., 301, 83.
16. O'Connell, R. W. 1986, in [34], p. 167.
17. Burstein, D. 1985, P.A.S.P., 97, 89.
18. Pickles, A. J. 1987, in Structure and Dynamics of Elliptical Galaxies, ed. T. de Zeeuw (Dordrecht: Reidel), in press.
19. Renzini, A. 1986, in [34], p. 213.
20. Wirth, A. and Shaw, R. 1983, A. J., 88, 171.
21. Freeman, K. C. 1986, in [34], p. 227.

22. Norman, C. A. 1987, this conference.

23. Winget, D. E., Hansen, C. J., Liebert, J., Van Horn, H. M., Fontaine, G., Rather, R. E., Kepler, S. O., and Lamb, D. Q. 1987, Ap. J. (Letters), 315, L77.

24. VandenBerg, D. A. 1985, Ap. J. Supp., 58, 711.

25. VandenBerg, D. A. and Laskarides, P. G. 1987, Ap. J. Suppl., 63.

26. Oemler, A. 1986, in [34], p. 197.

27. Eisenhardt, P. R. M., and Lebofsky, M. J. 1987, Ap. J., 316, 70.

28. Hamilton, D. 1985, Ap. J., 297, 371.

29. Bruzual, A. G. 1986, in [35], p. 263.

30. Wyse, R. F. G. 1985, Ap. J., 299, 593.

31. Larson, R. B., and Tinsley, B. M. 1978, Ap. J., 219, 46.

32. Thompson, L. A. 1986, Ap. J., 300, 639.

33. Rabin, D. M. 1980, Ph.D. Thesis, California Institute of Technology.

34. Stellar Populations, eds. C. Norman, A. Renzini, and M. Tosi (Cambridge: Cambridge University Press), 1986.

35. Spectral Evolution of Galaxies, eds. C. Chiosi and A. Renzini (Dordrecht: Reidel), 1986.

36. Djorgovski, S. 1987, this conference.

37. Baron, E., and White, S. D. M. 1987, preprint.

38. Wood, P. R. and Bessell, M. S. 1983, Ap. J., 265, 748.

STAR FORMATION IN ACTIVE GALAXIES AND QUASARS

Timothy M. Heckman
Astronomy Program
University of Maryland
College Park, Maryland
U.S.A.

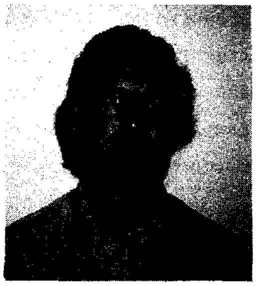

I review the observational evidence for a causal or statistical link between star formation and active galactic nuclei. The chief difficulty is in quantitatively ascertaining the star formation rate in active galaxies: most of the readily observable manifestations of star formation superficially resemble those of an active nucleus. Careful multi-wavelength spatially-resolved observations demonstrate that many Seyfert galaxies are undergoing star formation. Our survey of CO emission from Seyferts (interpreted in conjunction IRAS data) suggests that type 2 Seyferts have unusually high rates of star formation, but type 1 Seyferts do not. Recent work also suggests that many powerful radio galaxies may be actively forming stars: radio galaxies with strong emission-lines often have blue colors and strong far-infrared emission. Determining the star formation rate in the host galaxies of quasars is especially difficult. Multi-color imaging and long-slit spectroscopy suggests that many of the host galaxies of radio-loud quasars are blue and a cold interstellar medium has been detected in some quasar hosts.

1. Introduction

A relationship between star formation and the presence of an active galactic nucleus (AGN) might be expected on a number of different grounds. First, star formation might be a cause of nuclear activity. Indeed, Terlevich and Melnick [44] have proposed that star formation alone can account for the AGN phenomenon (no "monster" is necessary). Alternatively, Weedman [49] has suggested that starbursts and AGN´s are related in an evolutionary sense: the population of compact stellar remnants left behind by the starburst settle into the nucleus where they become the power source for subsequent activity. Second, star formation could be an effect of nuclear activity. The interaction between winds, jets, energetic particles, etc. produced by the AGN and the ISM of the surrounding galaxy could induce star formation [e.g. 5, 33, 39, 45]. Finally, star formation and nuclear activity may occur in parallel because they have a common cause. For example, both could be triggered by the deposition of cold gas into the circum-nuclear region.

I will adopt several perspectives designed to focus the present review. The emphasis will be on "classical" types of active galaxies (namely Seyfert galaxies, radio galaxies, and quasars). At least some of their phenomena require the presence of a compact active nucleus (a "monster"). This may not be the case for LINER´s or IR-bright galaxies. I will also concentrate on studies of large samples of active galaxies rather than on detailed investigations of individual cases since the paramount issue under consideration is whether star formation has any causal link to the general AGN phenomenon. Finally, the difficulty in discriminating decisively between the observational manifestations of star formation and of an AGN can not be over-emphasized. Both can produce strong emission-lines, blue colors, nonthermal radio emission, and thermal infrared and X-ray emission.

2. Star Formation in Seyfert Galaxies

i) Optical Colors

The bright nucleus of a Seyfert galaxy can affect the integrated color of the galaxy, complicating the interpretation of a comparison of Seyfert colors to those of normal galaxies. This problem will be particularly severe for type 1 Seyferts, since they have conspicuous blue quasar-like nuclei [e.g. 48]. Spatially-resolved color maps of samples of Seyferts

[25, 54] imply that the off-nuclear colors of the Seyferts (generally at distances > few kpc from the nucleus) are similar to the integrated colors of galaxies of moderately early Hubble type (E to Sbc). Since Seyferts are generally early type disk galaxies, these data suggest that the extra-nuclear regions of Seyferts are rather normal in terms of their stellar population.

The above data do not have adequate spatial resolution to assess the rate of circum-nuclear (kpc-scale) star formation. Attempts to model the spectral energy distribution of the light from this inner region in terms of starlight plus a "nonthermal" source [e.g. 19, 28] yield results that are consistent with a normal old stellar population. However, it is not clear how well the "nonthermal" component could be distinguished from light from OB stars.

ii) Optical Emission-Line Gas

In principle, the luminosity of the Balmer emission-lines in Seyferts could provide an estimate of the population of OB stars. However, the nuclear emission-lines are powered by the AGN (not by OB stars), and the AGN can also photoionize the ISM of the host galaxy. Thus, in order to use the optical emission-lines to study star formation, great care must be exercised in sorting out the effects of the AGN from those of OB stars. To this end, various empirical techniques have been employed [51].

Narrow-band imaging surveys of the ionized gas in Seyfert galaxies [e.g. 3, 18] reveal three main types of morphological features: smooth, centrally-concentrated ovals, complex filamentary structure, and systems of discrete knots associated with inner rings or with spiral arms. The <u>morphology</u> suggests that first type might be powered by the AGN and the third by OB stars. The other data summarized below supports this interpretation.

The relative strengths of the commonly observed optical emission-lines provide a powerful discriminant between gas which is photoionized by OB stars vs. gas that is photoionized by the much more energetic continuum of an AGN [2, 46]. The <u>line ratios</u> observed in the ionized gas around Seyfert nuclei frequently demand the presence of both sources of ionization, with the relative importance of each being strongly variable from place to place [e.g. 53].

The <u>kinematics</u> of the extra-nuclear gas in Seyferts provides important independent clues regarding the energy-source for the gas. Often, two kinematic components can be isolated: a disk-like structure engaged in simple rotation and a more complex component exhibiting strongly noncircular motions [cf. 53]. It is important to emphasize that these two respective kinematic components seem to correspond well to the gas which (as judged from the line ratios) is photoionized by OB stars and the gas which is ionized by the AGN.

The moral of the above summary is that a decomposition of the emission-line gas in Seyferts into components powered by the AGN and by OB stars is possible but is both difficult and time consuming. No statistically firm conclusions have yet been drawn regarding star formation in Seyferts vs. normal galaxies.

iii) Radio Continuum Emission

A large data set now exists concerning the nonthermal radio continuum emission from Seyfert galaxies (see [52] for a recent review). The interpretation of the origin of the radio plasma (jets from an AGN vs. the energetic processes associated with the evolution of massive stars) is still somewhat controversial, but the following classification/interpretive scheme seems reasonable.

The majority of the radio sources that are well-resolved spatially are classified as "Linear" and have a double, co-linear triple, or jet-like morphology. These L-type sources are most plausibly interpreted as plasma ejected by the AGN. A minority of the well-resolved radio sources are classified as "Diffuse" (round or oval morphologies). These D-type sources are coincident with the regions of star formation delineated in the emission-line gas by the techniques discussed above [51].

Thus, while the radio continuum data provide further evidence for star formation in some Seyfert galaxies, they do not as yet demonstrate whether or not Seyfert galaxies as a class have larger-than-average star formation rates.

iv) Infrared Continuum Emission

The nuclei of Seyfert galaxies have long been known as strong infrared sources [35]. More recently, IRAS has provided us with a large and homogeneous body of data concerning the global mid/far infrared (M/FIR) emission of Seyfert and normal galaxies. However until the physical origin of the M/FIR continuum is well understood, the IRAS data can not be used to reliably compare the star formation rate in Seyferts vs. normal galaxies. Unfortunately, several recent investigations have reached very different conclusions concerning the origin of the M/FIR emission from Seyferts.

Edelson and Malkan [10] have studied a sample of 29 bright Seyferts (nearly all type 1's), and have concluded that the M/FIR emission is produced by the AGN (in most cases it is nonthermal, but in other cases it is dust re-radiation of the nuclear nonthermal light). Dust re-radiation of light from the AGN is also favored by Kraemer and Harrington [20] in their detailed theoretical investigation of the type 2 Seyfert Mrk 3. In contrast, Rodriguez-Espinosa et al. [36] analysed a sample of 96 Seyferts and concluded that the M/FIR emission was powered by star formation. The strength of the M/FIR continuum then led them to conclude that Seyfert galaxies have unusually high rates of star formation compared to normal galaxies. Finally, Miley, Neugebauer, and Soifer [30], Ward et al. [47], and Rowan-Robinson (this volume) have concluded that the M/FIR continuum in Seyferts has several distinct components whose relative strength varies from galaxy to galaxy: 1. nonthermal nuclear radiation 2. thermal re-radiation of nuclear radiation 3. thermal re-radiation of the light from hot, young stars (the "starburst" component) 4. thermal re-radiation of the general diffuse starlight in the galaxy (the "cirrus" or "disk" component). Only the third component can be used to probe the star formation rate, and thus great care must be taken to correctly isolate this component.

The M/FIR spectral energy distribution provides a useful starting point to any attempt to de-compose the M/FIR continuum of a Seyfert galaxy into its component parts. Investigations of large samples of Seyfert galaxies [30] imply that the majority of the type 1 Seyfert galaxies have M/FIR "colors" like those of quasars but a significant minority have M/FIR colors like starburst galaxies. In contrast, the colors of the type 2 Seyferts are more evenly spread between those of quasars and starburst galaxies.

One plausible possibility is that the M/FIR emission in those Seyferts with "starburst"-type M/FIR colors is in fact powered by star formation. This hypothesis is strongly supported by Wilson's [51] discovery that Seyfert galaxies showing optical and/or radio evidence for star formation (see sections 2ii and 2iii) preferentially populate the starburst domain of the M/FIR color-color diagram. The nature of the infrared emission in the

Seyferts with quasar-like M/FIR colors is much less certain. It could be entirely nuclear (powered by the AGN) or it could be dominated by the AGN in the mid-IR ($\lambda < 25\mu m$), and by star formation in the far-IR ($\lambda > 60\mu m$). The latter appears to be the case in the well-studied type 2 Seyfert NGC1068 [43].

Let us assume for the moment that the far-IR is powered by star formation, and compare the far-IR properties of a well defined sample of Seyfert galaxies to a carefully chosen control sample of normal galaxies. Specifically, we have investigated an optically-selected sample of the 42 known Seyfert galaxies in the Revised Shapley-Ames Catalog (RSA). This list comes from J. Huchra (private communication). Our control sample consists of 42 non-Seyfert galaxies selected from the RSA to precisely match the Seyfert sample in Hubble type (including the presence of bars), absolute blue magnitude, and distance.

The main results of this comparison are as follows (we use $H_0 = 75$ throughout). First, the RSA Seyfert galaxies are on average two to three times as luminous as the non-Seyferts in the far-IR. The log-mean luminosities in solar units are 9.92 ± 0.10 vs. 9.52 ± 0.09 respectively -- a difference significant of the 99.7% confidence level. Second, the type 2 Seyfert galaxies are considerably more luminous on average than the type 1 Seyfert galaxies with respective log-mean luminosities of 10.13 ± 0.11 vs. 9.63 ± 0.15 (difference significant at the 99.3% confidence level). In fact, the Seyfert 1 galaxies considered alone are not significantly more luminous than the non-Seyferts (difference significant at only the 73% confidence level). The incidence rates of high far-IR luminosities in the three samples are strikingly different: while only about 5% of the non-Seyfert and type 1 Seyfert galaxies have luminosities in excess of 2×10^{10} $L_\odot$, nearly half the type 2 Seyferts do.

v) CO Emission from Seyfert Galaxies

To further assess the importance of star formation in the Seyfert phenomenon and gain more insight into the origin of the far-IR emission in Seyfert galaxies, we (Blitz, Miley, Wilson, and I) have recently conducted a survey of mm-wave CO emission from Seyferts. Including results from the literature, the sample consists of 55 Seyfert galaxies (of which 26 were detected), with 37 of these (18 detections) being Seyfert galaxies in the RSA. One of the main goals was to answer the question: "Do Seyfert galaxies obey the same relationship between the CO flux and the far-IR flux defined by normal and starburst galaxies?" If the answer is "yes" then it is plausible that the far-IR in Seyferts is powered by star formation. If the answer is "no" (in particular, if the Seyferts have an excess of far-IR luminosity at a given CO luminosity) then much of the far-IR is probably powered by the AGN.

The results of our analysis (Heckman et al. in preparation) are that 1) the Seyferts do follow the same far-IR/CO relation as normal and starburst galaxies; 2) the type 2 Seyfert galaxies have an excess of CO emission (normalized to the galaxy blue luminosity) compared to normal galaxies of similar Hubble type, while the type 1 Seyferts do not. Thus the CO properties of Seyfert galaxies are consistent with their far-IR properties discussed above; 3) those Seyfert galaxies with intrinsically strong CO emission generally exhibit optical and/or radio evidence for extra-nuclear star formation (see sections 2ii and 2iii).

vi) Summary

The available evidence suggests that type 2 Seyfert galaxies are characterized by a higher-than-average rate of star formation, while type 1 Seyfert galaxies are not. This is interesting because it provides clear evidence for intrinsic differences between the two types of Seyferts, and strongly constrains the timescale (massive star lifetime = few million years) over which the Seyfert 1 population could evolve into a Seyfert 2 population (and vice versa). More speculatively, it may be that the higher molecular gas content in the type 2's is related to nuclear material hypothesized to be responsible for obscuring the Broad Line Region [1, 21]. A plausible (though highly speculative) evolutionary scenario might be one in which the injection of gas into the circum-nuclear region of a galaxy leads first to a starburst plus a Seyfert 2 nucleus. As the molecular gas is depleted and the star formation wanes, the galaxy may evolve first into a type 1 Seyfert and finally back into a normal galaxy.

3. Star Formation in Radio Galaxies

Understanding star formation in radio galaxies is particularly important because they are often employed as probes of galaxy evolution out to large redshifts and are among the leading candidates for the "standard candle" that is the Holy Grail of observational cosmology [e.g. 37, 42].

The properties of radio galaxies at high redshifts are reviewed by

Djorgovski elsewhere in this volume. In summary, many radio galaxies at high redshifts appear to be undergoing star formation, possibly in a "burst" mode triggered by galaxy mergers [9, 24]. However, it is not yet clear whether there is any causal link between the star formation and the nuclear activity: radio-quiet galaxies show similar evidence for strong cosmological evolution in their star formation rate [cf. 23]. Another piece of the puzzle is the newly discovered population of faint blue radio galaxies at moderate redshifts which contributes significantly to radio source counts at low flux densities [22]. These may be distant examples of starburst galaxies [4], or perhaps Seyfert galaxies.

I will concentrate here on the evidence for star formation in classical (3CR or similar) radio galaxies at "low" redshifts ($z \lesssim 0.3$). Such radio galaxies can be broadly classified into two types, based primarily on their optical spectrum and secondarily on their radio morphology [14]. Class A radio galaxies have strong optical emission-lines (Seyfert-like), and usually have either "edge-brightened" Fanaroff and Riley [11] type II or compact radio sources. The Class A galaxies dominate the radio galaxy population at high radio powers (> 10E26 Watts/Hz at 178 MHz). The Class B radio galaxies have weak/absent optical emission-lines and have "edge-darkened" Fanaroff-Riley type I radio morphologies. These galaxies dominate at moderate radio powers (10E24 to 10E26 Watts/Hz).

My colleagues and I have discovered that it is the Class A radio galaxies that may be interesting from the standpoint of star formation. While Class B radio galaxies have integrated optical colors similar to those of elliptical galaxies, the colors of the Class A galaxies span a broad range blueward of the elliptical galaxies [12, 15, 40]. In some cases the blue colors may reflect the significant contribution of a very blue nonthermal nuclear source. However, our multi-color CCD data demonstrates that some Class A galaxies clearly have blue extra-nuclear colors, signifying recent or even on-going star formation.

Recent analysis of the IRAS data on radio galaxies provides further evidence for star formation in Class A radio galaxies: the Class A's have a median far-IR luminosity of about 4 x 10E10 $L_{\odot}$, compared to only 2 x 10E09 $L_{\odot}$ for the Class B's [29]. However, further work will be required to convincingly demonstrate that the far-IR continuum in radio galaxies is powered by star formation and not by the AGN.

A final tantalizing clue regarding star formation in radio galaxies is provided by their optical morphology. Heckman et al. [12] and Smith and Heckman [40] find that the Class A radio galaxies frequently (incidence rate = 40-50%) have distorted appearances. Hutchings [15] finds an even higher incidence rate in more distant and radio-powerful Class A galaxies. The tails, bridges, fans, shells, etc. suggest that many Class A radio galaxies may be merging or colliding with a disk galaxy. In contrast, the Class B radio galaxies rarely (incidence rate < 10%) exhibit such strong peculiarities. Are many low redshift Class A radio galaxies undergoing star formation triggered by a galaxy collision/merger?

4. Star Formation in Quasar Host Galaxies

The difficulties in discriminating observationally between the effects of star formation and an AGN are particularly acute in quasars, owing both to their large distances and to the dominance of the quasar over its host galaxy. Not surprisingly, the evidence in the literature for a link between star formation and the quasar phenomenon is ambiguous.

Optical imaging and longslit spectroscopic surveys of low redshift quasars have established that most are immersed in spatially-resolvable "fuzz" with properties consistent with those of a host galaxy. Malkan and colleagues [26, 27] concluded that the optical colors of the fuzz surrounding radio-quiet quasars were normal for early-type galaxies, consistent with the results summarized above for the type 1 Seyfert galaxies. In contrast, several lines of evidence suggest that the host galaxies of radio-loud quasars may have unusually young stellar populations. Both long-slit spectroscopy [6, 7, 13] and multicolor imaging data [15] imply that such host galaxies may often be bluer than normal giant elliptical galaxies. This is consistent with the older single aperture spectroscopy [31] which demonstrated that the spectral signature of an old stellar population was much weaker than would be expected if the hosts of radio-loud quasars were giant ellipticals. In a related vein, Smith et al. [41] have suggested that the strong propensity for quasars to reside in very luminous host galaxies might be due in part to a burst of star formation causally related to the turn-on of the quasar. The peculiar morphology of many quasar hosts [e.g. 16] is consistent with the quasar and putative starburst being triggered by a galaxy collision/merger.

While quasars are characteristically strong emitters in the far-IR, there is little evidence to date that this emission is generally powered by star formation and not by the quasar proper [32]. Observations of CO in low redshift quasars with strong far-IR emission would be very interesting in this regard. The peculiar type 1 Seyfert/quasar/infrared galaxy Mrk231 is in fact a strong CO source [38]. While CO has not yet been detected from a "classical" quasar, there is observational evidence that at least some radio quiet quasar host galaxies do have a cool interstellar medium: the 21cm line of HI has been detected from several low redshift quasars [8, 17].

We know next-to-nothing concerning star formation in high redshift quasars, a subject of considerable importance to our understanding of both galaxy formation and the strong cosmological evolution of quasars. Direct study of the stellar population of the host galaxies is impractical. However, an intriguing possibility is to search for evidence of massive star formation by looking for anomalous chemical abundances in the quasar gas clouds. Analysis of the broad emission-lines provides no clear evidence for strongly nonsolar abundances [34]. However, the material responsible for the Broad Absorption Lines in quasars (material that is clearly intrinsic to the quasars) may sometimes have very non-solar chemical abundances (e.g. carbon-to-hydrogen ratios at least ten times solar) [50]. This tantalizing possibility needs to be confirmed by further observations and more detailed models.

5. Conclusions and Future Prospects

The overall body of evidence linking star formation in some causal (or even statistical) sense to the AGN phenomenon is still only suggestive rather than compelling. Fortunately, we can look forward to significant progress in this important area of research over the next several years. The Hubble Space Telescope, with its superb angular resolution and ultraviolet sensitivity, will allow us to search for and quantitatively investigate star formation in and around AGN´s. This new capability is particularly important for investigating the host galaxies of quasars. The advent of infrared array detectors, mm-wave interferometers, and large single-dish mm-wave and sub-mm telescopes offer us the opportunity to probe the dust-shrouded regions of molecular gas in which star formation might occur in active galaxies. We already know such regions are frequently present in Seyfert galaxies, but much more detailed data are required to elucidate their relationship to the AGN phenomenon.

I would like to acknowledge the National Science Foundation, NASA's IRAS General Investigator Program, and the Alfred P. Sloan Foundation for their financial support of the research described above. I also thank the directors of the Moriond Workshop for the partial travel support they provided.

REFERENCES

[1] Antonnuci, R.R.J., and Miller, J.S. 1985, Ap. J., **297**, 621.
[2] Baldwin, J.A., Phillips, M.M., and Terlevich, R. 1981, PASP, **93**, 5.
[3] Balick, B., and Heckman, T.M. 1985, Astr. J., **90**, 197.
[4] Balzano, V.A. 1983, Ap. J., **268**, 602.
[5] Begelman, M.C. 1985, Ap. J., **297**, 492.
[6] Boroson, T.A., and Oke, J.B. 1984, Ap. J., **281**, 535.
[7] Boroson, T.A., Persson, S.E., and Oke, J.B. 1985, Ap. J., **293**, 120.
[8] Bothun, G.D., Heckman, T.M., Schommer, R.A., and Balick, B. 1984, Astr. J., **89**, 958.
[9] Djorgovski, S., Spinrad, HJ., Pedelty, J., Rudnick, L., and Stockton, A. 1987, Astr. J., in press.
[10] Edelson, R., and Malkan, M. 1986, Ap. J., **308**, 59.
[11] Fanaroff, B.L., and Riley, J.M. 1974, MNRAS, **167**, 31p.
[12] Heckman, T.M., Smith, E.P., Baum, S.A., van Breugel, W.J.M., Miley, G.K., Illingworth, G.D., Bothun, G.D., and Balick, B. 1986, Ap. J., **311**, 526.
[13] Hickson, P., and Hutchings, J.B. 1987, Ap. J. **312**, 518.
[14] Hine, R.G., and Longair, M.S., 1979, MNRAS, **188**, 111.
[15] Hutchings, J.B. 1987, preprint.
[16] Hutchings, J.B., Crampton, D., and Campbell, B. 1984, Ap. J., **280**, 41.
[17] Hutchings, J.B., Gower, A.C., and Price, R. 1987, Astr. J., **93**, 6.
[18] Keel, W.C. 1987, in Star Formation in Galaxies, ed. C. Persson (JPL: Pasadena).
[19] Koski, A.T. 1978, Ap. J., **223**, 56.
[20] Kraemer, S., and Harrington, P. 1986, Ap. J., **307**, 478.
[21] Krolik, J., andBegelman, M. 1986, Ap. J. Lett., **308**, L55.
[22] Kron, R.G., Koo, D.C., and Windhorst, R.A. 1985, Astr. Ap., **146**, 38.
[23] Lebofsky, M., and Eisenhardt, P. 1986, Ap. J., **300**, 151.
[24] Lilly, S., and Longair, M. 1984, MNRAS, **211**, 833.
[25] MacKenty, J.W. 1986, Ph.D. dissertation, Univ. of Hawaii.
[26] Malkan, M.A. 1984, Ap. J., **287**, 555.
[27] Malkan, M.A., Margon, B., and Chanan, G.A. 1984, Ap. J., **280**, 66.
[28] Malkan, M.A., and Filippenko, A.V. 1983, Ap. J., **275**, 477.
[29] Miley, G.K., Golombek, D., and Neugebauer, G. 1987, preprint.
[30] Miley, G.K., Golombek, D., and Neugebauer, G. 1987, preprint.
[31] Miller, J.S. 1981, PASP, **93**, 681.
[32] Neugebauer, G., Miley, G.K., Soifer, B.T., and Clegg, P.E. 1986, Ap. J., **308**, 815.
[33] Norman, C. 1987, in Star Formation in Galaxies, ed. C. Persson, (JPL: Pasadena).
[34] Osterbrock, D.E., and Mathews, 1986, Ann. Rev. Astr. Ap., **24**, 171.
[35] Rieke, G., and Lebofsky, M. 1979, Ann. Rev. Astr. Ap., **17**, 477.

[36] Rodriguez-Espinosa, J.M., Rudy R.J., and Jones B. 1987, Ap. J., **312**, 555.
[37] Sandage, A.R. 1972, Ap. J., **178**, 25.
[38] Sanders, D.B., Young, J.S., Scoville, N.Z., Soifer, B.T., and Danielson, G.E. 1987, Ap. J. Lett., **312**, L5.
[39] Sanders, R.H., and Bania, T.M. 1986, Ap. J., **204**, 341.
[40] Smith, E.P., and Heckman, T.M. 1987, in Radio Continuum Emission in Clusters of Galaxies, ed. J. Uson and C. O'Dea (NRAO: Charlottesville).
[41] Smith, E.P., Heckman, T.M., Bothun, G.D., Romanishin, W., and Balick, B. 1986, Ap. J., **306**, 64.
[42] Spinrad, H., and Djorgovski, S. 1987, in Proc. IAU Symp. #124: Observational Cosmology, ed. G. Burbidge, (D. Reidel).
[43] Telesco, C.M., Becklin, E.E., Wynn-Williams, G., and Harper, D.A. 1984, Ap. J., **282**, 427.
[44] Terlevich, R., and Melnick, J. 1985, MNRAS, **213**, 841.
[45] van Breugel, W.J.M., Filippenko, A.V., Heckman, T.M., and Miley, G.K. 1985, Ap. J., **293**, 83.
[46] Veuilleux, S., and Osterbrock, D.E. 1987, Ap. J. Suppl., **63**, 295.
[47] Ward, M.J., Elvis, M., Fabbiano, G., Carleton, N.P., Willner, S.P., and Lawrence, A. 1987, Ap. J., **315**, 74.
[48] Weedman, D.W. 1977, Ann. Rev. Astr. Ap., **15**, 69.
[49] Weedman, D.W. 1983, Ap. J., **266**, 479.
[50] Weymann, R.J., Turnshek, D.A., and Christiansen, W.A. 1985, in Astrophysics of Active Galaxies and QSO's, ed. J. Miller, (University Science Books: Mill Valley, CA).
[51] Wilson, A.S. 1987, in Star Formation in Galaxies, ed. C. Persson, (JPL: Pasadena).
[52] Wilson, A.S., and Heckman, T.M. 1985, in Astrophysics of Active Galaxies and QSO's, ed. J.S. Miller, (University Science Books: Mill Valley, CA).
[53] Wilson, A.S., Baldwin, J.A., Sun, S., and Wright, A.E. 1986, Ap. J., **310**, 121.
[54] Yee, H.K.C. 1983, Ap. J., **272**, 473.

THE RELATION BETWEEN VARIABILITY AND STAR FORMATION IN SEYFERT NUCLEI

Roberto TERLEVICH
Royal Greenwich Observatory
Herstmonceux, England

and

Jorge MELNICK
European Southern Observatory
Munich, Germany

The central hypothesis of this paper is that nuclear starbursts can reproduce the observed properties of Seyfert nuclei. We suggest that the so called Broad emission Line Region observed in Seyfert type 1 nuclei may be young supernova remnants evolving in the high density nuclear inter-stellar medium. The observed properties of the BLR (Size, Total energy, density, line widths) correspond to the expectations of the model. More importantly, the observed optical varibility properties of the BLR strongly suggest the SN origin.

1. Introduction The energy source of Active Galactic Nuclei (AGN) is usually ascribed to accretion onto a supermassive black hole sometimes called the "monster" [12,24,2]. For a long time, the alternative view that nuclear activity is the direct consequence of violent star formation in the nuclear region of spiral galaxies [25,8,11,18] has been considered wrong.

We have challenged the black hole scenario on grounds that most of the observations that are usually invoked as evidence for the existence of nuclear monsters can also be understood in terms of violent star formation activity [28,29]. We showed that the observational diagnostics which have traditionally been used to distinguish between "normal" (Starburst) and "active" emission-line nuclei (emission line ratios, radio and X-ray emission etc.) do not distinguish between starbursts and monsters [29].

A very important observational approach for probing the innermost regions of AGN's is the study of their variability. In "monster" models variability is ascribed to transient changes in some of the parameters like the accretion rate while in the starburst theory variability is the natural consequence of the final stages of stellar evolution, i.e. supernova outbursts and their associated young supernova remnants evolving in the high density nuclear interstellar medium [29].

Long term monitoring of AGN's with sufficient time coverage has over the past few years been carried out for a few galaxies, and has already yielded interesting results [30,21,23,32,7]. In this paper we will show that the observational evidence strongly support the starburst scenario.

2. The Evolution of Starbursts Within the life span (3 to 20 Myrs) of a massive star (100 to 10M$_\odot$) the Starburst model predicts a substantial evolution in the emitted spectrum of the young stellar cluster and its associated HII region [28]. There are two main phases : The stellar phase when the ionizing source is the normal stellar population, and the supernova phase when most of the ionization is provided by the supernova activity.

i - The stellar phase. For a given mass, the most important parameter affecting the evolution of a massive star is the mass-loss rate. Evolutionary models incorporating the effects of mass loss have been computed by a large number of authors [5]. Without exception, all authors find essentially the same basic difference between conservative ($\dot{M}$=0) and mass-losing models namely a change in the H and He-burning time scales and a blueward evolution when the products of nuclear burning reach the stellar surface [26].

Maeder (1983,1985) published models that give a consistent description of the evolution of massive stars. Very different evolutionary sequences are obtained from models of massive stars according to their initial masses and mass loss rates,

a) High mass-loss: ($M>25M_\odot$). Massive stars evolve initially towards the red (decreasing temperatures) but eventually the outer layers are peeled-off by stellar winds leaving exposed the nuclear burning layers. Subsequently as was the case for the early Tanaka [27] models, the stars evolve towards high temperatures and end their evolution as bare cores, near the He-ZAMS [26] where they reach the He-ZAMS at effective temperatures well in excess of 100,000 K. Stars more massive than $60M_\odot$ spend most of their He-burning life at the He-ZAMS. Stars less massive than this limit spend part of their He-burning life as red supergiants. However the mass loss in the red-supergiant phase completes the removal of the envelope and thus brings back the star to higher temperatures near the He-ZAMS also as a bare core. The evolutionary sequence is, according to Maeder:

0 - Of - (Eta Car/H-S var) - WN - WC - WO - SNIb

for stars more massive than 60Mo, and

0 - BSG - RSG - WN - WC - WO - SNIb

for stars with masses between 25Mo and 60Mo.

b) Low mass-loss: ($M<25M_\odot$) In this case stellar-winds are not sufficiently strong to remove the envelopes. As a consequence, stars spend all of the He-burning time in the RSG branch. The evolutionary stages are,

0 - BSG - RSG - YSG/Cepheids - RSG - SNII

Terlevich and Melnick (TM85) have computed evolutionary models for the emission line spectra of gaseous nebulae photoionized by coeval clusters of massive stars taking into account the effect of mass-loss in the stellar evolution. The ionizing spectrum of a starburst is dramatically affected by the presence of hot luminous massive stars near the He-ZAMS that have been called WARMERS by TM85 precisely because of this effect. These models show that when Warmers begin to appear in the cluster (i.e. after about 3 million years) the nebular spectrum changes in a very short time scale from a normal, low-excitation HII region (typical of nuclear starbursts) to a Seyfert or Liner spectrum. The theoretical predictions agree remarkably well with the observed line ratios in AGNs. See figures 7 to 11 in TM85 where this "qualitative" change is clearly illustrated.

We concluded in that paper, that the mere presence of strong high excitation forbidden lines in the nuclear spectrum of an early galaxy does not necessarily imply that photoionization is produced by a non-thermal source. Photoionization models of Starbursts with WARMERS give a very good description the observed emission line ratios in type 2 Seyfert and LINERS.

ii - The supernova phase. Both for high and low cases of mass-loss rate, observational considerations lead to the conclusion that massive stars end their evolution as supernova explosions that occur shortly after carbon ignition [15]. Supernovae are expected to be of two different types depending on the progenitor´s mass:

SN Ib-Those coming from high mass-loss progenitors (WARMERS) will give rise to a shock that expands from a non-degenerate carbon-oxygen core into the high velocity and low density pre-supernova wind blown bubble. Given the composition and density of the medium into which the shock expands, this type of event will presumably look like a sub-luminous type I supernova. The flash may last few weeks and have total energies probably below 10^{49} ergs. [35,34]. Following Wheeler et al [34] (WMS), at the time of explosion the surrounding wind blown bubble will consist of stellar wind out to 0.2pc for a $120M_\odot$ star embedded in a medium with density $10^{6}cm^{-3}$..

Regarding the geometry of the surrounding region, it is useful to remark the conditions of a burst of star formation in the nucleus of an early type spiral. The gravitational potential will confine the central gaseous component to a relatively thin disk. The most massive stars will presumably form in the central parts of the young stellar cluster. Wind from these stars whose relative distances are probably less than 0.2pc, will overlap and produce an extended super-bubble filled with hot gas. This bubble will extend further towards regions with steeper decreasing density gradients, in the case of an oblate spheroid this will presumably be along the rotation axis of the gas-cluster complex and not along its equatorial plane. The first supernovae will explode in this environment and the radially decreasing density gradient will accelerate the shock. If the remnant or remnants reach the edge of the disk a JET of matter should be ejected into the lower density outer regions were after some time a shock will be formed at large distances from the nucleus. UV radiation from the central cluster should leak also in the same direction, illuminating therefore any background gas. A similar geometry has been postulated for the nuclear region of M82[33]. It provides an explanation to the correlation observed between the mayor axis of linear radio sources and the mayor axis of the extended narrow line regions [31].

SN II-Low mass-loss progenitors will give raise to classical type II supernovae. These stars are more numerous and occupy a larger volume than the more massive ones. Most of the low-mass stars will populate the outer regions of the stellar cluster, outside the central wind blown super-bubble. The supernova envelope will expand out in the dense stellar wind of the red giant pre-supernova star. This produces a "flash" of energetic radiation that lasts a few weeks and emits 10^{49-50} ergs [4,9,10]. After this the supernova shell continues to expand until it reaches the edge of the wind blown bubble. The size of the bubble will be about 0.01pc for a typical 15M$_\odot$ star. Each star will have its individual bubble with no overlap between bubbles. The density in the interior of this bubble is low and the supernova remnant sweeps-up only a small amount of mass before encountering the dense and massive shell of shocked material at the edge of the bubble. This will produce a luminous phase with time-scales and luminosity depending on the density distribution of the surrounding material. In this high density environment the supernova remnant will deposit most of its kinetic energy in a short time scale and thus reach very high luminosities. For a 10^6 medium, this will be typically $2*10^9$ L$_\odot$ and a time scale of few years. Most of the luminosity will be emitted in the extreme UV/X-ray region of the spectrum.

WMS modelled the luminosity evolution of a 10^{52} erg/sec supernova ejecta expanding into a medium of uniform density $5*10^6$. They found that one year after the explosion the remnant reaches a peak luminosity of 10^9 solar luminosities. Thereafter, the luminosity drops by a factor of two after about 1,000 days.

3. <u>Variability time scales, total energy, sizes and line widths</u> From the previous discussion it is possible to see that during the SNII phase, i.e. when the ionizing flux is dominated by the SN activity, large variability is expected, particularly in systems with SN rates of about 1 per year. In general two typical total energies and time scales of variability are expected in the Starburst scenario during the Supernova phase:

(a) Flares of about 10^{49-50} ergs and lasting for few weeks coming from those supernovae whose progenitor is a red supergiant (SNII)

(b) About 10^{52} ergs total energy in longer term variations with time scales of order: $t \sim 1500$ days $n_6^{-0.4}$, and peak logaritmic luminosity: $\log L/L_\odot \sim 9.0 + 0.64 \log n_6$, were n_6 is the density of the interstellar medium in units of 10^6. The bubble will have about 0.01pc in radius implying a light travel time of about 30 days. Typical line widths at half maximum will be about 5000Km/s if the typical SN ejecta have initial velocities of about 10000Km/s.

We identify these rapidly evolving SN remnants as the Broad Line Region in AGNs.

4. Observational results Lyutyi [13,14])and Dibai and Lyutyi [6,7]) made extensive photometric observations of 16 galaxies since de late 1960s they found that the optical variability contains two components: a rapid "flare" component with characteristic time scales of tens of days and typical total energies of few 10^{49} ergs. This flares have a typical rise time of 10 days and a decay of 40 days with average absolute magnitude of -18.4 in galaxies like NGC4151 and NGC1275. The flares are superposed on a slower component with variability time scale of few years and similar amplitude to the flare component implying total energies of about 10^{51} ergs.

Dibai and Lyutyi [6]) also estimated the mean energy of the optical flares and their characteristic times for the 4 Syl galaxies with the best optical data.

NGC 5548	$E=4.5*10^{49}$ ergs	t=100days
NGC 1275	$E=0.6*10^{49}$ ergs	t=20 days
NGC 4151	$E=0.2*10^{49}$ ergs	t=30 days
NGC 3516	$E=0.1*10^{49}$ ergs	t=10 days

(Ho=100Km/s/Mpc)

Therefore the evidence presented by the optical monitoring of Lyutyi and collaborators supports the Starburst origin of the variability in AGNs.

Similar results can be found in more recent studies of variability. The comprehensive IUE monitoring of NGC4151 by Ulrich et al. [30]) reports variability in the broad CIV1550A with time scales of several weeks and luminosity in the variable component of CIV of about $2*10^{41}$ erg/sec, corresponding to total energies of about $5*10^{49}$ ergs in the ionizing continuum.

Another well studied Seyfert galaxy NGC1566 was found to show variations of 1300 days duration and total energies of order 10^{51} ergs [1]). We agree with Alloin et al that this result rules out SN flashes. The observed total energies and time scales correspond to the rapid evolution of a SNR in the high density environment. In fact not only the total luminosity but the peak luminosity and the observed light curve in NGC1566 is nicely described by the luminosity evolution of SNR in a high density cloud computed by WMS and mentioned at the end of section 2.

During the monitoring of NGC 5548, Peterson [22]) found that the increase in optical luminosity of the nucleus of this galaxy was accompanied by the appearance of a strong HeII 4686 emission line significantly broader than the Balmer lines. This was interpreted by Peterson and Ferland [20] as evidence that the gas producing the HeII emission was much closer to the central object and that the increase in luminosity was due to an accretion event of about $0.8M_\odot$ of material.

An important "coincidence" is that the rising and decaying time scales of the continuum and line fluxes in NGC 5548 are very similar to those of typical type II supernovae. Peterson's spectra show that the broad HeII line disappeared 260 days after the flare. Moreover, the excess energy emitted by the "flare" in the nucleus of NGC 5548 in emission lines and continuum is about $6.5*10^{49}$ ergs (for a distance of 50Mpc). This value corresponds closely to the energy which is emitted during a type II supernova event. Another "coincidence" is that the spectrum of Peterson and Ferland's "accretion event" looks remarkably similar to the pre-maximum spectrum of of the only known SN type II with a Wolf-Rayet progenitor, SN1983k. See figure 2 of Niemela et al [19]).

Therefore, the evidence presented suggest that Peterson has observed the explosion of a supernova in the nucleus of NGC 5548.

5. Conclusions Supernovae and their remnants are postulated in the starburst model to explain not only the existence of a broad line region and its variability but also the non-thermal radio emission and the X-ray emission from AGNs. The expected total energies and time scales associated with SN activity in the Starburst model are indeed observed in the monitoring of variable Seyfert nuclei. The "accretion event" in NGC 5548 reported by Peterson and Ferland may be the first direct observation of a supernova explosion in the nucleus of a Seyfert galaxy.

The starburst vs monster controversy continues. Further spectrophotometric monitoring of AGN variability with adequate temporal coverage and direct searches for nuclear supernovae are clearly very fruitful observational approaches to unravel the mystery of the origin of activity in the nuclei of galaxies.

References

1. Alloin,D.,Pelat,D.,Phillips,M.M.,Fosbury,R.A.E. and Freeman,K. 1986, Ap.J. 308,23
2. Begelman, M.C., 1985, in, "Astrophysics of Active Galaxies and Quasi-stellar Objects", ed. J.Miller (Mill Valley, University Science Books).
3. Chevalier,R.A. 1976, Ap.J. 208,826
4. Chevalier,R.A. 1982, Ap.J. 259,302
5. Chiosi, C. 1981 in "The most massive stars"(eds. D'Odorico et al) 261.
6. Dibai,E.A. and Lyutyi,V.M. 1976, Sov.Astron. Lett. 2,90
7. Dibai,E.A. and Lyutyi,V.M. 1984, Sov.Astron. 28,7
8. Field,G.B. 1964, Ap.J. 140,1434
9. Fransson,C. 1982, Astr.Ap 111,140
10. Fransson,C. 1984, Astr.Ap 133,264
11. Harwit,M. and Pacini, F. 1975 Astrophys. J. 200,L127
12. Lynden-Bell, D. 1969, Nature, 223, 690.
13. Lyutyi,V.M. 1977, Sov.Astron. 21,655
14. Lyutyi,V.M. 1979, Sov.Astron. 23,518
15. Maeder,A. and Lequeux,J. 1982, Astr.Ap. 114,409
16. Maeder,A. 1983, Aston.Astrop. 120,113
17. Maeder,A. 1985 private communiation
18. McCrea,W.H. 1976, in "The galaxy and the local group" ed Dickens,R.J. and Perry,J.E. (RGO Bull. 182)
19. Niemela, V.S., Ruiz, M.T. and Phillips, M.M. 1985, Ap.J. 289,52
20. Peterson B.M. and Ferland, G., 1986, Nature 324, 345.
21. Peterson, B.M. and Gaskell, C.M., 1986, A.J., 92, 552.
22. Peterson, B.M., 1987, Ap. J., 312, 79
23. Pronik, I.I. 1974 Sov. Astr. 16,628
24. Rees, M.J. 1984, Ann. Revs. Astron. Astrophys., 22, 471.
25. Shklovskii,I.S. 1960, Soviet Astr. 4,885
26. Stothers,R. and Chin,C.W. 1979, Ap.J. 233,267
27. Tanaka,S. 1966 P.A.S.J. 18,47
28. Terlevich, R. and Melnick, J. 1985, M.N.R.A.S., 213, 841. (TM85)
29. Terlevich, R, Melnick, J. and Moles, M. 1987, in IAU syposium N. 121, "Observational Evidences of Activity in Galaxies", ed. Khachikyan et al., (Reidel), p. 499.
30. Ulrich, M.H. et al. 1984, MNRAS, 206,221
31. Ulvestad,J.S.,Wilson,A.S. and Sramek,R.A. 1981 Ap.J. 247,419
32. Ulvestad,J.S. 1982, Ap.J. 259,96
33. Unger,S.W. et al 1985 in "Active Galactic Nuclei" (ed. J.E. Dyson) Manchester Univ. Press
34. Wheeler,J.C.,Mazurek,T.J. and Sivaramakrishnan,A. 1980, Ap.J. 237,781 (WMS),
35. Woosley,S.E. and Weaver,T.A. 1982, in "Supernovae:A survey of current research" ed Rees,M.J. and Stoneham,R.J.

STARBURSTS AND MERGERS AT LARGE REDSHIFTS, AND THE EVOLUTIONARY MECHANISMS OF POWERFUL RADIO–GALAXIES

S. Djorgovski
Harvard–Smithsonian Center for Astrophysics
60 Garden St.
Cambridge, MA 02138, USA.

Modern photometric, imaging, and spectroscopic data on powerful radio-galaxies, reaching up to the redshifts of ~ 1.8, show a dramatic evidence for evolution of stellar populations at large look-back times. The data suggest that the star formation in these systems occurs in massive starbursts, whose frequency and/or intensity diminishes in time. A plausible mechanism for the initiation of starbursts, suggested by the imaging and spectroscopic data, may be highly dissipative mergers of gas-rich galaxies at large redshifts. There are probably other processes involved, e.g., interactions of the radio plasma with the ambient gas in host galaxies, and the overall picture must be fairly complex. The processes governing galaxy evolution, most notably dissipative merging, are hard to separate from the process of galaxy formation. Newly found objects (Lyα galaxies) at $z \simeq 1.8$ have properties which can be interpreted as galaxies or small groups in the process of formation. These and other data are suggestive of, and fully consistent with, the idea that galaxy formation occurs at a range of redshifts, perhaps reaching as low as $z \simeq 1 - 2$. If this is the case, late-forming primeval galaxies have probably been detected.

Understanding of galaxy evolution is one of the centerpieces of modern cosmology. It is interesting on its own, galaxies being the bricks of the Universe at large scales, and it is necessary for most of the classical cosmological tests (Hubble diagrams, galaxy counts, etc.). To a first approximation, there are two kinds of evolutionary or formative effects for galaxies: (1) External or dynamical, when mergers violate the conservation of the comoving number-density of galaxies, and increase the luminosity of the dominant participant. This process is well described by the Schweizer equation, "$1 + 1 = 1$"; and (2) Internal, or spectral, due to the inevitable collective evolution of stellar populations and gas in galaxies [1–8]. The two processes may well be related, and it is one of the goals of this paper to show that such interplay is indeed detected for at least one kind of galaxies at large look-back times, *viz.*, those associated with powerful radio sources.

There are now several classes of observations which indicate or detect evolutionary effects in high-redshift galaxies: Butcher–Oemler–Dressler–Gunn effects [9,10], behaviour of faint galaxy counts [11], galaxy counts near quasars [12], etc. However, the most striking evidence for galaxy evolution comes from the photometric sudies of the 3C and "1-Jy" [13] samples of powerful radio galaxies, now reaching up to $z \simeq 1.85$, that is, to the look-back times of $\sim 65 - 80$ % of the Friedman time, depending on the cosmology [14,15]. These galaxies are at the low redshifts generally identified as gE or cD systems, and brightest members in groups or clusters, but not as luminous as the optically selected BCM's. Their radio sources are generally of Fanaroff-Riley type II, that is, with all the power from the radio lobes, and relatively weak or absent radio cores. Objects with optically luminous AGN or broad emission lines are excluded from these studies: we are interested primarly in the evolution of stellar populations at large look-back times.

Briefly put, at large redshifts ($z \geq 1$, say), these galaxies show systematically larger luminosities (up to $5^m - 7^m$) and bluer colors, than what would be expected from non-evolving populations at the same look-back times [16 – 25]. Their photometric properties in the observed range of wavelengths ~ 3500 Å $- 2.2$ μm (U to K bands) are consistently described by the evolutionary "μ" models by Bruzual [3–5], with exponentially declining star formation, and a range of e-folding times of 0.8 – 1.5 Gy. Passively evolving "c" models, in which all stars are formed in a relatively brief burst at the time of formation, are both too faint and too red to fit the data in the $UBVR(I?)$ bands. Similar results are found with population synthesis models by other authors [6–8]. There are far too many unknown parameters and built-in approximations in these models, as discussed elsewhere in this volume. Even so, it is very encouraging that it is possible to construct reasonable spectral evolution models which can fit the data, and make at least qualitative statements about possible star formation histories of galaxies in our samples.

The samples are well defined and almost completely identified, and thus any optical biases are highly unlikely. It is important to emphasize that the samples are selected in the radio, and there is no obvious evidence for a correlation between the radio fluxes and optical/IR photometric properties, which would cause the selection effects to mimic the evolutionary effects [25]. Nevertheless, such correlation may exist [26], and we must be careful not to extrapolate too far: these powerful radio-galaxies are very rare events, and their behaviour need not be representative of all gE and cD galaxies at large redshifts. They should not be too far off, since there are no systematic differences of 3C, 1-Jy and optically selected BCM galaxies with comparable redshifts in the near-IR [19,20,25]. Even if the flux selection was important, their very blue colors and large surface brightness provide a strong evidence that a substantial evolution of stellar populations is taking place in these objects: if their luminosity density was comparable to that of the nearby E's, they would not be detectable, because of the relativistic $(1+z)^{-4}$ dimming and the seeing effects [27]. It is thus probably fair to state that strong evolutionary effects, indicative of an extended star formation with rates increased in the past, are detected in the samples of powerful radio-galaxies, unusual as those samples may be.

The Bruzual μ models are meant to represent a smooth time average of multiple bursts of star formation, declining exponentially. In addition to that, we have averaging in the ensemble of objects: their collective behaviour is represented with an "average" $\mu = 0.5$ model (which has the SFR e-folding time of 1.44 Gy), and there should be some intrinsic scatter of data, corresponding to the random phases of bursts for individual objects. In order to demonstrate this, we construct three population synthesis models with different star formation rates (SFR), as shown in Figure 1. The model labeled "picket" consists of

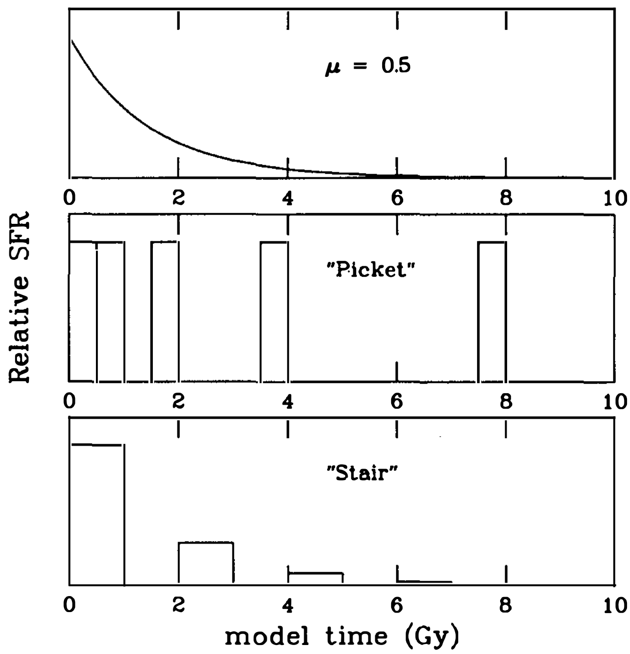

Figure 1. Schematic representation of star formation histories for three multi-burst synthesis models. The model predictions are compared with the data in Figure 2.

a sequence of starbursts 0.5 Gy long, and of equal strength, but with inter-burst times increasing exponentially. The model labeled "stair" consists of a sequence of starbursts 1 Gy long, with uniform inter-burst times of 1 Gy, but with intensities decreasing exponentially.

Figure 2 shows a comparison of the three models with the data on distant radio-galaxies [22]. The popular $\mu = 0.5$ model is indeed a time/ensemble average of the rough

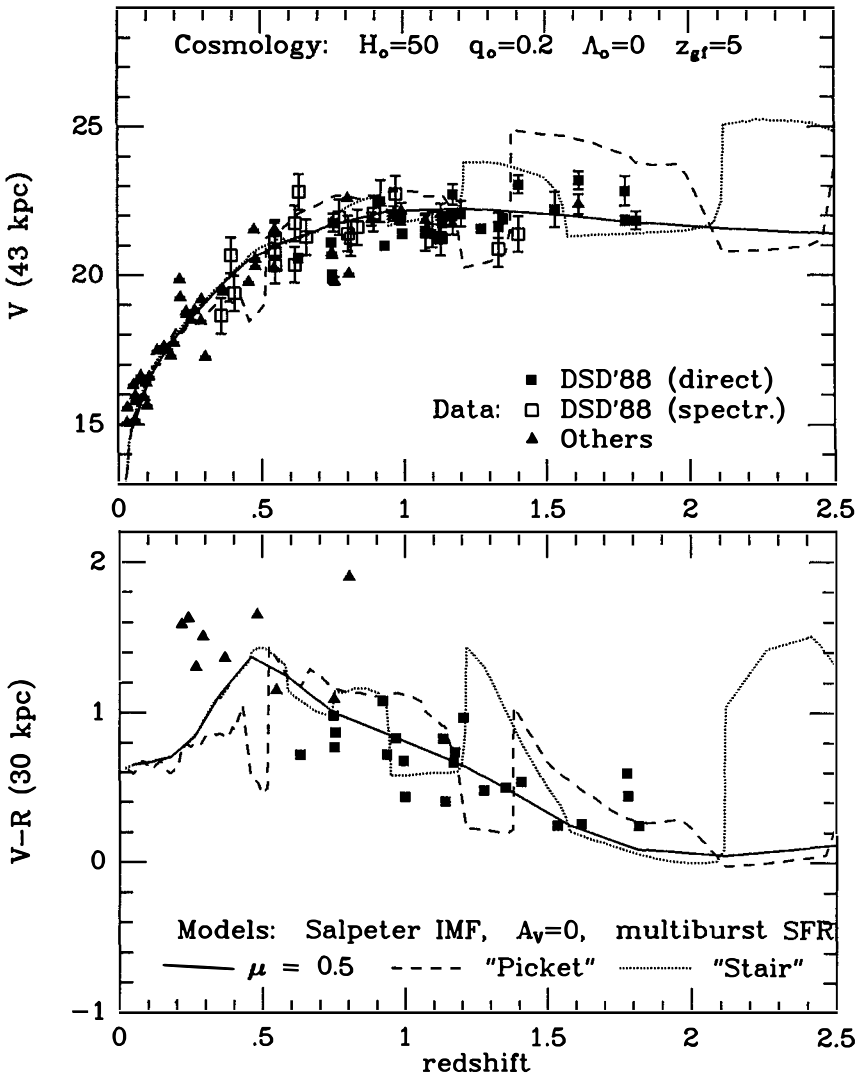

Figure 2. A comparison of the predictions of the three multi-burst synthesis models (Fig.1) with the magnitudes (top) and colors (bottom) of distant radio-galaxies. The data are from the study by Djorgovski, Spinrad, and Dickinson (DSD'88 = [22]). The cosmological parameters are indicated at the top. Typical error-bars for the colors are 0.2 – 0.4 mag. All models were scaled to $M_V = -22.6$ at $z = 0$ (the median luminosity of low-z 3C galaxies).

multi-burst models, and the SFR flicker in them can easily account for the cosmic scatter in the data. The true situation is probably a combination of the "stair" and "picket" schemes. Similar scenario was suggested by Lilly and Longair [18], and Eisenhardt and Lebofsky [20], on the basis of behaviour of $(V - K)$ colors: the passively evolving "c" (single initial burst) model is a good red envelope of the data, from which galaxies scatter blueward by amounts significantly exceeding the error-bars. Declining sequence of starbursts is thus a plausible explanation for the photometric behaviour of powerful radio-galaxies, up to $z \simeq 1.85$. What remains to be understood are the *causes* of the starbursts. Optical morphology and spatially resolved spectroscopy of ionized gas provide some clues.

The first modern CCD images of $z > 1$ radio-galaxies indicated that their shapes are very elongated or even multimodal [15,16,21–24,28–31]; under good seeing conditions, these structures are often resolved into two or more components [32]. This invited a comparison with the low-z merging doubles or db systems (Figure 3). A number of low-z radio-galaxies have such dual morphology, e.g., 3C40 = NGC 545/547, 3C278 = NGC 4782/4783, etc. [33]

Long-slit spectroscopy along the major axes of such systems resolved the low-ionization emission lines, principally [O II] 3727, both spatially and in velocity [14–16,23–25,28–31]. The emission-line gas is distributed generally in the same way as the underlying stellar continuum, and thus it must be locally ionized, by the UV continua of young stars, and/or gas cloud collisions. There is a good correspondence between the morphologies of emission-line gas, stellar continuum, and features in the gas velocity field (velocity shear;

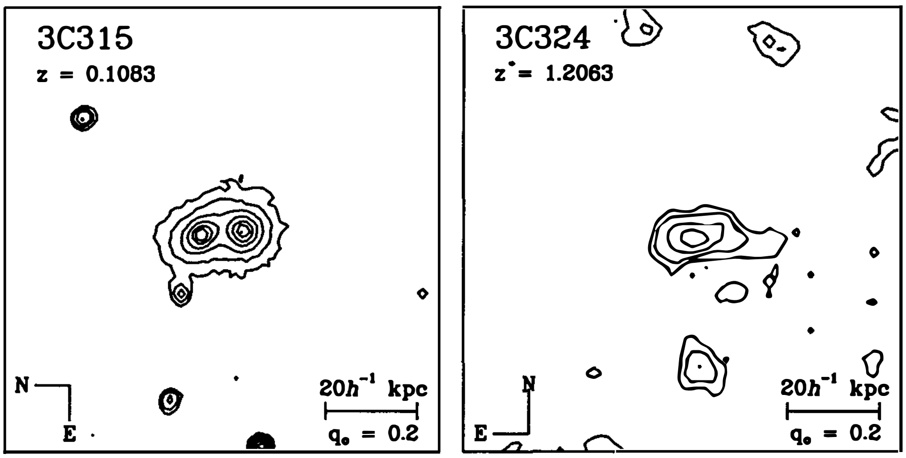

Figure 3. Multiple 3C galaxies at low and high redshifts, plotted on the same scale, as indicated by the bars in the lower right corners. Images of 3C324 obtained in a better seeing by Le Fèvre *et al.* [32] show it to consist of two brighter and one fainter components, not unlike the low-redshift system 3C315 shown here. Such tidally distorted doubles at low redshifts are commonly interpreted as galaxies in the process of merging. The data shown here were obtained in the R-band with a TI CCD at the Kitt Peak 4-m telescope.

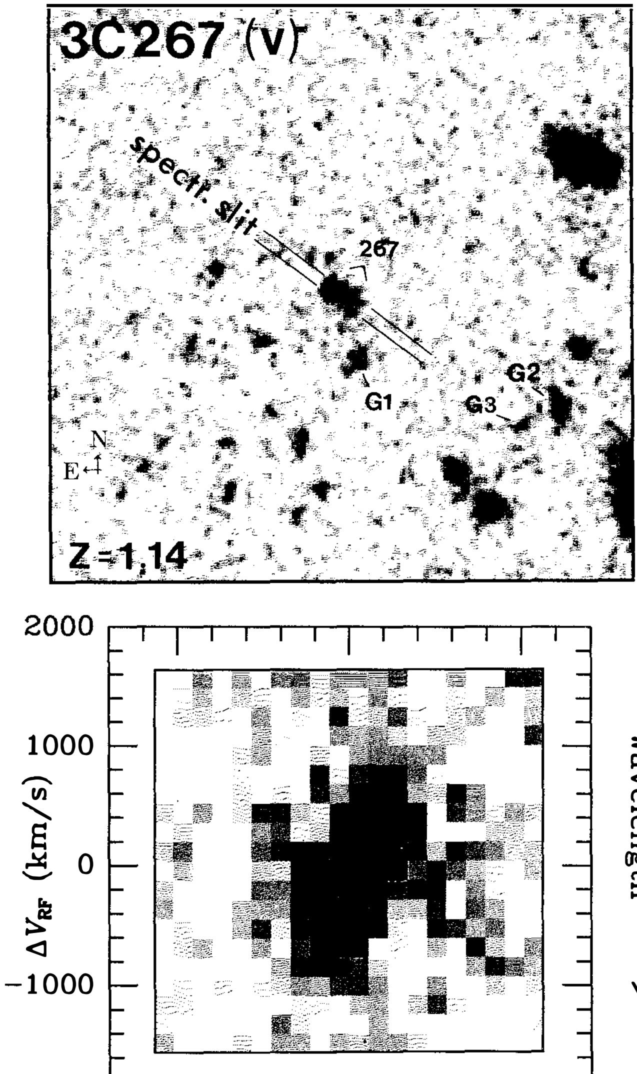

Figure 4. Top: V-band image of 3C267 ($z = 1.139$). The field size is 1 arcmin. The radio-source is identified with a marginally resolved double galaxy. Three other galaxies (G1–G3) show possible [O II] emission at the same redshift. These and other faint galaxies in the field may be members of an extermely distant rich cluster. Bottom: A section of a long-slit spectroscopic CCD frame of 3C267. The slit orientation is indicated on the top pannel. Shown here is the "phase space diagram" of the [O II] 3727 line, which is resolved both spatially, and in velocity. The two line components correspond to the two continuum components in the top image. Conversion of arcsec into kpc assumes a Friedman cosmology with $H_0 = 75$, $q_0 = 0.2$. The data were obtained at the Kitt Peak 4-m telescope.

velocity width, indicating either turbulence, or the shear along the line of sight; equivalent widths; ionization state). This is partly illustrated in Figure 4, on the example of 3C267, which clearly shows a bimodal structure, both in the spatial distributions of the continuum and emission-line gas, and the velocity structure in [O II] 3727.

The line luminosities of some of these galaxies reach $\sim 10^{10}\ L_\odot$, (or, $\sim 7 \times 10^{54}$ [O II] photons/sec), about two orders of magnitude higher than the largest luminosities of extended emission-line gas in low-z radio-sources [34]. We can use the synthetic spectra from the models which fit the colors and magnitudes of these galaxies, and compute the rates of ionizing photons generated by the young stars. Using the same models, cosmology, and scaling, we derive rates $\sim 10^{54} - 10^{55}$ ionizing photons/sec, assuming no internal extinction. A good conversion factor is hard to compute, but we estimate about 10 ionizing photons for every escaped [O II] 3727 photon. The ionization by stellar continua thus may be insufficient to account for the observed line fluxes; some other mechanisms are needed, and two possible candidates may be ionization in supernova shocks, and massive gas cloud collisions. One must also account for the large velocity fields observed in these systems, reaching $\sim$ 1000 km/sec in the rest-frame.

Such phenomena can be plausibly explained as spectacular, highly dissipative mergers of gas-rich galaxies at large redshifts. Mergers can stimulate the star formation, and feed the radio-source (which can feed back; see below). There is now a considerable body of evidence that galaxy mergers, starbursts, and non-thermal activity are mutually connected [31,35–48]. In the particular case of low-z powerful radio-galaxies, Heckman *et al.* [41] found that many or all of them show morphological signs indicative of past mergers: dust lanes, disturbed isophotes, tidal tails, shells, etc.

Merger-induced starbursts are now well documented in many low-z *IRAS* sources [40–47], but their conspicuous characteristic are copious amounts of dust, which reprocesses the primary UV photons generated by the young stars. The inferred IMF's in these starbursts are flatter with respect to the "normal", solar-neighborhood IMF [38,39,49,50]. This would be an important consideration for the synthesis models, but the objects which we see at large redshifts must involve somewhat different physics: they must be almost dust-free, since we observe them clear and bright in the rest-frame UV, where an analogue of Arp 220 may suffer $\sim 15^m - 20^m$ of extinction! We must be careful in extrapolating our low-z experience to the high-z galaxies discussed here: these are different, new phenomena, without direct counterparts at the low redshifts. (This, of course, does not exclude them as evolving progenitors of some common low-z objects, e.g., gE/cD galaxies.)

Typical SFR in these distant galaxies, inferred from the $\mu = 0.5$ model, scaled as to match the observed luminosities, are *several hundred* $M_\odot$/yr, for a range of plausible IMF's. This is larger than the rates inferred for the most luminous *IRAS* sources at low redshifts, although some $L_{bol} \simeq 10^{12}\ L_\odot$ sources may be close [43–47]. Assuming a normal IMF, such SFR would produce $\sim$ 1 supernova/yr. If the IMF is biased towards more massive stars, the SNR/SFR ratio would be higher, but that would be largely offset by the scaling with luminosity.

The energetics of the collisions is about right: The total available kinetic energy of the residual gas in such galaxies (using the same scaling as above) is at least $\sim 10^{59}$ erg, a sizable fraction of which may be dissipated, depending on the poorly known conversion efficiency factors. For a typical crossing (and starburst) time of $\sim 10^8$ yr, this is comparable to the energy input by the supernovæ of $\sim 10^{51}$ erg/yr [51,52]. A large fraction of that energy can then support the observed extended line emission, which may reach $\sim 10^{51}$ erg/yr; the remainder is probably deposited in the radio lobes, whose mechanical energy is of the similar order of magnitude [53]. The available data are thus at least semi-quantitatively consistent with the dissipative merger scenario.

However, the full picture must be more complex, as evidenced by the remarkable, newly discovered correlation between the optical and radio morphologies of distant radio galaxies [54,55]: there is a good correspondence between the orientation of optical isophotes (of the stellar continuum, or emission-line gas) and the radio-source axes, defined by the radio lobes. This is illustrated in Figure 5. Note that the correlation is between the orientations of principal axes of the optical and radio morphologies, and not of their positional coincidence: the radio lobes are generally, but not always, outside the visible optical images.

This effect clearly indicates that there is a fundamental, possibly symbiotic relation

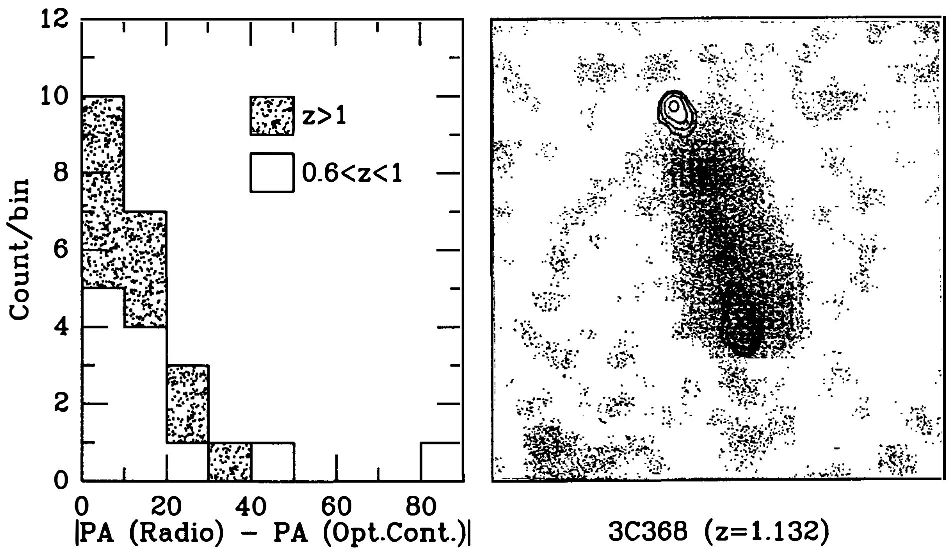

Figure 5. Alignment between the optical and radio axes of distant radio-galaxies: (Left) A histogram of position angle (PA) differences between the optical major axes and axes connecting the radio lobes for 3C galaxies with $z > 0.6$, from McCarthy *et al.* [54]. (Right) An example of the phenomenon is 3C368. Shown here are radio intensity contours over a narrow-band [O II] 3727 gray scale image, from Djorgovski *et al.* [30]. The field shown is 15 arcsec square, with N at the top, E to the left.

between the radio-sources and their host galaxies. Probably the most natural explanation is that star formation is somehow stimulated along the radio ejection axes. There is at least one known case at low redshifts, the Minkowski's Object [56,57] where interaction of a radio jet with a gas-rich dwarf galaxy appears to be causing a starburst. Several other interesting cases were reviewed by van Breugel [58], and references therein. However, the luminosities of, and star formation rates in the radio-galaxies discussed here surpass such cases by some two orders of magnitude, and that may be a problem with this hypothesis.

There are several possible mechanisms in which the flow of (sub?)relativistic plasma along the radio ejection axis may disturb the ISM of the parent galaxy. The jets themselves have much too small cross-sections, but they may be surrounded by larger turbulent regions, and may precess, and thus scoop a considerable volume. Also, there may be back-flows from the radio lobes, which could be highly turbulent, and have cross-sections of many kpc. Finally, there may be massive collimated galactic winds from the accretion disks around radio-source cores [59–61]. Enormous radio powers of 3C and 4C galaxies at large redshifts are suggestive of larger momentum transfers, which may account for more induced star formation than in any known low-z case; in addition, back then there was more gas to hit. The physics of this proposed mechanism is far from clear, and it is well worth further investigation: it is not even clear whether the highly supersonic flows of the radio plasma, or the galactic winds should stimulate or suppress star formation! A possible test would be to compare the near-IR and visible images of these sources: if most stars in elongated visible structures are formed *in situ*, in an interaction of radio-source plasma and ambient gas, they would be almost absent in the near-IR, where the older stars should dominate.

An alternative explanation may be that we are dealing with a physical selection effect, or a combined, symbiotic picture: There is a well-known problem of angular momentum loss in feeding of active nuclei [62]. Let us suppose that the most efficient way of powering a Fanaroff-Riley type II radio galaxy (powerful lobes, and a very weak core) involves a fuel transfer onto the central engine in a very narrow cone, along its principal axis; otherwise, some other type of AGN gets formed, e.g., with a radio-loud core or a luminous broad-line region. Then only the sources in which the fuel supplier is passing through the feeding cone (which would subsequently correspond to the jet/lobes axis) would trigger the formation of powerful radio lobes, which would be picked up in the 3C and 4C samples. In fact, some very special geometrical selection is probably inevitable: these are a few tens of the most powerful radio sources in $\sim 1/3$ of the observable Universe. A possible test of this admittedly very speculative hypothesis is to establish whether there is a radio-power threshold for the effect at any redshift. If we are dealing with some such selection effect, and the jet/backflow/wind-induced star formation is secondary, or relatively negligible, these galaxies would be less unusual, but just radio-loud representatives of a more common class of merging systems.

An alternative hypothesis to explain the observed properties of distant radio-galaxies, viz., massive cooling flows at large redshifts, was proposed by Fabian *et al.* [63]. It appears to be somewhat *ad hoc*, since we do not know that there were even rich clusters formed by then, let alone cooling flows; moreover, such hypothetical flows must have ceased at some intermediate redshift, otherwise these galaxies would be intrinsically *fainter* at those epochs than they are now [52]. Finally, the coolong flows hypothesis can hardly account for the good spatial and morphological corerspondence between the optical continuum, emission-line gas, and radio structure.

Another interesting fact is that there is a real redshift cutoff to the powerful (3C) sources [14,15], at $z \sim 2$. This was predicted from the models of source counts by Windhorst [64]. In other words, the powerful radio sorces first appear in the redshift range $z \sim 1 - 2$, in which we see the phenomena described above. It is intriguing that the same process, strongly dissipative mergers at large redshifts, may be responsible for the generation of powerful radio-sources, and aggregation of objects which may evolve into the present-day gE or cD galaxies. This is, perhaps, another small reason why mergers may be the primary trigger of the observed phenomena, with any possible feedback and interaction of the radio-source with its host galaxy following.

The question of galaxy evolution (or "growth") is not easily separable from the question of galaxy *formation*. (A convenient, if loose, definition of galaxy formation may be this: the time and process in which most of its gas forms its final constituent stars.) Even if we restrict ourselves to the narrow meaning of the term, the "original" dissipative collapse of classical ellipticals and bulges, the question is if there ever was a well defined and relatively short epoch of galaxy formation? There are now some signs of an emerging paradigm of gradual, or distributed galaxy formation, which combine both the new theoretical attitudes [65–67], and the new observations of fascinating objects which may be tentatively identified as galaxies forming at large redshifts [15,68–72]. I will briefly describe some intriguing high-z Lyα galaxies; more details are given elsewhere [68–78].

There are now several radio-galaxies known with redshifts above the atmospheric ozone limit for Lyα detection ($z > 1.6$), and from each of them we detect strong Lyα. These are in order of decreasing redshift: 3C 454.1, 326.1, 256, 239, 294, 194, 322, 470, 241, and "1-Jy" 1141+35 [14,15]. One or two of them (3C 256, possibly 239) have companion galaxies which also may have a moderate Lyα emission, which would be very interesting, showing that the phenomenon is not limited only to the enormosly powerful radio-sources. A subset of these galaxies (3C326.1, $z = 1.825$, and 3C294, $z = 1.779$; possibly also 3C 194, 68.2, and 222) have very interesting properties, which put them in a separate class, and tempt their identification as galaxies or small groups in the process of formation [15,68–72].

This new type of objects is distinguished by a very strong Lyα emission, resolved both spatially (over 10 – 15 arcsec, corresponding to > 100 kpc in the rest-frame) and in velocity ($\geq$ 1000 km/s velocity gradient or shear, with a comparable velocity width, suggestive of a high turbulence). Their continuum images have the same extent as the associatted Lyα clouds, blue colors, and lower luminosities and surface brightness than the other 3C galaxies at comparable redshifts. The appearance of both continuum and Lyα

is lumpy (Figure 6). The spectra are generally of low ionization (no C IV 1549 detected in 3C326.1, but some in 3C294). The inferred star formation rates (from the emission-line spectra and photometry) are a few hundred $M_\odot$/yr, which also suggests a large supernova rate. At least in the case of 3C326.1, the spectrum is very soft, and there is no radio core; this makes it unlikely that there is a "burried AGN" ionizing the gas, and some other mechanism is necessary. The observed Lyα fluxes from these galaxies are typically $\sim 10^{-15}$ erg/cm^2/sec, which in a $H_0 = 50$, $q_0 = 0$ Friedman cosmology at these redshifts translates to the rest-frame luminosities of $\sim 10^{55}$ Lyα photons/sec. Population synthesis models, scaled to $M_V = -23$ at $z = 0$, with the redshift of galaxy formation $z_{gf} = 5$, fail to produce sufficient numbers of ionizing photons bu 2 – 3 orders of magnitude, even assuming no internal extinction. However, the same models but with the $z_{gf} = 2$, produce ionizing photon fluxes comparable to the Lyα fluxes, and thus can account for at least a part of the observed emission. The answer is probably a combination of photoionization by young stars which we see, and collisional ionization in the supernova shocks, and in tentative inelastic collisions of infalling clouds or gas-rich fragments.

In other words, the properties of these objects are almost exactly what "textbook" primeval galaxies should look like! Except that: (1) they are "only" at $z \simeq 1.8$, rather than $z \simeq 5-10$, and (2) they have already well-formed radio sources. Both of these difficulties, as well as the question of the ionization balance, can be solved if one accepts that large galaxies can form at $z \simeq 2$. This is, in fact, what the modern theories of galaxy formation would like [66,67,79,80]. Figure 7 shows two snapshots from a cold dark matter (CDM) N-body simulation by Frenk *et al.* [80]. The resemblance of the merging group of protogalactic fragments at $z \simeq 1$ in this simulation, and the real 3C326.1 is striking. Some of the faint objects seen in the ultra-deep galaxy counts by Tyson and collaborators [11] may be similar protogalactic fragments, which have not merged yet.

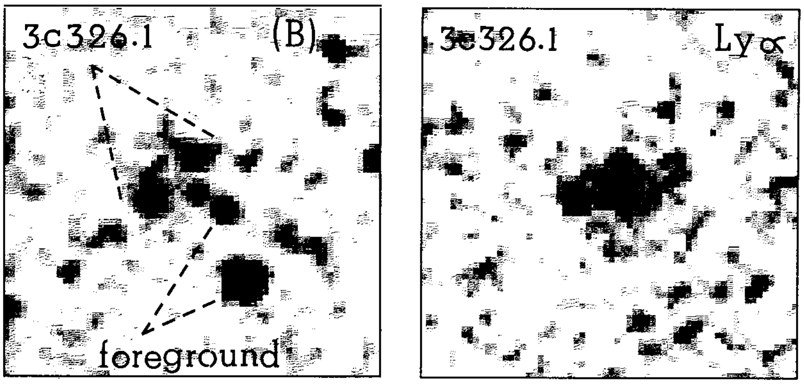

Figure 6. Images of 3C326.1 in the broad-band B continuum, which is free of any emission lines (left), and a narrow-band Lyα (right). The field sizes are 37.4 arcsec, with N at the top and E to the left. The data were obtained with a RCA CCD at the Kitt Peak 4-m telescope. Note the lumpy morphology in both images, and compare with the CDM simulation shown in Figure 7.

Of course, there are thousands of quasars known which are at even larger redshifts, and it is easy to find more. The comoving number density of QSO's does seem to peak near $z \sim 2-3$, with most distant QSO's known just at $z \geq 4$, and the appearance of QSO's may be closely following the appearance of galaxies. If there was any primordial clustering, it makes sense to look for galaxies near high-z quasars. The technique of Lyα imaging [76] was concieved to do that. To date, two interesting systems have been found using this method: a companion galaxy to the quasar PKS 1614+051, at $z = 3.215$ [76,77], and a pair of Lyα objects (or gravitationally lensed images of a single object) near the gravitational lens system MG 2016+112, at $z = 3.273$ [73,74].

The properties of the galaxy companion of PKS 1614+051 are described in more detail elsewhere [76,77,81]. Suffice to say that the object does have a marginally extended optical continuum, detected both spectroscopically and in a direct imaging, with $R_{cont} \simeq 24$, and no radio emission at a very low level ($\sim$ 30 μJy at 6 cm). This continuum is then plausibly interpreted as being mostly or entirely stellar. The Lyα gas is also extended, but in a different way from the underlying continuum; there are some suggestions of a tidal interaction with the neighbouring QSO. The object does have some nucleated C IV 1549 emission, which probably comes from a low-level active nucleus (the Lyα is narrow, so that the tentative active nucleus cannot be very dominant). Very little is known about the Lyα clouds in the MG 2016+112 system [73,74]. The important point is that (a) there are non-QSO objects, presumably galaxies, at $z > 3$, and (b) by the virtue of their large redshift, they must be still very young, no matter at which redshift they commenced forming.

Lyα photons clearly escape from all these objects without much difficulty; this is contrast with the findings for low-z dwarfs [82–84], where Lyα emission is weak or absent.

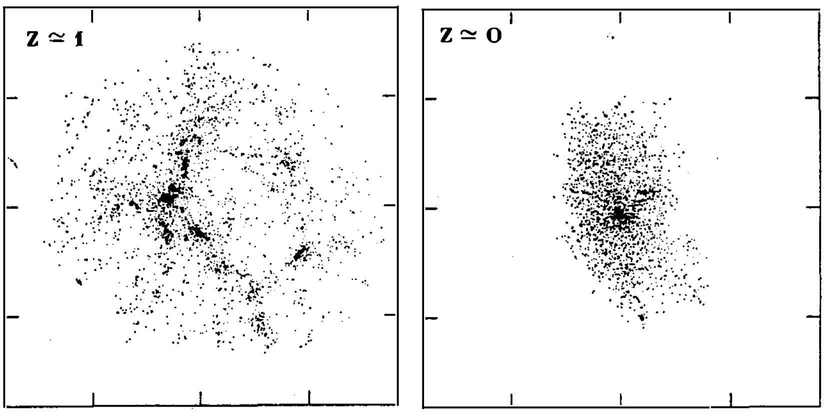

Figure 7. Two snapshots from a N-body CDM simulation of galaxy formation by Frenk *et al.* [80], corresponding to the redshifts of 1 (left) and 0 (right). A merging group of fragments at $z \simeq 1$ becomes a system quite like a cD galaxy at $z \simeq 0$. The tickmarks correspond to 1 Mpc intervals, assuming a $H_0 = 50$, $q_0 = 1/2$ Friedman cosmology. (Figure courtesy of Marc Davis.)

Apparently, there is very little dust in our high-z objects, suggesting that the reprocessing of the ISM in them is still at an early stage. Moreover, their enormous velocity fields make it possible for Lyα photons to escape absorption in the neutral gas. In any event, detection of distant (and possibly primeval) galaxies through Lyα emission is observational reality, and extrapolations of properties of low-z dwarfs to high-z giants may not be very pertinent, at least for the more massive and luminous systems.

Our group and others surveyed about 50 other QSO fields at $z > 2$, mostly at $z > 3$, and no other Lyα companion galaxies of comparable luminosity were found [71,78,81], although some very marginal detections are possible. The Lyα-luminous galaxies are scarce. It is possible that we are catching them in a brief period between the initial onset of star formation, and the generation of enough dust to efficiently trap the Lyα photons.

Finally, a few words on the formation of disks. The systems causing damped Lyα absorption are very plausible candidates for young disks at large redshifts [85–87]. Their optical luminosities may be too low for a direct detection in a near future. Almost primordial (proto?)disks may exist today: Malin–1 is a spectacular example [88]. And low-luminosity starburst dwarfs like I Zw 18, II Zw 40, or Mrk 36, were for a long time recognised as probable young galaxies, undegoing their first bursts of star formation [84,89,90].

The principal difficulty of the CDM theory of large-scale structure and galaxy formation (and many others) appeared to be the propensity to form galaxies too late, even at $z \simeq 1$. This is eminently possible, given the new data. Such large variation of z_{gf}, proposed earlier by Tinsley and Larson [91], and Silk and Wyse [65,92,93], is consistent with the photometric properties of distant radio-galaxies, as shown in Figure 8. A relatively quiescent formation of ellipticals out of smaller fragments at $z \sim 1 - 3$ could have well passed undetected in optical searches for primeval galaxies [94]. It is also possible that the bulk of primeval galaxy searches at $z \geq 5$ failed, because there were no luminous primeval galaxies that far back, and the smaller fragments which could have formed at $z \sim 5$ or earlier were too faint to detect with the available technology.

And so, I would like to advocate the view of galaxy formation not as a distant cataclysmic event, but rather as *an evolving sequence of processes*, which dominate formation of different objects at different cosmic epochs, and may overlap. The common denominator of most of them seems to be dissipative merging of gas-rich fragments, and star formation stimulated thereby. There is really no solid evidence that the bulk of stars in any given galaxy formed in a narrow time span at any particular redshift. While the bulk of the old populations is probably largely formed at $z > 1$, or perhaps even at $z \geq 3 - 5$, there are I Zw 18, Malin–1, and similar objects forming even now, and objects like Arp 220 doing things reminiscent of an earlier era. In the wise words of Toomre [95], these must be "just the statistical dregs of a once very common process". The exciting thing is that we are now begining to observe directly that very common process, as it occurs at large redshifts.

This paper is largely based on the work, data, and ideas by my able collaborators, Hy Spinrad, Mark Dickinson, Patrick McCarthy, Wil van Breugel, Michael Strauss, and others. They get the credit for the good data and interesting effects reported above, but I get the blame for the dubious interpretation and all errors. Thanks are due to the staffs of KPNO, Lick, MMT, CTIO, CFHT, and VLA observatories, for their tireless and highly professional help during numerous observing runs. Partial support from Harvard University and a AAS Travel Grant are gratefully acknowledged.

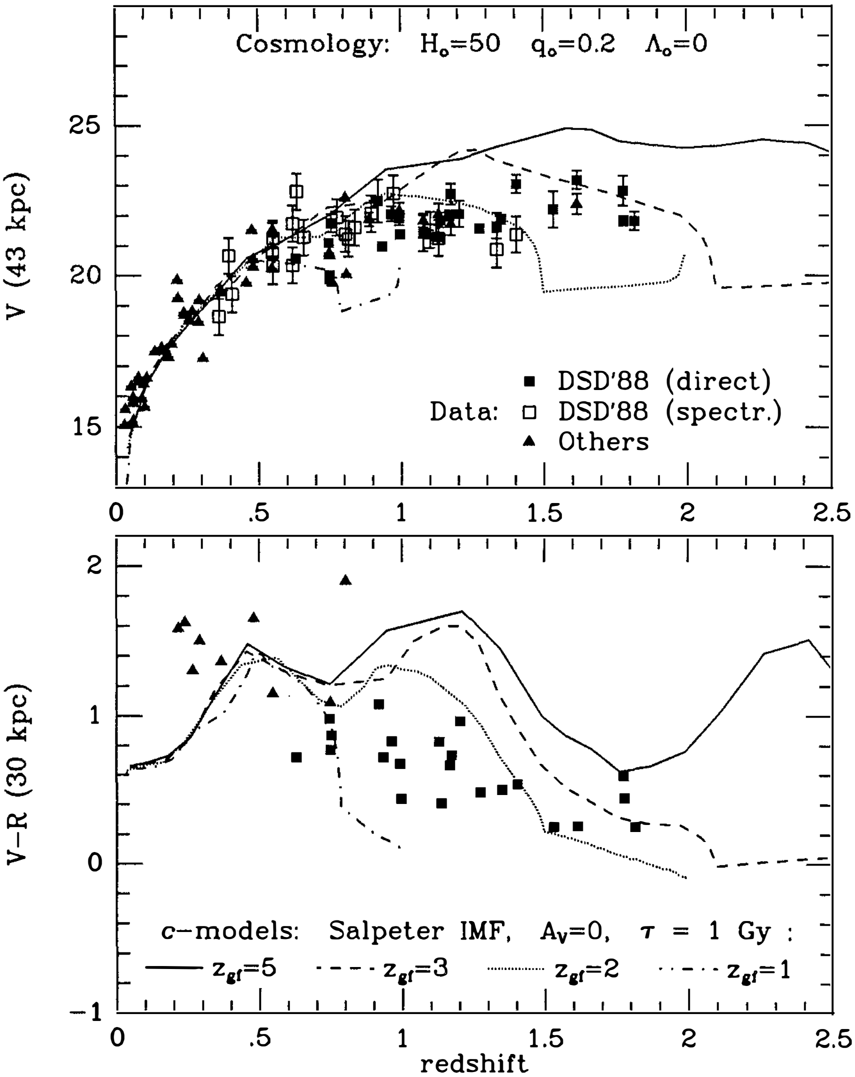

Figure 8. A comparison of population synthesis models with a range of galaxy formation redshifts (z_{gf}) with the photometric data on distant radio-galaxies, as in Fig. 2. Single-burst ("c") models, with the initial star formation phase of 1 Gy duration are shown here; similar results can be obtained with a set of μ-models and a range of z_{gf}. All models were scaled to $M_V = -22.6$ at $z = 0$. Galaxy formation at $z \sim 1 - 2$ is allowed by the data.

References:

1. Tinsley, B. 1986, *Fundam. Cosm. Phys.* **5**, 287.
2. Chiosi, C., and Renzini, A., (editors) 1986, *The Spectral Evolution of Galaxies.* Dordrecht: D. Reidel.
3. Bruzual, G. 1981, Ph. D. Thesis, University of California at Berkeley.
4. Bruzual, G. 1983, *Ap. J.* **273**, 105.
5. Bruzual, G. 1987, in *Nearly Normal Galaxies*, proceedings of the Santa Cruz Astrophysics Workshop, ed. S. Faber, p. 265. New York: Springer.
6. Arimoto, N., and Yoshii, Y. 1987, *Astron. Ap.* in press.
7. Guiderdoni, B., and Rocca–Volmerange, B. 1987, *Astron. Ap.* in press.
8. Rocca–Volmerange, B., and Guiderdoni, B., this volume.
9. Dressler, A., and Gunn, J. 1983, *Ap. J.* **270**, 7.
10. Dressler, A. 1987, in *Nearly Normal Galaxies*, proceedings of the Santa Cruz Astrophysics Workshop, ed. S. Faber, p. 276. New York: Springer.
11. Tyson, J.A., Seitzer, P., and Boeshaar, P. 1987, in preparation.
12. Tyson, J. A. 1986, *A. J.* **92**, 691.
13. Allington–Smith, J., *et al.* 1982, *M.N.R.A.S.* **201**, 331.
14. Spinrad, H., Djorgovski, S., Marr, J., and Aguilar, L. 1985, *P.A.S.P.* **97**, 932.
15. Spinrad, H. *et al.* 1988, in preparation.
16. Spinrad, H. 1986, *P.A.S.P.* **98**, 269.
17. Lilly, S., and Longair, M. 1982, *M.N.R.A.S.* **199**, 1053.
18. Lilly, S., and Longair, M. 1984, *M.N.R.A.S.* **211**, 833.
19. Lebofsky, M., and Eisenhardt, P. 1986, *Ap. J.* **300**, 151.
20. Eisenhardt, P., and Lebofsky, M. 1987, *Ap. J.* **316**, 70.
21. Djorgovski, S., Spinrad, H., and Marr, J. 1985, in *New Aspects of Galaxy Photometry*, ed. J.–L. Nieto, *Lecture Notes in Physics* **232**, p. 193. Berlin: Springer Verlag.
22. Djorgovski, S., Spinrad, H., and Dickinson, M. 1987, to be submitted to the *Ap. J.*
23. Djorgovski, S. 1987, in *Nearly Normal Galaxies*, proceedings of the Santa Cruz Astrophysics Workshop, ed. S. Faber, p. 290. New York: Springer.
24. Spinrad, H., and Djorgovski, S. 1984, *P.A.S.P.* **96**, 795.
25. Spinrad, H., and Djorgovski, S. 1987, in *Observational Cosmology*, proceedings of IAU Symposium 124, ed. G. Burbidge. Dordrecht: Reidel, in press.
26. Yates, M., Miller, L., and Peacock, J. 1986, *M.N.R.A.S.* **221**, 311.
27. Djorgovski, S. 1983, *J. Ap. Astron.* **4**, 271.
28. Spinrad, H., and Djorgovski, S. 1984, *Ap. J. Lett.* **280**, L9.
29. Spinrad, H., and Djorgovski, S. 1984, *Ap. J. Lett.* **285**, L49.
30. Djorgovski, S., Spinrad, H., Pedelty, J., Rudnick, L., and Stockton, A. 1987, *A. J.* **93**, 1307.
31. McCarthy, P. J. 1988, Ph. D. Thesis, University of California, Berkeley.
32. Le Fevre, O., Hammer, F., Nottale, L., and Mathez, G. 1987, *Nature* **326**, 268.
33. Djorgovski, S. 1985, Ph. D. Thesis, University of California at Berkeley.
34. Robinson, A., Binette, L., Fosbury, R., and Tadhunter, C. 1987, *M.N.R.A.S.* **227**, 97.
35. Larson, R., and Tinsley, B. 1978, *Ap. J.* **219**, 46.
36. Schweizer, F. 1986, *Science* **231**, 227.
37. Schweizer, F. 1987, in *Nearly Normal Galaxies*, proceedings of the Santa Cruz Astrophysics Workshop, ed. S. Faber, p. 18. New York: Springer.
38. Rieke, G., *et al.* 1980, *Ap. J.* **238**, 24.
39. Rieke, G., *et al.* 1985, *Ap. J.* **290**, 116.
40. Lonsdale, C., Persson, E., and Matthews, K. 1984, *Ap. J.* **287**, 95.
41. Heckman, T., *et al.* 1986, *Ap.J.* **311**, 526.
42. Joseph, R., and Wright, G. 1985, *M.N.R.A.S.* **214**, 87.
43. Joseph, R., this volume.
44. Harwit, M., Houck, J., Soifer, B., and Palumbo, G. 1987, *Ap. J.* **315**, 28.
45. Sanders, D., *et al.* 1986, *Ap. J. Lett.* **305**, L45.
46. Sanders, D., *et al.* 1987, *Ap. J. Lett.* **312**, L5.
47. Sanders, D., *et al.* 1987, *Ap. J.* in press.
48. Hutchings, J. 1983, *P.A.S.P.* **95**, 799.
49. Terlevich, R., and Melnick, J. 1981, *M.N.R.A.S.* **195**, 839.
50. Melnick, J., and Terlevich, R., this volume.

51. Silk, J. 1985, *Ap. J.* **297**, 9.
53. Pacholczyk, A. 1977, *Radio Galaxies.* Oxford: Pergamon.
52. Silk, J., Djorgovski, S., Wyse, R., and Bruzual, G. 1986, *Ap. J.* **307**, 415.
54. McCarthy, P.J., Van Breugel, W., Spinrad, H., and Djorgovski, S. 1987, *Ap. J. Lett.* **321**, L000.
55. Chambers, K., Miley, G., and van Breugel, W. 1987, *Nature*, in press.
56. van Breugel, W., Filippenko, A., Heckman, T., and Miley, G. 1985, *Ap. J.* **293**, 83.
57. Brodie, J., Bowyer, S., and McCarthy, P. 1985, *Ap. J. Lett.* **293**, L59.
58. van Breugel, W. 1986, *Can. J. Phys.* **64**, 392.
59. Heckman, T.M., Armus, L., and Miley, G.K. 1987, *A. J.* **93**, 276.
60. McCarthy, P.J., Heckman, T., and van Breugel W.J.M. 1987, *A. J.* **93**, 272.
61. Heckman, T., this volume.
62. Gunn, J. 1979, in *Active Galactic Nuclei*, C. Hazard and S. Mitton (eds.), p. 213. Cambridge: Cambridge University Press.
63. Fabian, A., Arnaud, K., Nulsen, P., and Mushotzky, R. 1986, *Ap. J.* **305**, 9.
64. Windhorst, R. 1984, Ph. D. Thesis, University of Leiden.
65. Silk, J., and Wyse, R. 1986, in *Structure and Evolution of Active Galactic Nuclei*, p. 173, ed. G. Giuricin *et al.*. Dordrecht: Reidel.
66. Baron, E., and White, S. D. M. 1987,*Ap. J.* in press.
67. Szalay, A., and Silk, J. 1987, preprint.
68. McCarthy, P., Spinrad, H., Djorgovski, S., Strauss, M., van Breugel, W., and Liebert, J. 1987, *Ap. J. Lett.* in press.
69. McCarthy, P., *et al.* 1986, *Bull. Am. Astron. Soc.* **18**, 903.
70. Strauss, M. *et al.* 1987, in proc. of the IAP Astrophysics Workshop *Primeval and High-Redshift Galaxies*, J. Bergeron and B. Rocca–Volmerange (eds.), in press.
71. Spinrad, H. 1988, in proc. of the IAP workshop *High-Redshift and Primeval Galaxies*, J. Bergeron and B. Rocca–Volmerange (eds.), in press.
72. Djorgovski, S. 1988, in proc. of the Erice workshop *Towards Understanding Galaxies at Large Redshifts*, ed. R. Kron and A. Renzini, in press. Dordrecht: Reidel.
73. Schneider, D., *et al.* 1986, *A. J.* **91**, 991.
74. Schneider, D., *et al.* 1987, *A. J.* **94**, 12.
75. Spinrad, H., Filippenko, A. V., Wyckoff, S., Stocke, J., Wagner, M., and Lawrie, D. 1985, *Ap. J. Lett.* **299**, L7.
76. Djorgovski, S., Spinrad, H., McCarthy, P., and Strauss, M. 1985, *Ap. J. Lett.* **299**, L1.
77. Djorgovski, S., Strauss, M., Perley, R., Spinrad, H., and McCarthy, P. 1987, *A. J.* **93**, 1318.
78. Djorgovski, S., Spinrad, H., McCarthy, P., and Strauss, M. 1988, in preparation.
79. Davis, M., Efstathiou, G., Frenk, C., and White, S. 1985, *Ap. J.* **292**, 371.
80. Frenk, C., White, S., Efstathiou, G., and Davis, M. 1985, *Nature* **317**, 595.
81. Hu, E., and Cowie, L. 1987, *Ap. J. Lett.* **317**, L7.
82. Hartmann, L., Huchra, J., and Geller, M. 1984, *Ap. J.* **287**, 487.
83. Hartmann, L., Huchra, J., Geller, M., O'Brien, P., and Wilson, R. 1987, *Ap. J.* in press.
84. Huchra, J., this volume.
85. Smith, H., Cohen, R., and Bradley, S. 1986, *Ap. J.* **310**, 583.
86. Wolfe, A., Turnshek, D., Smith, H., and Cohen, R. 1987, *Ap. J. Suppl. Ser.* **61**, 249.
87. Wolfe, A. 1987, in proc. of the *13th Texas Symposium on Relativistic Astrophysics*, p. 309, Singapore: World Scientific.
88. Bothun, G. D., Impey, C., Malin D. F., and Mould, J. R. 1987,*A. J.* **94**, 23.
89. Kunth, D., and Sargent, W. L. W. 1986,*Ap. J.* **300**, 496.
90. Huchra, J., Geller, M., Hunter, D., and Gallagher, J. 1982, in *Advances in Ultraviolet Astronomy*, Y. Kondo (ed.). Washington: NASA.
91. Tinsley, B., and Larson, R. 1979, *M.N.R.A.S.* **186**, 503.
92. Wyse, R. 1985, *Ap. J.* **299**, 593.
93. Wyse, R., and Silk, J. 1986, *Ap. J. Lett.* **319**, L1.
94. Koo, D. 1986, in *The Spectral Evolution of Galaxies*, C. Chiosi and A. Renzini (eds.), p. 419. Dordrecht: D. Reidel.
95. Toomre, A. 1977, in *The Evolution of Galaxies and Stellar Populations*, B. Tinsley and R. Larson (eds.), p. 420. New Haven: Yale University Observatory.

PECULIAR MORPHOLOGY FOR HIGH REDSHIFT 3C GALAXIES.

O. Le Fevre (1,2) and F. Hammer (2)

1 Canada-France-Hawaii Telescope Corporation
P.O.Box 1597, Kamuela, HI., 96743, USA

2 DAEC, Observatoire de Meudon, 92195 Meudon, France

Abstract

High spatial resolution of 3 3CR high redshift radio-galaxies are presented here. They are all resolved into a multi component structure. From the previously published case of 3C324 we infer that the 3CR sample of radio-galaxies with Z>1 is subjected to gravitational amplification effects. The overluminosity of those galaxies will then be partly due to gravitational amplification biasing our current estimates of the amount of evolution.

I. Introduction

The study of very high redshift galaxies is certainly of the highest importance to our understanding of galaxy evolution. The 3C radio-galaxies sample is by now the only one containing galaxies to redshifts as high as 1.82 and from recent studies (see [1] and reference included therein) we have learned that the high redshift 3CR sample with z>1 clearly shows large luminosity excess as compared to the low redshift BCG sample. Moreover those galaxies often shows elongated shapes and people have tend to explain their luminosity colors and shapes in terms of strong evolution of their stellar populations.

Undoubtedly this sample is subjected to strong selection effects since it is flux limited, and so distant that foreground contamination of the line of sight by galaxies or clusters of galaxies are becoming more likely [2]. We have also to keep in mind that the total sample of 3CR galaxies with z>1 is only twenty or so and therefore each galaxy is to be considered as a particular case.

In this paper we will present high spatial resolution imaging done at CFHT and from the case of 3C324 that we have presented as a probable case for gravitational lensing [3] we will show why we have to consider seriously the possibility of gravitational lensing as to explain at least part of the overluminosity of the 3CR high redshift galaxies.

II. New High Spatial Resolution Imaging at CFHT

Since June 1986 three high redshift radio-galaxies among the 3CR sample have been observed. The very sensitive RCA2 CCD at CFHT was used either at Prime or Cassegrain focii. The frames were processed in a standard way and calibrations in fields from [4] were used to derive the magnitudes.

As seen in fig 1 a,b,c the long exposures all gained from the superb image quality and stability over long integration times at CFHT. The seeing as measured on the CCD frames (FWHM) is as good as 0.6 arcsec for 3C13 and 0.7 arcsec for 3C256 and 3C324 for a typical integration time of one hour. For such faint and small galaxies the gain in spatial resolution has been crucial to separate and observe new components but also to detect faint ones.

The structures detected are interesting by several points. First it is obvious that for such distant galaxies their size is huge. Using a H0=50 and q0=0 cosmology, we found that these galaxies range in size from 60 to 100 kpc which is quite unusual in our neighborhood. The multiple structure is evident at least 3 close components are seen in each case, and their closeness means that it is impossible to see them with a seeing worst than 0.8 arcsec. The way the components are distributed is also very interesting, from fig 1 a and fig 2 a,b one can see that the components are aligned within a few degrees and moreover the central component is the brightest. This kind of structure is clearly unusual and calls a special attention. After describing the case of 3C324, we will show that a description in terms of gravitational lensing by foreground galaxies is to be considered.

III. The Case of 3C324: A New Gravitational Lens?

3C324 is a very exciting case since our first observation of its multiple structure. From interferential imaging we believe that it is a strong candidate for the first case of gravitational lensing of a distant galaxy by a foreground one [3].

From the spectra taken by [5], we inferred the existence of a line system at a different redshift than the radio-galaxy lines, i.e z=0.845 instead of z=1.206 [2]. Deep exposures were taken with two interferential filters one containing the OII emission line at z=0.845 and with one containing CII at z=1.206. From fig. 1 the differential behaviour of component A and the others is obvious. Fig. 1a shows the 4 components A,B,C and D plus the close galaxy E in a deep exposure in R band. In fig. 1b taken in the CII line at z=1.206 A is much fainter and combines with C to give the image C+A which centroid is in between the position of A and C in the R frame but closer to C. A is therefore not emitting in this line and we detect only its continuum. In OII A is proeminent while the other components are not detected in fig. 1c composite of two images with a 3 hours total exposure. Moreover, the R-I color index computed for each component is clearly different for A and the other components, i.e. 0.65 as compared to 1.07. From this data we concluded that A is probably a foreground spiral galaxy at a redshift z=0.845.

Taking into account the small separation angles between the components gravitational amplification of the background radio-galaxy must occur providing that the mass of the foreground galaxy is around 10**12 solar masses, a reasonable assumption as compared to its absolute magnitude ten times brighter than our own galaxy.

IV. Discussion: Implications on Galaxy Evolution at High Redshift

The interest in the high redshift 3CR galaxies sample is the hope to derive the amount of evolution in the stellar populations of these most distant galaxies. But before facing the problem of evolution one has to consider the biases possibly affecting such a small flux limited and very distant sample. As discussed in [2]:

- Gravitational lensing by foreground galaxies and clusters of galaxies may enhance the luminosity of 3C distant galaxies by several magnitudes in both optical and radio wavelength.

- A flux limited sample as 3C distant radio-galaxies should be strongly affected by gravitational lensing specifically because their radio-flux is very close to the 10 Jy detection limit.

These effects are actually at work in the 3C subsample of the twenty most distant galaxies with z>1. There is a significant excess of sources behind foreground galaxies (within a few arcsec) or clusters of galaxies (within a few arcmin) certainly acting as powerful gravitational deflectors. This leads us to think that the unusual observed properties of distant radio-galaxies are coming mainly from gravitational lensing rather than from physical properties (i.e. evolution and/or merging).

Our new imaging of distant 3CR galaxies fits well with this idea. Multiple components, their locations, brightnesses and colors are actually better explained by gravitational lensing effects [6]. From the case of 3C324 we may infer how taking into account this selection effect may change the general ideas on galaxy evolution at high redshift. If we correct the flux and color of 3C324 with respect to the foreground galaxy and the amplification, the real 3C324 should have a total magnitude lowered by 2 magnitudes and the R-I color index redder by 0.2 magnitudes. This is typically the order of magnitude of the strong evolution of the stellar populations.

One has to be careful when deriving the amount of evolution from observations of 3CR distant galaxies because:

- The galaxies are faint as a whole but with very faint components and needs sub-arcsec spatial resolution observations.

- Evolution is mixed with selection effects coming from gravitational lensing by foreground galaxies and clusters of galaxies which mimic evolution. In the same way a change in the value of the poorly constrained parameter q_0 could modify drastically our measure of the true evolution of distant galaxies [7].

We think that overluminosity of distant radio-galaxies is a mixture of evolution, gravitational lensing effects and q0 value, the two latter being due to the space curvature of our inhomogeneous universe. More high spatial resolution imaging and spectroscopy of 3CR galaxies are needed to precise this idea.

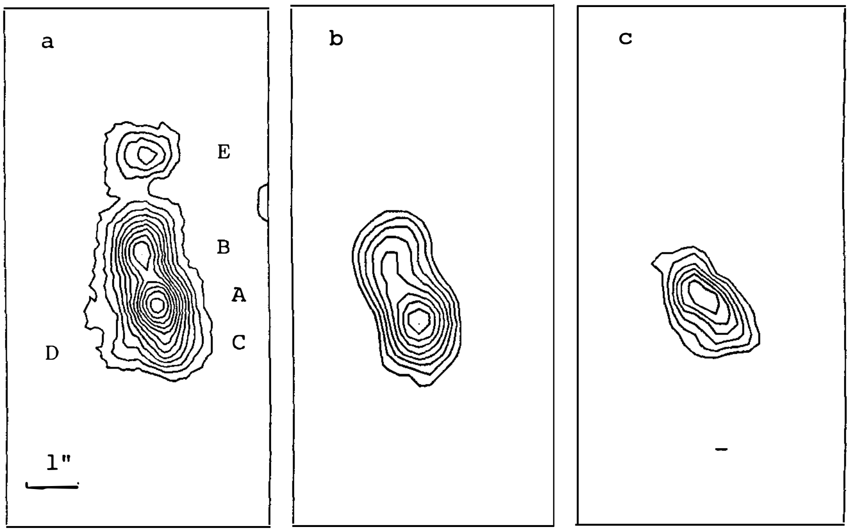

Fig. 1: (a) 3C324, R filter, CFHT F/8.
(b) 3C324, imaging in interferential filter including [CII] at Z=1.206.
(c) 3C324, filter including [OII] emission line at Z=0.845.

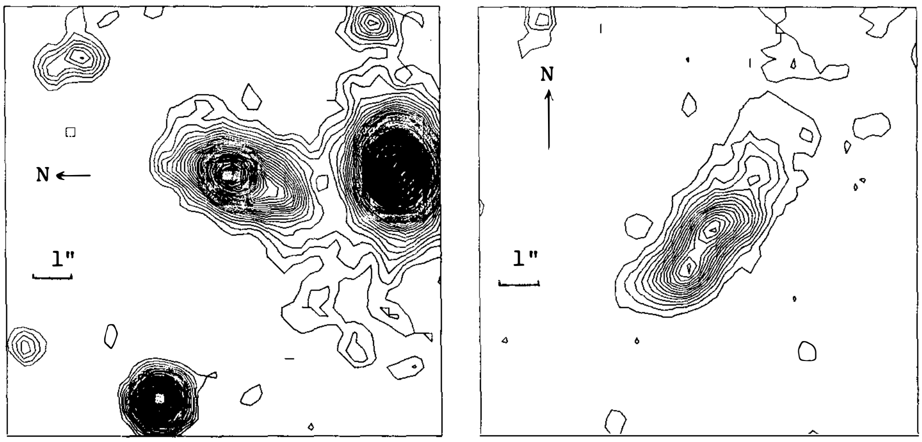

Fig. 2: (a) 313 Z=1.351, R filter, f/4.
(b) 3C256, Z=1.819, R filter, f/4.

REFERENCES

[1] Spinrad, H., Djorgovski, S. To appear in Proceedings of IAU Symposium n°124, "Observational Cosmology", G. Burbidge, ed., Reidel.

[2] Hammer, F., Nottale, L., Le fèvre, O., Astron. Astroph. 169, L1-L3 (1986).

[3] Le fèvre, O., Hammer, F., Nottale, L. Mathez, G., Nature, 326, 268-269 (1987).

[4] Christian, C., Waddell, P., McGonegal, R., SPIE Proc. no 627, 500-508 (1986).

[5] Spinrad, H., Djorgovski, G., Astrophys. J., 280, L9-L12 (1984).

[6] Le fèvre, O., Hammer, F., Nottale, L., in preparation (1987).

[7] Wampler, E.J., to appear in Astron. Astroph. (1987).

STARBURST GALAXIES IN DEEP RADIO SURVEYS

J. J. Condon
National Radio Astronomy Observatory[1]
Edgemont Road
Charlottesville, VA 22903
USA

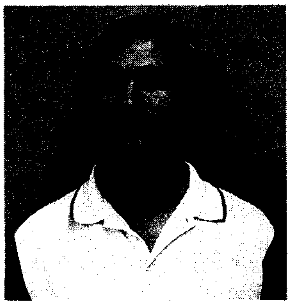

Abstract

Deep radio surveys reveal a rapidly increasing population of sources fainter than $S \approx 1$ mJy at $\nu = 1.4$ GHz. Its principal constituent appears to be spiral galaxies at cosmological redshifts: $\langle z \rangle \approx 0.8$. There is a tight correlation between the radio continuum and $\lambda = 60\ \mu$m far-infrared flux densities of spiral galaxies, so radio-selected spiral galaxies are intrinsically similar to *IRAS* galaxies, most of which are starburst galaxies. Evolutionary models based on the radio and far-infrared deep survey data indicate that starburst activity is evolving on cosmological time scales and accounts for about one-third of the 1.4 GHz discrete-source background.

---

[1] The National Radio Astronomy Observatory is operated by Associated Universities, Inc., under contract with the National Science Foundation.

1. Introduction

Nearly all radio sources stronger than $S \approx 1$ mJy at $\nu = 1.4$ GHz are associated with elliptical galaxies or quasars. The morphologies, sizes, and luminosities of these "classical" radio sources all point to supermassive compact objects as the ultimate energy source for their radio emission. The deepest radio surveys at $\nu = 1.4$ GHz detect far more sources with $S < 1$ mJy than expected from a simple extrapolation of the strong-source counts or from detailed evolutionary models of the radio sources produced by elliptical galaxies and quasars. These "unexpected" radio sources may represent an evolving population of spiral galaxies at cosmological redshifts, with most of their radio energy originating in starbursts.

The time scales for cosmological evolution are $> 10^9$ yr, and the duration of a starburst event may be $\approx 10^8$ yr. Both are much longer than the interval during which radio astronomical measurements have been made. Consequently the radio data can only present a "world picture" covering the surface of our past light cone, and the only way we can detect evolution with such data is by comparing different populations of radio sources observed at different lookback times. This essentially statistical problem of measuring evolution reduces to finding the evolving *radio luminosity function* $\rho(L|z)$ of spiral galaxies, where $\rho(L|z)dL$ is defined as the comoving density of radio sources with luminosities L to $L + dL$ at redshift z.

Radio flux-limited samples are well suited to such statistical investigations because: (1) Radio source samples are not confused by galactic stars. (2) Dust extinction in the parent galaxies of the sources themselves cannot hide emission from starbursts at radio wavelengths. (3) Most radio sources in starburst galaxies have featureless power-law spectra, so there are no uncertain redshift-dependent selection effects. (4) The most sensitive radio surveys could detect starburst galaxies known to exist locally even if they were moved to redshifts as high as $z \approx 1$. (5) Modern radio surveys are quite complete and reliable. The yield accurate flux densities and position uncertainties small enough ($\approx 1''$) that reliable optical identifications can be made by position coincidence even on deep CCD images. On the other hand, obtaining optical identifications and spectroscopic redshifts for all sources in a complete flux-limited sample is quite difficult. Consequently it is not possible to locate each source in the luminosity–redshift plane, and evolutionary *models* with only weak redshift constraints must be used to compare local and distant radio-source populations.

2. The Local Radio Luminosity Function

The local luminosity function $\rho(L|z = 0)$ of spiral galaxies at $\nu = 1.4$ GHz is based on sensitive VLA observations[1] of all spiral and irregular galaxies north of $\delta = -45°$ and brighter than $B_T = +12$ mag, the completeness limit of the *Revised Shapley-Ames Catalog.* The corresponding weighted luminosity function or "visibility function" $\phi(L|z = 0) \equiv L^{5/2}\rho(L|z = 0)$ is plotted in Figure 1, along with the local visibility function of E and S0 galaxies[2]. The visibility function weighting emphasizes those luminosity ranges that contribute the most sources to a flux-limited sample in the static Euclidean ($z \ll 1$) limit. For example, the local visibility function of elliptical galaxies has a maximum about two orders of magnitude higher than the peak local visibility function of spiral galaxies, so only about 1% of the strongest radio sources are found in spiral galaxies.

The peak of the spiral-galaxy local visibility function is at $L \approx 10^{22}$ W Hz^{-1}, indicating that typical *radio-selected* spiral galaxies are about an order of magnitude more luminous at radio wavelengths than our own galaxy. Most nearby spiral galaxies with 1.4 GHz luminosities $L \approx 10^{22}$ W Hz^{-1} have compact starburst cores[3] (e.g., NGC 520, NGC 660, NGC 3079, and NGC 7714) or extended disks with high star-formation rates[4] (e.g., NGC 1961, NGC 2146, NGC 3079, and NGC 4038); many are members of interacting systems[3]. They are *not* similar to "normal" optically selected spiral galaxies. In fact, since the $\lambda = 60\ \mu$m far-infrared and radio continuum flux densities of spiral galaxies are very strongly correlated[5], samples of radio-selected and *IRAS* spiral galaxies are almost identical.

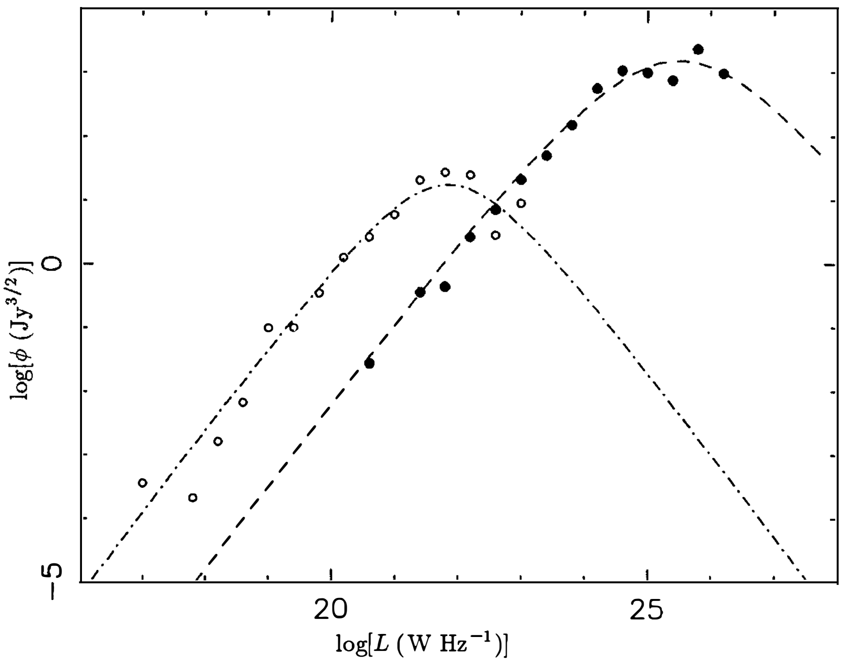

Figure 1. The local visibility functions of radio sources in spiral (open circles) and elliptical (filled circles) galaxies. The dash-dot and dashed curves are from the model described in Section 3.b. Note the sharp transition near $L \approx 10^{23}$ W Hz^{-1}. A Hubble constant $H_0 = 100$ km s^{-1} Mpc^{-1} is assumed throughout. Abscissa: log 1.4 GHz luminosity (W Hz^{-1}). Ordinate: visibility function (Jy$^{3/2}$).

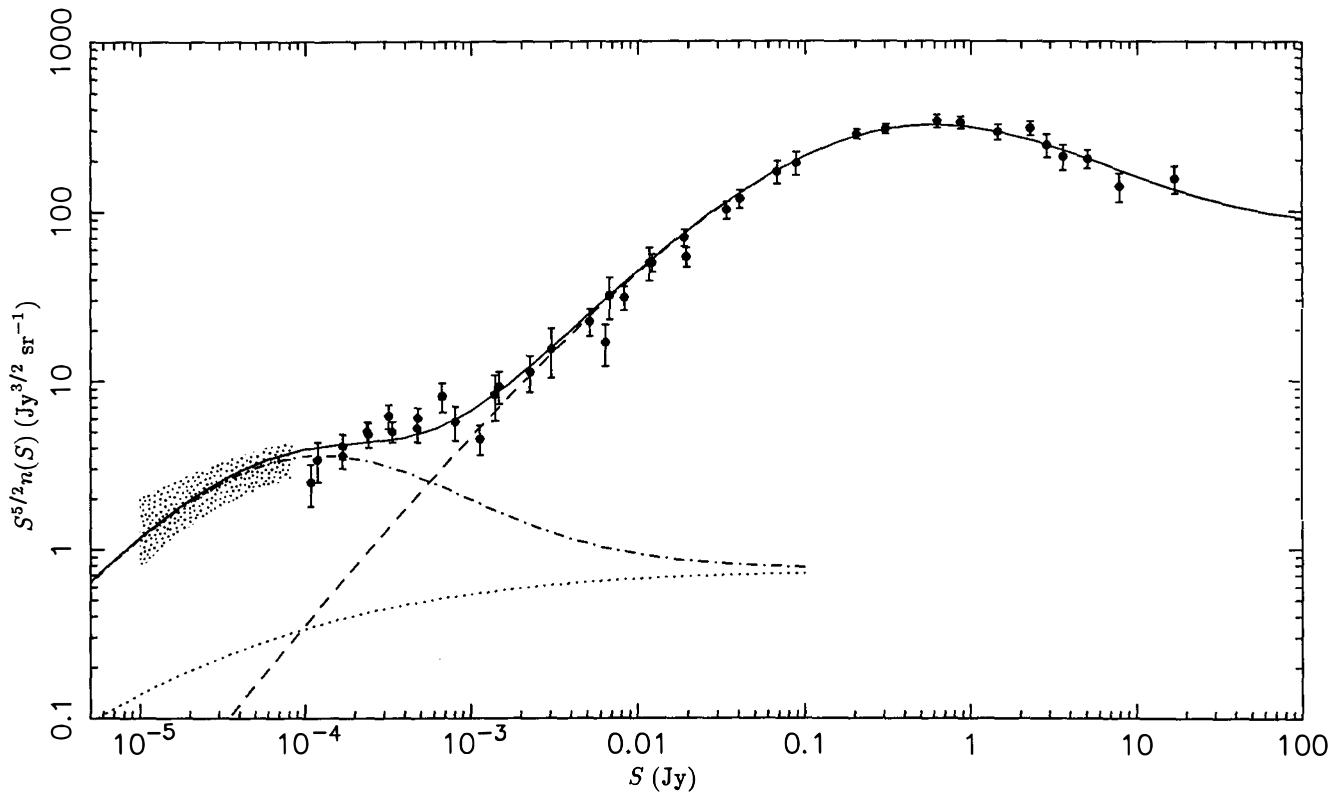

Figure 2. Weighted source count at $\nu = 1.4$ GHz. The evolutionary model described in Section 3.b. predicts the source counts contributed by elliptical galaxies (dashed curve), spiral galaxies (dash-dot curve), and their sum (solid curve). The dotted curve represents the source count that would be produced by ***nonevolving*** spiral galaxies only. Abscissa: flux density (Jy). Ordinate: weighted count (Jy$^{3/2}$ sr^{-1}).

3. Faint Radio Sources

3.a. The 1.4 GHz Source Count

The number $n(S)dS$ of sources per steradian with flux densities S to $S + dS$ is called the differential source count. The weighted 1.4 GHz source count $S^{5/2}n(S)$ is plotted in Figure 2. Points below $S = 1$ mJy are from the deepest VLA[6] and Westerbork[7] surveys, and the shaded area indicates the sky densities of sources estimated statistically[6]. Note the flattening $S^{5/2}n(S)$ below $S \approx 1$ mJy.

The sources with $S < 1$ mJy may be faint, but they are so numerous that they contribute significantly to the total background temperature T produced by extragalactic sources at $\nu = 1.4$ GHz. The Rayleigh-Jeans brightness temperature $T = [c^2/(2k\nu^2)] \int_S^\infty sn(s)ds$ from all sources stronger than S is plotted in Figure 3.

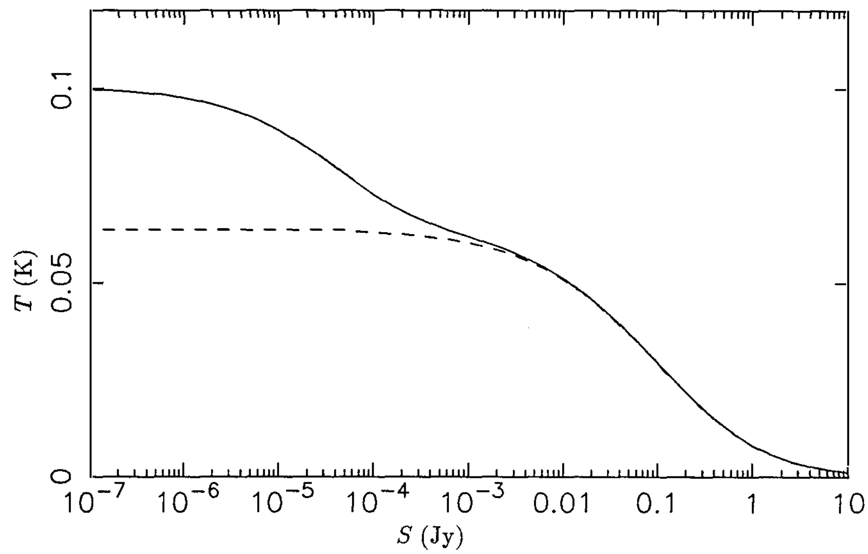

Figure 3. The extragalactic source background temperature T produced by all sources stronger than S at $\nu = 1.4$ GHz is indicated by the solid curve. From the model described in Section 3.b., the contribution from elliptical galaxies is shown by the dashed curve, and the difference between the solid and dashed curves is ascribed to spiral galaxies.

3.b. Evolutionary Models of the 1.4 GHz Source Count

Evolutionary models use the local luminosity function, source count, strong-source redshift distribution, plus the limited optical and infrared data available to constrain the evolution of the radio luminosity function. The contribution of sources associated with elliptical galaxies in one such model[8,9] is indicated by the dashed curve in Figure 2. While elliptical radio galaxies (and radio-loud quasars presumed to reside in elliptical galaxies) account for nearly all of the strong sources, they become a minority below $S \approx 1$ mJy. If the radio sources in spiral galaxies evolve at roughly the same rate as the radio sources in elliptical galaxies, they can account nearly all of the faintest radio sources (dash-dot curve in Figure 2), so that the total source count (solid curve) predicted by the model agrees with the data. This model also predicts that the median redshift of radio sources selected at $\nu = 1.4$ GHz is $\langle z \rangle \approx 0.8$ nearly independent of flux density for all $S < 10$ Jy — the faintest radio sources are not more distant, just intrinsically weaker. Most local low-luminosity radio sources are in spiral galaxies (Figure 1), so we *expect* that most faint ($S < 1$ mJy) radio sources are in spiral galaxies as well.

While this picture is consistent with the data, it is not unique and it depends on the unproven assumption that the radio-selected spiral galaxies evolve. Two alternative explanations for the large numbers of sub-mJy sources have been presented: (1) The faint sources are associated with *nonevolving* population of low-luminosity spiral galaxies at low ($z \approx 0.1$) redshifts[10]. The source count from a nonevolving population depends primarily on its local visibility function and only weakly on uncertain details of the assumed world model (e.g., the value of Ω). Nonevolving spiral galaxies can account for the observed faint-source population only if the local space density of radio-weak ($L < 10^{22}$ W Hz^{-1}) spiral galaxies is an order of magnitude higher than Figure 1 indicates. The new VLA data on bright spiral galaxies[1] appear to exclude this possibility. They yield only the source count contribution shown by the dotted line in Figure 2 for nonevolving spirals. Also the low redshifts predicted by the nonevolving model[10] are difficult to reconcile with the optical faintness of galaxies identified with sub-mJy sources[11]. (2) The faint radio sources may be a weakly evolving "new population" of blue radio galaxies[12] with luminosities $L \approx 10^{23}$ W Hz^{-1}. Such galaxies would be a new population because they are supposed to have a *local* space density $\approx$ 10 times that of the known spiral and elliptical galaxies shown in Figure 1. This high local space density of galaxies with $L \approx 10^{23}$ W Hz^{-1} has not been observed directly, but it was inferred from optical identifications of radio sources stronger than $S \approx 1$ mJy with distant galaxies[12]. Optically the blue radio galaxy identifications are about as luminous as bright spiral galaxies, and they "are often of peculiar compact morphology, sometimes interacting or merging"[12,13]. Only about 1/3 of the blue galaxies in a sample with $S > 1$ mJy have the optical and near-infrared colors characteristic of star-forming spiral galaxies[14]. The nearest ones (those with the lowest radio luminosities) are clearly spiral galaxies, but some of the more luminous ones may be broad-line radio galaxies (N-galaxies), photometrically misclassified elliptical galaxies, or misidentifications. The proportion of spiral galaxies in a radio-selected sample is expected to increase sharply at flux densities below $S \approx 1$ mJy (Figure 2), and the optical–near-infrared colors of sub-mJy source identifications confirm this expectation[15], so the main difference between this approach and the evolutionary model in Section 3.b. may only be a question of the local space density of radio-loud spiral galaxies, and not whether the faintest ($S < 1$ mJy) radio sources are really associated with spiral galaxies.

Two other pieces of evidence support the hypothesis that most of the faintest radio sources are in spiral galaxies: (1) the far-infrared source count and (2) the angular-size distribution of faint radio sources.

3.c. Comparison with the *IRAS* $\lambda = 60$ μm Source Count

An effective way to distinguish nearby radio-selected spiral galaxies from elliptical galaxies is by their far-infrared emission. Very few radio-selected elliptical galaxies are in the *IRAS* catalog of infrared sources with $S(60\ \mu\text{m}) \geq 0.5$ Jy, but there is a tight correlation between the far-infrared and radio flux densities of spiral galaxies[16]. Thus the contribution of spiral galaxies to the counts of faint radio sources may be estimated from the counts of faint far-infrared sources[17].

This infrared–radio correlation can be specified by the distribution of the statistic $u \equiv \log[S(60\ \mu\text{m})/S(1.4\ \text{GHz})]$. For an *infrared* flux-limited sample of spiral galaxies $\langle u \rangle = +2.15 \pm 0.15$ [16], so the $\lambda = 60$ μm source count extending to $S = 50$ mJy[18] constrains the $\nu = 1.4$ GHz radio source count down to $S \approx 0.35$ mJy. The distribution of u is narrow: $\sigma_u < 0.3$. If $\sigma_u = 0$, then the weighted source count $S^{5/2}n(S)$ scales exactly as $u^{3/2}$ and the infrared count implies that 20% of the observed sub-mJy radio sources are in spiral galaxies. If $\sigma_u > 0$, the fraction of radio sources in spiral galaxies must be even greater, and it may approach unity. In either case, the count of sub-mJy radio sources associated with spiral galaxies in this way exceeds the count predicted by the non-evolving model (dotted line in Figure 2).

3.d. The Relation Between Angular Size and Flux Density

The radio continuum emission from nearby radio-selected spiral galaxies is confined to those portions of the disk in which star formation is occurring[3,4]. In contrast, the radio sources produced by elliptical galaxies can extend far beyond the regions occupied by stars. The median angular size $\langle\theta\rangle$ of radio sources found at $\nu = 1.4$ GHz is a nearly constant $\langle\theta\rangle \approx 10''$ throughout the flux-density range $1 < S(\mathrm{mJy}) < 1000$. This corresponds to a linear size ≈ 40 kpc at the redshift distance of most radio sources (assuming $H_0 = 100$ km s^{-1} Mpc^{-1} and $\Omega = 1$). The angular sizes of cosmologically distant spiral galaxies are much smaller than this ($\theta \approx 2''$), so the majority of radio sources with $1 < S(\mathrm{mJy}) < 1000$ cannot be in spiral galaxies. If most sources fainter than $S \approx 1$ mJy are in spiral galaxies, the median angular size of these radio sources *must* be much smaller: $\langle\theta\rangle < 2''$. This prediction[8] has recently been confirmed observationally — the faintest radio sources selected at 1.4 GHz have $\langle\theta\rangle < 3''$ [19].

4. Discussion

An intense burst of star formation can increase the radio continuum luminosity of a spiral galaxy by an order of magnitude or more. Consequently, most spiral galaxies in radio flux-limited samples are starburst galaxies, just as *IRAS* galaxies are. Ordinary radio surveys would be as effective as far-infrared surveys for finding starburst galaxies, were they not dominated by radio-loud elliptical galaxies and quasars stronger than $S \approx 1$ mJy at $\nu = 1.4$ GHz. In contrast, radio surveys capable of detecting sources with $S \ll 1$ mJy are not dominated by sources in elliptical galaxies; they should be able to detect large numbers of starburst spiral galaxies at high redshifts. The evidence that they actually do includes (1) a flattening of the weighted source count below $S \approx 1$ mJy at $\nu = 1.4$ GHz, (2) the optical–near-infrared colors of galaxies identified with faint radio sources, (3) the deep far-infrared source count, and (4) the small median angular size of faint radio sources. Thus identifying sources found in the deepest radio surveys is probably an efficient way to find high-redshift starburst galaxies for further study.

If flux-limited samples of radio sources with $S < 1$ mJy at $\nu = 1.4$ GHz are primarily starburst galaxies, they can be used to show that the starburst phenomenon must evolve strongly with cosmological epoch. Statistical models[8,9] that explain the faint-source count by evolving the local radio luminosity function of spiral galaxies suggest that the median redshift of the faint sources is $\langle z \rangle \approx 0.8$.

REFERENCES

1. Condon, J. J. (1987). *Astrophys. J. Suppl.*, submitted.
2. Auriemma, C., Perola, G. C., Ekers, R., Fanti, R., Lari, C., Jaffe, W. J., and Ulrich, M. H. (1977). *Astron. Astrophys.* **57**, 41.
3. Condon, J. J., Condon, M. A., Gisler, G., and Puschell, J. J. (1982). *Astrophys. J.* **252**, 102.
4. Condon, J. J. (1983). *Astrophys. J. Suppl.* **53**, 459.
5. Helou, G., Soifer, B. T., and Rowan-Robinson, M. (1985). *Astrophys. J. Lett.* **298**, L7.
6. Mitchell, K. J., and Condon, J. J. (1985). *Astron. J.* **90**, 1957.
7. Oort, M. J. A. (1987). *Astron. Astrophys.*, submitted.
8. Condon, J. J. (1984). *Astrophys. J.* **284**, 44.
9. Condon, J. J. (1984). *Astrophys. J.* **287**, 461.
10. Subrahmanya, C. R., and Kapahi, V. K. (1983). *Proc. I.A.U. Symposium No. 104*, G. O. Abell and G. Chincarini, Eds. (Dordrecht: Reidel), p. 47.
11. Windhorst, R. (1986). *Highlights of Astronomy*, J. P. Swings, Ed. (Dordrecht: Reidel), p. 355.
12. Windhorst, R. (1984). Ph.D. thesis, University of Leiden.
13. Kron, R. G., Koo, D. C., and Windhorst, R. A. (1985). *Astron. Astrophys.* **146**, 38.
14. Thuan, T. X., Windhorst, R. A., Puschell, J. J., Isaacman, R. B., and Owen, F. N. (1984). *Astrophys. J.* **285**, 515.
15. Thuan, T. X., and Condon, J. J. (1987), in preparation.
16. Condon, J. J., and Broderick, J. J. (1986). *Astron. J.* **92**, 94.
17. Biermann, P., Eckart, A., and Witzel, A. (1985). *Astron. Astrophys.* **142**, L23.
18. Hacking, P., Condon, J. J., and Houck, J. R. (1987). *Astrophys. J. Lett.* **316**, L15.
19. Coleman, P. H., and Condon, J. J. (1985). *Astron. J.* **90**, 1431.

EVIDENCES FOR COSMOLOGICAL EVOLUTION OF ACTIVELY STAR FORMING GALAXIES

L. Danese [1], *G. De Zotti* [2], *A. Franceschini* [1], and *L. Toffolatti* [1]

[1] Dipartimento di Astronomia, Padova, Italy
[2] Osservatorio Astronomico, Padova, Italy

We have used the deepest surveys at radio and far infrared wavelengths to study the properties of starburst galaxies at cosmological distances. We find that all data require a substantial cosmological evolution of these sources. In the framework of a simple luminosity evolution model the required time scales are of the order of $\simeq 20\% \div 25\%$ of the Hubble time.

1. Introduction

Galaxies characterized by enhanced rates of star formation have long been recognized from morphological, photometric and spectroscopic studies in the optical band to comprise a non negligible fraction of field galaxies (Huchra, 1977). They usually show ultraviolet excess, radio and X-ray emissions larger than those of normal galaxies and strong mid- and far-infrared continua. A high fraction of them are observed in close binary or interacting systems (Balzano, 1983) and often display peculiar and distorted morphologies. Spectroscopically, they show narrow emission lines (half width $\simeq$ 150 Km/sec) and, generally, an intensity ratio $[OIII]\lambda5007 : H_\beta$ less than 3. Their very small $[NII]\lambda6584 : H_\alpha$ ratios suggest that photoionization by hot stars is very likely the primary energy-input mechanism (Balzano, 1983).

This paper deals with the problem of the cosmological evolution of this source population. For this analysis we have used the deepest surveys in various e.m. bands. In particular, optical identifications of deep samples of radio sources down to milliJansky and submilliJansky flux levels, (Kron, Koo & Windhorst, 1985) have revealed the emergence of a class of galaxies whose properties are consistent with those observed for starburst galaxies (Danese et al., 1987).

Since starburst regions are characterized by the presence of large amounts of dust, the far-IR IRAS band is the natural choice to analyse the properties of star-forming galaxies.

We show that all the available data from radio and far-IR bands can be accounted for by allowing actively star-forming galaxies to evolve on time scales of the order of $\simeq 20\% \div 25\%$ of the Hubble time ($H_0 = 50$ and $q_0 = 0.5$ have been adopted).

2. Starburst/Interacting galaxies in deep radio surveys

Data on bright radio sources ($S_{408} > 10$ mJy) are usually interpreted in terms of evolving flat- and steep-spectrum sources identified with elliptical+S0 galaxies and quasars (Peacock, 1985; Danese, De Zotti & Franceschini, 1985). At deeper flux levels, and down to at least 100 μJy, a striking outcome of the recent VLA deep surveys has been the discovery of a flattening in the slope of the differential counts (Condon & Mitchell, 1984; Windhorst, van Heerde & Katgert, 1984). Various suggestions have been made to explain this flattening: non evolving low luminosity sources, evolving spiral galaxies and a new class of blue galaxies with peculiar morphologies. We have explored in some detail the possibility that a population of actively star forming galaxies (we will refer to them in the following as Starburst/Interacting, or S/I, galaxies) is responsible for the upturn of the radio counts.

We have first derived the local radio luminosity functions of various galaxy populations, by using a bright subsample of the Uppsala General Catalogue including 1671 galaxies and complete to $m_{pg} = 14.5$. Complete information on radio fluxes at 2380 MHz is given by Dressel & Condon (1978), while the redshift distances for a large majority of the sources has been derived essentially from Palumbo, Tanzella-Nitti & Vettolani (1983) and Huchra et al. (1983). We have computed the contributions to the global luminosity function of some relevant classes of sources selected according to their different physical properties: spiral+irregular, elliptical+S0, Starburst/Interacting and Seyfert galaxies (Franceschini et al., 1987a). The S/I class in particular comprises non-Seyfert Markarians, Zwicky blue compacts and galaxies classified by Nilson (1973) as peculiars, disrupted, distorted, etc. By exploiting some of the richest radio selected samples, we have also determined the contributions of flat- and steep-spectrum radio sources (Toffolatti et al., 1987).

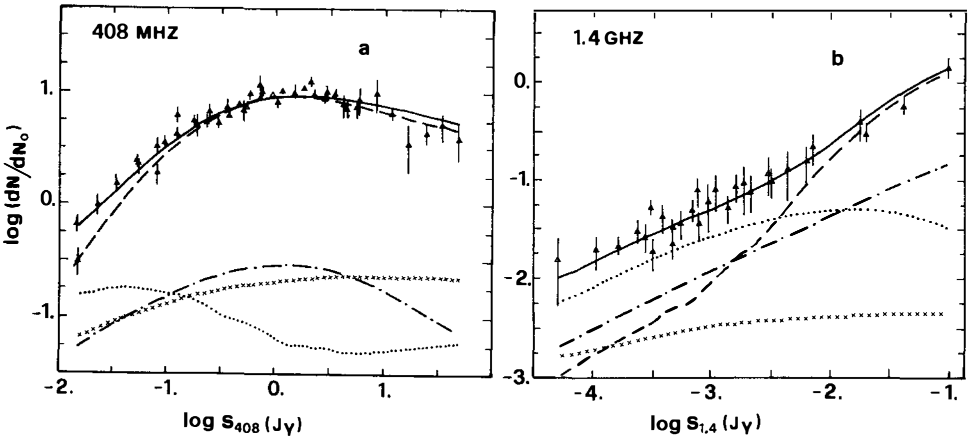

Figure 1. (a) Counts of radio sources at 408 MHz in the relative differential form ($dN_0 = 150 S_{408}^{-2.5} Jy^{-1} sr^{-1}$). The sources for the data points can be found in Danese, De Zotti & Franceschini (1985). The dashed and dot-dashed lines show the contributions of steep-spectrum and flat-spectrum E+S0+QSO; dotted lines and crosses are evolving Starburst/Interacting and unevolving spiral galaxies respectively. (b) Same as in Fig.(1a), but at 1.4 GHz.

Such careful determination of the various local luminosity functions (LLFs) has allowed us to work out a full model for the cosmological evolution of radio sources able to successfully reproduce all relevant radio data from the brightest to the faintest flux levels. We have adopted a simple scheme of luminosity evolution ($L(t) \propto exp[\tau(t) \cdot \kappa]$, τ being the look-back time and κ a constant) for both E+S0+QSO, S/I and Seyfert galaxy classes, while we have assumed no evolution for the spiral+irregular component (see for more details Danese et al., 1987). Figs. 1a and 1b show the best-fit contributions of these source populations to some crucial sets of data points. We can see that, while E+S0 galaxies and quasars dominate the bright source counts at both 408 MHz and 1.4 GHz, they clearly do not explain the upturn of counts below $S_{1.4} \sim 10$ mJy. Evolving normal spiral galaxies cannot, because of their low radio luminosities, contribute significantly in the flux range $1 < S_{1.4} < 10$ mJy, where the blue galaxies are found by Kron, Koo & Windhorst (1985) to be a sizeable fraction of the total identifications.

On the other hand, direct CCD imaging and spectroscopy (Kron, Koo & Windhorst 1985; Windhorst, Dressel & Koo, 1987) have revealed that indeed these blue galaxies, frequently showing morphological peculiarities which are indicative of interactions, are to be associated to a population of actively star forming galaxies, quite different from normal spirals. Hence, it has been natural to associate these sources to the Starburst/Interacting class defined above. As shown by the Fig.1 (dotted lines), a luminosity evolution of the S/I galaxies with time scales $\sim 20\% \div 25\%$ of the Hubble time is able to account for the observed flattening of the deep counts. Moreover, it also represents reasonably well the fraction of blue (S/I) to red (E+S0+QSO) galaxies identified in the Leiden-Berkeley deep surveys (Kron, Koo & Windhorst, 1985) over the entire flux range. It is also fairly well consistent with the available, still rather crude, information on the redshift distribution of the blue galaxies down to $F = 21$.

In conclusion, we confirm that the upturn of the mJy radio counts is likely to be ascribed to the emergence of an evolving population of actively star forming galaxies.

3. Interpretation of the far infrared IRAS data

A very tight correlation between radio and far infrared emissions for disk galaxies has been found by de Jong et al. (1985) and Helou et al. (1985) and is confirmed by the analysis of the optically selected sample by Franceschini et al. (1987a). Such correlation, commonly related to the star formation activity in these galaxies, implies that the substantial cosmological evolution of S/I galaxies required by the analysis of the radio counts would also show up in the far infrared surveys performed by the IRAS satellite. Actually, the far IR band, which is quite insensitive to emission processes not related to the presence of dust in star forming regions, is just ideal to study the statistical properties of actively star forming galaxies.

A positional correlation of galaxies from the optical sample described in Sect.3 with the IRAS Point Source Catalogue has allowed us to derive their 60 μm fluxes (or upper limits). The LLFs, the far-IR spectral indices and the radio to far-IR flux correlations for the various classes of galaxies have been obtained using survival analysis techniques (Franceschini et al., 1987a,b). Coupling these ingredients with models calibrated on radio data, we predicted the overall properties (counts, luminosity and redshift distributions, etc.) of far-IR selected galaxies.

It turned out that spiral+irregular and Starburst/Interacting galaxies dominate the 60 μm counts from 10 Jy to 50 mJy as given by Rowan-Robinson et al. (1986) and Hacking & Houck (1987), while the contribution from powerful radio galaxies, radio-loud and radio-quiet quasars is always negligible. Curves (d) and (c) in Fig.2 show respectively the contribution of S/I galaxies under the assumption of no evolution or of the evolution model used to fit the radio data, while curves (b) and (a) display the corresponding total counts, including contributions from non-evolving spiral+irr, Seyferts and E+S0's. It is clearly shown that the deep IRAS counts do require cosmological evolution. The evolution rate of S/I inferred

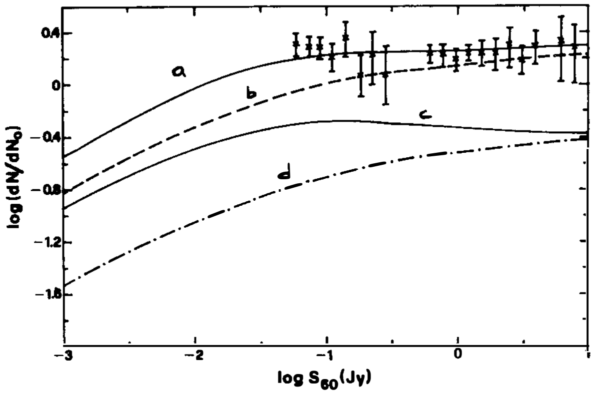

Figure 2. Differential counts at 60 μm normalized to 600 $S_{60}^{-2.5} Jy^{-1} sr^{-1}$. Data points are from Rowan-Robinson et al., (1986) and Hacking & Houck (1987). Curves (a) and (b) are the predicted total counts calculated for the cases of evolution and no-evolution of the Starburst/Interacting galaxies. The separate contributions of the latter class are shown as curves (c) and (d) for the cases of evolution and no-evolution, respectively.

from radio data is fully consistent with the data at 60 μm. Our interpretation is further supported by data from the IRAS selected sample of Lawrence et al. (1986) ($S_{60} \geq 0.85$ Jy), for which complete optical identifications and redshifts are available: for the 11 galaxies with 60μm luminosities $L_{60} > 10^{33}$ erg/s/Hz we have found an average $< V/V_{max} > \simeq 0.65 \pm 0.08$, which indicates the presence of an evolving population, although at 2σ level only. Further details can be found in Franceschini et al. (1987b).

5. Conclusions

We have shown that a great deal of information from radio and far infrared surveys strongly supports the idea that an evolving population of actively star forming galaxies is emerging at faint flux levels. This is the first clear indication of strong cosmological evolution effects, on time scales of the order of 20% $\div$ 25% of the Hubble time, not directly associated with nuclear activity.

So far we have not analyzed in detail the physical mechanisms originating the evolution. However, it is interesting to note that the inferred evolution time scales are similar to those for gas depletion within normal galaxies as determined by Larson & Tinsley (1978) and also suggested by Dopita (1985). An alternative possibility, proposed by Hacking, Condon & Houck (1987), is that starburst galaxies might be subject to a density evolution with cosmic time just due to the increased probability of galaxy collisions in the past denser universe.

REFERENCES

Balzano, V.A. 1983, *Ap. J.*, **268**, 602.

Condon, J.J., and Mitchell, K.J. 1984, *A. J.*, **89**, 610.

Danese, L., De Zotti, G., and Franceschini, A. 1985, *Astr. Ap.*, **161**, 1.

Danese, L., De Zotti, G., Franceschini, A., and Toffolatti, L. 1987, *Ap. J. (Letters)*, in press.

de Jong, T., Klein U., Wielebinski R., and Wunderlich, E. 1985, *Astr. Ap. (Letters)*, **147**, L6.

Dopita, M.A. 1985, *Ap. J. (Letters)*, **295**, L5.

Dressel, L.L., and Condon, J.J., 1978, *Ap. J. Suppl.*, **36**, 53.

Franceschini, A., Danese, L., De Zotti, G., and Toffolatti, L. 1987a, in preparation.

Franceschini, A., Danese, L., De Zotti, G., and Xu, C. 1987b, in preparation.

Hacking, P., and Houck, J.R. 1987, *Ap. J. Suppl.*, **63**, 311.

Hacking, P., Condon, J.J., and Houck, J.R. 1987, *Ap. J. (Letters)*, **316**, L15.

Helou, G., Soifer, B.T., and Rowan-Robinson, M. 1985, *Ap. J. (Letters)*, **298**, L7.

Huchra, J.P. 1977, *Ap. J. Suppl.*, **35**, 171.

Huchra, J.P., Davis, M., Latham, D., and Tonry, J. 1983, *Ap. J. Suppl.*, **52**, 89.

Kron, R.G., Koo, D.C., and Windhorst, R.A. 1985, *Astr. Ap.*, **146**, 38.

Larson, R.B., and Tinsley, B.M. 1978, *Ap. J.*, **219**, L46.

Lawrence, A., Walker, D., Rowan-Robinson, M., Leech, K.J., and Penston, M.V. 1986, *M.N.R.A.S.*, **219**, 687.

Nilson, P., 1973, *Uppsala General Catalogue of Galaxies*, Uppsala Astronomical Observatory, Uppsala.

Palumbo, G.C., Tanzella-Nitti, G., and Vettolani, G. 1983, *Catalogue of Radial Velocities of Galaxies*, Gordon and Breach, New York.

Peacock, R. 1985, *M.N.R.A.S.*, **217**, 601.

Rowan-Robinson, M., Walker, D., Chester, T., Soifer, T., Fairclough, J. 1986, *M.N.R.A.S.*, **219**, 273.

Toffolatti, L., Franceschini, A., De Zotti, G., and Danese, L. 1987, *Astr. Ap.*, in press.

Windhorst, R.A., van Heerde, G.M., and Katgert, P. 1984, *Astr. Ap. Suppl.*, **58**, 1.

Windhorst, R.A., Miley, G.K., Owen, F.N., Kron, R.G., and Koo, D.C. 1984, *Ap. J.*, **289**, 494.

Windhorst, R.A., Dressler, A., and Koo, D.C. 1987, in *IAU Symp. N° 124, Observational Cosmology*, eds. G. Burbridge and L.Z. Fang (Dordrecht:Reidel), in press.

Zamorani, G., Zitelli, V., and Marano B. 1986, in *IAU Symp. N.° 119, Quasars*, eds. G. Swarup and V.K. Kapahy (Dordrecht:Reidel), p. 33.

V. THE STARBURST PHENOMENON : MODELS AND THEORY

THE INITIAL MASS FUNCTION, STARBURSTS, AND THE MILKY WAY

John M. SCALO
Astronomy Department
University of Texas
Austin, TX 78712

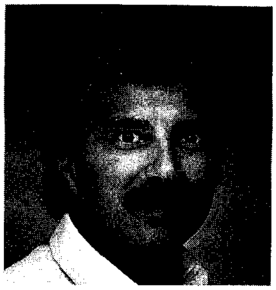

ABSTRACT

The evidence that the IMF varies significantly in galactic regions with enhanced star formation rates is critically examined. The shape of the large-scale IMF in normal late type galaxies appears to be uniform within the large uncertainties. Several arguments in favor of a deficiency of low mass stars in starburst regions are reviewed and found to be inconclusive, although, taken together, they do suggest such an effect.

Speculations concerning bimodal star formation are capable of explaining certain phenomena, such as radial abundance gradients and the local unseen matter, but also face a number of difficulties. In addition, it is concluded that there is as yet very little direct or indirect evidence in support of the hypothesis.

Two features in the Galactic present-day mass function can be interpreted as signatures of at least two past starbursts in the Milky Way, rather than a multimodal IMF. Two independent measures of the stellar age distribution support this interpretation. It is suggested that, rather than being bimodal, the characteristic mass of the IMF is a continuously increasing function of the massive star formation rate. This assumption may provide a means of incorporating the data on Milky Way bursts and starburst galaxies into a unified model, which could account for unseen matter, radial abundance gradients and other phenomena without invoking a bimodal or multimodal mechanism for which there is little evidence.

I. Introduction

The stellar initial mass function (IMF) is ideally defined as the frequency distribution of stellar masses for a group of coevally formed stars at birth. The importance of the IMF lies in its dual roles as a necessary input for studies of galaxy evolution and as a clue to the physical mechanisms controlling star formation. The IMF, together with the dependence of the rate of star formation on physical conditions, couples processes occurring on the scale of star clusters to processes occurring on a galactic scale.

Research on the IMF centers on two questions: 1. What is the form of the IMF in a given region of space? Empirically, attempts to answer this question consist of estimating the IMF from star counts or from indirect methods (colors, line strengths, elemental abundances, etc.) for the solar neighborhood, for star clusters and associations, and for galaxies. 2. How does the form of the IMF vary, if at all, between regions? Here the emphasis is on estimating differences in the IMF for, say, star clusters of different ages or metallicities, or galaxies of different morphological types, or regions of a given galaxy at different galactocentric distances, in order to learn something about the manner in which star formation depends on physical conditions. Unfortunately, despite a great deal of work on these questions, we are far from having any definitive answers. Determinations of the shape of the IMF have proved to be extremely difficult, and most evidence for variations in the IMF is marginal and ambiguous.

Galaxies and regions within galaxies experiencing enhanced star formation rates, or "starbursts" (see [1], [2] for reviews of selected types) provide an invaluable laboratory for studying IMF variations because their physical conditions often differ substantially from those in the solar neighborhood and in most "normal" galaxies (see, however, sec. 5 below). Not only is the star formation rate (SFR) larger by up to one or two orders of magnitude, but the resulting physical conditions, such as the intensity of the ultraviolet radiation field, the gas and dust temperature, and the velocity dispersion of interstellar clouds, are affected. Furthermore, star formation in starburst galaxies may be instigated by large scale processes, such as galaxy encounters, which are currently inoperative in most isolated galaxies. For these reasons starburst galaxies should provide prime targets in which to search for variations of the IMF with physical conditions.

The present paper attempts to summarize recent work on the IMF in starburst-like regions. I include in this category regions in which the current SFR per unit mass is thought to be significantly larger than in the solar neighborhood, so that star formation cannot continue at its present rate for more than a small fraction, say 10^{-1}, of the Hubble time. This definition includes the luminous galaxies undergoing global nuclear or extranuclear starbursts, blue compact dwarf galaxies, giant H II regions in some spiral and irregular galaxies, and perhaps spiral arms. I will concentrate on trying to clarify a few major issues without giving a comprehensive discussion of methods, uncertainties, and results. A detailed review of the IMF is given in [3]; briefer summaries concentrating on particular topics can be found in [4] and [5]. However, except for sec. 2, most of the arguments and conclusions of the present paper are not contained in, and often contradict the conclusions of, previous reviews.

2. <u>Does the Shape of the IMF Vary in "Normal" Galaxies?</u>

Before turning to starburst regions, it is useful to briefly consider what is known about IMF variations in "normal" galaxies.

Because of the large uncertainties in IMF estimates and because we will only be concerned with narrow mass ranges ($m \gtrsim 10\ m_\odot$ in most cases), the IMF per unit logarithmic mass interval will here be characterized by a power law of logarithmic slope Γ with lower and upper limits m_l and m_u. The existence of features in the IMF will be discussed in sec 5 below.

It is necessary to recognize that the absolute value of the slope Γ in a given region cannot currently be reliably estimated by any method. For example, various determinations for high mass stars in the solar neighborhood using star counts give values of Γ covering the range -1.0 to -2.2 [3,4]. The most important sources of uncertainty are incompleteness, treatment of reddening, and the degree to which convective overshoot and rotationally-induced mixing affect theoretical lifetimes and luminosities. Studies of the average Γ in young open clusters give a somewhat smaller range, $-1.8 \leq \Gamma \leq -1.2$ for $m \gtrsim 2\ m_\odot$, but the uncertainties due to small numbers, membership, age spread, mass segregation, and the effects of mixing on the mass-luminosity relation are still severe. (For tabular and graphical summaries of thse results, and references, see [3] and [4].) Estimates of Γ in galaxies based on indirect methods involving colors, ultraviolet fluxes, line strengths, chemical evolution modeling, etc., suffer uncertainties which are similar in magnitude. However, all these methods *can* be used to determine limits on *variations* in the IMF.

The most convincing, and perhaps surprising, evidence concerning IMF variations for massive stars on a galactic scale comes from studies of the luminosity functions (LFs) of galaxies.

Hoessel and coworkers [6] have derived LFs for a number of dwarf irregular galaxies. These LFs agree in shape, within the uncertainties, at the bright end where incompleteness problems are minimized. The very detailed study of galaxy LFs by Freedman [7] includes CCD data for seven spiral and irregular galaxies, supplemented with data from the literature for three additional irregulars. The resulting LFs shown in Figure 1 exhibit a remarkable similarity, with a dispersion in shapes $d\log N/dM_V$ of only $\pm$ 0.03. Freedman also finds no significant variations in slope with position or metallicity. Agreement between LFs of nearby galaxies was also found in [3], using inhomogeneous photographic data from the literature for two spirals and four irregulars.

Because of the steepness of the mass-luminosity relation, these empirical limits on LF slope variations only constrain the variation in the IMF slope to $\Delta\Gamma \lesssim \pm 0.5$. Nevertheless, within these broad limits, one must conclude that star counts yield no evidence for high-mass IMF variations within or among nearby galaxies. Certainly no trends are seen which depend on morphology or metallicity. In addition, Humphreys and McElroy [8] avoided the use of the LF by comparing the distribution of stars in the HR diagram with stellar evolutionary tracks and found good agreement between the LMC, SMC, and the solar neighborhood for very high-mass stars.

For smaller-mass stars, detailed studies exist only for the Large Magellanic Cloud [9-14]. LFs determined by Butcher [9] in the LMC halo and by Hardy *et al.* [13] in the LMC bar are shown in Figure 2, along with the solar neighborhood LF from [3]. A recent study of a region in the LMC

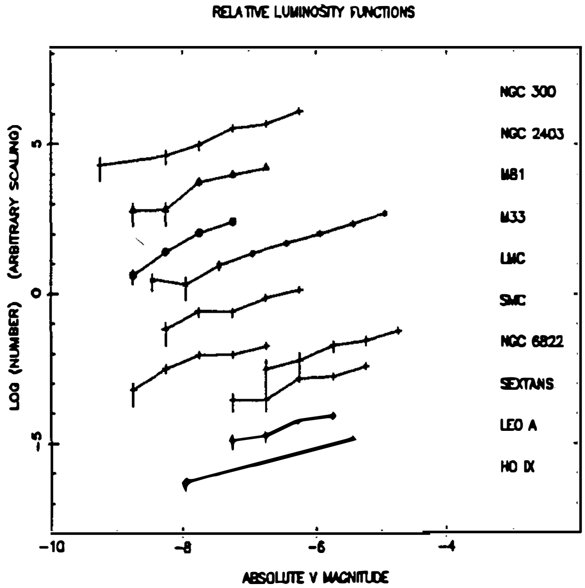

Figure 1. Luminosity functions of the brightest stars in several nearby galaxies, from [7].

disk south of the bar center [14] gives a very similar LF down to $M_V \approx +4$. These results suggest that the IMF in the LMC down to about 1.2 $m_\odot$ does not vary within the LMC and is similar to the solar neighborhood IMF. Looking forward to sec. 4 below, it should be emphasized that there is no suggestion of a deficiency of low-mass ($m \sim 2$-$4\ m_\odot$) stars in the LMC, where most of the star formation is believed to have taken place in two bursts, about 10^8 yr. and a few times 10^9 yr. ago [9-11, 13-15].

Evidence concerning the IMF in more distant galaxies must be based on indirect methods involving the matching of theoretical galaxy evolution calculations to observations of features in the integrated light of the galaxies, such as colors, hydrogen line equivalent widths, or ultraviolet fluxes. These methods give very uncertain results for the absolute value of the slope of the IMF, but can be applied to a statistical sample of galaxies yielding useful estimates of the *variation* in slope.

Kennicutt [16] examined the positions of 115 late-type spirals in the W(Hα) - (B-V) diagram and concluded that the slope was $\Gamma \approx -1.5$ with a dispersion of $\pm$ 0.3. Donas and Deharveng [17] attempted to match the observed ultraviolet fluxes of 40 spiral and irregular galaxies with galaxy evolution models and found $\Delta\Gamma < \pm$ 0.5. A recent paper by Buat *et al.* [18] considered IMF variations in 31 spiral and irregular galaxies for which both ultraviolet fluxes and Hα equivalent widths have been measured, and find $\Gamma \approx -1.6$. The dispersion in Γ for the entire sample is $\pm$ 0.4, or $\pm$ 0.25 for a subset of 17 Sbc and Sc galaxies. A weak trend of IMF flattening from late to early morphological types may be present, but uncertainties in the dependence of extinction on metallicity preclude any firm conclusion.

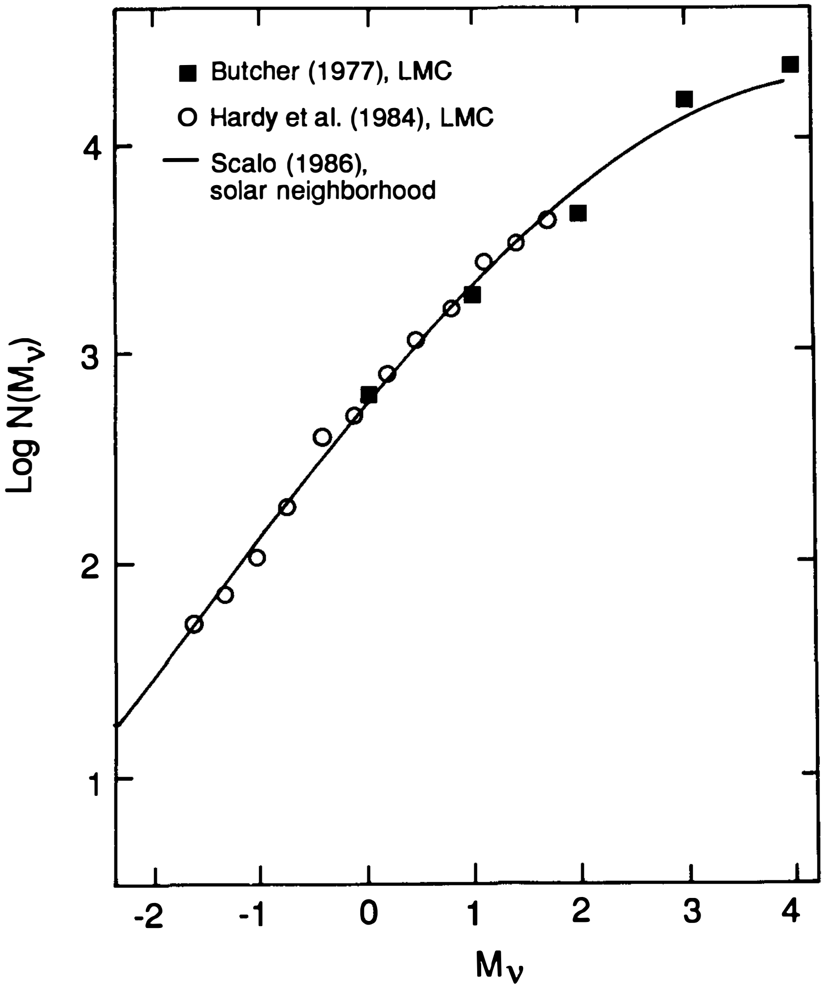

Figure 2. Determinations of the luminosity function in two regions of the Large Magellanic Cloud [9,13] are compared with the local Galactic luminosity function [3].

All the above indirect results refer to stars more massive than about 1.5 - 2 $m_\odot$. The quoted absolute values of Γ are uncertain by at least $\pm$ 0.4 due to uncertainties in the adopted upper mass limit, the treatment of internal extinction, and the theoretical evolutionary tracks.

A few additional studies, using different methods for a small sample of galaxies, are worthy of note because they concentrate on dwarf irregulars and blue compacts, objects which may be considered as starburst regions. Viallefond and Thuan [19] used W(Hβ), forbidden line strengths, and two visual continuum ratios to constrain the IMF and SFR in the blue compact dwarfs I Zw 36 and I Zw 18, and in the giant H II region NGC 5471 in M101. They found Γ -1.5 in I Zw 36 and I Zw 18, and $\Gamma \approx -2$ in NGC 5471. A method involving decomposition of the radio continuum spectrum into thermal and nonthermal components and a comparison with the far infrared luminosity yielded Γ -1.5 for six starburst nuclei, two blue compact dwarfs, and five giant H II regions [20]. An attempt to use oxygen yields to estimate Γ in the LMC, SMC, Mk 59, and NGC 6822 [21] gave $\Gamma = -1.6 \pm 0.3$. Similar studies for the LMC and SMC [22, 23] give $\Gamma = -2 \pm 0.5$ for both galaxies.

Although some of the results cited above are extremely uncertain, the general agreement suggests that the shape of the IMF does not differ among galaxies by more than $\Delta\Gamma \approx \pm 0.3$ to 0.5, in agreement with star counts. For some of the indirect results, and for star counts in the LMC, this conclusion applies to stars with masses as small as 1.5 - 2 $m_\odot$.

Nearly all of the numerous suggestions for systematic IMF variations in normal galaxies are based on indirect evidence which is either extremely uncertain, can be explained just as plausibly by other effects, or has not been corroborated by more recent work. The types of evidence on which these suggestions have been made include variations in mass-to-light ratios, excitation gradients in spiral galaxies, a Galactic gradient in the "infrared excess", yield variations in irregular and blue compact galaxies, radial abundance gradients, the metallicity distribution of local disk dwarfs, and the oxygen "enhancement" in metal-poor stars. Although systematic IMF variations may exist at some level, none of the above approaches have given a convincing demonstration of such variations. Because of the large scope of this topic, and since most of these questionable IMF variations are not directly related to starburst gålaxies, they will not be discussed here. A full discussion of these problems is given in [3].

3. Are Starburst Regions Deficient in Low-Mass Stars?

One of the most influential papers on starburst galaxies was the study of M82 and NGC 253 by Rieke *et al.* [24] who attempted to derive star formation history and IMF constraints by matching theoretical evolutionary models to a number of observed quantities such as $(M/L)_{bol}$, broad-band colors, CO band strength, Brα strength, and 2.2 μm flux. Their surprising conclusion concerning the IMF was that the number of stars with masses less than about 2-3 $m_\odot$ must be very small. The primary constraint responsible for this result was *not* the small $(M/L)_{bol}$ ratio, but the large 2 μm luminosity, presumably due to red giants and supergiants. With a normal IMF ($m_l \sim 0.1\ m_\odot$, say), most of the observed mass would have to be in low-mass stars; but stars with m $\lesssim 3\ m_\odot$ cannot have evolved to the giant phase within the derived age of the burst (~ 5 x 10^7 yr.), and there would not be sufficient numbers of higher-mass giants and supergiants to provide the 2 μm luminosity, which would be too small by a factor of about four.

A serious problem with the result is that it depends crucially on the derived extinction at 2 μm; if the extinction was overestimated by more than about a magnitude, then the required m_l could be substantially decreased [3]. In fact, the peak of the 2 μm emission is coincident with the optical knot denoted "A" in the study of M82 by O'Connell and Mangano [25], and the extinction there is only A_V

$\approx$ 2-4 [26], while Rieke *et al.* adopted A_V = 26. On the other hand the extinction at 2 μm adopted by Rieke *et al.* has been confirmed by recent Brγ and Paβ measurements [27]; this represents the extinction to the bulk of the ionized gas. Evidently the extinction is extremely inhomogeneous, and the optical knots may be "windows" looking into the starburst. In any case, given the coverage of the 2 μm region by optical knots, it seems likely that the effective extinction towards the giants and supergiants giving rise to the 2 μm emission was sufficiently overestimated by Rieke *et al.* that a severe deficiency of low-mass stars is not required; in fact, with a smaller extinction a small value of m_l is needed so that 2 μm radiation is not overproduced. It should also be noticed that burst constraints based on the inferred Lyman continuum flux will also be affected if the extinction was overestimated.

The work of Rieke *et al.* was followed by several other papers that suggested similarly large values of m_l in starburst regions; none of these results rely on the 2 μm flux as a constraint. One of the most convincing examples is the interacting starburst system Mk 171 for which the inferred value of m_l is at least around 10 $m_\odot$ if $\Gamma \approx -1.5$ [29]. This result is based primarily on the weakness of the Balmer absorption lines, indicating a relative scarcity of stars with spectral types late B or later. Another interesting result for this system is that the "effective temperature," a measure of the hardness of the ionizing radiation field, suggests an *upper* mass limit of only about 30 $m_\odot$, so the IMF is nearly a delta function. Weak Balmer absoprtion lines also give $m_l \sim$ 10 $m_\odot$ for the interacting system IC2153 [28]. An analysis of the extremely luminous interacting systems Arp 220 and NGC 6240 [30] gives the somewhat weaker result that $m_l \gtrsim$ 2-3 $m_\odot$ and/or $\Gamma > -1.5$. Indications of large m_l have also been found in blue compact dwarf galaxies. A study of I Zw36 [19] gives $m_l \sim 4$ $m_\odot$ if the SFR has been constant up to the present time; if instead the SFR was an instantaneous burst sometime in the past, the value of m_l could be much smaller. This illustrates the fact that the derived values of m_l in all the studies discussed here depend somewhat on the assumed time-dependence of the SFR. The blue compact dwarf ESO 338-IG04 may have an even larger $m_l \gtrsim$ 10 $m_\odot$ if $\Gamma \approx -2$ [31]. The limits on m_l in I Zw 36 and ESO 338-IG04 both are constrained primarily by the Hβ equivalent width, which measures the ratio of the number of O stars (through the ionizing flux required to give the Hβ strength) to the number of B and A stars (through the continuum flux at Hβ).

It is important to note that studies of starburst regions exist which do not require large values of m_l ; for example, modelling of I Zw 18 yields $m_l \lesssim 2$ [19].

More circuitous approaches have been used to infer large values of m_l in the arms of two spiral galaxies. An attempt to model the observed color distribution across the arms of M81 indicated that the arm colors and widths require essentially no stars more massive than about 10 $m_\odot$ [34]. However, this result depends on the uncertain subtraction of the underlying smooth disk light among other uncertainties. A detailed study of the M83 arms [35] resulted in SFRs, derived from Hα, which would be unreasonably large unless $m_l \sim$ 0.5-3$m_\odot$; another, more complicated argument in support of this result [35] is summarized in [3].

There are at least four additional indirect arguments which support the findings of large m_l in starburst galaxies.

First, the derived total SFRs in some starburst galaxies (including M82) are so great that the entire gas supply would be exhausted in a very short time ($\lesssim 10^7$ yr) unless the IMF is deficient in low mass stars [37,33]. While there is nothing unacceptable about producing gas-exhausted galaxies, such a situation might result in significant numbers of gas-exhausted galaxies dominated by B and A stars, which are not observed. However, this argument assumes that star formation would continue at its present rate until the gas is nearly used up, which seems unlikely, especially if a threshold gas density is required for star formation.

Second, some extreme starburst galaxies *may* have bolometric mass-to-light ratios as small as 0.01 or less (cf. [43]); such values require an IMF deficient in low-mass stars independent of the duration of the burst.

Third, Keel *et al.* [32] point out that once a star formation burst begins to subside, the timescale for decline of the Hα equivalent width will be significantly smaller than the time for the B-V color to increase, so one would expect to observe some blue, Hα-weak galaxies; yet none were found among their sample of interacting galaxies.

Finally, Bergvall [31] realized that, according to current ideas about stellar nucleosynthesis, the rather small (and uncertain) C/O ratio he measured in the blue compact dwarf ESO338-IG04 implies an IMF enriched in OB stars, in agreement with his conclusions based on photometric and spectral modelling. Small C/O ratios have also been estimated for a few other dwarf irregular and blue compact galaxies [31a]. Additional determinations of carbon abundances in a large sample of blue compact dwarfs could provide a valuable tool in the study of m_l variations in starburst regions.

Taken as a whole, then, the above evidence supports the idea that starburst regions tend to be deficient in low-mass stars, although individually the arguments are less than compelling. There is as yet little understanding of the physical processes which might be responsible for the effect. It has been suggested [3, 5, 38] that the characteristic stellar mass (mean or mode of the IMF) is an increasing function of the massive star SFR because of feedback in which the massive stars either heat the gas, thereby increasing either the minimum mass of opaque fragments [39] or the thermal Jeans mass [45], or ablate low mass fragments (see [41]). A discussion of these ideas is given in [38].

4. Is the IMF Bimodal?

An idea which has become quite popular in recent years is that there are two distinct mechanisms for star formation, each with its own IMF, the overall IMF being a superposition. This suggestion, which has become known as "bimodal star formation," would have important implications for star formation and galaxy evolution. In this section an attempt is made to summarize, as objectively as possible, the evidence for and against this proposal.

Herbig [44] noted that many associations of T Tauri stars exist which do not contain higher mass OB stars, while most OB associations do contain T Tauri stars, and suggested on this basis that some regions of star formation only produce low-mass stars. A counterexplanation is that star formation proceeds temporally from low-mass to high-mass stars, either because of physical effects, such as the gradual increase in gas temperature or turbulent velocity expected as the number of stars in an interstellar cloud complex increases or because of a purely statistical effect due to sampling from an IMF which decreases with increasing mass [45].

Van den Bergh [46] later suggested that the deficiencies of low-mass ($m \lesssim 1\ m_\odot$) stars which had been found in some open clusters could be interpreted as evidence for bimodal star formation; evidently some clusters were only capable of producing stars with $m \gtrsim m_\odot$. This idea, which is quite different than Herbig's suggestion, is the essence of most recent discussions of bimodal star formation. Unfortunately, the problems involved in estimating open cluster luminosity functions, primarily associated with mass segregation and membership assignment, turned out to be quite severe. A recent review of the problem [3] concludes that there are only a few well-studied open clusters (NGC 3293, M67, and NGC 2506) for which there remains evidence of a low-mass turnover in the IMF. Similarly, Larson [45] has argued that the IMFs of pre-main sequence stars found by Cohen and Kuhi [48] show that some star-forming regions which contain high-mass stars (e.g. Orion and NGC 2264) are deficient in low-mass stars compared to the Taurus region. However it now appears that incompleteness was the cause of the apparent low-mass turnovers, since the luminosity function for NGC 2264 [42] indicates an IMF which continues to increase to very small masses and has a shape similar to the field star IMF. The population of stars in the Orion cluster [50] also does not appear to show a deficiency of low-mass stars. Finally, sub-keV X-ray sources, which are thought to be associated with low-mass protostars, are seen in Orion [49a].

Gusten and Mezger [36], following an earlier suggestion [50], proposed that star formation in spiral arms only produces stars with masses greater than about 2-3 $m_\odot$, while interarm regions produce stars with all masses down to around 0.1 $m_\odot$. Assuming that the SFR rate in spiral arms is proportional to the frequency with which gas encounters the density wave pattern, differential rotation then ensures that the high-mass spiral arm mode of star formation will increase in dominance relative to the interarm mode at smaller galactocentric distances R. The assumed IMF is sketched in Figure 3. Gusten and Mezger show that such a bimodal IMF can account for the radial metallicity gradient in our Galaxy. The main effect is that the "locked-up fraction" of mass decreases at smaller R, increasing the effective yield of metals. In addition, this bimodal IMF model reduces the uncomfortably large Galactic star formation rates derived from thermal radio continuum fluxes (however, see below), since the Lyman continuum production rate per unit mass of stars formed is increased because a larger fraction of massive stars are formed.

The model of Gusten and Mezger is supported by the findings that only massive stars have formed in the arms of M81 [34] and M83 [35]. It should be noted, however, that the M83 results also require an *upper* mass cutoff at around 10-15 $m_\odot$.

No direct evidence that low-mass star formation is suppressed in spiral arms exists for the Milky Way. One might expect that some open clusters which have formed in Galactic spiral arms should be seen, and should be deficient in stars with $m \lesssim$ 2-3 $m_\odot$. The only known candidate for such an IMF is NGC 3293 [51]; a few additional clusters with possible low-mass IMF cutoffs have turnovers at ~ $1 m_\odot$, but the fraction of clusters represented by these cases is extremely small. This is not necessarily a severe problem, however, since if $m_l \sim$ 2-3 $m_\odot$, then clusters formed in spiral arms

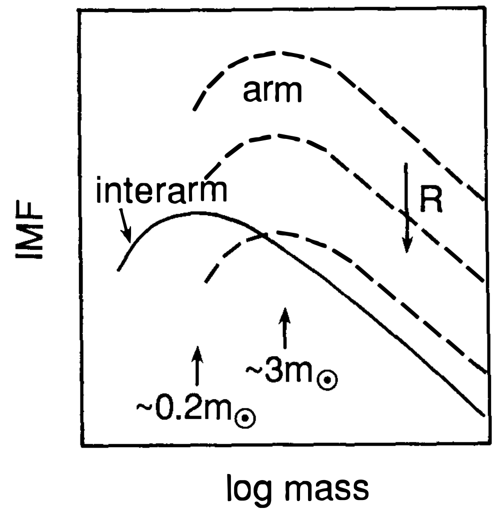

Figure 3. Schematic illustration of Gusten and Mezger's [36] bimodal IMF hypothesis. The higher-mass mode operates only in spiral arms with a relative amplitude that decreases with increasing galactocentric distance R.

more than about 2-5 x 10^8 yr ago would now consist entirely of stellar remnants and be difficult to observe except as a nearby cluster of white dwarfs.

Evidence for a localized deficiency of low-mass stars has been claimed for the Galactic H II region W33 [85] and several giant H II regions in the LMC and SMC [86] on the basis of a small ratio of total luminosity (from IR measurements) to ionizing flux (inferred from the radio continuum flux). However, besides a large number of other uncertainties which enter the estimate of this ratio from the observational data (see [85], [86]), the derived ratio depends sensitively on the assumed form of the IMF, which was taken from Miller and Scalo [54] with an upper mass limit $m_u = 60\ m_\odot$ in both studies. (The dependence of the ionizing flux on Γ and m_u is shown in Figures 56-58 of [3], while the dependence of the total luminosity on m_u for the IMF of [54] can be seen in Figure 7 of [85]). It appears that very modest changes in the adopted IMF shape and/or m_u can easily bring the predicted ratio into agreement with the observations for a normal m_l. The difference between the observed ratios in Galactic and LMC/SMC H II regions (about a factor of 2 to 4), if not due to variations in dust properties, geometry, resolution, etc., might be due to an enormous (factor of 100) difference in m_l, but can be more palusibly attributed to small differences in Γ and/or m_u.

Contrary to what has been claimed in the literature, CO observations of Galactic interstellar clouds provide no evidence supporting Gusten and Mezger's bimodal IMF model. The observation that warm molecular clouds, probably heated by massive stars, tend to be distributed like the giant HII regions which are associated with spiral arms while the cooler clouds are more uniformly distributed in the disk [e.g. 57] shows that high-mass star formation occurs primarily in spiral arms, *not* that low mass star formation is suppressed in arms, which is the essence of the proposed bimodal mechanism. Similarly, the existence of nearby clouds containing no high-mass stars and the fact that only a small fraction of massive clouds in the Galaxy contain giant HII regions only indicates that either star formation proceeds from small to large masses or that some regions do not form any high-mass stars, but certainly cannot be used to support a model which requires a scarcity of low-mass stars in spiral arms.

A feature in the local present-day mass function has been interpreted as a feature in the IMF and used to support the idea of bimodality [3,5]; in sec. 5 below it will be pointed out that an additional feature exists in the present-day mass mass function, and that both features can be more readily interpreted as evidence for past bursts of star formation without the necessity of IMF variations.

It is also not clear that bimodal star formation is actually required to explain the major observational motivations (radial abundance gradient, reduction in SFR) for the model.

Radial abundance gradients may be accounted for by other mechanisms. In particular, Lacey and Fall [53] have investigated chemical evolution models with radial gas flows in the disk, showing that the observed radial abundance gradient can be explained for a physically reasonable radial flow rate which does not contradict any observations. In addition, it should be noted that radial abundance gradients occur in some "flocculent" spirals, in which it is suspected that density waves are not the dominant cause of the spiral pattern (see [56] for a review of stochastic self-propagating star formation). If this is true, then one would have to postulate two separate mechanisms for producing abundance gradients in grand design and flocculent spirals, whereas radial flows are impartial in this regard.

The Galactic SFRs derived by Gusten and Mezger from free-free emission, which they thought to be too large, depend rather sensitively on the adopted shape of the high-mass IMF, which they took from Miller and Scalo [54]. This adopted IMF has an index $\Gamma \approx -2.5$ at 30 $m_\odot$, while *all* more recent determinations find $-2 \lesssim \Gamma \lesssim -1$ at about this mass (see [3, 4]. An increase in Γ by 0.5 would increase the predicted Lyman continuum flux and reduce the derived SFRs by nearly an order of magnitude (see Figures 56-58 in [3]). In fact, if $\Gamma \gtrsim -1.5$ at high masses, the derived SFRs are "too small", and one might then consider invoking an *excess* of low-mass stars in spiral arms to cure the discrepancy. In addition, the derived SFR depends on the adopted upper mass limit, which was 60 $m_\odot$ in Gusten and Mezger. It seems clear that the Galactic SFR derived from any measure of the Lyman continuum flux is sufficiently uncertain that it provides no motivation for a bimodal IMF.

A related issue is the "problem" that the estimated timescale τ_g to use up the gas in *some* normal galaxies at the current SFR is smaller than the present Hubble time, a result which has been cited as evidence for a bimodal IMF [e.g., 5, 56, 62]. For example, the value of τ_g for the Milky Way based on local star counts is about 3×10^9 yr, [3, 56, 57] with an uncertainty of a factor of about 3. SFRs estimated for normal spirals using either Hα strengths [16] or total luminosities derived from infrared measurements (see [57]) give mean values of $\tau_g \sim 3\text{-}5 \times 10^9$ yr, with a considerable spread. (It should be recalled, though, that uncertainties in extragalactic SFRs estimated by Hα and FIR luminosities are large [see also 58-61]). Recently Sandage [56] has considered the gas depletion timescales in the Milky Way, LMC, SMC, Sextans A, Local Group Im dwarfs, and

Virgo cluster Im dwarfs and finds τ_g (Gyr) = 4, 5, 11, 25, 16, and 10, respectively. Sandage points out that these timescales would be increased by a factor of about 10 (depending on the adopted IMF shape) if the IMF is cut off at a lower limit of 2 $m_\odot$, bringing τ_g comfortably above the Hubble time. However, Sandage's values of τ_g neglect the unknown contribution of molecular gas, which increases τ_g, and their normalization is based in large part on the LMC and SMC SFRs that Dennefeld and Tammann [60] derived from counts of supergiants in the H-R diagram. As discussed in [3], results derived from these counts are problematical and do not agree with other studies. Furthermore, the appropriate value of the Hubble time, τ_H, which Sandage took as 20 x 10^9 yr, is a matter of some dispute; if the Hubble time was 10 x 10^{10} yr, then the only galaxies studied by Sandage with $\tau_g < \tau_H$ would be the Milky Way and the LMC.

A more fundamental question is: Why does the result that $\tau_g < \tau_H$ for some galaxies present a problem? Miller and Scalo [54] felt that the uncomfortably small value of τ_g for the Milky Way would imply that we live at a "special time," an argument which now seems far from compelling, at least to this author. Similarly, Sandage [56] suggests that $\tau_g < \tau_H$ puts us "uncomfortably in a special epoch for viewing the Hubble sequence." However, given our lack of knowledge concerning the physics controlling the SFR in galaxies and the range in SFRs observed, it would seem natural to find at least some galaxies which are about to exhaust their gas or have already exhausted their gas. There is certainly evidence that some early-type galaxies were actively producing stars about 5 x 10^9 yr ago (see [61]); perhaps these objects were at one time irregulars or spirals which subsequently relaxed into their present forms when the stabilizing influence of gaseous dissipation was removed or because of a subsequent merger. The so-called anemic spirals [61a] might represent galaxies in which the condition $\tau_g < \tau_H$ once held. Also, if the optical sizes and surface brightnesses of disk galaxies are affected by the depletion of gas, as would occur, for example, for models in which star formation depends on a critical volume or column density threshold, the resulting objects might be under-represented in existing surveys because of selection effects [see 61b]. Whether or not these latter speculations have any merit, it is still not clear that the existence of galaxies with gas depletion timescales of a few billion years violates any observational constraints, or should even make us uncomfortable.

Finally, it is entirely possible that the galaxies with $\tau_g < \tau_H$ have suffered irregular star formation histories and that they happen to be observed today in a state of positive SFR fluctuation. That this is the case for the Milky Way will be argued in sec. 5. The statement by the present author [3] that this possibility is unlikely for the Milky Way because most of the contribution to the IMF comes from stars which have fairly large mean ages is fallacious; in fact the age distribution of stars has a strong peak at very small ($\lesssim 5$ x 10^8 yr) ages, as discussed below.

Larson [62, 5] has taken the bimodal IMF idea in a different direction. Larson investigated the consequence of assuming that there are two "modes" of star formation: a high mass mode which peaks at around 1.5-2 $m_\odot$ and was much stronger at early times, and a low-mass mode (mode mass $\approx$ 0.2 $m_\odot$) whose rate has been constant. The model is sketched in Figure 4. The motivation for this model is that the high-mass mode produces a large mass of remnants, mostly white dwarfs, which can account for the unseen mass in the solar neighborhood [see 63]. Larson's model is also capable

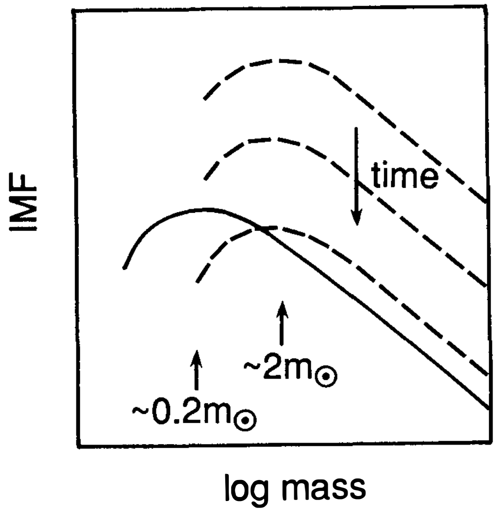

Figure 4. Schematic illustration of Larson's [62] bimodal IMF hypothesis. The relative amplitude of the higher-mass mode decreases with time.

of accounting for the observed age-metallicity relation (see [64]), the estimated SFRs in the inner regions of our galaxy and M33 without predicting more mass in low-mass stars than allowed by rotation curves, the increase of both metallicity and M/L with mass among giant ellipticals (*if* the amplitude and characteristic mass of the high-mass mode increase with galactic mass), and possibly the dark matter in galaxy halos. It also increases the timescales for gas consumption in our own and other spiral galaxies. Although independent evidence for a bimodal IMF is quite weak, as discussed above, the ability of Larson's model to simultaneously account for a number of poorly understood observational results makes it an attractive hypothesis.

As with the Gusten and Mezger proposal, there exist alternate ways of accounting for the main successes of the model. Rana [65] claims that it is possible to account for the unseen mass in the solar neighborhood using a time-independent IMF and a relatively constant birthrate; the major difference from previous work is simply the adoption of a larger scale height for lower-mass stars, based on [69]. Similarly, a number of proposals have been given to account for the stellar metallicity distribution. The feature in the present-day mass function at ~ 1.2 $m_\odot$ [3], which Larson interprets as the imprint of the high-mass mode, may more convincingly be interpreted as evidence for a past burst of star formation [72, 73] as discussed below. Also, there is probably a second feature in the present-day mass function.

Wyse and Silk [91] have shown that the V-R colors of 3CR radio sources as a function of redshift, which are blue at high redshift with a large spread in color, can be accounted for with an IMF which was deficient in low-mass stars at early epochs, as in Larson's model. However, an alternative explanation, that the colors are due to bursts of star formation at relatively recent epochs (z ~ 0.5 - 1.5), is also attractive [see 92]. Contrary to statements in [91], population synthesis studies of nearby early type galaxies suggest that such bursts did occur, that they produced a considerable fraction of the presently observed stars, and that their rapid post-burst evolution is easily capable of accounting for the red colors of low-z ellipticals [61]. Furthermore, the number of parameters required to produce the V-R spread is the same for each hypothesis. The question essentially boils down to: What is more plausible, a single epoch of star formation with a dispersion in IMF parameters, or a single IMF with a dispersion in burst epochs? The population synthesis results and the fact that merger-induced starbursts would naturally give a dispersion in burst epochs, along with lack of strong evidence for a variable IMF cutoff, suggests the latter choice. Very deep counts of galaxies indicate that if such bursts occurred at large redshift, the bursting galaxies must have been shrouded in dust [93].

A major difficulty with Larson's model is that it overproduces metals, giving a present $Z \approx 0.06$ using current theoretical nucleosynthesis yields, unless it is assumed that only stars with $m \lesssim 15\ m_\odot$ explode as supernovae [e.g. 65]. This assumption contradicts most attempts to match solar system abundance systematics, which require supernovae with a characteristic main sequence mass of around 25 $m_\odot$ [66], even if the high-mass IMF is as steep as in Miller and Scalo [54]. Furthermore, the main sequence mass of SN 1987a in the LMC is $19 \pm 3\ M_\odot$, and it produced 0.7 $m_\odot$ of iron and presumably larger amounts of other metals such as oxygen and silicon [67]. Another problem is that the model may predict an excessive number of visible white dwarfs, although uncertainties in white dwarf cooling rates may preclude a definitive test.

It is worth noting that the bimodal star formation models of Gusten and Mezger and Larson are actually quite different in both their assumed spatial and temporal locales and in their implications. Larson's model will not produce radial abundance gradients, and Gusten and Mezger's model will not produce unseen mass and the observed metallicity distribution (they assumed prompt early enrichment to match this constraint). It seems to this author that the simplest way to unify the two models, and to relate them to the suggested large values of m_l in starburst regions, is to abandon the term "bimodal" star formation and simply assume that the characteristic mass or mode mass m_o, of the IMF at a given place and time is an increasing function of the massive SFR [3]. Thus, m_o would be expected to be somewhat larger in spiral arms than between the arms, even larger in starburst galaxies, and perhaps largest in protogalaxy bursts. The distinction is important, since the term "bimodal" suggests that there are actually two different physical mechanisms which form stars (e.g. "spontaneous" and "induced" star formation, whatever these are taken to mean), while the continuously-varying m_o model makes no such claim. However, this alternative point of view suffers from most of the same problems and lack of convincing observational evidence as discussed above.

The discussion of this section is meant to show that, while suggestions of bimodal (or "variable-mode") star formation are capable of providing explanations for several galactic-scale phenomena, such as radial abundance gradients, unseen matter, and the age-metallicity relationship (or stellar metallicity distribution), alternate plausible explanations exist, and most of the observational evidence which has been cited in the literature as support for these models is either extremely weak, indeterminate, or has been misinterpreted. Personally, I suspect that the characteristic mass of the IMF *does* vary significantly in space and time, but must conclude that the only marginally convincing observational evidence for the effect comes from the study of the M83 spiral arms [35], the turnover in the IMF of the open cluster NGC 3293 at ~ 2-3 m$_\odot$ [51] and some of the evidence pertaining to the starburst regions discussed in sec. 3.

5. Was the Milky Way a Starburst Galaxy?

The present-day mass function (PDMF) of solar neighborhood main sequence stars, which is the luminosity function converted to a mass function and corrected for the presence of evolved stars, shows a definite feature at about 1.2 m$_\odot$ (see [3], [65]) which has been interpreted as evidence for the suggested "high-mass mode" of star formation [62, 3]. There is also strong evidence for a gap, or dip, in the frequency distribution of spectral types of main sequence stars between types FO and A5 [see 69-71]. Interpreting this feature as the minimum between two peaks, one at spectral type F2-F5 and the other around AO, the first peak corresponds to the PDMF feature at m ~ 1.2 m$_\odot$ while the

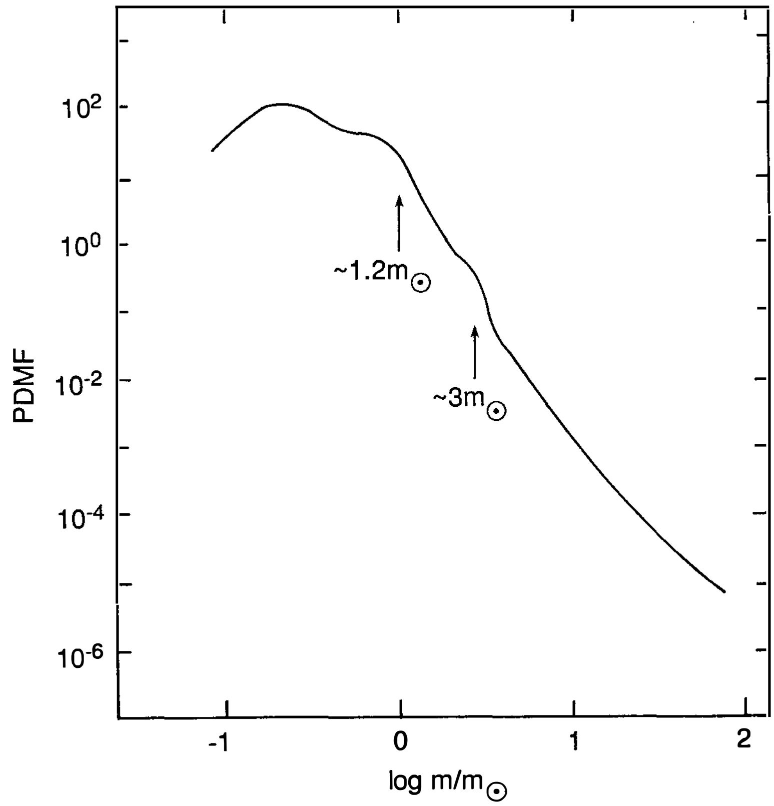

Figure 5. Present day mass function of main-sequence stars from [3] and [65], except for the feature at ~ 3 m$_\odot$, which is based on data in [3, 70, 71].

second occurs at m ~ 3 $m_\odot$. An inspection of published luminosity functions shows evidence of this second feature in 5 of the 7 luminosity functions compared in Fig. 3 of [3], at M_V ~ 0 to 1; the feature was smoothed out in [3] when estimating a representative curve through the data, and had not been noticed in any previous LF determinations. However the prominent feature in the spectral type distribution strongly suggests it is real.

The PDMF is sketched in Fig. 5 which is essentially a compromise between determinations in [3] and [65], but with the ~ 3 $m_\odot$ feature included. (Other features may be present, but are difficult to distinguish from noise in the PDMF curve; see [65]). Rather than interpret this PDMF in terms of a *tri*modal IMF, as would be the case if the SFR has been a smooth function of time, it is just as plausible to interpret each "ledge" or "knee" as representing the effect of a past burst of star formation [72, 73]. This is just the interpretation given to the knee in the LF of the LMC (see [9], [11]), and to the population synthesis results for a blue compact dwarf galaxy [73a].

As illustrated in Fig. 6, a burst beginning τ years ago results in a ledge in the PDMF near the mass whose main sequence lifetime is τ. The observed ledges in the PDMF, therefore, suggest that *the Milky Way has experienced two bursts of star formation*, one about 5 x 10^9 yr ago (the 1.2 $m_\odot$

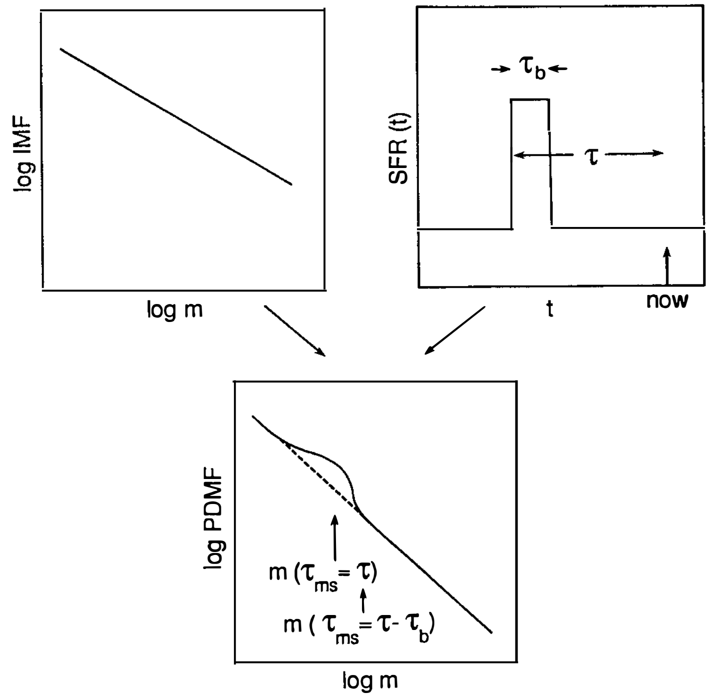

Figure 6. Schematic illustration of the effect of a starburst of duration τ_b, beginning at a time τ in the past, on a power law IMF. The burst produces a ledge in the present day mass function at the mass at which the main sequence lifetime equals τ.

feature), the other about 3 x 10^8 yr ago (the 3 $m_\odot$ feature). The older burst may consist of more than one burst, since the PDMF resolution in mass is poor. The measured amplitude and shape of the features allows an estimate of the duration of and enhancement in star formation during the bursts; details are given in [73].

If such bursts did occur in the Milky Way, then they should have left an imprint on the frequency distribution of stellar ages. In an earlier discussion of the stellar age distribution [3] it was noted that the raw distribution of chromospheric ages derived from the strength of the Ca H and K emission reversal in F and G stars [74] shows a marked deficiency of stars with ages of a few billion years, but the result was considered tentative for a number of reasons. However, after the present interpretation of the PDMF in terms of bursts was made, a detailed discussion of the chromospheric ages by Barry [75] appeared. The resulting age distribution is shown in Fig. 7. (Evolutionary corrections are not included, but are small for ages < 10 Gyr.) It is evident that the chromospheric age distribution provides independent evidence for the existence of bursts at about the predicted ages.

A second method for testing the burst hypothesis is possible using the frequency distribution of lithium abundances in red giants. (The method can only be used to probe the SFR at times $\gtrsim$ 1 Gyr in the past, as explained in [76].) The utility of this technique for probing the past SFR was demonstrated in [76], but only about 30 red giants with measured lithium abundances or upper limits were available at that time. Since then, Sneden [77] has accumulated lithium data for over 600 red giants. A preliminary inspection of the frequency distribution shows a peak at a lithium abundance corresponding to an age of 4-7 x 10^9 yr, as predicted, with some evidence for sub-peaks suggesting a few bursts in this interval, a feature which is also suggested by the chromospheric age distribution in Figure 7.

In summary, the available evidence supports the hypothesis that the features in the solar neighborhood PDMF are a result of at least two bursts of star formation. If this is true, then there is

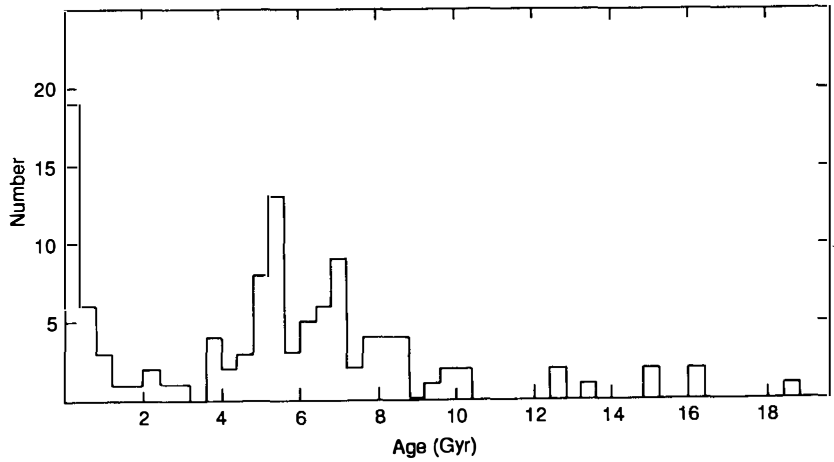

Figure 7. Frequency distribution of chromospheric ages for stars of spectral type middle F through G and luminosity class V, from [75].

no reason to interpret the PDMF features in terms of a multimodal IMF. It is, of course, possible that the IMF was peculiar during the bursts, especially considering the evidence presented in sec. 3, but the recovery of this information from the observed PDMF will require a much more accurate luminosity function and a detailed modelling of the shapes of the features. The age distributions from chromospheric activity and red giant lithium abundances already show that stars with masses in the 1-2 $m_{\odot}$ range were involved in the bursts.

The SFR history implied by the PDMF, the chromospheric age distribution, and possibly the lithium abundance distribution shows that the solar neighborhood has at least twice been involved in a starburst-like event, once very recently. Two lines of evidence suggest that one or both of these bursts were global Galactic starbursts rather than very localized events. First, the ages of the stars from the first burst are sufficiently large that their places of origin should have sampled a significant fraction of the disk. Second, the burst ages, while somewhat uncertain, are remarkably synchronous with the two bursts of star formation inferred for the LMC from the luminosity function [9-11, 14], the ratio of clump giants to main sequence stars [13], the lack of a subgiant branch [13], and the existence of a double asymptotic giant branch [15], although the lack of a subgiant branch [13], and the existence of a double asymptotic giant branch [15], although the lack of subgiants may require an age for the oldest burst somewhat smaller than 5 x 10^9 yr [13]. It is also possible that a larger number of bursts may give a better fit to the LMC luminosity function [11], a situation which may also prove to hold for the Milky Way.

These results for the Milky Way, a supposedly "normal" spiral, casts doubt on the traditional notion that the SFR in most galaxies (except dwarf irregulars) is a smooth function of time (for example, see Figure 10 in [56]). In fact, there is no observational evidence at all for smoothly-varying galactic SFRs, an idea which apparently became entrenched because galaxy photometric evolution *models* employ smoothly-varying SFRs for simplicity and also because it is often assumed in various applications that the SFR is proportional to some power of the gas density, even though there is virtually no justification for this assumption besides convenience. (A thorough review of the latter point is given in [88].) Several studies have derived constraints on the ratio R of the recent SFR to the past *average* SFR in the Milky Way (see [3] for a review) and samples of spiral and irregular galaxies [e.g. 16, 78, 79]. The results suggest that R is of order unity, but with a spread of about an order of magnitude. These studies are often quoted as showing that the SFR has been approximately constant in "normal" galaxies (like the Milky Way), while in fact a ratio R ~ 1 only shows that we are observing most galaxies at about their average rate of star formation, a situation which would occur even if the SFR was a quite irregular function of time, as long as the duty cycle is not too large. In fact the dispersion in SFRs at a given morphological type and/or gas content is fairly large, around a factor of five [e.g. 16, 83, 84], a result consistent with the fact that only about 10% of galaxies in an infrared complete sample have SFRs enhanced by more than a factor of about 5 [82]. Furthermore, statistics of starburst galaxies suggest that most spirals have suffered at least one optical starburst [e.g. 80], and that roughly half of galaxies with L > 10^{10} $L_{\odot}$ have undergone an infrared-bright phase [81]. It is therefore possible that "normal" galaxy SFRs are erratic and even unpredictable except in a statistical sense, and that "starburst" galaxies represent only the tip of the star formation iceberg. This possibility and the proclivity of several types of deterministic theoretical star formation-interstellar medium models for chaotic behavior is discussed in [72].

Combining the evidence for past Milky Way starbursts with the earlier suggestion that the characteristic mass of the IMF is a continuously increasing function of the SFR suggests a means for incorporating the existing analyses of starburst galaxies and the suggestions of Gusten and Mezger and Larson into a unified model, without invoking a bimodal or multimodal mechanism for which there is little evidence. For exmple, the remnants produced in the past Milky Way bursts might account for the local unseen matter, while a concentration of the bursts toward the central regions of the Galaxy (which is a tendency observed in starburst galaxies) would produce a metal abundance gradient. However, as discussed above, the question of whether or not either of these phenomena must actually be explained by a variation of the IMF remains an open one.

It is a pleasure to thank D. Barry, D. Lester, R. O'Connell, C. Telesco, S. Woosley, and H. Zinnecker for useful conversations and correspondence. I am especially grateful to Don Barry for allowing me to show his results prior to publication, and for encouraging my interest in star formation when I was an undergraduate at USC. This work was supported by NSF Grant AST-8619738.

References

1. Reike, G. H. 1985, in *Astrophysics of Active Galaxies and Quasi-Stellar*, ed. J. S. Miller (Mill Valley: University Science Books), p. 235.
2. Wynn-Williams, C. G. 1987, in *Star Forming Regions*, IAU Symp. No. 115, ed. M. Peimbert and J. Jugaku (Dordrecht: Reidel), p. 587.
3. Scalo, J. M. 1986, *Fund. Cos. Phys.*, **11**, 1.
4. Scalo, J. M. 1985, in *Luminous Stars and Associations in Galaxies*, IAU Symp. No. 118, ed. C.W.H. De Loore, A. J. Willis, and P. Laskarides (Dordrecht: Reidel), p. 451.
5. Larson, R. B. 1987, in *Stellar Populations*, ed. C. Norman, A. Renzini, and M. Tosí (Cambridge: Cambridge University Press), p. 101.
6. Hoessel, J. G. 1985, in *Luminous Stars and Associations in Galaxies*, IAU Symp. No. 118, ed. C.W.H. DeLoore, A. J. Willis, and P. Laskarides (Dordrecht: Reidel), p. 439.
7. Freedman, W. L. 1985, *Ap. J.*, **299**, 74.
8. Humphreys, R. M. and McElroy, D. B. 1985, *Ap. J.*, **284**, 565.
9. Butcher, H. 1977, *Ap. J.*, **216**, 372.
10. Stryker, L. L. and Butcher, H. R. 1981, in *IAU Colloq. No. 68*, ed. A. G. Davis Phillip and D. S. Hayes (Schenectady: Davis), p. 255.
11. Stryker, L. L. 1984, in *Structure and Evolution of the Magellanic Clouds*, IAU Symp. No. 108, ed. S. van den Bergh and K. de Boer, p. 79.
12. Hardy, E. 1979, *Astron. J.*, **83**, 319.
13. Hardy, E., Buonnanno, R., Corsi, C. E., Jancs, K. A., and Schommer, R. A. 1984, *Ap. J.*, **278**, 592.
14. Ardeberg, A., Linde, P., Lindgren, H. and Lynga, G. 1985, *Astr. Ap.*, **148**, 263.
15. Frogel, J. A. and Blanco, V. M. 1983, *Ap. J. (Letters)*, **274**, L57.
16. Kennicutt, R. C. 1983, *Ap. J.*, **272**, 54.
17. Donas, J. and Deharveng, J. R. 1984, *Astr. Ap.*, **140**, 325.
18. Buat, V., Donas, J., and Deharveng, J. M. 1987, *Astr. Ap.*, **180**, 12.
19. Viallefond, F. and Thuan, T. X. 1983, *Ap. J.*, **269**, 444.
20. Sramek, R. A. and Weedman, D. W. 1986, *Ap. J.*, **302**, 640.
21. Alloin, D., Collin-Souffrin, S., Joly, M., and Vigroux, L. 1979, *Astr. Ap.*, **78**, 200.
22. Matteucci, F. and Chiosi, C. 1983, *Astr. Ap.*, **123**, 121.
23. Rocca-Volmerange, B., Lequeux, J., and Maucherat-Joubert, M. 1984, *Astr. Ap.*, **104**, 177.
24. Rieke, G. H., Lebofsky, M. J., Thompson, R. I., Low, F. J., and Tokunaga, A. T. 1980, *Ap. J.*, **238**, 24.

25. O'Connell, R. W. and Mangano, J. J. 1978, *Ap. J.*, **221**, 62.
26. O'Connell, R. W. and Nelson, C. 1987, in preparation.
27. Lester, D. 1987, personal communication.
28. Olofsson, K., Bergvall, N., and Ekman, A. 1984, *Astr. Ap.*, **137**, 327.
29. Augarde, R. and Lequeux, J. 1985, *Astr. Ap.*, **147**, 273.
30. Rieke, G. H., Cutri, R. M., Black, J. H., Kailey, W. F., McAlary, C. W., Lebofsky, M. J., and Elson R. 1985, *Ap. J.*, **290**, 116.
31. Bergvall, N. 1986, preprint.
31a. Dufour, R. J. 1986, *Publ. A. S. P.*, **98**, 1025.
32. Keel, W. C., Kennicutt, R. C., Hummel, E., and van der Hulst, J. M. 1987, *Ap. J.*, in press.
33. Belfort, P., Mochkovitch, R., and Dennefeld, M. 1987, *Astr. Ap.*, **176**, 1.
34. Bash, F. N., and Visser, H.C.D. 1981, *Ap. J.*, **247**, 488.
35. Jensen, E. B., Talbot, R. J., and Dufour, R. J. 1981, *Ap. J.*, **243**, 716.
36. Güsten, R., and Mezger, P. G. 1983, *Vistas in Astronomy*, **26**, 159.
37. Kronberg, P. P., Biermann, P., and Schwab, F. R. 1985, *Ap. J.*, **291**, 693.
38. Silk, J. 1987, in Star Forming Regions, IAU Symp. No. 115, ed. M. Peimbert and J. Jugaku (Dordrecht: Reidel), p. 663.
39. Silk, J. 1977, *Ap. J.*, **214**.
40. Larson, R. B. 1985, *M.N.R.A.S.*, **214**, 379.
41. Klein, R. I., Sandford, M. T., and Whitaker, R. W. 1983, *Ap. J. (Letters)*, **271**, L69.
42. Adams, M. T., Strom, K. M., and Strom, S. E. 1983, *Ap. J. Suppl.*, **53**, 893.
43. Joseph R. D., and Wright, G. S. 1985, *M. N. R. A. S.*, **214**, 87.
44. Herbig, G. 1962, in *Advances in Astronomy and Astrophysics*, **1**, 47.
45. Elmegreen, B. G. 1985, in *Birth and Infancy of Stars*, ed. R. Lucas, A. Omant, and R. Stora, p. 257.
46. van den Bergh, S. 1973, in *Stellar Ages*, ed. G. Cayrel de Strobel and A. M. Delplace (Paris: Obs. de Paris - Meudon), p. XL-1..
47. Larson, R. B. 1982, *M.N.R.A.S.*, **200**, 1159.
48. Cohen, M. and Kuhi, L. V. 1979, *Ap. J. Suppl.*, **41**, 743.
49. Walker, M. P. 1969, *Ap. J.*, **155**, 447.
49a. Montmerle, T. 1987, this volume.
50. Mezger, P. G. and Smith, L. F. 1977, in *Star Formation*, IAU Symp. No. 75, ed. T. de Jong and A. Maeder (Dordrecht: Reidel), p. 133.
51. Herbst, W. and Miller, D. P. 1983, *Astron. J.*, **87**, 1478.
52. Solomon, P. M., Sanders, D. B., and Rivolo, R. 1985, *Ap. J. (Letters)*, **292**, L19.
53. Lacey, C. G., and Fall, S. M. 1985, *Ap. J.*, **290**, 154.
54. Miller, G. E., and Scalo, J. M. 1979, *Ap. J. Suppl.*, **41**, 513.
55. Seiden, P. E., and Gerola , H. 1982, *Fund. Cos. Phys.*, **7**, 241.
56. Sandage, A. 1986, *Astr. Ap.*, **161**, 89.
57. Young, J. S. 1987, in *Star Formation in Galaxies*, ed. C. J. Lonsdale Persson, p. 197.
58. Lonsdale Persson, C. J., and Helou, G. 1987, in *Star Formation in Galaxies*, ed. C. J. Lonsdale Persson, p. 99.
59. Cox, P., and Mezger, P. G. 1987, in *Star Formation in Galaxies*, ed. C. J. Lonsdale Persson, p. 23.
60. Dennefeld, M., and Tammann, G. A. 1980, *Astr. Ap.*, **83**, 275.
61. O'Connell, R. W. 1988, this volume.
61a. van den Bergh, S. 1976, *Ap. J.*, **206**, 883.
61b. Phillips, S., and Disney, M. 1986, *M.N.R.A.S.*, **221**, 1039.
62. Larson, R. B. 1986, *M.N.R.A..S.*, **218**, 409.
63. Bahcall, J. N. 1986, in *Dark Matter in the Universe*, IAU Symp. No. 117, ed. J. Kormendy and G. R. Knapp (Dordrecht: Reidel).
64. Wyse, R. F., and Silk, J. 1987, *Ap. J. (Letters)*, **313**, L11.
65. Rana, N. C. 1987, *Astr. Ap.*, in press.
66. Weaver, T. A., and Woosley, S. E. 1980, *Ann. N.Y. Acad. Sci.*, **336**, 335.
67. Woosley, S. E., in preparation.
68. Robin, A., and Creze, M. 1986, *Astr. Ap.*, **157**, 71.
69. Houck, N. 1978, in *The H-R Diagram*, IAU Symp. 80, ed. A. G. Davis Philip and D. S. Hayes, p. 91.
70. Vereshchagin, S. V. 1982, *Pis'ma Astr. Zhurn.*, **8**, 546.
71. Piskunov, A. E., and Vereshchagin, S. V. 1986, preprint.

72. Scalo, J. M. 1987, Proc. Erice Summer School, *Galaxies at High Redshift.*
73. Scalo, J. M. 1987, in preparation.
73a. Thuan, T. X. 1987, this volume.
74. Vaughan, A. H., and Preston, G. W. 1980, Publ. A. S. P., **92**, 385.
75. Barry, D. C. 1987, preprint.
76. Miller, G. E., and Scalo, J. M. 1980, *Ap. J.*, **239**, 953.
77. Sneden, C. 1987, in preparation.
78. Gallagher, J. S., Hunter, D. A., and Tutukov, A. V. 1984, *Ap. J.*, **284**, 544.
79. Thronson, H. A., and Telesco, C. M. 1986, *Ap. J.*, **311**, 98
80. Balzano, V. A. 1983, *Ap. J.*, **268**, 602.
81. Soifer, B. T., Sanders, D. B., Neugebauer, G., Danielson, G. E., Persson, C. J., Madore, B. F., and Persson, S. E. 1986, *Ap. J. (Letters)*, **301**, L41.
82. de Jong, T., and Brink, K. 1987, in *Star Formation in Galaxies*, ed. C. J. Lonsdale Persson, p. 323.
83. Donas, J., Deharveng, J. M., Laget, M., Millard, B., and Huguenin, D. 1987, *Astr. Ap.*, **180**, 12.
84. Kennicutt, R. C., and Kent, S. M. 1983, *A. J.*, **88**, 1094.
85. Haschick, A. D. and Ho, P. T. P. 1983, *Ap. J.*, **267**, 638,
86. Jones, T. J., Hyland, A. R., Straw, S., Harvey, P. M., Wilking, B. A., Joy, M., Gatley, J., and Thomas, J. A. 1986, *M.N.R.A.S.*, **219**, 609.
87. Ho, P. T. P. and Haschick, A. D. 1981, *Ap. J.*, **248**, 622.
88. Freedman, W. L. 1984, Ph.D. dissertation, Univ. Toronto.
89. Soifer, B. T., Houck, J. R. and Neugebauer, G. 1988, *Ann. Rev. Astr. Ap.*, in press.
90. Wyse, R. F. G. and Silk, J. 1987, *Ap. J. (Letters)*, **319**, L1.
91. Djorgovski, S. 1987, this volume.
92. Tyson, J. A. 1987, preprint.

STAR FORMATION RATES AND STARBURSTS

Richard B. Larson
Yale Astronomy Department
Box 6666
New Haven, Connecticut 06511
U.S.A.

ABSTRACT

Understanding star formation rates in galaxies requires understanding both the rate at which molecular clouds form and the efficiency of star formation in these clouds. The efficiency of star formation is probably limited mainly by the destruction of star-forming clouds by ionization, and molecular clouds probably form by a combination of large-scale gravitational instabilities and cloud accretion processes. These hypotheses lead to quantitative predictions that agree well with observational estimates of both the efficiency of star formation and the timescale for converting gas into stars. The predicted timescale depends mainly on the surface density of gas in a galaxy, and the predicted star formation rate per unit area is proportional to the square of the gas surface density, similar to the original Schmidt law. A burst of star formation requires an exceptionally high gas surface density; this results in both a short timescale and a high efficiency for star formation. The gas feeding a starburst must be assembled rapidly into the starburst region, and this requires a violent large-scale disturbance to the interstellar medium in a galaxy, such as that produced by a tidal interaction or merger with another galaxy.

1. INTRODUCTION

A "starburst" may be defined as a star-forming event in a galaxy during which the star formation rate (SFR) is much higher than normal. Before we can understand starbursts, we must therefore first understand something about "normal" star formation; we need to know, for example, what star formation rates normally occur in galaxies, and how the SFR depends on galactic properties such as gas content and Hubble type. More fundamentally, we wish to understand the processes by which stars form and the parameters that determine the SFR. Many possible determining parameters have been suggested; for example it has often been assumed, following Schmidt[1)], that the SFR depends predominantly on the gas density. It has also been suggested that various dynamical processes and timescales play an important role in determining the star formation rate in galaxies[2,3)]. If we can understand what controls the SFR in normal circumstances, we can then hope to understand what changes in conditions are required to produce a starburst.

2. CHARACTERISTICS OF NORMAL STAR FORMATION

In normal spiral galaxies, star formation is a slow, orderly, and well-regulated process. It is slow or inefficient in that the timescale for turning gas into stars, $\tau_{gas} = |M_{gas}/\dot{M}_{gas}|$, is typically estimated[4–7)] to be of the order of several times 10^9 years, which is more than an order of magnitude longer than any of the relevant dynamical timescales. For example, both the growth time for large-scale gravitational instabilities and the timescale for density-wave compression of the interstellar medium are of the order of 10^8 years, and the time required for giant molecular clouds to grow by accretion processes is at most a few times 10^8 years (see Section 4). The timescale for the internal evolution of molecular clouds is even shorter, about 10^7 years or less. Thus typically less than ten percent, and probably only a few percent, of the interstellar matter in a galaxy condenses into stars in the time required for giant molecular clouds to form and evolve.

Normal star formation is also a well-regulated process, as is suggested by the fact that spiral galaxies generally have very similar gas consumption timescales τ_{gas}. The value of τ_{gas} is not very different for different Hubble types, although there appears to be a slow systematic increase of τ_{gas} with Hubble type among the later types. These characteristics are shown by the recent results of Donas et al.[6)] based on ultraviolet flux measurements of a large number of galaxies: the median estimated value of τ_{gas} is about 2.5 Gyr, and most galaxies have gas lifetimes within a factor of 2 of this median. As a function of Hubble type, the median value of τ_{gas} increases from about 1.5 Gyr for Sbc galaxies to 4.5 Gyr for Irr galaxies; within most types the dispersion in τ_{gas} is less than a factor of 2, and is comparable to the accuracy of measurement. We note that an increase of τ_{gas} with Hubble type is actually required to account for the larger gas contents of the later-type galaxies. The numerical values quoted above are based on assuming a conventional IMF, and would be increased if the IMF contains less than the standard proportion of low-mass stars, for example if it is bimodal[8,9].

If star formation is normally a slow, well-controlled process whose rate is determined within narrow limits by the large-scale properties of galaxies, then it seems likely that the SFR is regulated by a negative feedback effect. It has long been clear that star formation influences the interstellar medium in various ways that can affect the star formation rate; in principle both negative and positive feedback effects can occur, and numerous theories of both self-regulating[10–14] and self-propagating[15–18] star formation have been proposed. However, the low efficiency and the well-regulated nature of normal star formation suggest that the dominant feedback effect is negative. The efficiency of star formation must be maintained at typically only a few percent, and this is a strong requirement for the regulating mechanism, which may provide a clue to its nature.

3. WHAT REGULATES STAR FORMATION?

Much attention has been devoted to the possible influence of stellar winds and supernovae on star formation; however, as has been noted at this workshop[19], both cloud destruction (negative feedback) and cloud compression (positive feedback) effects can occur, and not even the sign of the net effect is clear. In any case, a more important feedback effect is almost certainly that produced by the ionizing radiation from hot stars, since by the time the dynamical effects of shocks driven by winds or supernovae have become significant, much of the gas in a star-forming cloud containing massive stars will already have been either ionized or accelerated and dispersed by the effects of ionization[20,21]. Thus the primary mechanism limiting the efficiency of star formation, at least in regions of massive star formation, is probably the destruction of star-forming clouds by the effects of ionization.

Unlike the uncertain effects of supernovae and stellar winds, the feedback effect of ionization on star formation is unambiguously negative, since dense cool molecular gas that might otherwise have formed stars is converted into hot ionized gas that cannot form stars. Even if ionization-driven shocks compress residual cloud gas and cause secondary star formation[15], much more gas is ionized than is turned into stars in this way. The rate of cloud destruction by ionization can be calculated without much uncertainty because the physics involved is simple, and the resulting ionization rate depends only weakly on the properties of the cloud and the dynamics of the evolving HII region. A newly formed group of stars containing at least one O star can readily ionize many times its own mass of gas: for example, Whitworth[22] has estimated that even if only 4 percent of the mass of a molecular cloud condenses into stars with a standard IMF, enough ionizing photons are emitted by these stars to completely ionize the rest of the cloud. This is just what is needed to account for an efficiency of star formation of the order of a few percent.

More detailed treatments of the dynamics of evolving HII regions lead to very similar conclusions. Tenorio-Tagle[23)] has pointed out that during much of the evolution of a typical HII region, the gas ionized from a star-forming cloud streams away from the cloud in a "champagne flow" with velocities that can reach 30 km/s or more. Numerical calculations of the evolution of HII regions including the champagne phase show that typically about 1% of the ionizing photons emitted by the associated O stars create new electron-proton pairs that are evaporated from the cloud[24,25)]. This makes ionization a very effective cloud destruction mechanism: if a conventional IMF is assumed and the stellar ionizing photon emission rates given by Güsten and Mezger[26)] are used, the mass of gas ionized is then predicted to be about 20 times the mass of the stars formed, in good agreement with the earlier estimate by Whitworth[22)]. The associated rate of cloud dispersal is probably sufficient to destroy most giant molecular clouds within 10^7 years[20,27)].

These results mean that the efficiency of star formation is predicted to be small, at least when averaged over a region large enough to contain significant numbers of O stars. Defining the efficiency of star formation as the ratio of "output", taken as the mass of stars formed, to "input", taken as the mass going into star-forming clouds, we obtain

$$\text{efficiency } \varepsilon = \text{stellar mass / cloud mass} \sim 0.05.$$

The uncertainty in this prediction may be a factor of 2 to 4, but is probably not as large as an order of magnitude. The predicted efficiency could be too low if a significant fraction of O stars end their lives no longer closely associated with their birth clouds, in which case their radiation might no longer contribute effectively to the destruction of these clouds. However, the destructive effects of radiation from O stars include not only direct ionization but also the dissociation of molecular gas and the acceleration and dispersal of neutral gas by ionization-driven shock fronts, and this removes additional material from star-forming clouds. Eventually stellar winds and supernovae may also contribute to cloud destruction, but they are probably less important than ionization because by the time their effects become significant, ionization has already done most of the damage that will be done[20,21)]. Because of these additional destructive effects, the efficiency of 5% predicted above is perhaps more likely to be an overestimate than an underestimate.

These expectations are in good agreement with observational determinations of the efficiency of star formation in giant molecular clouds. The efficiency estimated from observations generally ranges between 1 and 10 percent, and values of a few percent are typical[28–31)]. An additional estimate based on the relation between cloud mass and maximum stellar mass[32)] yields an efficiency of about 4 percent. It should be noted that all of these estimates are based, as is the theoretical prediction, on the assumption that low-mass stars always form together with massive stars in the proportions predicted by a conventional IMF. If the IMF actually contains a smaller proportion of low-mass stars[33)], for example if it is bimodal, then both the predicted and the "observed" efficiency of star formation are reduced by the same factor, which could be large[9)].

If the efficiency of star formation can be considered known, then the total star formation rate in our Galaxy can be predicted in order of magnitude, given the total mass in molecular clouds and the estimated lifetime of these clouds. The total mass of molecular clouds in our Galaxy is about 2×10^9 solar masses[34)], and the typical lifetime of these clouds as estimated both from the timescale for internal evolution and from the spread in ages of the associated young stars is of the order of 2×10^7 years[35)]. The rate of cycling of matter through giant molecular clouds must then be of the order of 100 solar masses per year, and if 5% of this mass goes into stars, the predicted total SFR for our Galaxy is about 5 solar masses per year. This is similar to the total SFR of ~ 6 solar masses per year estimated from observations of thermal radio emission[26)]. Thus, understanding the efficiency of star formation takes us a long way toward understanding star formation rates in galaxies. We still need to understand the rate of formation of giant molecular clouds, and we address this question in the next section.

In addition to controlling the efficiency of star formation, the dispersal of star-forming clouds by the effects of ionization may play another fundamental role: it may account for most of the observed interstellar turbulent or cloud motions, and may explain why their velocity dispersion is almost universally in the range 5 – 10 km/s. The above results imply that interstellar matter is processed frequently through HII regions: the total rate of production of ionizing photons in our Galaxy[26)] is sufficient to re-ionize the entire interstellar medium once every 5×10^7 years , and locally the timescale for cycling of matter through HII regions is about 10^8 years. The gas evaporated from a cloud at an ionization front streams away from the front at a velocity comparable to the sound speed in the ionized gas, i.e. about 11 km/s; in a champagne flow, velocities up to ~ 30 km/s can be achieved. Residual neutral gas can also be accelerated[36)] by the "rocket effect" to velocities up to ~ 10 km/s, and can form a massive shell[21,27,37)] expanding at a velocity of ~ 6 – 10 km/s; such shells are actually observed around some HII regions. Thus it seems likely that nearly all of the gas in a region where O stars form is accelerated to velocities of the order of 10 km/s. The observed velocity dispersions of interstellar clouds can be reproduced by a coagulation/fragmentation model[51,80)] for the formation and destruction of molecular clouds (see below) if molecular clouds are broken up by star formation into fragments moving with velocities of 10 – 12 km/s, just as is expected owing to the effects of ionization.

4. WHAT DRIVES STAR FORMATION?

The formation of stars evidently requires the prior formation of gravitationally bound molecular clouds, so we need to understand the mechanisms of molecular cloud formation and their associated timescales. Many processes probably play a role in the formation of giant molecular clouds, but the ones that are probably most important are:

(1) Large-scale gravitational instabilities in the interstellar medium

Gravitational instabilities occurring primarily in the gas component of a disk galaxy have been proposed as a mechanism for producing spiral structure in galaxies[38-40] and also as a mechanism for initiating or organizing star formation on the scale of spiral arms[2,18,41-44]. In a cloudy interstellar medium, the concentration of gas into spiral arms can promote the accumulation of small clouds and diffuse gas into large clouds, leading to the formation of giant molecular clouds and cloud complexes arrayed along spiral arms. For a thin gas layer with a velocity dispersion c_g and an average surface density μ_g, the growth time for a gravitational instability is[43,45]

$$\tau \sim c_g / \pi G \mu_g \sim 5 \times 10^7 \, \mathrm{yr}$$

where the local values $c_g \sim 6$ km/s and $\mu_g \sim 8$ M_{sun}/pc^2 have been substituted. If the stability parameter $Q_g = c_g \kappa / \pi G \mu_g$ is approximately equal to 2, as expected for marginal stability ($Q_g \sim 2.3$ locally), the growth time τ is approximately $2\kappa^{-1}$ where κ is the epicyclic frequency.

(2) Density-wave compression of the interstellar medium

Regular spiral patterns may be produced by density waves in galactic disks, and density waves may sometimes trigger star formation, although there is little unambiguous evidence for this[2,46]. Interstellar matter entering a density wave experiences systematic compression, and both rapid cloud growth and gravitational instabilities can result, leading to the formation of giant molecular clouds in spiral arms[47]. The timescale for processing gas through density-wave arms is approximately

$$\tau \sim 2\pi R / V \sim 2 \times 10^8 \, \mathrm{yr},$$

where R and V are the galactic radius and rotation speed, and local values have again been used. This timescale is not greatly different from that for gravitational instability, and indeed the two timescales should be related, since any self-sustaining density wave must also rely significantly on the self-gravity of the gas and may be regarded as an organized form of gravitational instability.

(3) Accretion in a galactic shear flow

A process that probably also plays a role in the formation of giant molecular clouds in a differentially rotating galaxy is the growth of clouds by gravitational accretion in a shearing gas layer[42,48]. The approximate accretion rate for a cloud of mass M may be calculated, assuming a smooth shear flow and neglecting turbulent motions, as

$$dM/dt \;\cong\; (2GM)^{2/3} A^{-1/3} \mu_g$$

where μ_g is again the surface density of the gas layer and A is the Oort constant specifying the shear rate. The time required for a cloud to grow to a mass M is then

$$\tau \;\sim\; 3(2G)^{-2/3}(AM)^{1/3} \mu_g^{-1} \;\sim\; 10^8 \text{ yr},$$

where a cloud mass of 10^5 M_{sun} has been assumed and local values of μ_g and A have been used. More rapid cloud growth would be expected in spiral arms where μ_g is enhanced. Thus the timescale for the growth of molecular clouds by gravitational accretion is comparable, at least in the absence of random cloud motions, to the timescale for gravitational instability. In fact, both processes probably occur together, leading to the accretional growth of giant molecular clouds in spiral arms formed by gravitational instabilities[42].

(4) Cloud coagulation by random collisions

Even without help from gravity, random collisions can lead to cloud growth if clouds stick together when they collide; such a process has been suggested as a way of forming giant molecular clouds[49,50], and it can be particularly important in spiral arms[47,51,52]. It has also been suggested that collisions between molecular clouds may play a direct role in triggering star formation[53]. In general, collisions between small clouds are likely to result in cloud destruction rather than growth[54], but a massive gravitationally bound molecular cloud may survive collisions with smaller clouds and grow by accreting them. Adopting conventional values for cloud parameters, the time required for random collisions to build up a cloud of mass M is

$$\tau \;\sim\; 7 \times 10^6 M^{1/3} \;\sim\; 3 \times 10^8 \text{ yr}$$

for a cloud mass of 10^5 M_{sun}; again, a shorter timescale should apply in spiral arms where the space density of clouds is enhanced. The timescale for cloud growth by random collisions is thus longer than that for gravitational accretion, but not by a large factor, so that random collisions probably also contribute significantly to the formation of giant molecular clouds.

In summary, the condensation of interstellar matter into star-forming clouds is probably initiated mainly by large-scale gravitational instabilities, since this process has the shortest timescale of those considered above; on smaller scales, both systematic and random accretion processes probably play a role in the buildup of individual giant molecular clouds. All of the timescales involved are of the order of 10^8 years, so it seems reasonable to conclude that the interstellar medium is processed into giant molecular clouds in a time that is locally of the order of 10^8 years. If 5% of the mass that goes into giant molecular clouds condenses into stars, as was estimated above, the timescale τ_{SF} for processing interstellar matter into stars is then 20 times longer than the timescale τ_{CF} for cloud formation, i.e.

$$\tau_{SF} = \varepsilon^{-1}\tau_{CF} \sim 20\,\tau_{CF} \sim 2\text{ Gyr.}$$

The star formation timescale τ_{SF} could be somewhat longer than this if the formation of molecular clouds is itself an inefficient process, i.e. if part of the interstellar medium avoids becoming condensed into molecular clouds by the processes discussed above. However, the efficiency of molecular cloud formation in our Galaxy is evidently not small since a substantial fraction, perhaps as much as half, of the interstellar medium is in the form of molecular clouds.

For comparison with the above theoretical prediction, the total SFR in our Galaxy estimated by Güsten and Mezger[26)] for a typical conventional IMF is approximately 6 M_{sun}/yr; assuming a total gas content of $5 \times 10^9\,M_{sun}$, this implies a star formation timescale τ_{SF} of about 8×10^8 yr, or allowing for gas recycling, a gas consumption time τ_{gas} of about 1.3 Gyr. For other spiral and irregular galaxies, somewhat longer median gas consumption timescales of about 2 to 4 Gyr have been estimated[4–7)]. These observational estimates agree well with the prediction that $\tau_{SF} \sim 2$ Gyr, which implies that $\tau_{gas} \sim 3$ Gyr. Once again, we note that both the predicted and the "observed" star formation timescales are based on a conventional IMF, and they would be increased by the same possibly larger factor if the IMF contains less than the standard proportion of low-mass stars.

5. WHAT CONTROLS THE STAR FORMATION RATE?

If the efficiency of star formation is fixed, then the rate of star formation depends only on the rate of molecular cloud formation. Many of the cloud formation processes discussed above have timescales that vary inversely with the surface density μ_g of the gas in a galactic disk. The growth time for gravitational instabilities is proportional to c_g/μ_g, so if the velocity dispersion c_g of the gas is always close to the "universal" value of ~ 10 km/s, the growth time depends only on μ_g and is proportional to μ_g^{-1}. Density-wave triggering of star formation would depend partly on galactic dynamics, but as was noted above, density-wave effects must also depend significantly on the self-gravity of the gas; thus an important parameter should still be the gas surface density μ_g. The timescale for cloud growth by gravitational accretion in a shearing gas layer is again proportional to μ_g^{-1}, with a weaker dependence on the Oort constant A, varying as $A^{1/3}$. Finally, if typical cloud properties do not vary, the timescale for cloud growth by random collisions is inversely proportional to the average gas density, and if variations in scale height are also not important, this implies an inverse proportionality to μ_g.

Thus, the most important parameter determining the star formation timescale τ_{SF} in a galaxy is probably the gas surface density μ_g. For most of the relevant cloud formation mechanisms, the associated timescale is at least approximately proportional to μ_g^{-1}; thus we expect that, at least to a first approximation,

$$\tau_{SF} \propto \mu_g^{-1}.$$

If dependences on other parameters are not important, we then predict that the star formation rate per unit area in a galactic disk satisfies

$$\mathrm{SFR/area} = \mu_g / \tau_{SF} \propto \mu_g^2.$$

This is essentially the relation first proposed by Schmidt[1], expressed here in terms of the gas surface density (as was done by Schmidt[55] in his 1963 paper). It is important to note that this predicted relation applies only to quantities averaged over regions with dimensions of at least a kiloparsec, since the underlying physical processes, such as large-scale gravitational instabilities, operate only on length scales of the order of a kiloparsec or larger. Many efforts have been made to verify the Schmidt law from observations, but the results of these tests have been ambiguous because they depend on the spatial resolution of the data used[56]. Consistency with a Schmidt law with an exponent in the range 1 – 3 has often been claimed, but the correlation between the SFR per unit area and the gas surface density actually improves and its slope becomes steeper when the data are averaged over larger regions. For example, when the data for M33 and M31 are binned with a resolution of 500 pc they yield an exponent of about 2.3, considerably larger than the exponent derived from higher-resolution data[56].

Using data for entire galaxies, Donas et al.[6] have plotted the star formation rate per unit area versus average gas surface density for a large number of galaxies. A clear correlation is seen, although with considerable scatter; the authors state that this correlation is consistent with a linear relation of the form SFR/area $\propto \mu_g$, but the dependence actually appears steeper than this and more consistent with a relation of the form SFR/area $\propto \mu_g^2$. Thus the available data support a strong dependence of the SFR per unit area on the surface density of gas, at least when these quantities are averaged over sufficiently large areas.

It is worth recalling some of the properties of galactic models in which a universal star formation law of the form SFR/area $\propto \mu_g^2$ is assumed to hold throughout the evolution of a galaxy or part of a galaxy[1]. At late times when most of the gas has been converted into stars, models of this type predict that the gas surface density becomes nearly the same everywhere and independent of the total surface density. This contrasts with models in which the SFR depends only linearly on the gas content, which predict that the gas surface density remains proportional to the total surface density. Observations show that the surface density of gas in spiral and irregular galaxies generally has similar values everywhere, and is not proportional to the total surface density; the apparent relative constancy of μ_g was taken as one of the original pieces of evidence for a quadratic dependence of the SFR on gas content[1].

A second prediction is that the past average SFR exceeds the present SFR by a factor equal to the ratio of the total surface density to the present gas surface density. In the solar neighborhood this ratio is about 8, so that the quadratic model predicts

$$\text{average SFR} \sim 8 \times \text{present SFR}.$$

If the same model applies everywhere, a large value for this ratio is predicted for galactic disks generally. This prediction conflicts with interpretations of the photometric properties of galaxies based on the assumption of a conventional IMF, which imply that the SFR in most galactic disks has remained nearly constant with time[57]. Indeed, the adoption of a Schmidt law with *any* exponent much larger than zero is incompatible with a conventional IMF unless most galactic disks have acquired most of their mass by infall and their gas content has not changed much with time. Present evidence does not appear to support the required high rates of gas infall[33]. In the solar neighborhood, if the SFR has decreased strongly with time as predicted above, then the IMF derived from star counts is bimodal and has a second peak at a mass of 1.2 to 1.5 solar masses[8,58]. Models with a bimodal IMF and an SFR that declines rapidly with time, at least for massive stars, appear to be consistent with all of the available constraints and even have some advantages over conventional models, including the ability to account readily for unseen mass in galaxies as stellar remnants[8].

We note that if, at earlier times in the evolution of galactic disks, the velocity dispersion c_g of the gas was substantially larger than 10 km/s, then the growth time $\tau \sim c_g/\pi G\mu_g$ for gravitational instabilities would have varied less with time than predicted above, resulting in a weaker time-dependence of the SFR. As a limiting case, it could be imagined that the stability parameter $Q_g = c_g\kappa/\pi G\mu_g$ remains constant with time as μ_g decreases[44], so that if κ does not change much with time, the timescale $\tau \sim c_g/\pi G\mu_g$ does not vary much either. The SFR would then follow a Schmidt law with an exponent of unity. The discrepancy with a conventional IMF noted above would then still exist but in a less extreme form. Probably an intermediate case is most realistic, in which case the time evolution of a galaxy might be best represented by a Schmidt law with an exponent intermediate between 1 and 2.

Of course, a simple Schmidt law cannot be expected to provide more than a very crude first approximation to galactic evolution. Such effects as very strong density waves, galaxy interactions, or large-scale gas flows might well alter simple predictions. Some observed properties of galaxies, such as the central hole in the gas layer of some galaxies and the highly variable gas contents of early-type galaxies, clearly cannot be explained by simple models assuming a Schmidt law and neglecting gas flows. A central hole in the gas layer could result from a bar-like distortion of a galactic disk, which can efficiently remove angular momentum from the gas and cause it to flow toward the center, thus evacuating part of the disk. The widely variable gas contents of early-type galaxies probably result from a variety of gas removal and accretion processes. Whatever dynamical processes may operate, if the gas surface density is still an important parameter determining the SFR, anything that redistributes gas in galaxies and concentrates it in some places can have an important effect on the SFR. If a Schmidt law with any exponent larger than unity is applicable, compressing a given amount of gas into a smaller region will increase the total SFR. Such large-scale gas compression processes may play a crucial role in producing starbursts.

6. WHAT CREATES STARBURSTS?

To account for the properties of the most extreme starbursts, two important modifications to normal star formation processes appear to be required: (1) The star formation timescale must be reduced by at least two orders of magnitude to account for the very short timescales of 2×10^7yr or less that have been inferred for many starbursts[59–62]. (2) The efficiency of star formation must also be considerably increased, since in some well-studied cases such as M82 a star formation efficiency of at least 50% in the starburst region has been inferred[60,63–65]; moreover, in extreme starburst systems a substantial fraction of the entire galactic gas content may be consumed during the burst[61,66–68].

Our discussion of star formation processes in Section 4 suggests that a very short star formation timescale τ_{SF} requires a very high gas surface density μ_g. For example, if $\tau_{SF} \propto \mu_g{}^{-1}$, then a reduction of τ_{SF} from (say) 2.5×10^9 yr to 2×10^7 yr requires a corresponding increase in μ_g by two orders of magnitude from 8 to 1000 M_{sun}/pc^2. Thus we expect that starbursts should occur in regions with exceptionally high gas surface densities. This expectation is consistent with recent data[69] showing that the central starburst regions of some compact dwarf galaxies have HI surface densities above 120 M_{sun}/pc^2 that are higher than are found anywhere else, and with the fact that the surface density of molecular gas[65] near the center of M82 exceeds 500 M_{sun}/pc^2. In the possible starburst galaxy Arp 220, the central surface density of molecular gas has the extraordinarily high value[70] of 5000 M_{sun}/pc^2. It may also be relevant that the hot core regions of some nearby giant molecular clouds such as OMC1 and M17SW, which are presently actively forming massive stars and thus may be regarded as "mini-starburst" regions, have exceptionally high surface densities[35)] of the order of 1000 M_{sun}/pc^2. The most active site of massive star formation in our Galaxy, the molecular-cloud/HII-region complex W49A, has an extremely compact molecular core with a mass of $\sim 10^5$ M_{sun} and a surface density of $\sim 10^4$ M_{sun}/pc^2 in which an intense burst of star formation has very recently taken place[71)].

The further requirement of a high efficiency of star formation in starbursts may be satisfied if star formation takes place on a timescale short compared with the time required for the negative feedback effect due to ionization to become important. Delayed feedback plays a key role in some formal models of starbursts[72)] because such a delay can allow overshoot of an equilibrium to occur. If the primary feedback mechanism limiting the efficiency of star formation is ionization, as proposed in Section 3, there is a delay time provided by the finite evolutionary lifetimes of the ionizing stars; if we define the delay time as the time required for the emission of half of the ionizing photons that will ever be emitted, this time is about 3×10^6 yr for a cluster of O stars with a normal IMF. If star formation occurs within a time interval shorter than this, less than half of the stellar ionizing photons will be emitted while the stars are still forming, and the negative feedback effect of ionization will accordingly be reduced; if the reduction is by a factor of two, the efficiency of star formation can increase from 5% to 10%. Similarly we estimate that if the duration of star formation is only 10^6 years, its efficiency can be as high as 20%, while if star formation is completed in only 3×10^5 years the efficiency can be as high as 50%.

We note that an efficiency of star formation of the order of 50% or more is required for the formation of a bound cluster of stars[28,29)], so starbursts with sufficiently short timescales may also produce massive bound star clusters. Indeed, the formation of globular clusters almost certainly occurs in starbursts[44,73,74)].

If the surface density of a gas layer is locally as high as 1000 M_{sun}/pc^2, the growth time for gravitational instabilities is 7×10^5 yr for a gas velocity dispersion near the "universal" value of ~ 10 km/s; the predicted timescale increases in proportion to the velocity dispersion. If the duration of star formation in the starburst region is also 7×10^5 yr, the efficiency of star formation as estimated above can be as high as $\sim 30\%$. In fact, the efficiency can be higher than this because the individual star-forming clouds in a starburst region almost certainly have higher densities and shorter timescales than the starburst region as a whole, just as do the individual giant molecular clouds in a spiral arm. If the cloud surface densities are a few times larger and their timescales a few times shorter than the above values, then a star formation efficiency exceeding 50% can be achieved. The overall star formation timescale τ_{SF} may then be decreased by as much as *three* orders of magnitude when the gas surface density is increased by two orders of magnitude to ~ 1000 M_{sun}/pc^2. Values for τ_{SF} as small as 2×10^6 yr would then result, easily satisfying all of the observational constraints even for extreme starbursts. We conclude that an increase in the surface density of the gas in a galaxy or in part of a galaxy to ~ 1000 M_{sun}/pc^2 would essentially guarantee a starburst with a very short timescale and a high efficiency of star formation.

If the gas fueling a starburst is turned into stars on a timescale shorter than 10^7 years, the gas must also be *assembled* into the starburst region in a comparably short time if it is to accumulate faster than it is consumed. If a large amount of gas is involved, such rapid accumulation can be achieved only by moving the gas with large velocities, and therefore a violent large-scale disturbance of the interstellar medium in a galaxy is required. For example, in the well-studied galaxy M82 the starburst region contains about 2×10^8 M_{sun} of gas; if we assume for illustration that this amount of gas is compressed from 100 to 1000 M_{sun}/pc^2 within a period of only 10^7 yr, then a velocity of at least 55 km/s is required. More generally, if the gas fueling a starburst is self-gravitating and the velocity with which it condenses does not exceed the virial speed V, then there is a maximum gas inflow rate $\dot{M}_{max}$ that depends only on V and is given by

$$\dot{M}_{max} \sim V^3/G.$$

For example, values for V of 50, 100, and 150 km/s yield values for $\dot{M}_{max}$ of about 30, 200, and 700 M_{sun}/yr. The latter numbers are comparable to the star formation rates inferred for extreme starburst galaxies, so we conclude that gas velocities of at least 100 to 150 km/s are required to provide a high enough fueling rate for the most extreme starbursts.

Clearly, then, a strong starburst cannot occur in a normal quiescent spiral galaxy where departures from circular motion do not exceed ~ 10 km/s. Starbursts often appear to occur near the centers of galaxies, and this means that some large-scale dynamical disturbance must cause the gas in a galaxy to lose angular momentum and fall rapidly toward the center, or that gas with little angular momentum must fall in from outside the galaxy. Two possible effects that could act to transfer angular momentum and allow gas to fall rapidly toward the center of a galaxy are: (1) a bar-like distortion in the mass distribution, and (2) a tidal interaction or merger with a companion galaxy. In both cases the departure from axial symmetry in the mass distribution produces gravitational torques that alter the angular momentum distribution of the gas; for example, a trailing spiral distortion in the mass distribution acts to transfer angular momentum outward, allowing matter to flow inward[75–77]. Numerical simulations have confirmed the effectiveness of both bars[78–80] and tidal interactions[81,82] in redistributing angular momentum and allowing gas to accumulate near the center of a galaxy. Observations show that the galaxies with the highest star formation rates are, in fact, almost exclusively either barred galaxies[83] or interacting or merging systems[34,59,62,74,84–86]. In most cases, when adequate spatial resolution is available, the region of most active star formation is found to be located near the center of the galaxy.

Starbursts caused by violent dynamical disturbances were almost certainly much more frequent and important during the early evolution of galaxies than they are at present. Not only would the average surface density of gas in galaxies have been higher then, but the young galaxies would have been less regular and symmetrical in structure, and interactions and mergers would have been much more frequent[87]. Elliptical galaxies and spheroidal systems in general may even have formed by a series of mergers of smaller systems, and much of the star formation in them may have taken place in a sequence of bursts triggered by the mergers[88]. Such a picture may account for the clumpy appearance and the photometric properties of several candidate protogalaxies that have recently been discovered[89,90].

REFERENCES

1. Schmidt, M., 1959. *Astrophys. J.*, **129**, 243.
2. Larson, R. B., 1977. In *The Evolution of Galaxies and Stellar Populations*, eds. B. M. Tinsley and R. B. Larson, p. 97. Yale University Observatory, New Haven.
3. Larson, R. B., 1980. *Phil. Trans. Roy. Soc. Lond. A*, **296**, 299.
4. Larson, R. B., Tinsley, B. M., and Caldwell, C. N., 1980. *Astrophys. J.*, **237**, 692.
5. Kennicutt, R. C., 1983. *Astrophys. J.*, **272**, 54.
6. Donas, J., Deharveng, J. M., Laget, M., Milliard, B., and Huguenin, D., 1987. *Astron. Astrophys.*, in press.
7. Young, J. S., 1987. In *Star Formation in Galaxies*, ed. C. J. Persson, in press. U. S. Government Printing Office, Washington.
8. Larson, R. B., 1986. *Mon. Not. Roy. Astron. Soc.*, **218**, 409.
9. Sandage, A., 1986. *Astron. Astrophys.*, **161**, 89.
10. Talbot, R. J., and Arnett, W. D., 1975. *Astrophys. J.*, **197**, 551.
11. Norman, C., and Silk, J., 1980. *Astrophys. J.*, **238**, 158.
12. Franco, J., and Shore, S. N., 1984. *Astrophys. J.*, **285**, 813.
13. Silk, J., 1987. In *Star Forming Regions*, IAU Symposium No. 115, eds. M. Peimbert and J. Jugaku, p. 663. D. Reidel, Dordrecht.
14. Dopita, M. A., 1987. In *Nearly Normal Galaxies: From the Planck Time to the Present*, ed. S. M. Faber, in press. Springer-Verlag, New York.
15. Lada, C. J., Blitz, L., and Elmegreen, B. G., 1978. In *Protostars and Planets*, ed. T. Gehrels, p. 341. University of Arizona Press, Tucson.
16. Herbst, W., and Assousa, G. E., 1978. In *Protostars and Planets*, ed. T. Gehrels, p. 368. University of Arizona Press, Tucson.
17. Seiden, P. E., and Gerola, H., 1982. *Fundamentals of Cosmic Physics*, **7**, 241.
18. Elmegreen, B. G., 1985. In *Birth and Infancy of Stars*, eds. R. Lucas, A. Omont, and R. Stora, p. 215. North-Holland, Amsterdam.
19. Wiklind, T., 1987. This volume.
20. Yorke, H. W., Bodenheimer, P., and Tenorio-Tagle, G., 1982. *Astron. Astrophys.*, **108**, 25.
21. McKee, C. F., 1986. *Astrophys. Space Sci.*, **118**, 383.
22. Whitworth, A., 1979. *Mon. Not. Roy. Astron. Soc.*, **186**, 59.
23. Tenorio-Tagle, G., 1979. *Astron. Astrophys.*, **71**, 59.
24. Bodenheimer, P., Tenorio-Tagle, G., and Yorke, H. W., 1979. *Astrophys. J.*, **233**, 85.
25. Tenorio-Tagle, G., Yorke, H. W., and Bodenheimer, P., 1979. *Astron. Astrophys.*, **80**, 110.
26. Güsten, R., and Mezger, P. G., 1983. *Vistas in Astron.*, **26**, 159.
27. Mazurek, T. J., 1980. *Astron. Astrophys.*, **90**, 65.
28. Elmegreen, B. G., 1983. *Mon. Not. Roy. Astron. Soc.*, **203**, 1011.

29. Wilking, B. A., and Lada, C. J., 1985. In *Protostars and Planets II*, eds. D. C. Black and M. S. Matthews, p. 297. University of Arizona Press, Tucson.
30. Myers, P. C., Dame, T. M., Thaddeus, P., Cohen, R. S., Silverberg, R. F., Dwek, E., and Hauser, M. G., 1986. *Astrophys. J.*, **301**, 398.
31. Nakajima, T., Nagata, T., Nishida, M., Sato, S., and Kawara, K., 1986. *Mon. Not. Roy. Astron. Soc.*, **221**, 483.
32. Larson, R. B., 1982. *Mon. Not. Roy. Astron. Soc.*, **200**, 159.
33. Larson, R. B., 1987. In *Stellar Populations*, eds. C. A. Norman, A. Renzini, and M. Tosi, p. 101. Cambridge University Press, Cambridge.
34. Solomon, P. M., Rivolo, A. R., Mooney, T. J., Barrett, J. W., and Sage, L. J., 1987. In *Star Formation in Galaxies*, ed. C. J. Persson, in press. U. S. Government Printing Office, Washington.
35. Larson, R. B., 1981. *Mon. Not. Roy. Astron. Soc.*, **194**, 809.
36. Bedijn, P. J., and Tenorio-Tagle, G., 1981. *Astron. Astrophys.*, **98**, 85.
37. Beltrametti, M., Tenorio-Tagle, G., and Yorke, H. W., 1982. *Astron. Astrophys.*, **112**, 1.
38. Goldreich, P., and Lynden-Bell, D., 1965. *Mon. Not. Roy. Astron. Soc.*, **130**, 125.
39. Toomre, A., 1981. In *The Structure and Evolution of Normal Galaxies*, eds. S. M. Fall and D. Lynden-Bell, p. 111. Cambridge University Press, Cambridge.
40. Carlberg, R. G., and Freedman, W. L., 1985. *Astrophys. J.*, **298**, 486.
41. Elmegreen, B. G., and Elmegreen, D. M., 1983. *Mon. Not. Roy. Astron. Soc.*, **203**, 31.
42. Larson, R. B., 1983. *Highlights of Astronomy*, **6**, 191.
43. Elmegreen, B. G., 1987. *Astrophys. J.*, **312**, 626.
44. Larson, R. B., 1987. In *Globular Cluster Systems in Galaxies*, IAU Symposium No. 126, eds. A. G. D. Philip and J. E. Grindlay, in press. D. Reidel, Dordrecht.
45. Larson, R. B., 1985. *Mon. Not. Roy. Astron. Soc.*, **214**, 379.
46. Elmegreen, B. G., 1987. In *Star Forming Regions*, IAU Symposium No. 115, eds. M. Peimbert and J. Jugaku, p. 457. D. Reidel, Dordrecht.
47. Tomisaka, K., 1987. *Publ. Astron. Soc. Japan*, **39**, 109.
48. Toomre, A., 1987. In preparation.
49. Kwan, J., 1979. *Astrophys. J.*, **229**, 567.
50. Scoville, N. Z., and Hersh, K., 1979. *Astrophys. J.*, **229**, 578.
51. Casoli, F., and Combes, F., 1982. *Astron. Astrophys.*, **110**, 287.
52. Kwan, J., and Valdes, F., 1987. *Astrophys. J.*, **315**, 92.
53. Scoville, N. Z., Sanders, D. B., and Clemens, D. P., 1986. *Astrophys. J.*, **310**, L77.
54. Lattanzio, J. C., Monaghan, J. J., Pongracic, H., and Schwarz, M. P., 1985. *Mon. Not. Roy. Astron. Soc.*, **215**, 125.
55. Schmidt, M., 1963. *Astrophys. J.*, **137**, 758.
56. Freedman, W. L., 1986. In *Luminous Stars and Associations in Galaxies*, IAU Symposium No. 116, eds. C. W. H. de Loore, A. J. Willis, and P. Laskarides, p. 61. D. Reidel, Dordrecht.
57. Kennicutt, R. C., 1987. In *Stellar Populations*, eds. C. A. Norman, A. Renzini, and M. Tosi, p. 125. Cambridge University Press, Cambridge.
58. Scalo, J. M., 1986. *Fundamentals of Cosmic Physics*, **11**, 1.
59. Larson, R. B., and Tinsley, B. M., 1978. *Astrophys. J.*, **219**, 46.
60. Rieke, G. H., Lebofsky, M. J., Thompson, R. I., Low, F. J., and Tokunaga, A.T., 1980. *Astrophys. J.*, **238**, 24.
61. Rieke, G. H., Cutri, R. M., Black, J. H., Kailey, W. F., McAlary, C. W., Lebofsky, M. J., and Elson, R., 1985. *Astrophys. J.*, **290**, 116.
62. Kennicutt, R. C., Keel, W. C., van der Hulst, J. M., Hummel, E., and Roettiger, K. A., 1987. *Astron. J.*, **93**, 1011.
63. Knapp, G. R., Phillips, T. G., Huggins, P. J., Leighton, R. B., and Wannier P. G., 1980. *Astrophys. J.*, **240**, 60.
64. Kronberg, P. P., Biermann, P., and Schwab, F. R., 1985. *Astrophys. J.*, **291**, 693.

65. Lo, K. Y., Cheung, K. W., Masson, C. R., Phillips, T. G., Scott, S. L., and Woody, D. P., 1987. *Astrophys. J.*, **312**, 574.
66. Houck, J. R., Schneider, D. P., Danielson, G. E., Beichman, C. A., Lonsdale, C. J., Neugebauer, G., and Soifer, B. T., 1985. *Astrophys. J.*, **290**, L5.
67. Sanders, D. B., and Mirabel, I. F., 1985. *Astrophys. J.*, **298**, L31.
68. Belfort, P., Mochkovitch, R., and Dennefeld, M., 1987. *Astron. Astrophys.*, **176**, 1.
69. Comte, G., 1987. This volume.
70. Scoville, N. Z., Sanders, D. B., Sargent, A. I., Soifer, B. T., Scott, S. L., and Lo, K. Y., 1986. *Astrophys. J.*, **311**, L47.
71. Miyawaki, R., Hayashi, M., and Hasegawa, T., 1986. *Astrophys. J.*, **305**, 353.
72. Struck-Marcell, C., and Scalo, J. M., 1987. *Astrophys. J. Suppl.*, **64**, 39.
73. Larson, R. B., 1987. In *Nearly Normal Galaxies: From the Planck Time to the Present*, ed. S. M. Faber, in press. Springer-Verlag, New York.
74. Schweizer, F., 1987. In *Nearly Normal Galaxies: From the Planck Time to the Present*, ed. S. M. Faber, in press. Springer-Verlag, New York.
75. Lynden-Bell, D., and Kalnajs, A. J., 1972. *Mon. Not. Roy. Astron. Soc.*, **157**, 1.
76. Larson, R. B., 1984. *Mon. Not. Roy. Astron. Soc.*, **206**, 197.
77. Norman, C. A., 1987. This volume.
78. Sorensen, S.-A., Matsuda, T., and Fujimoto, M., 1976. *Astrophys. Space Sci.*, **43**, 491.
79. Schwarz, M. P., 1984. *Mon. Not. Roy. Astron. Soc.*, **209**, 93.
80. Combes, F., and Gerin, M., 1985. *Astron. Astrophys.*, **150**, 327.
81. Icke, V., 1985. *Astron. Astrophys.*, **144**, 115.
82. Noguchi, M., and Ishibashi, S., 1986. *Mon. Not. Roy. Astron. Soc.*, **219**, 305.
83. Hawarden, T. G., Mountain, C. M., Leggett, S. K., and Puxley, P. J., 1986. *Mon. Not. Roy. Astron. Soc.*, **221**, 41P.
84. Joseph, R. D., and Wright, G. S., 1985. *Mon. Not. Roy. Astron. Soc.*, **214**, 87.
85. Sanders, D. B., Scoville, N. Z., Young, J. S., Soifer, B. T., Schloerb, F. P., Rice, W. L., and Danielson, G. E., 1986. *Astrophys. J.*, **305**, L45.
86. Young, J. S., Kenney, J. D., Tacconi, L., Claussen, M. J., Huang, Y.-L., Tacconi-Garman, L., Xie, S., and Schloerb, F. P., 1986. *Astrophys. J.*, **311**, L17.
87. Toomre, A., 1977. In *The Evolution of Galaxies and Stellar Populations*, ed. B. M. Tinsley and R. B. Larson, p. 401. Yale University Observatory, New Haven.
88. Tinsley, B. M., and Larson, R. B., 1979. *Mon. Not. Roy. Astron. Soc.*, **186**, 503.
89. Baron, E., and White, S. D. M., 1987. *Astrophys. J.*, in press.
90. Djorgovski, S., 1987. This volume.

STARBURSTS AND THEIR DYNAMICS

Colin A. Norman
Space Telescope Science Institute
and
Johns Hopkins University

Detailed mechanisms associated with dynamical process occurring in starburst galaxies are considered including the role of bars, waves, mergers, sinking satellites, self-gravitating gas and bulge heating. Our current understanding of starburst galaxies both observational and theoretical is placed in the context of theories of galaxy formations, Hubble sequence evolution, starbursts and activity, and the nature of quasar absorption lines.

1. INTRODUCTION

Starburst systems are dynamically very interesting. In the low luminosity range we find turbulent, chaotic motions of stars and gas in dwarf galaxies, in barred galaxies the starburst mode is enhanced by about a factor of two and in the powerful infrared starburst galaxies, interactions between galaxies appear to be an obvious driving force behind the burst mode. Over this vast range of luminosities there are some quite elementary considerations of a dynamical nature that may clarify some of the physics. The physics of starburst systems can be made as complex as one wishes and the focus here on dynamical processes is obviously for the sake of clarity and at the expense of completeness. We do not yet know if there is one specific starburst mechanism. In fact, I shall assume the contrary and set out the various possibilities. Angular momentum transport by bars and spiral waves are treated, outlining the essential processes associated with any such non-axisymmetric distrubance in a dissipative medium. The central point is that outside corotation gas will flow outward to the outer Lindblad Resonance and inside corotation it will flow inwards to the inner Lindblad Resonance(s) or the nucleus, in the absence of this latter resonance. The effects of interaction are treated by analysing the effects of mergers which are clearly appropriate to the powerful sources and in the somewhat more intermediate cases we use results from work on sinking satellites. Here it is obvious that a satellite galaxy can readily reach the centre of an L_* galaxy but in doing so, considerable disk damage may result. A few remarks are made here on how flat disk-like system may in fact become bulges.

In the central regions of objects such as Arp 220 the starburst mode is so strong that a significant fraction of the central bulge is being turned into stars. This logically leads us into considerations of galaxy formation from the starburst point of view, evolution of galaxies along the Hubble sequence, the relation between starbursts and activity, and the nature of quasar absorption lines that may be associated with the environments of starburst system and their huge bipolar outflows. For very interesting considerations of the nature of the interstellar medium and the actual details of the star formation process one should study the contributions to this volume by Ikeuchi and Larson. What help do we have other than studying starbursts in our quest for a serious theory of galaxy formation? One very interesting approach we can take is to assume that we have actually *seen* the protogalaxies.

Protospirals we associate with the damped Lyman alpha system seen by Wolfe and colleagues (Wolfe *et al.* 1986). These systems have column densities of $\sim 10^{22}$ cm^{-2} and cover 20% of the sky at a redshift of 2–3. The estimated mass density of the system is sufficient to account for all the luminous matter in the universe within a factor of 2. Protoellipticals would be the objects found by Djorgovskii, Spinrad and others (Djorgovskii *et al.* 1987) by deep imaging with filters of emission line regions around distant 3CR sources. Quite possibly these could be merging protospirals producing elliptical galaxies and initiating the triggering of an active nucleus. One interesting point here is that the radio axis appears to be aligned with the axis of emission-line gas whereas at low redshift it is, in fact, orthogonal (Chambers *et al.* 1987). Evolutionary tracks of galaxies may eventually be calculable and even at this very early stage it is worthwhile to think of galaxies evolving in some parameter space. This image is clear enough but what is the best parameter space in which to think of this evolution. The classic Hubble sequence is that of bulge to disk. According to Sandage (1983) "anyone who has looked through a telescope" would clearly classify galaxies according to the surface brightness of the bulge. The total luminosity of the bulge gives a one parameter fairly for the Hubble sequence as outlined by Meisels and Ostriker (1984). Recent studies of elliptical galaxies (Davies *et al.* 1987) and spiral galaxy bulges (Dressler 1987) show that some of the fundamental parameters are constrained to lie on a plane that is similar for both elliptical and bulges (of early type galaxies). The essential physics here is that binding energy increases with mass. The larger system are more tightly bond with respect to the virial theorem. Does this then mean that larger systems have dissipated more (Djorgovskii 1986)? Even though we don't have details about the hyper-plane along which galaxies evolve we will crudely assume it exists and we hypothesize that we may learn much about the speed and trajectory on this hyper plane from studying starburst systems.

2. WAVES AND BARS IN GAS-RICH DISKS

Conventional stellar bars driving gas flows generate rapid inflow near the bar. The nature of the periodic orbits changes near resonances and this sharp change cannot be achieved by the gas and shocks develop driving further flow inwards. Spiral waves, which can, in reality, be dominated by the self gravity of the gas, produce a more gradual outflow than a bar. There resonances can damp the waves and thus inhibit the inflow. For purely stellar supported waves they are absorbed at the Inner Lindblad Resonance. We further note that a rapid rise of $\sigma(r)$ towards the centre reflects the wave. As shown by Lubow (1987), a five percent ratio of gas to stars results in effective Q parameters both for the stars and gas of comparable amplitude due to the low temperature and scale height of the dissipative gas layer. At a ratio of 15% the gas dominates the wave self gravity by nearly an order of magnitude. Modelling the central disk of NGC 1068 the wave surface density increases as $r^{-\alpha}$, with $\alpha \sim 3/2$ and this *strong* increase towards the centre can result in a strong central concentration of shocks and star formation. This is most interesting. Starbursts seem to occur more frequently in later type systems with gas rich disks and there is clearly some strong wave driving by, for example, a companion. Is the feedback positive or negative? The wave amplitude can be self limited due to cloud collisions. This negative feedback situation can probably be overcome and turned into a positive feedback starburst situation by sufficiently increasing the angular momentum flow rate so that the gas inflow rate $\dot{M}$ is high enough to overcome this. There is a possibility here of a natural threshold, due to say cloud-cloud collisions, that is to be overcome so that the mode is that of a *burst*. As discussed previously Norman (1987) we consider a disk with an ensemble of clouds and a general non-axisymmetric perturber. Cloud collisions are analysed as straight $\langle n\sigma v \rangle$ collisions to give a collision rate γ. Following a straightforward analysis derived as a dissipative version of Lynden-Bell and Kalnajs we find the angular momentum flow rate is

$$\dot{h} = 2m^2\gamma k^2 S^2(\Omega - \Omega p)/\Omega^4$$

with characteristic time scale of inflow

$$\tau^{-1} = \dot{h}/h = 2\gamma m^2 \left[\frac{S}{\Omega^2 R_h^2}\right]^2 \left[\frac{\Omega - \Omega p}{\Omega}\right] (kR_h)^2$$

Away from resonances, the wave-driven viscosity will beat the ordinary collisional viscosity ($\nu \sim \frac{1}{3}\ell v$) if the wave amplitude is greater than

$$\left(\frac{S}{\Omega^2 R_h^2}\right) > \frac{1}{\sqrt{3}m(n\sigma R_n)} \approx \frac{\ell}{\sqrt{3}mR_h}$$
$$\gtrsim 3\%$$

where $\ell/R_n \sim h/R_h \sim 0.1$ and $m = 2$. The combination of enhanced cloud collision and large amplitude perturbations can give very greatly enhanced inflow by at least an order of magnitude.

Using standard $n\sigma v$ estimates with wave amplitudes of order 10% we find an inflow timescale for the centre of Arp 220 of $\approx 2 \times 10^7$ year and for a normal Sa galaxy of $\gtrsim 10^9$ years. There are many ideas of what actually gives the mass function but let us calculate here the interesting possibility that it is cloud-cloud collisions (Scoville 1986). Using numbers from Arp 220 from (Scoville *et al.* 1986a) we divide the $10^{10}\ M_\odot$ of gas in the central region ($\lesssim 3$ kpc) of Arp 220 with 10^5 objects of $10^5\ M_\odot$ with radius of 5 pc and velocity dispersion of 20 km s^{-1}! Assuming a star formation efficiency of $\sim$ 10%, the stars formation rate becomes 10^2 OB star per year.

Bars exhibit a strongly non-linear gas response and it is necessary to perform detailed numerical calculations to obtain precise estimates. The time scale for gas inflow is of order $\sim (3-10)\tau_{rot}$. Larson (1985) has estimated the time scale to be $\tau \sim m\tau_{rot}(M_{halo}/M_{disk})(\delta\Sigma_d/\Sigma_d)^{-2}$ and for a general wave with pitch angle j he has estimated a timescale $\tau \sim m(\Sigma_d/G(\delta\Sigma_d)^2)$ $(V_{rot}/\sin j \cos j)$ which both give estimates of time scales similar to those made above.

3. SELF-GRAVITATING GAS IN CENTRAL REGIONS

Masses of molecular gas such as these inferred from the CO observations of starburst galaxies show that the central potential well may, in fact, be dominated by the gas itself or at least very significantly affected. For such systems the condition for instability to form a massive bar in the gas itself is $T/W \lesssim 0.14$ (Ostriker and Peebles 1973) that depends in detail on the actual mass distribution. This will give a very rapid transfer of angular momentum by, for example, interaction with the halo. The timescale for decay or slow down of such a bar and consequent mass inflow is short.

$$\tau_{decay} \sim 10^1 - 10^{1.5}\tau_{rot}(M_{bar}/M_{halo})$$

including the effect of strong shocks and dynamical friction giving

$$\tau_{decay} \sim 3 \times 10^6 - 10^7\ yr$$

on scale of order $\sim$ 1 kpc. It is therefore very important to map the central regions in CO with submillimetre interferometers to accurately establish the mass distribution in the gas and to search for linear offset shocks as indication of the presence of barred galaxies.

A most interesting effect due to such a massive central concentration of molecular clouds is the enhanced two-body star cloud heating rate whereby stars are heated by "collisions" with clouds. The velocity dispersion obtained by stars in, say, the centre of Arp 220 is

$$\sigma \approx 160 \left(\frac{\sigma_{d,gas}}{10^5 \, M_\odot \, pc^{-2}} \right)^{1/4} \left(\frac{t}{10^8 yr} \right)^{1/4} km \; s^{-1}.$$

Thus a significant number of metal-rich population II stars can be heated to form a bulge in, of order the lifetime of the starburst $\sim 10^8$ yr. This is quite possibly relevant to the very metal-rich halo stars in our Galactic Bulge found by Whitford and Rich (1986), the formation of very thick inner disks and once again the possibility of evolution along the Hubble Sequence.

In the spherical case of a gas rich dwarf galaxy, protoelliptical galaxy, or the central region of a star bursting bulge we have a novel cooling flow problem with a pressure loaded polytrope of cooling molecular gas. Massive accretion $\dot{M} \sim 10 - 100 \, M_\odot$ yr^{-1} can occur, as will massive star formation and self regulation of the accretion can occur due to the energy input from star formation.

The cloud-cloud collision rate is considerably enhanced by orbit crossing. In triaxial systems the box orbits can cross and if gas is following these orbits they will suffer very enhanced dissipation (Lake and Norman 1983). If a black hole is grown in the central region of galaxies the orbits will go from being regular box orbits to stochastic orbits to regular tube orbits. Norman and May (1985) found that for a hole to core mass ratio of 10^{-3} to 10^{-1} the orbits in a dominant nuclear bar will be predominantly stochastic.

4. INTERACTION OF DISKS WITH GAS-RICH DWARFS/COMPANIONS

Spiral galaxies are very responsive to satellites and consequently can trap them into merging on short time scales. Their fate is to reach to the central bulge regions on a time scale estimated by Quinn and Goodman (1986) to be

$$\tau_{sink} \sim 4 \times 10^9 \left(\frac{10^9 \, M_\odot}{M_{satellite}} \right) \left(\frac{v_c}{220 \; km \; s^{-1}} \right) \left(\frac{r_c}{10kpc} \right)^2 \left(\frac{3}{\ln \Lambda} \right) yr$$

This is a very crude estimate since the interplay of effects here is very subtle—dynamical friction, resonance effects and horseshoe orbits. Sometimes even the sign is difficult to ascertain! The normal descent of a satellite is a damped vertical oscillation to the plane and then a radially inward motion to the nucleus. Very considerable damage is done to the disks during this process and the morphology of the underlying galaxies shows the signature of this essential process occurring. Here, once again, the issues of bulge building, disk heating, starbursts and activity, damaged galaxies and Hubble sequence evolution are all intertwined. There are certainly not obviously enough gas rich satellites to produce all the active and starburst systems that we see. These basic fuel units may however have been much more numerous in the past and associated with quasar absorption lines (c.f. Silk and Norman 1981, Ikeuchi and Norman 1987). However, at the current epoch it may be that merging generates bridges and tails which then form break up into small, cold (i.e. low velocity dispersion) objects in the potential well of the merged system and which then form such satellites as described above.

As cosmological simulations have shown (c.f. Roos and Norman 1979) merging occurs mainly in broad sub clumps. The relative velocity of merging galaxies must be less than their internal velocity dispersion, i.e. $v_{rel} \lesssim 1.1\sigma_{gal}$. The process of violent relaxation occur during merging since AU/U $\sim$ 1 where U is the internal energy of the galaxy. Assume that the interstellar media of the two galaxies are, as is usual, dominated by a multi-phase medium with a cool dense component in the form of massive clouds. Elliptical galaxies will be produced when $n_{cl}\sigma_{cl}v_{cl}t_{cross} \sim$ few, and the end result will be a spiral galaxy when the value of $n_{cl}\sigma_{cl}v_{cl}t_{cross} \gg 1$ and a slow settling occurs. The first possibility gives huge initial bursts of star formation of order $(10^{10}\, M_\odot/t_{cross}) \approx 10\, M_\odot\ \mathrm{yr}^{-1}$ and the second is the most likely for a regular starburst mode. In this content it is interesting to look at Sandage's (1986) recent galaxy formation proposal in a new light *not* of the rate of star formation but the value of $n_{cl}\sigma_{cl}v_{cl}t_{cross} \gg 1$. To form galaxies this way the merging must be normally that of protogalaxies. Stellar merging only is impossible. The merging of gas rich proto galaxies is crucial. As discussed extensively by (Silk and Norman 1981) the galaxies must consist of bound subclumps since one needs the properties of both the ballistic orbits to maintain the triaxiality and the dissipative collisions to generate the binding energy and such features as colour gradients.

5. GALAXY EVOLUTION AND ACTIVITY

A major theme of current theoretical astrophysic is to achieve a better understanding of the Hubble sequence and of the evolution of galaxies in that classification scheme. Satellite interactions with say Sc gas rich disks can act to grow the bulge at the expense of the depletion of the satellite population and the significant heating even damage of the disk possibly to form a thick disk. Elliptical galaxies are found in more spectacular mergers of spiral protogalaxies. The rate of evolution along the Hubble sequence is given by

$$\frac{M_{int}}{t_{int}} \approx \dot{M}_{bulge}$$

corresponding to an increase in the bulge to disk ratio. From careful study of current starbursts and those accessible to the Hubble Space Telescope at redshifts greater than unity much can be learned from the observation of the milder form of the galaxy formation process at the present epoch, that occurs in a more dramatic form at redshifts of, say, 5.

Starbursts giving bulge building will probably naturally give growth of a central mass concentration such as a black hole and its associated star cluster. Scoville and Norman (1987) have shown how even the long standing problem of the nature of the broad emission line region of active galaxies and quasars can be realised in such a scenario. Most of the mechanisms for fuelling and triggering activity are similar to those invoked here concerning the driving of the starburst mechanism namely bars, orbit scattering, waves in the dissipative gascons component, massive cloud, supernovae near black holes and accretion disk around black holes, etc. Very efficient star formation in dense clouds with box-orbits are expected in star bursts. There is a big advantage for massive dense, bound star clusters that may be found in star bursts. These can rapidly spiral into the central regions on a timescale $\bar{\tau} \sim t_{dyn}$ $(M_{core}/M_{cluster})$. Tidal disruption can occur *but* the fuel can be carried much closer to the centre. This process could be greatly enhanced by collapse.

Huge collinated outflows of momentum and energy from an active nucleus can trigger star formation in the surrounding medium. This is seen to happen in M51, NGC 1068, Minkowski's object, and Centaurus-A. One way to view this is to calculate the increased pressure that a cloud feels when shocked by a jet or when it orbits into a jet. The conventional pressure in the interstellar medium is $P_{ism} \sim 10^{-12}$ dyne cm^{-2} whereas the pressure in a jet at ≈ 100 pc is

$$P_{jet} \sim 10^{-9}\left(\frac{L_{jet}}{N^{12}ergs^{-1}}\right)\left(\frac{(100pc)^2}{A}\right)\left(\frac{10^4kms^{-1}}{v_{jet}}\right) dyne\ cm^{-2} \gg P_{ism}.$$

Such an increase in pressure is similar to the effects of a cloud-cloud collision. Clouds orbiting into a jet will be triggered just as massive OB stars appear to be triggered in spiral arcs. Similarly ageing effects should be seen as newly formed stars move away from the triggered jet, just as for the spiral wave case.

The active nucleus itself can significantly affect the interstellar medium. The ionisation balance in clouds can change by an order of magnitude due to the strong X-ray radiation bathing the molecular clouds. This directly lengthens the ambipolar diffusion time since it is proportional to the ionisation balance.

Starbursts themselves can directly feed the monster. Massive OB stars on radial, chaotic or box orbits can have lifetimes to supernova τ_{SN}, significantly less than the crossing time. Thus high pressures and strong momentum inputs can be derived from nuclear supernovae. Since all the mechanisms for triggering and fuelling a starburst are the same as those envisaged for active galaxies and quasars and furthermore the mass supply rates are of order 10^2 $M_\odot$ yr^{-1} it seems hard to avoid inducing activity in a starburst nucleus.

6. QUASAR ABSORPTION LINES

Metallic quasar absorption lines are *not* like the halo of our own Galaxy (Danly, Blades and Norman 1987). What are they? They could well be star burst systems. York *et al.* (1987) have argued that dwarf galaxies could account for *some* of the systems. However, a more likely possibility considered here is that they are associated with the huge bipolar outflows found by Heckman *et al.* (1987). These are systems with large covering factors (linear extents out to $\sim 10^2$ kpc), low ionisation, low temperature, filamentary strucure, metal rich, created at the epoch of significant star formation and undoubtedly more common at the epoch of both galaxy and active galaxy formation, say, a redshift $z \sim 5$.

7. SUMMARY AND CONCLUSIONS

Bars, waves and interactions can certainly drive an outward angular momentum flow and inward mass flow. In gas-rich systems there is an interesting threshold effect below which a negative feedback effect is operating to saturate the wave amplitude and above which a positive feedback effect is possible that drives an ever increasing mass flux. The star formation processes are associated with cloud-cloud collisions or some other dissipative process in the gaseous component of the disk.

The starburst phenomenon may well allow us to understand phenomenon seen at high redshift quite possible associated with protogalaxies namely the damped Lyman alpha disks

(Wolfe *et al.* 1986), highly disturbed star forming 3CR sources observed in emission lines by Djorgovskii *et al.* (1987) and features of quasar absorption lines associated with, say, gas-rich dwarfs.

Starburst theory and observation allows a deeper understanding of the evolution along the Hubble sequence particularly with respect to bulge formation, mass and angular momentum flow, flux of gas into stars and the expulsion of metal-rich material into the environments of galaxies. Activity of a galactic nucleus and starbursts are intimately associated.

An interesting observational question is what are post starburst system really like? Is bulge building really occuring in some system at the current epoch? The two central theoretical questions that have been addressed here are what are the fundamental parameters associated with the Hubble sequence and how would one go about computing tracks and secondly how this work does in fact tie in with all our current thinking on galaxy formation, the nature of quasar absorption line and the understanding of the intergalactic medium.

It is a pleasure to thank the organiser of the Moriand conference for such a stimulating gathering and for the participants for interesting discussions and encouragement in particular S. Ikeuchi, R. Larson, and B. Pagel.

REFERENCES

Chambers, K., Miley, G. and van Breugel, W. 1987, preprint.

Danly, L., Blades, C. and Norman, C. 1987, preprint.

Davies, R. L., Burstein, D., Dressler, A., Faber, S. M., Lynden-Bell, D., Terlevich, R., Wegner, G. in Proceedings of IAU Symposium *124* on *Observational Cosmology*, ed. G. R. Burbidge, and A. Hewitt (Dordrecht, Reidel), 1987.

Djorgovskii, 1986, Ph.D. Thesis, University of California, Berkeley.

Djorgovskii, S., Spinrad, H., Pedelty, J., Rudnick, L. and Stockton, A. 1987, preprint.

Dressler, A. 1987, preprint.

Heckman, T. M., Armus, L. and Miley, G. K. 1987, *A. J.*, **92**, 277.

Lake, G. and Norman, C. 1983, *Ap. J.*, **270**, 51.

Larson, R. B. 1985, *M.N.R.A.S.*, **214**, 379.

Lubow, S. 1987, in preparation.

Lynden-Bell, D. and Kalnajs, A. 1971, *M.N.R.A.S.*, **157**, 1.

Meisels, A. and Ostriker, J. P. 1984, *A. J.*, **89**, 1451.

Norman, C. and May, A. 1985, unpublished.

Norman, C. A. 1987, preprint.

Ostriker, J. P. and Peebles, P. J. E. 1973, *Ap. J.*, **186**, 467.

Quinn, P. J. and Goodman, J. 1986, *Ap. J.*, **309**, 472.

Roos, N. and Norman, C. 1979, *Astr. Ap.*, **76**, 75.

Sandage, A., 1983 in Internal Kinematics and Dynamics of Galaxies IAU *100*, p. 367, ed. E. Athanassoula.

Sandage, A. 1986, *Astr. Ap.*, **161**, 89.

Scoville, N. Z., Sanders, D. B., Sargent, A. I., Soifer, S. L. 1986a, *Ap. J. (Letters)*, **311**, L47.

Scoville, N. Z., Sanders, D. B., Clemens, D. P. 1986b, *Ap. J. (Letters)*, **310**, L77.

Scoville, N. Z. and Norman, C. A. 1987, in preparation.

Silk, J. and Norman, C. 1981, *Ap. J.*, **247**, 59.

Wolfe, A., Turnshek, D., Smith, H. E. and Cohen, R. D. 1986 *Ap. J. Suppl.*, **61**, 249.

York, D. G., Dopita, M., Green, R. and Bechtold, J. 1986, *Ap. J.*, **311**, 610.

FEEDBACK AND STARBURSTS

Tommy Wiklind
Onsala Space Observatory
S-439 00 Onsala, Sweden

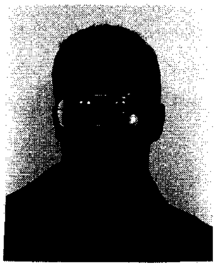

A simple phenomenological model of the regulatory coupling between the SFR and the molecular gas fraction is presented. The model can in a qualitative way explain both the constant SFR observed in most galaxies and the starbursting behaviour seen in some systems.

Formation of massive stars are thought to have both a positive and a negative feedback on further stellar formation. A sudden increase in the gas available for star formation will cause a strong increase in the SFR lasting for $\sim 3 \cdot 10^7$ yrs. Both the SFR and the molecular gas fraction will then perform damped oscillations over a period of a few $\times$ 10^8 yrs. This general behaviour is valid for a large range of parameter values.

1. Introduction

Since the work of Searle, Sargent and Bagnuolo in 1973 [14] it is well known that some galaxies undergo transient periods of greatly enhanced star formation rate (SFR). Although the number of known starburst galaxies has been rapidly increasing in the last few years, they still constitute a minority. Most late type galaxies, including our own, exhibit nearly constant SFR's [18, 17, 6]

In our Galaxy stars are formed in molecular clouds, which usually are several orders of magnitude more massive than their corresponding Jeans mass. If these clouds would all be undergoing gravitational collapse and forming stars, the SFR would be around 10^3 $M_\odot$/yr. The observed SFR is about 3 $M_\odot$/yr [11, 6]. Hence, star formation appears to be regulated and maintained at a low efficiency over long time intervals. Several sources of such regulation have been proposed [e.g. 3]. One of these is feedback from OB-stars on the ambient interstellar medium.

On the one hand, expanding OB-associations can be understood as a dispersal of the parent molecular cloud, containing most of the binding mass, by the first formed OB-stars [10]. On the other hand, OB-associations often occur in sub-groups with monotonically changing ages [e.g. 1], which has been interpreted by Elmegreen and Lada [4] as propagating star formation driven by a previous generation of OB-stars. A striking example of such self-propagating star formation can be found in the Shapley III constellation in the LMC [2] where the lack of rotational shear has preserved the ring-like symmetry.

The feedback from OB-stars is thus both positive, in that it induces star formation, and negative, in that it inhibits further star formation by destroying the molecular cloud. I will here show that a simple phenomenological model of the SFR, with these feedbacks incorporated exhibits both a steady state and a bursting behaviour when perturbed.

2. Description of the model

The major asset with a simple phenomenological model is its qualitative description of a complex physical situation. In order to retain simplicity we will keep the number of parameters to an absolute minimum and try to assign reasonable numerical values to them.

We will use two coupled rate equations for the SFR (ψ) and the molecular gas fraction, MGF (D).

$$\dot{D} = \varepsilon_1 - \gamma_1 D \psi \tag{1}$$

$$\dot{\psi} = (-\varepsilon_2 + \gamma_2 D)\,\psi \tag{2}$$

Obviously, this system has a stationary point at

$$(D_0, \psi_0) = (\varepsilon_2/\gamma_2, \varepsilon_1\gamma_2/\varepsilon_2\gamma_1) \tag{3}$$

The rates of the negative and positive feedback are given by the parameters γ_1 and γ_2, respectively. Since these are closely related to the main sequence lifetime of massive stars we will assign a numerical value of 10^{-6} yrs^{-1} to both of them. The MGF is assumed to increase by various accretion processes which are clumped together in the single parameter ε_1. The time to form a GMC by random collisions of small molecular clouds is 10^8–10^9 yrs [9], and we will here use 10^{-9} yrs^{-1} as a typical 'accretion' rate. The observed SFR is moderated by the short main sequence lifetime of the massive stars. This is implemented through ε_2, which is taken to be 10^{-6} - 10^{-7} yrs^{-1}.

Similar one-zone models have also been presented by others [15, 7, 5]. Scalo and Struck-Marcell [13] have modelled a feedback regulated interstellar cloud evolution.

3. Stability

From stability analysis it turns out that the model is dynamically and structurally stable against perturbations in either the MGF or the SFR. Both variables will perform damped oscillations around their equilibrium value. The response of the SFR to a sudden increase in the MGF will be strong and burst-like, lasting for $(2\text{-}4)\cdot 10^7$ yrs, and phaseshifted relative to the MGF by approximately $3\cdot 10^7$ yrs, cf. figure 1.

A change of the numerical values of the parameters ε_1, ε_2, γ_1 and γ_2, within reasonable ranges, will not change the stability but rather the damping and oscillatory times. By introducing a time delay for the dispersion of the ambient molecular cloud of a few Myrs, the response of the system to a disturbance is enhanced, cf. figure 2. However, if a similar time delay is also introduced for the induction of star formation, the enhancement is counteracted and the response is then similar to the case with no time delay at all.

In the solution of the linearized equations it is possible to define a damping time t_D and an oscillatory period T as

$$t_D = 2\varepsilon_2/\varepsilon_1\gamma_2 \tag{4}$$

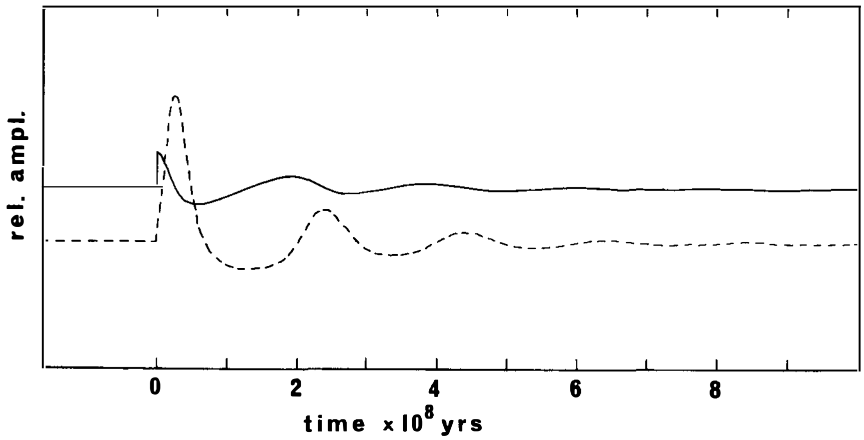

Figure 1. *An increase in the MGF (full drawn line) at time zero with two times the equilibrium value, gives rise to a strong response in the SFR (dashed line). The parameter values are:* $\varepsilon_1=10^{-9}$ *yrs*$^{-1}$, $\varepsilon_2=10^{-7}$ *yrs*$^{-1}$ $\gamma_1=\gamma_2=10^{-6}$ *yrs*$^{-1}$.

$$T = 4\pi\varepsilon_2/[\varepsilon_1\gamma_2\sqrt{(4\varepsilon_2^2/\varepsilon_1\gamma_2) - 1}\,] \tag{5}$$

In figure 3 t_D and T are plotted vs. changes in the parameter values. From these plots one can deduce the effect of different parameter values on the model. It is evident that the model is stable for large variations of the parameter values.

4. Applications

A simple model like this has no direct applications apart from giving a qualitative picture of possible feedback mechanisms. However, in a numerical simulation of star formation due to cloud-cloud collisions in an interacting galaxy, Noguchi and Ishibashi [12] found the SFR to increase by a factor ~8 relative to the equilibrium value, and also temporal oscillations in the global SFR with amplitudes and durations similar to those in the present model.

By initially decreasing the MGF, or similarly inhibiting the SFR, the response of the system will be oscillations in the MGF and the SFR as before, but with a time delay of several 10^7 yrs for the first burst of the SFR. An intriguing result from IR observations of interacting galaxies [8, 16] is that out of 73 pairs showing starburst activity only 1 has such activity in both galaxies. The cause of this effect is not known, but the present model shows that large phase differences in the SFR are possible when one system experiences

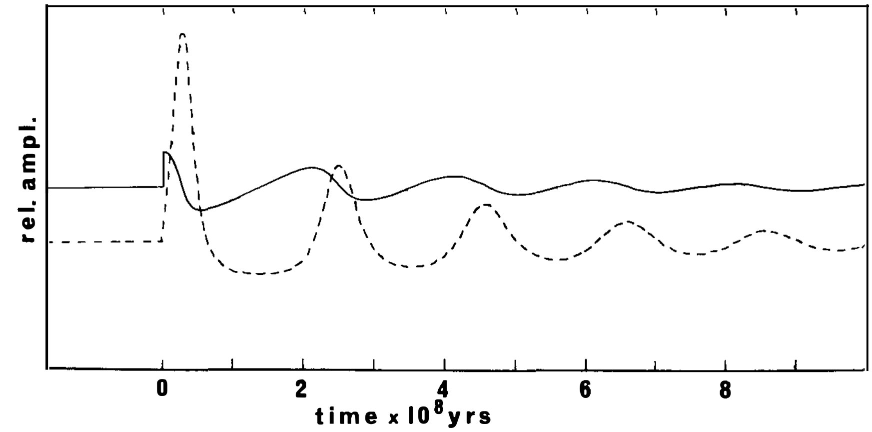

Figure 2. *Same as in figure 1, but with a time delay of $5 \cdot 10^6$ yrs for the dispersal of the ambient molecular cloud.*

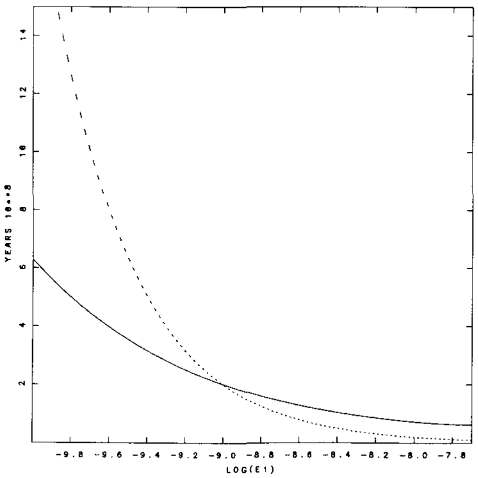

Figure 3. *The damping time t_D, dashed line, and the oscillatory period T, full drawn line, defined from solution of the linearized model. The numerical values are choosen as in figure 1, and then varied one at a time.*

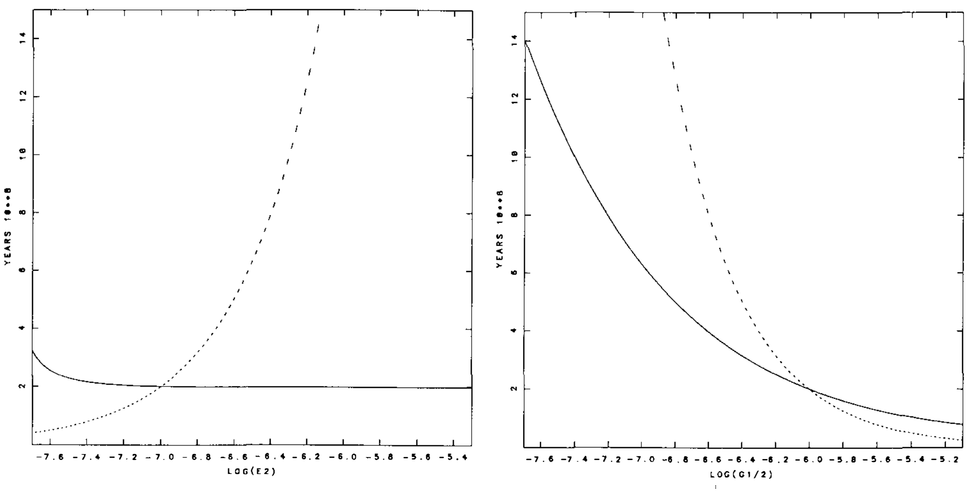

an increase in the MGF, or the SFR, and the other system a decrease.

Hence a simple phenomenological model, containing only a few parameters, can give a qualitative picture of the regulatory coupling between the MGF and the SFR. The system has a stationary point which is stable against perturbations, and when disturbed the inherent properties of the regulatory coupling lead to a burstlike behaviour of the SFR, with timescales agreeing with observed gas consumption rates in starburst galaxies.

References

1. Blaauw, A., 1964, Ann. Rev. Astron. Astrophys., 2, 213
2. Dopita, M.A., Mathewson, D.S. and Ford, V.L., 1985, Ap. J., 297, 599
3. Downes, D., 1986, IAU Symp. no. 115, Star Forming Regions, eds. M. Peimbert and J. Jugaku, Reidel
4. Elmegreen, B.G. and Lada, C.J., 1977, Ap. J., 214, 725
5. Ferrini, F. and Marchesoni, F., 1984, Ap. J., 287, 17
6. Gallagher, J.S., Hunter, D.A. and Tutukov, A.V., 1984, Ap. J., 284, 544
7. Ikeuchi, S. and Tomita, H., 1983, Publ. Astron. Soc. Jap., 35, 77
8. Joseph, R.D., Meikle, W.P.S., Robertson, N.A. and Wright, G.S., 1984, M.N.R.A.S., 209, 111
9. Kwan, J., 1979, Ap. J., 229, 567
10. Lada, C.J., 1986, IAU Symp. no. 115, Star Forming Regions, eds. M. Peimbert and J. Jugaku, Reidel
11. Mezger, P.G., Mathis, J.S. and Panagia, N., 1982, Astron. Astrophys., 105, 372
12. Noguchi, M. and Ishibashi, S., 1986, M.N.R.A.S., 219, 305
13. Scalo, J.M. and Struck-Marcell, C., 1986, Ap. J., 301, 77
14. Searle, L., Sargent, W.L.W. and Bagnuolo, W.G., 1973, Ap. J., 179, 427
15. Shore, S.N., 1981, Ap. J., 249, 93
16. Telesco, C.M., Wolstencroft, R.D., Done, C. and Arp, H.C., 1987 preprint
17. Tosi, M., 1982, Ap. J., 254, 699
18. Twarog, B.A., 1980, Ap. J., 242, 242

STAR FORMATION AND SPECTROPHOTOMETRIC EVOLUTION OF HIGH REDSHIFT GALAXIES

Brigitte ROCCA-VOLMERANGE* and Bruno GUIDERDONI
Institut d'Astrophysique de Paris
98 bis, bd Arago F-75014 Paris

* also Laboratoire Rene Bernas
Universite de PARIS XI F-91306 Orsay

Abstract One clue to understand galaxies at large redshifts and, by extension, starburst galaxies, is to assume that they evolve as nearby galaxies and to build evolutionary models to be constrained by observations on a large redshift scale. The present status of far-UV emissivity of giant elliptical galaxies is firstly reviewed, since this range is fundamental to study past star formation and is detected in visible for $z \geq 0.5$. Based on recent improvements in spectrophotometric models, possible scenarios of star formation histories for bursting and normal galaxies are proposed. Special attention is given to the evolutionary modelisation of a single burst, which will be helpful to study starbursts at large redshifts.

Introduction

First developments on understanding starbursts in galaxies arised from models of stellar populations built to reproduce colors of extremely blue galaxies consuming a large fraction of gas on a short timescale and characterized by a dominant young massive stellar population (Searle et al., 1973, Larson and Tinsley, 1978). More recently, observations from the IRAS satellite, in the far–infrared wavelength range, extended the notion of starbursts in galaxies and more precisely in distant galaxies, to a large scale. Moreover, smaller bursts of star formation in galaxies can also explain the fraction of blue galaxies in cluster cores, which increases with redshift (Butcher and Oemler, 1984, and references therein).

So, before estimating significant parameters of a burst of star formation (M/L ratio, present rate, initial mass function,..), it is necessary to separate the contribution of "normal evolution", the effect of the cosmology and the effect of the dust in the underlying galaxy. That is the crucial and general problem of the analysis of high–redshift galaxies. Bursts which concern the totality or a large fraction of the galaxy and its environment have to be studied from preferential rest–frame wavelength ranges: they are extreme–UV and far–infrared on the one hand, and near–infrared ($\lambda \leq 5\mu m$) on the other hand, respectively informing on massive, main sequence stars and on supergiant stars.

Models tentatively reproduce, at any age, "normal evolution" of galaxies of the Hubble Sequence from far–UV light (1200 Å) to near infrared ($\sim 1\mu m$). We propose models which give intrinsic evolution effects by varying a limited number of free parameters: essentially the time-scale of the gas consumption. Careful attention will be given to the far–UV light emitted by elliptical or inner bulges of spiral galaxies, the most detectable objects at large distances in visible broad–band filters.

We search for the observational characteristics of a young elliptical galaxy to compare (or eventually substract) to a starburst galaxy and thus to define the intrinsic properties of starbursts.

We review the present status including our new analysis of the far–UV light emitted by giant elliptical galaxies in section 1. Section 2 will present models of evolution of normal galaxies. Results on colors and magnitudes of high–redshift galaxies will be given in section 3 and our preliminary conclusion on the amount of galactic evolution as defined by our UV–hot and UV–cold models, will be given in the last section.

I. An evolutionary scenario for the "UV excess"

An important literature has been published on various interpretations given to the apparent excess of UV light emitted by early–type galaxies : either massive stars (Wu et al., 1980) or hot evolved stars (Bertola et al., 1982, Deharveng et al., 1982) among which horizontal branch stars and more recently post asymptotic giant branch stars (Renzini, 1985) are the favorite candidates.

a) The main properties of this far–UV light emitted essentially by nuclei of elliptical or SO galaxies and detected by the ANS, OAO and IUE satellites, are :

i) An important variation from one galaxy to another one (Bertola et al., 1982, Nesci and Perola, 1985, and references therein).

ii) Variations are observationally limited by the maximum values of the well–known elliptical galaxies of the Virgo cluster M87 (Bertola et al., 1980) and NGC4649 (Bertola et al., 1982).

iii) In gas–rich galaxies such as NGC5102, where star formation is detected (Van den Bergh, 1976), a definition of the UV excess is not significant.

In Rocca-Volmerange and Guiderdoni 1987, hereafter RVG, we propose a new analysis of the IUE spectra of early– type galaxies, using the best spectral resolution ($\leq$ 10 Å) of the instruments and the stellar atlases (Wu et al., 1983, Heck et al., 1983, Gunn and Stryker,1983),treated in the same way as the spectra of galaxies, to interpret stellar emissivity. Three important results related to the history of the star formation are obtained in our sample of gas-poor galaxies:

iv) From the spectral range 2500 Å to 3000 Å, a dominant stellar component of F stars with an age of 3 to 10 Gyrs is detected in the nuclei of these galaxies. UV stellar continua do not present discontinuities with the visible, favoring a scenario of continuous star formation process.

v) A faint emissivity at 2000 Å is observed for all galaxies. This is the range of maximum emission of A stars. The horizontal branch stars which have essentially the A type (Caloi et al., 1986) cannot be the main contributors to the far–UV emission.

vi) In some cases, an UV excess is detectable (cases of M87, NGC3115) and in other cases, any UV excess is not detectable (cases of M32 and NGC4382). But with this new analysis, UV excess is only significant below 2000 Å . If its origin is stellar, it corresponds to very hot stars. The fact that it is not observed in all galaxies does not favor the hypothesis of evolved stars according to a standard scenario. Moreover, in each case, it may be explained by the accretion of a small amount of gas : cooling–flows are detected in M87 and a stripped dwarf galaxy companion has been detected in the typical isolated SO galaxy NGC3115 (de Vaucouleurs et al., 1976, Hanes and Harris, 1986). This could supply the galaxy with a low amount of gas according to the accretion model of Silk and Norman, 1979. For NGC 3115, another explanation to the UV excess is difficult to find.

The lack of UV emissivity of M32 can be explained by the sweeping of the gas content during the crossing of the disk of M31 while, in the case of NGC4382 which is relatively blue and in pair with another giant galaxy, interaction could have stripped the gas from the nucleus.

b) As a conclusion of the previous analysis, the origin of the UV excess can be star formation, and the evolution of this massive stellar component at large look–back times will be strongly different from that of an evolved stellar component, as calculated in the "HB1" and "HB2" models of Bruzual, 1981 and we propose to model the UV emissivity with an evolutionary scenario of star formation with given IMF and age. An extended grid of μ–models was proposed by Bruzual, 1983. These models were also based on star formation scenarios but a complete fit from far–UV to visible needed the simultaneous variation of several parameters (IMF, rates). If the UV emissivity is related to the presence or lack of a small amount of gas, a precise origin of this gas is impossible to determine and consequently one difficulty is to parametrize any environmental interaction which is in principle randomly distributed during the life of the galaxy. To answer this problem, we proposed two extreme models "UV-cold" and "UV-hot" ellipticals respectively fitting the extreme cases (maximum for M87 and null for NGC4382), as analyzed by RVG (figures 1ab).

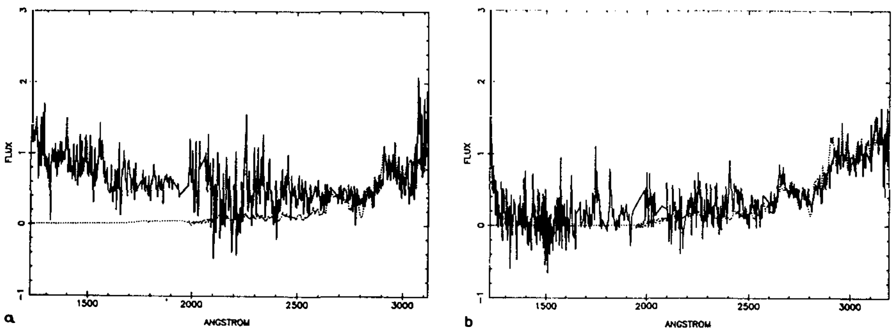

Figure 1. A comparison of the IUE spectra of M87 (a) and NGC4382 (b) with a F8V star. Stellar fluxes are normalized at 3000 Å to galactic ones in absolute units:10^{-14}erg cm^{-2}s^{-1} Å^{-1} .

Such scenarios have to be tested with an evolutionary model. The adopted star formation laws are the following ones:

– the upper limit is well represented by a star formation law proportional to the gas content, with a high efficiency: $\tau_*(t) = 1g(t)$ with $g(t) = M_{gas}(t)/M_{tot}$. This is the UV–hot (h) model.

– the lower limit in extreme UV light is simply given by an exponentially decreasing star formation law, independent of the gas content: $\tau_*(t) = \exp(-t)$. This is the UV–cold (c) model.

$\tau_*(t)$ is in $M_\odot$ Gyr^{-1} by $M_\odot$ unit, and t is in Gyr unit. The present age of the galaxy t_g is $\geq$ 13 Gyrs. Calculations are proposed in Guiderdoni and Rocca–Volmerange, 1987a, hereafter GRV and a comparison with models is given in figure 2.

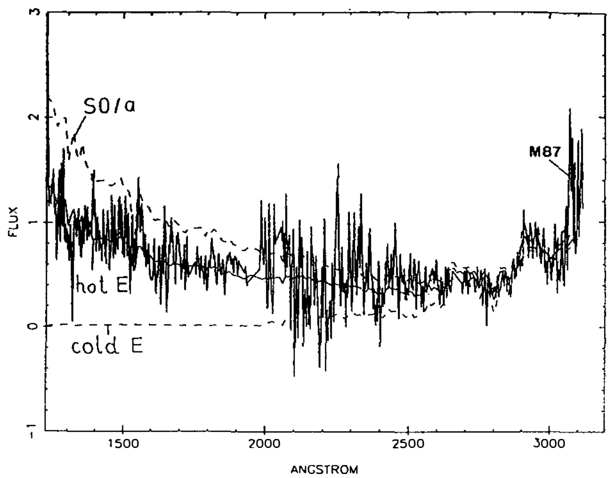

Figure 2. Comparison of the synthetic spectra of cold (c) and hot (h) elliptical galaxies at an age 13Gyrs, with the observational spectrum of the nucleus of M87 (Bertola et al, 1980). M87 has one of the largest UV excesses.

For comparison, another exponentially decreasing star formation law is also considered: $\tau_*(t) = 0.4\exp(-0.4t)$. this model (h') reproduces the maximum UV excess of M87 with a time-scale of the star formation longer than (h), inducing colors in visible which are bluer than normal E galaxies. We will also introduce a 1Gyr burst model (b): $\tau_*(t) = 1$ for t$\leq$ 1Gyr and null later. It reproduces a null UV-excess with a shorter time-scale than (c), inducing redder colors in visible and infrared.

II. Models of galactic evolution

a) Photometric evolutionary models

Photometric models were initiated by Tinsley, 1972, and Searle et al., 1973, to interpret visible photometry of galaxies and the Hubble sequence in color–color diagrams. An explanation of the bluest galaxies by bursts of star formation was also given by Searle et al., 1973, and Larson and Tinsley, 1978.

Such models were improved with a nebular component (Huchra, 1977), with a metal–deficiency effect and far–UV colors (Rocca-Volmerange et al., 1981) and more recently with a continuous metallicity effect (Arimoto and Yoshii, 1986).

But a model to analyze apparent magnitudes and colors of high–redshift galaxies needs the addition of a spectral library of stars and the coupling with a cosmological model. It was firstly carried out by Bruzual, 1981, whose model has been used for many interpretations.

At present, several improvements relatively to these previous models are in GRV.
— A complete stellar library from 1200 Å to $\sim$ 1μm, used with the best resolution $\leq$ 10Å ,exists from the IUE satellite (Wu et al., 1983, Heck et al., 1983) and visible (Gunn and Stryker, 1983) spectral Atlases. The library of Bruzual, 1981, models had no flux at $\lambda \leq$ 2000Å for stars with a type later than F and an average wavelength step = 50Å in visible.
— The nebular component (continuum and emission lines) may have a stronger effect at high redshift than estimated for nearby galaxies (Huchra, 1977) and is added according to a standard HII region from Stasińska, 1984, models.
— The extinction effect, tightly correlated to dust and gas, modifies the apparent spectrophotometry of galaxies, especially in UV light and when galaxies are more gaseous than now.
— The sensitivity of the results to the effective temperature of the giant branches is now well known (Renzini, 1985). In our models, we propose to vary T_{eff} with stellar masses according to the models of Sweigart and Gross, 1978, deduced from the Yale isochrones. We also take into account the evolutionary phase of the Asymptotic Giant Branch, from Iben and Truran, 1978, and Renzini and Voli, 1981, and the Horizontal Branch stars, according to Sweigart and Gross, 1976. Details are given in GRV.

b) Star formation parameters

Various histories are proposed in models of evolution : correlation of the star formation rate (SFR) with the gas content HI or H_2, exponentially–decreasing or constant. From Schmidt's (1963) law to the models of Dopita, 1985, fitting the sample of galaxies from Donas and Deharveng, 1984, observed in UV-light with the OAO satellite (Code and Welch, 1982), SFRs are generally assumed to be proportional to a power of the gas density, more specifically of the surface density (Larson, this conference) with a possible threshold effect (Elmegreen, 1979, Dopita, 1985, Guiderdoni, 1987). But to estimate the variation of the gas content is difficult since it depends on the efficiency of the star formation but also on the gas ejected by stars and on possible exchanges with the environment (accretion flow, cooling flows, galactic winds, etc...).

The parameter which gives a good image of the large scale phenomenon of star formation rate is the time scale of the gas consumption. Table 1 gives the adopted time scales (Guiderdoni, 1986, Guiderdoni and Rocca–Volmerange, 1987b); corresponding star formation histories and possible morphological types are also given.

$r_*(t)$	t_* (Gyr)	Type
burst 1 Gyr	0.63	
$1 \exp -1t$	1.0	UV–cold E/SO
$0.37 \exp -0.37t$	2.7	UV–hot E/SO
$0.4g(t)$	2.3	SO/a
$0.3g(t)$	3.0	Sa
$0.2g(t)$	4.5	Sb
$0.1g(t)$	9.1	Sc
0.048	13.2	Sd
$4.0 \times 10^{-4}t^2$	16.8	Im

Table 1.
Star formation histories, time scales of the gas consumption t_* and possible morphological types adopted in our models (GRV).

SFR(t)	g	M/LB	U-B	B-V	V-R	R-I	191Ø-B	246Ø-B	SFR/<SFR>
burst 1Gyr	Ø.173	1Ø.6	Ø.56	Ø.94	Ø.77	Ø.61	5.Ø4	2.89	Ø.ØØ
exp-t	Ø.178	9.7	Ø.62	1.Ø1	Ø.88	Ø.75	5.Ø8	2.96	Ø.ØØ
Ø.37exp-Ø.37t	Ø.168	8.1	Ø.48	Ø.92	Ø.84	Ø.73	1.43	1.69	Ø.Ø2
Ø.4g(t)	Ø.Ø1Ø	6.7	Ø.4Ø	Ø.89	Ø.83	Ø.73	Ø.73	1.19	Ø.Ø5
Ø.3g(t)	Ø.Ø25	6.2	Ø.3Ø	Ø.63	Ø.3Ø	Ø.71	Ø.24	Ø.77	Ø.1Ø
Ø.2g(t)	Ø.Ø77	5.7	Ø.17	Ø.74	Ø.75	Ø.67	-Ø.2Ø	Ø.38	Ø.22
Ø.1g(t)	Ø.265	5.1	Ø.Ø3	Ø.62	Ø.67	Ø.6Ø	-Ø.54	Ø.Ø3	Ø.5Ø
Ø.Ø48	Ø.37Ø	3.8	-Ø.Ø8	Ø.51	Ø.58	Ø.51	-Ø.83	-Ø.25	1.ØØ
4.ØE-Ø4t**2	Ø.572	2.2	-Ø.21	Ø.37	Ø.46	Ø.37	-1.2Ø	-Ø.6Ø	2.98

Table 2. Gas density g, M/L ratio, visible and UV colors, present/past SFR calculated for our various star formation laws at 15.5 Gyrs.

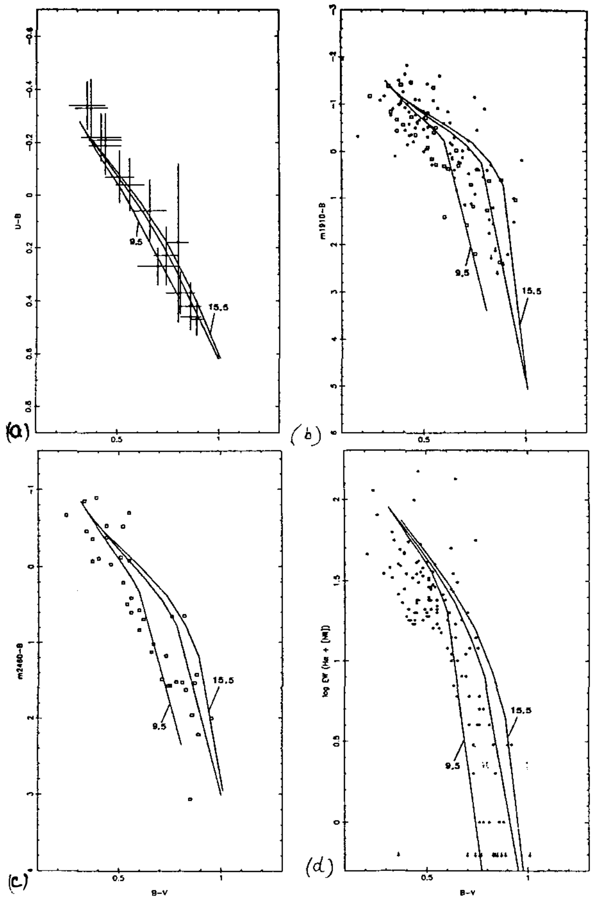

Figure 3. Comparison of three isochrone sequences (9.5Gyrs, 12.5Gyrs, 15.5Gyrs) for various SF laws of table 1 with observational colors. Sources of observations and caracteristics of the photometric systems are in GRV.

Several IMFs have been proposed in the literature. They essentially differ for massive stars: $dN(m)/d\log m \propto m^{-x}$ with x=1.35 (Salpeter, 1955), 2.3 (Miller and Scalo, 1979), 2.0 (Lequeux, 1979). A recent, complete analysis of the present observations (Scalo, 1986) gives x=1.7. In our models we adopt this value for $2M_\odot \le m \le 80M_\odot$. Slopes for less massive stars are more uncertain because of incomplete counts and dependence on past star formation. We adopt values from Tinsley, 1980: x=0.25 for $0.1M_\odot \le m \le 1M_\odot$ and from Salpeter, 1955, x=1.35 for $1M_\odot \le m \le 2M_\odot$.

As a first approximation, we adopt one unique metallicity, the solar one which is reached in less than 1 Gyr (Rocca–Volmerange, 1987a). In our UV and visible studies, the results are more sensitive to the age effect than to the metallicity effect, as confirmed by Bica and Alloin, 1986, Moreover integrated photometry of distant galaxies includes all the components (halo, disk and bulge) and their average metallicity could be not far from solar.

III. Evolution of high–redshift galaxies

a) Rest–frame colors and spectra

Main results of colors and gas content at 15.5 Gyrs for the adopted star formation histories, which are outputs of our models (GRV), are given in table 2. The comparison of these models at three ages with observed galaxies of the Hubble sequence in visible and far–UV colors is shown in figures 3abc. Equivalent widths of ($H\alpha$ + [NII]) lines are given in fig.3d, assuming a fraction 0.8 of the total ionizing energy being absorbed by grains or escaping from the galaxy.

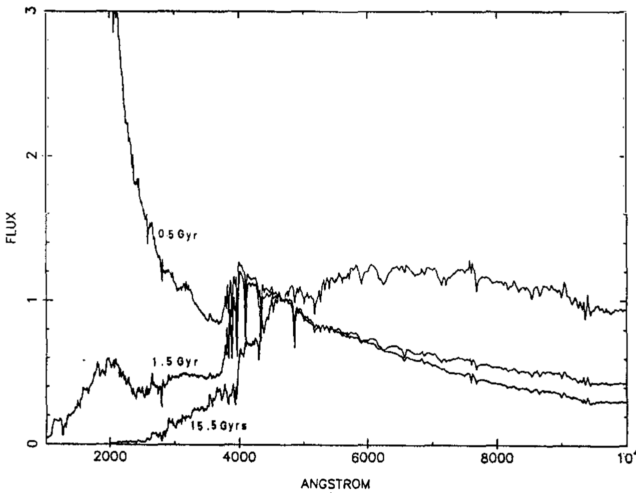

Figure 4a

Three types of galaxies will be presented:

- Stellar continua of a bursting galaxy (figure 4a). The duration of the burst is 1Gyr. Three ages are shown: 0.5 Gyr, 1.5 Gyr and 15.5 Gyrs. The IMF is from Scalo, 1986, as previously described.

- The stellar energy distribution of an Sb galaxy can be modeled as shown in fig.4b. The star formation rate by mass of galaxy is 0.4 $M_{gas}(t)/M_{tot}$. Nebular continuum and lines are also calculated.

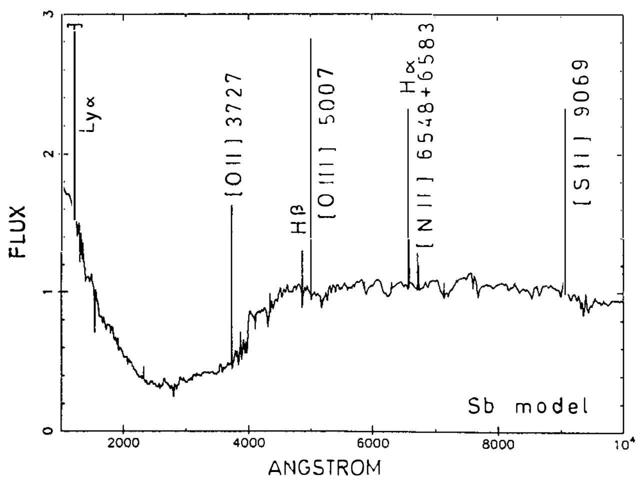

Figure 4b

- Elliptical galaxies, the brightest ones, can be detected at large distances. Fig 4c presents synthetic spectra for our two UV–hot and UV–cold models at 13 Gyrs.

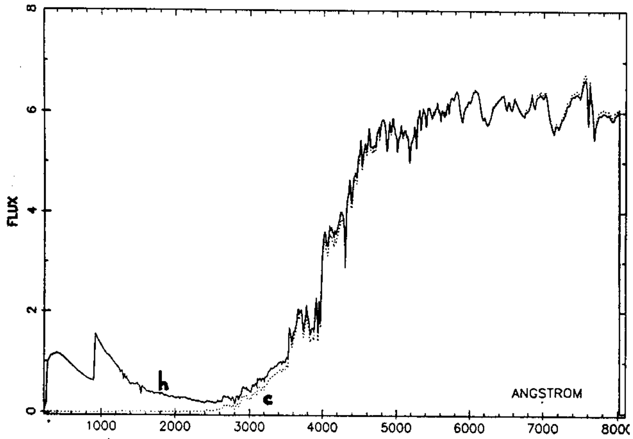

Figure 4c

A comparison of such synthetic spectra with observations is needed before using them as rest-frame typical spectra. One difficulty of any comparison is to have identical apertures with the different instruments. Two examples of well known elliptical galaxies M87 and NGC 4649, published by Bertola et al, 1980, 1982 are fairly fitted from far-UV light to visible by our UV-hot model at the age 13Gyrs (Rocca-Volmerange, 1987b). Figure 5 shows that agreement is quite satisfying for adopting these time scales for the gas consumption and it also confirms that UV excess of such galaxies has most likely a star formation origin.

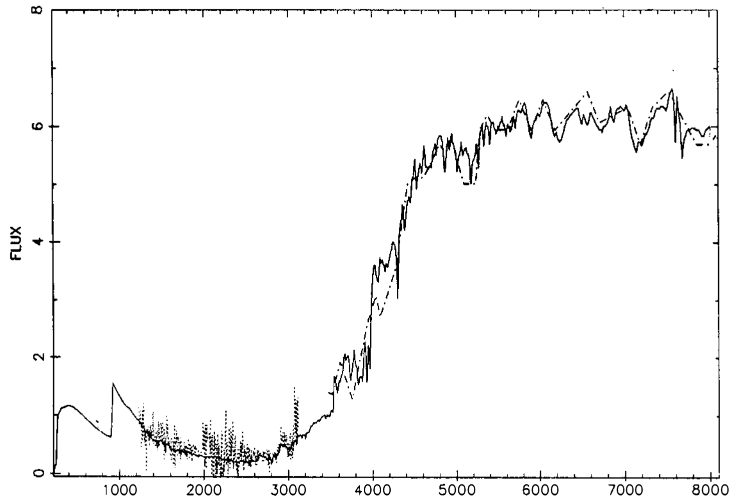

Figure 5. Comparison of the UV-hot (h) elliptical model at 13 Gyrs with observational spectrum of M87 from Bertola et al, 1980. Normalisations are at 3000Å (IUE spectrum) and 5400Å (visible).

b) Evolution effect at high redshift

Friedman-Lemaître cosmological models associated to our evolutionary model of stellar population give spectra and emission lines of galaxies with different types at various cosmological ages. Colors may be easily calculated by these spectra through filters. Apparent magnitudes and colors of distant galaxies are given in tables (Guiderdoni and Rocca-Volmerange, 1987b), for various photometric systems: Johnson, 1965, Thuan and Gunn, 1976, Kron, 1980, Koo, 1981, and through filters of the Wide Field Camera and Faint Object Camera of the Space Telescope (Paresce, 1985, Griffiths, 1985). They are published for timescales of table 2 to reproduce morphological types of the Hubble Sequence from bursts and elliptical to irregular galaxies. One example for V and B-V is shown in figure 6.

The results of our models can be summarized as follows : The elliptical galaxies which have significant changes in their star formation histories need an evolution factor

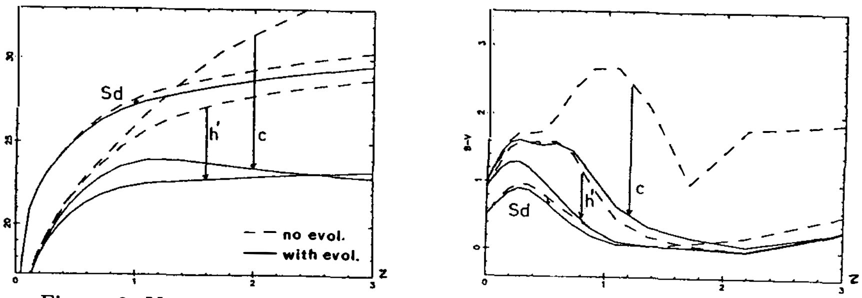

Figure 6. V and B-V versus z for a spiral galaxy (Sd) and for SO/elliptical galaxies (UV–hot (h') and UV–cold (c) models), calculated with (full line) and without (dashed line) evolution. The UV–hot case (h) roughly similar to (c) according to fig.4c is not shown.

to be taken into account at large look–back times. The redshift limit beyond which evolution is detectable varies from 0.7 (in the U band) to 0.9 in visible. The evolutionary correction strongly increases beyond $z \simeq 1$, and reaches several magnitudes (GRV).

The irregular and late spirals have a uniform and almost constant with time SFR. So no evolution factor is necessary to interpret the observations. This remark will be useful for most faint galaxies observed in large field surveys, for which the disk components are probably dominant.

A comparison of our models with Bruzual models, calculated in the conditions of the μ–model (μ = 0.6) and of the burst (b) is presented in figure 7 for the two visible colors in which differences are the most conspicuous.

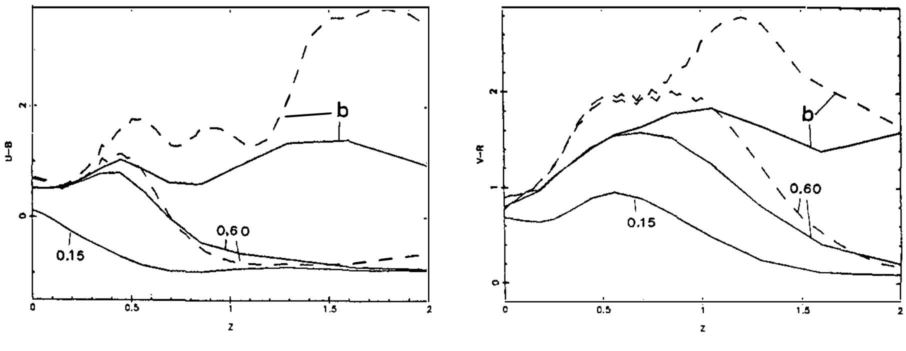

Figure 7. Comparison of Bruzual models,1981 (dashed lines) and GRV, 1987 (full lines) when calculated with identical star formation parameters: burst (b), μ models with μ=0.6 and 0.15. Extinction and nebular component are not included.

c) Comparison with observations

A comparison is possible with some sample of high–redshift galaxies: bright cluster members (Kristian et al, 1978) and optical counterparts of 3CR radiogalaxies observed by Djorgovski et al., 1987. Figures 8 and 9 present V and R photometry for two sets of cosmological parameters (H_0=50 km s^{-1} Mpc^{-1}, Ω_0=0.1 and 1, λ_0=0), and three star formation histories: (c) and (h') with an active evolution and 1Gyr burst (b) with a passive evolution. From a comparison with observations, it is clear that 3CR radiogalaxies follow scenarios of active evolution of star formation. This is in agreement with the detection of several components (Le Fevre, this conference) as well as the intensity of the [OII] lines or the velocity fields of such radiogalaxies (Djorgovski et al, 1987) from which it is concluded to interaction or merging processes. These processes drastically increase the surface density of gas and induce a high-efficiency process of star formation (Larson, this conference) during a time scale long enough to be simulated by the continuous (h') and (c) models.

Another interesting point is that M87, which is a radiogalaxy, also follows (figure 5) an active scenario of star formation (h), intermediate between (h') and (c), at an age 13Gyrs from 1200 Å to 8000 Å, without any sign of rough interaction with the intergalactic medium as hot galactic winds. Then such merging 3CR radiogalaxies which would have to appear as monsters due to their interacting mass are in fact well simulated in magnitude as in colors by the same star formation rate *by mass unit* than the giant and not merging radiogalaxy M87. Better comparisons have to be realized with other radiogalaxy samples such as the "1 Jy" sample (Allington–Smith et al., 1985, Lilly et al., 1985). These radiogalaxies, well bracketed by the two (h') and (c) continuous star formation models, do not present caracteristics of a starburst but are likely representative of *normal* galaxies with a high surface density of gas for a long time scale.

The present question is: Does it exist giant galaxies with a lower gaseous surface density which would be located between the (c) and (b) models in the magnitude–z or color–z diagrams. This sample of 3CR radiogalaxies could be a biased sample in magnitude. From figure 9, it is clear that galaxies between the burst curve (b) and the (h') and (c) curves with evolution cannot be detected if their surface brightness is insufficient. It is also possible that an amplification factor due to gravitational lensing (Hammer and Nottale, 1986) as well as the contribution of the active component to the total energy could modify the apparent stellar energy distribution in a way which is difficult to estimate. However the amplification effect does not modify colors and evolution is detectable in several colors as shown in GRV.

To summarize, the 3CR radiogalaxy sample presents in the rest–frame UV and visible colors (not affected by amplification) a scenario of star formation similar to M87. To know if this stage of merging radiogalaxy is a sign of formation by merging or an occasional phenomenon will only be possible from infra–red colors with a look–back

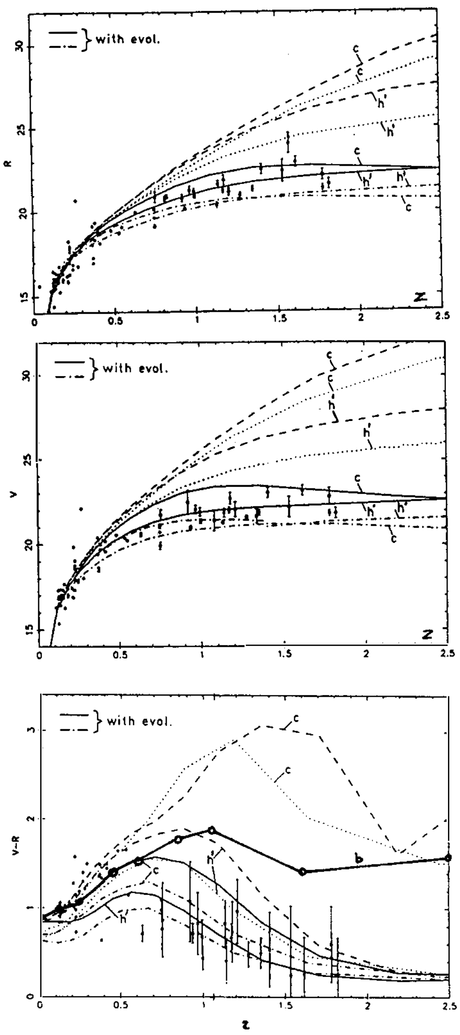

Figures 8 and 9. Apparent V and R magnitudes and V-R color versus redshift calculated with our UV–hot (h') and cold (c) and ($H_0 = 50, \Omega_0 = 0.1, \lambda_0 = 0, z_{for} =$ 5Gyrs) cosmological parameters: with (thick lines) and without (dashed lines) evolution. Another cosmological model with $\Omega_0 = 1$ is also shown with (dot-dashed lines) and without (dotted lines) evolution. Observations are from Kristian et al, 1978 (dots) and Djorgovski et al, 1987 (squares). Normalisation is the absolute magnitude at rest M_B=-22. The (b) model is also mentioned (open dots) in figure 9.

time corresponding to earlier phases (Lilly and Longair, 1984, Eisenhardt and Lebofsky, 1987).

Conclusion

A short review of the scenarios of star formation history, needed to reproduce the normal evolution of galaxies in the rest frame, is given. The characteristics of a "normal" evolution must be well known before the extension to characteristics of intense bursts.

For high-redshift galaxies, because of large look-back times, emission in the rest-frame UV range at the is detected in visible, so we concentrate our analysis on recent evolutionary ideas of the UV light emitted by elliptical galaxies.

We also present some new developments:

i) in our model which simulates the evolution of galaxies of the Hubble Sequence with a minimum number of free parameters, and predicts apparent magnitudes in various photometric systems,

ii) in fitting on a large wavelength range (1200Å –8000Å) the spectrum of M87 with an active scenario of star formation. No evidence of violent interaction with external medium (hot galactic winds for example) appears for the last 13 Gyrs.

iii) in concluding that 3CR radiogalaxies at large z evolve in colors and magnitudes as giant elliptical galaxies.

References

Allington-Smith, J.R., Lilly, S.J., Longair, M.S., 1985,*M.N.R.A.S.* ,213,243

Arimoto, N., Yoshii, Y., 1986, *Astron.Astrophys.*, 164, 260

Bertola, F., Capaccioli, M., Holm, A.V., Oke, J.B., 1980, *Astrophys. J. Letters*, 237, L65

Bertola, F., Capaccioli, M., Oke, J.B., 1982, *Astrophys.J.*, 254, 494

Bica, E., Alloin, D., preprint,1986.

Bruzual, G., 1981, Ph.D. Thesis, University of California, Berkeley

Bruzual, G., 1983,*Rev. Mex. Astron. Astrof.*, 8, 63

Butcher, H., Oemler, A.,Jr., 1984, *Astrophys.J.*,285,426

Caloi, V., Castellani, V., Danziger,J., Gilmozzi, R., Cannon, R.D., Hill,P.W. Boksenberg,A., 1986, *M.N.R.A.S.*, 222, 55

Code, A.D., Welch, G.A., 1982, *Astrophys.J.*, 256, 1

Deharveng, J.M., Joubert, M., Monnet, G., Donas, J., 1982, *Astron.Astrophys.*, 106, 16

de Vaucouleurs, G., de Vaucouleurs, A., Corwin, H.G., 1976, Second Reference Catalogue of Bright Galxies (Austin University of Texas Press).

Dekel, A., Silk , J., 1986, *Astrophys.J.*,303,39

Donas, J., Deharveng, J.N., 1984, *Astron. Astrophys.*, 140, 325.

Dopita, M., 1985, *Astrophys. J.*, 295, L5.

Djorgovski, S., Spinrad, H., Marr, J., 1984, in New Aspects of Galaxy Photometry, J.L. Nieto (ed.), Springer Verlag, p. 193

Djorgovski, S., Spinrad, H., Dickinson, M., 1987, preprint

Elmegreen, B.G., 1979, *Astrophys.J.* 231,372.

Forman, W., Jones, C., Tucker, W., 1985, *Astrophys. J.*, 293, 102

Griffiths, R., 1985, Wide Field and Planetary Camera Instrument Book, *STScI*, NASA/ESA

Guiderdoni, B., 1986, These de Doctorat de l'Universite de Paris VII

Guiderdoni, B., 1987, *Astron.Astroph.*, 172, 27.

Guiderdoni, B., Rocca–Volmerange, B., 1987a,(GRV),*Astron. Astrophys.*, in press.

Guiderdoni, B., Rocca–Volmerange, B., 1987b,*Astron. Astrophys.*, submitted

Gunn, J.E., Stryker, L.L., Tinsley, B.M., 1981, *Astrophys.J.* , 249, 48.

Gunn, J.E., Stryker, L.L., 1983, *Astrophys.J. Supp. Series*, 52,121 , 249, 48.

Hammer, F.,Nottale, L.,1986, *Astron. Astrophys.*, 167, 1

Hanes, D.A., Harris, W.E., 1986, *Astrophys. J.*, 304, 599.

Heck, A., Egret, D., Jaschek, C., 1984, Battrick., B., ESA SP-1052.

Huchra, J.P., 1977, *Astrophys. J.*, 217, 928

Iben, I.Jr., Truran, W.J.,1978, *Astrophys. J.*, 220,980

Koo,D.C.,1981, Ph.D. thesis, University of California, Berkeley

Kristian, J., Sandage, A., Westphal, J.A., 1978,*Astrophys. J.*,221,383

Kron, R.G., 1980, *Astrophys. J. Supp. Series*,43,305

Larson, R.B., 1974, *M.N.R.A.S.*, 164, 585

Larson, R., Tinsley, B.M., 1978,*Astrophys. J.*, 219, 46

Eisenhardt, P.R.M.,Lebofsky, M.J., 1987,*Astrophys. J.* 316,70

Lequeux, J., 1979, *Astron. Astrophys.*, 80, 35

Lilly, S.J., Longair, M.S., 1984, *M.N.R.A.S.*, 211, 833

Lilly, S.J., Longair, M.S., Miller, L., 1985, *M.N.R.A.S.*, 214,109

Mathews, W.G.,Baker, J.C., 1971, *Astrophys.J.*, 170,241.

Miller, G.E., Scalo, J.M., 1979, *Astrophys. J. Supp. Series*, 41, 513

Nesci, R., Perola, G.C., 1985, *Astron.Astrophys.*, 145, 296

Noorgaard-Neilsen, H.V., Kjaergaard, P., 1981, *Astron.Astrophys.*, 93, 290

O'Connell, R.W., 1976, *Astrophys.J.*, 206, 370.

Paresce, F., 1985, Faint Object Camera Instrument Book, *STScI*, NASA/ESA

Renzini, A., Voli, R., 1981, *Astron. Astrophys.*, 94, 175

Renzini, A., 1985,in Spectral Evolution of Galaxies, ed. Renzini and Chiosi.

Rocca–Volmerange, B., Lequeux, J., Maucherat–Joubert, M., 1981, *Astron. Astrophys.*, 104, 177

Rocca–Volmerange, B., Guiderdoni, B., 1987a,(RVG), *Astron. Astrophys.*, 175, 15

Rocca–Volmerange, B., 1987a, Proceedings of the ESO Workshop :Stellar Evolution of the Outer Halo of Our Galaxy, Ed. M.Azzopardi,in press

Rocca–Volmerange, B., 1987b,submitted

Rose, J.A., 1985, *Astron.J.*, 90, 1927
Salpeter, E.E., 1955, *Astrophys. J.*, 121, 161
Scalo, J.M., 1986,*Fundamental of Cosmic Physics*, 11,1
Schmidt , M.,1963, *Astrophys. J.*,137,758
Searle, L., Sargent, W.L.W., Bagnuolo, W., 1973, *Astrophys. J.* , 179, 427
Silk, J., Norman, C., 1979, *Astrophys. J.*, 234, 86
Stasińska, G., 1984, *Astron. Astrophys. Suppl. Series*, 55, 15
Sweigart, A.V., Gross, P.G., 1976, *Astrophys. J. Suppl. Series*, 32, 367
Sweigart, A.V., Gross, P.G., 1978, *Astrophys. J. Suppl. Series*, 36, 405
Thuan, T.X., Gunn, J.E., 1976, *Pub. Astron. Soc. Pac.*, 88, 543
Tinsley, B.M., 1972, *Astron. Astrophys.*, 20, 383.
Tinsley, B.M., 1980, *Fund. Cosmic. Physics*, 5, 287.
Van den Bergh, S., 1976, *Astron.J.*, 81, 795
Wu, C.C., Faber, J.M., Gallagher, J.S., Peck, M., Tinsley, B.M.,1980, *Astrophys. J.*, 237,290
Wu et al., 1983, NASA News n° 22.

GALACTIC EVOLUTION AND FRAGMENTATION BURSTS IN THE PROTOHALO

A. Di Fazio
Osservatorio Astronomico di Roma
V. le del Parco Mellini, 84 I-00136 ROMA, Italy.

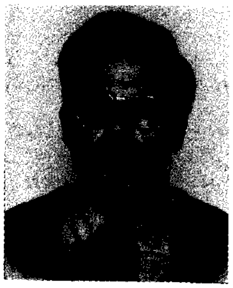

The primordial evolution of the galactic halo is investigated, using a multifluid fragmenting-radiative evolution model. A new theory of fragmentation (1), supported by a suitable treatment of the radiative properties of the primordial halo gas (accounting also for the formation of molecular hydrogen and for its cooling effect) is used to predict the mass spectrum of the first stellar generation and to study the primordial fragmentation activity. The first stars form in the range (40, 1000) solar masses, most likely in the protoglobular clusters. Strong fragmentation bursts appear after 200 Myr (about 1.2 galactic free-fall times).

1. Introduction.

The main goal of this paper is to determine the main physical characteristics of the evolution of the primordial galactic halo. In particular, when and where are the first stars born, what is their mass spectrum, what are the first self-gravitating, pre-stellar structures formed. In Sect. 2, we shall see how we can set up a multi-fluid calculation, in order to accomplish our goal. At the same time, it will be shown what treatment is suitable to describe the radiative activity of the protohalo's low density and temperature gas medium, using other specific works in the literature (2,3). Sect. 3 will display the results, together with a short discussion.

It is well known that the above described problems are intensively debated subjects. One of the main reasons for this is that global models with complete and sufficiently refined treatment of the relevant physical processes are rarely found in the literature. The main questions subject to scientific 'polemics' are: i) whether the first stars are low or high mass (and thus should or should not still be present now as a zero-heavy-element population); ii) whether the first star formation activity is a highly efficient and fast process (protohalo star burst); iii) whether the globular clusters are necessarily a pre-galactic generation or can reasonably be another protohalo fragmentation generation.

2. Radiative multifluid model.

The system is followed after the time of exit from linearity (decoupling from the Hubble flow). It is schematized as an initially pure gas sphere, of primordial chemical composition (e.g., X=0.25, Y=0.75) and at a temperature $100<T<1000\ ^{\circ}K$. In these conditions, the system is very far from equilibrium. The equation of state accounts for the ionization of the material and for the molecular hydrogen formation process. The cooling function is divided into two parts: the first one is due to free-bound and free-free transitions and to Thomson scattering on the atomic hydrogen and helium, the second one to the roto-vibrational transitions of the hydrogen molecule. The opacity function adopted is described and discussed in (2), together with the relevant processes. As the gas starts collapsing under its own gravity, it is also gravitationally unstable and it begins to fragment. Following a recent work on fragmentation by gravitational instability (1), which allows to compute the evolution of the fragments' mass spectrum and the instantaneous fragmentation rate, we describe the birth of a condensed phase in our collapsing system. The previous work did not account for molecular hydrogen and had a rougher treatment for the cooling function, as well as for the equation of state and for the radiation losses. The dynamical and thermodynamical description of the two phases (gas+fragments) is accomplished by following a spherical system of fragments. Like in (1), the fragments are coupled to the gas via the fragmentation law (determined by the instant local state of matter) and the conservations of energy, momentum, and mass. The differential equations governing the system are the same as in (1), with the following exceptions: i) the cooling function has an additive term like that described in (3) (for the molecular hydrogen contribution, Smith's fit accounts for 3 vibrational and 20 rotational levels); ii) a Saha equation describes the abundance of molecular hydrogen and the fraction is scaled down by a factor accounting for NLTE; iii) the latent heats of ionization and dissociation are accounted for.

The initial conditions chosen for the protogalactic cloud are: $T_o = 100\,^{\circ}K$; $R_o = 30$ Kpc; $M_{tot} = 10^{11}\,M_{\odot}$; $M_{gas} = 0$. Generations of fragments are born when the fragmentation process comes to a halt due to the low density induced by gas exhaustion (see 1).

3. Results

The results are shown in Fig.s 1 to 5. Fig. 1 displays: i) (short-dashed line) the velocity dispersion (in units 9 Km/sec) of the second generation fragments (protoglobular clusters, see Fig.3); ii) (long-dashed line) the gas temperature (in units 1000 °K); iii) the gas temperature of (1), that was computed without molecular hydrogen cooling; all quantities are vs. time in free-fall time units (140Myr). Fig. 1

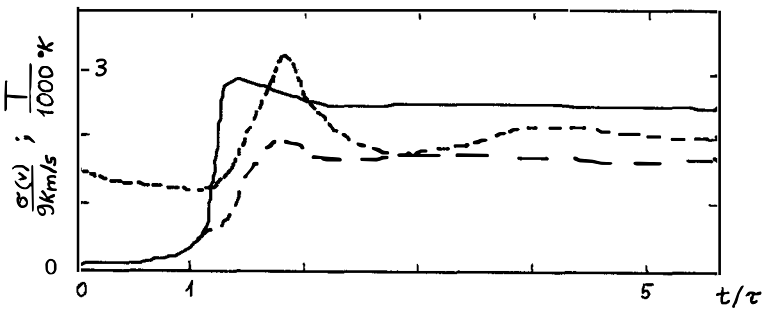

An adiabatic behaviour is obviously followed by the fragments velocity dispersion (the fragment system's internal energy in random orbits behaves adiabatically), while the gas temperature reaches very soon a quasy-isothermal phase around 1800 °K.

It is interesting to see what happens to the system as a whole. First, in about 160 Myr, it gives birth to a first generation of fragments whose masses can be seen in fig 2 (mass spectrum).

Fig. 2

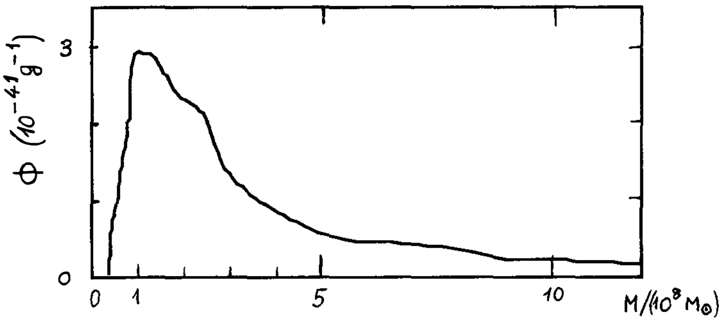

This figure, like all the mass function figures in this paper, plots the number of fragments per unit mass interval in arbitrary units. Here, the mass is in units of $10^8 M_\odot$. These fragments are even more unstable than in (1), due to the cooling effect of the molecular hydrogen produced. The following fragmentation process gives birth to the generation whose mass function is displayed in Fig. 3. This generation can represent the primeval family of protoglobular clusters . (The mass is in units of $10^5 M_\odot$).

Fig. 3

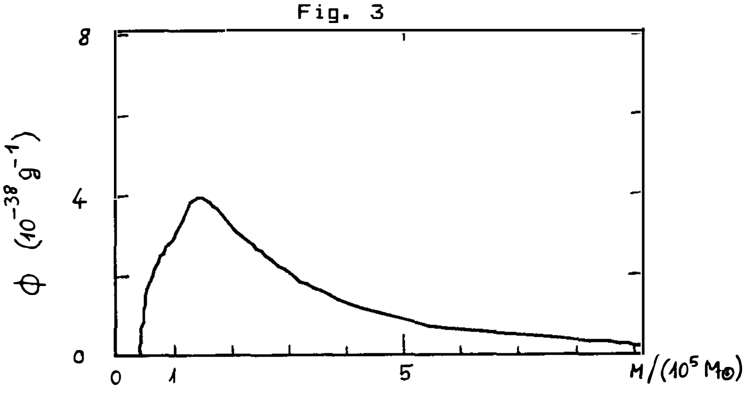

Although the shape is slightly different than in (1), the peak mass differs only for a small factor from (1). This is due to the onset of a radiative pseudo-equilibrium during the collapse. Further fragmentation (the state of the gas in the various fragments is constantly followed in time) leads to the third generation fragments. The majority of these objects forms in only 60-70 Myr, and their mass spectrum is shown in Fig. 4

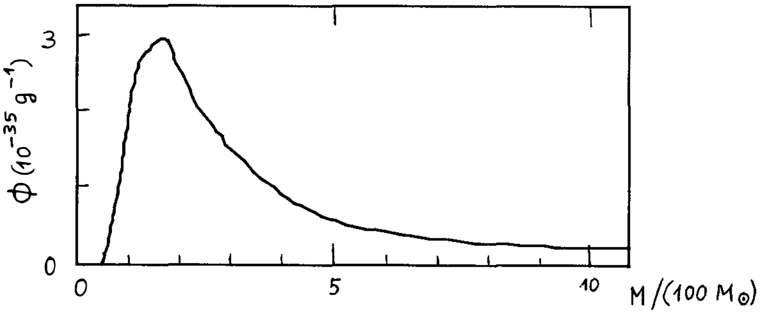

(The mass unit is 100 $M_\odot$). Here the H_2 cooling has lowered (with respect to Ref. 1) the min mass to 45 solar masses; the shape in the high mass tail has not changed. We see that the objects whose mass is histogrammed in 4 are very likely to be the first stars (the previous generations' masses are too large). If these calculations are detailed enough to give good orders of magnitude (which is very likely) we note that these primordial heavy stars would last only 2 or 3 Myr, before they explode and enrich the interstellar medium with the first non-cosmological elements heavier than helium. It is interesting to compare these mass functions to the observed ones for a wide class of objects (like explained in Ref. 4). In particular, the protoglobular initial mass function, in Fig. 3, resembles very closely (in shape) the present mass spectrum of the globular cluster family of our galaxy and of M31. Finally, we can examine the behaviour of the fragmentation rate in the last generation. Fig. 5 displays the fragmentation rate (in units 210 $M_\odot$/yr) vs. time in free-fall times. Two quite violent bursts of star formation are evident at 1.2 and 2.2 free-fall times. Similar, but more detailed and completely NLTE calculations, supported also by a suitable transport equation in hydrodynamical environment, will be performed in (5).

Fig. 5

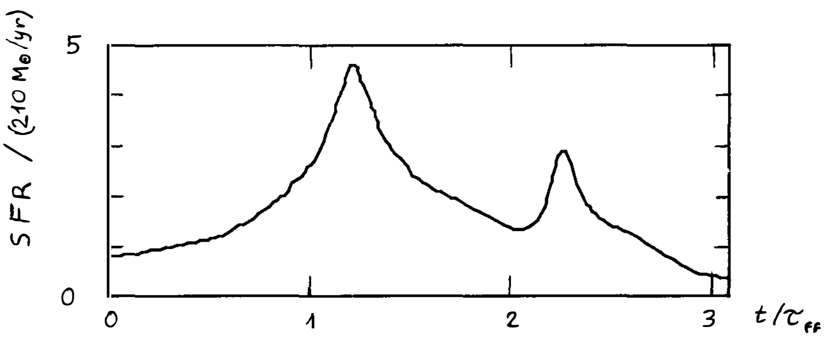

References.

(1). Di Fazio, A. 1986 Astron. Astrophys. 159, 840

(2). Capuzzo Dolcetta, R., Di Fazio, A., Palla, F. 1985 Astron. Astrophys. 145, 290

(3). Smith, J.K. 1980 Astrophys. J. 238, 840

(4). Di Fazio, A., Capuzzo Dolcetta, R. 1987 Astron. Astrophys. in press

(5). Di Fazio, A., Capuzzo Dolcetta, R., Menshikov, A., Shustov, B., Tutukov, A. 1987 in press.

A MODEL FOR THE STAR FORMATION RATE IN SPIRAL GALAXIES

Federico FERRINI°, Daniele GALLI°
Francesco PALLA*, Steven N.SHORE+
°Istituto di Astronomia, Pisa, Italia
*Osservatorio Astrofisico Arcetri, Italia
+New Mexico Tech., Socorro, USA

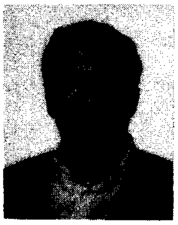

A non-linear phase-coupling model is proposed for the evolution of galaxies with disk and halo components. A particular emphasis is given to the determination of the star formation rate; a simple hypothesis on the connection between spiral density wave and cloud phase generates a sequence of star formation histories, in close correspondence to the Hubble types. Two star burst mechanisms are also included.

It is well known, and particularly underlined in this Conference, that galaxies do not evolve as closed systems. Indeed their gaseous and stellar components are not immutable properties: galaxies of different type have about the same age but they turned the gas into stars at different rates [1] .

The star formation rate (SFR) is the consequence of the internal dynamics of the gas, stars and clouds, and also of external perturbations.

In the simple model of the evolution of normal, isolated disk galaxies the SFR is treated as a simple function of the gas content which, if not replenished via infall of the halo gas, is rapidly depleted, yielding an exponentially decreasing SFR [1] . More sophisticated models have been presented [2] that couple the disk evolution to that of the halo and that consider various modes of induced star formation (cloud-cloud collisions, density wave triggering, etc.), in addition to spontaneous processes. This way non local and non linear effects that cooperate in the star formation history of the galaxy can be incorporated in the modelling.

The governing equations of our model are the following:

$$\frac{d}{dt}s_{1H} = K_1 g_H^n - r_1 s_{1H}$$

$$\frac{d}{dt}s_{2H} = K_2 g_H^n - r_2 s_{2H}$$

$$\frac{d}{dt}g_H = -(K_1 + K_2) g_H^n + r_1' s_{1H} + r_2' s_{2H} - f g_H$$

$$\frac{d}{dt}s_{1D} = a_1 s_{2D} c_D + H_1 c_D^2 - r_1 s_{1D}$$

$$\frac{d}{dt}s_{2D} = a_2 s_{2D} c_D + H_2 c_D^2 - r_2 s_{2D}$$

$$\frac{d}{dt}g_D = -\mu g_D^m + H' c_D^2 + r_1' s_{1D} + r_2' s_{2D} + a' s_{2D} c_D + f g_H$$

$$\frac{d}{dt}c_D = \mu g_D^m - (a_1+a_2+a') s_{2D} c_D - (H_1+H_2+H') c_D^2$$

$$\frac{d}{dt}(g_H Z_H) = p_Z r_2 s_{2H} - Z_H(K_1 + K_2)g_H^n - Z_H f g_H$$

$$\frac{d}{dt}[(g_D + c_D)Z_D] = p_Z r_2 s_{2D} + f g_H Z_H - Z_D(a_1 + a_2)s_{2D}c_D - $$
$$-Z_D(H_1 + H_2)c_D^2$$

Star Formation Rates:

$$= (K_1+K_2)g_H^n \qquad \text{(halo)}$$

$$= (H_1+H_2)c_D^2 + (a_1+a_2)s_{2D}c_D \qquad \text{(disk)}$$

where s_1, s_2 are stars with mass respectively lower or higher than 4 $M_\odot$, g and c are diffuse gas and clouds phases; the indices H and D refer to halo and disk populations.

The microphysics of the intervening processes is described by the rate coefficients. As a first step we determine the value of the rates in the solar neighborhood [2,3] . The results are shown in Figures 1 and 2. We note that the metallicity evolution of the disk is well reproduced; furthermore a relevant contribution to the total mass of the disk and the halo comes from the 'remnant' phase, dead stars and low mass stars that do not replenish the gas or cloud phases.

A second point of interest is to understand if galaxies of different Hubble type present a series of histories of star formation. The systematic trend of higher star formation for early types in the first stages of evolution and a reversed situation at the present time might explain the main properties of the Hubble classification scheme [4] . In our model the influence of the large scale dynamics, i.e. the spiral density wave, corresponds to the variation of the parameters related to the formation and destruction of clouds [5] . The consequence of this simple hypothesis is plotted in Figure 3.

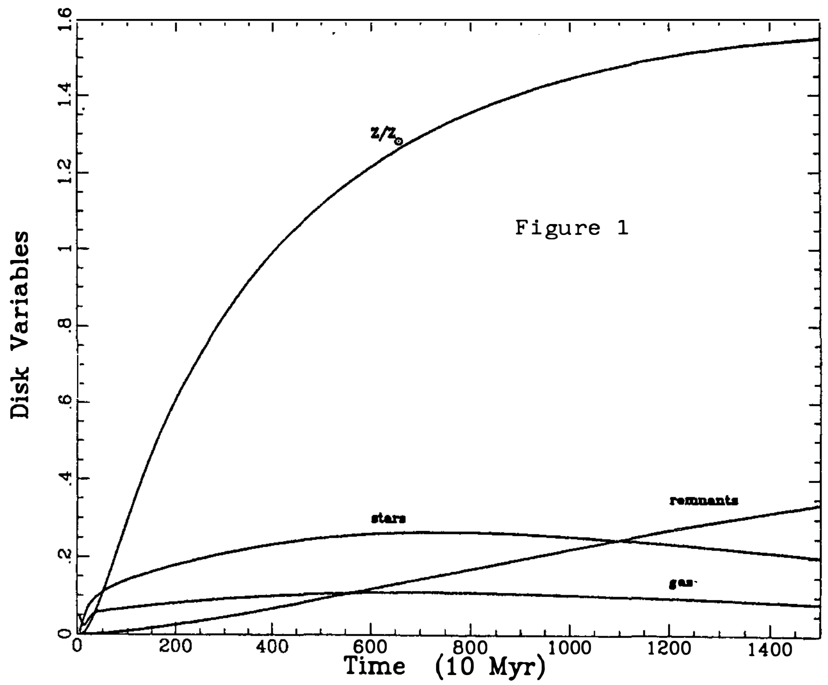
Figure 1
Disk Variables
Time (10 Myr)
Z/Z$_\odot$
stars
remnants
gas
0
.2
.4
.6
.8
1
1.2
1.4
1.6
200
400
600
800
1000
1200
1400

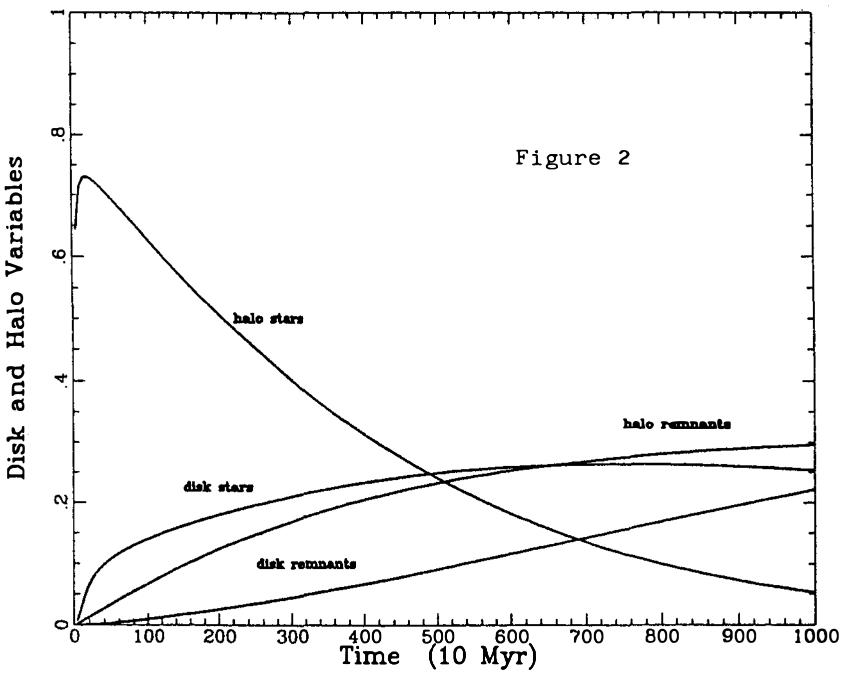
Figure 2
Disk and Halo Variables
Time (10 Myr)
halo stars
halo remnants
disk stars
disk remnants
0
.2
.4
.6
.8
1
100
200
300
400
500
600
700
800
900
1000

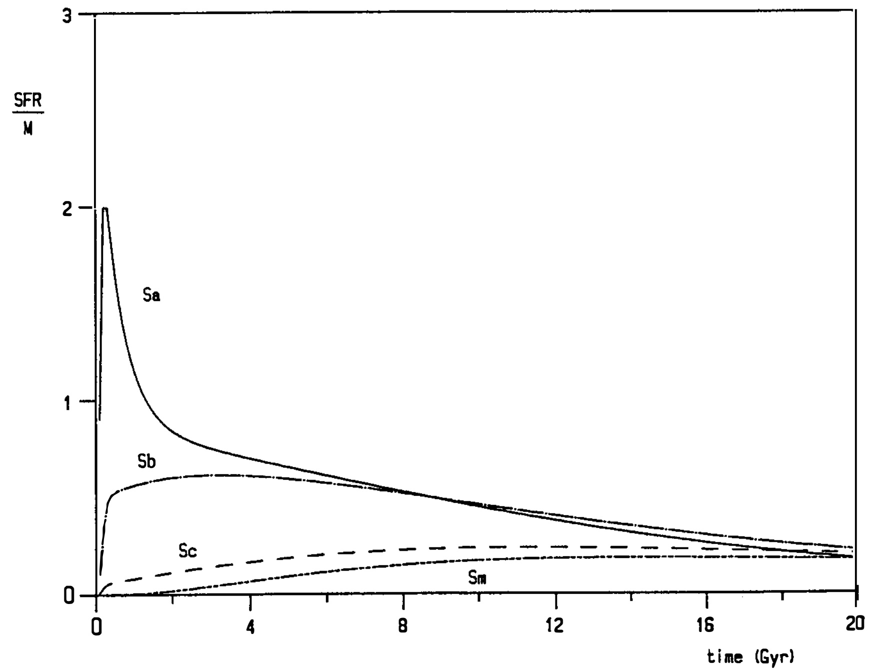

Figure 3. SFR per unit mass vs. time, as calculated form the multiphase model for different Hubble types.

The third step is to investigate on the possibility that bursts of star formation can appear in such a scheme, as suggested in previous works by Shore [6] and Ferrini et al. [7]. Several authors have analized in great detail the limit cycle property that the feedback models intrinsically present, covering a large parameter space [8]. We note that generally their mathematical formulation represents a restriction of our model described here. Using the set of rates adopted for normal galaxies does not lead to a burst in the SFR. However, the presence of small disturbances to the system of the type discussed by Ferrini and Marchesoni [9] that mimick interactions with external galaxies or tides induced by cluster galaxies allows the appearance of a burst behaviour (noise induced phase transition). The important point to stress is that the external action needs not to be particularly strong.

A second natural bursting mechanism is due to direct stripping of the gas by merging or collision with galaxies. Figure 4 shows a typical behaviour of the system. The two curves represent the SFR of the standard model (Milky Way) when gas and clouds are completely removed at 1 and 3 Gyr respectively. The restitution of matter from evolving stars is sufficient to fade the system to allow a consistent and rapid increase in the SFR.

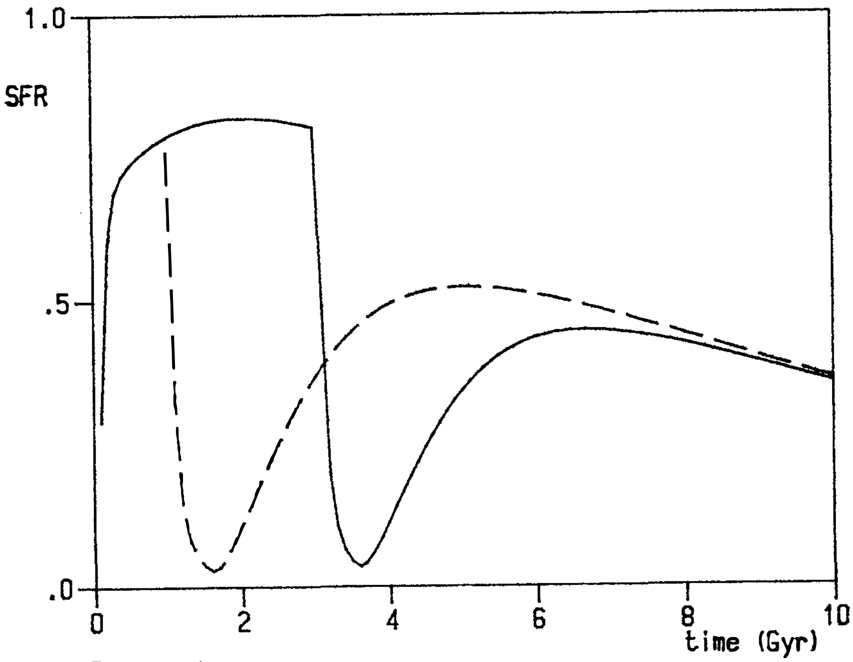

Figure 4.

We conclude underlying the fact that any of the behaviors above shortly indicated is ruled not by a sinlge rate, but by the combination of various ones. This has two important aspects: what happens in a complex system like a galaxy is a concert of several physical mechanisms; to understand the behaviour of the system we need not to know in great detail the physics of all of them, but to have indication on their relative importance;

References

[1]- Tinsley, B.M. 1980, Fundamentals Cosmic Phys., 5, 287.
[2]- Ferrini, F. Palla, F., Shore, S.N. 1987, in Star Forming Regions, IAU Symp. n.115, eds. M.Peimbert, J.Jugaku, p.701 (Dordrecht, Reidel).
Shore, S.N., Ferrini, F., Palla, F. 1987, Astrophys.J., May 15.
[3]- Galli, D. 1987, Astron.Astrophys., submitted.
[4]- Sandage, A. 1986, Astron.Astrophys., 161, 89.
[5]- Ferrini, F., Galli, D. 1987, Astron.Astrophys., submitted.
[6]- Shore, S.N. 1981, Astrophys.J., 249, 93.
" " 1983, Astrophys.J., 265, 202.
[7]- Ferrini, F., Marchesoni, F., Shore, S.N. 1985, Adv.Chem. Phys., LXII, 493.
[8]- Ikeuchi, S., Tomita, H. 1983, Pub.Astron.Soc.Jap.,33,23.
Ikeuchi, S., Habe, A., Tanaka, Y.D. 1984, Mon.Not.R. Astron.Soc., 207, 909.
Bodifée, G., de Loore, C. 1985, 142, 297.
Scalo, J.M., Struck-Marcell, C. 1986, Astrophys.J.,301,77.
Barbaro, G., Mazzei, P. 1987, preprint.
[9]- Ferrini, F., Marchesoni, F. 1984, Astrophys.J., 287, 17.

NON-EQUILIBRIUM COOLING OF A HOT PRIMORDIAL GAS CLOUD

Francesco Palla[1] and Hans Zinnecker[2]
[1]Osservatorio Astrofisico di Arcetri, Firenze, Italy
[2]Royal Observatory, Blackford Hill, Edimburgh EH9 3HJ, Scotland

ABSTRACT

Star formation in clouds of primordial composition may be a rather inefficient process if the gas is not able to cool to low temperatures, as in present day molecular clouds, within a free fall time. In particular, various schemes of galaxy and globular cluster formation envisage a situation where the gas is heated to temperatures of the order of a million degrees K, and then cools rapidly, but gets trapped to $T \sim 10^4$K, due to the existence of the Ly-α barrier in the cooling function, assuming ionization equilibrium. Here, we suggest the possibility of removing this difficulty by investigating the chemical and thermal properties of a gas that is far from equilibrium.

1. Introduction

How does a gas cloud of primordial composition after being heated to a high temperature ($T>10^4$ K) cool to a low temperature ($T<10^4$ K) without getting trapped at $T\sim10^4$ K, where hydrogen recombines and Ly-α cooling is quenched? This is an important question whose answer is of critical importance for star formation, for example, in various schemes of galaxy formation [(1)] (pancake, explosive, biased) where shock heating plays a role, or in the recent theory of globular cluster formation proposed by Fall and Rees [(2)].

The problem arises because in the assumption that hydrogen recombines in equilibrium the degree of ionization drops dramatically at $T<10^4$ K. Only few electrons remain for the excitation of neutral hydrogen, that would provide the photons responsible for the energy loss of the gas: this is the so-called Ly-α barrier. However, it is long known[(3,4)] that, when hot gas of solar composition starts to recombine, the ionization equilibrium (EQ) is not maintained, i.e. the recombination timescale lags behind the ionization timescale, yielding a much higher electron abundance at the critical temperature $T<10^4$ K. A similar non-equilibrium (NEQ) recombination applies to a gas of primordial composition, with dramatic consequences for the formation of molecular species and for the cooling efficiency.

Molecular hydrogen is the main coolant of the gas mixture and its formation in the gas phase via H^- and H_2^+ ions requires a non negligible fraction of electrons and protons [(5)]. Therefore, the NEQ recombination would provide favorable conditions for an efficient formation of the intermediary species and hence of H_2 [(6-8)]. The amount of H_2 formed in this way can be determined only by a numerical time-dependent calculation, following in detail the coupled thermal and chemical evolution of gas. However, our contribution here will be to reduce the complexity of the problem at hand to the key processes that can be understood without numerical integration.

2. Chemistry of the NEQ gas

We discuss here the main channels for the formation in the gas phase of H_2 and HD. The general network sketched in Figure 1[9] is modified by the introduction of other reactions relevant to the particular conditions of the NEQ gas.

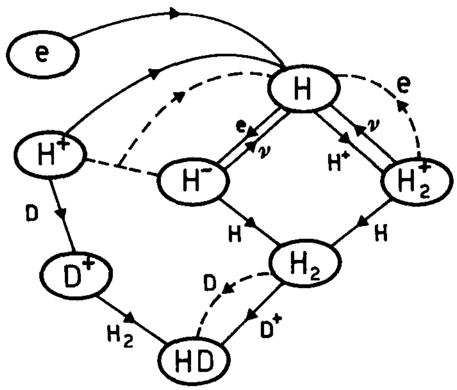

Figure 1. Chemical network of the NEQ gas. The dashed lines represent the reactions discussed in the text.

2a. H^- chemistry

Formation: the only viable formation reaction for H^- is by radiative association:

$$H + e \longrightarrow H^- + \gamma \quad ; \quad k_1 = 1.8\text{x}10^{-18} \cdot T \text{ cm}^3 \text{ s}^{-1} \qquad (1)$$

The alternative route via H_2 and e has a rate coefficient between 5 and 20 times smaller than that of reaction (1). Note, however, that k_1 is also small and that this reaction represents the bottleneck for H_2 formation : the H^- formation timescale is indeed much longer than any destruction mechanism.

Destruction: there are several ways to destroy H^-, but the most important are those involving associative detachment due to H atoms, and mutual neutralization with H+ ions:

$$H^- + H \rightarrow H_2 + e \; ; \quad k_{2a} = 1.3\times10^{-9} \; cm^3 \, s^{-1} \tag{2a}$$
$$H^- + H \rightarrow 2H + e \; ; \quad k_{2b} = 5.3\times10^{-20} \; T^{2.2} \, e^{-8750/T} \; cm^3 \, s^{-1} \tag{2b}$$

$$H^- + H^+ \rightarrow 2H \; ; \quad k_{3a} = 4\times10^{-6} \; T^{-0.5} \; cm^3 \, s^{1} \tag{3a}$$
$$H^- + H^+ \rightarrow H_2^+ + e ; \quad k_{3b} = 10^{-8} \; T^{-0.4} \; cm^3 \, s^{-1} \tag{3b}$$

H^- can also be efficiently destroyed by collisions with electrons, yielding two electrons back to the gas and maintaining the ionization fraction high. Competition between (2a) and (2b) favors the first reaction, characterized by a rate coefficient 100 to 700 times larger than that of (2b) in the temperature interval 10^4-6000 K. Analogously, reaction (3a) proceeds much faster than (3b), the ratio of the rates being approximately constant over the same temperature interval and equal to 160. However, notice that while reaction (2a) is the driving channel to form H_2 , reaction (3a) favors a mutual neutralization of the hydrogen ions: an efficient molecular formation depends therefore on the competition between these reaction. From their rates we get:

$$\frac{D(2a)}{D(3a)} = \frac{k_{2a} \, H^- \, H}{k_{3a} \, H^- \, H^+} \simeq \frac{2\times10^{-2}}{x} \, , \tag{4}$$

where x is the ionization fraction and $H^+ = e$.

So, as long as $x \sim 10^{-2}$, recombination of H^- with H^+ prevails: the higher ionization degreee of NEQ maintained between 10^4 and 6000 K has the net effect of slowing down the formation of H_2 molecules. It is correct to assume that in NEQ H^- ions are more abundant than in EQ, but their conversion to molecules is opposed by recombination.

2b. H_2^+ chemistry

Formation: radiative association of H and H^+ and charge exchange between H_2 and H^+ are the routes for H_2^+ formation:

$$H + H^+ \rightarrow H_2^+ + \gamma \; ; \quad k_{5a} = 1.9\times10^{-23} \; T^{1.8} \; cm^3 \, s^{-1} \tag{5a}$$
$$H_2 + H^+ \rightarrow H_2^+ + H \; ; \quad k_{5b} = 2.4\times10^{-9} \; e^{-21200/T} \; cm^3 \, s^{-1} \tag{5b}$$

A third channel involves H^- and H^+, as in reaction (3b). Its rate coefficient is large, but the concentration of H^- compared to either H or H_2 is always small enough to make its contribution negligible. From (5a) and (5b) it is clear that a higher ionization fraction will promote an enhancement of the H_2^+ abundance.

Destruction: H_2^+ is destroyed by the reverse of reaction (5b) and by dissociative recombination:

$$H_2^+ + H \rightarrow H_2 + H^+ \quad ; \quad k_{6a} = 6\times10^{-10}\ cm^3 s^{-1} \qquad (6a)$$
$$H_2^+ + e \rightarrow 2H \quad ; \quad k_{6b} = 2.3\times10^{-6}\ T^{-0.4}\ cm^3 s^{-1} \qquad (6b)$$

the process of mutual neutralization of H_2^+ and H^- being negligible compared to (6a) or (6b). We then obtain:

$$\frac{D(6a)}{D(6b)} = \frac{k_{6a}}{k_{6b}} \quad \frac{H_2^+ \ H}{H_2^+ \ e} \simeq \frac{10^{-2}}{x} \qquad (7)$$

This result is very similar to that found in (4), and we have the same limit on the ionization fraction for H_2^+ to effectively contribute to the formation of H_2.

The results given in (4) and (7) allow us to make an estimate of the abundance of H_2 formed in NE and to compare it to what expected in EQ. The H_2 concentration can be simply related to the degree of ionization, at the temperature where the recombination of H^- and H_2^+ into H atoms no longer occurs. It can be shown that:

$$f_{H_2}(NEQ) \cong \frac{x(NEQ)}{x(EQ)} \ f_{H_2}(EQ) \cong \frac{x(NEQ)}{x(EQ)} \ \Gamma(T)\ x(EQ) = \Gamma(T)\ x(NEQ)$$
$$\gtrsim 5\times10^{-3} \quad \text{at} \quad T=6000\ K$$

where $\Gamma(T)$ increases as T decreases, so that Λ_{H_2} remains nearly constant at lower temperatures.

2c. HD chemistry

Preferred routes for the formation of HD are the deuterium analogues of reactions (2a) and (6a) and

$$H^+ + D \rightarrow H + D^+$$
$$\quad\quad \hookrightarrow +H_2 \rightarrow HD + H \qquad (8)$$

Reaction (8) is the driving one in present-day diffuse molecular clouds, where the protons are provided by cosmic rays. In addition, since HD has a dipole moment, it can be formed by direct radiative association of H and D. However, we like to point out another reaction that is usually dismissed in interstellar clouds of normal composition, due to the existence of an energy barrier ($\Delta E/k = 404$ K)[10], namely:

$$H_2 + D \rightleftarrows HD + H + \Delta E \qquad (9)$$

Under the conditions of the NEQ recombining gas, where the gas is cooling from high temperatures, the problem of the energy barrier is overcome and at temperatures where the ionization degree has dropped considerably reaction (9) becomes the main route for the formation of HD. All cosmological deuterium can be converted into HD and it is conceivable that the fractional abundance of HD can be as high as 10^{-5} - 10^{-4}.

In summary, we schematically propose three regimes for the chemical evolution of the NEQ recombining gas below 10^4 K:

(i) between 10^4 K and 6000 K molecular hydrogen is formed, but a rate reduced by the destruction of the intermediary species H^- and H_2^+;

(ii) below 6000 K H_2 forms via the well known reactions (2a) and (6a) at a rate much higher than it would if EQ applies;

(iii) formation of HD occurs most effectively when the gas is mainly neutral via conversion of H_2 molecules.

3. Cooling function

The chemical network so far discussed, together with the conditions established by NEQ, has profound implications on the cooling properties of the gas.

In figure 2 we show how the usual cooling function for an opticlly thin gas of primordial composition (the dot-dasched curve labelled EQ) is modified by relaxing the assumption of ionization equilibrium. The resulting solid line is due to the combination of three different regimes: excitation of discrete levels of atomic hydrogen (Ly-α cooling), and vibro-roto transitions of excited H_2 and HD molecules. Contrary to the usual assumption, Ly-α cooling does not shut off at $T \lesssim 10^4$ K: the drop beyond the peak at T~16000 K [11] is a not as dramatic as in EQ, and one can estimate that, when T ~ 7000 K and x is still of the order of 0.1, the cooling function has decreased by less than 3 orders of magnitude, against more than 6 in EQ. It is the prolonged Ly-α cooling that allows the gas to overcome the barrier. H_2 cooling takes over Ly-α cooling at a temperature that depends on the fractional abundance of H_2: the curves shown in Figure 2 are computed for $f_{H_2} = 10^{-3}$ a value in the range predicted by the estimate derived in 2b. Data are taken from Lepp and Shull [12] (LS) and the two densities should bracket the typical conditions of protoglobular cluster gas clouds. Note, however, that recent calculation by Dove and Mandy [13] of the collision-induced dissociation rate of H_2 at low densities ($<10^2$ cm^{-3}) found values smaller than those used by LS by as much as 1500 times, at temperatures below 5000 K. Therefore, the curves of Λ_{H_2} could be shifted upward in the diagram.

Finally, at the lowest temperatures (T<200 K), HD cooling takes over H_2 cooling, as shown in the figure. Data are taken from Dalgarno and Wright[14], but a recent revision of that calculation yields a cooling rate enhanced by a factor of 3.

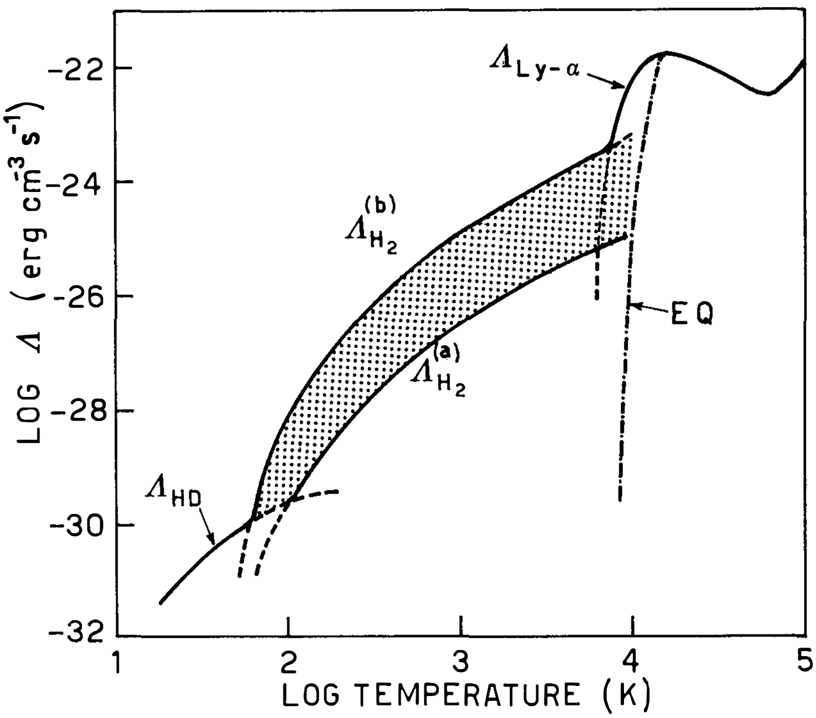

Figure 2. Cooling function of the primordial NEQ gas. Curve (a) refers to n = $= 10^0$ cm^{-3} ; curve (b) is for n = 10^2 cm^{-3}.

4. Conclusions

The main conclusions of this discussion are:

(1) at $T < 10^4$ K molecular hydrogen formation via H^- and H_2^+ does occur, but due

to the high degree of ionization, destruction processes of the intermediaries limit strongly the efficiency of its formation;

(2) active H_2 formation starts to occur once $x \lesssim 10^{-2}$ that in NEQ corresponds to $T \sim 6000$ K;

(3) due to the ionization fraction, Ly-α photons provide enough radiation to overcome the temperature barrier at $T \lesssim 10^4$ K and to cool the gas to T~6000K, where cooling due to vibro-rotational transitions of H_2 takes over;

(4) further cooling is provided at low temperatures (T<200 K) by HD molecules that can lower the gas temperature to a few tens of degrees K;

(5) cooling by H_2 and HD is strong enough that there is no need to invoke the contribution of heavy elements to reach low temperatures in the primordial gas. In this way, fragmentation and star formation could have proceeded unimpeded by thermal constraints in the same fashion as in present day conditions.

It is a pleasure to thank R. Stanga at E.S.O. for his precious collaboration. We also thank I. Scala for typing the manuscript and A. Lepri for preparing the drawings.

References

1) Silk, J., Astrophys. J. 297, 1 (1985).
2) Fall, S.M., and Rees, M.J., Astrophys. J. 298, 18 (1985).
3) Kafatos, M., Astrophys. J. 182, 433 (1973).
4) Shapiro, P.R., and Moore, R.T., Astrophys. J. 207, 460 (1976).
5) Palla, F., Salpeter, E.E., and Stahler, S.W., Astrophys. J. 271, 632 (1983).
6) Izotov, Yu., and Kolesnik, I.G., Sov. Astron. 28, 15 (1984).
7) MacLow, M.M., and Shull, J.M., Astrophys. J. 302, 585 (1986).
8) Shapiro, P.R., and Kang, H., preprint (1986).
9) Dalgarno, A., in "Molecular Astrophysics" eds. G.H.F. Diercksen et al., Reidel Publ. Co., 15 (1985).
10) Watson, W.D., Astrophys. J. (Letters) 182, L73 (1973).
11) Dalgarno, A., and McCray, R., Ann. Rev. Astr. Astrophys. 10, 375 (1972).
12) Lepp, S., and Shull, J.M., Astrophys. J. 270, 578 (1984).
13) Dove, J.E., and Mandy, M.E., Astrophys. J. (Letters) 311, L93 (1986).
14) Dalgarno, A., and Wright, E.L., Astrophys. J. (Letters) 174, L49 (1972).

MAGNETIC FIELD GENERATION AND STAR FORMATION IN PROTOGALAXIES

Ralph E. Pudritz
Department of Physics
McMaster University
Hamilton, Ontario L8S 4M1
Canada

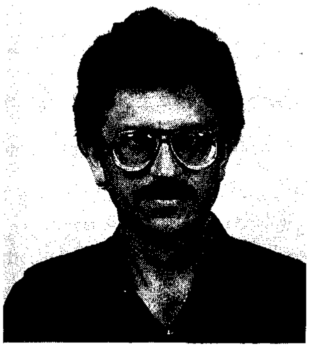

If the first generation of stars forms just after protogalaxies have aquired their spin, then star formation in this epoch must overcome an angular momentum barrier nearly as severe as that in our own galactic disk. This paper outlines work done in collaboration with Joseph Silk on the resolution of this problem by magnetic braking. While seed magnetic fields in the protogalactic gas can be no more than about 10^{-18} Gauss, we show that very high fields (10^{-6} Gauss) can be generated by dynamo action within one protogalactic free-fall time. The requirement is that strong cloud-cloud collisions should characterize the state of the galaxy at this time. High fields are generated in the shocked gas layers that form as a consequence of such collisions. The predictions are in agreement with the high galactic halo magnetic field strengths which have been inferred from Faraday rotation measures observed towards radio loud quasars.

1. Introduction

When and how the first stars formed is of critical importance for an understanding of galactic formation and structure. While significant progress has been made in the theory of spherical collapse in primordial clouds as it pertains to star formation [1], important differences enter if stars form after protogalactic gas has aquired its spin. Primordial star formation after this epoch requires that the specific angular momentum of protogalactic gas be reduced by four orders of magnitude in order that stellar type objects can form (the present galactic angular momentum problem requires a five to six decade reduction from $10^{23} cm^2 s^{-1}$ to $10^{17} cm^2 s^{-1}$). The specific angular momentum of protogalaxies is a well calculated number. The mechanism worked out by Hoyle and later Peebles [2,3], involves tidal torques between linear density fluctuations in the expanding universe. It is the strong quadropole moments of these fluctuations that leads to the spin-up torque. Primordial star forming regions then would have acquired far too much angular momentum to allow purely spherical protostellar collapse to occur.

What is the spin-down torque which must be operative if primordial star formation is to go through under these circumstances? Our proposal [4] is that magnetic braking is the dominant means of solving this primordial angular momentum problem. Magnetic field generation takes place in shocked gas layers that form in the course of cloud-cloud collisions in the protogalactic halo. Oblique high Mach number shocks generate strongly vortical gas motions. If the dynamo conditions are met, exponential growth of the seed magnetic field will ensue. Constraints on the physical nature of the clouds can be drawn from the requirement that the internal timescales in these layers be short enough that a dynamically important field can be grown within a free-fall time of the protogalaxy. This will secure the formation of galactic halo stars. The ratio of the magnetic braking to free-fall time scale in the external medium around the primordial protostar scales as the ratio of the magnetic to the gravitational energy density of the braking cloud. Therefore braking and subsequent star formation in a galactic halo requires that field be amplified from 10^{-18} to 10^{-6} Gauss within a free-fall time. This paper sketches a natural protogalactic model that has these features.

2. Observational Support

Recent VLA observations have shown that after the galactic background has been subtracted, a large excess extragalactic Faraday rotation of more than 30 rad m^{-2} is observed towards radio loud quasars [5]. This excess RM is strongly correlated with the occurance of optical absorption, which Kronberg and Perry suggested was due to a population of discrete intervening clouds. High resolution optical spectroscopy allows a good estimate of the column density of absorbing intervening material to be made. In concert with the RM determinations, these measurements allow the field strengths in the intervening objects to be estimated, since $RM = 0.81 \int_0^{z_e} (n_e B_{||}/[1+z]^2) dl(z)$ rad m^{-2}. Here $B_{||}$ is the line of sight magnetic field (in μG), n_e is the electron density (cm^{-3}), dl is the path length (pc) and z_e the redshift of the emitting source.

The model that best fits the observations requires that the dominant intervenor have scales $R \simeq 50$ kpc, electron densities $n_e \simeq 10^{-3}$, and an astonishingly high magnetic field $B \simeq 2\mu G$. Furthermore the observations indicate that the RM evolves as $(1+z)^{0.9\pm0.6}$ out to $z_e = 2$. The obvious possibility that the Lyman clouds are the intervenors is eliminated by the fact that they would have to contain magnetic fields 25 times larger than is permitted by equipartition with their gas pressure. These galactic halo fields may be quite tangled in principle. The net RM is analogous to a random walk along the line of sight so that a null measurement is highly unlikely. These observations have two important theoretical consequences:

1. Strong dissipation must have occurred in galactic halo since strong dissipationless field generation mechanisms fail by ten orders of magnitude to reach these values.
2. The regions in which these fields are generated can be much smaller than the 50 kpc characteristic of a galactic halo.

Such a strong magnetic field in galactic halos could not have arisen by the expulsion of magnetic flux which was generated in a galactic disk. Flux conservation alone would predict that field generated in a disk and convected into the halo by something like localized galactic fountain flows would be reduced by at least a hundred from this value. In this view then, halo fields are the fossil bones of strongly dissipative processes that must have been prevalent during the formation of the galaxies.

3. Seed Fields

A primary ingredient in this picture is to reliably estimate what the primordial seed magnetic field could have been. If one rules out mechanisms that involve unsubstantiated particle physics theories, one is left with two mechanisms *which must operate* at the epoch when protogalaxies spin-up. Mishustin and Ruzmaikin [6] showed that Compton drag on the ionized rotating gas characteristic of protogalaxies after recombination would lead to field generation. The point is that Compton drag by the homogenous, background of residual radiation in the post-recombination epoch is far larger for electrons than ions. The resulting slight charge separation in the rotating protogalaxy leads to the flow of an electric current which generates a magnetic field. For a Hubble constant of $h_{50} = H_o/50kms^{-1}Mpc^{-1}$ the seed field is

$$B_{Comp} = 0.94 \times 10^{-23}(1+z_f)^{5/2}\Omega^{-1/2}h_{50}^{-1}(\Omega_{gal}/10^{-14}s^{-1})Gauss \tag{1}$$

Here, Ω_{gal} is the rotation frequency of the protogalaxy and z_f is the epoch of galaxy formation. If this epoch occurs at a redshift of 10 say, the field generated is only 10^{-20} Gauss.

A related process which also must occur after protogalaxies begin to rotate is the Biermann Battery [7]. In differentially rotating fluids, isobars and equipotential surfaces are slightly different. In a conducting fluid this means that a minute current can flow which in all other circumstances except this cosmological one, is entirely too small to worry about. Theory shows that the field grows linearly in time until Ohmic losses cut in. We show elsewhere [4] that if this dissipation is turbulent, then the seed field achieves an amplitude of

$$B_{Bier} = 0.68 \times 10^{-18}(\Omega/10^{-14}s^{-1})Gauss \tag{2}$$

where the mean molecular weight of the primordial metal-free gas was taken to be $\mu = 0.59$. Clearly, these well understood mechanisms are incapable of explaining high galactic halo field strengths.

4. Dynamo Action

A dynamo involves exponential growth of the field if there is a sufficiently strong source of vortical fluid motion for the field to draw on. Doroshkevich [8] points out that since the fluctuations which are thought to give rise to galaxies are all irrotational, then the only way to generate vorticity is to have dissipative processes such as oblique shocks operative. Exponential growth of the field components occurs in an e-folding time scale, denoted t_{dyn}. Growth of the toroidal field proceeds by shearing of the poloidal field component. This in turn is regenerated from the toroidal field by vortical gas motions in a stratified medium (the so-called $\alpha - effect$). Linearized instability analysis is used to calculate the dynamo time scale in thin layers [9,4]. The fastest growing mode of the field occurs in a time

$$t_{dyn} = \frac{4}{3}\left(\frac{32\eta_T}{\alpha^2(r\Omega')^2}\right)^{1/3} \tag{3}$$

where Ω is the vorticity that is associated with the layer, η_T is the 'turbulent ' diffusivity that erodes the growing field and the electric field component induced by the vortical gas motions is $\alpha\mathbf{B}$. Estimates need to be made of the coefficients η_T and α. Different scalings for these quantities may arise depending on the model for the motions of the stirred gas [9,10]. Adopting the latter model,

$$\alpha = 0.25M_T^2 z_o \Omega \tag{4}$$

$$\eta_T = M_T^2 z_o^2 \Omega \tag{5}$$

where z_o is the width of the shocked gas layer, and M_T is the Mach number characterizing the turbulent gas motions in the shock. Subsituting (4) and (5) into (3) yields,

$$t_{dyn} = 10.5M_T^{2/3}\Omega^{-1} \tag{6}$$

Growth of the field continues until its energy density starts to become comparable to the gravitational energy density in the layer. The field now retards the very motions that are responsible for its generation and the problem becomes non-linear. At this time magnetic braking becomes powerfully effective. Although this theory cannot follow the problem in the nonlinear regime, it predicts when braking turns on.

In order that 25 e-foldings of the field can occur within a free-fall time of the protogalactic halo the vorticity time scale must be much smaller than that characterizing the gas motions in the galaxy as a whole. The central question becomes one of finding a natural protogalactic model whose whose shocked subcomponents are endowed with fast internal time scales.

5. Primordial Star Forming Regions

The basic model considered here consists of a collection of identical self-gravitating gaseous spheres with radius L, density ρ_i and internal velocity dispersion σ_i. These clouds fall into a protogalactic potential well that is specified at each radius r, by the density ρ, and a velocity dispersion σ. The size of the clouds is dictated by tidal truncation by the protogalactic potential, so that $\rho_i L \simeq \rho r$. The velocity dispersions for the cloud and the protogalaxy can be simply estimated using the Virial theorem, which gives $(\sigma_i/\sigma)^2 = (\rho_i L^2/\rho r^2)$. Self gravitating clouds at $10^{4o}K$ have internal velocities of $\sigma_i \simeq 10 kms^{-1}$ and are stable against collapse. This will be taken as the basic model for the clouds falling into the protogalactic potential. Galactic potentials can be characterized by Virial temperatures of order $10^{6o}K$ so that $\sigma \simeq 100 kms^{-1}$. The size of the unshocked clouds is

$$\frac{L}{r} = \left(\frac{\sigma_i}{\sigma}\right)^2 \simeq 10^{-2} \tag{7}$$

Thus, a 50 kpc halo will be filled with 500 pc clouds moving at a few hundred kms^{-1}.

These clouds must inevitably undergo cloud-cloud collisions which in general are oblique. Shocks with maximum of Mach 10 will be driven into the clouds so that ultimately, highly flattened merged objects will be produced. Such collisions have been studied by means of a 3-D hydro code and flattened bars persist for at least 5 free-fall times [11]. For non-rotating clouds, cloud dispersal rather than merging occurred for Mach numbers higher than 12. While rotation effects can reduce this critical number for dipersal, the effect will not be too large. This is evidence that cloud-cloud collisions in the protogalaxy will produce flattened objects with vortical motions that will persist for many dynamical time scales. The vorticity in such a layer may then be estimated as $\Omega = (\nabla_T R)(\sigma/z_o)$ where the first factor is the deformation tensor for the distorted colliding clouds. The ratio of the dynamo time-scale to the free-fall time (from rest to the protogalactic centre) in the halo can then be calculated, ie

$$\frac{t_{dyn}}{t_{ff}} = 0.084 \left(\frac{M_T^{2/3}}{(\nabla_T R)} \right) \left(\frac{(\sigma_i/\sigma)}{10^{-1}} \right)^2 \frac{z_o}{L} \tag{8}$$

where equations (6) and (7) have been used. Given the uncertainties in the detailed shock properties it is safe to say that if the merged clouds are compressed by at least a factor of five then this protogalactic model generates magnetic field and hence solves the primordial angular momentum problem within a protogalactic free-fall time. Thin, self-gravitating layers will fragment. If the shocked gas can cool in a time shorter than its free-fall time scale, the fragment masses can be driven down to below $10^7 M_\odot$. The basic star forming units would then be the globular clusters. A possible test of these ideas would be to look for cluster formation and high magnetic field strengths in dwarf irregular galaxies which are known to be associated with large HI clouds.

I am indebted to Dick Bond, Bill Harris, Roman Juszkiewicz, and John Lattanzio for many stimulating discussions.

References

1. Palla, F., Salpeter, E.E., and Stahler, S.W. 1983, Ap. J., **271**,632.
2. Hoyle, F. 1949, in *Problems of Cosmical Aerodynamics,* p. 195.
3. Peebles, P.J.E. 1969, Ap. J., **155**, 393.
4. Pudritz, R.E. and Silk, J. 1987, Ap. J., submitted.
5. Welter, G.L., Perry, J.J., and Kronberg, P.P. 1984, Ap. J.,**279**, 19.
6. Mishustin, I.N. and Ruzmaikin, A.A. 1972, JETP, **34**, 233.
7. Roxburgh, I.W. 1966, MNRAS, **132**, 201.
8. Doroshkevich, A.G. 1973, Sov. Astr, **16**, 986.
9. Zweibel, E.G. 1986, in *Proc. Summer School on Interstellar Processes,* Wyoming, (D. Reidel), in press.
10. Pudritz, R.E. 1981, MNRAS, **195**, 897.
11. Lattanzio, J.C. and Henriksen, R.N. 1987, preprint, CITA.

SOME CLUES ABOUT GALAXY FORMATION FROM THE PROPERTIES OF NEARBY ELLIPTICAL GALAXIES

S. Djorgovski
Harvard–Smithsonian Center for Astrophysics
60 Garden St.
Cambridge, MA 02138, USA.

Observed correlations between the global properties of nearby galaxies can provide some valuable hints about the physics of galaxy formation. I briefly explore the significance of the "fundamental plane" of elliptical galaxies and bulges. From the equations of the plane, one derives a scaling relation of mass-to-light ratios with the mass: $(M/L) \sim M^{\alpha}$, where $\alpha = 1/(6\pm2)$. The fact that (M/L) is a function of galaxy mass signifies that the formation of ellipticals and bulges was at least partly dissipative. More interestingly, the fact that $\alpha > 0$ indicates that more massive (and thus more metal-rich) proto-ellipticals were either less efficient in forming stars overall, and/or that they had steeper initial mass functions in the average. Several theoretical mechanisms may interplay in producing this trend, but their relative dominance and the net effects are far from clear. A much better understanding of the physics of star formation is needed, before we can fully unravel the dissipative processes of galaxy formation.

Understanding of galaxy formation is one of the fundamental tasks of modern cosmology. Probably the most interesting and challenging approach is to look for very young or primeval galaxies at large redshifts, and there are now some exciting prospects that such objects or their signatures may finally have been seen [1 – 9]. However, it is quite possible that we will not be able to observe directly the formation of a bulk of the galaxy population in any forseeable future, but rather of some extraordinarly luminous or otherwise unusual objects. Many interesting clues can be gathered from observations and models of large scale structure, Lyα clouds, and the cosmic microwave background [10 – 12]. There is also a third approach, namely, to try to deduce something about galaxy formation from the systematics and correlations of properties of mature galaxies and galaxy families at low reshifts [13 – 19]. Old spheroidal systems (ellipticals and bulges) make good "fossiles", since their global properties were likely and largely set at their formation epochs. Probably a good name for this approach would be the ***paleontocosmology*** (or perhaps, "the Silk road"), and its task is as easy and straightforward as reconstructing the whole dinosaur, skin color and all, from a single petrified rib bone.

Most of the recent efforts concentrated in interpreting the cooling diagrams (virial tempereature *vs.* the density, in some guise or another). The separation of galaxy families or Hubble types, and galaxy groups and clusters in such diagrams can provide some interesting leads about the roles of dissipation and galactic winds in galaxy formation [13 – 19]. The purpose of this contribution is to dig for some paleontocosmological clues within a single species of galaxies, viz., the normal ellipticals.

In the past couple of years, a significant progress has been made in investigating the fundamental properties of elliptical galaxies, and their interdependence. The principal new discovery is that the variance of global properties, including luminosity (L), radius (R), mass (M), surface brightness (I), luminosity or mass density (ρ_L or ρ_M), velocity dispersion (σ), and metallicity indices) is exhausted almost entirely by two variables [20 – 24]. In the space of these parameters, ellipticals and bulges lie on a plane, which can be defined as:

$$R \sim \sigma^{1.4\pm0.15}\ I^{-0.9\pm0.1}. \tag{1}$$

A useful representation of this "fundamental plane" is its projection on the (log σ, log I) plane of observables [21,22], which is but a version of the cooling diagram. The position of a galaxy in that plane may be related to the degree of dissipation during its formation.

The key for understanding the fundamental plane may be through the behaviour of mass-to-light ratios (M/L); I am indebted to Sandra Faber for inspiring me to think in this way [23]. In general, for a family of galaxies bound by the Newtonian gravity, the following relation must apply:

$$R \sim \sigma^2\ I^{-1}\ (M/L)^{-1}. \tag{2}$$

The difference between the powers of σ and I in the observed Eq.(1), and the virial Eq.(2) is then telling us something about the behaviour of (M/L), viz.,

$$(M/L) \sim \sigma^{0.6\pm0.15} I^{-0.1\pm0.1}. \tag{3}$$

Substituting the observed Eq.(1) into the virial relation $M \sim \sigma^2 R$, we obtain:

$$M \sim \sigma^{2.4\pm0.15} I^{-0.9\pm0.1}. \tag{4}$$

We can thus express the (M/L) as:

$$(M/L) \sim M^{\alpha}, \tag{5}$$

where $\alpha = 1/(6\pm2)$, in a good agreement with expressions derived by other authors [23,25]. This dependence is illustrated in Figure 1. The derivation of Eq.(5) from the fundamental plane is much cleaner than deriving it directly from the regression of (M/L) vs. M: the cumulative error-bars of the derived M and (M/L) are very large, and correlated, whereas the Eq.(1) has relatively small errors. The relation has lots of residual scatter, because of the presence of a second parameter. The data are not quite good enough to state whether this scatter increases with the mass, or whether it correlates well with the metallicity.

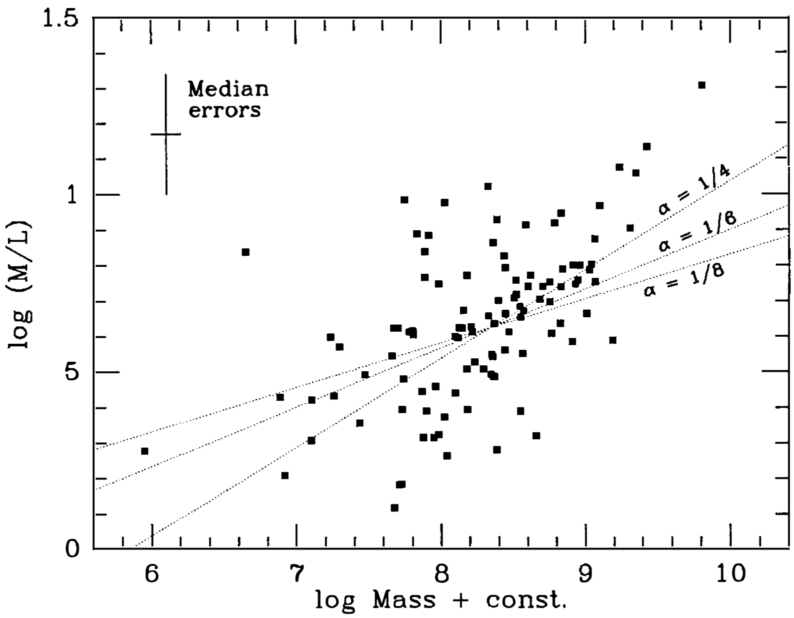

Figure 1. The trend of (M/L) ratios, taken from the sample of Djorgovski and Davis [21], plotted against the virial mass (computed as $M \sim \sigma^2 R$). The (M/L) ratios were computed for the red light within the r_e isophotes. The range of slopes derived in Eq.(5) is shown with the dotted lines. The least-squares regression through the points gives the slope α_{LS} = 0.18, and the correlation coefficients 0.82 (linear) and 0.56 (Spearman rank).

The Eq.(5) has two very important implications:

(♠) *The formation of elliptical galaxies must have been at least partly dissipative*; otherwise, the (M/L) would not be a function of mass. If ellipticals formed via non-dissipative stochastic merging of smaller fragments (like in most N-body experiments), the data should be fitted by a "virial plane", as in Eq.(2), but without the (M/L) term. The relations are close, though, since the α is small: as Faber *et al.* [23] say, the virial theorem provides the only tight constraint on the structure of elliptical galaxies. Note also that the "original" relation was probably steeper ($\alpha_{formation} > \alpha_{now}$) and stronger, since post-formation mergers would tend to flatten the slope of Eq.(5), and increase the scatter.

(♣) *The more massive galaxies were less efficient in forming* $\sim 1\ M_\odot$ *stars*, which contribute most of the observed light as the red giants now; *either they were less efficient in forming stars overall, and/or they have had steeper IMF's* (i.e., more dwarf-dominated). The first possibility may be more important if the stars formed in gravitationally dominant preexisting dark halos [26], and the second one if the barions dominate mass densities in the inner regions (probably more likely). This is more-or-less in a direct contradiction with the intuitive expectations voiced in many models of dissipative galaxy formation; fortunately such expectations were functionally irrelevant for the models.

The consequence (♠) is not surprizing. There are many good reasons to believe that galaxy formation was at least partly dissipative: the large baryonic density contrast between galaxies and the large-scale structure, the metallicity-luminosity relation, the metallicity gradients, the cooling diagram, the phase-space density argument, etc. [13 – 19; 27 – 34]. A plausible picture may include vigorous merging of gas-rich fragments and violent relaxation in their collective field. Such process wold satisfy all of the data, and lead to the characteristic observed surface brightness profiles, $I(r) \sim r^{-2}$, which can be well reproduced in numerical simulations of galaxy formation by a (mostly?) nondissipative collapse and violent relaxation [35,36]. The intrinsic stochasticity of the formative and post-formation merging may well account for the subtle, but definite variation in the observed surface brightness profiles [22,37,38], and for the complete lack of correlations between the parameters describing the radial and azimuthal shapes of light distribution in ellipticals, between themselves or with the parameters of the fundamental plane [21,22].

The consequence (♣) is more interesting and challenging. Two possible physical causes come to mind: (♡) protogalactic clouds ("galaxlets") would collide faster in potential wells of more massive galaxies, and the induced shocks will be stronger; (♢) the metallicity will be higher in more massive galaxies, since they are swept less by their own winds and/or the ram-pressure of any diffuse intergalactic gas that may have been present. Importance of galactic winds for the classical, dense ellipticals is not clear. In addition to those primary differences, any number of complex feedback processes may be operating [15,17,33,39,40].

The dependence of the star formation efficiency, and the IMF slope on the strength of shocks to which protostellar clouds in forming galaxies may be subjected is almost completely unknown. It is not even clear whether the shocks would stimulate or suppress the star formation! While the compression in slow inelasic collisions may trigger some star formation, strong cloud collisions are likely to be disruptive, and at large impact velocities (> 100 km/s, or so) collisional ionization may suppress the star formation [41 – 46].

The influence of metallicity on the shape of the IMF is perhaps more tractable; still, the data are controversial [47]. McClure *et al.* [48] find that metal-rich globular clusters have flatter IMF's, in agreement with the effect discussed here. On the other hand, Terlevich and Melnick [49,50] find the opposite trend for the extragalactic H II regions and blue starburst galaxies, at least for the upper end of the IMF. Finally, Freedman [51] finds no trend with metallicity for the nearby resolbed galaxies. The upper end of the IMF may be irrelevant here: those stars contribute a small fraction of the total mass.

Theoretical arguments are twofold: There may be important differences in the cooling mechanisms: in metal-poor systems, the H_2 cooling will dominate, and preferentially low-mass stars will form; while in metal-rich systems, the Lyα cooling will dominate, and preferentially high-mass stars will form [19,33,52]. This would imply shallower slopes in more metal-rich (and thus more massive) galaxies [53], in a contradiction to the effect reported here. Then, there may be a number of negative feedback mechanisms inherent to the star formation, once the massive stars have formed. Their photospheric UV radiation, and the supernova shocks may disrupt and ionize the remaining protostellar clouds, and thus suppress the subsequent star formation [18,19,33,39,40,53].

Apparently, we must have a much better understanding of star formation in a range of physical conditions if we are to understand better the physics of galaxy formation. Improved models of galaxy formation incorporating both the gravitational and dissipative effects are needed [54 – 57]. Several other tests can be done or redone with modern data: a repeat of the classical study by Fish on the relation between the binding energies and masses of elliptical galaxies [58]; inferences on the duration of the epoch of galaxy formation from the range in mean densities of ellipticals; etc. They will be explored in a future paper.

I am indebted to Marc Davis for many stimulating discussions, and support at the earlier stages of this project. I was greatly inspired by the numerous papers on galaxy formation by Joe Silk, and conversations with Richard Larson and Sandra Faber. Partial support from Harvard University and a AAS Travel Grant are gratefully acknowledged.

References:

1. Smith, H., Cohen, R., and Bradley, S. 1986, *Astrophys. J.* **310**, 583.
2. Wolfe, A., Turnshek, D., Smith, H., and Cohen, R. 1987, *Astrophys. J. Suppl. Ser.* **61**, 249.
3. Wolfe, A. 1987, in proc. of the *13th Texas Symposium on Relativistic Astrophysics*, p. 309, Singapore: World Scientific.
4. Djorgovski, S. *et al.* 1987, *Astron. J.* **93**, 1318.
5. Djorgovski, S., Spinrad, H., McCarthy, P., and Strauss, M. 1985, *Astrophys. J. Lett.* **299**, L1.
6. McCarthy, P. *et al.* 1987, *Astrophys. J. Lett.* in press.
7. Spinrad, H. 1988, in proc. of the IAP workshop *High-Redshift and Primeval Galaxies*, J. Bergeron and B. Rocca–Volmerange (eds.), in press.

8. Djorgovski, S. 1988, in proc. of the Erice workshop *Towards Understanding Galaxies at Large Redshifts*, ed. R. Kron and A. Renzini, in press. Dordrecht: Reidel.
9. Spinrad, H. *et al.* 1988, in preparation.
10. Davis, M., Efstathiou, G., Frenk, C., and White, S. 1985, *Astrophys. J.* **292**, 371.
12. Tytler, D. 1987, in proc. of the *13th Texas Symposium on Relativistic Astrophysics*, p. 304, Singapore: World Scientific.
11. Vittorio, N., and Silk, J. 1984, *Astrophys. J. Lett.* **285**, L39.
13. Faber, S. 1982, in "Astrophysical Cosmology", *Pontif. Acad. Scripta Varia* #48, pp. 191 and 219.
14. Silk, J. 1983, *Nature* **301**, 574.
15. Silk, J. 1984, in *The Big Bang and Georges Lemaitre*, p. 279, Dordrecht: Reidel.
16. Blumenthal, G., Faber, S., Primack, J., and Rees, M. 1984, *Nature* **311**, 517.
17. Silk, J. 1985, *Astrophys. J.* **297**, 9.
18. Silk, J., and Wyse, R. 1986, in *Structure and Evolution of Active Galactic Nuclei*, p. 173, ed. G. Giuricin *et al.*. Dordrecht: Reidel.
19. Silk, J. 1986, in *Spectral Evolution of Galaxies*, p. 15, ed. C. Chiosi and A. Renzini. Dordrecht: Reidel.
20. Dressler, A. *et al.* 1987, *Astrophys. J.* **313**, 42.
21. Djorgovski, S., and Davis, M. 1987, *Astrophys. J.* **313**, 59.
22. Djorgovski, S. 1987, in *Structure and Dynamics of Elliptical Galaxies*, IAU Symposium No. 127, ed. T. de Zeeuw, in press. Dordrecht: Reidel.
23. Faber, S. *et al.* 1987, in *Nearly Normal Galaxies*, p. 175, New York: Springer.
24. Dressler, A., 1987, *Astrophys. J.* **317**, 2.
25. Faber, S., and Jackson, R. 1976, *Astrophys. J.* **204**, 668.
26. White, S., and Rees, M. 1978, *M.N.R.A.S.* **183**, 341.
27. Larson, R. 1974, *M.N.R.A.S.* **166**, 585.
28. Larson, R. 1975, *M.N.R.A.S.* **173**, 671.
29. Tinsley, B., and Larson, R. 1979, *M.N.R.A.S.* **186**, 503.
30. Ostriker, J. 1980, *Comm. Astrophys.* **8**, 177.
31. Struck-Marcel, C. 1981, *M.N.R.A.S.* **197**, 487.
32. Silk, J., and Norman, C. 1981, *Astrophys. J.* **247**, 59.
33. Silk, J. 1985, *Astrophys. J.* **297**, 1.
34. Carlberg, R. 1986, *Astrophys. J.* **310**, 593.
35. Villumsen, J. 1982, *M.N.R.A.S.* **199**, 493.
36. van Albada, T. 1982, *M.N.R.A.S.* **201**, 939.
37. Djorgovski, S. 1985, Ph. D. Thesis, University of California at Berkeley.
38. Djorgovski, S., Davis, M., and Kent, S. 1985, in *New Aspects of Galaxy Photometry*, Lecture Notes in Physics #232, p. 257, ed. J.–L. Nieto. Berlin: Springer Verlag.
39. Larson, R., this volume.
40. Silk, J. 1987, in *Star–Forming Regions*, IAU Symposium No. 115, p. 663, eds. M. Peimbert and J. Jugaku. Dordrecht: Reidel.
41. Tohline, J. 1980, *Astrophys. J.* **239**, 417.
42. Chièze. J., and Lazareff, B. 1980, *Astron. Astrophys.* **91**, 290.
43. Hausman, M. 1981, *Astrophys. J.* **245**, 72.
44. Scalo, J., and Pumphrey, W. 1982, *Astrophys. J. Let.* **258**, L29.
45. Struck-Marcell, C. 1982, *Astrophys. J.* **259**, 127.
46. Palla, F., Salpeter, E., and Stahler, S. 1983, *Astrophys. J.* **271**, 632.
47. Scalo, J. 1986, *Fundam. Cosm. Phys.* **11**, 1.
48. McClure, R., *et al.* 1986, *Astrophys. J. Lett.* **307**, L49.
49. Terlevich, R., and Melnick, J. 1981, *M.N.R.A.S.* **195**, 839.
50. Melnick, J., and Terlevich, R., this volume.
51. Freedman, W. 1985, *Astrophys. J.* **299**, 74.
52. Silk, J. 1977, *Astrophys. J.* **211**, 638.
53. Silk, J. 1977, *Astrophys. J.* **214**, 718.
54. Carlberg, R. 1984, *Astrophys. J.* **286**, 403.
55. Carlberg, R. 1984, *Astrophys. J.* **286**, 416.
56. Carlberg, R., Lake, G., and Norman, C. 1986, *Astrophys. J. Lett.* **300**, L1.
57. Carlberg, R. 1987, preprint.
58. Fish, R. 1964, *Astrophys. J.* **139**, 284.

VI. INSTRUMENTAL PROSPECTS

THE INFRARED SPACE OBSERVATORY

C. J. Cesarsky
SAp/CEN-SACLAY
91191 Gif sur Yvette Cedex, France

M. S. Kessler
ESTEC, Noordwijk, The Netherlands

The Infrared Space Observatory (ISO) is a satellite which is under development at ESA ; it will be launched into an elliptical orbit of period 24 hours by an Ariane rocket in 1992 or 1993. In addition to a cryogenically cooled telescope with an effective aperture of 60 cm, ISO will carry four complementary focal plane instruments : a camera (3-17 μm), a photopolarimeter (3-200 μm), and two spectrometers which together cover the range 3-180 μm. The expected lifetime of ISO is 18 months. Two thirds of ISO observing time will be available to general astronomical community.

1/ INFRARED ASTRONOMY, STARBURSTS AND GALAXY EVOLUTION

Thanks to a combination of technological advances in instrumentation and to the advent of the space era, our perception of the universe has enormously expanded in the last few years. In the field of extragalactic astronomy, and particularly for the study of galactic evolution, the greatest harvest of highly relevant data brought about by space astronomy is, in our opinion, that of the IRAS satellite, launched in 1983.

IRAS surveyed the whole sky in four wide energy bands (12 µm, 25 µm, 60 µm, 100 µm). Well over 75 % of the 60 µm sources are extragalactic (Soifer et al. 19 Few elliptical and SO galaxies appear as strong infrared sources in the IRAS catalogue, while late type spiral galaxies are by far the most frequently detected galaxy type. The most interesting and unexpected result is that the range of variation of galaxy infrared luminosities is much greater than that of the blue light ; infrared bright galaxies exhibit bolometric luminosities in excess of $10^{12}L_\odot$, and are the dominant population in the local universe at $L_{bol}>2x10^{11}L_\odot$. These high luminosities are attributed to the starburst phenomena, already discovered through optical observations, and imply that this effect is of paramount importance in shaping galactic evolution. This has indeed been the central point of discussion in these "Rencontres de Moriond".

Exciting as they are, the IRAS results suffer from many limitations, which most often make it difficult to interpret them unambiguously through physical models. We are left wondering about the emissivities of IRAS sources in the wavelength ranges outside the IRAS bands ; we would like to know in more detail the spatial and spectral distribution of the radiation, in some cases its degree of polarization ; and of course we would welcome an increase in sensitivity to be able to detect even more remote bright sources, or to explore better the realm of intrinsically faint sources, such as dwarf and elliptical galaxies. For these purposes, a second generation infrared mission is needed, with a set of complementary focal plane instruments, and the possibility to point for long times in a given direction. Indeed, the European Space Agency is now developing such a project, ISO (see below).

Let us give a few examples of how ISO can help solve some of the problems discussed at this meeting.
We have seen how difficult it is to separate, with a good degree of certainty, the infrared emission of IRAS galaxies into its various components :

photospheric emission, emission from dust surrounding evolved stars, interstellar emission, starbursts, active nuclei (see papers presented by M. Rowan-Robinson and by T. Heckman).

With observations at higher spatial and spectral resolution, it will become possible, in our own galaxy, to isolate the interstellar cirrus component, whose signature is expected to be the "unidentified" lines, probably due to PAH (Policyclic Aromatic Hydrocarbons) emission. Then, the real nature of the "disk component" of far away galaxies will be revealed. Spatial resolution will allow to distinguish between nuclear and disk emission ; spectral resolution and polarimetry will help to disentangle a starburst component from an active nucleus component in the center of galaxies.

An infrared mission with spectroscopic capabilities could take a high resolution spectrum of a nearby HII region over the widest possible range ; this spectrum would then be used as a template to compare with spectra or parts of spectra of other galactic HII regions, of HII regions in nearby galaxies and of total emission from distant galaxies. With the capability for pointed observations, it becomes possible to make thorough studies of interesting regions, and to perform variability studies on quasars and active nuclei.

High sensitivity maps of star formation regions, supplemented with polarization data to allow discrimination of intrinsic sources from reflexion nebulae, will bring new information on the low mass end of the Initial Mass Function (see paper by Scalo).

Also, interesting discoveries can be made on faint sources. For instance, it may be possible to detect, and even to map, the hot dust emission in some of the HII and blue compact galaxies discussed at this meeting by J. Melnick and T.X. Thuan, since it is known that even in such possibly pristine objects the interstellar matter is contaminated with nucleosynthetic products from stars.

Obviously, interacting galaxies will be a key topic (e.g. talks by R. Joseph, P. Belfort) . For instance, it will be possible, through maps at wavelengths > 10 μm, to identify the region where starbursts are taking place.

2/ THE ISO SATELLITE

The satellite consists of a payload module and a service module. These modules are coupled by a composite-material framework, which serves as a load path between them while decoupling them thermally. ISO is 5.2 m high, 2.3m wide and weights around 2300 kg at launch.

The basic spacecraft functions are provided by the service module. These include the structure and the load path to the launcher, the solar array and power conditioning subsystem, a data-handling and telecommunication subsystem using two antennas, and the attitude and orbit control subsystem. The last provides the three-axis stabilisation, to an accuracy of a few arc seconds, and raster scan facilities needed for the mission. It consists of sun sensors, star trackers, a quadrant star sensor on the telescope axis, gyros, reaction wheels and a hydrazine reaction control system. The nominal down-link bit rate is 33 kbps.

The payload module (see figure 1) is essentially a large cryostat. Inside the vacuum vessel is a toroidal tank filled with about 2000 l of superfluid helium, which will provide an in-orbit lifetime of at least 18 months. Some of the infrared detectors are directly coupled to the helium tank and are at a temperature of around 2 K. Apart from these, all other units are cooled using the cold boil-off gas from the liquid helium. This gas is first routed through the optical support structure, where it cools the telescope and the scientific instruments to a temperature of 3-4 K. The gas is then passed along the baffles and radiation shields before being vented to space. Mounted on the outside of the vacuum vessel is a sunshield, which prevents the sun from ever shining directly on the cryostat. The solar array is carried by this sunshield.

Suspended in the middle of the tank is the telescope, which is a Ritchey-Chrétien configuration with an effective aperture of 60 cm and an overall f/ratio of 15. A weight-relieved fused-silica primary mirror and a solid fused-silica secondary mirror have been selected. The optical quality of these mirrors is adequate for diffraction-limited performance at a wavelength of 5 μm. Stringent control of straylight, particularly from bright infrared sources outside the telescope's field of view, is necessary in order to ensure that the system sensitivity is not degraded. This is accomplished by imposition of viewing constraints and by means of the sunshade and the cassegrain and main baffles.

The scientific instruments are mounted on the opposite side of the optical support structure to the primary mirror, each one occupying an 80° segment of the cylindrical volume available. The 20 arc minute total unvignetted field of view of the telescope is distributed radially to the four instruments by a pyramid mirror. Each experiment receives a 3 arc minute unvignetted field, centred on an axis at an angle of 8.5 arc minutes to the main optical axis.

The baseline orbit of ISO has a 24-hour period, a perigee height of 1000 km, an apogee height of 70000 km, and an inclination of 5° to the equator. The foreseen launch date is 1992-1993, and the expected mission duration is 18 months.

3/ SCIENTIFIC INSTRUMENTS

ISO's instrument complement consists of an imaging photo-polarimeter, a camera and two spectrometers. The characteristics and scientific capabilities of these instruments are summarised in the table. Each instrument is being built by a consortium of institutes using national non-ESA funding and will be delivered to ESA for in-orbit operation. In keeping with the observatory nature of ISO, the individual instruments are being optimised to form a complete, complementary and versatile package. The four instruments view adjacent areas of the sky and switching between them will be accomplished by re-pointing the satellite. In principle, only one will be operated at a time ; however, when the camera is not the main instrument, it will be used in a parallel mode. The long-wavelength channel of the photometer will be used during satellite slews to make a serendipitous survey at 200 μm of much of the sky.

In fig. 2, the expected sensitivities of the instruments are displayed. (Note that these figures differ from those published in the first issue of the ISO newsletter ISO Info ; this change reflects the improvement in performance expected since ESA decided to launch ISO into a 24 hour orbit, which is out of the Earth's radiation belts for 75% of the time).

It is interesting to point out : that the spatial resolution achievable by ISOCAM matches that of millimeter wave interferometers at OVRO and at IRAM ; that SWS allows to study kinematics down to a resolution of ~ 10 km/sec ; that the sensitivity of the LWS will enable it to obtain spectra of all sources detected by IRAS at 60 μm and 100 μm, with resolution R=250 ; and that the photometer, not only has much greater sensitivity and versatility than IRAS, but also expands the wavelength range down to 3 μm and up to 200 μm.

4/ SCIENCE WITH ISO

In the present development phase, scientific aspects of ISO are followed by the ISO Science Team (IST), appointed by ESA. The IST is chaired by Martin Kessler, who is the ISO Project Scientist ; in addition to the four PI's, the IST contains five mission scientists : Th. Encrenaz, H. Habing, M. Harwit, A. Moorwood and J.L. Puget. Scientists interested in obtaining additional information on ISO should address their questions to IST members, and should ask Martin Kessler to add their name to the mailing list for "ISO Info".

ISO is expected to make major contributions in a large variety of fields of astrophysics, encompassing not only galaxies and quasars, but also stars and interstellar medium, planets, asteroïds and comets. The observing programme will be elaborated in the two years preceding launch. Two thirds of the observing time will be open to the scientific community, via the submission of proposals and selection, by peer review. The remaining time will be reserved for the groups who provide the instruments, for the Mission Scientists and for the Observatory Team who operate the satellite. During scientific use, the satellite will always be in contact with the ground segment, however, it is planned to minimise real time modifications to the observing programme in order to maximise the overall efficiency of the satellite. Within a few hours of an observation being completed, the guest observer will be provided with a "quick-look" output adequate for judging the scientific quality of the data. A final product with more detailed data reduction and calibration will be supplied later. This product will be the one from which the guest observer makes his astronomical analysis.

We end with a message to the reader of this article, who is a potential ISO user : the time to start thinking how you will take advantage of ISO is now !

Reference

Soifer, B.T., Houck, J.R. and Neugebauer, G., 1987, preprint.

ISO

Instrument and Principal Investigator	Main Function	Wavelength (Microns)	Spectral Resolution	Spatial Resolution	Outline Description
ISOCAM (C. Cesarsky, CEN-Saclay, F)	Camera and Polarimetry	3 - 17	Broad-band, Narrow-band, and Circular Variable Filters	Pixel f.o.v.'s of 1.5, 3, 6 and 12 arc seconds	Two channels each with a 32x32 element detector array
ISOPHOT (D. Lemke, MPI für Astronomie, Heidelberg, D)	Imaging Photo-polarimeter	3 - 200	Broad-band and Narrow-band Filters. Near IR Grating Spectrometer with R=100	Variable from diffraction - limited to wide beam	Four sub-systems: i) Multi-band, Multi-aperture photo-polarimeter (3-110 μm) ii) Far-Infrared Camera (30-200 μm) iii) Spectrophotometer (2.5-12 μm) iv) Mapping Arrays (3 bands at 4, 11 and 22 μm)
SWS (Th. de Graauw, Lab. for Space Research, Groningen, NL	Short-wavelength Spectrometer	3 - 45	1000 across wavelength range and 3×10^4 from 15 - 30 μm	7.5x20 and 12x30 arc seconds	Two gratings and two Fabry-Pérot Interferometers
LWS (P. Clegg, Queen Mary College, London, GB)	Long-wavelength Spectrometer	45-180	200 and 10^4 across wave-length range	1.65 arc minutes	Grating and two Fabry-Pérot Interferometers

Characteristics of Scientific Instruments

TABLE 1

Fig. 1 - ISO Payload Module.

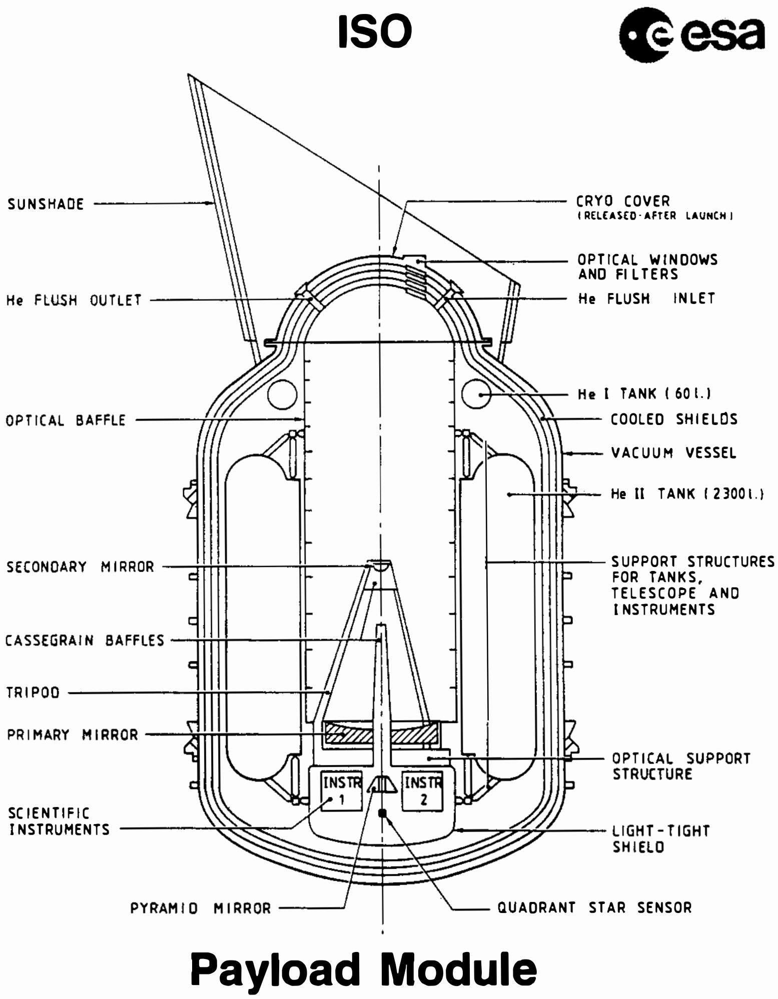

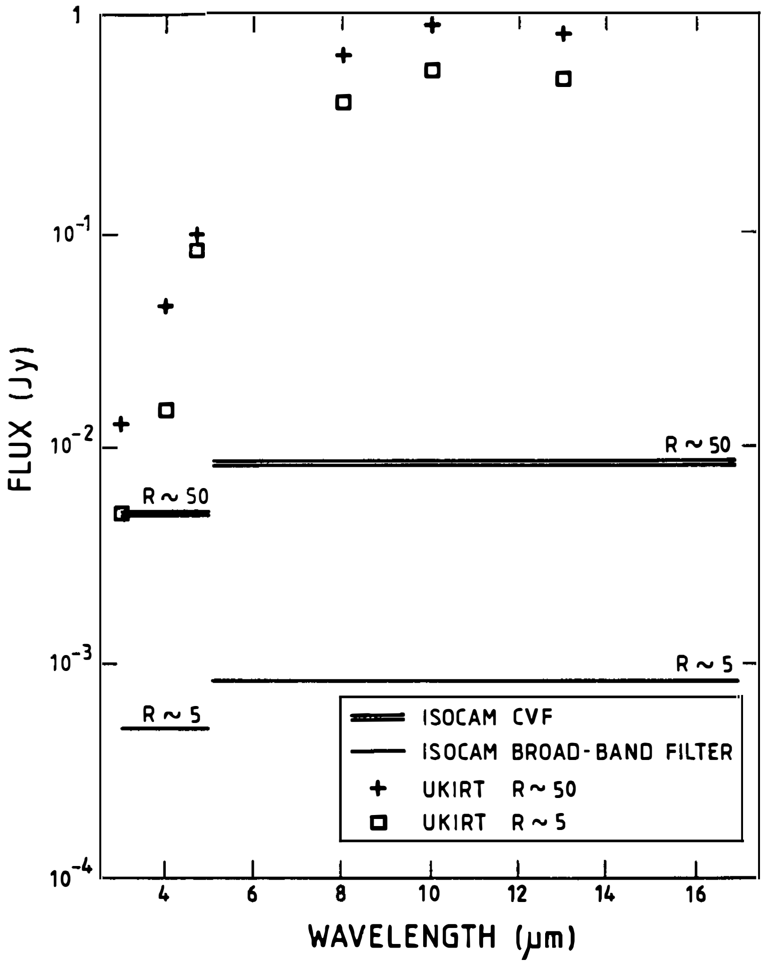

Fig. 2a - Flux detectable by ISOCAM at a signal-to-noise ratio of 10 in an integration time of 100 secs for broad band (resolving power ~ 5) filters and narrow band (resolving power ~ 50) circular variable filters. A point source has been assumed. For comparison purposes, the performance of current instruments operating on UKIRT at or near the quoted resolution is given . A 5 arc second field of view has been assumed for these instruments.

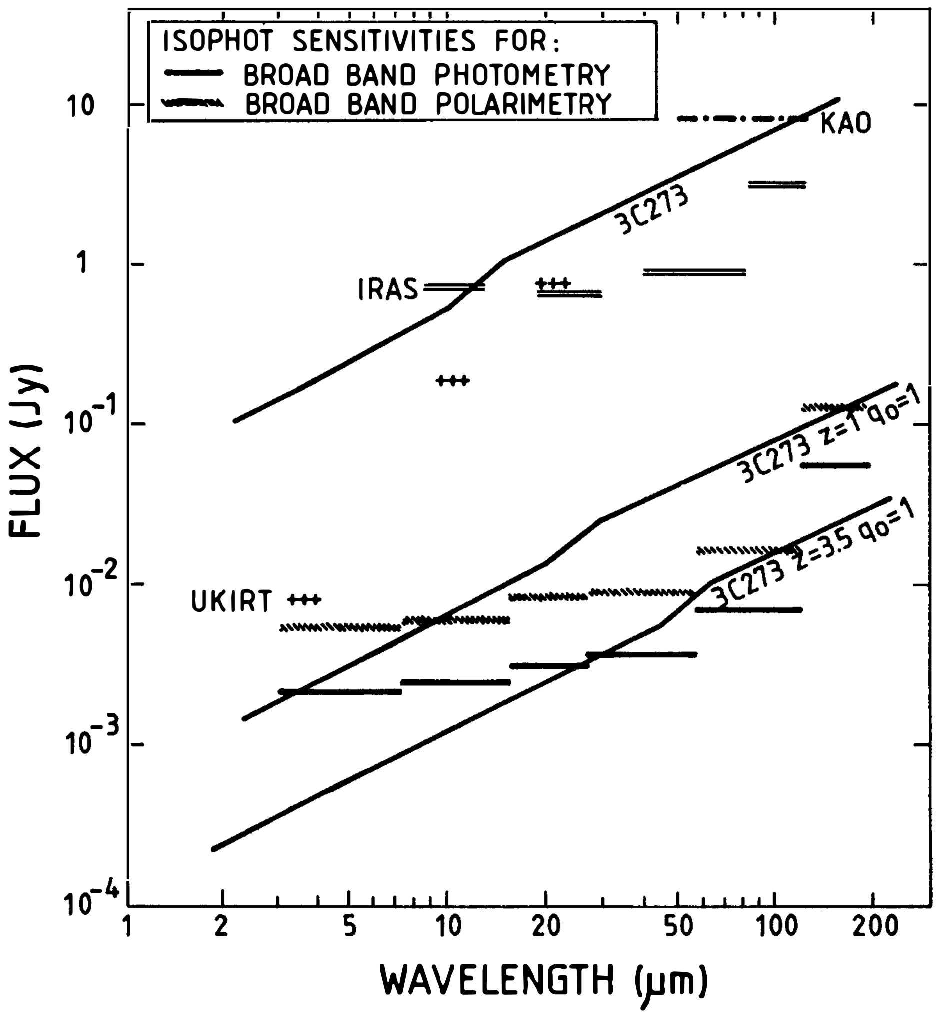

Fig. 2b - Flux detectable with ISOPHOT at a signal-to-noise ratio of 10 in an integration time of 100 secs in two of its different operating modes (broad band photometry and broad band polarimetry). For comparison purposes, the sensitivities of IRAS (survey mode), the KAO and UKIRT are also given.

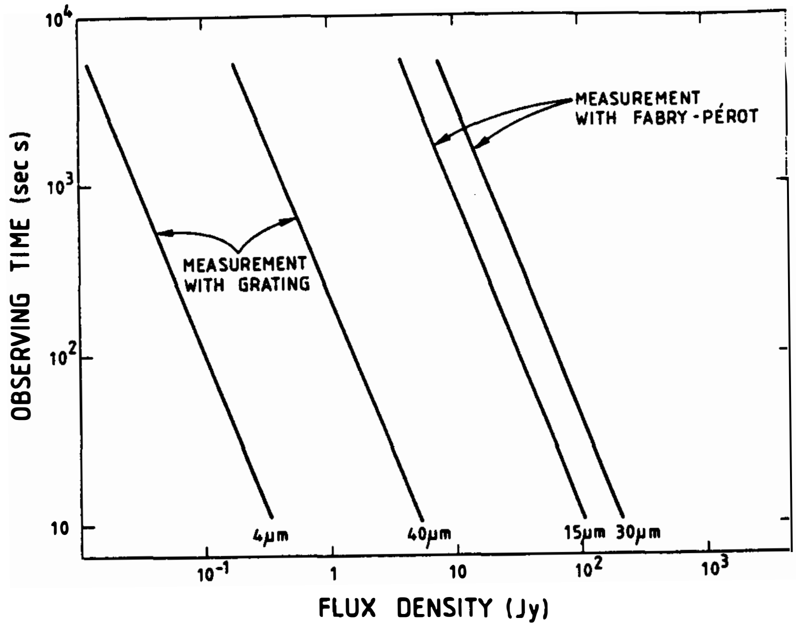

Fig. 2c - Observing times required for SWS to detect IR flux within a spectral element at a signal-to-noise ratio of 10. The cases shown are (i) Measurement in grating mode with a resolving power of 1000 at wavelengths of 4 and 40 µm and (ii) Measurement in Fabry-Pérot mode with a resolving power of 30000 at wavelengths of 13 and 30 µm. (A number of spectral elements are measured simultaneously while in grating mode).

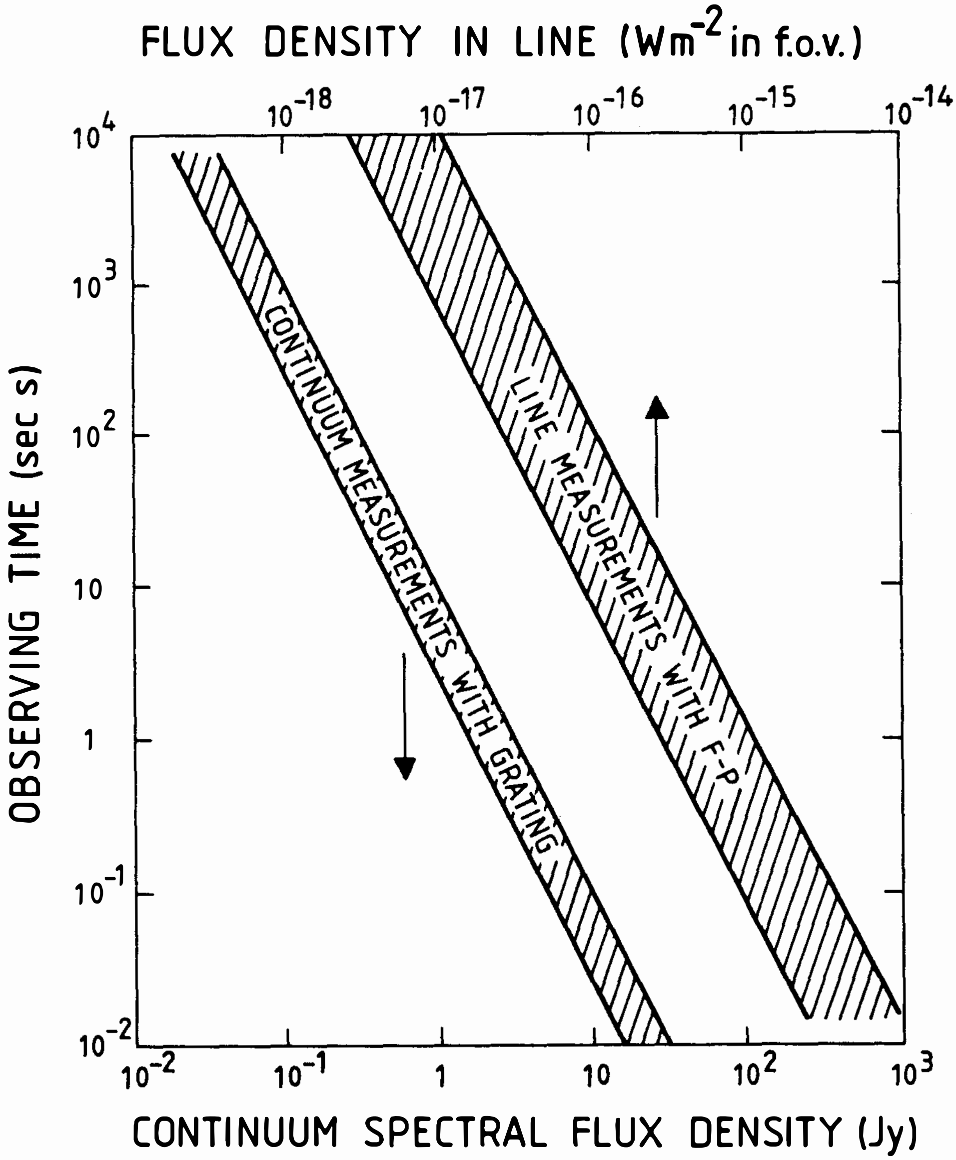

Fig. 2d - Observing times required for LWS to detect IR flux within a spectral element at a signal-to-noise ratio of 10. Use of integrating amplifiers has been assumed. The cases shown are (i) Measurement in grating mode with a resolving power of 200 and (ii) Measurement in Fabry-Pérot mode with a resolving power of 10000. The spread in each case is due to the variation in instrument efficiency across its operating range of 45-180μm.

ULTRAVIOLET OBSERVATIONS OF STARBURST SYSTEMS WITH ASTRO AND THE HUBBLE SPACE TELESCOPE

Robert W. O'CONNELL
Astronomy Department
University of Virginia
Charlottesville, VA 22903 USA

ABSTRACT

The Hubble Space Telescope and Astro missions will open up a new domain of research in ultraviolet astronomy with not only greatly increased sensitivity, but also fundamentally new capabilities in UV imaging, polarimetry, and high time resolution. The scientific potential of these instruments for applications to starburst galaxies and related problems is reviewed.

I. Introduction

Ultraviolet astronomy is still in its infancy. Much UV data is already available, particularly in the form of International Ultraviolet Explorer spectra, but because of small apertures of limited observing times, UV experiments have yet to reach the sensitivity levels routinely achieved at visible wavelengths on the ground. This will change dramatically in the near future. For example, the working limit of the IUE low resolution spectrograph is $m_\lambda(2000\ A) \sim 14$ for point sources, but the limit of the Hubble Space Telescope Faint Object Camera will be $m_\lambda(2000\ A) \sim 26$, a factor of 60,000 fainter.

Clearly, a vast, new domain will soon open up in UV astronomy. This is also true if one considers the kind of observations which will be possible. Most UV astronomy experiments to date have been broad-band photometers and spectrographs. Excluding planetary missions, no polarimetry or high time resolution photometry and very little direct imaging has been done. (Among the notable pioneering experiments in UV imaging are two from groups here in France: the SCAP 2000 balloon camera [1], and the Spacelab Very Wide Field Camera [2]). The HST and Astro facilities offer powerful capabilities in all three areas.

I have chosen not to review the visible or near infrared capabilities of HST because I believe these are well known to most people here (many of whom were probably feverishly preparing HST proposals until the Challenger accident). On the other hand, UV science, particularly non-spectroscopic, is likely to be less familiar. I have also chosen to concentrate on HST and Astro as being of most near-term interest, though I should note that other major UV experiments-- e.g. Lyman-- may become available later in the 1990's, and the Soviet Mir astrophysics module may have significant UV capability.

I will usually quote magnitude in the monochromatic magnitude system, $m_\lambda(\lambda) = -2.5 \log F_\lambda - 21.1$, where $[F_\lambda]$ = erg s^{-1} cm^{-2} A^{-1}, and surface brightnesses in the corresponding units: $\mu_\lambda = m_\lambda + 2.5 \log A$, where A is the source area measured in $arcsec^2$.

II. Scientific Advantages of the Ultraviolet

The great scientific potential of the ultraviolet for extragalactic problems arises mainly from the following considerations:

1. Sensitivity to hot sources. Hot stars and many nonthermal sources are brighter in the UV than the visible. Unreddened B0 stars, for instance, have $m_\lambda(1500\ A) - V = -4.5$. They can therefore be studied to much fainter thresholds than in the visible. For composite souces such as galaxies, temperature resolution is greatly improved. Equally important in many applications is the contrast between hot sources and cool background light. For example, a hot horizontal branch star will be brighter than a K2 giant of equal V magnitude by 16 magnitudes (a factor of 2.5×10^6) at 1500 A; the contrast between a nonthermal galaxy nucleus and the surrounding stellar population will be typically 6-7 mags better at 1500 A than at 5500 A. As a result, the detection of "submerged" active nuclei or starbursts (e.g. the starburst nucleus in M83 [3]) will be greatly facilitated in the UV.

2. Rich UV line spectra. The many resonance and other important transitions in the UV have proved to be of enormous astrophysical value for the study of stellar atmospheres, circumstellar material, and the interstellar medium in our own and other galaxies. Of special interest to this conference are the C IV (1500 A) and Si IV (1400 A) features, important diagnostics of stellar temperature and stellar winds and also prominent in AGN's. Observations of Ly-α have been limited to date by the strong geocorona but will be of great interest with the new UV observatories, especially for low-to-moderate redshift systems. In the spectral region below 1100 A accessible to HUT, the O VI (1034 A) feature is a key diagnostic of gas in the 10^{5-6} K range, spectral structure across the Lyman discontinuity at 912 A in the restframe can provide important constraints on the IMF in starburst galaxies and neutral hydrogen covering factors in AGN's, and the He I and He II resonance lines (584 A and 304 A, respectively, in the restframe) may be observable in high redshift systems.

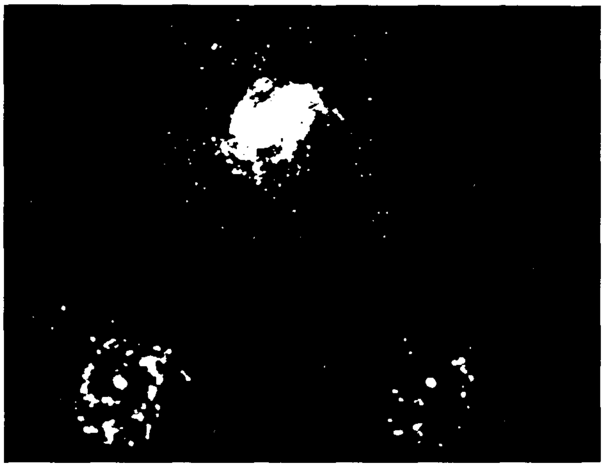

Figure 1: An example of the improved detectability of hot sources in the UV: the starburst nucleus of the barred spiral galaxy M83. The upper panel is a ground-based, visual-band photograph taken with the Kitt Peak 4-m telescope (courtesy R. Dufour). The bar of M83 is prominent. The two lower panels are UV images taken with the 38-cm prototype of the Ultraviolet Imaging Telescope during a sounding rocket flight [3]. Both exposures were 25 sec long, with broad band filters centered at 2360 A (left hand panel) and 1540 A (right hand panel). A starburst nucleus is revealed by the UV images and produces about 20% of the total UV flux of the galaxy. The cool stars of the bar have been suppressed in the UV. Note that the major axis of the star-burst nucleus is perpendicular to the bar. H II regions in the spiral arms are UV-bright. The dynamic range of the original images is not well represented in this reproduction.

3. Sensitivity to interstellar dust. Interstellar dust grains in various environments can be studied to great advantage in the UV through their absorptive scattering, and polarization properties. The 2175 A absorption feature is a convenient indicator of the amount of extinction to a source as well as a clue to the physical nature of grains. Scattered UV light from dust may prove to be a sensitive probe of cool circumgalactic material [e.g. 4]. While very large extinction can certainly limit UV observations in some cases, many starforming extragalactic system have proven to have surprisingly small E(B-V)'s and are UV-bright.

4. The dark UV sky. In directions typical of extragalactic pointings, the sky background in space reaches m_λ(2000 A) $\sim$ 26 mag arcsec^{-2}, which is a factor 40 darker than at any wavelength at excellent ground-based sites. This represents an unprecedented new opportunity to study low surface brightness objects. Taking into account the UV/V energy distribution of potential targets, one finds that in certain circumstances UV surface photometry can permit detection of regions with equivalent V-band brightnesses of $\mu(V) \sim 35$ mag arcsec^{-2}, or over 100,000 times fainter than the ground-based sky [5].

III. HST and Astro Instrumentation

I presume the HST needs little introduction. It is a free-flying 2.4-m telescope developed by NASA and ESA which will orbit at an altitude of $\sim$ 500 km. It is intended to be a permanent observatory with a lifetime of at least 15 years. Although return to Earth is no longer contemplated, it can be serviced on-orbit at regular intervals, and instruments can be replaced if desirable. Currently under development for replacement of first generation instruments after perhaps 5 years of operation are an imaging spectrograph and a near infrared instrument. By virtue of its optics and pointing system, HST offers superb image quality, with a 70% encircled energy radius of only 0.06 arcsec at 3500 A. HST will support a vigorous General Observer program throughout its lifetime. A full description is available in [6] and the handbooks issued by the Space Telescope Science Institute. HST is currently scheduled for a November 1988 launch.

Astro is a Spacelab observatory consisting of three co-aligned, simultaneously operating UV telescopes mounted on the ESA-supplied Instrument Pointing System. It is operated in the payload bay of the Shuttle at an altitude of ∿ 300 km and can be refurbished between missions. The telescopes, designed by different PI groups, were selected from ∿ 200 Spacelab proposals submitted in 1978, of which fewer than 10 have survived. Astro was originally scheduled for three 8-10 day missions in 1986-7, the first of which (March 1986) was to have involved extensive observations of Halley's comet, with a set of three follow-on missions likely. A Guest Observer program amounting to about 50% of the available time on later missions was planned. Two Astro missions are on the current Shuttle manifest, the first scheduled for January 1989. The ultimate program will depend in large part on user demand. A description of the facility is available in two "Space Science and Applications Notices" issued by NASA Headquarters in December 1985.

The six HST instruments were selected in 1977. The Fine Guidance Sensors serve as point source astrometry instruments as well as star trackers. Detector characteristics and other salient features of the other first generation instruments follow:

Faint Object Camera: Image intensifiers plus TV camera, photon counting. $\lambda\lambda$1150-6500. Min. pixel 0.007 arcsec, oversamples PSF. Max field 44 x 44 arcsec. Carries filters and polarizers. Objective prism and grating for low resolution spectroscopy.

Faint Object Spectrograph: 512-diode Digicons, photon counting. $\lambda\lambda$1150-8500. Resolution 100-1000. Min. aperture 0.1 arcsec; max 0.5 x 2.0 arcsec. Carries polarizers. Time resolution 20 ms.

High Resolution Spectrograph: 512-diode Digicons, solar blind, photon counting. $\lambda\lambda$1100-3200. Resolution $2 \times 10^3 - 10^5$. Aperture sizes 0.25-2.0 arcsec.

High Speed Photometer: Photomultipliers (2 solar blind), photon counting. $\lambda\lambda$1200-8000. Aperture sizes 0.4-1.0 arcsec. Time resolution 10 μs. Carries filters and polarizers.

Wide Field/Planetary Camera: CCD Mosaic, 1600 x 1600 pixels, analog readout. $\lambda\lambda$1150-11000. Min. pixel 0.04 arcsec. Max field 2.6 x 2.6 arcmin. Carries filters and polarizers. Objective grating for slitless spectroscopy.

The *Astro* facility consists of the following:

Hopkins Ultraviolet Telescope (A. Davidsen, Johns Hopkins University, PI): 90-cm telescope, primary coated with iridium, plus Rowland spectrograph. Intensified 1024 element Reticon detector, solar blind, photon counting. $\lambda\lambda$420-1850. Resolution $\sim$ 500. Min. aperture 9 arcsec dia; max 18 x 120 arcsec. Time resolution 1 ms.

Ultraviolet Imaging Telescope (T. Stecher, Goddard Space Flight Center, PI): 38-cm telescope. Intensified film cameras, solar blind, 2000 frames per mission. $\lambda\lambda$1150-3300. Pixel size 1.2 arcsec. Internal image motion compensator, 0.2 arcsec stability. Field 40 arcmin diameter. Carries 11 filters plus objective grating for slitless spectroscopy.

Wisconsin Ultraviolet PhotoPolarimeter Experiment (A. Code, University of Wisconsin, PI): 50-cm telescope plus spectropolarimeter. Intensified dual 1024 element Reticon detector, solar blind, analog readout. $\lambda\lambda$1300-3300. Resolution $\sim$ 500. Min. aperture 1.5 arcsec dia; max. 50 x 50 arcsec. Carries Lyot filters and wave plates to measure all Stokes parameters simultaneously across spectral range.

IV. Capabilities of the Instruments

There is obviously some redundacy among these eight instruments, but each also has unique and powerful capabilities.

The *HST* instruments are designed to take advantage of *HST*'s large aperture, excellent image quality, photometric stability, and long lifetime, which permits integrations lasting many orbits if necessary. The 70% encircled energy radius at 3500 A corresponds to 0.2 pc at M31 or 5 pc at the distance of the Virgo cluster. As a consequence, _HST_ will be an extraordinarily powerful tool for the analysis of stellar populations and AGN's in nearby galaxies. With the FOC, the S/N = 10 limit for a point source in a 10 hour integration at 2000 A is $m_\lambda \sim 26.5$. If the source were an unreddened B0 star, the equivalent V magnitude limit would be 30.3 (cf. Sec. II). This is a factor ~ 40 fainter than reached to date by even the most heroic ground-based efforts. Most _HST_ observing programs will not involve such long integrations, however. For the Wide Field Camera, the limiting magnitude for a 30 minute integration at 2500 A is $m_\lambda \sim 21.5$, or V(B0) ~ 24.5. With the FOS, a 30 minute integration at a resolution of 1200 yields S/N = 10 per A for a source with m_λ(2000 A) ~ 18.4 or V(B0) ~ 22.2.

The _Astro_ instruments were designed to have capabilities complementary to _HST_'s and to be highly productive during missions of short duration. HUT extends the wavelength coverage of _HST_ to the EUV region $\lambda\lambda$420-912, which is essentially unexplored. While the interstellar medium is expected to be opaque for longer pathlengths in this regime, nonetheless observations of some important hot sources are clearly possible [7]. The region 912-1150 A, also not available to _HST_, is of great astrophysical interest, as noted in Sec. II, for both nearby objects and high redshift systems (where the Lyman continuum $\lambda_{rest} < 912$ A becomes visible). WUPPE provides an unmatched capability for efficient, high precision polarimetry throughout its spectral range. UIT, HUT, and WUPPE all employ "solar-blind" detectors, which provide strong rejection of visible light. This is highly desirable to eliminate the effects of scattered light in the spectrographs and is extremely important to suppress filter "red leaks" in many extragalactic UV imaging applications.

A key complementary feature which is shared by all three _Astro_ instruments is a larger field of view than their _HST_ counterparts. WUPPE and HUT can employ aperture sizes of 2000-2500 arcsec^2 whereas the _HST_ spectrographs are limited to 1 arcsec^2 (FOS) and 4 arcsec^2 (HRS). For extended sources, such as the inner regions of starburst galaxies, this means that HUT, for example, is 25 times faster than the FOS at 1700 A despite its small aperture.

The UIT's field of view is 180 times larger than that of the Wide Field Camera. For point sources, its limiting magnitude is about the same as the WFC, i.e. m_λ(2500 A) $\sim$ 21.8 or V(BO) $\sim$ 24.8 in 30 minutes. UIT's extended source threshold is about 20 times fainter than that of the WFC in a 30 min integration if the threshold is defined by the surface brightness of a source yielding a signal equal to the detector noise per unit area. These values are μ_λ(UIT) = 25.8 and μ_λ(WFC) = 22.3 at 2500 A. The unexpectedly good performance of the UIT results from fewer reflections in the optical train, a detector with low equivalent readout noise, and its use of high efficiency, broad band UV filters. However, it should be noted that, as with all photographic detector systems, UIT's photometric S/N is limited to about 20.

As a result of its high efficiency design, the Astro complement can return a surprisingly large amount of information even in the relatively short duration of a 6-8 day Shuttle mission. In 6 days of science operations, Astro will be able to make 192 target pointings (2 per orbit). The total field area covered by UIT in this period, for example, is equivalent to 18 years of WFC exposures (to the same UV limiting magnitude for point sources) if the WFC is able to take UV exposures on one of every three target pointings (1 per orbit). On the other hand, there will be many situations where the higher spatial or spectral resolution of HST or its capacity for extended integrations or long-term monitoring of variable sources is crucial. Taken together, HST and Astro provide a powerful, balanced, and strongly complementary UV observational capability.

V. UV Observations of Starburst and Related Systems

HST and Astro ultraviolet observations will make important, perhaps decisive, contributions to many of the problems discussed at this meeting. A brief list of some sample observing programs follows, and many others will readily occur to the reader. General discussions of UV science may be found in many conference proceedings, notably [6,8,9].

MASSIVE STARS IN OUR OWN AND NEARBY GALAXIES

Individual spectra $\lambda\lambda$900-3200: Lyman lines, O VI, C IV, Si IV; abundances atmospheric structure, winds.

Polarimetry: winds and extended atmospheres.

Initial mass function: resolve star forming regions in nearby galaxies (HST); UV photom/imagery improves temperature discrimination.

INTERSTELLAR MEDIUM IN NEARBY GALAXIES

Absorption line spectroscopy against hot stars/AGN's; abundances, temperatures, velocity fields; nature of hot halos; local ISM in the Lyman continuum, 400-912 A (HUT).

Dust: extinction law, polarization/scattering properties; λ2175 feature; grain characteristics in different environments.

Supernovae remnant/planetary nebula surveys using C IV imagery.

ULTRAVIOLET EXCESS COMPONENT IN OLD STELLAR POPULATIONS

Identify and study the nature of this hot component in E galaxies and spiral bulges by resolving individual stars in nearby galaxies (HST), by studying its spatial distribution in various galaxy types (UIT), and by spectroscopy.

DEEP UV SURVEYS (FILTER IMAGING AND SLITLESS SPECTROSCOPY)

Hot stars in nearby galaxies: massive or highly evolved low mass objects (horizontal branch, post-AGB, etc).

Low surface brightness blue dwarf galaxies with $\mu_\lambda > 26$

Clusters of galaxies (UIT): integrated UV photometry for all morphological types; Ly-α fluxes for $z \gtrsim 0.04$; emission lines from cooling flows; thorough samples of nearby clusters are necessary for interpretation of high redshift data.

Starburst and Ly-α emission objects to $z \sim 2$.

Primeval galaxies at $z \sim 2$-4 recognized by unusual colors or spectra in the restframe Lyman continuum.

Note: all surveys benefit from the extremely dark UV sky (cf. Sec. II).

AGN'S AND QSO'S

Nature of continuum radiation: UV spectral shapes; polarization

Nonthermal jets (UV imaging).

Physics of ionized medium: absorption and emission lines; O VI, Ly-α, N V, C IV; spatial resolution of nuclear emission line regions (HST).

Neutral hydrogen covering factors from spectral shape at $\lambda_{rest} \lesssim 912$ A.

EUV features (He I, He II $\lambda\lambda$584,304; Lyman edge; Lyman continuum) in high redshift objects; intergalactic absorption.

Identification of very low luminosity AGN's in nearby galaxies.

STARBURST SYSTEMS

Spatial resolution of bursting region in nearer systems.

Spatial resolution of parent system in more distant systems (HST); nature of parents/burst mechanism.

Integrated UV spectra of bursts: abundances, stellar winds, dynamics of gas and stars in bursting region; IMF and star formation history.

Detection of low luminosity starburst nuclei through improved UV contrast against dominant, old populations.

Circumgalactic material in tidally interacting and merger systems; hot gaseous components in absorption or emission line spectra; stellar or cool, dusty components by very low surface imaging (to $\mu(V) \gtrsim 30$ equivalent).

VI. Conclusion

HST and Astro offer not just greatly improved sensitivity for ultraviolet astronomy, but fundamentally new capabilities in the essentially unexplored areas of UV imaging, polarimetry, and high time resolution, These, taken together with the high density of astrophysical information in the ultraviolet, promise a rich scientific return in short order once Space Shuttle launches resume.

This work was supported in part by NASA grants NAG 5-700 and NAG 5-838.

REFERENCES

1. Donas, J., Milliard, B., Laget, M., and Deharveng, J. M. 1981, Astr. Ap., 97, L7.
2. Courtes, G., Viton, M., Sivan, J.-P., Decher, R., and Gary, A. 1984, Science, 225, 179.
3. Bohlin, R. C., Cornett, R. H., Hill, J. K., Smith, A. M., and Stecher, T. P. 1983, Ap. J. (Letters), 274, L53.
4. Stecher, T. P., Bohlin, R. C., Hill, J. K., and Jura, M. A. 1982, Ap. J. (Letters), 255, L99.
5. O'Connell, R. W. 1987, submitted to A. J.
6. Hall, D. N. B. 1982, The Space Telescope Observatory, NASA CP-2244 (Baltimore: Space Telescope Science Institute).
7. Malina, R. F., Bowyer, S., and Basri, G. 1982, Ap. J., 262, 717.
8. Longair, M. S., and Warner, J. W., Scientific Research with the Space Telescope (IAU Colloquium 54) (NASA CP-2111), 1979.
9. Mead, J. M., Chapman, R. D., and Kondo, Y., The Future of Ultraviolet Astronomy Based on Six Years of IUE Research (NASA CP-2349), 1984.

AXAF AND XMM: THE X-RAY OBSERVATORIES FOR THE 1990s

A.C. Fabian

Institute of Astronomy

Cambridge

United Kingdom

The Advanced X-ray Astronomy Facility (AXAF) of NASA and the X-ray Multi-Mirror Mission (XMM) of ESA will be the major X-ray observatories of the late 1990s. Their potential for studies of galaxies is enormous.

1 Introduction

The X-ray observatories of the 1980s - the *Einstein Observatory* and EXOSAT - together with Tenma and Ginga have laid the basis for X-ray imaging and spectroscopy. Most classes of cosmic object have been detected as X-ray sources and spectral lines found in the brighter ones.

The early 1990s will see the production of the ROSAT Survey containing up to 10^5 sources over the whole sky. This survey will extend to about 2 keV and have a spatial resolution of $\sim$ 10 arcsec (Trumper 1984). Spectral information will be obtained in about 4 'colour bands'. The next obvious steps are to pursue higher spatial resolution, higher spectral resolution and wider spectral bandwidth. NASA's Advanced X-ray Astronomy Facility (AXAF) and ESA's X-ray Multi-Mirror Mission (XMM - sometimes known as the X-ray Spectroscopy Mission) aim to achieve these goals in a complementary manner. Both will have a bandwidth extending above 8 keV, which gives access to the important iron Kα line complex at $\sim$ 6.5 keV, and much greater collecting area than previous missions. AXAF, one of NASA's Great Observatories, is designed for high spatial resolution and will give sub-arcsecond imaging. XMM, one of ESA's Cornerstones, is designed for high spectroscopic throughput. These long-lived observatories, together with other intermediate experiments expected to be launched by NASA, Japan, the USSR, Italy and others, will mean that the late 1990s will be rich in X-ray data.

X-rays are the primary energy output for most forms of compact objects, binary stars, active galaxies and diffuse hot gas. Such gas is a common feature in the Universe and is well observed where it is trapped in the potential wells of clusters and galaxies. The major emission lines of hot thermal gas are shown in Fig. 1. A gas of cosmic abundance at 10^7 K radiates about 60 per cent of its emission as lines. AXAF and XMM will measure the abundances of such gas to better than 20 per cent. This has obvious implications for studies of the chemical enrichment and recycling of gas in galaxies. In the last Section of this talk I shall discuss further how X-ray observations are essential to many galactic studies and how they may relate to star formation and starbursts.

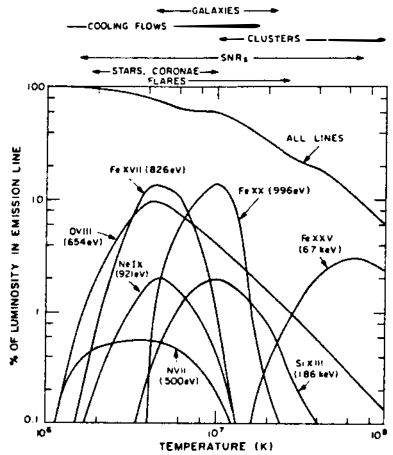

Figure 1. Fractional contribution of emission lines to equilibrium thermal gas emission as a function of temperature.

2 The Instruments

2.1 AXAF

AXAF is the top recommendation of the Field Report and currently under study by NASA. It is to be a space observatory with a lifetime exceeding 15 yr, with periodic refurbishment by the Space Station.

The telescope consists of 6 nested Wolter I mirrors of 1.2m maximum diameter and 10m focal length. An on-axis point-spread function of 0.65 arcsec diameter is achievable (Van Speybroeck et al. 1987; Schwartz *et al.* 1987) and images can be positioned to within 1 arcsec. 4 focal-plane instruments together with transmission gratings study the spatial and spectral content of the images. A detailed description of these instruments is given in SPIE, Vol. 597, pp 232 - 281 (1985).

a) *CCD Imaging Spectrometer (ACIS; G. Garmire P.I.).*

A CCD array gives high angular resolution (0.5 arcsec) and moderate spectral resolution ($\sim$ 150 eV) over the energy range of 0.1 to 10 keV. Single photon quantum efficiencies of up to 90 per cent can be obtained so that the effective area will be $\sim 600\,\mathrm{cm}^2$ over the 0.5 keV band. Point sources of $\leq 10^{-15}\,\mathrm{erg\,cm^{-2}\,s^{-1}}$ can be detected in exposures of 10^5 s.

b) *High Resolution Camera (HRC; S. Murray P.I.).*

The detector is a CsI-coated microchannel plate which has a high angular resolution, low background and large field-of-view. This means that it will be the preferred instrument for diffuse sources. Some modest energy resolution is achieved at low energies (≤ 2 keV).

c) *Bragg Crystal Spectrometer (BCS; C. Canizares P.I.).*

Spectral resolving powers of 200 - 2000 are obtained over the 0.5 - 8 keV band and 50 - 80 over 0.14 - 0.5 keV. An effective collecting area of $\sim 4 - 60\,\mathrm{cm}^2$ gives a minimum detectable line flux of $\sim 4 - 30 \times 10^{-6}\,\mathrm{ph\,cm^{-2}\,s^{-1}}$.

d) *X-ray Calorimeter (XRS; S. Holt P.I.).*

This is an innovative idea which is currently being tested in the laboratory. The temperature increase that occurs as a small crystal absorbs an X-ray is measured by the change in electrical resistance. This should give a high quantum efficiency and a resolving power of ~ 1000 at 6 keV.

e) *Low Energy Transmission Grating (LETGS; A. Brinkman P.I.).*

The grating operates over the 2 - 140 A range giving $\Delta\lambda = 0.05$ Å with an effective area of $\sim 20 - 30\,\mathrm{cm}^2$.

f) *High Energy Transmission Grating (HETGS; C. Canizares P.I.).*

Here the energy band is 0.4 to 8 keV with R $\sim$ 100 to 1000 and an effective area of $\sim 10 - 200\,\mathrm{cm}^2$.

AXAF will have a spatial resolution which is $\sim$ 4 to 8 times better than that achieved with the Einstein Observatory and will be $\sim$ 10 - 50 times more sensitive.

2.2 *XMM*

XMM is ESA's major X-ray mission for the future as recommended by the 'HORIZON 2000' report (1984). It is currently planned for launch in 1998 by Ariane IV into a deep-Earth orbit similar to that of EXOSAT.

It is envisaged that the payload consists of 4 telescope modules each of which is composed of 58 Wolter 1 nested telescopes. The focal length is 7.5 m and the outermost shell diameter is 0.7 m providing an energy range of 0.1 - 15 keV. This will give between 6000 and 3000 cm^2 effective telescope area between 1 and 8 keV with a spatial resolution of $\sim$ 30 arcsec half-energy-width. Broad-band spectroscopy is the major goal of XMM. This will be achieved with a range of possible instruments. The model payload currently being studied contains:

a) A CCD array as the prime detector on all 4 telescopes.

b) A imaging gas scintillation proportional counter on all 4 telescopes.

c) Reflection gratings permanently fixed to 2 telescopes covering the energy range 0.4 to 2.5 keV to give a resolution of $\sim$ 300 and effective area $\sim 400\,cm^2$ at 1 keV.

d) Bragg crystal spectrometers on 2 telescopes to give a resolution of $\sim$ 1000 around the K lines of iron and oxygen.

An optical monitor telescope that can detect objects down to $\sim$ 23 mag at 2000 - 6000Å is included as part of the payload. Further descriptions of some of the instruments can be found in the Proceedings of the ESA Workshop on XMM (ESA SP-239).

2.3 A COMPARISON

The two missions have different emphasis and are optimized accordingly. AXAF has a superior spatial resolution to XMM ($\leq$ 1 arcsec vs $\sim$ 30 arcsec) whilst XMM has the superior effective area. (Fig. 1; $\sim 4000\,cm^2$ vs $\sim 1000\,cm^2$ at 2 keV - note that the reflection gratings on XMM reduce the total effective area from that of 4 modules to 3). Both missions will achieve a point-source sensitivity better than $\sim 2.10^{-15}\,erg\,cm^{-2}\,s^{-1}$ in the 0.5 - 8 keV band in 6 hours observing time; AXAF will go deeper than $10^{-15}\,erg\,cm^{-2}\,s^{-1}$ in $10^5\,s$. This corresponds to a flux level of $\sim$ 100 pJy. Detailed spectra below 2 keV and just around the iron complex at 6.5 keV of isolated point sources and, on a one arcmin scale, of extended sources can be rapidly obtained with XMM. AXAF will give sharp images and spectra on a subarcsecond scale and, with the high energy grating, it will give detailed spectra up to 8 keV.

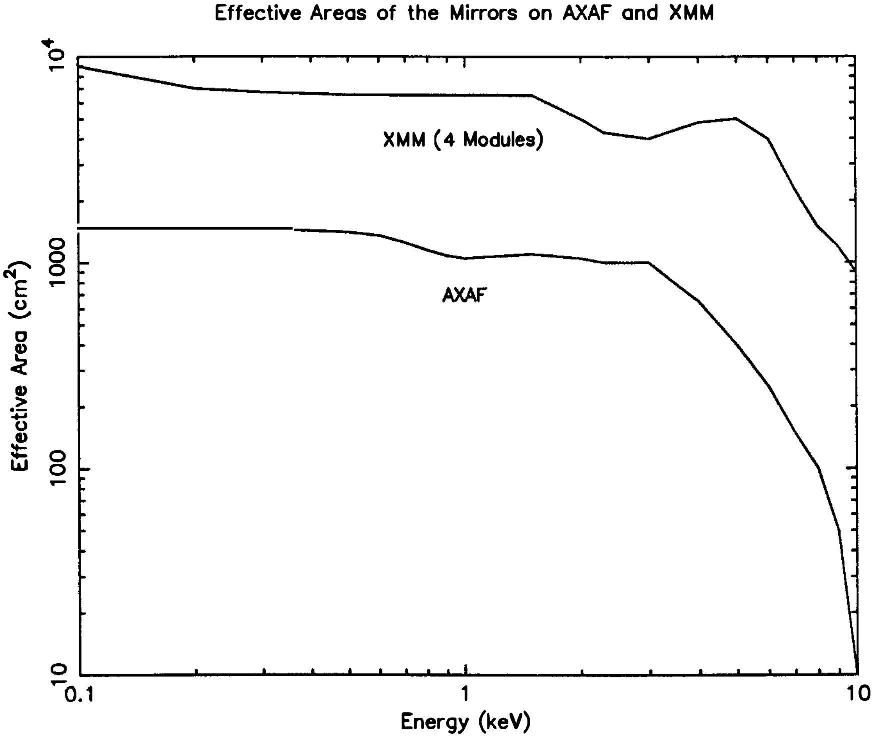

Figure 2. Effective total areas of the telescopes on AXAF and XMM. The reflection gratings mounted in front of 2 of the XMM modules reduce the effective area for imaging to 75% of that shown here.

3. AXAF and XMM for GALAXIES and STARBURSTS

A limit of $10^{-15}\,\mathrm{erg\,cm^{-2}\,s^{-1}}$ is shown in Fig. 2 and compared with the classes of X-ray source expected in galaxies, groups and clusters. Objects that will be detected include:

a) bright stars, RS CVn systems and catacylsmic variables in the Magellanic Clouds;

b) most supernova remnants in the Local Group;

c) the brightest X-ray binaries in the Virgo supercluster;

d) normal spiral galaxies out to the distance of the Coma cluster;

e) bright elliptical and lenticular galaxies out to redshifts of 0.2;

f) groups and clusters out to redshifts of 2 or more.

The study of the internal X-ray structure of most galaxies will require the high spatial resolution of AXAF, although useful overall spectra and timing infomation will of course be obtained with XMM.

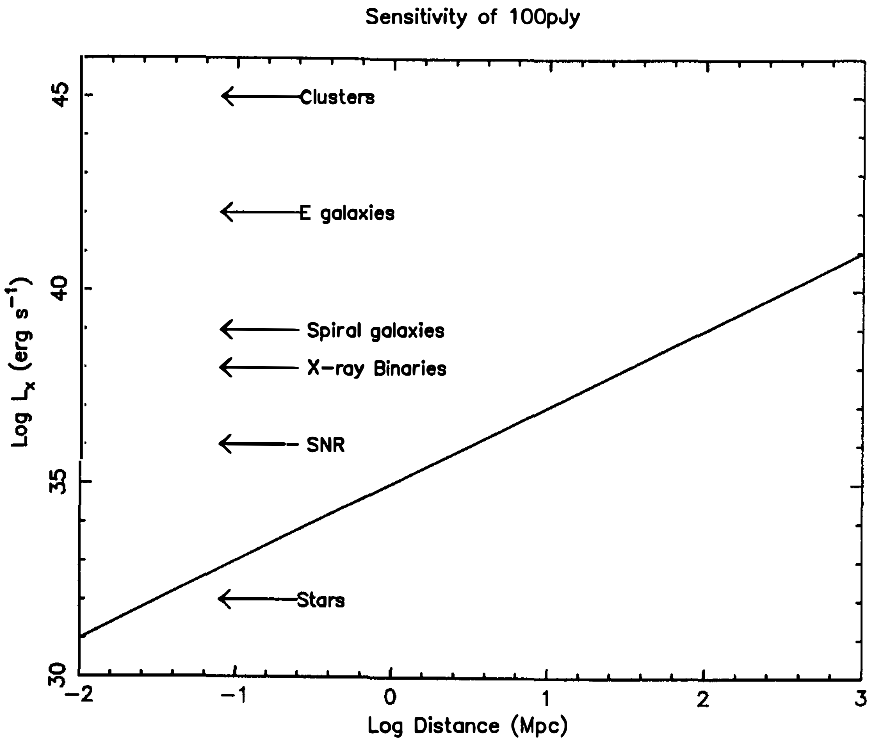

Figure 3. Detectability of various X-ray sources as a function of distance. The solid line indicates a detection threshold of 100 pJy. Maximum observed luminosities for different classes of X-ray source are shown. No cosmological effects are included - they are relatively unimportant out to redshifts of 0.2.

Star forming regions produce X-rays, as discussed elsewhere in this Volume by T. Montmerle. Young stars and especially T Tauri stars, flare stars and OB stars are all X-ray sources with X-ray luminosities, L_x, up to $10^{34}\,\mathrm{erg\,s^{-1}}$. Supernova remnants and pulsars appear to have $L_x \leq 10^{37}\,\mathrm{erg\,s^{-1}}$, at least in our Galaxy. Massive X-ray binaries probably dominate the X-ray output of massive star forming regions with $L_x \leq 10^{39}\,\mathrm{erg\,s^{-1}}$. A comparison of M31, the Milky Way, the LMC, SMC and NGC 5408 indicate that the mean L_x increases as metal abundance decreases (Markert *et al.* 1977; Stewart *et al.* 1982). This may be a result of a decrease in Wolf-Rayet activity at low abundance. Any detailed predictions of the expected X-ray luminosities requires some assumptions about the frequency of massive close binaries but they are possibly very common (see e.g. Fabian 1986).

Peculiar and starburst galaxies appear to be X-ray bright (Weedman *et al.* 1981, Fabbiano *et al.* 1982), with X-ray-to-optical luminosity ratios that are substantially higher than those for

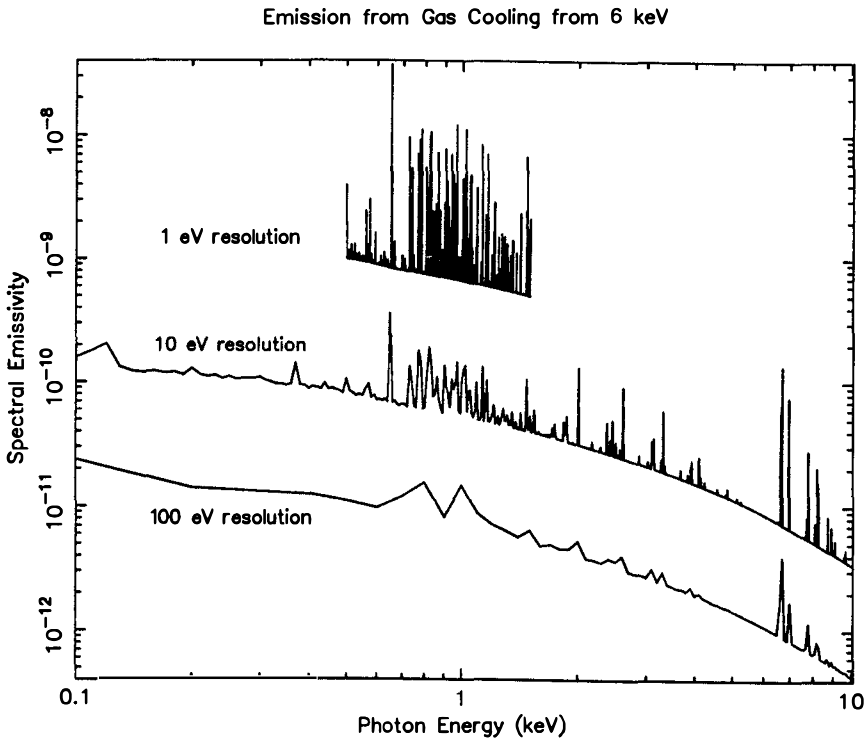

Figure 4. Total energy spectrum of gas cooling from 6 keV at 1, 10 and 100 eV resolution. This is similar to the spectrum expected from a cooling flow. The abundances of the elements are taken to be 0.4 Solar.

normal spiral galaxies like M31. The extragalactic HII region NGC 5408 (Stewart *et al.* 1982) and NGC 5204, which is a companion to M101 (Fabbiano & Panagia (1983), are both extreme in this respect and probably contain large populations of massive X-ray binaries. A strong correlation of X-ray luminosity with blue luminosity in 13 'normal' spiral galaxies detected with the *Einstein Observatory* has been reported by Fabbiano *et al.* (1984), suggesting that the X-ray emission is produced by young systems. Further studies of the Starburst galaxies NGC 253 (Fabbiano & Trinchieri 1984) and M82 (Watson *et al.* 1984) show,in addition to some point sources, extended diffuse X-ray emission that is probably associated with hot outflows.

Spectroscopic results on galaxies that can be expected are:

a) redshifts (to ~ 1 per cent) and abundances (primarily of the elements C through to Fe and Ni; to an accuracy better than 20 percent) for E and S0 galaxies, and clusters. This will readily show the chemical enrichment and recycling of interstellar and intracluster gas. The distribution of clusters of galaxies with redshift, and thus their evolution, will be measured.

b) gas motions 300 $\mathrm{km\,s^{-1}}$ in the nearest clusters. Optical filaments observed in the cores of some cooling flows show velocity widths of more than 500 $\mathrm{km\,s^{-1}}$. Galaxy wakes and stripped gas must have velocities up to $\sim 2000\,\mathrm{km\,s^{-1}}$. Subsonic turbulence of the gas and large scale rotation may generate velocities of $\sim 500\,\mathrm{km\,s^{-1}}$.

c) cooling flows out to substantial redshifts and of quasar 'fuzz' (see Fig. 4 and my other contribution to this volume). Dissipative galaxy formation in which a significant fraction of the gas constituting a galaxy is at its virial temperature will give luminous sources below 1 keV.

d) the spectra of stars, starbursts and X-ray binaries over almost two decades of energy. This may be an important source of hard ionizing radiation in dense gas clouds.

e) absorption studies of the interstellar and intracluster medium (including dust). These give the chemical abundances of the cold (recombined) gas in galaxies from the strengths of the photoelectric edges. X-rays can effectively be used to map the hot and cold gas distribution and composition in suitable galaxies.

The large effective area at 8 keV means that iron line spectroscopy will become routine. (The Tenma satellite found iron line emission from most classes of X-ray source, Makishima 1986). Iron abundance gradients in clusters and groups can be studied (taking into account resonance line scattering, Gilfanov *et al.* 1987). The mass profiles of elliptical and S0 galaxies and of groups and clusters of galaxies will also become a straightforward measurement. Detailed maps can therefore be made of 'dark matter'. The cores of objects such as Arp 220, our Galactic Centre and other highly obscured regions can be examined in detail. Finally the massive X-ray binary population of our Galaxy, and other nearby galaxies, can be mapped in detail.

Acknowledgements

I thank the Project Scientists for AXAF and XMM, Martin Weisskopf and Tone Peacock respectively, and Claude Canizares for help with the details, Peter Thomas for help with TeX and Roderick Johnstone for help with producing Figure 4.

References

Fabbiano, G., Feigelson,E. & Zamorani, G., 1982. *Astrophys. J.*, **256**, 397.
Fabbiano, G. & Panagia, N., 1983. *Astrophys. J.*, **266**, 568.
Fabbiano, G., Trinchieri, G. & Macdonald, A., 1984. *Astrophys. J.*, **284**, 65.
Fabbiano, G. & Trinchieri, G., 1984. *Astrophys. J.*, **286**, 491.
Fabbiano, G. & Trinchieri, G., 1985. *Astrophys. J.*, **296**, 430.
Fabian, A.C., 1986. in *Star-Forming Dwarf Galaxies and related objects*, ed. D. Knuth, T.X. Thuan and J. Tran Thanh Van, Editions Frontieres.
Fabian, A.C., 1987. *Astrophys. Lett*, in press.
Gilfanov, M.R.,Syunyaev, R.A. & Churazov, E.M., 1987. Preprint.
Makishima, K., 1986. in *The Physics of Accretion onto Compact Objects*, ed. K.O. Mason, M.G. Watson & N.E. White, 249 (Springer-Verlag).
Markert, T.H., Canizares, C.R., Clark, G.W., Hearn, D.R., Li, F.K., Sprott, G.F. & Winkler, P.F., 1977. *Astrophys. J.*, **218**, 801.
Schwartz, D.A. *et al.*, 1987. in SPIE Proceedings *X-ray Instrumentation in Astronomy*, ed J.L. Culhane, **597**.
Stewart, G.C., Fabian, A.C., Terlevich, R.J. & Hazard, C., 1982. *Astrophys. J.*, **200**, 61.
Trumper, J., 1984. in *X-ray and UV Emission from Active Galactic Nuclei*, 254 (MPE).
Watson, M.G., Stanger, V. & Griffiths, R.E., 1984. *Astrophys. J.*, **286**, 144.
Weedman, D.W., Feldman, F.R., Balzano, V.A., Ramsey, L.W., Sramek, R.A. & Wu, C.C., 1981. *Astrophys. J.*, **248**,105.
Van Speybroeck, L. *et al.*, 1987. in SPIE Proceedings *X-ray Instrumentation in Astronomy*, ed J.L. Culhane, **597**.

VII. SUMMARY

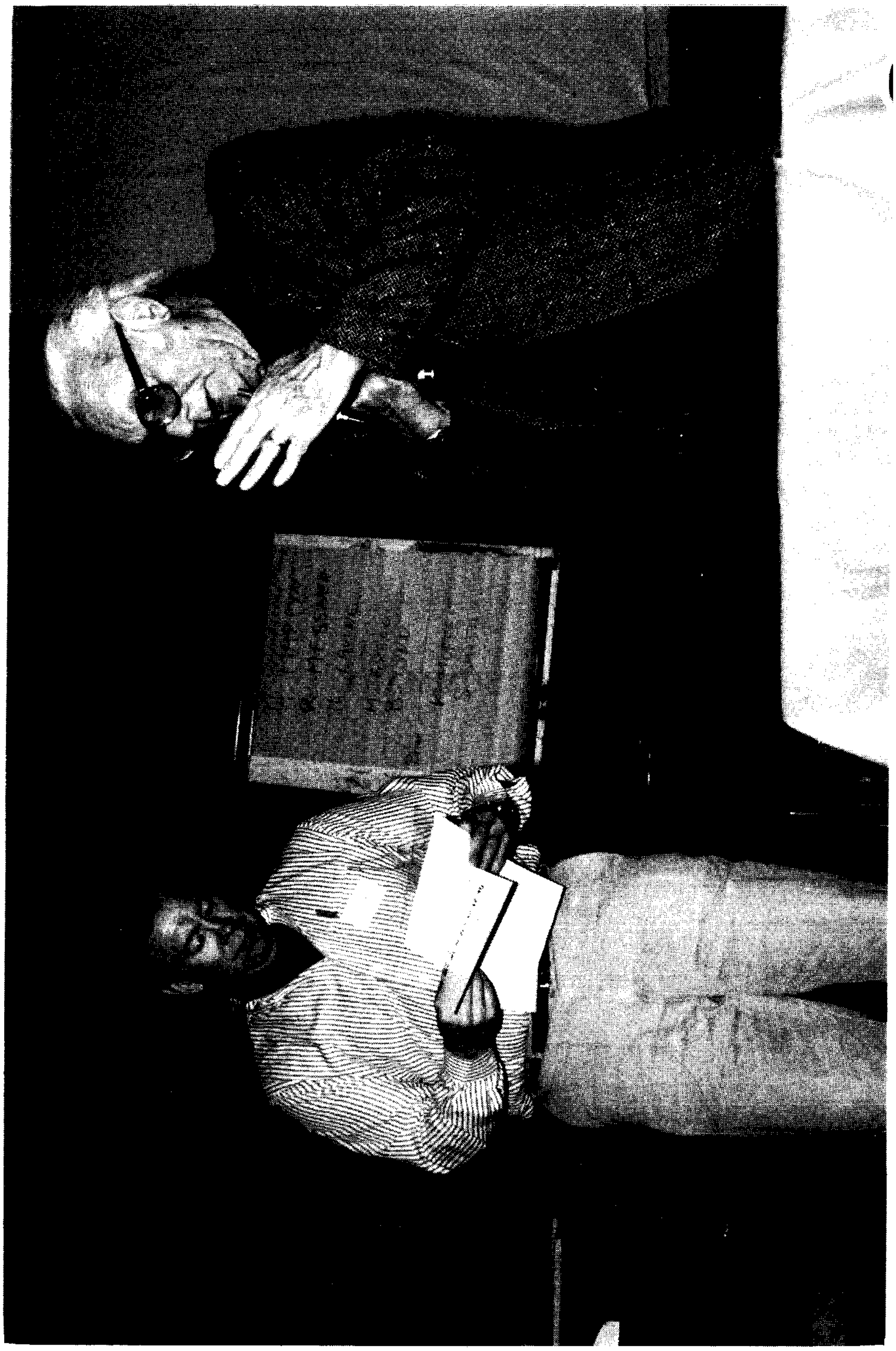

SUMMARY TALK
XXIInd RECONTRE DE MORIOND
WORKSHOP ON STARBURSTS AND GALAXY EVOLUTION

David N. SCHRAMM
The University of Chicago
and
Fermi National Accelerator Laboratory

Abstract

The Astrophysics Meeting had three separate subtopics. The first, and perhaps most dramatic, was the Supernova and the observations of neutrinos from it. The second, the question of dark matter in the Universe. The third, the primary topic of the meeting, the question of star bursts and their role in galactic evolution. In this summary I will briefly mention all three.

1. Introduction

The 1987 Moriond Astrophysics Conference, while formally on the subject of star bursts and their role in galactic evolution also had important contributions with regard to the subject of dark matter, and most dramatically had the excellent luck of having occurred shortly after supernova SN 1987A in the Large Magellanic Cloud, and the consequent detection of neutrinos from that event. In particular, experimentalists from each of the underground experiments, Kamioka in Japan, IMB in the U.S., the Mont Blanc detector in Italy, and the Baksan detector in the Soviet Union, were all represented. Thus, this summary will mention each of these three topics.

2. Supernova 1987A

At this meeting, we were fortunate to have a major, possibly historical, session on the recent supernova. At the time of the meeting, there were still many uncertainties and rumors wandering through the audience, with telegrams and phone calls bringing new, and often contradictory, information. With the hindsight that is obtained by writing this report a couple months after the meeting, one now has a fairly clear picture of what went on in SN 1987A, although, even at this stage, there are still many questions, and much excitement awaits us.

The facts are, on February 23, Supernova 1987A exploded. It was first seen on the 24th, but the photographs show that it was indeed approximately sixth magnitude at 10h UT on February 23, and did not seem to be visible an hour earlier to an observer who was sensitive at approximately eighth magnitude. The star that blew up, has now been reasonably well determined, as a star in the Sanduliac Catalog which was a blue super giant. Although initially there were some questions as to why a blue, rather than a red star should blow up. It now appears to be easy to understand within standard stellar evolution, that the low metalicity Large Magellanic Clouds can have stars in the 15–20$M_\odot$ range blow up while blue rather than red stars. This can occur due to either the stars in that range never having moved fully over to the red, as discussed by Brunish and Truran[1], or having an evolved star that was in the red move over to the blue in one of its oscillations across the top of the HR diagram, as has been discussed by Woosley[2]. Thus the light curve of the supernova itself has continued to rise slowly over the 60 days since the explosion, reaching third magnitude at the time of this report. This continual rise, coupled with the rapid early expansion, was at first perplexing since it did not seem to fit the standard light curve concepts. However, when it is recognized that the star that blew up is definitely a blue star with a relatively compact envelope compared to a red super giant, and if an additional energy source, such as a rotating pulsar inside or radioactive heating is included, one can understand the behavior. Future evolution of the light curve, its subsequent fall and the interior mantle inside of recently-produced heavy elements and possibly the new born neutron star all remain exciting observational possibilities. For the physicist, the most exciting aspect of the supernova has been the detection of neutrinos. This is the first example of extra-solar system neutrinos, and thus marks a major event in astronomy.

At this conference we were fortunate enough to have representatives from each of the groups that reported neutrino detections[3]. In particular, the Kamioka group from Japan, the IMB group from the United States, the Mt. Blanc group from Italy, and the Baksan group from the Soviet Union. Table 1 summarizes the reported neutrino detections. While

Table 1: Neutrino Data		
Time (UT) February	Detector (threshold*/size)	# of Events (E-range/Duration)
23 2h 52m	Mt. Blanc (7 MeV/90 T)+	5 (6–10 MeV/7 sec)
"" ±1 min	Kamioka (8 MeV/2.14 kT)	2 (7–12 MeV/10 sec)
""	IMB (30 MeV/5 kT)	none reported
""	Baksan (11 MeV/130 T)+	none reported
23 7h 35m (± min)	Kamioka (7 MeV/90 T)	11 (7–35 MeV/13 sec)
23 7h 35m	IMB (30 MeV/5 kT)	8 (20–40 MeV/4 sec)
""	Baksan (11 MeV/130 T)+	3 (12–17 MeV/10 sec)
""	Mt. Blanc (7 MeV/90 T)+	2 (7–9 MeV/13 sec)
sum of pulses	Homestake ν_e (0.7 MeV/615 T)**	consistent with background
	Optical	
23 9h 25m	lack of sighting	$m_v \gtrsim 8$ magnitude
23 10h 40m	photograph	$m_v = 6$ magnitude
24 10h 53m	discovery	$m_v = 4.8$ magnitude

*Threshold is when efficiency drops to $\lesssim 50\%$ (sub-threshold events are therefore possible).

+These detectors are liquid scintalators with $H_{2n+n}C_n$, thus have $\sim$ 1.39 more free protons than H_2O detectors of same mass.

**The Homestake detector is only sensitive to ν_e's. It is made of C_2Cl_4.

all groups are in agreement that there was an event at 7h 35m UT on February 23, there is some question about an earlier event seen at the Mt. Blanc detector at 2h 52m UT. When the IMB detection of the second event is used to calibrate the Kamioka clock and Kamioka looks back at the earlier time, it has two events in the 8-second window around the earlier Mt. Blanc detection. However, with the detector more than 20 times bigger, one might expect a somewhat larger number of events. I will return in a moment to the possible discrepancies here.

The latter, well-confirmed event fits remarkably well with expectations for a standard core collapse of a massive star. From the early 1970s it was realized that the cores of all massive stars would essentially be at the Chandrasekhar mass for their final collapse. This is because the evolution of these massive stars, once they get beyond carbon burning, is dominated by neutrino emission. Thus, the core evolves as if it is decoupled from the outer edge of the star, the neutrinos stream straight through. Each of these stars goes through successive burning stages until it produces a 1.4$M_\odot$ iron core. Since there is no further nuclear energy to be released from iron, the iron core collapse becomes catastrophic. It is the collapse of this iron core down to the neutron-star densities and conditions that yields a supernova, and also yields a huge emission of neutrinos. In fact, in order to get down to a neutron star state, the core must radiate the binding energy of a neutron star, which for 1.4$M_\odot$ is about 2×10^{53} ergs. Since the energy of the supernova itself, its hydrodynamics and luminosity in electromagnetic radiation is only the order of 10^{51} ergs, the bulk of the binding energy must be emitted as neutrinos. (Gravitational waves have been shown to make up less than one percent of the emitted energy.) In the early 1970s, it was also known (see, for example, Schramm and Arnett 1974) that the typical energy of the electron neutrinos emitted from such a collapse would be about 10 MeV, and that the other neutrino species would be emitted through neutral current processes. For mu and tau neutrinos, the opacities were somewhat lower than electron neutrinos due to only neutral-current contributions, thus their temperatures and their energies, would be somewhat higher. In the recent detailed calculations of Mayle, Wilson, and Schramm[6], it was found that the mu and tau neutrinos were coming out with average energies of about 20 MeV and the electron anti-neutrinos approximately midway between 10 and 20 MeV, starting low and gradually rising with time. Thus, it had been expected for a long time that if a collapse did occur it should be a significant neutrino burst.

The actual structure of the burst comes in two parts. The first, the neutralization where essentially all of the protons in the core are converted to neutrons. This produces approximately 10^{57} 10 MeV electron neutrinos, yielding about 2×10^{52} ergs. The remaining 90% of the binding energy comes off in neutrino–anti-neutrino pairs via $e^+e^- \rightarrow \nu\bar{\nu}$. Via neutral currents, it has been known since the mid-1970s that all types of neutrinos would be produced in this emission. Since the detectors are most sensitive to $\bar{\nu}_e$s, that means they are only sensitive to about 1/6 of the emitted neutrinos from the supernova. Using this fact, one can trivially estimate[5] the number of counts one expects in a $\bar{\nu}_e$ detector of any given size for a SN in LMC, 50 kpc away. For example, one expects for the Kamioka detector with 2140 tons of water, approximately 10 $\bar{\nu}_e$ captures. For the Mt. Blanc detector, with 90 tons of scintillator, one expects about 1/2 a capture from a collapse[4,5]. The IMB detector is somewhat more problematic because its threshold is so high that it is only getting the high-energy tail. The high-energy tail is slightly more model dependent than the bulk energetic arguments mentioned above. In Mayle, Wilson and Schramm, it was shown that the high-energy tail would have a slightly higher characteristic temperature than the peak of the distribution, thus enhancing the ability of IMB to see events. If we use the Mayle, Wilson and Schramm[6] calculations and the cross sections for anti-neutrino capture[5], one estimates that about six counts would be expected in the 5,000 ton IMB detector. Thus, from the observations shown in Table 1, it is clear that the second burst fits remarkable well with what one expects.

In addition to the $\bar{\nu}_e$ captures there would also be some electron scattering possibilities. All of the neutrino types are able to scatter off electrons, however, their cross sections for this process are all very small. At 10 MeV the cross section for electron neutrinos scattering off electrons is a factor of $\sim$ 80 below the cross section for anti-neutrino capture[5]. The cross section for ν_μ scattering is down by another factor of six below the electron neutrino scattering. However, there are five times as many free electrons in a water Cherenkov detector as there are free protons. Thus, the huge cross section difference is suppressed somewhat. In addition, there are slightly more electron neutrinos because of the neutralization burst at the beginning of the collapse. Neutronization burst only lasts, in the standard models, a few tens of milliseconds, whereas the rest of the neutrinos come out over several seconds in the standard models with the length of time depending on assumptions about collapse hydrodynamics, total binding energy to be emitted, etc. Thus, there might be a slightly greater possibility of electron scattering events in the first fraction of a second of the detected neutrino burst. In fact, Kamioka did see two events pointed toward the LMC in their initial time bins. One would have expected from a collapse event that produced 10 $\bar{\nu}_e$s approximately 0.7 neutrino $\nu_e - e$ scatterings and a comparable rate for the sum of all other neutrinos scattering off of electrons. Thus a total of about 1–1.5 electron scatterings. We see two or possibly three electron scattering events in the Kamioka data. It is thus not out of line with what one expects, especially considering statistics of small numbers. The fact that the Davis ^{37}Cl experiment has not seen any excess counts argues that there is not any significant excess of electron neutrinos in this collapse event and that the electron neutrinos have energies

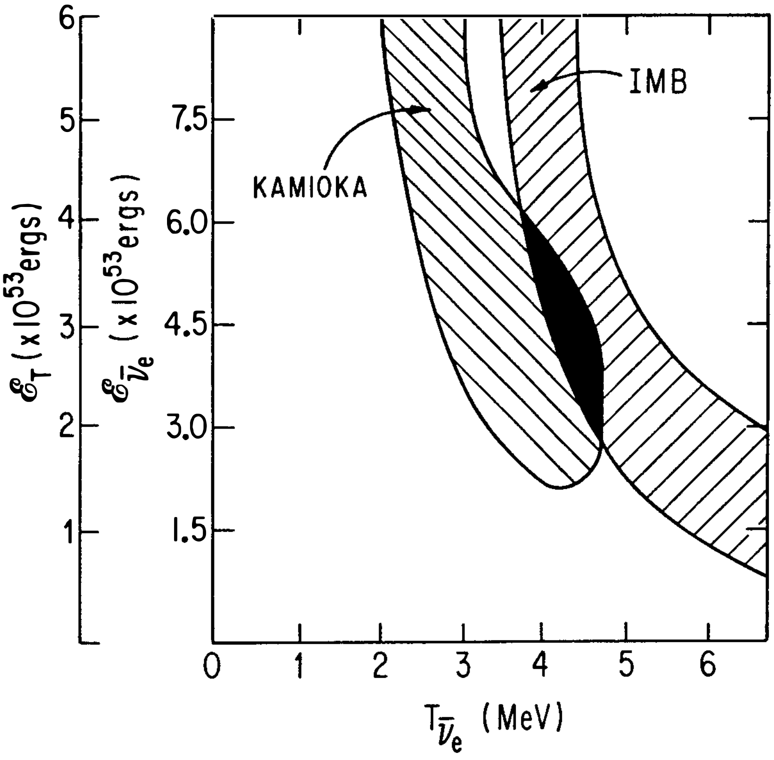

Figure 1: Neutrino Temperature and energy emitted as implied by Kamioka and IMB data[5].

approximately what one would expect, since the cross section for a ^{37}Cl neutrino capture is a very steep function of energy, $E^{3.7}$. Although, for a standard model, one does not expect the chlorine experiment to have any significant counts above the normal low rate from the Sun.

If we deconvolute the observed number of events and their mean energy to say what temperature and luminosity the Kamioka and IMB bursts imply, we find that they imply a temperature for the $\bar{\nu}_e$ of approximately 4 MeV and a total luminosity emitted in all types of neutrinos of 2 to 4 $\times$ 10^{53} ergs. A remarkable agreement with what simple model estimates, made over ten years ago, would have predicted (see, for example, Freedman, Schramm and Tubbs[7], or the Proceedings of the DUMAND Conference[8]). Figure 1 shows the temperature and emitted energies of Kamioka and IMB burst and the overlap region. Note that the central temperature value for Kamioka is below the central value for IMB. It is possible that instead of these both sampling the same temperature, they're really sampling slightly different temperature distribution, since in the Mayle, Wilson and Schramm models, the temperature of the high-energy tail is a little bit higher than the peak temperature.

If we apply the same temperature total energy emitted analysis to the first event reported by Mt. Blanc, we get a curious result. The temperature to fit the events is down around 1

MeV and the luminosity is up greater than a few $\times 10^{54}$ ergs. That is, it is greater than the rest mass energy of a neutron star. The luminosity–temperature distribution would imply events that might also be difficult for Kamioka to see, since the temperature is so low and Kamioka's threshold is higher than Mt. Blanc's. (It is clear that small statistical variations in the Mt. Blanc implied temperature toward the lower side would yield a distribution that would be difficult for Kamioka to see.) Therefore, experimentally one can not rule out that Mt. Blanc was seeing a real event and Kamioka was just unlucky due to the low temperature of the distribution Mt. Blanc was sampling. At the same time, the temperature was so low that the higher thresholds of IMB and Baksan prevented detection. However, the temperature and energy characteristics that such an event would have are very difficult to understand in any reasonable theoretical model, while the Kamioka–IMB burst fits standard theory extraordinarily well. Of particular concern is the total energy emitted which would imply a very large massive object.

There is the curiosity that room-temperature gravitational wave detector[9] in Italy and also the room-temperature gravitational wave detector in Maryland di report noise coincident with the Mt. Blanc event. However, these room-temperature detectors would have required several thousand masses of energy in gravitational waves for an event in the Magellanic Clouds to produce a detectable signal. The alternative is either to say that something very bizarre took place initially and it somehow converted to a rather normal collapse, after five hours, or to say that the earlier burst was unrelated to the LMC event, in which case the huge energies implied could be reduced, and the other event could be very near-by but hidden in a dust cloud so that it produced nothing optically. However, this latter case would require the amazing coincidence that this strange event occurred at approximately the same time as the Supernova in LMC. Thus, without further evidence, I'm inclined to take the Eddington view that any observation in astronomy that is not confirmed by theory is suspect. However, this should not be interpreted as any fault on the part of experimentalists at Mt. Blanc who have done a fantastic job, and who had the foresight to realize the importance of neutrinos from supernovae.

As far as the physics that can be obtained from this neutrino event, much has been written. In fact, the number of papers on neutrino mass far exceeds the number of events that have been seen. However, when it really comes down to it, there will always be some model dependence. In addition, one has to not only interpret whether or not the late counts in Kamioka are due to the intrinsic spread of the emitted burst or due to a finite mass, or should be dismissed for some obscure reason and whether the width of the burst is due to a finite neutrino mass or intrinsic-ness, or in fact whether a finite neutrino mass has compressed the width of the burst due to, for example, the higher energy neutrinos being emitted later than the lower energy neutrinos, as occurs in the Mayle, Wilson, Schramm models. In fact, when all of the data is combined, I believe that all one can fairly state is that the mass implied is probably less than about 30 eV, which is not as good as the experimental limits from tritium decay[10]. Any statements with regard to finite neutrino masses are clearly model dependent. Any statements about a mass of a neutrino other than $\bar{\nu}_e$ are very difficult to make, due to the extremely low cross sections for all other events. Although some limits can be set on mixing with finite masses, I think it would be difficult to use the SN 1987A to rule out cosmologically significant masses for the mu- and tau-neutrino.

There is an interesting physical result that can be obtained on the number of neutrino flavors. This comes from the fact that the neutrinos, through neutral currents, are emitted in all flavors and yet a finite detection occurred in $\bar{\nu}_e$'s, so the number of flavors cannot be too large or the number of $\bar{\nu}_e$'s detected would be reduced below the observed result. In another paper[11] presented at this conference, it was shown that that limit is approximately 7 neutrino flavors, which is not as good as one can do cosmologically, but is comparable to current experimental limits and further confirms that the total number of families seems to be small.

From the total energetics and the fact that anti-neutrinos were emitted in significant numbers, one can also set limits on the axion coupling constant[12]. By using the zone where the neutrinos are emitted, the limit on the axion coupling constant, $f > 10^9$ GeV, comparable to the limits that came from red giants[13]. However, if one takes into account axion emission from the core of the star, where neutrinos don't get out but axions do, this limit can be strengthened considerably, and severely tightens the limits on the axion coupling constant[12].

The limits on neutrino mixing were discussed prior to the supernova explosion by Walker and Schramm[14]. The fact that some ν_e's were detected seems to rule out the standard adiabatic MSW mixing scenario. However, non-adiabatic MSW that does not solve solar neutrinos can still be allowed.

A trivial statement is the fact that neutrinos made it to us from the LMC constrains the lifetime times gamma to sufficiently large values that neutrinos probably made it to us from the sun, unless there was some sort of optimized mixing[15].

3. Dark Matter

At this conference, Krauss presented a review talk on dark matter, and there were several mentions of dark matter throughout. The dark matter questions of cosmology have been reviewed extensively at other places[17]. The important point here is that in the last year or so, neutrinos have reemerged as a possible candidate for dark matter if they have masses of 20 to 30 eV. The most likely candidate would be the tau-neutrino since it is the neutrino associated with the heaviest family. The reemergence of neutrinos has occurred due to the fact that Turok, Schramm, Brandenburger and Kaiser[18,19] have shown that galaxies are able to form sufficiently rapidly in hot dark matter models, if the initial perturbations are in the form of strings rather than random adiabatic fluctuations. While the cold matter model has the advantage of being easy to do calculations and thus has very definitive predictions, these predictions apparently seem to be causing it problems in that it has difficulty in fitting the large-scale cluster–cluster correlation functions and the large-scale velocity fields. Of course, the large-scale velocity fields are extraordinarily debatable at the present time. Clearly, more definitive work with new catalogs and unbiased selection techniques are needed before the final nails can be driven into the cold matter coffin.

An important point that has been emphasized by Freese and Schramm[19] is that big bang nucleosynthesis seems to imply that there are dark baryons, and in fact, the bulk of the baryons appear to be dark. It was emphasized by Gott, Gunn, Schramm, and Tinsley[20] in 1974 that baryon densities in big bang nucleosynthesis are in very good agreement with the dynamical densities implied by binaries and small groups, which include dark halos. Thus, it is reasonable, though not compulsory, to assume that the halos are baryonic rather than made out of some exotic dark matter candidate. At this conference, we heard a very nice argument by Andy Fabian[21] with regard to X-rays which favor baryonic halos. We also heard arguments by Zinneker that it is possible to form low mass, low luminosity objects which would make excellent baryonic dark halos and slip through the loophole that Olive and Hegyi[23] left with regard to baryonic halo matter. Obviously, much more remains to be done with regard to the dark matter questions.

4. Star Bursts and Galactic Evolution

The central topic of this conference had to do with the astronomically interesting phenomenon, the star burst, where large numbers of massive stars are produced in a short time. This phenomenon makes for very interesting observations, since massive stars are easy to see, and they also produce lots of energy yielding HII regions, etc. In addition, star-forming regions are famous for their infrared emission and the new IRAS survey certainly added much information about this phenomenon and star formation in general in other galaxies.

One of the problems that I encountered in the many presentations at this meeting, was that in this area, as opposed to cosmology, there is so much information that one worries whether or not we're going to miss the main processes because absorbed in the details. In particular, I have to worry whenever I see problems that involve hydrodynamics, magnetic fields, and turbulence, that we may be finding ourselves in the famous conundrum formulated by Steve Wolfram on cellular automata. Namely that while many cellular automata have the property that they converge to some final result independent of the initial conditions, there is a sub-class of such cellular automata where the final result is totally dependent on the initial conditions in the microscopic way. Certain physical problems such as weather may fall into this sub-set. For example, the classic statement, 'what is the effect of a butterfly flapping its wings in the amazon jungle on the weather in Les Arcs?' might not be totally irrelevant. However, even if it is proven that the solutions to the kinds of problems being studied are indeed of the initial-condition dominated variety, we should not stop exploring for macroscopic trends. Just as one might be able to understand global or continental weather patterns while one cannot predict in detail the weather tomorrow.

With these caveats, let us look at what the questions are that emerged and what are the things that we have accomplished.

1. What is the standard IMF? Are there bumps? What is the nature of the high mass end? What about a high- and/or low-mass cutoff? What is the role of mass loss, Wolf–Rayet stars, etc. in estimating the IMF? These topics were addressed by Scalo[24], Thuan[25], Larson[26], de Fuzio[27], Chieze[28], Conti[29], and Maeder[30]. Others addressed the possibility of bimodality with a bump at the high end[31,25], or a large low-end peak[21,22]. There was also the question of whether the IMF was varied in models when the real culprit is some other parameter[24,16]. The questions of whether the IMF depended on galaxy type or metalicity were also discussed[24–27,31,32]. The resolution to all these problems requires a fundamental physical understanding of chaos, hydrodynamics, atomic physics, thermodynamics, etc. Until such understanding occurs we may be stuck with our present empirical approach.
2. The Role of Star Bursts. Do they play a role in 'normal' galaxy evolution[24,33,34]? (They seem to be found in all galaxies.) Are they always triggered by dynamical interactions, or does normal evolution also produce them35? Rowan–Robinson[36] showed that IRAS galaxies don't always show interactions, but could dust obscuration hide it? Ikeucki[37] and Montmerle[38] discussed the role of infall shocks, etc.
3. Relation of Star Bursts to Active Galactic Nuclei (AGN). There was much discussion related to AGN's. Is the AGN a central monster or multiple flashes? AGN's were discussed

by Joseph[39], Fabian[21], Norman[40], Terlevich[41], and Heckman[42].

4. Ellipticals. An active question centered around whether or not ellipticals formed from collisions, as shown in the simulations of Combes[35] in colliding spirals, or in the mergers of smaller galaxies as shown by Norman[40].
5. Relation of IRAS Galaxies and Star-Burst Galaxies. Rowan–Robinson[36] separated the IRAS galaxies into three components: disk-like, seyfert-like, and star burst. Thus, he implied that not all IRAS galaxies are star-burst galaxies contrary to some people's preconceptions.
6. Energy Flow. The question of 'where does the star-burst energy go' was discussed in detail by Ikeuchi[37], Zinnecker[22], Montmerle[38], and Heckman[42]. Effects such as chimneys, shocks and general flows, or just heating were mentioned. In addition, the angular momentum flow during galaxy and star-burst formation was discussed[43].
7. Galactic Evolution in Cosmology. Several speakers[33,44–46] attempted to model galactic evolution in enough detail to use galaxies for cosmological studies. Potentially, the impact is very high, however, more needs to be done.

In general, I was struck by how much had become known since I last looked in detail at some of the galactic evolution questions, but also by how many of the questions that we asked a decade ago are still relevant questions today.

This was clearly a successful conference due not only to the fine work of the organizing committee but also to the luck of the gods for the supernova going off just the week before.

5. Acknowledgements

I wish to acknowledge the hospitality of the Max Planck Institut in Munich and an Alexander von Humboldt award. This work was supported in part by the NSF at the University of Chicago and by the NASA at Fermilab.

6. References

1. W. Brunish and J. Truran, *Astrophys. J.*, 1983.
2. S. Woosley, University of California, Santa Cruz preprint, 1987.
3. A. Savaadra, *Proc. XXII Recontre de Moriond*, 1987; A. Pomansky, ibid; J. VanDerVelde, ibid; K. Tanaka, ibid.
4. R. Schaefer, ibid.
5. D. Schramm, *Comments on Nuclear and Particle Physics*, submitted, 1987.
6. R. Mayle, J. Wilson, and D. Schramm, *Astrophys. J.*, in press, 1987.
7. D. Freedman, D. Schramm, and D. Tubbs, *Ann. Rev. Nucl. Part. Sci.* **27**, 167, 1977.
8. *Proc. DUMAND Symposium*, ed. A. Roberts, Fermilab, 1977.
9. U. Amaldi, *Proc. XXII Recontre de Moriond*, 1987.
10. Kunde, *Proc. XXI Recontre de Moriond*, 1986.
11. D. Schramm, *Proc. XXII Recontre de Moriond*, 1987.
12. K. Olive and J. Ellis, CERN preprint, 1987; R. Mayle, J. Wilson, J. Ellis, K. Olive, D. Schramm, and G. Steigman, in preparation, 1987.
13. D. Dearborn, D. Schramm, and G. Steigman, *Phys. Lett.* B, submitted, 1987.
14. T. Walker and D. Schramm, in press, 1987.
15. J. Frieman and K. Freese, SLAC preprint, 1987.
16. L. Krauss, *Proc. XXII Recontre de Moriond*, 1987.
17. D. Schramm, ibid, and references therein.

18. N. Turok, D. Schramm, R. Brandenburger, and N. Kaiser, FNAL preprint, 1987.
19. K. Freese and D.N. Schramm, *Nucl. Phys.* **B233**, 167, 1984.
20. J. Gott, J. Gunn, D. Schramm, and B. Tinsley, *Astrophys. J.*, 1984.
21. A. Fabian, *Proc. XXII Recontre de Moriond*, 1987.
22. H. Zinneker, ibid.
23. K. Olive and D. Hegyi, *Nature*, 1985.
24. J. Scalo, *Proc. XXII Reçontre de Moriond*, 1987.
25. T. Thuan, ibid.
26. R. Larson, ibid.
27. A. de Fazio, ibid.
28. C. Chieze, ibid.
29. P. Conti, ibid.
30. A. Maeder, ibid.
31. P. Mezger, ibid.
32. J. Lequieux, ibid.
33. A. Djorgorski, ibid.
34. R. O'Connell, ibid.
35. F. Combes, ibid.
36. M. Rowan–Robinson, ibid.
37. I. Ikeuchi, ibid.
38. T. Montmerle, ibid.
40. C. Norman, ibid.
41. R. Terlevich, ibid.
42. H. Heckman, ibid.
43. R. Pulritz, ibid.
44. E. Athansoula, ibid.
45. B. Rocca–Volerauge, ibid.
46. E. Ferrari, ibid.

AUTHOR INDEX

LIST OF PARTICIPANTS

ARNAULT, P.	Institut d'Astrophysique, Paris, France
ATHANASSOULA, E.	Observatoire de Marseille, Marseille, France
BELFORT, P.	Institut d'Astrophysique, Paris, France
BERGVALL, N.	Uppsala Astronomical Observatory, Uppsala, Sweden
BOSMA, A.	Observatoire de Marseille, Marseille, France
BUAT, V.	Observatoire de Marseille, Marseille, France
CASPERS, H.	Sterrewacht Leiden, Leiden, The Netherlands
CESARSKY, C.	CEN Saclay, Gif-sur-Yvette, France
CHIEZE, J. P.	CEA, Bruyères-le-Chatel, France
CHIEZE-TURCK, S.	CEN Saclay, Gif-sur-Yvette, France
CHINI, R.	MPI für Radioastronomie, Bonn, West Germany
COMBES, F.	Ecole Normale Supérieure, Paris, France
COMTE, G.	Observatoire de Marseille, Marseille, France
CONTI, P.	University of Colorado, Boulder, USA
DANESE, L.	Universita di Padova, Padova, Italy
DI FAZIO, A.	Osservatorio Astronomico, Roma, Italy
DJORGOVSKI, S.	California Institute of Technology, Pasadena, USA
DONAS, J.	Observatoire de Marseille, Marseille, France
FABIAN, A.	University of Cambridge, Cambridge, United Kingdom
FERRINI, F.	Istituto di Astronomia, Pisa, Italy
FRITZE, U.	University of Göttingen, Göttingen, West Germany
GONZALEZ-RIESTRA, R.	IUE - Vila Franca, Madrid, Spain

HARVEY, P.	Université de Grenoble, Grenoble, France
HECKMAN, T.	University of Maryland, College Park, USA
HEYVAERTS, J.	Observatoire de Meudon, Meudon, France
HIPPELEIN, H. H.	MPI für Astronomie, Heidelberg, West Germany
HUCHRA, J.	Center for Astrophysics, Cambridge, USA
IKEUCHI, S.	Tokyo Astronomical Observatory, Tokyo, Japan
JOSEPH, R.	Imperial College, London, United Kingdom
KEEL, W.	Sterrewacht Leiden, Leiden, The Netherlands
KLAAS, U.	MPI für Astronomie, Heidelberg, West Germany
LARSON, R.	Yale University, New Haven, USA
LE FEVRE, O.	Canada-France-Hawaii Telescope Corporation, Kamuela, USA
LEQUEUX, J.	Observatoire de Marseille, Marseille, France
LORTET, M. C.	Observatoire de Meudon, Meudon, France
MAEDER, A.	Observatoire de Geneve, Sauverny, Switzerland
MARTIN, J. M.	Observatoire de Meudon, Meudon, France
MASEGOSA, J.	Inst. de Astrofisica de Andalucia, Granada, Spain
MELNICK, J.	European Southern Observatory, Garching, West Germany
MEZGER, P.	MPI für Radioastronomie, Bonn, West Germany
MIRABEL, I.	University of Puerto Rico, San Juan, Puerto Rico
MONTMERLE, T.	CEN Saclay, Gif-sur-Yvette, France
MOSS, C.	University of Cambridge, Cambridge, United Kingdom
NORMAN, C.	Space Telescope Science Institute, Baltimore, USA
O'CONNELL, R.	University of Virginia, Charlottesville, USA
PAGEL, B.	Royal Greenwich Obervatory, Hailsham, United Kingdom

PALLA, F.	Osservatorio Astrofisico Arcetri, Firenze, Italy
PANTELAKI, I.	Rice University, Houston, USA
PUDRITZ, R.	McMaster University, Hamilton, Canada
RADFORD, S.	Université de Grenoble, Grenoble, France
REEVES, H.	CEN Saclay, Gif-sur-Yvette, France
ROCCA-VOLMERANGE, B.	Institut d'Astrophysique, Paris, France
ROWAN-ROBINSON, M.	Queen Mary College, London, United Kingdom
RYTER, C.	CEN Saclay, Gif-sur-Yvette, France
SCALO, J.	University of Texas, Austin, USA
SCHRAMM, D.	University of Chicago, Chicago, USA
SCHWERING, P.	Sterrewacht Leiden, Leiden, The Netherlands
SOUCAIL, G.	Observatoire de Toulouse, Toulouse, France
TENORIO-TAGLE, G.	European Southern Observatory, Garching, West Germany
TERLEVICH, R.	Royal Greenwich Observatory, Hailsham, United Kingdom
THUAN, T. X.	University of Virginia, Charlottesville, USA
WIKLIND, T.	Onsala Space Observatory, Onsala, Sweden
WOLSTENCROFT, R.	Royal Observatory, Edinburgh, United Kingdom
ZAMORANO, J.	Dept. de Astrofisica, Madrid, Spain
ZINNECKER H.	Royal Observatory, Edinburgh, United Kingdom